

# 231

## Topics in Current Chemistry

### Editorial Board:

A. de Meijere · K.N. Houk · H. Kessler · J.-M. Lehn  
S.V. Ley · S.L. Schreiber · J. Thiem · B.M. Trost  
F. Vögtle · H. Yamamoto

**Springer**

*Berlin*

*Heidelberg*

*New York*

*Hong Kong*

*London*

*Milan*

*Paris*

*Tokyo*

# Elemental Sulfur and Sulfur-Rich Compounds II

Volume Editor: Ralf Steudel

With contributions by  
B. Eckert · R. Okazaki · R. Steudel · N. Takeda  
N. Tokitoh · M.W. Wong



Springer

The series *Topics in Current Chemistry* presents critical reviews of the present and future trends in modern chemical research. The scope of coverage includes all areas of chemical science including the interfaces with related disciplines such as biology, medicine and materials science. The goal of each thematic volume is to give the nonspecialist reader, whether at the university or in industry, a comprehensive overview of an area where new insights are emerging that are of interest to a larger scientific audience.

As a rule, contributions are specially commissioned. The editors and publishers will, however, always be pleased to receive suggestions and supplementary information. Papers are accepted for *Topics in Current Chemistry* in English.

In references *Topics in Current Chemistry* is abbreviated *Top Curr Chem* and is cited as a journal.

Visit the TCC home page at <http://www.springerlink.com>

ISSN 0340-1022

ISBN 3-540-40378-7

DOI 10.1007/b11909

Springer-Verlag Berlin Heidelberg New York

Library of Congress Catalog Card Number 74-644622

This work is subject to copyright. All rights are reserved, whether the whole or part of the material is concerned, specifically the rights of translation, reprinting, reuse of illustrations, recitation, broadcasting, reproduction on microfilms or in any other ways, and storage in data banks. Duplication of this publication or parts thereof is only permitted under the provisions of the German Copyright Law of September 9, 1965, in its current version, and permission for use must always be obtained from Springer-Verlag. Violations are liable for prosecution under the German Copyright Law.

Springer-Verlag is a part of Springer Science+Business Media

[springeronline.com](http://springeronline.com)

© Springer-Verlag Berlin Heidelberg 2003

Printed in Germany

The use of general descriptive names, registered names, trademarks, etc. in this publication does not imply, even in the absence of a specific statement, that such names are exempt from the relevant protective laws and regulations and therefore free for general use.

Cover design: KünkelLopka, Heidelberg/design & production GmbH,  
Heidelberg

Typesetting: Stürtz AG, 97080 Würzburg

02/3020 ra - 5 4 3 2 1 0 - Printed on acid-free paper

---

## Volume Editor

Prof. Dr. Ralf Steudel

Technische Universität Berlin  
Institut für Anorganische  
und Analytische Chemie / Sekr. C2  
Straße des 17. Juni 135  
10623 Berlin, Germany  
*E-mail: steudel@schwefel.chem.tu-berlin.de*

## Editorial Board

Prof. Dr. Armin de Meijere

Institut für Organische Chemie  
der Georg-August-Universität  
Tammannstraße 2  
37077 Göttingen, Germany  
*E-mail: ameijer1@uni-goettingen.de*

Prof. Dr. Horst Kessler

Institut für Organische Chemie  
TU München  
Lichtenbergstraße 4  
85747 Garching, Germany  
*E-mail: kessler@ch.tum.de*

Prof. Steven V. Ley

University Chemical Laboratory  
Lensfield Road  
Cambridge CB2 1EW, Great Britain  
*E-mail: svl1000@cus.cam.ac.uk*

Prof. Dr. Joachim Thiem

Institut für Organische Chemie  
Universität Hamburg  
Martin-Luther-King-Platz 6  
20146 Hamburg, Germany  
*E-mail: thiem@chemie.uni-hamburg.de*

Prof. Dr. Fritz Vögtle

Kekulé-Institut für Organische Chemie  
und Biochemie der Universität Bonn  
Gerhard-Domagk-Straße 1  
53121 Bonn, Germany  
*E-mail: voegtle@uni-bonn.de*

Prof. K.N. Houk

Department of Chemistry and  
Biochemistry  
University of California  
405 Hilgard Avenue  
Los Angeles, CA 90024-1589, USA  
*E-mail: houk@chem.ucla.edu*

Prof. Jean-Marie Lehn

Institut de Chimie  
Université de Strasbourg  
1 rue Blaise Pascal, B.P.Z 296/R8  
67008 Strasbourg Cedex, France  
*E-mail: lehn@chimie.u-strasbg.fr*

Prof. Stuart L. Schreiber

Chemical Laboratories  
Harvard University  
12 Oxford Street  
Cambridge, MA 02138-2902, USA  
*E-mail: sls@slsiris.harvard.edu*

Prof. Barry M. Trost

Department of Chemistry  
Stanford University  
Stanford, CA 94305-5080, USA  
*E-mail: bmtrost@leland.stanford.edu*

Prof. Hisashi Yamamoto

School of Engineering  
Nagoya University  
Chikusa, Nagoya 464-01, Japan  
*E-mail: j45988a@nucc.cc.nagoya-u.ac.jp*

## **Topics in Current Chemistry Also Available Electronically**

For all customers who have a subscription to Topics in Current Chemistry, we offer the electronic version via SpringerLink free of charge. Please contact your librarian who can receive a password for free access to the full articles by registering at:

<http://www.springerlink.com>

If you do not have a subscription, you can still view the tables of contents of the volumes and the abstract of each article by going to the SpringerLink Homepage, clicking on “Browse by Online Libraries”, then “Chemical Sciences”, and finally choose Topics in Current Chemistry.

You will find information about the

- Editorial Board
- Aims and Scope
- Instructions for Authors
- Sample Contribution

at <http://www.springeronline.com> using the search function.

---

## Preface

Despite more than 200 years of sulfur research the chemistry of elemental sulfur and sulfur-rich compounds is still full of “white spots” which have to be filled in with solid knowledge and reliable data. This situation is particularly regrettable since elemental sulfur is one of the most important raw materials of the chemical industry produced in record-breaking quantities of ca. 35 million tons annually worldwide and mainly used for the production of sulfuric acid.

Fortunately, enormous progress has been made during the last 30 years in the understanding of the “yellow element”. As the result of extensive international research activities sulfur has now become the element with the largest number of allotropes, the element with the largest number of binary oxides, and also the element with the largest number of binary nitrides. Sulfur, a typical non-metal, has been found to become a metal at high pressure and is even superconducting at 10 K under a pressure of 93 GPa and at 17 K at 260 GPa, respectively. This is the highest critical temperature of all chemical elements. Actually, the pressure-temperature phase diagram of sulfur is one of the most complicated of all elements and still needs further investigation.

Sulfur compounds have long been recognized as important for all life since sulfur atoms are components of many important biologically active molecules including amino acids, proteins, hormones and enzymes. All these compounds take part in the global geobiochemical cycle of sulfur and in this way influence even the earth’s climate. In interstellar space, on other planets as well as on some of their moons have elemental sulfur and/or sulfur compounds also been detected. The best known example in this context is probably Jupiter’s moon Io, first observed by Galileo Galilei in 1610, which according to modern spectroscopic observations made from the ground as well as from spacecrafts is one of the most active bodies in the solar system with quite a number of sulfur volcanoes powered by sulfur dioxide and spraying liquid sulfur onto the very cold surface of this moon.

The general importance of sulfur chemistry is reflected in the long list of monographs on special topics published continuously, as well as in the huge number of original papers on sulfur related topics which appear every year. Regularly are international conferences on organic and inorganic sulfur chemistry held, and specialized journals cover the progress in these areas.

In Volumes 230 and 231 of *Topics in Current Chemistry* eleven experts in the field report on the recent progress in the chemistry and physics of elemental

sulfur in the solid, liquid, gaseous and colloidal form, on oxidation products of elemental sulfur such as polyatomic sulfur cations and sulfur-rich oxides which both exhibit very unusual structures, on classical reduction products such as polysulfide dianions and radical anions as well as on their interesting coordination chemistry. Furthermore, the long homologous series of the polysulfanes and their industrial significance are covered, and novel methods for the removal of poisonous sulfur compounds from wastegases and wastewaters in bioreactors taking advantage of the enzymatic activities of sulfur bacteria are reviewed. In addition, the modern ideas on the bonding in compounds containing sulfur-sulfur bonds are outlined.

The literature is covered up to the beginning of the year 2003. A list of useful previous reviews and monographs related to the chemistry of sulfur-rich compounds including elemental sulfur is available on-line as supplementary material to these Volumes.

As the guest-editor of Volumes 230 and 231, I have worked for 40 years in basic research on sulfur chemistry, and I am grateful to my coworkers whose names appear in the references, for their skillful experimental and theoretical work. But my current contributions to these Volumes would not have been possible without the continuous encouragement and assistance of my wife Yana who also took care of some of the graphical work. The constructive cooperation of all the co-authors and of Springer-Verlag, Heidelberg, is gratefully acknowledged.

Berlin, April 2003

Ralf Steudel

---

## Contents

<b>Quantum-Chemical Calculations of Sulfur-Rich Compounds</b> M. W. Wong .....	1
<b>Molecular Spectra of Sulfur Molecules and Solid Sulfur Allotropes</b> B. Eckert · R. Steudel .....	31
<b>Inorganic Polysulfanes <math>H_2S_n</math> with <math>n&gt;1</math></b> R. Steudel .....	99
<b>Inorganic Polysulfides <math>S_n^{2-}</math> and Radical Anions <math>S_n^{\bullet-}</math></b> R. Steudel .....	127
<b>Polysulfido Complexes of Main Group and Transition Metals</b> N. Takeda · N. Tokitoh · R. Okazaki .....	153
<b>Sulfur-Rich Oxides <math>S_nO</math> and <math>S_nO_2</math></b> R. Steudel .....	203
<b>Author Index Volumes 201–231 .....</b>	231
<b>Subject Index Vol. 230 .....</b>	241
<b>Subject Index Vol. 231 .....</b>	245

---

## **Contents of Volume 230**

### **Elemental Sulfur and Sulfur-Rich Compounds I**

**Volume Editor: Ralf Steudel**

ISBN 3-540-40191-1

#### **Solid Sulfur Allotropes**

R. Steudel · B. Eckert

#### **Liquid Sulfur**

R. Steudel

#### **Speciation and Thermodynamics of Sulfur Vapor**

R. Steudel · Y. Steudel · M. W. Wong

#### **Homoatomic Sulfur Cations**

I. Crossing

#### **Aqueous Sulfur Sols**

R. Steudel

#### **Biologically Produced Sulfur**

W. E. Kleinjan · A. de Keizer · A. J. H. Janssen

# Quantum-Chemical Calculations of Sulfur-Rich Compounds

Ming Wah Wong

Department of Chemistry, National University of Singapore, Science Drive, 3,  
117543, Singapore, Singapore  
E-mail: [chmwmw@nus.edu.sg](mailto:chmwmw@nus.edu.sg)

**Abstract** In this chapter, we review the application of quantum-chemical calculations to a range of sulfur-rich compounds, including disulfane, polysulfanes, sulfur clusters and their cations, anions and protonated forms, as well as sulfur-sulfur three-electron bonded systems. Special emphasis is placed on their roles in understanding the molecular structures, thermochemical properties, chemical bonding and reaction mechanisms of this class of compounds.

**Keywords** Sulfur clusters · Quantum chemical calculations · Ab initio · DFT · Structure · Bonding · Hemibonds · Cations · Anions · Halides · Polysulfanes · Spectra

1	Introduction . . . . .	2
2	Computational Methods . . . . .	2
3	Disulfane $H_2S_2$ and its Derivatives. . . . .	4
4	Polysulfanes $H_2S_n$ . . . . .	7
5	Sulfur Clusters $S_n$ . . . . .	11
6	Cluster Anions $S_n^{--}$ and $S_n^{2-}$ . . . . .	16
7	Cluster Cations $S_n^{++}$ and $S_n^{2+}$ . . . . .	18
8	Protonated Sulfur Clusters $HS_n^+$ . . . . .	21
9	Three-Electron S-S Bonds . . . . .	23
10	Concluding Remarks . . . . .	26
	References . . . . .	26

## 1 Introduction

The field of quantum chemistry has witnessed dramatic developments in the past decades, which led to the emergence of many novel theoretical techniques. Theoretical calculations using a variety of computational methods, ranging from force field, semiempirical [1], ab initio [2] to density functional [3] methods, have been reported for numerous sulfur-rich compounds. These quantum-chemical calculations were employed to determine molecular structures, vibrational frequencies and one-electron properties. They were also used to investigate problems related to reaction energies and thermochemical data. In particular, they have been used extensively to make predictions of bond dissociation energies, ionisation energies, electron affinities, appearance energies, proton affinities and enthalpies of formation. Several quantum-chemical studies aimed to explore potential energy surfaces, particularly the characterization of transition states, which allow the determination of activation energies and thus the understanding of the mechanism of complex reactions.

Many of the sulfur-rich compounds considered in this chapter are unstable reactive species so that important properties such as geometrical structures, vibrational spectra and reaction energies are difficult to obtain experimentally and remain uncertain. In these cases, theory is particularly suited to provide the necessary complementary information to understand and interpret the experimental observations for these systems.

## 2 Computational Methods

Before 1980, force field and semiempirical methods (such as CNDO, MNDO, AM1, etc.) [1] were used exclusively to study sulfur-containing compounds due to the lack of computer resources and due to inefficient quantum-chemical programs. Unfortunately, these computational methods are rather limited in their reliability. The majority of the theoretical studies under this review utilized ab initio MO methods [2]. Not only ab initio MO theory is more reliable, but also it has the desirable feature of not relying on experimental parameters. As a consequence, ab initio MO methods are applicable to any systems of interest, particularly for novel species and transition states.

The choice of basis set in ab initio calculations has been the subject of numerous theoretical studies. Early SCF calculations utilized mainly split-valence basis sets such as 3-21G and 4-31G. The importance of inclusion of *d* polarization functions on sulfur atoms has been stressed by several authors. For instance, Suleimenov and Ha found that the omission of *d* polarization functions leads to a substantially lower barrier for the internal rotation ( $\sim 16$  kJ mol<sup>-1</sup> for the central bond of H<sub>2</sub>S<sub>4</sub>) and produces an unrealistically large S-S bond length for the most stable rotamer [4]. In general, the use of

split-valence polarized basis sets (e.g. 6-31G\*) is sufficient for the purpose of geometry optimisation. Inclusion of diffuse functions is desirable for studying anions and three-electron bonded species. Magnusson and Schaefer noted that multiple *d* functions are particularly important for second-row atoms if they are in high formal oxidation states [5]. For calculations of very large system, the use of the effective core potential (ECP) provides an alternative to the more demanding all-electron basis sets. In the ECP basis sets, the effect of the inner (or core) electrons is approximated by a set of potential functions.

For “normal” sulfur-containing compounds, the Hartree-Fock (HF) method reproduces the experimental geometries reasonably well. However, for systems containing highly electronegative elements and systems containing hypervalent atoms, optimisations at a correlated level lead to significant changes in geometries from the HF results. For example, HF calculations failed to predict the short S-S bond length in FSSF [6]. Furthermore, it failed to predict the correct stability order of the two S<sub>2</sub>F<sub>2</sub> isomers (FSSF and F<sub>2</sub>S=S). Incorporation of the electron correlation at the MP2 level of theory resolved the two major defects in the HF results.

To obtain a satisfactory evaluation of relative energies, especially for the computation of activation barriers, higher levels of theory than those needed to obtain the underlying geometries are usually required. MP2 is the most economical and popular method of incorporation electron correlation. For a more accurate theoretical estimate, higher-level of correlation treatment such as QCISD(T) or CCSD(T) theory is desirable.

Extensive comparisons of experimental frequencies with HF, MP2 and DFT results have been reported [7–10]. Calculated harmonic vibrational frequencies generally overestimate the wavenumbers of the fundamental vibrations. Given the systematic nature of the errors, calculated raw frequencies are usually scaled uniformly by a scaling factor for comparison with the experimental data.

To predict thermochemical data with an accuracy of  $\pm 8$  kJ mol<sup>-1</sup>, quantum-chemical calculations using high-level correlation methods, such as QCISD(T) and CCSD(T), in conjugation with very large basis sets are required. The Gaussian series of theories (G1, G2 and G3) by Pople et al. [11] as well as the complete basis set (CBS) methods of Petersson et al. (e.g. CBS-4, CBS-Q, CBS-APNO, etc.) [12] are the most popular composite methods for computing thermochemical data. In these composite methods, a basis-set additivity approximation is employed to obtain an effective energy corresponding to the QCISD(T) level with a very large basis set. The methods G1, G2 and G3 as well as their variants have been applied to many molecular systems and in most cases quite successful.

Quantum-chemical calculations which utilize the density functional theory (DFT) are now perhaps amongst the most frequently performed because of their relatively low cost and high accuracy. Structural results obtained from DFT based methods are often as good as those derived from MP2 calculations. It is well documented that DFT methods, especially those involving hybrid functionals such as B3LYP, B3P86 and B3PW91, yield reliable

structures and vibrational frequencies for organic and inorganic compounds as well as transition metal complexes [13]. It seems that DFT has adopted the role of a standard tool for the prediction of molecular structures. For instance, the new variants of G3, namely G3X and G3X(MP2) [14], utilize the B3LYP/6-31G(2df,p) level for geometry optimisations as well as for frequency calculations.

In this review, we consider the application of quantum-chemical calculations to a range of sulfur-rich compounds. The empirical, semiempirical and ab initio MO calculations published before 1980 are considered rather inadequate. Therefore, theoretical calculations before 1980 will not be mentioned in detail here.

### 3 Disulfane H<sub>2</sub>S<sub>2</sub> and its Derivatives

The S-S bond between two divalent sulfur atoms plays an important role as the main stabilizer of the tertiary structure of many proteins. The simplest chemically stable compounds of this class are HSSH and CH<sub>3</sub>SSCH<sub>3</sub>. The structures of these two disulfanes have been established by microwave spectroscopy and electron diffraction experiments.

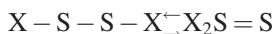
H<sub>2</sub>S<sub>2</sub> (hydrogenpersulfide), the smallest member of the polysulfane series [15], has been studied extensively by molecular spectroscopy and theoretical calculations [16] (and references therein). By now, accurate knowledge of its structure, torsional potential and vibrational modes has been established. Ab initio calculations readily reproduce these properties [17]. The value of the SSH angle in hydrogen disulfide was a subject of controversies for some time. However, recent experiments led to a different value which is in favour of the ab initio calculated value [17].

Early SCF studies [18, 19] on dimethyl disulfane (CH<sub>3</sub>SSCH<sub>3</sub>) employed medium-sized basis sets to predict its molecular structure and electronic properties. These studies demonstrated the importance of adding *d* polarization functions to the double-zeta type of basis sets. Li et al. have calculated the adiabatic ionisation energy of dimethyl disulfane using high-level G2(MP2) theory [20]. Their calculated value of 8.15 eV is in pleasing agreement with their measured value (8.18±0.03 eV), determined from pulsed molecular beam photoionisation mass spectrometric experiments. In contrast to the neutral disulfane which has only one stable structure of C<sub>2</sub> symmetry, the CH<sub>3</sub>SSCH<sub>3</sub><sup>+</sup> radical cation has two stable planar conformations: the *trans* (C<sub>2h</sub>) and the *cis* (C<sub>2v</sub>) form. The *trans*-conformer is predicted to be slightly more stable, by 16 kJ mol<sup>-1</sup>. The G2(MP2) rotational barriers around the S-S bond of CH<sub>3</sub>SSCH<sub>3</sub> are predicted to be 47 (*trans*) and 24 (*cis*) kJ mol<sup>-1</sup>, respectively.

It is well established that disulfur difluoride (S<sub>2</sub>F<sub>2</sub>) exists in two isomeric forms, the nonplanar disulfane FSSF and the branched thiosulfoxide form F<sub>2</sub>S=S, with the latter found to be the more stable isomer. Both isomers have been characterized by microwave spectroscopy, mass spectrometry, infrared and Raman spectroscopy as well as photoelectron spectra [6] (and refer-

ences therein). Marsden and co-workers re-determined the structures of both  $S_2F_2$  isomers based on a joint analysis of electronic diffraction data and rotational constants reported in the literature [6]. Extensive ab initio calculations were also carried out for both FSSF and  $F_2S=S$  in parallel with their experimental work. Reliable prediction of the molecular geometry of FSSF represented a major challenge to quantum-mechanical calculations a decade ago. Early semiempirical calculations [6] (and references therein) are rather poor in reproducing the experimental S-S bond length. SCF calculations employing a triple-zeta basis set with multiple polarization functions also failed to reproduce the spectacularly short S-S distance. It is too long by 45 pm even at the Hartree-Fock limit. On the other hand, inclusion of electron correlation at the MP2 level led to a substantial improvement to the geometry predicted for FSSF. At the SCF level, FSSF is predicted to be more stable than  $F_2S=S$ , though by decreasing amounts as the basis quality improved. Experimentally the opposite order has been established.

Solouki and Bock reported the first theoretical study on the isomerization reaction



of several disulfanes ( $X=H, F, Cl$ ) using semiempirical CNDO calculations [21]. A more comprehensive study employing ab initio and density functional calculations was reported subsequently by Bickelhaupt, Sola and Schleyer [22]. The disulfane isomers are found to be more stable than the corresponding thiosulfoxides, and  $X_2S=S$  becomes less stable with respect to  $XSSX$ , and the S-S bond elongates along the series  $X=F, Cl, CH_3$  and H. These authors interpreted their results by means of a natural population analysis (e.g. the interaction between the formal disulfur moiety  $S_2^{2-}$  and the two univalent substituents X). The bonding in the hypervalent  $X_2S=S$  species is similar to the bonding in the nonhypervalent  $XSSX$  and does not involve a special role for the sulfur-3d orbitals. Schleyer et al. also showed that the DFT and conventional ab initio results on optimised structures and isomerization energies agree well.

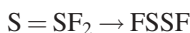
The relative stabilities of  $RSSR$  and  $R_2S=S$  for  $R=OH$  and  $SH$  have been determined by Stedel and co-workers [23, 24]. At the MP2/6-311G\*\*//HF/6-311G\*\*+ZPE level of theory,  $(HO)_2S=S$  (thiosulfurous acid) is just 13 kJ mol<sup>-1</sup> less stable than the chain-like isomer  $HOSSOH$  (dihydroxydisulfane) [23]. For  $R=SH$ ,  $(HS)_2S=S$  is less stable than the corresponding trisulfane  $HSSSH$  by 132 kJ mol<sup>-1</sup> (MP2/6-31G\*\*//HF/4-31G) [24].

Thionylfluoride  $F_2S=S$  is one of the few examples of a stable compound containing an S=S double bond. Stedel et al. explored the stabilities of organic thiosulfoxides  $R_2S=S$  ( $R=H, Me, Pr, All$ ), using ab initio MP2/6-311G\*\* calculations [25]. These authors determined the structures and energies of organic thiosulfoxides as well as the activation energies for their formation from the corresponding disulfanes.  $H_2S=S$  is calculated to be 143 kJ mol<sup>-1</sup> less stable than  $HSSH$ , and separated by an activation barrier of 210 kJ mol<sup>-1</sup>. Likewise,  $Me_2S=S$  is 84 kJ mol<sup>-1</sup> higher in energy than

MeSSMe and inhibited to isomerise by a significantly larger isomerization barrier of  $340 \text{ kJ mol}^{-1}$ . Thus, both  $\text{H}_2\text{S}=\text{S}$  and  $\text{Me}_2\text{S}=\text{S}$  are predicted to be kinetically stable toward unimolecular isomerization and should be experimentally observable in the gas phase or after matrix isolation. HF/6-31G\* calculations indicate that the allyl analogue has a similar  $\text{R}_2\text{S}=\text{S}/\text{RSSR}$  energy difference but a substantially lower activation barrier ( $110 \text{ kJ mol}^{-1}$ ) for rearrangement [25].

The existence of organic thiosulfoxides  $\text{X}_2\text{S}=\text{S}$  ( $\text{X}=\text{H}$ ,  $\text{CH}_3$  and  $\text{C}_2\text{H}_5$ ) was proven recently by Flammang et al. using a combination of tandem mass spectrometry methodologies in conjunction with neutralization-reionisation and ion-molecule reactions [26]. The corresponding radical cations were also observed in the MS experiments. Ab initio calculations at the MP2/6-311+G\*\*//MP2/6-31G\*+ZPE level were also employed to investigate the potential energy surface for isomerization of the ionised disulfanes. Flammang et al. found that the ionised thiosulfoxides ( $\text{X}_2\text{SS}^+$ ) and disulfanes ( $\text{XSSX}^+$ ) are stable energy minima, with the disulfane isomers being more stable (by 91, 65 and  $59 \text{ kJ mol}^{-1}$  for  $\text{X}=\text{H}$ ,  $\text{CH}_3$  and  $\text{C}_2\text{H}_5$ , respectively). The energy difference between the two isomers is significantly smaller than with their neutral counterparts. In sharp contrast to the neutral RSSR molecules, the  $\text{RSSR}^+$  radical cations are calculated to have a *trans*-planar chain conformation, which can be explained by the formation of a three-electron  $\pi$  bond. Isomerization of  $\text{XSSX}^+$  to  $\text{X}_2\text{SS}^+$ , via a simple 1,2-X shift, is calculated to have a moderate energy barrier ( $197$ ,  $262$  and  $233 \text{ kJ mol}^{-1}$  for  $\text{X}=\text{H}$ ,  $\text{CH}_3$  and  $\text{C}_2\text{H}_5$ , respectively). Thus, the calculated kinetic stabilities support the observation of both isomeric ionic structures.

The isomerization of disulfanes to thiosulfoxides has been studied by several groups [17, 21, 23, 27–29]. The theoretical estimates of their activation energies indicate that the unimolecular uncatalysed isomerization of disulfanes to thiosulfoxides will not take place at low temperatures. With such a high energy barrier, interconversion of  $\text{F}_2\text{S}=\text{S}$  and FSSF via an unimolecular rearrangement is unlikely to happen under the normal experimental conditions. Therefore, Schleyer et al. proposed an alternative bimolecular mechanism for which lower-energy transition states can be conceived. The effect of solvation on the rearrangement reaction



has been investigated by Toro-Labbe using DFT calculations [29]. Their result suggests that this intramolecular rearrangement reaction is thermodynamically and kinetically more favourable in solution.

Cooper et al. [30] were successful in rationalizing the striking variation in the S-S equilibrium bond lengths of FSSF ( $189.0 \text{ pm}$ ), ClSSCl ( $195.0 \text{ pm}$ ) and HSSH ( $205.5 \text{ pm}$ ) using the spin coupled (modern valence bond) theory. In the disulfur dihalides, but not for HSSH, incipient hypercoordinate character is observed at sulfur, with two partial  $\pi$ -like interactions in approximately perpendicular planes, and some antibonding character in the S-X ( $\text{X}=\text{F}$  or  $\text{Cl}$ ) bonds. In other words, it is the form of  $\pi$ -like orbitals that is most rele-

vant to the experimental observation of a short S-S separation and of relatively long S-F bonds in FSSF. The degree of delocalisation of electron density from the  $\pi$ -like orbital onto the neighbouring sulfur atom follows the order expected from the S-S bond lengths, i.e. FSSF > ClSSCl > HSSH.

The SS bond in thiosulfoxides may be considered as either “double” or “semipolar” depending on the electronegativity of the substituents [25]; see Scheme 1.



Scheme 1

The calculated (MP2/6-311G\*\*) S-S bond distances for  $\text{H}_2\text{SS}$  and  $\text{Me}_2\text{SS}$  are 201.8 and 200.3 pm, respectively. The experimental value for  $\text{F}_2\text{S}=\text{S}$  is 185.6 pm, while the thiosulfite  $(\text{RO})_2\text{S}=\text{S}$  has an S-S bond length of 190.1 pm. These data can be rationalized in terms of the inductive effect of R on the polarisable sulfur atoms.

## 4

### Polysulfanes $\text{H}_2\text{S}_n$

It is well established that sulfur compounds as well as elemental sulfur have the tendency to form long chain molecules. All of these substances can be regarded as derivatives of the hydrogen polysulfanes (or polysulfanes)  $\text{H}_2\text{S}_n$ . Polysulfanes form a long series of homologous chain-like molecules since the number  $n$  can assume any value. S-S and S-H bonds are frequently found in chemical and biological systems. Thus, polysulfanes have been the subject of numerous experimental and theoretical studies (for a recent review, see [15]).

The lower members of the polysulfane series with  $n=2-6$  have been prepared as pure compounds, while all members with  $n$  values up to 35 have been detected by  $^1\text{H-NMR}$  spectroscopy in so-called “crude sulfane” [31]. The gas-phase structures of the first three members of the polysulfane series are well established from either microwave spectra ( $\text{H}_2\text{S}_2$  [32],  $\text{H}_2\text{S}_3$  [33]) or high-level ab initio MO calculations ( $\text{H}_2\text{S}_4$  [34]). Systematic ab initio studies of the structures, vibrational frequencies and heats of formation of  $\text{H}_2\text{S}_n$  with  $n$  up to 6 have also been reported [4, 16].

While  $\text{H}_2\text{S}_2$  adopts a conformation of  $C_2$  symmetry similar to that of  $\text{H}_2\text{O}_2$ ,  $\text{H}_2\text{S}_3$  and probably also  $\text{H}_2\text{S}_4$  exist as equilibrium mixtures of several conformational isomers of almost identical energy. All polysulfane molecules are characterized by torsional angles at the S-S bonds of  $\sim 90^\circ$  ( $\pm 10^\circ$ ), but these angles may be positive or negative resulting in the different conformational isomers. Thus, hydrogen trisulfide,  $\text{H}_2\text{S}_3$  may exist in two confor-

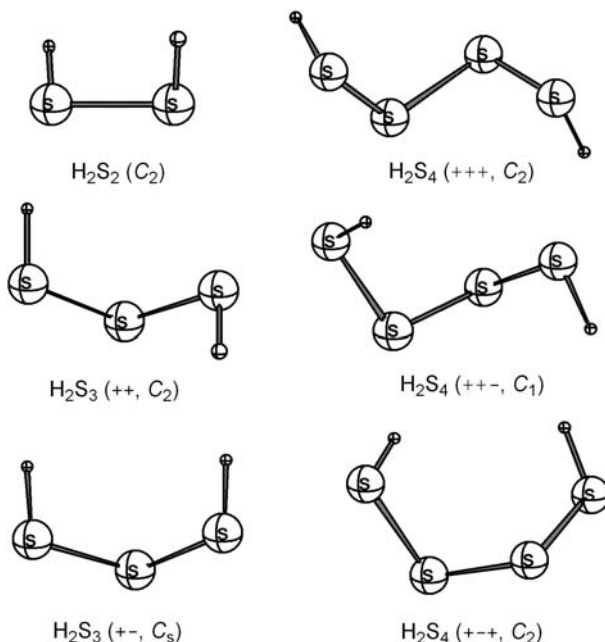


**Fig. 1** Conformers of  $\text{H}_2\text{S}_2$ ,  $\text{H}_2\text{S}_3$  and  $\text{H}_2\text{S}_4$

mations: *trans* (motif ++,  $C_2$  symmetry) and *cis* (+-,  $C_s$  symmetry) (Fig. 1). The best theoretical treatments of  $\text{H}_2\text{S}_3$  correspond to the MP2/MC-311G(d,p) and QCISD/MC-311G(d,p) calculations of Winnewisser, Cremer and co-workers [35]. Both conformers were found to lie very close in energy, with a slight preference of the *trans*-form, by  $1.0 \text{ kJ mol}^{-1}$ . This theoretical prediction was nicely confirmed by their experiments, which yielded an estimate of  $1.3 \text{ kJ mol}^{-1}$  for the *cis/trans* energy difference. The relative stability of the *trans*-conformer was attributed to the favourable alignment of S-H bond dipoles. The increase in S-S bond lengths on going from  $\text{H}_2\text{S}_2$  to  $\text{H}_2\text{S}_3$  can be explained by the anomeric delocalisation of electron lone pairs at the terminal sulfur atoms. The *trans*-form of  $\text{H}_2\text{S}_3$  was first characterized by millimetre wave and infrared Fourier transform spectroscopy [35]. Subsequently, the gas-phase molecular structures of both *cis*- and *trans*-forms were finally characterized by their rotational spectra [32]. The MP2/MC-311G(d,p) structural parameters are in pleasing agreement with the observed  $r_s$  structures. In addition, the ratio of the calculated dipole moments  $\mu(\text{cis})=2.02 \text{ D}$  and  $\mu(\text{trans})=0.68 \text{ D}$ , is also in excellent accord with the experimental ratio of 2.7.

The structures, energies, torsional barriers and vibrational spectra of three rotamers of tetrasulfane,  $\text{H}_2\text{S}_4$ , have been examined by Drozdova, Miaskiewicz and Steudel at the MP2/6-311G\*\* level [34]. Surprisingly, the *cis-trans* conformation (motif ++-; symmetry  $C_1$ ) is found to be most stable, followed by the all-*cis* form (+-+; symmetry  $C_2$ ), while the helical all-

*trans* (motif +++; symmetry  $C_2$ ) is least stable, by 0.7 kJ mol<sup>-1</sup> (Fig. 1). This energy increases to 2.4 kJ mol<sup>-1</sup> at the CCSD(T)/ANO-DZ//MP2-6-311G\*\* level of theory [36]. This calculated stability order demonstrates that the frequently cited statement that “the structure of highest symmetry is the most stable one” is not always correct. It is worth noting that organic polysulfanes R-S<sub>n</sub>-R with  $n=4-7$  and 9 exist as either helical or non-helical rotamers in the solid state [37]. The predicted *cis*- and *trans*-rotational barriers of H<sub>2</sub>S<sub>4</sub> are 32 and 27 kJ mol<sup>-1</sup> (31 and 24 kJ mol<sup>-1</sup> at the CCSD(T)/ANO-DZ//MP2-6-311G\*\* level of theory [36]). The geometries of the two rotational transition states display an interesting bond distance pattern: the central S-S bond is considerably elongated while the terminal S-S bonds are shortened. This bond alternation was explained by a hyperconjugation between the  $3p_\pi$  lone pairs at the two terminal sulfur atoms with the  $\sigma^*$  molecular orbital of the two central sulfur atoms [34].

The general structural features of long-chain polysulfanes can be deduced from the MP2/6-31G\* geometries of the helical structures of H<sub>2</sub>S<sub>n</sub> ( $n=1-6$ ) [4]. The S-S bond lengths agree well with the commonly accepted value of S-S single bond (206 pm). The calculated ellipticities, which reflect the  $\pi$  characters, of the sulfur chain bonds are close to zero. However, the calculated AIM bond orders are  $\sim 1.28$ . All bond angles are calculated to be between 107.0° and 107.5°, while the dihedral angles are between 79.0° and 90.4°. These dihedral angles are largely governed by the requirement of the minimal repulsions between lone pairs on the sulfur atoms.

Suleimenov and Ha have used high-level G2 and CBS-Q ab initio methods to study the thermochemical properties of gaseous polysulfanes (H<sub>2</sub>S<sub>n</sub>,  $n=1-6$ ) [4]. The enthalpy of formation were calculated from atomisation energies and from enthalpies of dehydrogenation reactions such as shown in Eq. (1):



The G2 enthalpies of formation using the atomisation enthalpies are significantly different from the experimental values, but the CBS-Q values are in good agreement with the experimental data. In distinct contrast, G2 theory performs extremely well comparing to the CBS-Q theory for the calculation of the heats of formation obtained from the enthalpies of dehydrogenation reactions. This can be explained partially by the cancelling out of empirical corrections for polysulfane hydrogenation reactions at the G2 level. The calculated mean bond energies (*B.E.*) from CBS-Q calculations are *B.E.*(H-S)=348 kJ mol<sup>-1</sup> and *B.E.*(S-S)=266 kJ mol<sup>-1</sup>.

The gas-phase acidities  $\Delta G_{\text{acid}}(298 \text{ K})$  of the first four members of the polysulfanes H<sub>2</sub>S<sub>n</sub> ( $n=1-4$ ) have been investigated by Otto and Stuedel using high-level G2 and G2(MP2) methods [38]. Although hydrogen sulfide H<sub>2</sub>S is known to be a weak acid in water with a  $\text{p}K_{\text{a}}$  value of 7, in the gas-phase the higher polysulfanes are predicted to be strong proton donors. The gas-phase acidities are defined as the Gibbs energies of the deprotonation reaction and are computed follows (in kJ mol<sup>-1</sup>):

$\text{H}_2\text{S}$  (1444),  $\text{H}_2\text{S}_2$  (1406),  $\text{H}_2\text{S}_3$  (1370),  $\text{H}_2\text{S}_4$  (1347)

The latter values may be compared to those of other strong Brønsted acids like gaseous  $\text{HNO}_2$  (1396),  $\text{HCl}$  (1371) and  $\text{HBr}$  (1332), the gas-phase acidities of which are given in parentheses. It is worth noting that the G2 acidities of  $\text{H}_2\text{S}$  and  $\text{H}_2\text{S}_2$  (1446 and 1407  $\text{kJ mol}^{-1}$ ) are in very good agreement with the experimental values ( $1443\pm 8$  and  $1418\pm 13$   $\text{kJ mol}^{-1}$  [39]). The monoanions  $\text{HS}_n^-$ , i.e. the conjugate bases of  $\text{H}_2\text{S}_n$ , are found to exhibit an interesting bond length pattern: the S-S bond adjacent the S-H bond being the longest and the terminal S-S bond significantly shorter. The calculated NBO atomic charges indicate that the negative charge is delocalised over all sulfur atoms. The bond length pattern and charge distribution were explained in terms of a hyperconjugation between the  $3p$  lone pair at the terminal sulfur atom and the antibonding  $\sigma^*$  molecular orbital of a neighbouring bond. The stabilities of the  $\text{HS}_n^-$  anions are responsible for the high acidities of the polysulfanes. Higher sulfanes  $\text{H}_2\text{S}_5$  and  $\text{H}_2\text{S}_6$  are expected to be even stronger acids [38].

Wong et al. [40] examined the relative stability of the branched isomer  $(\text{HSS})_2\text{S}=\text{S}$  of hexasulfane  $\text{H}_2\text{S}_6$ . The calculated G3X(MP2) enthalpy difference between these two isomers is found to be surprisingly low: 53  $\text{kJ mol}^{-1}$ . For comparison, the small thiosulfoxide molecules like  $\text{H}_2\text{S}=\text{S}$  and  $\text{Me}_2\text{S}=\text{S}$  are much less stable with respect to their unbranched isomers  $\text{HSSH}$  and  $\text{MeSSMe}$ , by 140 and 80  $\text{kJ mol}^{-1}$ , respectively [33, 34]. The stabilization of the branched  $\text{H}_2\text{S}_6$  structure was attributed to the neighbouring S-S bonds. As reflected in the optimised geometry, the four S-S bonds in the branched polysulfane chain are pairwise much longer (233 pm) and much shorter (202 pm) than the bond distances of  $208.1\pm 0.1$  pm calculated for helical  $\text{H}_2\text{S}_6$ . This structural feature and the stabilizing effect can readily be explained by a  $\pi^*-\pi^*$  interaction.

Papadopoulos et al. investigated the structure-polarization relationship in a series of polysulfanes using several semiempirical (MNDO and MNDO/d) and ab initio (MP2/STO-3G\*\*++ and MP2/[ $3s2p/7s5p2d$ ]) methods [41]. They studied the effect of changes of the geometry of  $\text{H}_2\text{S}_n$  ( $n$  up to 50) on their polarizabilities and second hyperpolarizabilities. Several models for  $\text{H}_2\text{S}_n$  were considered. A remarkable variation of the hyperpolarizabilities with the molecular geometry of  $\text{H}_2\text{S}_n$  was found. As sulfur is involved in derivatives with nonlinear electric properties, this structure-polarization relationship may be used as a tool for designing nonlinear optical materials.

The S-S bond dissociation energies of  $\text{H}_2\text{S}_2$ ,  $\text{H}_2\text{S}_3$  and  $\text{H}_2\text{S}_4$  have been studied by Steudel et al. at the CCSD(T)//6-311+G(2df,p) level [42]. The calculated enthalpies  $\Delta H^\circ$  for the dissociation at the central bonds at 298 K are 247, 201 and 159  $\text{kJ mol}^{-1}$ , respectively. The lower stability of the tri- and tetrasulfanes towards homolytic S-S cleavage is attributed to the stability of the generated  $\text{HSS}^\cdot$  radical which is stabilized by the formation of a three-electron  $\pi$  bond.

## 5 Sulfur Clusters $S_n$

Sulfur is unique in its propensity to catenation. It is well established that sulfur atoms avoid the formation of double bonds (at temperatures near 298 K) by joining its atoms into  $S_n$  rings (cyclosulfur,  $n=6, 7$  or  $8$ , for example) or high molecular weight chains  $S_n$  (catena-sulfur) instead of  $S_2$  molecules ( $S=S$ ). In fact, sulfur is the element with the largest number of solid allotropes. More than 30 crystalline allotropes are known, most of which are composed of homocyclic rings [43–45]. As a result, a large number of electronic structure studies have been devoted to sulfur clusters in the past two decades, using mainly *ab initio* and density functional methods with various levels of sophistication. There are several systematic studies on a range of cluster size:  $S_2$ – $S_{13}$  by Hohl, Jones, Car and Parrinello (MD/DFT) [46],  $S_2$ – $S_8$  by Laitinen, Pakkanen and co-workers (HF/MZ and HF/DZP) [47,48],  $S_2$ – $S_{12}$  by Raghavachari, Rohlfing and Binkley (MP3/6-31G\*\*/HF/3-21G\*) [49, 50],  $S_4$ – $S_8$  by Dixon and Wasserman (MP2/MC-DZP//HF/MC-DZP) [51],  $S_3$ – $S_{13}$  by Yilmaz and Erkoç (MNDO) [52],  $S_3$ – $S_8$  by Warren and Gimarc (MNDO and MP2/MC-DZP) [53],  $S_5$ – $S_8$  rings by Cioslowski, Szarecka and Moncrieff (B3LYP/6-311G\* and MP2/6-311G\*) [54],  $S_2$ – $S_{11}$  by Au and co-workers (B3LYP/6-31G\*) [55],  $S_2$ – $S_{12}$  by Millefiori and Alparone (CCSD(T)/aug-cc-pVDZ//B3LYP/cc-pVDZ) [56],  $S_6$ – $S_{16}$  by Peter (B3PW91/6-311+G(3df)) [57],  $S_2$ – $S_{20}$  by Ludwig, Behler, Klink and Weinhold (B3LYP/6-31+G\* and MP2/6-31+G\*) [58],  $S_2$ – $S_{18}$  by Jones and Ballone (Monte Carlo/DFT) [59], and  $S_2$ – $S_{10}$  by Steudel, Steudel and Wong (G3X(MP2)) [60].

In 1986, Schaefer et al. reported the first extensive *ab initio* calculations of  $S_3$  [61]. SCF and CISD calculations indicated that the global minimum is the ring  $D_{3h}$  form. The more sophisticated CASSCF and MR-CISD calculations, on the other hand, favoured the open bent structure of  $C_{2v}$  symmetry. The preference of the open form was subsequently confirmed by several other theoretical investigations [62–65]. The  $D_{3h}$  structure is calculated to be 31–44 kJ mol<sup>-1</sup> less stable than the open  $C_{2v}$  structure, depending on the method of calculation and the level of theory applied [56, 59–65]. The best estimate of the S-S bond length of the  $C_{2v}$  form is 193.2 pm (CCSD(T)) [65] and the bond angle is 117°. Compared with the multireference calculations, DFT methods adequately describe the structure and PES of  $S_3$ .

$S_4$  represents one of the best studied  $S_n$  clusters [46, 51, 55, 56, 59, 60, 66–68]. The structures and relative energies of the  $S_4$  isomers are extremely sensitive to the level of theory being employed. As a result, several different isomers have been proposed as the global energy minimum of  $S_4$ . The controversial problem is further complicated by the fact that the rectangular  $D_{2h}$  structure is predicted as the global minimum by MP2 [49], MD-DFT [46] and MC-DFT [59] calculations. The best earlier investigation of  $S_4$  corresponds to the two-configuration CISD calculations of Quelch, Schaefer and Marsden [66]. Recent high-level G3X(MP2) and CCSD(T)/aug-cc-pVTZ [60] calculations confirmed that the singlet *cis*-planar  $C_{2v}$  structure is the lowest-energy structure on the  $S_4$  PES, with the *trans*-planar  $C_{2h}$  isomer significant-

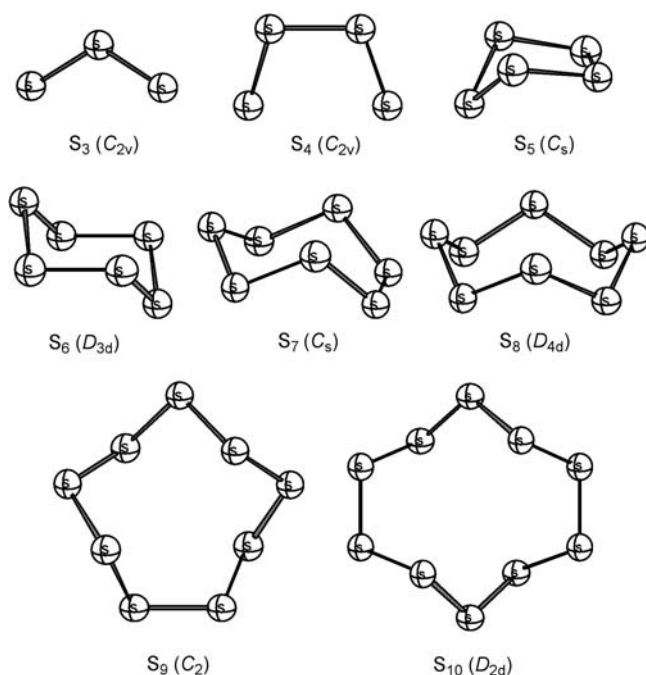


**Fig. 2** Ground-state structures of  $S_n$  clusters ( $n=1-10$ )

ly higher in energy. The rectangular  $D_{2h}$  geometry is not an equilibrium structure, but corresponds to a transition state which interconverts two *cis*-planar forms. Based on several theoretical studies, the relative energies of the various  $S_4$  isomers are in the order  $C_{2v} < C_{2h} < C_s < D_{2d} < D_{3h}$ . The most stable triplet  $S_4$  is predicted to lie close in energy to the singlet ground state ( $50 \text{ kJ mol}^{-1}$ ) and has an open  $C_{2v}$  geometry.

Wong et al. [60] recently calculated the electronic and vibrational spectra of several  $S_4$  isomers in an effort to provide a more definitive assignment of the spectra of the various observed  $S_4$  isomers. The calculated transition energies of the  $C_{2v}$  and  $C_{2h}$  isomers (566 and 634 nm, respectively) match very well with the UV-vis spectra of the observed green and red absorbing  $S_4$  isomers [69–71]. The branched ring  $S_3=S$  of  $C_s$  symmetry is predicted to absorb at 240 nm. Thus, it can be concluded that the assignment of  $S_3=S$  as the red light absorbing isomer [70] is probably incorrect.

Most theoretical calculations on  $S_5$  [49, 50, 54, 55, 59, 60] indicate that this homocycle exists exclusively in a highly fluxional  $C_s$  conformation (half-boat) (Fig. 2), and undergoes a facile pseudorotation through a  $C_2$  structure (twist-boat). The computed barrier to this pseudorotation amounts to less than  $2 \text{ kJ mol}^{-1}$ . It is worthwhile to note that LDA calculations predicted the  $C_2$  structure to be a minimum that is almost isoenergetic with its  $C_s$  counterpart [46]. The diradical chain structure of  $S_5$  lies significantly higher in energy than the ring form [49, 50, 55, 59, 60].

As expected, the hexagonal chair form of  $S_6$  with  $D_{3d}$  symmetry, occurring in the solid hexasulfur, is the most stable form of hexasulfur, due to its minimal strain. The boat conformer of  $C_{2v}$  symmetry is  $\sim 50$  kJ mol $^{-1}$  less stable than the chair form [54]. The  $D_{3d} \rightarrow C_{2v}$  interconversion requires to overcome a barrier of ca. 125 kJ mol $^{-1}$ . A structure of  $C_2$  symmetry, which is a local minimum at the HF/3-21G\* level [49, 50], is not a stationary point at higher levels of theory [54, 55].

There are two possible  $C_s$  conformations of the  $S_7$  homocycle: *exo* and *endo*. The *exo* global minimum (Fig. 2) lies  $\sim 15$  kJ mol $^{-1}$  below the *endo*-form. Both conformers undergo facile pseudorotation through  $C_2$  transition states, with barriers of less than 4 kJ mol $^{-1}$  [54]. The *exo*-conformer possesses the geometry found in the sulfur allotropes  $\gamma$ - $S_7$  and  $\delta$ - $S_7$  [72]. This  $C_s$  structure has four bonds near the length of a normal S-S bond and one rather long bond of  $\sim 215$  pm with a dihedral angle of  $0^\circ$ .

Among the various sulfur allotropes,  $S_8$  is the most stable form at STP conditions. It exists as a highly symmetrical  $D_{4d}$  cyclic (crown-shaped) structure, which is well characterized by numerous quantum-chemical calculations. The structures and energies of  $S_8$  isomers have received recent theoretical attention due to the interest in the phase transition occurring in liquid sulfur at 159 °C. Cioslowski et al. [54], Au et al. [55] and Wong et al. [40] explored various possible isomers of  $S_8$ . In addition, Cioslowski et al. provided a comprehensive characterization of the interconversions of the ring conformers [54]. The  $S_8$  isomers considered include the  $C_2$  (*endo-exo* ring),  $C_2$  (twist ring),  $D_{2d}$  (boat)  $C_{2h}$  (chair),  $C_2$  (cluster),  $C_1$  ( $S_7=S_{axial}$ ) and  $C_1$  ( $S_7=S_{equatorial}$ ) structures as well as several open-chain and branched forms. The eight-membered crown- $S_8$  ( $D_{4d}$ ) is confirmed to be the global energy minimum by different levels of theory. Interestingly, a cluster structure with a spiraling chain of 8 atoms ( $C_2$  symmetry), studied previously by Jones and Hohl [73], is predicted to lie close in energy (33 kJ mol $^{-1}$ ) to the crown- $S_8$  minimum [40]. This cluster species is characterized by two three-coordinate atoms and a rectangular arrangement of four sulfur atoms (with bond lengths of 193 and 281 pm) at the formal chain-ends. This unusual cluster geometry was rationalized in terms of a weak  $\pi^*-\pi^*$  bond between the two  $\pi^*$  molecular orbitals of the chain-end groups. Surprisingly, a cuboid structure of  $D_{4h}$  symmetry, consisting of four parallel oriented  $S_2$  molecules interacting by four  $\pi^*-\pi^*$  bonds, is calculated to be a local energy minimum at the MP2/6-31G\* level [40]! However, at the higher levels of theory, B3LYP/6-31G(2df) and QCISD/6-31G\*, this cuboid structure represents a transition state which interconverts two boat-like structures [40].

The most stable isomer of  $S_9$  ( $C_2$  symmetry, Fig. 2) was first predicted by Hohl et al. [46] and was found experimentally in the  $\alpha$ - $S_9$  sulfur allotrope [74]. The calculated lowest-energy structures of  $S_{10}$ ,  $S_{11}$  and  $S_{12}$  correspond to  $D_{2d}$ ,  $C_2$  and  $D_{3d}$  rings. The DFT calculations of these larger rings [46, 49, 50, 57–60] correctly reproduce the observed X-ray structures [75]. The ground-state structures of  $S_3$ – $S_{10}$  are summarized in Fig. 2. The structures and bonding of even larger sulfur rings,  $n=13$ – $20$ , have recently been reported by Peter [57], Ludwig and co-workers [58], and Jones and Ballone [59].

Accurate molecular structures can readily be obtained using a hybrid density functional in conjugation with a flexible basis set. Peter has successfully reproduced the experimental structural parameters of the sulfur rings  $S_6$  to  $S_{14}$  using the B3PW91/6-311+G(3df) [57]. The calculated bond lengths are within 1 pm and the bond angles are within  $2^\circ$ . The vibrational spectra of most sulfur clusters are known [76]. Calculated vibrational spectra can be used to confirm experimental findings and to guide experimentalists to search for novel species. For comparison with experiment, calculated harmonic vibrational frequencies are normally scaled by a uniform scaling factor to account for the overestimation of the computed frequencies at a particularly level of theory [7–10]. For all the calculated frequencies reported for sulfur clusters [49–51, 57], there is an overall good agreement between the scaled computed and experimental values.

Jones and Ballone examined the trend of mean bond energies and structures for the rings  $S_2$ – $S_{18}$ . The calculated variation of bond energy per atom with increasing  $n$  indicates that even-numbered molecules are generally more stable than odd-numbered, with  $S_8$ ,  $S_{12}$ ,  $S_{14}$ ,  $S_{16}$  and  $S_{18}$  being particularly stable. Structures with dihedral angles  $\sim 90^\circ$  are found to be most stable. Ring structures are found to have a strong preference to be singlet states, and the HOMO-LUMO gaps are large and remarkably uniform ( $\sim 210$  kJ mol $^{-1}$ ). Chains are generally less stable than rings. The authors also noted that the most stable calculated structures of the larger clusters may not correspond to those found in crystalline allotropes. For instance, the form of  $S_{18}$  with the calculated lowest energy is not found in the crystalline forms of  $\alpha$ - $S_{18}$  or  $\beta$ - $S_{18}$  [59].

Based on 68 isomers of sulfur clusters  $S_n$  ( $n=3$ – $11$ ), Au et al. have shown that two-fold coordination is generally favoured in sulfur clusters [55]. Structures with atom(s) in one-fold and three-fold coordinations are higher in energy. As a consequence, many large sulfur clusters exist as monocyclic rings while the open-chain forms are significantly less stable.

Millefiori and Alparone calculated the dipole polarizabilities of  $S_n$  clusters up to  $n=12$  using the HF, B3LYP and CCSD(T) methods [56]. They found that

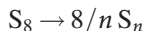
1. The bond energy per atom increases with the size of the cluster and reaches the asymptotic limit for a relatively small  $n$  value.
2. The mean dipole polarizability  $\langle\alpha\rangle$  monotonically increases with  $n$  and linearly correlates with the molecular volume.

From the calculated energies of the disproportionation reaction



they concluded that  $S_2$ ,  $S_6$  and  $S_8$  are particularly stable, in agreement with experiments.

The thermodynamic properties of sulfur clusters have been investigated by Steudel et al. [60] who examined the reaction enthalpies of the interconversion reactions



using the high-level G3X(MP2) theory. Comparing their calculated values with the different sets of experimental gas-phase thermodynamic data indicates that the best agreement corresponds to the vapour pressure measurement by Rau et al. [77]. All the G3X(MP2) values are within 7 kJ mol<sup>-1</sup> of the experimental values except for S<sub>5</sub>. The G3X(MP2) reaction enthalpies are significantly better than those reported previously at the MP2 [51], MP4 [49] and B3LYP [54] levels.

Branched sulfur rings of the type S<sub>n</sub>=S and diradical chains S<sub>n</sub>•• are important intermediates in high-temperature sulfur chemistry. Steudel, Steudel and Wong investigated the branched ring (S<sub>n-1</sub>=S) and the triplet diradicals of S<sub>n</sub>•• (n=1–10) at the G3X(MP2) level [60]. In general, the branched rings favour an exocyclic S=S bond in an axial position. The relative energy of the branched species depends strongly on the size of the system. For the S<sub>5</sub> system, S<sub>4</sub>=S is significantly less stable than the 5-membered homocycle, by 120 kJ mol<sup>-1</sup>. On the other hand, the branched isomer lies just ~30 kJ mol<sup>-1</sup> above the corresponding S<sub>n</sub> global energy minimum for S<sub>8</sub> and S<sub>9</sub>. The larger branched systems are stabilized by the π\*–π\* interaction. The conformations of the triplet diradicals (C<sub>2</sub> symmetry) are best described as a helical chain with two almost planar S<sub>4</sub> terminal units. The geometry of this terminal S<sub>4</sub> moiety is similar to that of the structure of S<sub>4</sub>, which is characterized by two short S-S bonds joined by a relatively long central bond in a *cis* arrangement. For all the long-chain S<sub>n</sub>•• biradicals, the S-S bond distances in the terminal S<sub>4</sub> units are 193, 224 and 202 pm. The four sulfur atoms in the S<sub>4</sub> unit are not exactly coplanar, but with a small torsional angle of 7–9°. For S<sub>8</sub>, the calculated relative enthalpy of the triplet-chain structure (154 kJ mol<sup>-1</sup>) is in excellent agreement with the experimental value of 152 kJ mol<sup>-1</sup> for radical formation in liquid sulfur [78].

Using the first-principles molecular-dynamics simulation, Munejiri, Shimojo and Hoshino studied the structure of liquid sulfur at 400 K, below the polymerization temperature [79]. They found that some of the S<sub>8</sub> ring molecules homolytically open up on excitation of one electron from the HOMO to the LUMO. The chain-like diradicals S<sub>n</sub>•• thus generated partly recombine intramolecularly with formation of a branched S<sub>7</sub>=S species rather than *cyclo*-S<sub>8</sub>. Furthermore, the authors showed that photo-induced polymerization occurs in liquid sulfur when the S<sub>8</sub> chains or S<sub>7</sub>=S species are close to each other at their end. The mechanism of polymerization of sulfur remains a challenging problem for further theoretical work.

## 6 Cluster Anions $S_n^{\cdot-}$ and $S_n^{2-}$

Amongst the singly-charged sulfur cluster anions  $S_n^{\cdot-}$ , the thiozone anion  $S_3^{\cdot-}$  has attracted the most attention as this radical anion had been identified as the key chromophore of the brilliant blue pigment of “Lapis Lazuli” (ultramarine) [80]. Furthermore,  $S_3^{\cdot-}$  was identified as a stable paramagnetic species in the reaction of elemental sulfur with partially hydroxylated magnesium oxide. Several theoretical studies have been reported for the  $S_3^{\cdot-}$  radical anion. The earliest SCF calculation was carried out by Hinchliffe [81], who reported the ground-state open  $C_{2v}$  geometry and its one-electron properties. Subsequently, von Niessen and co-workers considered the geometry and relative stability of the triangular  $D_{3h}$  isomer of  $S_3^{\cdot-}$  [82, 83]. In addition, they predicted the adiabatic and vertical electron affinities of  $S_3$ . The most elaborate calculations of  $S_3^{\cdot-}$  have been published by Koch, Natterer and Heinemann [65]. These authors employed highly correlated MRCI and CCSD(T) wavefunctions together with a large atomic natural orbital (ANO) basis set to investigate the ground state as well as the low-lying electronic states. These calculations confirmed that the  $C_{2v}$  form is the global minimum on the  $S_3^{\cdot-}$  potential energy surface, and the  $D_{3h}$  isomer is considerably higher in energy, by 167–176 kJ mol<sup>-1</sup>. This computed energy difference is significantly larger than for the corresponding neutral  $S_3$  molecule, by 21–25 kJ mol<sup>-1</sup>. The MRCI+Q/ANO6532 calculation yielded  $S_3$  bond lengths of 200.2 pm and a bond angle of 115.1° for the  $C_{2v}$  form of  $S_3^{\cdot-}$ . The presence of the additional electron in the open form of  $S_3^{\cdot-}$  leads to a lengthening of the S-S bonds by 65 pm and a concomitant decrease of the bond angle by 2.7°. These geometrical changes can be rationalized using a molecular orbital argument [65]. The adiabatic electron affinity of thiozone computed at the MRCI+Q/ANO7643 level (2.10 eV) is in perfect agreement with the photoelectron spectroscopy result of Nimolos and Ellison (2.093±0.025 eV) [84]. Due to the required multireference character of the calculations of the neutral, the single-reference CISD+Q and CCSD(T) calculations yield electron affinities which are some 0.2 eV too high. The calculated vertical transition energy of the strong  $\tilde{C}^2A_2 \rightarrow \tilde{X}^2B_1$  transition (2.1 eV) agrees well with the observed strong band in ultramarine at 600 nm (=2.07 eV) [85].

In a rather surprising report, Dehnicke et al. observed the  $S_6^{\cdot-}$  radical anions in the orange-red needles of  $Ph_4P^+S_6^{\cdot-}$ , prepared by the reaction of  $H_2S$  and tetraphenylphosphonium azide in the presence of trimethylsilyl azide at 20 °C [86]. The  $S_6^{\cdot-}$  ions have a disordered chair structure, characterized by two long S-S bonds of 263 pm connecting the  $S_3$  units. The average S-S distance in the two  $S_3$  fragments is 206.0 pm, comparable to that of a typical S-S single bond. To understand the nature of the  $S_6^{\cdot-}$  chair structure in  $Ph_4P^+S_6^{\cdot-}$ , density functional calculations of the cyclic  $S_6^{\cdot-}$  were also performed. The calculated symmetrical chair conformation, with  $C_{2h}$  symmetry, resembles the observed X-ray structure. It is composed of two loosely bound  $S_3$  fragments with  $d(S-S)=207.5$  pm, connected via two long S-S bonds of

246.0 pm. However, this structure does not represent an energy minimum on the PES but corresponds to a transition state for the interconversion of two distorted  $C_2$  chair forms, which lie 8.4 kJ mol<sup>-1</sup> lower in energy. The  $S_3$  fragments in this  $C_2$  structure are connected through a short (212.5 pm) and a long bond (294.3 pm). In contrast to the DFT result, ab initio MP2/6-31+G\* computations favour the  $C_{2h}$  chair conformation over the  $C_2$  form by 2 kJ mol<sup>-1</sup>. In light of this small energy difference between the chair conformations, more definitive calculations are required to establish the correct stability order. Perhaps, the environment effects may also play a decisive role in determining the geometry of  $S_6^{4-}$  in the crystal. It is important to note also that the most stable gas-phase  $S_6^{4-}$  structure has a chain-like geometry according to simulated annealing calculation. The  $C_2$  isomer lies 10 kJ mol<sup>-1</sup> higher in energy [86].

A comprehensive study of the singly-charged radical anions of sulfur clusters with up to nine atoms  $S_n^-$  ( $n=1-9$ ) has been carried out by Hunsicker, Jones and Ganteför [87, 88]. This study focused on the energy difference between the charged and neutral systems. The authors employed photoelectron detachment measurements using a pulsed arc cluster ion source (PACIS) which yielded vertical detachment energies (VDE) for transitions from the ground state of the ions to states of the neutral clusters. For the theoretical work, they employed density functional calculations with simulated annealing to structures and energies of the open and cyclic forms of the cluster anions  $S_n^-$ . In general, the most stable structures of  $S_n^-$  have at least one bond being strained or broken by the presence of the additional electron. The ground states of  $S_5^-$ ,  $S_7^-$ ,  $S_8^-$  and  $S_9^-$  belong to this family. Several sulfur cluster anions are calculated to have chain-like structures. Structures with a *cis*-planar tetramer at one or both terminal ends are found for  $S_4^-$  to  $S_9^-$ . In  $S_4^-$ , it corresponds to a *cis*-planar structure with  $C_{2v}$  symmetry. For cluster anions with even values of  $n$ , they correspond to the most stable isomers. In agreement with the experimental observation, the chain-like isomers are calculated to have higher electron affinities, compared to the ring-like structures. Although the cyclic structures are generally more stable than the chain structures, the environment used to generate the larger clusters ( $n>7$ ) favours the formation of the latter in a cluster beam.

Vibrational fine structure was resolved for  $n=1-3$  and 6 [88]. In particular, the observed frequencies allow the identification of both ring and chain isomers of  $S_6^-$  and  $S_7^-$ . It is of interest to note that the only wavenumber measured for the neutral  $S_6$  structure ( $570\pm 32$  cm<sup>-1</sup>) is significantly higher than both the calculated and observed Raman wavenumbers of the  $D_{3d}$  isomer of  $S_6$  and falls in a pronounced gap of the spectrum of this isomer.

In polysulfide solutions there exist chainlike  $S_n^{2-}$  dianions with practically arbitrary chain lengths  $n$ . Berghof, Sommerfeld, and Cederbaum have investigated the onset of stability in the  $S_n^{2-}$  ( $n=2-8$ ) series of dianions based on SCF calculations with the DZPD basis set [89]. The isolated chainlike  $S_n^{2-}$  isomers were found to exhibit twisted structures, and the onset of electronic stability (with respect to electron autodetachment) was predicted to occur at  $n=7$ . Branched isomers were found to be electronically more stable than the

corresponding chain-like isomers but are expected to be more sensitive to fragmentation. For all chain-like clusters, the bond lengths and bond angles are rather independent on the cluster size and the position within the chain. The typical bond length is  $208 \pm 1$  pm, and the typical bond angle is close to the tetrahedral ( $\pm 2^\circ$ ). As a result, all chainlike  $S_n^{2-}$  resemble twisted chains. A population analysis revealed that the two excess charges are essentially localized at the terminal atoms of the sulfur chains such that the inner atoms carry only small amounts of negative charge.

## 7

### Cluster Cations $S_n^+$ and $S_n^{2+}$

Although  $S_n^+$  cluster cations were detected up to  $n=56$  by Martin [90] in the gas phase, the structures of these radical cations are hardly known except for  $S_5^+$ . Theoretical investigations on cationic sulfur clusters are also rare. The most comprehensive investigation corresponds to a recent DFT study by Au et al. [91]. They examined the structures and energies of various possible isomers of  $S_n^+$  cations ( $n=3-13$ ) using the B3LYP/6-31G\* theory. The majority of the cationic clusters are composed of two-coordinate atoms; those with one- and three-coordinate atoms are higher in energy. Interestingly, the most stable isomer of some cationic clusters is found to have a structure slightly different from that of the corresponding neutral cluster. For instance, the most stable neutral  $S_7$  is a 'chair' structure of  $C_s$  symmetry, but upon ionisation the  $C_s$  structure becomes a saddle point. The preferred  $S_7^+$  ring structure is of  $C_2$  symmetry. Among the various most stable  $S_n^+$  structures, those of  $S_3^+$ ,  $S_4^+$ ,  $S_5^+$ ,  $S_6^+$ ,  $S_9^+$ ,  $S_{10}^+$  and  $S_{12}^+$  are structurally similar to the neutral counterparts.

The smaller cluster ions  $S_3^+$ ,  $S_4^+$  and  $S_5^+$  have been examined by Zakrzewski and von Niessen at the HF/6-31+G\* level [82]. The lowest cationic states are predicted to be  ${}^2B_2$ ,  ${}^2B_{1u}$  and  ${}^2A''$  for  $S_3^+$  ( $C_{2v}$ ),  $S_4^+$  ( $D_{4h}$ ) and  $S_5^+$  ( $C_s$ ), respectively. The ionisation processes may result in significant structural relaxation leading to the sequence of states different from that of the vertical states. The calculated lowest adiabatic ionisation energies, using the CI method with a very large ANO basis set, are 9.53, 8.05, and 8.20 eV for  $S_3^+$ ,  $S_4^+$  and  $S_5^+$ , respectively.

Cioslowski, Szarecka, and Moncrieff studied the conformations of  $S_5^+$ ,  $S_6^+$  and  $S_8^+$  rings employing both UB3LYP/6-311G\* and UMP2/6-311G\* calculations [92, 93]. As with the neutral, the  $S_5^+$  homocyclic radical cation exists in only one conformer of  $C_s$  symmetry [92]. A structure with  $D_{3d}$  symmetry is predicted to be the global energy minimum for the  $S_6^+$  species [92]. This chair-like structure is somewhat less puckered than that of neutral  $S_6$ . The  $C_{2v}$  boat-like conformer is 21-29 kJ mol $^{-1}$  less stable than the  $D_{3d}$  minimum. The *endo-exo* conformer ( $C_s$  symmetry) is the lowest-energy conformer of  $S_8^+$ , with several other structures lying close in energy, within 28 kJ mol $^{-1}$  [93]. A conformational analysis of the cyclic  $S_8^+$  ion demonstrated that the structure is very sensitive to the level of theory used, which leads to significant discrepancies between the UB3LYP and UMP2 results [93].

UB3LYP theory predicts four minima of  $S_8^+$  which possess  $C_s$ ,  $C_{2h}$ ,  $D_2$  and  $C_2$  symmetries. At the UMP2 level of theory, no stationary point corresponding to the  $C_2$  minimum can be located and two new local minima with  $D_{4d}$  and  $D_2$  symmetries appear. The  $S_8^+$  conformers are found to be very prone to pseudorotation and are predicted to interconvert readily. For this reason, Cioslowski et al. refer to  $S_8^+$  as a fluxional species [93]. Interestingly, they found that the structures corresponding to local minima are not directly interconvertible.

Double ionisation of neutral molecules often leads to remarkable structural and energetic changes [94]. This is readily demonstrated in some of the doubly-charged ions of sulfur clusters. The equilibrium geometry of  $S_2^{2+}$  was first reported by Balaban and co-workers at the HF/6-31G\* level [95]. Subsequently, Jurek et al. have employed multireference CASSCF and CASPT2 calculations to examine the potential energy curves of the ground state and some low-lying excited states of  $S_2^{2+}$  [96]. As with the isoelectronic dication analogue  $O_2^{2+}$ , which is well established experimentally and theoretically, the electronic ground state of  $S_2^{2+}$  is  $^1\Sigma_g^+$ . Due to the strong Coulomb repulsion in this ion,  $S_2^{2+}$  is predicted to be a metastable species. In agreement with its experimental observation,  $S_2^{2+}$  is calculated to be a strongly bound species, with a sizable barrier of 263 kJ mol<sup>-1</sup> to dissociation into two  $S^+$  ions [96]. The  $^3\Sigma_u^+$ ,  $^3\Delta_u$ , and  $^3\Pi_u$  excited states are also calculated to be metastable with sufficiently high barriers to dissociation. As with  $O_2^{2+}$  [97],  $S_2^{2+}$  is predicted to have a remarkably short bond distance of 178.9 pm, ascribed to a formal S≡S triple bond. For comparison, the equilibrium internuclear distance ( $r_e$ ) of neutral  $S_2$  is 188.9 pm, which corresponds to a standard S=S double bond. The short SS bond in the  $S_2^{2+}$  dication arises from the removal two antibonding electrons from neutral  $S_2$ . It is of interest to note also that the triply charged ion  $S_2^{3+}$  has been observed by Coulomb explosion experiments and its existence is confirmed readily by the multireference calculations by Jurek et al. [96].

According to Walsh, triatomic molecules with 12–16 valence electrons are expected to be linear [98]. Unexpectedly, ab initio calculations up to the QCISD(T)/TZ2P level by Schaefer et al. demonstrated that the  $S_3^{2+}$  dication is the first 16-valence electron triatomic species with an equilateral triplet ground state ( $^3A'$ ) of  $D_{3h}$  symmetry [99]. Its bond length is 203 pm. Five other  $S_3^{2+}$  isomers have been examined. The most stable singlet state is of  $C_{2v}$  symmetry and has a bond angle of  $\sim 72^\circ$ . It lies 45 kJ mol<sup>-1</sup> above the triplet ground state. The classic linear singlet state ( $^1\Sigma_g^+$ ) is calculated to be a minimum on the  $S_3^{2+}$  potential energy surface, but it lies  $\sim 70$  kJ mol<sup>-1</sup> above the triangular triplet structure. SCF calculations of Pyykkö predicted a slightly bent geometry ( $174^\circ$ ) for the 'linear' species [100]. Fragmentation of  $S_3^{2+}$  to  $S_2^+$  and  $S^+$  is calculated to be an exothermic reaction, by 94 kJ mol<sup>-1</sup> [99].

The structures and stabilities of several  $S_n^{2+}$  dications are well established. Red, yellow or blue solutions are obtained if sulfur is added to  $SO_3$ -containing sulfuric acid (oleum). Gillespie et al. have suggested that the colours are due to the nonadecasulfur dication  $S_{19}^{2+}$ , octasulfur dication  $S_8^{2+}$ , and tetra-

sulfur dication  $S_4^{2+}$  [101]. The  $S_4^{2+}$  dication has originally been identified by magnetic circular dichroism [102] and was subsequently isolated as  $S_4(SO_3F)_2$  and characterized [101]. The  $S_4^{2+}$  dication possesses a square planar structure, with a quasi-aromatic  $6\pi$  four-membered ring. Several ab initio studies have addressed the geometric and electronic structure of  $S_4^{2+}$  [103–109]. The best theoretical treatment corresponds to the MP2/6-31G\* calculation by Janssen [108]. The calculated S-S bond length is 206.5 pm, in fair agreement with the experimental data (198.0–2.015 pm). The  $D_{4h}$  structure of  $S_4^{2+}$  is a stable minimum at all levels of theory [108]. The alternative  $C_{2v}$  geometry is considerably higher in energy and possesses two imaginary vibrational frequencies.

Organic  $6\pi$  four-membered rings are unknown. On the contrary, several  $6\pi$  four-membered inorganic rings have been prepared. Well-known examples are the  $S_4^{2+}$  dication, and its analogues  $S_2N_2$ ,  $Se_4^{2+}$  and  $Te_4^{2+}$ . Janssen and van Zandwijk have addressed the question of whether inorganic  $6\pi$  electron four-membered rings are in general more stable than organic rings. To this end, they have investigated systematically a number of four-membered rings containing second-row atoms and found several of these systems to possess a planar (aromatic) configuration [108, 110]. Furthermore, they demonstrated that several factors, viz. the presence of substituents, repulsive 1,2- and 1,3-interactions, and bond length, contribute to the conformational preferences.

Krossing et al. calculated the gas-phase dimerization energy for the  $2 S_2^+ - S_4^{2+}$  system at various levels of theory [109, 111]. They found that the dimerization energy depends strongly on the size of the basis set and the correlation method used (ranging from 217 to 522 kJ mol<sup>-1</sup>). The Møller-Plesset perturbation theory (MP $n$  with  $n=2-4$ ) performs moderately and diverges. The inclusion of polarization  $d$ - and  $f$ -functions is crucial in the energetic description of this strongly delocalised ion. The best estimate of the dimerization enthalpy ( $\Delta H_{298}$ ) of  $S_2^+$  is 257 kJ mol<sup>-1</sup> [111]. This result is achieved using the compound methods (e.g. CBS-Q and G2), the computationally very expensive CCSD(T) level extrapolated to the complete basis set limit, or by employing hybrid DFT calculations with flexible basis sets, e.g. B3PW91/6-311+G(3df).

The  $S_8^{2+}$  dication, like  $S_8$ , is cyclic, but the conformation changes markedly upon oxidation, with a sulfur atom flipping from the *exo*- to the *endo*-position. Earlier semiempirical [112, 113] and Hartree-Fock calculations [106, 114] predicted a strong transannular bond linking the two nonbonded sulfur atoms with localized positive charges. In particular, Bader et al., based on the analysis of the Laplacian ( $\nabla^2_\rho$ ) at the bond critical point, demonstrated that the cross-ring bond in  $S_8^{2+}$  exhibits the characteristics of closed-shell interaction ( $\nabla^2_\rho > 0$ ) as opposed to other S-S bonds, which exhibit characteristics typical of shared interactions ( $\nabla^2_\rho < 0$ ) [106]. The computed geometry of  $S_8^{2+}$  is extremely sensitive to the electron correlation effects. In sharp contrast to the Hartree-Fock result, the transannular interaction is completely missing in the correlated MP2 and BLYP calculations published by Cioslowski and Gao [114]. These authors attributed the exaggeration of transannular

interactions observed within the HF approximation to an excessive localization of positive charge. At the MP2/6-311G\* level, the *endo-exo* ring conformer is favoured over the *endo-endo* and *exo-exo* conformations, by 39 and 49 kJ mol<sup>-1</sup>, respectively. Cioslowski and Gao noted that none of the HF, MP2 and BLYP methods are capable of reproducing the experimental solid-state geometries of S<sub>8</sub><sup>2+</sup> [115, 116] which is almost certainly distorted to a large degree by crystal packing and counterion effects. However, in a more recent theoretical study [117], Crossing, Passmore and co-workers have shown that a satisfactory calculated geometry of gaseous S<sub>8</sub><sup>2+</sup> can be obtained using the B3PW91 or MPW1PW91 density functional in conjugation with the 6-311G(2df) basis set. It was concluded that the new MPW1PW91 level of theory provides a well-balanced description of electron correlation so that even the 3-21G\* basis set is sufficient to model the geometry of S<sub>8</sub><sup>2+</sup>. The transannular bond is calculated to lie in a very shallow minimum. The predicted enthalpy of formation ( $\Delta H_f^\circ$ ) of S<sub>8</sub><sup>2+</sup> is 2151 kJ mol<sup>-1</sup>. The most favourable gas-phase dissociations correspond to 2 S<sub>4</sub><sup>+</sup> and S<sub>2</sub><sup>+</sup>+1/2 (S<sub>5</sub><sup>+</sup>+S<sub>7</sub><sup>+</sup>). The bonding analysis based on the theory of atoms in molecules (AIM) indicates that there are bonds between all atoms, one transannular bond for which a Raman stretch has been observed. In addition, the analysis confirmed that the extra bond formed in S<sub>8</sub><sup>2+</sup> is highly delocalised. The positive charge is found delocalised over all atoms, decreasing the Coulomb repulsion between positively charged atoms. The bonding in S<sub>8</sub><sup>2+</sup> was explained in terms of a  $\sigma$ -bonded S<sub>8</sub> framework with additional bonding and charge delocalisation occurring by a combination of transannular  $\pi^*-\pi^*$  and  $p^2 \rightarrow \sigma^*$  bonding.

Li, Liu and Lu investigated the electronic structures and the possible aromaticity of some 10 $\pi$ -electron systems, including the S<sub>6</sub><sup>2+</sup> dication, at the HF/6-31G\* level [118]. The optimised S-S bond length of S<sub>6</sub><sup>2+</sup> is 210 pm. Based on the analysis of the bonding characteristics in terms of the canonical molecular orbital and the Foster-Boys localized molecular orbital, they concluded that S<sub>6</sub><sup>2+</sup> is of weak aromaticity. This is due to the occupation of the weak antibonding MOs. As a consequence, the bond strengths of the 10 $\pi$ -electron systems decrease with respect to their 6 $\pi$ -electron counterparts.

## 8

### Protonated Sulfur Clusters HS<sub>n</sub><sup>+</sup>

Relatively little is known about the protonated forms of sulfur clusters (S<sub>n</sub>H<sup>+</sup>). The only experimental study corresponds to the spectroscopic investigation by Abboud, Yáñez and coworkers [68]. These authors determined the gas-phase basicities of S<sub>6</sub> and S<sub>8</sub> using Fourier transform ion cyclotron resonance spectroscopy (FT-ICR). In addition, the structures and energies of various possible S<sub>6</sub>H<sup>+</sup> isomers were examined using the G2(MP2,SVP) theory. Surprisingly, the global energy minimum corresponds to a distorted five-membered ring structure with the hydrogen bonded to the exocyclic sulfur atom (Fig. 3). The chair-shaped six-membered ring species, derived

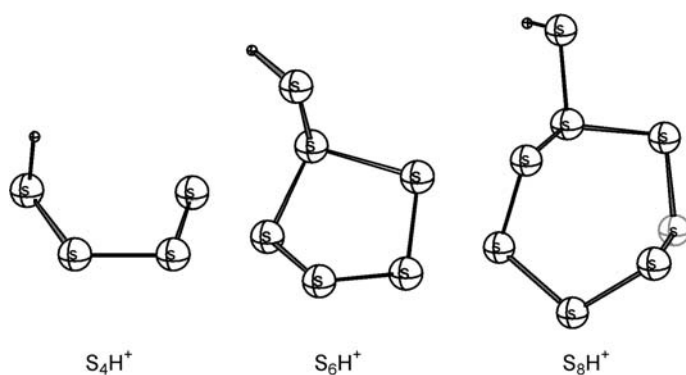


**Fig. 3** Structures of  $S_4H^+$ ,  $S_6H^+$  and  $S_8H^+$

from the most stable form of  $S_6$  is less stable, by 8 kJ mol<sup>-1</sup>. Four additional  $S_6H^+$  isomers were located with a common feature of an almost planar  $S_4$  moiety attached to the  $S_2H$  subunit. The calculated basicity of  $S_6$  (735 kJ mol<sup>-1</sup>) is somewhat high compared to the measured value of 702 kJ mol<sup>-1</sup>.

Abboud et al. explored also the potential energy hypersurface (PES) of  $S_8H^+$  at the HF/3-21G(d) level and found that the global minimum has similar characteristics as  $S_6H^+$  [68]. The lowest-energy structure of  $S_8H^+$  is a distorted seven-membered ring with an exocyclic  $SH^+$  group (Fig. 3). Thus, the most stable protonated forms of both  $S_6$  and  $S_8$  can be considered as an  $SH^+$  group attached to a cyclic moiety. The characteristics of the  $S_4H^+$  PES were found to be rather different from those of  $S_6H^+$  and  $S_8H^+$ . The global minimum of  $S_4H^+$  corresponds to the protonated form of the *cis*-isomer of  $S_4$ , which is the global minimum of this planar molecule. Higher-energy isomers of  $S_4H^+$  arising from the protonation of the puckered four-membered and branched rings of  $S_4$  have also been located. Based on the computed G2(MP2) proton affinities,  $S_4$  is predicted to be slightly more basic than  $S_6$ .

The PES of the protonated  $S_3$  molecule has been investigated by density functional calculations at the BP/DZVP level by Mineva et al. [119]. These authors considered 13 plausible protonated  $S_3H^+$  isomers derived from both the open-chain and cyclic forms of  $S_3$  but only four structures corresponding to energy minima on the PES were located. The *trans*-planar chain structure  $SSSH^+$  is the preferred protonated form; but the *cis*-planar chain, the branched and the cyclic forms correspond also to minima on the PES. A strong correlation is found between the absolute chemical hardness (reactivity indices) [120] and the relative stability of the various  $S_3H^+$  isomers. It is interesting to note that the relative stability of the cyclic form with respect to the *trans*-planar chain increases on going from  $O_3H^+$  to  $Se_3H^+$  and reverses for  $Te_3H^+$ .

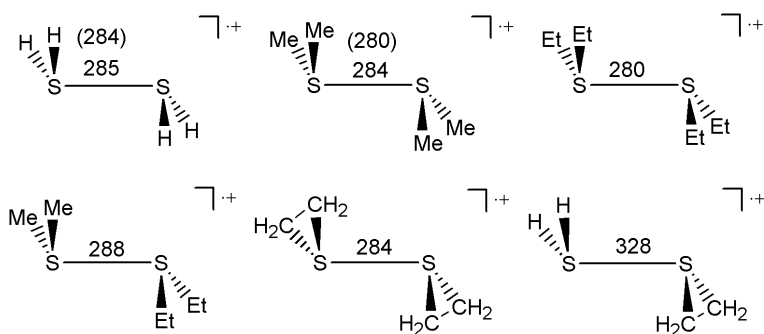


**Fig. 4** Structures of the three-electron hemibonded radical cations  $[R_2S:.SR_2]^+$ . The S-S bond lengths (HF/6-31G\*, with the MP2/6-31G\* values in parenthesis) are given in pm

## 9 Three-Electron S-S Bonds

The two-centre three-electron bond,  $2c-3e$  or  $(\sigma)^2(\sigma^*)^1$ , was first described by Pauling in 1931 [121]. Since the three-electron bond has a formal bond order of  $1/2$ , Gill and Radom referred this type of bond as three-electron hemibond [122], which may be distinguished from the three-electron sesquibond in which all three electrons occupy bonding molecular orbitals so that the formal bond order is  $1\frac{1}{2}$ . The radical cation  $[H_2S:.SH_2]^+$ , the prototype system of the three-electron S:S hemibond, has been the subject of several theoretical studies, mainly by Gill, Radom and co-workers [122, 123], Clark [124–126], McKee, Illies and co-workers [127–129], and Ortiz et al. [130, 131]. This hemibonded species is characterized by a rather long S-S bond of 284 pm (MP2/6-31G\*), 95 pm longer than that in the  $S_2$  molecule and 78 pm longer than in disulfane  $H_2S_2$ . It favours an *anti*-conformation with  $C_{2h}$  symmetry (Fig. 4). In line with the large S-S bond length is the low bond energy of the SS hemibond in  $[H_2S:.SH_2]^+$ . The best theoretical estimate of the gas-phase bond dissociation energy is 120 kJ mol<sup>-1</sup>, based on the calculated G2 dissociation energy of  $[H_2S:.SH_2]^+$  to  $H_2S+H_2S^+$  [128]. For comparison, the S-S bond dissociation energy in  $H_2S_2$  is 260 kJ mol<sup>-1</sup> [42, 132].

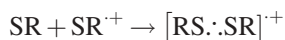
In sharp contrast to the stable  $[H_2S:.SH_2]^+$  radical cation, the isoelectronic neutral radicals  $[H_2S:.SH]$  and  $[H_2S:.Cl]$  are very weakly-bound van der Waals complexes [125]. Furthermore, the unsymmetrical  $[H_2S:.ClH]^+$  radical cation is less strongly bound than the symmetrical  $[H_2S:.SH_2]^+$  ion. The strength of these three-electron bonds was explained in terms of the overlap between the donor HOMO and radical SOMO. In a systematic study of a series of three-electron bonded radical cations [126], Clark has shown that the three-electron bond energy of  $[X:.Y]^+$  decreases exponentially with AIP, the difference between the ionisation potentials (IP) of X and Y. As a consequence, many of the known three-electron bonds are homonuclear, or at least involve two atoms of similar IP.

A simple qualitative model of the three-electron hemibond in  $[X:\cdot X]^+$ , based on the Hückel approximation, has been proposed by Gill and Radom [122]. This qualitative model predicts that the strength of the hemibond should vary in proportion to the Hückel parameter  $\alpha$ , which can be replaced by the HOMO energy in X because a good correlation is found between  $E_{\text{HOMO}}(X)$  and  $D_e(X-X^+)$ . This model readily rationalizes the marked substituent effect on the strength of the hemibond. In particular, electron-withdrawing substituents are found to have a strengthening effect.

For the hemibonded radical cations containing hydrogen, e.g.  $(\text{NH}_3)_2^+$ , the stabilities depend not only on the bond dissociation energies of the hemibonds but also on the relative stabilities of the hydrogen-bonded isomers. Therefore, Gill and Radom examined the hydrogen-bonded isomers for several first- and second-row homonuclear hemibonded systems [122]. The hydrogen-bonded systems are found to be the preferred isomers for all the first-row systems, such as  $(\text{NH}_3)_2^+$ . In contrast, the second-row hemibonded species  $[\text{H}_2\text{S}:\cdot\text{SH}_2]^+$  is more stable than its hydrogen-bonded isomer  $[\text{H}_2\text{SH}\cdots\text{SH}]^+$  by 50 kJ mol<sup>-1</sup> (HF/6-31G\*). In fact, this hydrogen-bonded isomer does not correspond to an energy minimum at the MP2/6-31G\* level. Thus, it is likely that the three-electron hemibonded species is the only minimum on the PES of  $\text{H}_4\text{S}_2^+$ .

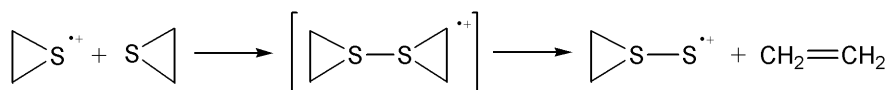
Asmus et al. unambiguously identified a variety of  $[\text{R}_2\text{S}:\cdot\text{SR}_2]^+$  radical cations in solution and measured their optical absorption spectra using pulse radiolysis techniques [133]. They proposed that the spectrum of  $[\text{H}_2\text{S}:\cdot\text{SH}_2]^+$  arises from the  $\sigma \rightarrow \sigma^*$  transition in the three-electron S:S hemibond. Based on a molecular orbital analysis, Clark ascribed the observed transition from a nonbonding orbital, which has both sigma and lone-pair character, to the sulfur-sulfur  $\sigma^*$  MO [124]. Illies et al. [128] performed CIS/6-31G\* calculations to determine the lowest excitation energy for  $[\text{H}_2\text{S}:\cdot\text{SH}_2]^+$  as well as for the complex  $[\text{H}_2\text{S}:\cdot\text{SH}_2]^+ \cdot 4\text{H}_2\text{O}$ . They found the solvent effects lead to a blue shift of  $\lambda_{\text{max}}$  of 45 nm. The calculated transition energy of the cation-water complex (396 nm) is in pleasing agreement with the observed  $\lambda_{\text{max}}$  value in solution (370 nm).

The substituted radical cations  $[\text{Me}_2\text{S}:\cdot\text{SMe}_2]^+$ ,  $[\text{Et}_2\text{S}:\cdot\text{SEt}_2]^+$  and  $[\text{Et}_2\text{S}:\cdot\text{SMe}_2]^+$  (Fig. 4) have been studied by Illies, McKee and co-workers using a combined experimental/theoretical approach [127–129]. Mass spectrometry experiments on the gas-phase association reactions



yielded reaction enthalpies which can be compared with calculated bond enthalpies. Both DFT and PMP4 (“P” indicates spin-projected MP4) methods have been employed to determine the reaction enthalpies. In all cases, there is a good agreement between theory and experiment. The calculated B3LYP/6-31G\* bond energies (298 K) for  $[\text{Me}_2\text{S}:\cdot\text{SMe}_2]^+$ ,  $[\text{Et}_2\text{S}:\cdot\text{SEt}_2]^+$  and  $[\text{Et}_2\text{S}:\cdot\text{SMe}_2]^+$  are 127, 117, 105 kJ mol<sup>-1</sup>, respectively. As expected from the qualitative prediction, the S:S three-electron bond energy is smaller for the unsymmetrical hemibonded system compared to the symmetrical systems.

The ion-molecule reaction between thiirane and its radical cation to form a thiirane sulfide radical cation and ethylene has been studied by Qin, Meng and Williams [134]. ESR studies using a low-temperature solid-state Freon radiolysis technique provided compelling evidence that the hemibonded dimer radical cation of thiirane is an intermediate in this so-called “sulfur-transfer” reaction; see Scheme 2.

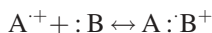


**Scheme 2**

An analogous sulfur transfer reaction has been proposed for the thermal decomposition of neutral thiirane to give ethylene and elemental sulfur, on the basis of ab initio calculations at the G3(MP2) level of theory [135].

Gill, Weatherall and Radom [123] calculated the energetics of the formation of the thiirane dimer radical cation and found that the hemibond strength of this dimer ion is  $127 \text{ kJ mol}^{-1}$  (MP2/6-31G\*/HF/6-31G\*+ZPE), comparable to that of the parent analogue  $[\text{H}_2\text{S}\cdot\cdot\text{SH}_2]^+$  ( $112 \text{ kJ mol}^{-1}$  at the same level of theory). Thus, their theoretical result nicely confirmed the experimental observation of this hemibonded system. Gill et al. also examined a closely related mixed dimer radical cation of thiirane and hydrogen sulfide. In agreement with the qualitative prediction, based on ionisation energies of the neutral monomers, the S-S bond of this mixed radical cation is considerably weaker ( $47 \text{ kJ mol}^{-1}$ ). The strength of this S-S three-electron hemibond is readily reflected in the comparison of the S-S bond lengths ( $328 \text{ pm}$  vs  $285 \text{ pm}$  in  $[\text{H}_2\text{S}\cdot\cdot\text{SH}_2]^+$ , see Fig. 4).

The ab initio calculations of various three-electron hemibonded systems [122, 123] indicated that the inclusion of electron correlation corrections is extremely important for the calculation of three-electron bond energies. The Hartree-Fock (HF) error is found to be nonsystematic and always large, sometimes of the same order of magnitude as the bond energy. According to valence bond (VB) and MO theories, the three-electron bond is attributed to a resonance between the two Lewis structures



These two resonance hybrids are mutually related by charge transfer. Hiberty, Shaik and co-workers [136] explained the HF bias in the three-electron bond energies in terms of two deficiencies:

1. Poor description of the individual resonance structures at bonding distances
2. Overestimation of the resonance energy

These authors proposed a “uniform mean-field HF” (UMHF) procedure which involves orbital occupancy constraints and correction of resonance energy by non-empirical factors. This UMHF method yields the dissociation energies of three-electron systems in satisfactory agreement with accurate calculation performed in the same basis set.

## 10

### Concluding Remarks

Extensive quantum chemical calculations have been reported for sulfur-rich compounds in the past two decades. These calculations were used to investigate molecular structures and spectroscopic properties, as well as to understand the nature chemical bonding and reaction mechanism. Many high-level ab initio calculations were used for interpretation of experimental data and for providing accurate predictions of molecular structures and thermochemical data where no reliable experimental values are available. In recent years, density functional calculations have been extensively tested and used on many first- and second-row compounds. These proven DFT methods look promising for larger systems because for their computational efficiency.

With the availability of sophisticated computational methods, combined with the ever increasing speed of computers and the latest parallel computing technology, quantum chemical calculations with chemical accuracy for larger systems are now readily available. Thus, computational chemistry will play a major role in solving many of the unresolved and challenging problems in sulfur chemistry.

**Acknowledgements** The author is indebted to Professor Ralf Steudel for many enlightening discussions and his encouragement through the years. This work was supported by the National University of Singapore.

### References

1. J.J. Stewart, in: *Reviews in Computational Chemistry*, Vol. 1 (K. B. Lipkowitz, D. B. Boyd, Eds.), Wiley-VCH, 1990, Chapter 2
2. W.J. Hehre, L. Radom, P. v. R. Schleyer, J.A. Pople, *Ab Initio Molecular Orbital Theory*, Wiley, New York, 1986
3. R.G. Parr, W. Yang, *Density Functional Theory of Atoms and Molecules*, Oxford University Press, New York, 1989
4. O.M. Suleimenov, T.K. Ha, *Chem. Phys. Lett.* 1998, 290, 451
5. E. Magnusson, H.F. Schaefer, *J. Chem. Phys.* 1985, 83, 5721
6. C.J. Marsden, H. Oberhammer, O. Losking, H. Willner, *J. Mol. Struct.* 1989, 193, 233
7. J.A. Pople, A.P. Scott, M.W. Wong, L. Radom, *Isr. J. Chem.* 1993, 33, 345
8. A.P. Scott, L. Radom, *J. Phys. Chem.* 1996, 100, 16502
9. M.W. Wong, *Chem. Phys. Lett.* 1996, 256, 391
10. I. Bytheway, M.W. Wong, *Chem. Phys. Lett.* 1998, 282, 219
11. L.A. Curtiss, K. Raghavachari, P.C. Redfern, V. Rassolov, J.A. Pople, *J. Chem. Phys.* 1998, 109, 7764; and references therein

12. J.W. Ochterski, G.A. Petersson, J.A. Montgomery, Jr., *J. Chem. Phys.* **1996**, *104*, 2598; and references therein
13. W. Koch, M.C. Holthausen, *A Chemist's Guide to Density Functional Theory*, Wiley-VCH, New York, **2000**
14. L.A. Curtiss, P.C. Redfern, K. Raghavachari, J.A. Pople, *J. Chem. Phys.* **2000**, *114*, 108
15. R. Steudel, *Top. Curr. Chem.* **2003**, *231*, in print
16. P. Birner, H.J. Kohler, A. Karpfen, H. Lischka, *J. Mol. Struct. (THEOCHEM)* **1991**, *72*, 223
17. C.J. Marsden, B.J. Smith, *J. Phys. Chem.* **1988**, *92*, 347
18. M. Honda, M. Tajima, *J. Mol. Struct. (THEOCHEM)* **1986**, *136*, 93
19. T.-K. Ha, *J. Mol. Struct. (THEOCHEM)* **1985**, *122*, 225
20. W.-K. Li, S.-W. Chiu, Z.-X. Ma, C.-L. Liao, C. Y. Ng, *J. Chem. Phys.* **1993**, *99*, 8440
21. B. Solouki, H. Bock, *Inorg. Chem.* **1979**, *16*, 127
22. F.M. Bickelhaupt, M. Sola, P. v. R. Schleyer, *J. Comput. Chem.* **1995**, *16*, 465
23. K. Miaskiewicz, R. Steudel, *J. Chem. Soc. Dalton Trans.* **1991**, 2395
24. R.S. Laitinen, T.A. Pakkanen, R. Steudel, *J. Am. Chem. Soc.* **1987**, *109*, 710
25. R. Steudel, Y. Drozdova, K. Miaskiewicz, R.H. Hertwig, W. Koch, *J. Am. Chem. Soc.* **1997**, *119*, 1990
26. P. Gerbaux, J.-Y. Salpin, G. Bouchoux, R. Flammang, *Int. J. Mass Spectrom.* **2000**, *195/196*, 239
27. D.N. Harpp, K. Steliou, C.J. Cher, *J. Chem. Soc. Chem. Commun.* **1980**, 825
28. D. Das, S. C. Whittenburg, *J. Phys. Chem.* **1999**, *103*, 2134
29. P.K. Chattaraj, P. Pérez, J. Zevallos, A. Toro-Labbé, *J. Mol. Struct. (THEOCHEM)* **2002**, *580*, 171
30. D.R. Alleres, D.L. Cooper, T.P. Cunningham, J. Gerratt, P. B. Karadakov, M. Raimondi, *J. Chem. Soc. Faraday Trans* **1995**, *91*, 3357
31. J. Hahn, *Z. Naturforsch., Part B* **1985**, *40*, 263
32. J. Hahn, P. Schmidt, K. Reinartz, J. Behrend, G. Winnewisser, K.M.T. Yamada, *Z. Naturforsch. B* **1991**, *46*, 1338
33. M. Liedtke, M.T. Yamada, G. Winnewisser, J. Hahn, *J. Mol. Struct.* **1997**, *413/414*, 265
34. Y. Drozdova, K. Miaskiewicz, R. Steudel, *Z. Naturforsch., Part B* **1995**, *50*, 889
35. M. Liedtke, H. Saleck, M.T. Yamada, G. Winnewisser, D. Cremer, E. Kraka, A. Dolgner, J. Hahn, *J. Phys. Chem.* **1993**, *97*, 11204
36. Y. Steudel, R. Steudel, private communication of unpublished results, **2003**
37. R. Steudel, *Chem. Rev.* **2002**, *102*, 3905
38. A.H. Otto, R. Steudel, *Eur. J. Inorg. Chem.* **1999**, 2057
39. <http://webbook.nist.gov/chemistry>
40. M.W. Wong, Y. Steudel, R. Steudel, *Chem. Phys. Lett.* **2002**, *364*, 387
41. S.G. Raptis, S. M. Nasiou, I. N. Demetropoulos, M. G. Papadopoulos, *J. Comput. Chem.* **1998**, *19*, 1698
42. R. Steudel, Y. Steudel, K. Miaskiewicz, *Chem. Eur. J.* **2001**, *15*, 3281
43. R. Steudel, B. Eckert, *Top. Curr. Chem.* **2003**, *230*, in print
44. R. Steudel, *Top. Curr. Chem.* **1982**, *102*, 149
45. R. Steudel, in: *Studies in Inorganic Chemistry*, Vol. 5 (A. Müller, B. Krebs, eds.), Elsevier, Amsterdam, **1984**, p.3, and references therein
46. D. Hohl, R.O. Jones, R. Car, M. Parrinello, *J. Chem. Phys.* **1988**, *89*, 6823
47. R.S. Laitinen, B. Randolph, T.A. Pakkanen, *J. Mol. Struct. (THEOCHEM)* **1987**, *8*, 658
48. R.J. Suontamo, R.S. Laitinen, T.A. Pakkanen, *J. Mol. Struct. (THEOCHEM)* **1994**, *313*, 189
49. K. Raghavachari, C.M. Rohlfing, J. S. Binkley, *J. Chem. Phys.* **1990**, *93*, 5862
50. K. Raghavachari, C.M. Rohlfing, J. S. Binkley, *Int. J. Mass Spectrom. Ion Proc.* **1990**, *102*, 313
51. D.A. Dixon, E. Wasserman, *J. Phys. Chem.* **1990**, *94*, 5772
52. H. Yilmaz, S. Erkoc, *J. Mol. Struct. (THEOCHEM)* **1991**, *231*, 63
53. D.S. Warren, B. M. Gimarc, *J. Phys. Chem.* **1993**, *97*, 4031

54. J. Cioslowski, A. Szarecka, D. Moncrieff, *J. Phys. Chem. A* **2001**, *105*, 501
55. M.D. Chen, M.L. Liu, H.B. Luo, Q.E. Zhang, C.T. Au, *J. Mol. Struct. (THEOCHEM)* **2001**, *548*, 133
56. S. Millefiori, A. Alparone, *J. Phys. Chem. A* **2001**, *105*, 9489
57. L. Peter, *Phosphorus, Sulfur, Silicon Relat. Elem.* **2001**, *168*, 287
58. R. Ludwig, J. Behler, B. Klink, F. Weinhold, *Angew. Chem. Int. Ed.* **2002**, *41*, 3199
59. R.O. Jones, P. Ballone, *J. Chem. Phys.* **2003**, *118*, 9257
60. R. Steudel, Y. Steudel, M.W. Wong, *Top. Curr. Chem.* **2003**, *230*, in print
61. J.R. Rice, R.D. Amos, N.C. Handy, T.J. Lee, H.F. Schaefer, *J. Chem. Phys.* **1986**, *85*, 963
62. T. Fueno, R.J. Buenker, *Theor. Chim. Acta*, **1988**, *73*, 123
63. A. S. Brown, V.H. Smith, *J. Chem. Phys.* **1993**, *99*, 1837
64. G. Orlova, J. D. Goddard, *J. Phys. Chem. A* **1999**, *103*, 6825
65. W. Koch, J. Natterer, C. Heinemann, *J. Chem. Phys.* **1995**, *102*, 6159
66. G.E. Quelch, H.F. Schaefer, C.J. Marsden, *J. Am. Chem. Soc.* **1990**, *112*, 8719
67. W. von Niessen, *J. Chem. Phys.* **1991**, *95*, 8301
68. J.-L.M. Abboud, M. Essefar, M. Herreros, O. Mó, M.T. Molina, R. Notario, M. Yáñez, *J. Phys. Chem. A* **1998**, *102*, 7996
69. G.D. Brabson, Z. Mielke, L. Andrews, *J. Phys. Chem.* **1991**, *95*, 79
70. P. Hassanzadeh, L. Andrews, *J. Phys. Chem.* **1992**, *96*, 6579
71. Boumedién, J. Corset, E. Picquenard, *J. Raman Spectrosc.* **1999**, *30*, 463
72. R. Steudel, J. Steidel, J. Pickardt, F. Schuster, R. Reinhardt, *Z. Naturforsch., Part B* **1980**, *35*, 1378
73. R.O. Jones, D. Hohl, *Int. J. Quantum Chem.: Quantum Chem. Symp.* **1990**, *24*, 141
74. R. Steudel, K. Bergemann, J. Buschmann, P. Luger, *Inorg. Chem.* **1996**, *35*, 2184
75. R. Steudel, B. Eckert, *Top. Curr. Chem.* **2003**, *230*, in print
76. B. Eckert, R. Steudel, *Top. Curr. Chem.* **2003**, *231*, in print
77. H. Rau, T.R.N. Kutty, J.R. F. Guedes de Carvalho, *J. Thermodyn.* **1973**, *5*, 833
78. H. Radscheit, J.A. Gardner, *J. Non-Cryst. Solids* **1980**, *35& 36*, 1263
79. S. Munejiri, F. Shimojo, K. Hoshino, *J. Phys.: Condens. Matter* **2000**, *12*, 7999
80. D. Reinen, G.-G. Lindner, *Chem. Soc. Rev.* **1999**, *28*, 75
81. A. Hinchliffe, *J. Mol. Struct. (THEOCHEM)* **1981**, *85*, 207
82. V.G. Zakrzewski, W. von Niessen, *Theor. Chim. Acta* **1994**, *88*, 75
83. W. von Niessen, P. Tomasello, *J. Chem. Phys.* **1987**, *87*, 5333
84. M.R. Nimolos, G.B. Ellison, *J. Phys. Chem.* **1986**, *90*, 2574
85. G.-G. Lindner, *Doctoral Dissertation*, Marburg, **1994**
86. B. Neumüller, F. Schmock, R. Kirmse, A. Voigt, A. Diefenbach, F.M. Bickelhaupt, K. Dehnicke, *Angew. Chem. Int. Ed. Engl.* **2000**, *39*, 4580
87. G. Ganteför, S. Hunsicker, R.O. Jones, *Chem. Phys. Lett.* **1995**, *236*, 43
88. S. Hunsicker, R.O. Jones, G. Ganteför, *J. Chem. Phys.* **1995**, *102*, 5917
89. V. Berghof, T. Sommerfeld, L. S. Cederbaum, *J. Phys. Chem.* **1998**, *102*, 5100
90. T.P. Martin, *J. Chem. Phys.* **1984**, *81*, 4426
91. M.D. Chen, M.L. Liu, J.W. Liu, Q.E. Zhang, C.T. Au, *J. Mol. Struct. (THEOCHEM)* **2002**, *582*, 205
92. J. Cioslowski, A. Szarecka, D. Moncrieff, *Int. J. Quantum Chem.* **2002**, *90*, 1049
93. J. Cioslowski, A. Szarecka, D. Moncrieff, *Mol. Phys.* **2002**, *100*, 1559
94. L. Radom, M.W. Wong, P.M.W. Gill, *Adv. Mass Spectrom.* **1989**, *11*, 702
95. A. Balaban, G. R. DeMare, R.A. Poirier, *J. Mol. Struct. (THEOCHEM)* **1989**, *183*, 103
96. M. Urban, G.H.F. Diercksen, M. Jurek, *Mol. Phys.* **1998**, *94*, 199
97. M.W. Wong, R.H. Nobes, W.J. Bouma, L. Radom, *J. Chem. Phys.* **1989**, *91*, 2971
98. A. Walsh, *J. Chem. Soc.* **1953**, 2260, 2266, 2288, 2296 and 2301
99. C.J. Marsden, G.E. Quelch, H.F. Schaefer, *J. Am. Chem. Soc.* **1992**, *114*, 6802
100. P. Pyykkö, *Chem. Phys Lett.* **1989**, *162*, 349
101. R.J. Gillespie, J. Passmore, P.K. Ummat, O. C. Vaidya, *Inorg. Chem.* **1971**, *10*, 1327
102. P.J. Stephens, *J. Chem. Soc. Chem. Commun.* **1969**, 1496
103. J. Kao, *Mol. Struct. (THEOCHEM)* **1980**, *63*, 293

104. F.L. Skrezenek, R.D. Harcourt, *Theor. Chim. Acta* **1985**, *67*, 271
105. R.D. Harcourt, F.L. Skrezenek, *J. Mol. Struct. (THEOCHEM)* **1987**, *151*, 203
106. T.-H. Tang, R.F.W. Bader, P.J. MacDougall, *Inorg. Chem.* **1985**, *24*, 2047
107. L.J. Saethre, O. Gropeh, *Can. J. Chem.* **1992**, *70*, 348
108. R.A. Janssen, *J. Phys. Chem.* **1993**, *97*, 6384
109. I. Krossing, *Top. Curr. Chem.* **2003**, *230*, in print
110. G. van Zandwijk, R.A. Janssen, H. M. Buck, *J. Am. Chem. Soc.* **1990**, *112*, 4155
111. H.D.B. Jenkins, L.C. Jitariu, I. Krossing, J. Passmore, R. Suontamo, *J. Comput. Chem.* **2000**, *21*, 218
112. N.C. Baird, *J. Comput. Chem.* **1984**, *5*, 35
113. K. Tanaka, T. Yamabe, H. Teramae, K. Fukui, *Nouv. J. Chim.* **1979**, *3*, 379
114. J. Cioslowski, X. Gao, *Int. J. Quantum Chem.* **1997**, *65*, 609
115. C.G. Davies, R.J. Gillespie, J.J. Park, J. Passmore, *Inorg. Chem.* **1971**, *10*, 2781
116. R.J. Gillespie, J. Passmore, *Acc. Chem. Res.* **1971**, *4*, 413
117. T.S. Cameron, R.J. Deeth, I. Dionne, H. Du, H. D. B. Jenkins, I. Krossing, J. Passmore, H. Roobottom, *Inorg. Chem.* **2000**, *39*, 5614
118. J. Li, C.-W. Liu, J.-X. Lu, *J. Mol. Struct. (THEOCHEM)* **1993**, *280*, 223
119. T. Mineva, N. Russo, E. Sicilia, M. Toscano, *J. Chem. Soc. Faraday Trans.* **1997**, *93*, 3309
120. J.L. Gazquez, in *Structure and Bonding*, (K. Sen, Ed.), Springer, Berlin, **1993**, Vol. 80, p. 27
121. L. Pauling, *J. Am. Chem. Soc.* **1931**, *53*, 3225
122. P.M.W. Gill, L. Radom, *J. Am. Chem. Soc.* **1988**, *110*, 4931
123. P.M.W. Gill, P. Weatherall, L. Radom, *J. Am. Chem. Soc.* **1989**, *111*, 2782
124. T. Clark, *J. Comput. Chem.* **1981**, *2*, 261
125. T. Clark, *J. Comput. Chem.* **1982**, *3*, 112
126. T. Clark, *J. Am. Chem. Soc.* **1988**, *110*, 1672
127. A.J. Illies, P. Livant, M.L. McKee, *J. Am. Chem. Soc.* **1988**, *110*, 7980
128. Y. Deng, A.J. Illies, M.A. James, M.L. McKee, M. Peschke, *J. Am. Chem. Soc.* **1995**, *117*, 420
129. M.A. James, M.L. McKee, A.J. Illies, *J. Am. Chem. Soc.* **1996**, *118*, 7836
130. P.F. Fernandez, J.V. Ortiz, E. A. Walters, *J. Chem. Phys.* **1986**, *84*, 1653
131. J.V. Ortiz, *Chem. Phys. Lett.* **1987**, *134*, 366
132. N. Matsunaga, D.W. Rogers, A. A. Zavitsas, *J. Org. Chem.* **2003**, *68*, 3158, and publications cited therein
133. K.-D. Asmus in *Sulfur-Centered Reactive Intermediates in Chemistry and Biology*, (C. Chatgililoglu, K.-D. Asmus, eds.), Plenum Press, New York, **1990**, p.155
134. X.-Z. Qin, Q.-C. Meng, F. Williams, *J. Am. Chem. Soc.* **1987**, *109*, 6778
135. Y. Steudel, R. Steudel, M.W. Wong, *Chem. Eur. J.* **2002**, *8*, 217
136. P.C. Hiberty, S. Humbel, D. Danovich, S. Shaik, *J. Am. Chem. Soc.* **1995**, *117*, 9003



# Molecular Spectra of Sulfur Molecules and Solid Sulfur Allotropes

Bodo Eckert<sup>1</sup> · Ralf Steudel<sup>2</sup>

<sup>1</sup> Fachbereich Physik, Universität Kaiserslautern, 67663 Kaiserslautern, Germany  
*E-mail: eckert@physik.uni-kl.de*

<sup>2</sup> Institut für Chemie, Sekr. C2, Technische Universität Berlin, 10623 Berlin, Germany  
*E-mail: steudel@schwefel.chem.tu-berlin.de*

**Abstract** Molecular spectroscopy is one of the most important means to characterize the various species in solid, liquid and gaseous elemental sulfur. In this chapter the vibrational, UV-Vis and mass spectra of sulfur molecules with between 2 and 20 atoms are critically reviewed together with the spectra of liquid sulfur and of solid allotropes including polymeric and high-pressure phases. In particular, low temperature Raman spectroscopy is a suitable technique to identify single species in mixtures. In mass spectra cluster cations with up to 56 atoms have been observed but fragmentation processes cause serious difficulties. The UV-Vis spectra of S<sub>4</sub> are reassigned. The modern XANES spectroscopy has just started to be applied to sulfur allotropes and other sulfur compounds.

**Keywords** Vibrational spectra · Electronic spectra · Mass spectra · XANES spectra · Photolysis

1	Introduction . . . . .	32
2	UV-Vis Spectra. . . . .	33
2.1	Gaseous Sulfur . . . . .	33
2.2	Liquid Sulfur . . . . .	36
2.3	Sulfur Solutions . . . . .	39
2.4	Solid Sulfur Allotropes. . . . .	40
3	Vibrational Spectra. . . . .	42
3.1	Small Sulfur Molecules (S <sub>2</sub> , S <sub>3</sub> , S <sub>4</sub> , S <sub>5</sub> ) . . . . .	42
3.1.1	Disulfur S <sub>2</sub> . . . . .	42
3.1.2	Trisulfur S <sub>3</sub> . . . . .	43
3.1.3	Tetrasulfur S <sub>4</sub> . . . . .	43
3.1.4	Pentasulfur S <sub>5</sub> . . . . .	43
3.2	Sulfur Rings S <sub>6</sub> to S <sub>20</sub> . . . . .	43
3.2.1	S <sub>8</sub> . . . . .	43
3.2.1.1	The Free S <sub>8</sub> Molecule . . . . .	44
3.2.1.2	Crystals of $\alpha$ -S <sub>8</sub> . . . . .	45
3.2.1.3	External Modes and the Torsional Vibration $\nu_9$ . . . . .	49
3.2.1.4	Bending Vibrations . . . . .	52
3.2.1.5	Stretching Vibrations. . . . .	55
3.2.1.6	Effects of Isotopic Impurities. . . . .	57
3.2.1.7	Overtone and Combination Vibrations. . . . .	62

3.2.1.8	High-Pressure Studies . . . . .	63
3.2.1.9	Crystals of $\beta$ -S <sub>8</sub> . . . . .	64
3.2.1.10	Crystals of $\beta$ -S <sub>8</sub> . . . . .	65
3.2.2	S <sub>6</sub> . . . . .	65
3.2.3	S <sub>7</sub> . . . . .	68
3.2.4	S <sub>9</sub> . . . . .	70
3.2.5	S <sub>10</sub> and S <sub>6</sub> ·S <sub>10</sub> . . . . .	70
3.2.6	S <sub>11</sub> . . . . .	73
3.2.7	S <sub>12</sub> and S <sub>12</sub> ·CS <sub>2</sub> . . . . .	73
3.2.8	S <sub>13</sub> . . . . .	75
3.2.9	S <sub>14</sub> . . . . .	76
3.2.10	S <sub>15</sub> , S <sub>18</sub> , S <sub>20</sub> , and Other Large Rings (S <sub>x</sub> ) . . . . .	77
3.3	Polymeric Sulfur. . . . .	79
3.4	High-Pressure Allotropes of Sulfur . . . . .	82
3.5	General Observations. . . . .	85
4	Mass Spectra . . . . .	88
5	XANES Spectra . . . . .	90
	References . . . . .	92

### List of Abbreviations and Symbols

S <sub>π</sub>	Mixture of soluble sulfur rings other than S <sub>8</sub>
S <sub>∞</sub>	Polymeric sulfur dissolved in liquid sulfur (mixture of very large rings and very long chains)
S <sub>μ</sub>	Polymeric insoluble sulfur usually prepared from liquid sulfur
DOS	Density of states
IR	Infrared
FTIR	Fourier transform infrared
LD	Lattice dynamics
MD	Molecular dynamics
Me	Methyl group
STP	Standard temperature-pressure (conditions)
UBFF	Urey-Bradley force field
XANES	X-ray absorption near edge structure

## 1

### Introduction

Elemental sulfur is one of the best investigated chemical elements but it represents also one of the most complex systems. The large number of its allotropes (ca. 30 [1]) and their peculiar behavior on melting, vaporization

and under pressure made it necessary to investigate this element by as many types of molecular spectroscopy as possible to identify the molecular species present. In this chapter the results of these investigations are reviewed.

Most informative in this context is vibrational spectroscopy since the number of signals observed depends on the molecular size as well as on the symmetry of the molecule and, if it is part of a condensed phase, of its environment. In particular, Raman spectroscopy has contributed much to the elucidation of the various allotropes of elemental sulfur and to the analysis of complex mixtures such as liquid and gaseous sulfur.

UV-Vis spectroscopy may also provide valuable information if small molecules are studied. However, the *photochemical sensitivity* of many sulfur-containing molecules may trigger changes in the composition of the sample during irradiation. For instance, this phenomenon has been observed in Raman spectroscopy using the blue or green lines of an argon ion laser which sometimes decompose sensitive sulfur samples with formation of S<sub>8</sub> [2, 3]. Reliable spectra are obtained with the red lines of a krypton ion or a He-Ne laser as well as with the infrared photons of a Nd:YAG laser.

Similarly, the *thermal sensitivity* of sulfur allotropes makes mass spectrometry of elemental sulfur and sulfur-rich compounds difficult especially with the conventional electron impact ionization. Nevertheless, valuable information has been obtained by this technique also.

Despite the fact that natural elemental sulfur contains 0.75% of the isotope <sup>33</sup>S [4] with a nuclear spin of  $I = 3/2$  no NMR spectra of elemental sulfur have ever been reported. Such spectra are however well-known for compounds containing just one or two sulfur atoms [5]. Electron spin resonance spectra of irradiated elemental sulfur samples and of quenched sulfur vapor have been reviewed elsewhere [6–8].

## 2 UV-Vis Spectra

### 2.1 Gaseous Sulfur

Sulfur vapor contains all molecules with between 2 and 8 atoms which are related by temperature- and pressure-dependent equilibrium reactions:



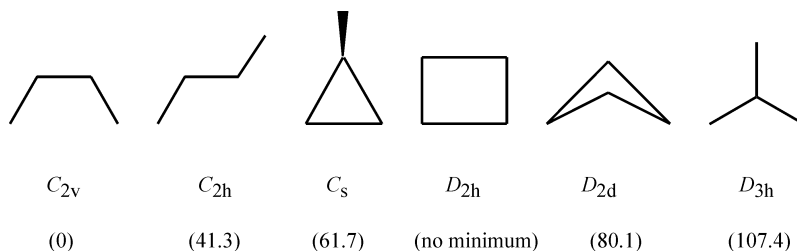
Some of these species occur as several isomers, and in addition larger molecules like S<sub>9</sub> and S<sub>10</sub> are present in trace amounts [9]. The acyclic species S<sub>2</sub>, S<sub>3</sub>, and S<sub>4</sub> absorb visible light while all larger molecules are cyclic or polymeric and absorb only in the near UV with a wing into the violet region of the visible spectrum. Therefore, these species are more or less yellow at 25 °C. However, at temperatures below 160 K pure *cyclo*-S<sub>8</sub> is colorless which demonstrates that the wing on the longer wavelength side of the UV absorption band is caused by vibrational broadening which, of course, disappears

at low temperatures. Other sulfur allotropes are either also colorless at liquid nitrogen temperature (e.g.,  $S_{12}$ ,  $S_{20}$ ,  $S_{\mu}$ ) or their deep yellow color at 25 °C becomes much lighter at 77 K (e.g.,  $S_6$ ,  $S_7$ ,  $S_{10}$ ) [10].

Below 250 °C the spectrum of saturated sulfur vapor consists of unresolved absorption bands at 210, 265, and 285 nm caused by the electronic transitions of *cyclo*- $S_8$  [11]. These bands have also been observed for  $S_8$  solutions in organic solvents and for thin films of solid  $S_8$  (see below).

At temperatures above 350 °C saturated sulfur vapor exhibits three electronic absorption bands in the visible range at 400, 530, and 625 nm. Meyer et al. [12] first convincingly assigned the 400 nm band to  $S_3$  and Braune et al. [13] assigned the much weaker 530 nm band to  $S_4$  which was later confirmed by several authors [14–16]. The third band at 625 nm is still weaker and was suspected to originate from a second isomer of  $S_4$  [8] which was later confirmed [17]. Meyer claimed that  $S_3$  is deep cherry-red in hot sulfur vapor [12]. The  $S_4(C_{2v})$  absorption in the green region (500–590 nm) results in a purple-red complimentary color while the  $S_4(C_{2h})$  absorption in the red region (625 nm) should yield a blue-green appearance [18] if this isomer could be observed separately.

Ab initio MO and DFT calculations have revealed that  $S_4$  can exist as six isomers on the potential energy hypersurface. Their connectivities and relative energies (in  $\text{kJ mol}^{-1}$ ) [9] are shown in Scheme 1.



**Scheme 1**

The large energy differences between the global minimum structure of  $C_{2v}$  symmetry and the other isomers indicate that equilibrium sulfur vapor will contain only minute amounts of the latter, even at very high temperatures. However, under non-equilibrium conditions as in electrical discharges or by illumination with a laser as in Raman spectroscopy unstable isomers may be formed and detected.

Wong et al. [9] calculated the wavelengths of the lowest-energy electronic transitions of  $S_2$ ,  $S_3$ , and of the three most stable isomers of  $S_4$  from ab initio MO theory as follows (wavelengths in nm; oscillator strengths in parentheses):

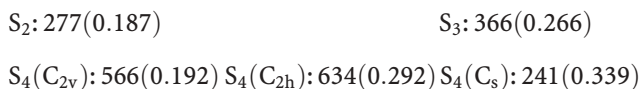


**Table 1** Harmonic fundamental modes of the three most stable isomers of  $S_4$  with infrared and Raman intensities calculated at the B3LYP/6-31G(2df) level of theory [9]. Symmetrical modes (of symmetry  $A$ ) are shown in italics. For the connectivities of the  $S_4$  isomers, see Scheme 1. Experimental wavenumbers are given for comparison; assignments according to [9] using experimental data from [17, 76]

Symmetry:	$C_{2v}$ <sup>a</sup>	$C_{2h}$ <sup>a</sup>	$C_s$ <sup>a</sup>	Matrix infrared spectra (12 K) [17]	Resonance Raman spectra (hot vapor) [76]
$\nu_1$	674 w/76	649 0/100	665 vs/26	683 ( $S_{\bar{r}}=S$ ) <sup>d</sup>	678 ( $C_{2v}$ ) <sup>b</sup> 635 ( $C_{2h}$ ) <sup>c</sup> 601 ( $C_{2v}$ ; $2\times\nu_4$ ) <sup>b</sup>
$\nu_2$	649 vs/13	637 vs/0	541 m/100	662 ( $C_{2v}$ ) 642 ( $C_{2h}$ ) <sup>e</sup>	575 (?) <sup>b,c</sup>
$\nu_3$	373 w/100	471 0/51	390 s/50	-	400 ( $C_{2h}$ ; $2\times\nu_4$ ) <sup>c</sup> 375 ( $C_{2v}$ ) <sup>b</sup>
$\nu_4$	330 vw/35	225 0/55	308 m/27	-	322 sh ( $C_{2v}$ ; $\nu_5+\nu_6$ ) <sup>b</sup> 303 ( $C_{2v}$ ) <sup>b</sup>
$\nu_5$	207 vw/1	124 w/0	215 w/52	-	-
$\nu_6$	104 vw/33	93 vw/0	164 vw/41	-	-

<sup>a</sup> Wavenumbers (unscaled;  $\text{cm}^{-1}$ ) and relative infrared/Raman intensities as follows. Infrared intensities: very strong-strong-medium-weak-very weak-0. Raman intensities: 0–100 (sh: shoulder). In the case of the centrosymmetric point group  $C_{2h}$  the rule of mutual exclusion applies

<sup>b</sup> Observed in the spectra excited with blue-green light (488–530 nm)

<sup>c</sup> Observed in the spectra excited with red light (647 nm)

<sup>d</sup> Observed only after annealing of the matrix at 38 K;  $n \geq 4$  [17]

<sup>e</sup> The other Raman lines calculated for this species at 471 and 225  $\text{cm}^{-1}$  may have been obscured by the strong lines of  $S_8$ ,  $S_7$ , and  $S_6$  near 475  $\text{cm}^{-1}$  (stretching) and 213/232/263  $\text{cm}^{-1}$  (totally symmetrical bending) in the Raman spectra of sulfur vapor

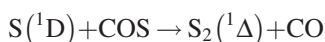
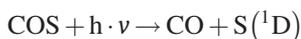
The wavelengths obtained for  $S_2$  and  $S_3$  agree reasonably well with the experimental spectra. From the  $S_4$  data it follows that the isomer absorbing at 530 nm is of  $C_{2v}$  symmetry and the one absorbing near 625 nm is of  $C_{2h}$  symmetry, while the three-membered branched ring of  $C_s$  symmetry must be colorless. The data also indicate that the unstable  $C_{2h}$  isomer of  $S_4$  has probably been detected in equilibrium sulfur vapor only because of its high oscillator strength.

Billmers and Smith recorded the UV-Vis absorption spectra of sulfur vapor at various pressures (9–320 Torr or 1.2–42.7 kPa) and temperatures (670–900 K) but failed in obtaining the correct reaction enthalpy for the interconversion of  $S_3$  and  $S_4$  from the absorption intensities [19]. The molar extinction coefficient of  $S_3$  at 400 nm exceeds that of  $S_4$  at 520 nm by more than one order of magnitude. While the  $S_3$  absorption band at 360–440 nm exhibits a vibrational fine structure, the two broad  $S_4$  absorption bands at

480–600 nm and at 610–660 nm are lacking any fine structure. Meyer et al. compiled the vibrational assignment of the  $S_3$  absorption bands [20].

The 520 nm absorption of  $S_4$  has also been observed in the spectrum of certain red-colored ultramarine samples [21]; the assignment of this band to the  $C_{2v}$  isomer of  $S_4$  is supported by the simultaneously observed Raman line at  $678\text{ cm}^{-1}$  which represents the symmetrical stretching vibration of the terminal SS bonds of this molecule (see Table 1 below).

High-temperature sulfur vapor at low pressure is said to be pale-violet due to the presence of  $S_2$  [22]. The  $S_2$  molecule in its triplet ground state has also been produced by photolysis of  $H_2S_2$  [23],  $S_2Cl_2$  [20, 24], and  $Me_2S_2$  [25], for example. The  $S_2$  vapor spectrum is characterized by the Schumann-Runge bands ( ${}^3\Sigma_u^- \leftarrow {}^3\Sigma_g^-$  transition;  $\nu_{00}=316\text{ nm}$  [26]) which at high temperatures extend from the UV into the visible region and beyond due to vibrational splittings (250–700 nm) [27, 28]. The electronic spectrum and the electronic states of  $S_2$  have been reviewed in 1965 by Barrow et al. [29]; the electronic energy levels of  $S_2$  were tabulated by Meyer et al. in 1972 [30] and by Huber and Herzberg in 1979 [26]. For more recent studies, see [25, 31, 32]. Singlet  $S_2({}^1\Delta)$  has also been produced by photolysis of sulfur compounds such as  $H_2S$  and  $COS$  [33]:



## 2.2

### Liquid Sulfur

At all temperatures liquid sulfur consists of a complex mixture of all homocycles from  $S_6$  to at least  $S_{35}$  and of larger polymeric molecules of cyclic and chain-like structure (collectively termed as  $S_\infty$ ) [34]. At temperatures above  $250\text{ }^\circ\text{C}$  smaller molecules such as  $S_5$ ,  $S_4$ ,  $S_3$ , and  $S_2$  are also likely components of the liquid as the composition of the equilibrium vapor demonstrates [9] (see above). In addition, branched rings and chains are probably minor components at temperatures near the boiling point of  $445\text{ }^\circ\text{C}$  [35] (see below).

At the melting point of  $120\text{ }^\circ\text{C}$  liquid sulfur is yellow due to its components  $S_8$ ,  $S_n$ , and  $S_\infty$ . The symbol  $S_n$  stands for all species soluble in  $CS_2$  at  $20\text{ }^\circ\text{C}$  except  $S_8$ . With increasing temperature the color of the liquid changes via orange and dark-red to dark red-brown [36]. The saturated sulfur vapor shows the same colors. Several research groups have tried to use absorption spectroscopy in the UV-Vis region to detect and identify the molecular species responsible for the color changes of liquid sulfur [11, 14, 37–39]. Because of the extremely high absorbance of sulfur one usually obtains spectra characterized by a steep absorption edge even if very thin films are investigated. At  $120\text{ }^\circ\text{C}$  melt temperature this edge begins to rise at  $480\text{ nm}$  ( $2.6\text{ eV}$ ) and is very steep near  $450\text{ nm}$  (path length  $0.1\text{ mm}$ ). With increasing tem-

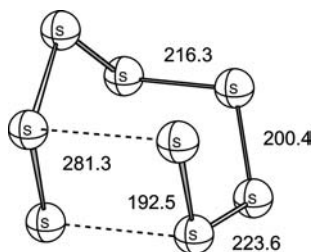
perature the edge shifts to larger wavelengths. This red-shift is explained by the increasing excitation of molecular vibrations resulting in a broadening of the absorption bands of  $S_8$ . This view is in agreement with the measured activation energy for the red-shift of  $10 \pm 1 \text{ kJ mol}^{-1}$  [40]. From about  $400 \text{ }^\circ\text{C}$  a strong increase of the absorption in the region of  $950 \pm 100 \text{ nm}$  (ca.  $1.3 \text{ eV}$ ) is observed resulting in shoulders at the absorption edge. This absorption band has been assigned to the chain-end atoms of free radicals  $S_n^\cdot$  since the temperature dependence of this absorption is about the same as that of the ESR signal intensity [14, 39] (while in reality it is slightly smaller). The band gap between the valence and conduction bands of liquid sulfur is  $3.65 \text{ eV}$  at  $150 \text{ }^\circ\text{C}$ ; it slightly decreases with increasing temperature [39]. For spectra of liquid sulfur under high pressure recorded in the range  $450\text{--}700 \text{ nm}$ , see [41]. Increasing pressure shifts the polymerization temperature to lower values and the absorption edge to larger wavelengths.

The spectra of very thin films of liquid sulfur exhibit absorptions which are not present in the spectrum of pure *cyclo*- $S_8$ . Even at as low a temperature as  $145 \text{ }^\circ\text{C}$  a shoulder at  $360 \text{ nm}$  is observed which has been assigned to  $S_6$  [14]. This absorption band can also be seen in the spectra of liquid sulfur at  $250 \text{ }^\circ\text{C}$  [14, 37] and in the spectrum of the melt quenched from  $250 \text{ }^\circ\text{C}$  [20, 37]. The assignment to  $S_6$  is rather unlikely since this molecule has practically no absorption in this region [42]. Furthermore, the  $S_6$  concentration at  $145 \text{ }^\circ\text{C}$  is only  $0.8\%$  [43]. Most probably the  $360 \text{ nm}$  band is caused by the collective absorption of the macromolecular components of  $\pi$ -sulfur, i.e., by the rings larger than  $S_8$  which have higher extinction coefficients at  $360 \text{ nm}$  than the smaller rings [42]. For example, *cyclo*- $S_{12}$  has its longest wavelength absorption maximum at  $317 \text{ nm}$  [42]. However, Tamura et al. [38] found a linear correlation between the absorbance at  $380 \text{ nm}$  ( $3.25 \text{ eV}$ ) and the polymer content of the melt quenched from temperatures in the region  $160\text{--}300 \text{ }^\circ\text{C}$  as determined by Koh and Klement [44]; they consequently assigned this band to the central atoms in the polymeric chains of  $S_\infty$ . Most likely both the long chains and the large rings contribute to this absorption.

At temperatures of  $300\text{--}700 \text{ }^\circ\text{C}$  an additional absorption was observed at  $400 \text{ nm}$ , and in the region of  $500\text{--}900 \text{ }^\circ\text{C}$  another one at  $520 \text{ nm}$  [14]. By comparison with the spectra of sulfur vapor [3] as well as with the spectra of photolytic dissociation products of  $S_3Cl_2$  and  $S_4Cl_2$  the absorption at  $520\text{--}530 \text{ nm}$  was assigned to the *cis*-planar isomer of the  $S_4$  molecule (see above) and the  $400\text{--}410 \text{ nm}$  band to the bent  $S_3$  molecule [20, 30]. The saturated sulfur vapor contains about  $1 \text{ mol}\%$  each of  $S_3$  and  $S_4$  at  $500 \text{ }^\circ\text{C}$  but about  $10 \text{ mol}\%$  each at  $1000 \text{ }^\circ\text{C}$  [3, 45]. Below  $300 \text{ }^\circ\text{C}$  these species are practically absent and therefore do not play any significant role in liquid sulfur. The deep red-brown color of sulfur melts at temperatures above  $400 \text{ }^\circ\text{C}$  has to be assigned to the molecules  $S_3$  (greenish-yellow),  $S_4$  ( $C_{2v}$ , purple-red), and the short-chain diradicals  $S_x^{\cdot}$  which will also contribute to the color. The latter are expected to absorb at various wavelengths owing to their widely differing chain-lengths.

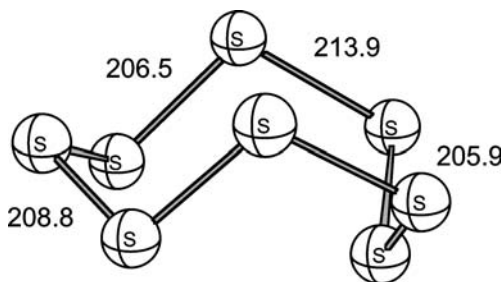
In addition to the chain-like and cyclic species discussed so far the presence of branched rings and chains in sulfur vapor and in liquid sulfur has been discussed [46] but no conclusive *experimental* evidence for such iso-

mers is presently available. For example, an isomer of *cyclo-S<sub>8</sub>* could be a candidate since ab initio MO calculations at the very high G3X(MP2) level of theory place the lowest energy isomer of S<sub>8</sub> at only  $\Delta G^\circ_{298}=28$  kJ mol<sup>-1</sup> above the eight-membered ring of *D*<sub>4d</sub> symmetry [35]. This isomer is of *C*<sub>2</sub> symmetry [47] and has the structure of a partly opened ring or a cluster-like spiral (bond lengths in pm):



The concentration of this species in liquid sulfur was estimated from the calculated Gibbs energy of formation as ca. 1% of all S<sub>8</sub> species at the boiling point [35]. In this context it is interesting to note that the structurally related homocyclic sulfur oxide S<sub>7</sub>=O is known as a pure compound and has been characterized by X-ray crystallography and vibrational spectroscopy [48, 49]. Similarly, branched long *chains* of the type -S-S-S(=S)-S-S- must be components of the polymeric S<sub>∞</sub> present in liquid sulfur at higher temperatures since the model compound H-S-S-S(=S)-S-S-H was calculated to be by only 53 kJ mol<sup>-1</sup> less stable at the G3X(MP2) level than the unbranched helical isomer of H<sub>2</sub>S<sub>6</sub> [35].

In addition to the branched rings and chains, cyclic S<sub>8</sub> conformations of lower symmetry than *D*<sub>4d</sub> are also likely components of liquid sulfur. For example, the following *exo-endo* isomer of S<sub>8</sub> (*C*<sub>s</sub> symmetry) is by just 28 kJ mol<sup>-1</sup> ( $\Delta G^\circ_{298}$ ) less stable than the ground state conformation and therefore its relative concentration in liquid sulfur and sulfur vapor at the boiling point will also be 1% of all S<sub>8</sub> species [35].



The HOMO/LUMO gaps of these isomeric sulfur molecules of branched rings and chains are considerably smaller than that of the crown-shaped S<sub>8</sub> ring [35]. Therefore, the UV-Vis spectra of these species are expected to exhibit absorption bands at longer wavelengths than the ground state structure

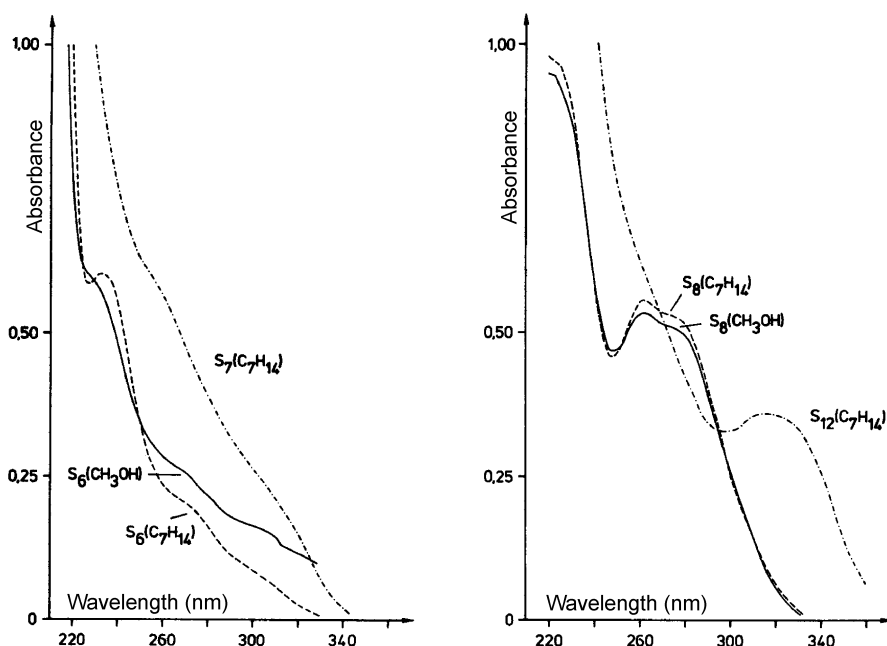


**Fig. 1** Absorption spectra of  $S_6$  and  $S_7$  (left) as well as of  $S_8$  and  $S_{12}$  (right) in methanol and methylcyclohexane ( $C_7H_{14}$ ) at 20 °C [42]

of  $S_8$ . In addition, these species possess a dipole moment in contrast to the  $S_8$  ring of  $D_{4d}$  symmetry. All of these species can be expected to be present in liquid sulfur at high temperatures [35].

Isomeric forms of *cyclo*- $S_6$  and *cyclo*- $S_7$  can also be suspected as components of liquid sulfur at high temperatures. However, their relative energies have not yet been calculated on a high enough level of theory to obtain reliable data.

### 2.3

#### Sulfur Solutions

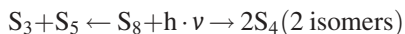
The UV-Vis absorption spectra of the homocyclic molecules  $S_n$  with  $n = 6-10, 12, 15,$  and  $20$  have been recorded in methylcyclohexane and/or methanol solutions at 20 °C in the range 200–360 nm [42]. Representative examples of the spectra are shown in Fig. 1. Their molar extinction coefficients ( $\epsilon$ ) at 254 nm in methylcyclohexane solution linearly increase with the ring size as the following data demonstrate (20 °C):

$$S_6: \epsilon = 2400 \quad S_7: \epsilon = 5550 \quad S_8: \epsilon = 6420 \quad S_{12}: \epsilon = 13710$$

Therefore, the corresponding coefficients of other molecules may be estimated by interpolation.

It is interesting to note that the longest wavelength absorption band of these homocycles more and more shifts to lower energies as the molecular size increases. This effect can most clearly be seen in the spectrum of  $S_{12}$ .

When  $S_8$  solutions in cyclopentane ( $1 \text{ mmol l}^{-1}$ ) were irradiated by 308 nm laser pulses four novel absorption bands at 325, 400, 530, and 640 nm appeared [50]. The absorptions assigned to  $S_3$  (400 nm) and  $S_4$  (530 nm) decayed within microseconds. The other two peaks also disappeared very rapidly but their origin remained unexplained in 1985. However, it is now evident that the 640 nm absorption is due to the presence of the  $C_{2h}$  isomer of  $S_4$ . Evidently,  $S_8$  decomposes by the following reactions:



It seems feasible that the 325 nm band originates from  $S_5$  the UV spectrum of which is still unknown.

Irradiation of *cyclo*- $S_8$  dissolved in  $CS_2$  by a high-pressure mercury lamp at 20 °C produces the homocycles  $S_7$ ,  $S_6$ ,  $S_{12}$ ,  $S_9$ ,  $S_{10}$ , and probably  $S_5$  in concentrations decreasing in this order. Irradiation of  $S_6$  in  $CS_2$  gives mainly  $S_8$  and  $S_7$  while irradiation of  $S_7$  generates  $S_8$  and  $S_6$ . Similarly, photolysis of  $S_{12}$  in  $CS_2$  yields  $S_8$ ,  $S_7$ , and  $S_6$  [51]. For these reasons UV-Vis spectra of compounds containing S-S bonds must be recorded with caution not to trigger decomposition reactions.

## 2.4

### Solid Sulfur Allotropes

The color of a perfect dielectric is due to optical transitions of valence electrons to the conduction band. In the case of isolated  $S_8$  molecules these transitions occur between the occupied  $\pi^*$  (HOMO) and the unoccupied  $\sigma^*$  (LUMO) molecular orbitals which in the crystal form the valence and conduction bands, respectively. Since the van der Waals interaction between  $S_8$  molecules in the crystalline allotropes is rather weak, the widths of the conduction and valence bands will be rather small. The minimal photon energy at which such transitions are allowed (the absorption threshold) is the width of the forbidden gap of an insulator. In the case where the onset of the optical absorption falls into the visible photon energy range, the color of the crystal is determined by the photon energy of the absorption threshold and by the spectral distribution of the intensity of the transitions. The HOMO/LUMO gap of isolated  $S_8$  molecules has recently been estimated by high-level ab initio MO calculations as 4.9 eV [35]. From the longest wavelength absorption maximum of  $S_8$  molecules in solution (280 nm) one obtains 4.4 eV. In liquid sulfur the real part of the complex dielectric constant has a peak at 4.3 eV [38]. The solid allotrope  $\alpha$ - $S_8$ , however, is an indirect band gap material, i.e., electronic absorptions are assisted by phonon processes besides pure electronic transitions over the direct gap. A careful evaluation of the optical absorption edge in orthorhombic sulfur at STP conditions yielded 2.61 eV for the indirect gap and 4.43 eV for the direct gap [52]. The mean

phonon energy was reported as 0.117 eV ( $\sim 944 \text{ cm}^{-1}$ ) which is two times the wavenumber of the stretching vibration at  $472 \text{ cm}^{-1}$ . In addition, it was found that selenium impurities have a considerable effect on the absorption edge [52]. Under high pressure, the absorption edge shows a red shift due to broadening of the valence and conduction bands which results in a narrowing of the energy gap,  $E_{\text{gap}}$ . The pressure dependence of the optical absorption edge,  $dE_{\text{gap}}/dp$ , has been investigated several times [53–57]. The slope of  $dE_{\text{gap}}/dp$  is slightly non-linear and of the order of  $0.05\text{--}0.1 \text{ eV GPa}^{-1}$  below 10 GPa, depending on the method of evaluation of the gap energy. Discontinuities in  $dE_{\text{gap}}/dp$  have been attributed to structural phase transitions [56, 57], and the photo-induced amorphization of  $\alpha$ -S<sub>8</sub> under pressure could be correlated to the red shift of the absorption edge [58].

Commercial elemental sulfur is usually of “bright-yellow” color at 20 °C [36]. Pure orthorhombic  $\alpha$ -S<sub>8</sub> is, however, of greenish-yellow color at 20 °C but totally colorless at 77 K while commercial sulfur often remains pale-yellow at this temperature [59]. The reasons for this different behavior are two-fold. Commercial samples are never pure S<sub>8</sub> but besides traces of organic impurities they always contain S<sub>7</sub> in concentrations of between 0.1 and 0.5% [59]. Sulfur found as a mineral in Nature sometimes also contains S<sub>7</sub> but in addition traces of selenium are quite often present (up to 680 ppm Se, probably as S<sub>7</sub>Se molecules) [60]. These minor components influence the color of the samples at ambient and low temperatures in the sense that a more orange-type of yellow (“egg-yellow”) is recognized.

The various solid sulfur allotropes are all more or less yellow at 20 °C but the scale ranges from the deep orange-yellow of S<sub>6</sub> to the pale yellow of S<sub>12</sub>. The color also depends on the particle size: As finer the particles as lighter the color impression. Chemically produced S<sub>8</sub> has in fact occasionally been obtained as a colorless material at room temperature which only slowly turns yellow as the initially tiny crystals grow [61]. The sample temperature is also of decisive influence (thermochromic effect) [10] (see above).

The origin of the small S<sub>7</sub> content of all commercial sulfur samples is the following. Elemental sulfur is produced either by the Frasch process (mining of sulfur deposits) or by the Claus process (partial oxidation of H<sub>2</sub>S) [62]. In each case *liquid* sulfur is produced (at ca. 140 °C) which at this temperature consists of 95% S<sub>8</sub> and ca. 5% other sulfur homocycles of which S<sub>7</sub> is the main component. On slow cooling and crystallization most of the non-S<sub>8</sub> species convert to the more stable S<sub>8</sub> and to polymeric sulfur but traces of S<sub>7</sub> are built into the crystal lattice of S<sub>8</sub> as solid state defects. In some commercial samples traces of S<sub>6</sub> or S<sub>9</sub> were detected in addition. The “S<sub>7</sub> defects” survive for years if not forever at 20 °C. The composition of the commercial samples depends mainly on the cooling rate and on other experimental conditions. Only recrystallization from organic solvents removes S<sub>7</sub> and, of course, the insoluble polymeric sulfur and produces pure  $\alpha$ -S<sub>8</sub> [59].

The reflectance spectra of solidified liquid sulfur previously equilibrated at temperatures of between 120 ° and 440 °C have been measured at 25 °C and color pictures of these solidified melts were published [63]. These data were used to explain the yellow, orange and red colors of the sulfur flows on

Jupiter's moon Io on which a number of very active sulfur volcanoes have been discovered [64]. These volcanoes are powered by  $\text{SO}_2$  gas which forces the liquid sulfur from its underground deposits to the surface.

A thin film of  $\alpha\text{-S}_8$  exhibits an absorption maximum at 285 nm with a large wing extending to 350 nm at 25 °C [20]. The absorption is so strong that crystals of  $\alpha\text{-S}_8$  are opaque below 350 nm. The electronic absorption spectrum of  $\alpha\text{-S}_8$  is fairly well known [65–68]. The lowest energy electronic transition of  $\alpha\text{-S}_8$  was calculated as 324 nm (3.83 eV) [67] and as 3.6 eV [66, 68].

If the colorless crystals of  $\alpha\text{-S}_8$  immersed in liquid nitrogen are irradiated by sunlight they turn intense yellow within a few minutes [10]. The origin of this color is unknown but most probably it is caused by one of the isomers of  $\text{S}_8$ , maybe the one of  $C_2$  symmetry shown above.

If hot sulfur melts or hot sulfur vapors at low pressure are frozen at low temperatures highly colored samples are obtained which may be black, green or red depending on the temperature and pressure conditions and on the rate of quenching [69]. These colors originate from the small molecules and radicals, present at high temperatures, which become trapped in the solid sample. At room temperature these samples turn yellow, provided the sulfur has been very pure.

The optical properties of solid  $\text{S}_6$  have been studied by ab initio MO calculations of the energy band structure [70] but no experimental data for solid  $\text{S}_6$  are known.

### 3 Vibrational Spectra

#### 3.1 Small Sulfur Molecules ( $\text{S}_2$ , $\text{S}_3$ , $\text{S}_4$ , $\text{S}_5$ )

##### 3.1.1 *Disulfur* $\text{S}_2$

Raman spectra of  $\text{S}_2$  in its triplet ground state have been recorded both in sulfur vapor and after matrix isolation using various noble gases. The stretching mode was observed at  $715\text{ cm}^{-1}$  in the gas phase [46], and at  $716\text{ cm}^{-1}$  in an argon matrix [71]. From UV absorption and fluorescence spectra of sulfur vapor the harmonic fundamental mode of the  $\text{S}_2$  ground state was derived as  $\omega_e = 726\text{ cm}^{-1}$ . The value corrected for anharmonicity is  $720\text{ cm}^{-1}$  [26, 27]. Earlier reports on the infrared absorption spectrum of  $\text{S}_2$  in matrix isolated sulfur vapor [72] are in error: the observed bands at 660, 668 and  $680\text{ cm}^{-1}$  are due to  $\text{S}_4$  [17] and other species [73].

### 3.1.2

#### *Trisulfur S<sub>3</sub>*

Raman spectra of  $^{32}\text{S}_3$  and  $^{34}\text{S}_3$  have been recorded using sulfur vapor [74] while infrared spectra were measured after matrix isolation in solid argon [75]. The  $\text{S}_3$  molecule is of  $C_{2v}$  symmetry. Therefore, all fundamental modes are Raman and infrared active. The Raman spectra excited by lasers emitting at wavelengths of between 407 and 515 nm are mainly resonance enhanced. Accordingly, a large number of combination bands was observed. The three fundamental modes of  $^{32}\text{S}_3$  ( $^{34}\text{S}_3$ ) occur at  $\nu_1 = 581(564) \text{ cm}^{-1}$  (symmetrical stretching) [74],  $\nu_2 = 281(273) \text{ cm}^{-1}$  (bending) [74], and, from infrared spectra,  $\nu_3 = 680(660) \text{ cm}^{-1}$  (asymmetrical stretching) [75]. In matrix isolation experiments several different sites were occupied by the  $\text{S}_3$  molecules resulting in slightly differing wavenumbers for its vibrations [75]. Force constants have also been calculated [74].

### 3.1.3

#### *Tetrasulfur S<sub>4</sub>*

Raman spectra of  $\text{S}_4$  were recorded using saturated and unsaturated sulfur vapor [76] while infrared spectra were measured after matrix isolation of sulfur vapors in solid argon [17, 75]. The assignment of these spectra is complicated by the occurrence of at least two isomers of  $\text{S}_4$  and by the simultaneous presence of other species like  $\text{S}_2$ ,  $\text{S}_3$  and, probably, branched rings of the type  $\text{S}_n=\text{S}$  with  $n \geq 4$ . The two isomers of  $\text{S}_4$  observed so far are of  $C_{2v}$  and  $C_{2h}$  symmetry; see Scheme 1 above. Their calculated and—as far as known—observed fundamental modes are given in Table 1. As can be seen from these data, for none of the isomers the full set of six fundamental modes has been observed yet. The claimed existence of the three-membered branched ring isomer of  $\text{S}_4$  ( $\text{S}_3=\text{S}$ ) of  $C_s$  symmetry in sulfur vapor [76] or in matrix isolated samples [17] has recently been shown to be in error [9].

For a more detailed discussion of the vibrational spectra of  $\text{S}_4$ , see [9].

### 3.1.4

#### *Pentasulfur S<sub>5</sub>*

Vibrational spectra of  $\text{S}_5$  have not been reported.

## 3.2

### *Sulfur Rings S<sub>6</sub> to S<sub>20</sub>*

#### 3.2.1

##### *S<sub>8</sub>*

The vibrational spectrum of orthorhombic  $\alpha\text{-S}_8$  is the best studied amongst the various sulfur allotropes. Experimental as well as theoretical investiga-

tions have produced a large amount of data. Therefore, the Raman and infrared spectra of  $S_8$  will be discussed first.

### 3.2.1.1

#### The Free $S_8$ Molecule

An eight-membered ring molecule has  $3 \times 8 - 6 = 18$  intramolecular vibrations [77]. Since the molecular symmetry of  $S_8$  belongs to the point group  $D_{4d}$  the representation of the internal vibrations is given by

$$\Gamma_{\text{int}} = 2A_1 + B_1 + B_2 + 2E_1 + 3E_2 + 2E_3$$

Vibrations of the symmetry class  $A_1$  are totally symmetrical, that means all symmetry elements are conserved during the vibrational motion of the atoms. Vibrations of type  $B$  are anti-symmetrical with respect to the principal axis. The species of symmetry  $E$  are symmetrical with respect to the two in-plane molecular  $C_2$  axes and, therefore, two-fold degenerate. In consequence, the free molecule should have 11 observable vibrations. From the character table of the point group  $D_{4d}$  the activity of the vibrations is as follows: modes of  $A_1$ ,  $E_2$ , and  $E_3$  symmetry are Raman active, modes of  $B_2$  and  $E_1$  are infrared active, and  $B_1$  modes are inactive in the free molecule; therefore, the number of observable vibrations is reduced to 10.

The first successful calculation of the fundamental modes and their assignment came from Scott et al. in 1964 [78] based on a Urey-Bradley force field (UBFF) with six force constants. The force constants were calculated from ten fundamental frequencies observed by Raman and IR spectroscopy at that time. In addition, Steudel et al. [79–81] reported force constant calculations applied on the cyclic molecules  $S_6$ ,  $S_7$ ,  $S_8$ ,  $S_8O$ , and  $S_{12}$  respectively. It was found that the force constants for a given type of vibration (stretching, bending, torsion) are almost uncoupled. For example, the force constant responsible for the stretching vibration is mainly characterized by the contribution due to the variation of the bond lengths. Accordingly, the various types of vibrations are energetically well separated: stretching  $\sim 410$ – $480 \text{ cm}^{-1}$ , bending  $\sim 150$ – $250 \text{ cm}^{-1}$ , torsion  $\sim 90 \text{ cm}^{-1}$ . Although most of the frequencies could be reproduced within a few wavenumbers, the calculated value of the  $E_2$  bending vibration showed a relatively large difference of about  $+10 \text{ cm}^{-1}$  to the observed value of about  $152 \text{ cm}^{-1}$  [78, 79].

The frequencies of the  $S_8$  ring have also been calculated by means of MD methods [82]. Since the intramolecular potential utilized corresponds to that of Scott et al. the calculated value of the  $E_2$  bending mode again deviates from the experimental wavenumber. Attempts to reproduce the wavenumber of this mode by additional force constants were not successful [79]. The origin of this peculiarity is still unknown and may trigger a new approach to the intramolecular potential in  $S_8$ . On the other hand, by means of a general valence force field (GVFF) including 14 (!) force constants which have been fitted to 22 experimental frequencies of  $^{32}S_8$  and  $^{34}S_8$  the deviation was enormously reduced ( $\leq 1.5 \text{ cm}^{-1}$ ) [83]. Furthermore, frequencies of the harmonic

vibrations obtained by ab initio quantum chemical calculations (e.g., [84, 85]) match the experimental spectra only if empirical scaling factors are introduced which depend on the method of calculation.

In the UBFF calculations as well as in the molecular dynamics simulations the experimental wavenumber of the  $B_1$  stretching vibration ( $\sim 411 \text{ cm}^{-1}$ ) could only be reproduced by introducing of an additional force constant which accounts for the interaction of vibrations of adjacent bonds [78, 82]. This can reasonably be understood in terms of the bond alternation since the stretching of one bond forces the neighboring bonds to shorten [79, 80]. Over the period of a stretching vibration the valence electrons undergo a rearrangement which causes a weakening of the stretched bond and a strengthening of the adjacent bonds. The force constants derived for  $S_8$  were found to be transferable to other highly symmetrical homocycles such as  $S_6$  and  $S_{12}$ , for example [80, 86].

Raman intensities of the molecular vibrations as well as of their crystal components have been calculated by means of a bond polarizability model based on two different intramolecular force fields ([87], the UBFF after Scott et al. [78] and the GVFF after Eysel [83]). Vibrational spectra have also been calculated using velocity autocorrelation functions in MD simulations with respect to the symmetry of intramolecular vibrations [82].

### 3.2.1.2

#### Crystals of $\alpha$ - $S_8$

In the crystal, the total number of vibrations is determined by the number of atoms per molecule,  $N$ , and the number of molecules per primitive cell,  $Z$ , multiplied by the degrees of freedom of each atom:  $3ZN$ . In the case of  $\alpha$ - $S_8$  ( $Z=4$ ,  $N=8$ ) this gives a total of 96 vibrations (!) which can be separated in  $(3N-6)-Z = 72$  intramolecular or "internal" vibrations and  $6Z = 24$  intermolecular vibrations or lattice phonons ("external" vibrations). The total of the external vibrations consists of  $3Z = 12$  librational modes due to the molecular rotations,  $3Z-3 = 9$  translational modes, and 3 acoustic phonons, respectively.

The vibrations of the free molecule can be correlated with the vibrations of the crystal by group theoretical methods. Starting with the point group of the molecule ( $D_{4d}$ ), the irreducible representations (the symmetry classes) have to be correlated with those of the site symmetry ( $C_2$ ) in the crystal and, as a second step, the representations of the site have to be correlated with those of the crystal factor group ( $D_{2h}$ ) [89, 90]. Since the  $C_2$  point group is not a direct subgroup of  $D_{4d}$  of the molecule and of  $D_{2h}$  of the crystal, the correlation has to be carried out in successive steps, for example:

$$D_{4d} \rightarrow D_4 \rightarrow D_2 \rightarrow C_2 \rightarrow C_{2v} \rightarrow D_{2h}$$

molecule     $\rightarrow$     site     $\rightarrow$     crystal

The transformation of the irreducible representations of the molecular point group to those of the site is connected with a reduction of the symme-

**Table 2** Correlation of the molecular point group of  $S_8$  with the factor group of the orthorhombic crystal ( $D_{4d} \rightarrow C_2 \rightarrow D_{2h}$ ) [88]

Molecule				Site	Crystal <sup>a</sup>		
Vibration <sup>b</sup>	Energy (cm <sup>-1</sup> ) <sup>c</sup>	Activity <sup>d</sup>	$D_{4d}$	$\rightarrow$	$C_2$	$\rightarrow$	$D_{2h}^{24}$
$\nu_1$ (s)	476	Ra	$2A_1$	$\rightarrow$	2a	$\rightarrow$	$2a_g + 2b_{1g} + 2a_u + 2b_{1u}$
$\nu_2$ (b)	218.5						
$\nu_3$ (s)	(424)	ia	$B_1$	$\rightarrow$	a	$\rightarrow$	$a_g + b_{1g} + a_u + b_{1u}$
$\nu_4$ (b)	243	IR	$B_2$	$\rightarrow$	b	$\rightarrow$	$b_{2g} + b_{3g} + b_{2u} + b_{3u}$
$\nu_5$ (s)	471	IR	$2E_1$	$\angle$	2a	$\rightarrow$	$2a_g + 2b_{1g} + 2a_u + 2b_{1u}$
$\nu_6$ (b)	191				2b	$\rightarrow$	$2b_{2g} + 2b_{3g} + 2b_{2u} + 2b_{3u}$
$\nu_7$ (s)	476	Ra	$3E_2$	$\angle$	3a	$\rightarrow$	$3a_g + 3b_{1g} + 3a_u + 3b_{1u}$
$\nu_8$ (b)	152.5				3b	$\rightarrow$	$3b_{2g} + 3b_{3g} + 3b_{2u} + 3b_{3u}$
$\nu_9$ (t)	86						
$\nu_{10}$ (s)	444	Ra	$2E_3$	$\angle$	2a	$\rightarrow$	$2a_g + 2b_{1g} + 2a_u + 2b_{1u}$
$\nu_{11}$ (b)	248				2b	$\rightarrow$	$2b_{2g} + 2b_{3g} + 2b_{2u} + 2b_{3u}$
$R_z$	-	(ia)	$A_2$	$\rightarrow$	b	$\rightarrow$	$b_{2g} + b_{3g} + b_{2u} + b_{3u}$
$R_x, R_y$	-	(Ra)	$E_3$	$\angle$	a	$\rightarrow$	$a_g + b_{1g} + a_u + b_{1u}$
					b	$\rightarrow$	$b_{2g} + b_{3g} + b_{2u} + b_{3u}$
$T_z$	-	(IR)	$B_2$	$\rightarrow$	b	$\rightarrow$	$b_{2g} + b_{3g} + b_{2u} + b_{3u}^e$
$T_x, T_y$	-	(IR)	$E_1$	$\angle$	a	$\rightarrow$	$a_g + b_{1g} + a_u + b_{1u}^e$
					b	$\rightarrow$	$b_{2g} + b_{3g} + b_{2u} + b_{3u}^e$

<sup>a</sup> Modes of  $a_u$  symmetry are inactive, g = gerade modes are Raman active, u = ungerade modes are IR active

<sup>b</sup> s = stretching, b = bending, t = torsional vibration of the molecule

<sup>c</sup> Experimental wavenumbers of  $S_8$  in  $CS_2$  solution at room temperature [78, 79]. Calculated value for  $\nu_3$  in brackets

<sup>d</sup> Ra = Raman active, IR = infrared active, ia = inactive molecular vibration. R and T denote rotations and translations, respectively

<sup>e</sup> A set of three acoustical modes ( $b_{1u}, b_{2u}, b_{3u}$ ) with zero energy at the center of the Brillouin zone must be subtracted from the number of observable IR absorptions

try elements. The physical meaning is that the (static) crystal field enforces its lower symmetry on the molecule. In consequence, the selection rules for optical activity are changed (Table 2). For example, the  $\nu_3$  stretching vibration, inactive in the free molecule (symmetry class  $B_1$ ), becomes Raman and IR active in the crystal. In the case of the degenerate vibrations of the  $S_8$  ring ( $E_1, E_2, E_3$ ) the degeneracy is removed by the correlation procedure (Table 2). The fact that the primitive cell contains four interacting molecules leads to a resonance splitting of the molecular vibrations [91]. Each intramolecular vibration then has four components in the crystal and, since the degeneracy of the vibrations of  $E_1, E_2$ , and  $E_3$ , respectively, is lost, these modes split into eight crystalline components (Table 2).

The factor group  $D_{2h}$  of orthorhombic  $S_8$  includes an inversion operation; therefore, the g-u exclusion principle works resulting in modes of either Raman (gerade, g) or infrared activity (ungerade, u).

Summarizing, in the crystal there are 36 Raman active internal modes (symmetry species  $a_g$ ,  $b_{1g}$ ,  $b_{2g}$ ,  $b_{3g}$ ) and 26 infrared active internal modes ( $b_{1u}$ ,  $b_{2u}$ ,  $b_{3u}$ ) as well as 12 Raman active and 7 infrared active external vibrations (librations and translations). Vibrations of the type  $a_u$  are inactive because there appears no dipole moment along the normal coordinates in these vibrations of the crystal.

The spectral distribution of the three types of internal vibrations is in accordance with that of the free molecule. The factor group splitting is relatively large for the doubly degenerate torsional vibration  $\nu_9$  ( $\sim 25$   $\text{cm}^{-1}$ ) and for the bending modes  $\nu_8$  and  $\nu_6$  ( $\sim 11$  and  $\sim 16$   $\text{cm}^{-1}$ , respectively). Therefore, the crystal field effects cannot be treated as a small perturbation on the internal potential. The external modes extend over the spectral range 25–77  $\text{cm}^{-1}$  which is close to the components of the torsional vibration, if not overlapping with them (see below). Experimentally as well as theoretically the intensities of the vibrations obey the following order with respect to their molecular symmetry:

$$A_1 \sim E_2 \sim E_3 > B_2 \sim E_1 > B_1 \text{ (Raman)}$$

$$E_1 \sim B_2 > E_2 \sim E_3 \sim A_1 > B_1 \text{ (infrared)}$$

The first Raman and infrared studies on orthorhombic sulfur date back to the 1930s. The older literature has been reviewed before [78, 92–94]. Only after the normal coordinate treatment of the  $S_8$  molecule by Scott et al. [78] was it possible to improve the earlier assignments, especially of the lattice vibrations and crystal components of the intramolecular vibrations. In addition, two technical achievements stimulated the efforts in vibrational spectroscopy since late 1960s: the invention of the laser as an intense monochromatic light source for Raman spectroscopy and the development of Fourier transform interferometry in infrared spectroscopy. Both techniques allowed to record vibrational spectra of higher resolution and to detect bands of lower intensity.

Since then, the vibrational spectrum of  $S_8$  has been the subject of several studies (Raman: [79, 95–100], infrared: [101, 102]). However, because of the large number of vibrations in the crystal it is obvious that a full assignment would only be successful if an oriented single-crystal is studied at different polarizations in order to deconvolute the crystal components with respect to their symmetry. Polarized Raman spectra of samples at about 300 K have been reported by Ozin [103] and by Arthur and Mackenzie [104]. In Figs. 2 and 3 examples of polarized Raman and FTIR spectra of  $\alpha$ - $S_8$  at room temperature are shown. If the sample is exposed to low temperatures the bandwidths can enormously be reduced (from several wavenumbers down to less than 0.1–1  $\text{cm}^{-1}$ ) permitting further improvements in the assignment.

Polarized Raman and infrared spectra of orthorhombic  $S_8$  at low temperatures were reported by Gautier and Debeau (30–50 K) [106] and by Becucci et al. (< 20 K) [107]. Since natural sulfur is composed of isotopomers of the  $S_8$  molecules (see below), the vibrational spectra of isotopically pure  $\alpha$ - $^{32}S_8$  ( $^{32}S$  purity >99.95%) as well as of natural sulfur have been investigated in

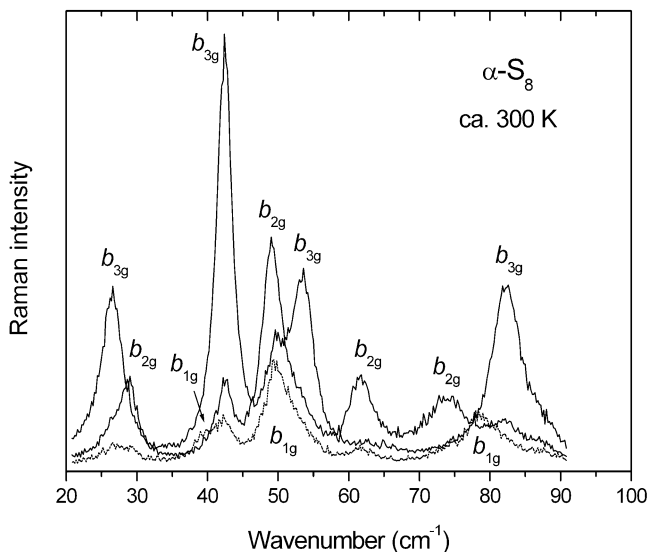


**Fig. 2** Raman spectra of a single-crystal of orthorhombic  $S_8$  at three different polarizations in which the off-diagonal elements of the Raman scattering tensor are non-zero ( $b_{1g}$ ,  $b_{2g}$ ,  $b_{3g}$ ), after [105]. However, Raman intensities of other polarizations like  $a_g$  components ( $\sim 54 \text{ cm}^{-1}$ ) penetrate in the spectra due to optical anisotropy in the crystal

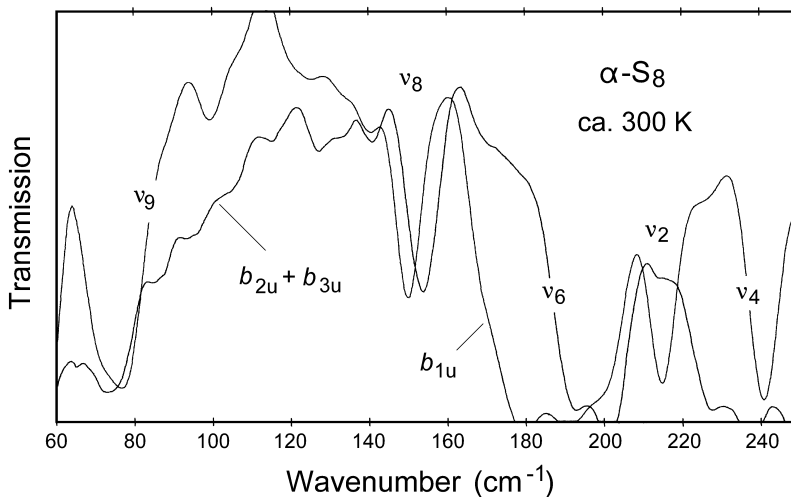


**Fig. 3** Single beam IR transmission spectra of a single-crystal of orthorhombic  $S_8$  at two polarizations ( $b_{1u}$   $\sim$  parallel to crystal  $c$  axis,  $b_{2u}+b_{3u}$   $\sim$  perpendicular to  $c$ ) showing the strong absorption of the IR active vibrations  $v_4$  and  $v_6$  (resolution:  $2 \text{ cm}^{-1}$ ), after [105]. Sample thickness  $\sim 450 \mu\text{m}$

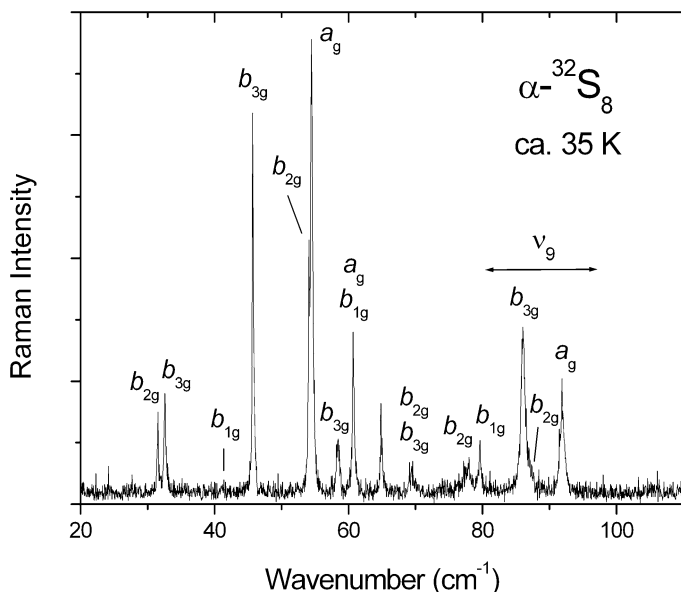


**Fig. 4** Raman spectrum of the external and torsional vibrations of a single crystal of  $\alpha$ - $^{32}\text{S}_8$  (resolution:  $<0.1\text{ cm}^{-1}$ ), after [110]

the most recent study of Becucci et al. with high accuracy (Raman: ca.  $\pm 0.1\text{ cm}^{-1}$ , FTIR: ca.  $\pm 0.01\text{ cm}^{-1}$ ) and high resolution (Raman:  $\sim 0.2\text{ cm}^{-1}$ , FTIR:  $< 0.05\text{ cm}^{-1}$ ). As a result, some previously doubtful assignments could be corrected and, additionally, isotopic line splitting of internal modes has been observed (see below) [107–109].

### 3.2.1.3

#### External Modes and the Torsional Vibration $\nu_9$

Figures 4 and 5 show the Raman and IR spectra of  $\alpha$ - $\text{S}_8$  in the range up to about  $100\text{ cm}^{-1}$ . A comparison of these spectra with those presented in Figs. 2 and 3 reveals that the linewidths are much smaller at low temperatures (ca.  $0.02$ – $0.2\text{ cm}^{-1}$ ). The wavenumbers and assignments of the external and torsional modes as reported by Gautier and Debeau [106] and Becucci et al. [107] are listed in Table 3. The spectra in Figs. 4 and 5 clearly demonstrate that there is no gap between the external vibrations and the crystal components of the lowest internal vibration  $\nu_9$ . Moreover, at about  $76\text{ cm}^{-1}$  an IR active lattice mode appears between two components of the fundamental  $\nu_9$  at  $74\text{ cm}^{-1}$  and  $79\text{ cm}^{-1}$ , respectively.

The classification of external modes into librations and translations was ensured by group theoretical considerations and by comparison of expected with observed intensities in the vibrational spectra [107]. In addition, it was

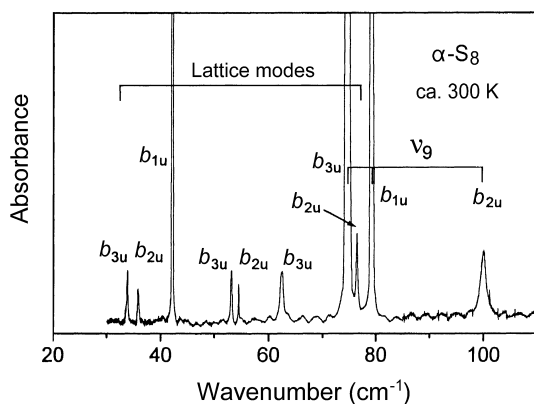


**Fig. 5** FTIR absorbance spectrum of the external and torsional vibrations of a single crystal of  $\alpha$ -S<sub>8</sub> (resolution: 0.03 cm<sup>-1</sup>, sample thickness ca. 350  $\mu$ m), after [107]

argued that the energy of librational modes should be lower than that of the translational modes [95, 106]. However, this assignment has to be regarded as only tentative since lattice dynamical calculations of the eigenvectors of the external modes showed that the modes will have at least a partially mixed character [111–113].

The components of the low lying Raman doublet ( $b_{2g}$ ,  $b_{3g}$ ) at about 30 cm<sup>-1</sup> exhibit a different temperature dependence which gives rise to a reverse assignment at 300 K [103, 104] in comparison to the low temperature studies (< 20 K); see Figs. 2 and 3. In fact, the bands overlap at about 50 K [114].

The intermolecular modes have been studied theoretically by lattice dynamical methods in the harmonic approximation [111, 113, 115–117] as well as by molecular dynamics simulations [118]. Various models based on a Buckingham 6-exp atom-atom potential have been applied: rigid-body [113, 116] and rigid-shell models [115], rigid-body including charge transfer [111], and flexible molecule models [116–118]. In the flexible molecule models of Kurittu [116] and Gramaccioli and Filippini [117] the intramolecular degrees of freedom were allowed to be excited and to couple with the external vibrations. A mixing of external-internal character was found for the lattice modes ( $b_{2g} \sim 65$  cm<sup>-1</sup>,  $b_{2u} \sim 76$  cm<sup>-1</sup>,  $b_{2g} \sim 78$  cm<sup>-1</sup>) and for two components of the  $\nu_9$  mode ( $b_{2g} \sim 87$  cm<sup>-1</sup>,  $b_{2u} \sim 100$  cm<sup>-1</sup>) [116]. Interestingly, the eigenvectors of an external mode at about 62.5 cm<sup>-1</sup> ( $b_{3u}$ ) were calculated as being dominated by contributions of the internal degrees of freedom. According to the theoretical predictions, the mixing of eigenvector components of  $\nu_9$  with intermolecular degrees of freedom is also expressed by the pressure and temperature dependence of the frequencies of the  $\nu_9$  components which have been studied experimentally. For example, the pressure dependent frequency shifts of the Raman active components of  $\nu_9$  (ca. 6–7 cm<sup>-1</sup>/GPa) were found intermediate to the shifts obtained for lattice phonons (ca.

**Table 3** Assignment and wavenumbers ( $\text{cm}^{-1}$ ) of the external and torsional vibrations of  $\alpha$ -S<sub>8</sub> based on polarization dependent studies [106, 107]. In the first two columns the type and symmetry classes of the molecular and crystal vibrations, respectively, are given. The wavenumbers of the vibrations are listed in the columns “infrared” and “Raman” corresponding to the order of symmetry species given in the second column (crystal). natS means orthorhombic S<sub>8</sub> with natural isotopic composition, while <sup>32</sup>S stands for isotopically pure <sup>32</sup>S crystals (purity >99.95%)

Vibration	Infrared <sup>a</sup>		Raman <sup>a</sup>	
	Crystal <sup>a</sup>	natS	<sup>32</sup> S	natS
<b>Molecule<sup>b</sup></b>				
<b>Librations</b>				
R <sub>z</sub>	<i>b</i> <sub>2u</sub> , <i>b</i> <sub>3u</sub>	35, 34	35.80, 33.83	30, 30
A <sub>2</sub> (ia)	<i>b</i> <sub>2g</sub> , <i>b</i> <sub>3g</sub>	35.74, 33.76		31.4, 32.6
R <sub>x</sub> , R <sub>y</sub>	<i>b</i> <sub>1u</sub> , <i>b</i> <sub>2u</sub> , <i>b</i> <sub>3u</sub>	44, 45, 47	~41.75, 53.13, 54.48	45, 40, 46, 46
E <sub>3</sub> (Ra)	<i>a</i> <sub>g</sub> , <i>b</i> <sub>1g</sub> , <i>b</i> <sub>2g</sub> , <i>b</i> <sub>3g</sub>		54.51	54.5, 40.8, ? <sup>c</sup> , 45.6
<b>Translations</b>				
T <sub>z</sub>	<i>b</i> <sub>2u</sub> , <i>b</i> <sub>3u</sub>	74, 57	76.37, 62.32	67, 70
B <sub>2</sub> (IR)	<i>b</i> <sub>2g</sub> , <i>b</i> <sub>3g</sub>			
T <sub>x</sub> , T <sub>y</sub> <sup>d</sup>	<i>a</i> <sub>g</sub> , <i>b</i> <sub>1g</sub> , <i>b</i> <sub>2g</sub> , <i>b</i> <sub>3g</sub>	- <sup>d</sup>	- <sup>d</sup>	56, 61, 56, 61
E <sub>1</sub> (IR)				60.0 <sup>e</sup> , 60.8 <sup>e</sup> , 69.2, 58.4
<b>Torsions</b>				
<i>v</i> <sub>9</sub>	<i>b</i> <sub>1u</sub> , <i>b</i> <sub>2u</sub> , <i>b</i> <sub>3u</sub>	78, 96, 89 <sup>f</sup>	78.47/79.62 <sup>g</sup> , 99.96, 79.10, 99.79, 74.43	92, 79, 79, 86
E <sub>2</sub> (Ra)	<i>a</i> <sub>g</sub> , <i>b</i> <sub>1g</sub> , <i>b</i> <sub>2g</sub> , <i>b</i> <sub>3g</sub>	74.12/74.62 <sup>g</sup>		91.6, 79.2, ~87 <sup>h</sup> , 86.0
Temperature (K)		34	< 20	30
Reference		[106]	[105, 107, 109]	[106]

<sup>a</sup> Infrared active are modes of symmetry *b*<sub>1u</sub>, *b*<sub>2u</sub>, *b*<sub>3u</sub>, and Raman active are those of symmetry *a*<sub>g</sub>, *b*<sub>1g</sub>, *b*<sub>2g</sub>, *b*<sub>3g</sub>

<sup>b</sup> (ia) = inactive, (Ra) = Raman active, and (IR) = infrared active molecular vibrations

<sup>c</sup> Not resolvable due to line broadening in the crystal of natural isotopic composition

<sup>d</sup> Acoustic modes (*b*<sub>1u</sub>, *b*<sub>2u</sub>, *b*<sub>3u</sub>) with ~ 0  $\text{cm}^{-1}$  <sup>e</sup> Assignment unclear <sup>f</sup> Doubtful, not observed in recent studies

<sup>g</sup> Isotopic line splitting in natural  $\alpha$ -S<sub>8</sub> <sup>h</sup> Shoulder on stronger *b*<sub>3g</sub> component

5–10  $\text{cm}^{-1}/\text{GPa}$ ) and for bending vibrations (ca. 0.5–4  $\text{cm}^{-1}/\text{GPa}$ ) [109, 119, 120].

In addition, theoretically calculated dispersion curves and Raman intensities have been reported as well as results of neutron scattering experiments [113, 115].

The density of states (DOS) of lattice phonons has been calculated by lattice dynamical methods [111]. The vibrational DOS of orthorhombic  $\text{S}_8$  up to about 500  $\text{cm}^{-1}$  has been determined by neutron scattering [121] and calculated by MD simulations of a flexible molecule model [118, 122].

Up to now, the intermolecular potential models are only fair in reproducing the wavenumbers of the external modes. Although various refinements have been made, none of the models seems to be superior to the others. More recently developed intermolecular potentials have been applied to structural and thermodynamical studies but not to the analysis of the vibrational spectra [122–125].

#### 3.2.1.4

##### Bending Vibrations

Of the five bending vibrations of the  $\text{S}_8$  molecule three are Raman active ( $\nu_2$ ,  $\nu_8$ ,  $\nu_{11}$ ) and two are IR active ( $\nu_4$ ,  $\nu_6$ ). Most of the Raman active modes in the crystal could clearly be resolved in spectra at low temperatures and by polarization measurements. For example, Fig. 6 shows the Raman active factor group components of the  $\nu_8$  mode obtained at three different polarizations. In Fig. 7 an analogous IR spectrum is presented.

Figures 8 and 9 shows a part of the bending region at low temperature containing the components of  $\nu_8$  (150–160  $\text{cm}^{-1}$ ) and  $\nu_6$  (190–200  $\text{cm}^{-1}$ ). The  $\nu_6$  vibration, IR active in the free molecule, has weak components in the Raman spectrum. According to theoretically calculated Raman intensities, which almost perfectly fit the experimental spectrum, the  $b_{1g}$  component has a very low scattering cross-section [87] and is accidentally degenerate with the  $b_{2g}$  component at ca. 188  $\text{cm}^{-1}$ . The IR active components of  $\nu_6$  cause strong absorptions in the IR spectrum even if the crystalline sample used for transmission studies is as thin as  $\sim 400 \mu\text{m}$  [107, 109].

The strongest line in the Raman spectrum of  $\alpha\text{-S}_8$  at ambient and low temperature is the  $a_g$  component of the  $\nu_2$  mode (Fig. 10). The IR absorbance was expected to be low; however, the  $b_{1u}$  component is of moderate intensity. The most intense absorption bands in the IR spectrum are the two components of the  $\nu_4$  mode ( $b_{2u}$ ,  $b_{3u}$ ) which obscure two weakly absorbing components of  $\nu_{11}$ , leaving only the  $b_{2u}$  component at 253  $\text{cm}^{-1}$  observable (Fig. 9). Although  $\nu_{11}$  is Raman active in the isolated molecule, the crystal components are not very intense in the Raman spectrum (Fig. 10) according to the calculated intensities [87]. In contrast to the strong absorption of the IR active components of  $\nu_4$ , its  $b_{2g}$  and  $b_{3g}$  counterparts are very weak in the Raman spectrum (Fig. 10), which is again in excellent agreement with the calculated intensities.

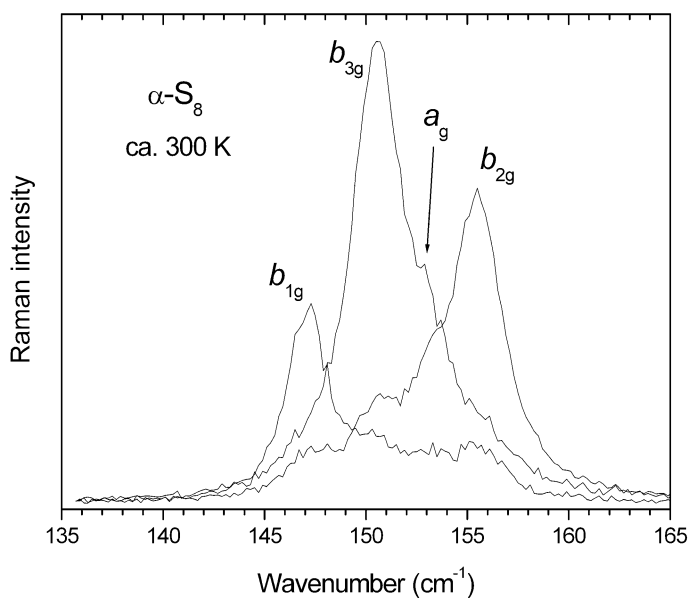


**Fig. 6** Polarized Raman spectra of the bending vibration  $\nu_8$  ( $b_{1g}$ ,  $b_{2g}$ ,  $b_{3g}$ ) in a single crystal of  $\alpha$ - $S_8$  each showing the penetration of modes of other polarizations as weak shoulders, after [105]

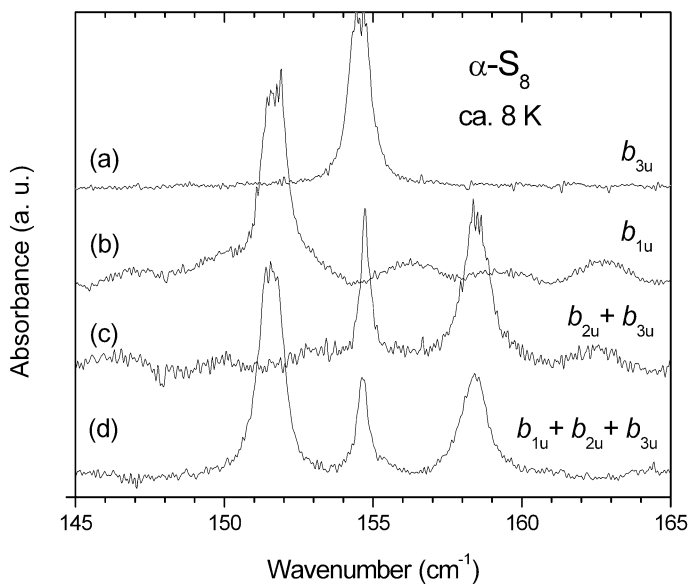


**Fig. 7** Polarized FTIR absorbance spectra of the bending vibration  $\nu_8$  in single crystals of  $\alpha$ - $S_8$  ((a) natural  $\alpha$ - $S_8$ , thickness  $\sim 1$  mm, (b)–(d)  $\alpha$ - $^{32}S_8$ , thickness  $\sim 400$   $\mu\text{m}$ , resolution  $< 0.05$   $\text{cm}^{-1}$ ), after [105, 109]

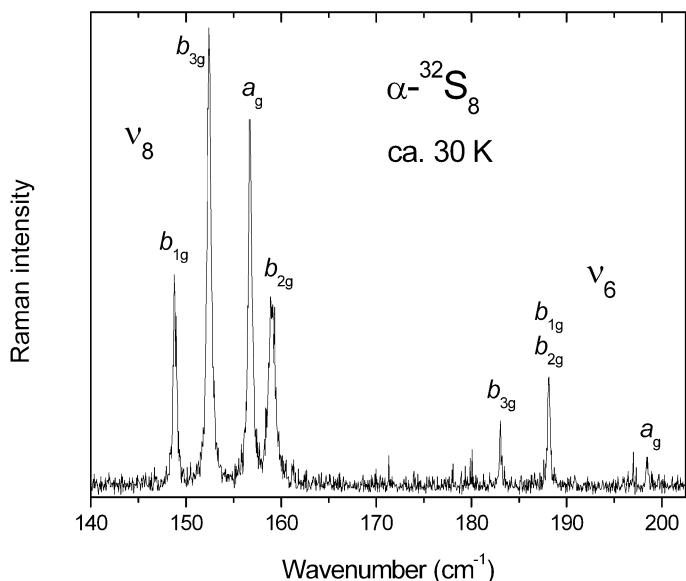


**Fig. 8** Raman spectrum of the bending region in the range of  $\nu_8$  and  $\nu_6$  in single crystalline  $\alpha\text{-}^{32}\text{S}_8$  (resolution  $< 0.1\text{ cm}^{-1}$ ), after [110]

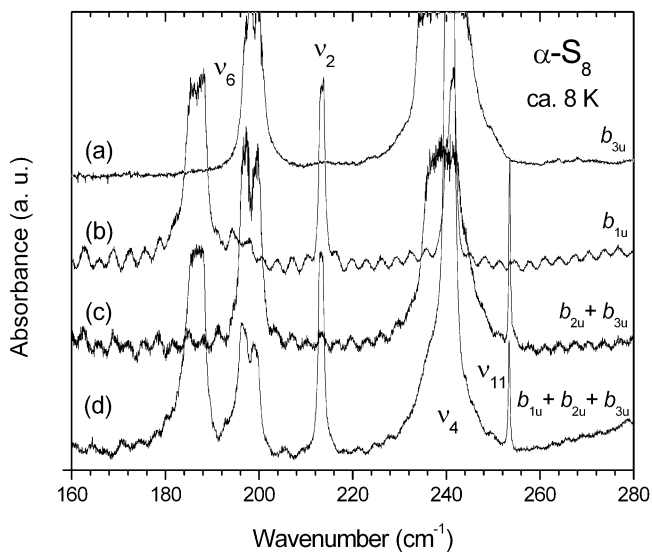


**Fig. 9** Polarized FTIR absorbance spectra of the bending region in the range of  $\nu_6$ ,  $\nu_2$ ,  $\nu_4$ , and  $\nu_{11}$ , respectively ((a) natural  $\alpha\text{-S}_8$ , thickness  $\sim 1\text{ mm}$ , (b)–(d)  $\alpha\text{-}^{32}\text{S}_8$ , thickness  $\sim 400\text{ }\mu\text{m}$ , resolution  $< 0.05\text{ cm}^{-1}$ ), after [105, 109]

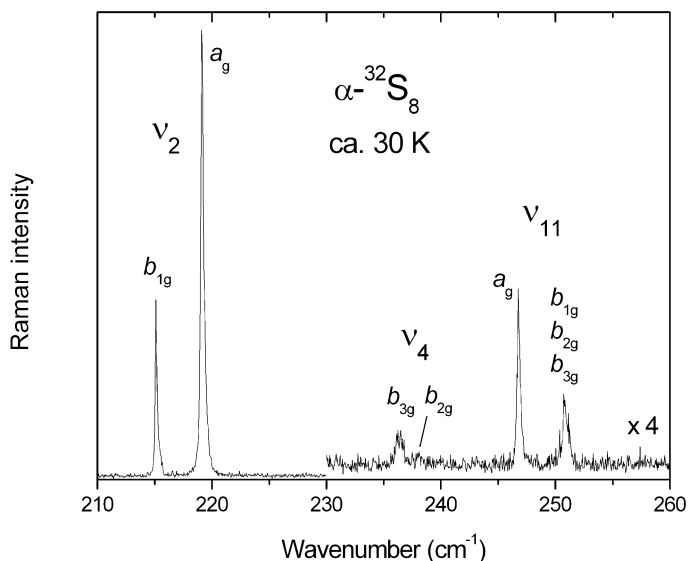


**Fig. 10** Raman spectrum of the bending region in the range of  $\nu_2$ ,  $\nu_4$ , and  $\nu_{11}$ , respectively (resolution  $< 0.1 \text{ cm}^{-1}$ , single crystal), after [110]. The intensity in the range 230–260  $\text{cm}^{-1}$  is enhanced by a factor of 4

### 3.2.1.5

#### Stretching Vibrations

The most prominent feature in the region of the stretching vibrations ( $410\text{--}480 \text{ cm}^{-1}$ ) is the signal near  $475 \text{ cm}^{-1}$  which is composed of ten components in the Raman spectrum and of seven components in the IR spectrum. Even at low temperatures and high spectral resolution ( $< 0.1 \text{ cm}^{-1}$ ) the factor group components are difficult if not impossible to resolve. However, according to the calculated Raman intensities [87] the most intense lines are those of  $a_g$  symmetry as can be seen in Fig. 11. Although Gautier and Debeau [106] proposed a complete assignment for all symmetry species, it must be stated that the assignment of the weak components is doubtful due to the penetration of the strong  $a_g$  components in other polarization geometries (suitable for  $b_{1g}$ ,  $b_{2g}$ ,  $b_{3g}$ ). In addition, accidental degeneracies of the weak components have likely to be taken into account. A similar problem arises in the IR spectrum. The strongest lines are expected for the components of  $\nu_5$  which is IR active in the free molecule ( $E_1$  symmetry). Analogously, the strong absorbing components of  $\nu_4$  at  $240 \text{ cm}^{-1}$  obscure the weakly absorbing components of the molecular Raman active modes of  $\nu_{11}$ . Therefore, the shoulder at  $477 \text{ cm}^{-1}$  might be assigned to the  $b_{1u}$  component of  $\nu_1$ , see Fig. 12.

The stretching vibration  $\nu_{10}$  at about  $440 \text{ cm}^{-1}$  has four Raman active components in the crystal. However, in the low temperature spectra there is

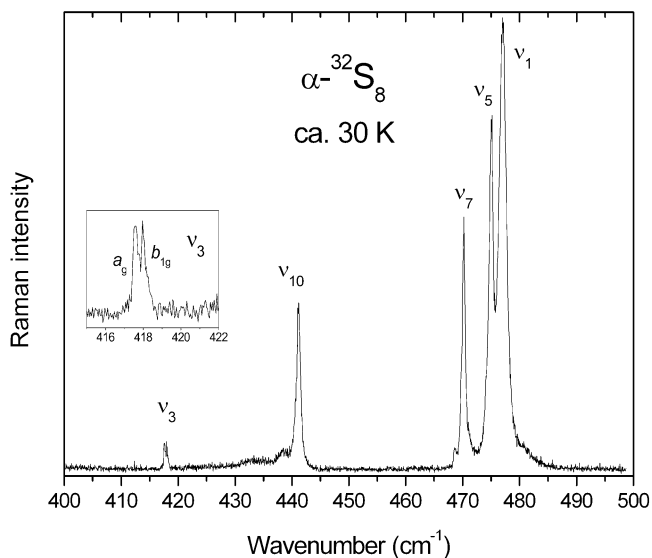


**Fig. 11** Raman spectrum of the stretching vibrations in single crystal  $\alpha\text{-}^{32}\text{S}_8$  (resolution  $< 0.1\text{ cm}^{-1}$ ), after [110]

only one sharp peak visible due to the  $a_g$  component accompanied by weak and broad bands at lower energy (Fig. 11). The band shape of the IR absorption of  $\nu_{10}$  is similar; the absorption is mainly caused by the  $b_{2u}$  component, while the  $b_{1u}$  and  $b_{3u}$  components are of low intensity.

The  $\nu_3$  mode observed at about  $415\text{ cm}^{-1}$  is inactive in the free molecule and, therefore, the factor group components are very weak in the Raman

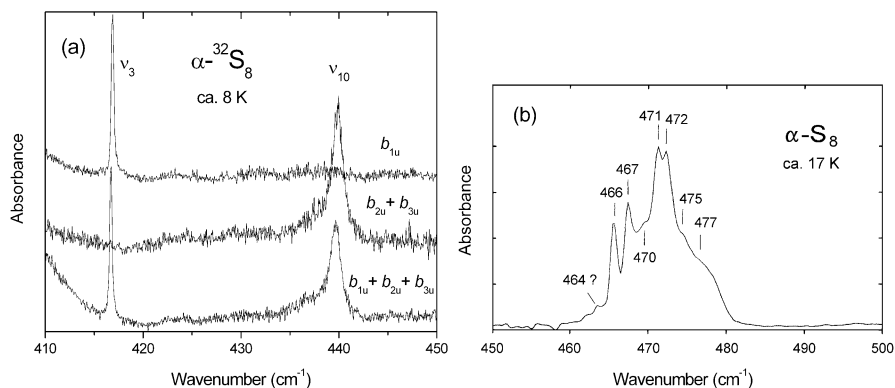


**Fig. 12** FTIR absorbance spectra of the stretching vibrations in single crystals of  $\alpha\text{-S}_8$ . (a) Polarized spectra of  $\nu_3$  and  $\nu_{10}$  in  $\alpha\text{-}^{32}\text{S}_8$  (resolution  $< 0.05\text{ cm}^{-1}$ ), after [105, 109], (b) unpolarized spectrum of the strong absorbing manifold of components of  $\nu_7$ ,  $\nu_5$ , and  $\nu_1$ , respectively, in natural  $\alpha\text{-S}_8$  (resolution  $\sim 0.5\text{ cm}^{-1}$ ), after [109]

and IR spectra. The infrared absorption ( $b_{1u}$ ) shows a pronounced line splitting in sulfur samples of natural isotopic composition (see below).

Most of the many modes of  $\alpha$ -S<sub>8</sub> have been assigned to their symmetry class. However, some strong infrared absorptions ( $\nu_4 \sim 240 \text{ cm}^{-1}$ ,  $\nu_5 \sim 470 \text{ cm}^{-1}$ ) and weak Raman lines ( $\nu_{11} \sim 250 \text{ cm}^{-1}$ ) as well as signals originating from accidental degeneracies (e.g.,  $\nu_1$ ,  $\nu_5$ , and  $\nu_7$  at around  $475 \text{ cm}^{-1}$ ) were difficult to assign.

The wavenumbers of the internal modes have been calculated by LD [116, 117] and MD methods [118]. In general, the results are in qualitative agreement with the observed signals and factor group splittings. However, the results are not sufficient to improve the assignment of modes based on experimental studies. For example, the Raman active components of  $\nu_9$  were reported to have a factor group splitting of  $2 \text{ cm}^{-1}$  (MD [118], LD [117]) and  $8 \text{ cm}^{-1}$  (LD [116]) while the splitting is in fact  $12 \text{ cm}^{-1}$ . These deviations are probably caused by the inadequate intermolecular potential, as discussed above. The splitting of modes of higher energy is much better reproduced by the theoretical models. The observed wavenumbers and their assignments have been discussed in detail elsewhere [109].

### 3.2.1.6

#### Effects of Isotopic Impurities

Natural sulfur is composed of the four stable isotopes  $^{32}\text{S}$ ,  $^{33}\text{S}$ ,  $^{34}\text{S}$ , and  $^{36}\text{S}$  with natural abundances of 95.02, 0.75, 4.21, and 0.02%, respectively [4]. Since the vibrational frequencies depend on the masses and force constants, the isotopic impurities are expected to have observable effects on the vibrational spectrum. For example, if the S<sub>8</sub> ring is infected by only one  $^{34}\text{S}$  atom ( $^{34}\text{S}_1^{32}\text{S}_7$ ) the mass variation is  $^2/_{64} \sim 3\%$  in the case of an S-S stretching vibration and  $^2/_{256} \sim 0.8\%$  in the case of external vibrations [126]. Although  $^{34}\text{S}$  is present only with 4.21%, the probability to find one  $^{34}\text{S}$  atom in a ring of composition  $^{34}\text{S}_1^{32}\text{S}_7$  is 23.6% as calculated by binomial statistics. Accordingly, the isotopomer  $^{32}\text{S}_8$  has a natural probability of only 66.5%. On the other hand, 94% of the heteronuclear rings arise from the  $^{34}\text{S}$  isotope which, therefore, can be treated as the main isotopic impurity in natural sulfur ( $^{\text{nat}}\text{S}_8$ ). Every fourth S<sub>8</sub> molecule in the primitive cell of orthorhombic S<sub>8</sub> is a  $^{34}\text{S}_1^{32}\text{S}_7$  isotopomer, and 10% of the molecules in  $^{\text{nat}}\text{S}_8$  are of other heteronuclear compositions.

The presence of isotopic impurities causes clear effects in the vibrational spectra. Almost all modes studied so far show frequency shifts on  $^{32}\text{S}/^{34}\text{S}$  substitution [81, 107]. The average shift of the internal modes is ca.  $0.6 \text{ cm}^{-1}$ , and of the external modes it is  $0.1\text{--}0.3 \text{ cm}^{-1}$  (Tables 3, 4 and 5). Furthermore, the isotopomers which are statistically distributed in crystals of natural composition can act as additional scattering centers for the phonon propagation. Therefore, in such crystals the lifetime of the phonons is shortened in comparison with isotopically pure crystals and, as a conse-

**Table 4** Assignment and wavenumbers ( $\text{cm}^{-1}$ ) of the bending vibrations in  $\alpha$ -S<sub>8</sub> based on polarization dependent studies [106, 107]. The Table has to be read like Table 3

Vibration	Infrared		Raman	
	natS	<sup>32</sup> S	natS	<sup>32</sup> S
Molecule	Crystal			
$\nu_8$	151, 158, 155	151.4, 158.2, 151.59, 158.40,	159, 150, 161, 154	156.2, 148.4, 158.6,
$E_2$ (Ra)	$a_{1g}, b_{1g}, b_{2g}, b_{3g}$	154.51	154.67	152.0
$\nu_6$	187, 197, 199	185.0/188.0 <sup>a</sup> , 186.6, 196.7,	199, 188, 188, 183	199.0, 188.4, 188.4,
$E_1$ (IR)	$a_g, b_{1g}, b_{2g}, b_{3g}$	196.2/197.4 <sup>a</sup> , 199.2 ?/199.7 <sup>a</sup>	199.2	183.1
$\nu_2$	213	212.4/213.7 <sup>a</sup>	221, 217	219.1, 215.1
$A_1$ (Ra)	$a_g, b_{1g}$			
$\nu_4$	238, 239	234.4, ?	239, 236	238.6, 236.2
$B_2$ (IR)	$b_{2g}, b_{3g}$			
$\nu_{11}$	253, 254, 256	?, 253.21, ?	249, 249, 253, 253	246.8, 251.4, 251.4,
$E_3$ (Ra)	$a_g, b_{1g}, b_{2g}, b_{3g}$	240±1, 253.46,	249, 249, 253, 253	251.4
Temperature (K)	34	240±5	30	< 20
Reference	[106]	[105, 107, 109]	[106]	[105, 107, 109]

<sup>a</sup> These modes show a line splitting in crystals of natural isotopic composition. [109]

**Table 5** Assignment and wavenumbers ( $\text{cm}^{-1}$ ) of the stretching vibrations of  $\alpha$ -S<sub>8</sub> based on polarization studies [106, 107]. The Table has to be read like Table 3

Vibrations	IR		Raman	
	natS	<sup>32</sup> S	natS	<sup>32</sup> S
Molecule	Crystal			
$\nu_3$	$b_{1u}$	408	417.11 / 415.54 <sup>a</sup>	416.82
$B_1$ (ia)	$a_{1g}, b_{1g}$			419, 420
$\nu_{10}$	$b_{1u}, b_{2u}, b_{3u}$	431, 437, 435	440.2, 440.2, ~437	439.4 sw <sup>?</sup> , 439.8, 441, 434, 441, 443
$E_3$ (Ra)	$a_{1g}, b_{1g}, b_{2g}, b_{3g}$			440.3, ~433, 438.2, ~440
$\nu_5$	$b_{1u}, b_{2u}, b_{3u}$	464, 466, 465	472.3, 469.5, 473.8	472.4, 469.7, 474.8
$E_1$ (IR)	$a_{1g}, b_{1g}, b_{2g}, b_{3g}$			470, 473, 472, 468
$\nu_7$	$b_{1u}, b_{2u}, b_{3u}$	472, 476, 471	465.6, 471.2, 467.4	467.2, 471.3, 468.6
$E_2$ (Ra)	$a_{1g}, b_{1g}, b_{2g}, b_{3g}$			474, 473, 472, 472
$\nu_1$	$b_{1u}$	476	470.1	478.0
$A_1$ (Ra)	$a_{1g}, b_{1g}$			476.8, 477.5, (480)
Temperature (K)		50	< 20	-
Reference		[106]	[105, 107, 109]	[105, 107, 109]

<sup>a</sup> This mode has been observed as a multiplet in crystals of natural isotopic composition [108, 109]

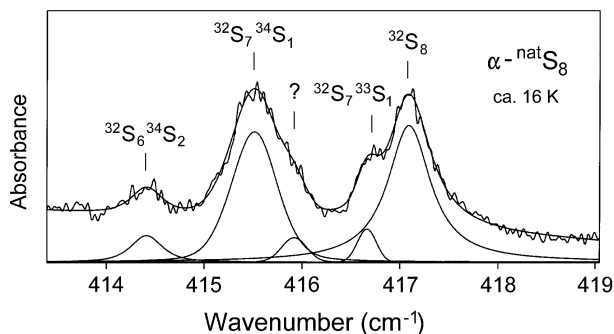


**Fig. 13** Isotopic line splitting of the  $\nu_3$  stretching vibration in single crystalline  $\alpha\text{-natS}_8$  (see also Fig. 12(a)), after [108, 109]. The origin of each absorption band is indicated by an isotopomer present in crystals of natural composition. While the  $^{32}\text{S}_8$  absorption could be fitted by a Lorentzian band profile, the remaining peaks were dominated by the Gaussian contribution in the Voigt band shapes (*solid lines* below the spectrum). The sum result of fitting the isotopic absorption bands is inserted in the measured spectrum as a *solid line*

quence, the bandwidth of the Raman and absorption lines is increased [127–129]. Phonon relaxation processes in  $\alpha\text{-}^{32}\text{S}_8$  and  $\alpha\text{-natS}_8$  have been studied by high resolution Raman and FTIR techniques [108, 114, 130]. By evaluation of the temperature dependence of the Lorentzian band profiles it was found that the relaxation of the modes is mainly due to three-phonon processes in both the natural and isotopically pure crystals. However, while the wavenumbers of the modes are affected by the isotopic impurities, the impact on bandwidths is mode-selective, and this observation was explained for internal vibrations in terms of resonant scattering processes [114, 130].

Isotopic line splitting has been studied by MD simulations on a free  $\text{S}_8$  ring [131] but has been observed only for IR active internal vibrations [107, 108]. For example, the IR active  $b_{1u}$  component of the molecular inactive  $\nu_3$  mode ( $\sim 416\text{ cm}^{-1}$ ) is composed of at least five absorptions in the natural crystal which can be assigned to the most abundant isotopomers (Fig. 13) [108, 109]. As can be seen by comparison of Fig. 13 with Fig. 12(a), the band origin of the  $b_{1u}$  vibration in natural sulfur crystals which corresponds to the  $^{32}\text{S}_8$  ring is shifted by about  $0.3\text{ cm}^{-1}$  towards higher energy with respect to the band origin in  $\alpha\text{-}^{32}\text{S}_8$ . Moreover, the relative intensities do not reflect the natural abundance of the isotopomers [108]. However, wavenumber shifts and intensity changes have been interpreted in terms of a resonance interaction [109]. Since a mixing of the eigenvector components of  $\nu_3$  with the much stronger bands at  $475\text{ cm}^{-1}$  was assumed, the interpretation of isotope effects is much easier in the case of the torsion vibration  $\nu_9$ .

Due to the large factor group splitting of about  $25\text{ cm}^{-1}$  the bands of the torsional vibration are well separated (Fig. 5) and the isotope effect on the frequency was calculated to about  $0.6\text{ cm}^{-1}$  [131]. Figure 14 clearly demonstrates the broadening and splitting of the  $b_{3u}$  and  $b_{1u}$  components of  $\nu_9$  as

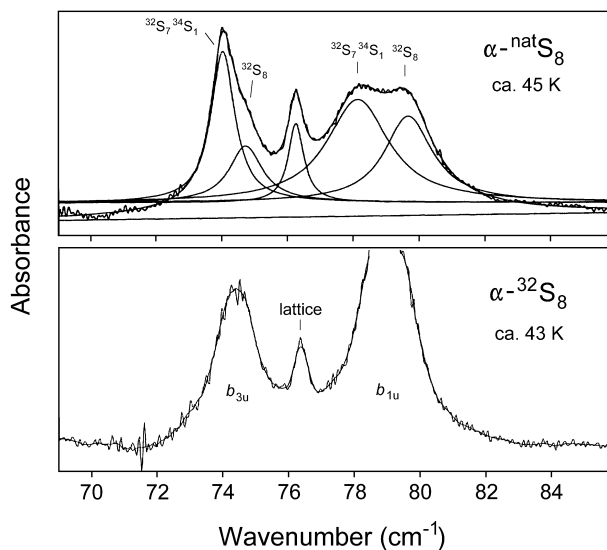


**Fig. 14** FTIR absorbance spectra of the  $b_{3u}$  and  $b_{1u}$  components of the torsional vibration  $\nu_9$  in single crystals of  $\alpha\text{-natS}_8$  (top) and  $\alpha\text{-}^{32}\text{S}_8$  (bottom), after [105, 109]. In the  $\alpha\text{-}^{32}\text{S}_8$  crystal, the  $b_{1u}$  component is strong absorbing which led to a cut-off. The solid line in the  $\alpha\text{-}^{32}\text{S}_8$  spectrum is a result of soft smoothing, while the solid lines in the  $\alpha\text{-natS}_8$  spectrum resulted from a fit to Voigt profiles

well as the wavenumber shifts and considerable intensity changes. As the bands in the natural crystal can be fitted each by two Lorentzian band-shapes, only the main impurity  $^{34}\text{S}_1^{32}\text{S}_7$  has to be taken into account. In an isotopically pure  $^{32}\text{S}_8$  ring, the  $\nu_9$  vibration has  $E_2$  symmetry. Substitution of a  $^{32}\text{S}$  atom by  $^{34}\text{S}$  leads to a change of molecular symmetry from  $D_{4d}$  to  $C_s$  which removes the two-fold degeneracy of  $\nu_9$  (Fig. 15); however, the distortion is small [131]. The two  $\nu_9$  vibrations of  $^{34}\text{S}_1^{32}\text{S}_7$  are of  $A'$  and  $A''$  symmetry. In the crystal, each mode splits in two components ( $A'$  corresponds to  $a_u$  and  $b_{3u}$ ,  $A''$  to  $b_{1u}$ ,  $b_{2u}$ ), c.f. Fig. 15. Thus, in the natural crystal the  $b_{1u}$  and  $b_{2u}$  components mentioned above are provided by the  $^{32}\text{S}_8$  rings (66%) as well as by the  $^{34}\text{S}_1^{32}\text{S}_7$  rings (24%). Since one molecule of the primitive cell is a  $^{34}\text{S}_1^{32}\text{S}_7$  isotopomer, resonance interaction occurs between the components of the same symmetry class leading to line splitting [109].

From an energetic point of view, the bands at higher wavenumbers can be assigned to the  $^{32}\text{S}_8$  rings. However, the intensities were found as ca. 0.65:1 (pure : infected) instead of 2.8:1 which would be expected from the natural abundance of the isotopomers. These discrepancies were solved by applying the mathematical formalism utilized in the treatment of intramolecular Fermi resonance (see, e.g., [132]). Accordingly, in the natural crystal we have to deal with vibrational coupling between isotopomers in the primitive cell of the crystal [109].

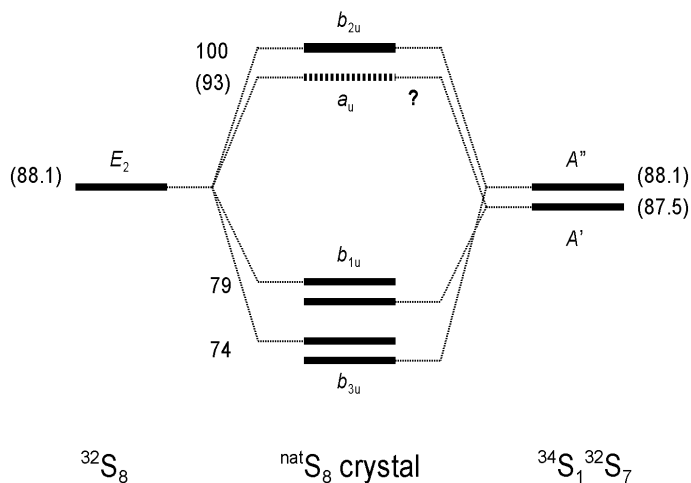


**Fig. 15** Energy level scheme of the isotopic line splitting of  $\nu_9$  in terms of the free molecules ( ${}^{32}\text{S}_8$  and  ${}^{34}\text{S}_1{}^{32}\text{S}_7$  as the main contributions) and of the orthorhombic crystal with natural abundance of isotopomers, after [109]. Numerical values are observed wavenumbers (in  $\text{cm}^{-1}$ ), values in brackets came from MD simulations on free rings [131] and in the case of  $a_u$  from LD calculations [116, 117]

### 3.2.1.7

#### Overtones and Combination Vibrations

The large number of modes in orthorhombic  $\text{S}_8$  results in a manifold of overtones and combination bands in the vibrational spectra [133]. As an ex-

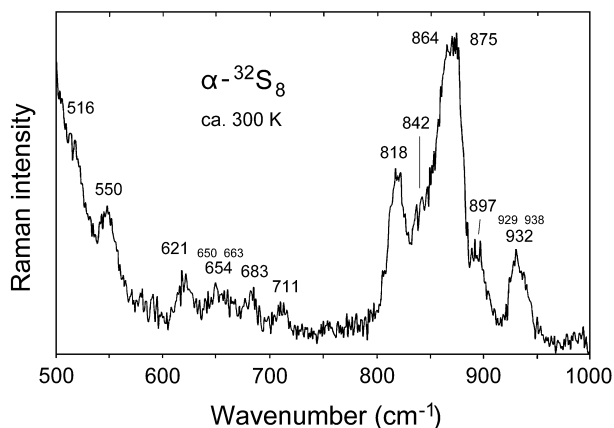


**Fig. 16** Raman spectrum of two-phonon processes in single crystalline  $\alpha$ - ${}^{32}\text{S}_8$  in the range 500–1000  $\text{cm}^{-1}$ , after [109]. The strong bands in the range 800–950  $\text{cm}^{-1}$  result from combinations of components of the stretching vibrations

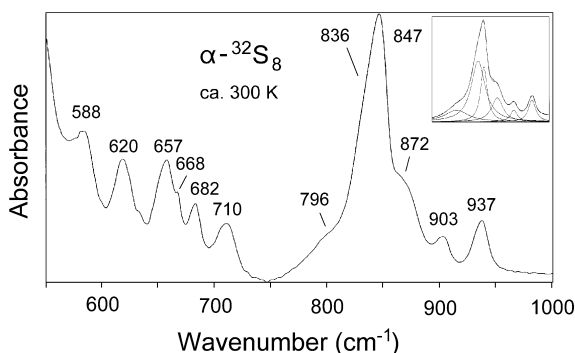


**Fig. 17** FTIR absorbance spectrum of two-phonon processes in single crystalline  $\alpha$ - $^{32}\text{S}_8$  in the range 550–1000  $\text{cm}^{-1}$ , after [109]. The strong bands in the range 800–950  $\text{cm}^{-1}$  result from combinations of components of the stretching vibrations. The *insert* shows a numerical deconvolution of the prominent spectral feature between 750–950  $\text{cm}^{-1}$

ample, Figs. 16 and 17 show such signals in the spectral range 500–1000  $\text{cm}^{-1}$ . The assignment of these bands is difficult due to the large number of possible processes. The intensities of the combinations are about 1% compared to the fundamental modes. The combinations are more intense at higher temperatures because of the thermal population of the phonon DOS.

Important contributions on the Raman side came after 1970 which could make use of the well established assignment of the fundamentals in interpreting the spectra [97–99, 134]. The most complete studies on two- and three-phonon processes have been carried out by Harvey and Butler (Raman, only  $g \times g$  combinations assigned) [100] and by Eckert (Raman and IR) [109].

### 3.2.1.8

#### High-Pressure Studies

Application of high pressure causes the spectrum of a crystal to expand since the “springs” are stiffened as a consequence of the potential anharmonicity. The pressure effect on the external modes is stronger because of the weaker intermolecular potential. For molecular crystals like  $\alpha$ - $\text{S}_8$  a scaling law for the pressure dependence of the inter- and intramolecular force constants was predicted [135]. Generally, in the Grüneisen concept a dimensionless parameter  $\gamma$  relates the phonon frequency  $\omega$  of a crystal to its volume  $V$  by  $\omega \propto V^{-\gamma}$ . In the model of Zallen for molecular crystals, external modes should have  $\gamma_{\text{ext}} \sim 2$  and internal modes should behave according to  $\gamma_{\text{int}} \sim \omega_{\text{int}}^{-2}$ .

Several studies confirmed the high-pressure response of sulfur crystals by Raman [109, 119, 120, 135–137] and IR spectroscopy [109, 138]. Accordingly, external and torsional vibrations have values for the mode Grüneisen parameter around 2, and the parameters of the bending and stretching vibra-

tions are frequency dependent spanning a range from 0.2 to 0.005. Moreover, it was predicted that the high energetic factor group components of internal modes should have a stronger dependence on pressure (and temperature) variation which was confirmed, too [109].

In addition, intensity changes under increasing pressure have been observed. For example, the most intense Raman line at STP conditions is the  $a_g$  component of  $\nu_2$  ( $\sim 220\text{ cm}^{-1}$ ), but at about 2 GPa the intensity decreases in favor of the  $a_g$  component of  $\nu_1$  ( $\sim 475\text{ cm}^{-1}$ ) which on further compression gains more intensity (about a factor of 2 at 5 GPa) [120]. This behavior was explained by the anisotropy of the crystal's compressibility [139] and differences in the components of the Raman tensor of the two modes [87] with respect to the crystal axes [109].

The pressure dependence of wavenumbers has been investigated theoretically by LD methods on the basis of a Buckingham 6-exp potential. In the studies of Pawley and Mika [140] and Dows [111] the molecules were treated as rigid bodies in order to obtain the external modes as a function of pressure. Kurittu also studied the external and internal modes [141] using his deformable molecule model [116]. The force constants of the intramolecular potential (modified UBFF) were obtained by fitting to the experimental wavenumbers. The results of these studies are in qualitative agreement with the experimental findings.

### 3.2.1.9

#### Crystals of $\beta$ -S<sub>8</sub>

For monoclinic  $\beta$ -S<sub>8</sub> Raman, infrared as well as neutron scattering data have been reported. Besides more qualitative studies [94,121,142–145], Gautier and Debeau had published a detailed analysis of the Raman spectrum of  $\beta$ -S<sub>8</sub> at different temperatures [146]. At 373 K the spectrum of the internal vibrations above  $100\text{ cm}^{-1}$  is qualitatively similar to that of orthorhombic S<sub>8</sub> at and above 298 K (Fig. 18, top) in accordance with previous Raman and IR studies [94]. The region of the torsional and external modes, however, is characterized by one broad band with more or less distinct peaks ( $\sim 34, 42, 82\text{ cm}^{-1}$ ) and a few shoulders, typical for a disordered structure (Fig. 19, top). At the order-disorder transition at 198 K remarkable changes occurred in both spectral regions, and at low temperature (40 K) some of the internal modes split into doublets while in the low frequency range a rich pattern of well resolved lines appeared. Since  $\beta$ -S<sub>8</sub> contains 6 molecules per primitive cell (factor group C<sub>2</sub>), the prominent totally symmetric  $\nu_2$  vibration, for example, showed four Raman components. Gautier and Debeau proposed an explanation of the spectral features on the basis of molecules on general and pseudo-centric positions in the unit cell of  $\beta$ -S<sub>8</sub>. However, a partial accidental degeneracy of modes has to be taken into account. Since the authors could not obtain oriented single crystals of  $\beta$ -S<sub>8</sub>, no analysis of the spectra by means of different polarization geometries could be performed [146].

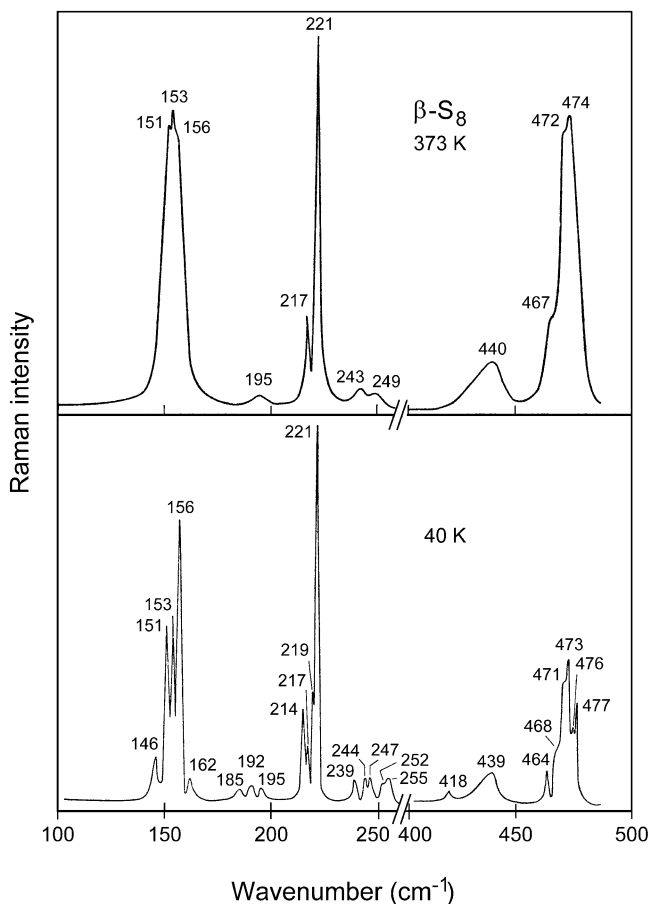


**Fig. 18** Raman spectra of the stretching and bending vibrations of  $\beta$ -S<sub>8</sub> at two different temperatures corresponding to the twofold disorder of one-third of the molecules (373 K) and to the ordered structure (40 K), after [146]. Spectral resolution was 0.75 cm<sup>-1</sup>

### 3.2.1.10

#### Crystals of $\beta$ -S<sub>8</sub>

To the best of our knowledge, no vibrational spectra of this allotrope have been reported.

### 3.2.2

#### S<sub>6</sub>

The chair-like S<sub>6</sub> molecule is of D<sub>3d</sub> symmetry [147] and due to the center of inversion in this point group the rule of mutual exclusion applies. Therefore,

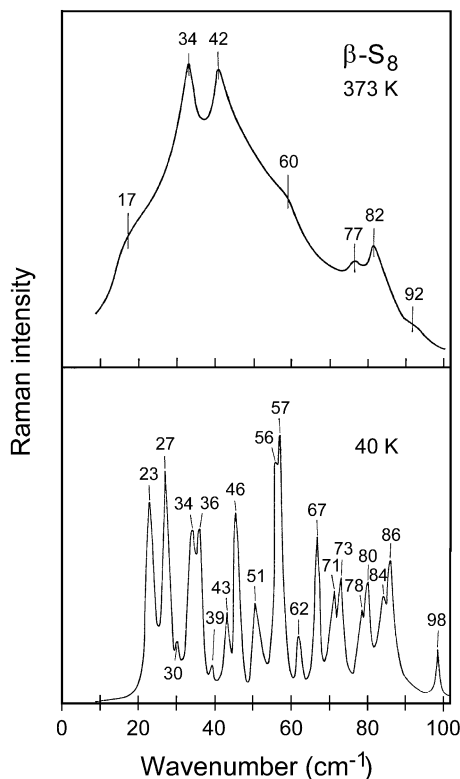


**Fig. 19** Raman spectra of the torsional and external vibrations of  $\beta$ - $S_8$  at two different temperatures showing the dramatic change due to the order-disorder transition, after [146]. Spectral resolution was  $0.75 \text{ cm}^{-1}$

of the 12 intramolecular vibrational degrees of freedom only 5 are infrared active and 6 are Raman active. However, twofold degeneracies reduce the number of observable fundamental modes to 3 in the IR spectrum ( $1A_{2u}$  and  $2E_u$ ) and 4 in the Raman spectrum ( $2A_{1g}$  and  $2E_g$ ); a mode of  $A_{1u}$  symmetry is inactive. In addition, several combination modes have been observed as well as lattice modes for solid  $S_6$ . While the librational lattice modes are Raman active ( $a_g, e_g$ ), the translational modes ( $a_u, e_u$ ) are acoustic phonons and, therefore, not observable in the IR spectrum. Since the primitive cell of rhombohedral  $S_6$  contains only one molecule the intramolecular modes have no factor group splitting in the crystal spectra. The reduction of symmetry ( $D_{3d} \rightarrow C_{3i}$ ) causes the  $A_{1u}$  mode to gain IR activity in the crystal (symmetry class  $a_u$ ).

While the Raman spectrum of  $S_6$  has been investigated many times and at different conditions, the infrared spectrum is less well known and only two reports can be found in the literature [148, 149]. In Table 6 the observed signals are listed together with their assignments, and Fig. 20 shows the very

**Table 6** Infrared and Raman spectra of  $S_6$  in the solid state and in  $CS_2$  solution at 20 °C with assignments according to [148, 149, 151]. Wavenumbers in  $cm^{-1}$ ; relative intensities: very strong-strong-medium-weak-very weak

Infrared, solid	Infrared, solution	Raman, solid	Raman, solution	Symmetry class		Assignment <sup>a</sup>
				Molecule	Crystal	
-	-	79 s		$E_g$	$e_g$	Libration <sup>b</sup>
-	-	106 w <sup>c</sup>		$A_{2g}$	$a_g$	Libration <sup>b</sup>
180 s				$E_u$	$e_u$	Torsion
		202 s	204 w	$E_g$	$e_g$	Bending
		262 s	266 w	$A_{1g}$	$a_g$	Bending
313 s	312 m			$A_{2u}$	$a_u$	Bending
(390 vw) <sup>d</sup>				$A_{1u}$ or $CS_2$	$a_u$ or $CS_2$	(Stretching)
		448 s	451 w	$E_g$	$e_g$	Stretching
463 s	462 s			$E_u$	$e_u$	Stretching
		471 vs	476 m	$A_{1g}$	$a_g$	Stretching
520 w	515 vw					313+202
593 m	590 w					390+202
607 w						463+202
764 w						448+313
840 m	852 m					448+390

<sup>a</sup> Bending and torsion modes are heavily mixed

<sup>b</sup> Assignment of the symmetry class based on the observed pressure dependence of Raman intensities has been performed on group theoretical considerations with respect to the molecular geometry [150]

<sup>c</sup> Observed at -90 °C [151]

<sup>d</sup> Observed on the wing of the  $CS_2$  bending mode. Occurs in violation of the selection rules of the point group  $D_{3d}$  but is IR active under the  $C_{3i}$  factor group of the crystal. Could also be a combination vibration or caused by the  $CS_2$  impurity which was present in the sample (see text)

simple low-temperature Raman spectrum of  $S_6$ . Systematic studies on the temperature dependence of the Raman spectrum have been published [150]. However, the assignment of the very weak IR band at  $390\text{ cm}^{-1}$  to the inactive  $A_{1u}$  mode is still somewhat uncertain (see below).

Wong [152] predicted the wavenumbers of the harmonic fundamental modes of isolated  $S_6$  molecules by ab initio calculations at the CIS/6-311+G(2df) level as follows: 478, 460, 440, 354, 324, 263, 203,  $163\text{ cm}^{-1}$ . While the wavenumbers of all directly observable modes (Table 6) agree with these calculated numbers within  $17\text{ cm}^{-1}$ , the inactive  $A_{1u}$  mode assigned at  $390\text{ cm}^{-1}$  [148] disagrees by  $36\text{ cm}^{-1}$ , indicating an erroneous assignment. This mode has been claimed to be observable as a weak IR band on the high frequency side of the wing of the  $CS_2$  bending fundamental (which is usually located at the same wavenumber of  $390\text{ cm}^{-1}$  [153]).  $CS_2$  was present in the sample which was prepared by spraying a  $CS_2$ -solution of  $S_6$  on a CsBr window. It is quite possible that both IR absorptions observed near  $390\text{ cm}^{-1}$

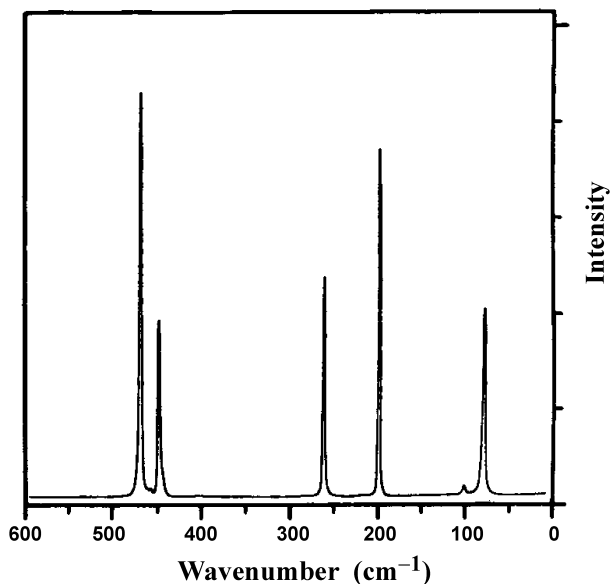


**Fig. 20** Raman spectrum of solid  $S_6$  at  $-90\text{ }^\circ\text{C}$ . The lines at  $84$  and  $106\text{ cm}^{-1}$  represent lattice modes [151]

originate from the  $CS_2$  bending mode as has been observed in the case of  $S_{12}\cdot CS_2$  [79]. Two combination vibrations observed in the infrared spectra of  $S_6$  have been assigned using the  $390\text{ cm}^{-1}$  absorption as a fundamental mode [148] (see Table 6). However, if this absorption were due to the combination vibration  $180+202\text{ cm}^{-1}$  ( $e_u+e_g$ ) or, most likely, due to  $CS_2$  the assignments of two other combination vibrations in Table 6 would change accordingly. Thus, it is obvious that the infrared spectrum of  $S_6$  needs to be reinvestigated.

Force constants of  $S_6$  have been calculated from the data in Table 2 using the general valence force field (GVFF) [148, 149] as well as the Urey-Bradley force field [80] (UBFF) although there is insufficient data to evaluate all the interaction constants since no isotopomers of  $S_6$  have been measured by vibrational spectroscopy. The stretching and bond interaction force constants were reported as  $f_r = 2.24$  and  $f_{rr} = 0.53\text{ N cm}^{-1}$ , respectively [149]. However, because of the uncertainty regarding the  $A_{1u}$  mode of  $S_6$  the published force constants [80, 148, 149] may be unreliable.

### 3.2.3

#### $S_7$

The free  $S_7$  molecule is of  $C_s$  symmetry but in its various solid allotropes it occupies sites of  $C_1$  symmetry [154]. In any case, in these point groups all fundamental modes are infrared and Raman active and no degeneracies occur. Four allotropes of  $S_7$  ( $\alpha$ ,  $\beta$ ,  $\gamma$ ,  $\delta$ ) have been identified by Raman spec-

**Table 7** Raman and infrared spectra of cycloheptasulfur (wavenumbers in  $\text{cm}^{-1}$ , Raman intensities in brackets, abbreviations: b broad, sh shoulder, v very, s strong, m medium, w weak). Raman lines below  $100 \text{ cm}^{-1}$  are lattice vibrations [81]

Raman				IR			Assignment
$\alpha$ -S <sub>7</sub>	$\beta$ -S <sub>7</sub>	$\gamma$ -S <sub>7</sub>	$\delta$ -S <sub>7</sub>	in CS <sub>2</sub>	solid ( $\alpha$ )	in CS <sub>2</sub>	
530(4)	528(6)	523(4)	527(3)	-	526sh	-	A''
518(44)	518(42)	510(24,b)	518(21)	520m	513 vs	518 vs	A'
514(21,sh)	511(25,sh)	-	510(8,sh)	515sh	-	-	360+155
481(87)	480(88)	481(58)	480(44)	485 s	480 s	482 m	A'
459(13)	459(13)	459(6)	460(6)	462 w	461 m	463 s	A''
420(1, b)	420(1, b)	420(1, b)	419(2, b)	-	-	-	239+185
400(85)	400(87)	400(48)	400(100)	402 m-s	400 vs	obscured by CS <sub>2</sub>	A'
-	395(28,sh)	-	396(30,sh)	-	-	-	A''
-	362(45)	364(64)	363(19)	362 s	-	-	A'
355(52)	358(37)	-	358(15)	-	357 vw	-	242+49
-	-	292(6)	-	-	-	-	
285(13)	285(17)	285(8)	285(5)	289 w	282sh	288 vw	A''
270(12)	270(14)	274(16)	270(9)	274 w	270 vs	270 s	A'
241(sh)	-	242(82)	-	-	-	-	A'+A''
239(59)	239(71)	237(20, sh)	239(53)	238 vs	235 s	236 s	A'+A''
-	-	199(4)	201(1)	-	194 m	195 m	A'
185(24)	185(35)	-	185(26)	174 m	-	-	A''
180(22)	182(30,sh)	178(47)	-	-	180 m <sup>a</sup>	-	A''
-	-	159(11)	-	-	-	-	59+62
157(45)	155(48)	151(62)	155(25)	153 s <sup>a</sup>	-	-	A'
150(8)	-	-	150(5)	-	-	-	79+79
145(13)	146(16)	143(17,sh)	147(5)	-	146 m <sup>a</sup>	-	A''
95(12)	93(22)	85(40)	93(18)	-	-	-	
79(100)	80(100)	79(55)	80(80)	-	-	-	
-	75(39,sh)	71(19)	75(28)	-	-	-	
-	68(20)	62(80)	68(10)	-	-	-	
57(81)	60(93)	59(81)	60(29)	-	-	-	
52(81)	55(70)	54(79)	56(39)	-	-	-	
-	47(32)	49(100)	50(14)	-	-	-	
41(12)	39(38)	39(12)	40(13)	-	-	-	
33(10)	33(13)	-	33(7)	-	-	-	
-	19(25)	-	20(13)	-	-	-	

<sup>a</sup> After [155]

troscopy, but their spectra differ only slightly in wavenumbers and relative intensities [81]. Since solid S<sub>7</sub> is unstable at 20 °C, spectra are difficult to record unless the sample is cooled to -100 °C, for instance. However, in CS<sub>2</sub> solution S<sub>7</sub> is stable at room temperature in the dark. In Table 7 the Raman and infrared spectra of S<sub>7</sub> solutions and of the various solid allotropes are given as far as known [81, 155]. Only the crystal structures of  $\gamma$ -S<sub>7</sub> and  $\delta$ -S<sub>7</sub> have been determined [154].

As an example, the Raman spectrum of  $\alpha$ -S<sub>7</sub> is shown in Fig. 21.

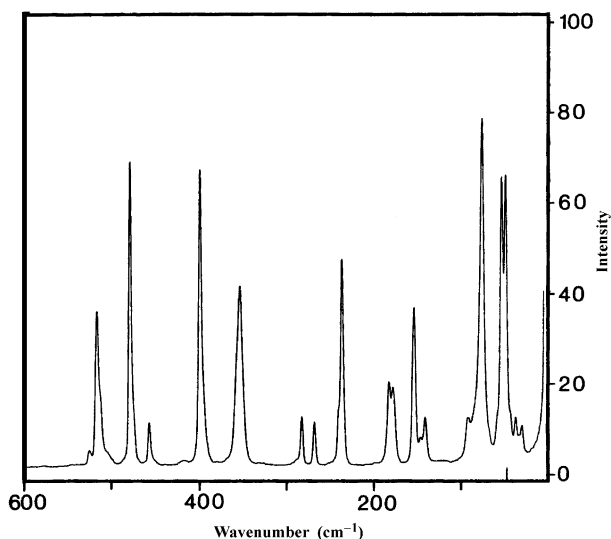


**Fig. 21** Raman spectrum of  $\alpha$ -S<sub>7</sub> at  $-100$  °C [81]

### 3.2.4

#### S<sub>9</sub>

Raman spectra of solid S<sub>9</sub> have revealed that this compound crystallizes as two allotropes, termed  $\alpha$ -S<sub>9</sub> and  $\beta$ -S<sub>9</sub>; see Fig. 22 [156, 157]. These allotropes were obtained by recrystallization from different solvents or at different temperature and concentration conditions but often mixtures of the two forms were observed. No detailed assignment of the recorded Raman lines has been published so far (see Table 8) and consequently no force constant calculation for S<sub>9</sub> is available. The crystal and molecular structures of  $\alpha$ -S<sub>9</sub> were determined by X-ray diffraction on single crystals [157]. The molecular symmetry is C<sub>2</sub> but the site symmetry is C<sub>1</sub>. Therefore, no degeneracies are expected. The nine SS stretching modes of S<sub>9</sub> give rise to 7 Raman lines in the 414–485 cm<sup>-1</sup> region. The symmetrical SSS bending mode is observed as a very strong line at 181/188 cm<sup>-1</sup>. In sulfur homocycles the wavenumber of this mode is indicative of the ring size [156]. The similarity of the spectra of  $\alpha$ - and  $\beta$ -S<sub>9</sub> support a similar molecular conformation for the  $\beta$ -allotrope as was found in the  $\alpha$ -form. On the other hand, the Raman spectra of S<sub>9</sub> are different enough from those of all other sulfur homocycles that an unequivocal identification is possible.

### 3.2.5

#### S<sub>10</sub> and S<sub>6</sub>·S<sub>10</sub>

In the monoclinic crystals of *cyclo*-decasulfur the molecules occupy sites of C<sub>2</sub> symmetry although the molecular symmetry is close to D<sub>2</sub> [151, 158]. In-

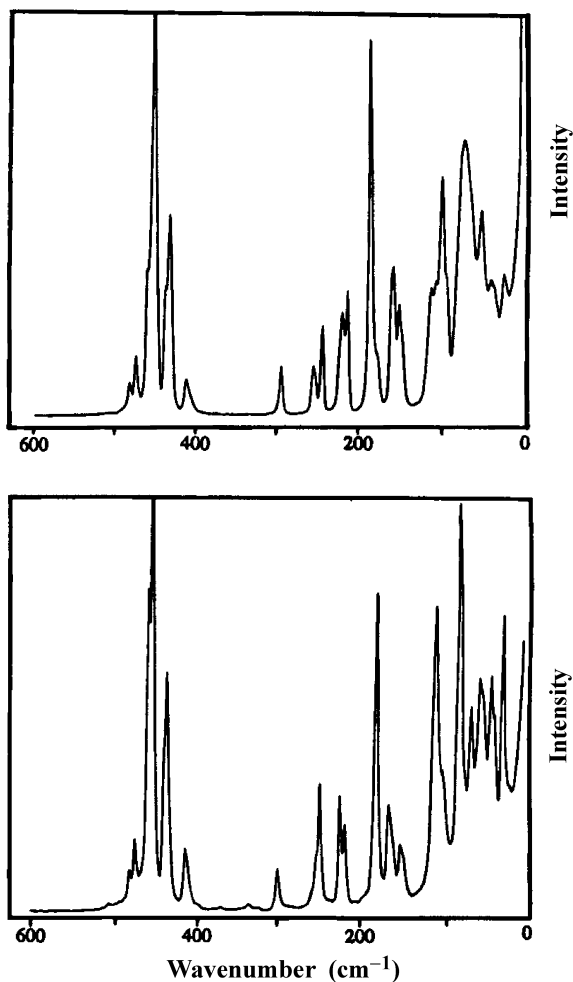


**Fig. 22** Raman spectra of  $\alpha$ -S<sub>9</sub> (top) and of  $\beta$ -S<sub>9</sub> (bottom) at  $-100$  °C [157]

frared and Raman spectra of solid S<sub>10</sub> have been recorded but no assignment of the spectra has been published [151, 159]. The SS stretching modes are found in the region 400–500 cm<sup>-1</sup> and all other modes occur below 260 cm<sup>-1</sup>. Interestingly, S<sub>10</sub> is a constituent of another allotrope of composition S<sub>6</sub>·S<sub>10</sub> in which layers of S<sub>6</sub> and S<sub>10</sub> molecules alternate with each other [151]. In these crystals the site symmetries are C<sub>i</sub> for S<sub>6</sub> and C<sub>2</sub> for S<sub>10</sub>. The vibrational spectra of S<sub>6</sub>·S<sub>10</sub> crystals are practically a superimposition of the spectra of the two components. Wavenumbers are given in Table 9.

**Table 8** Wavenumbers of the Raman lines of  $\alpha$ - and  $\beta$ -S<sub>9</sub> at  $-100$  °C ( $\text{cm}^{-1}$ ; relative intensities in parentheses; sh = shoulder) [157]. Columns 1+2: stretching modes, columns 3+4: bending modes, columns 5+6: bending, torsion and lattices modes

1	2	3	4	5	6
$\alpha$ -S <sub>9</sub>	$\beta$ -S <sub>9</sub>	$\alpha$ -S <sub>9</sub>	$\beta$ -S <sub>9</sub>	$\alpha$ -S <sub>9</sub>	$\beta$ -S <sub>9</sub>
485 (10)	483 (11)	297 (13)	300 (12)	117 (31)	114 (76)
477 (16)	476 (20)	256 (12)	251 sh	111 sh	
463 sh	460 (93)	245 (23)	248 (36)	104 (58)	104 sh
454 (100)	454 (100)	222 (26)	224 (32)	100 sh	84 (100)
442 sh	440 sh	215 (31)	218 (23)	78 (67)	71 (37)
436 (49)	437 (68)	188 (90)	181 (88)	57 (50)	61 (46)
416 (11)	414 (18)	181 sh		46 (33)	59 sh
		161 (37)	167 (27)	43 sh	47 (38)
		155 (28)	153 (15)	41 sh	44 sh
		151 sh		27 (35)	33 (53)

**Table 9** Raman spectra ( $-90$  °C;  $500$ – $100$   $\text{cm}^{-1}$ ) and infrared spectra (CsI disc;  $25$  °C) of S<sub>10</sub> and S<sub>6</sub>S<sub>10</sub>. Wavenumbers in  $\text{cm}^{-1}$ , relative Raman intensities in parentheses [151]

S <sub>10</sub> ; Raman	S <sub>6</sub> S <sub>10</sub> ; Raman	S <sub>10</sub> ; IR	S <sub>6</sub> S <sub>10</sub> ; IR
495(6)			
487(16)	489(4)	482 w	483 w
481 sh	479(69)		
469(36)	466(38)	456 vw	461 vs
466 sh	461 sh		
	455 sh		
	451(21)		
425(5)	428(19)		
403(2)	408(4)		
			387 vw <sup>a</sup>
			310 m
	272(31)		
255(5)	265(3)		264 vw
246 sh	249(6)		
243(24)	240(15)	244 sh	242 vs
		239 vs	240 sh
231(3)	228(3)	226 sh	231 sh
	225(1)	220 s	221 m
	207(17)		211 s
	201 (19)	204 m-s	207 sh
178(31)	172(29)		
155(2)	145(3)		
131(20)	136(10)		
100(19)	103(26)		

<sup>a</sup> May be caused by traces of CS<sub>2</sub>

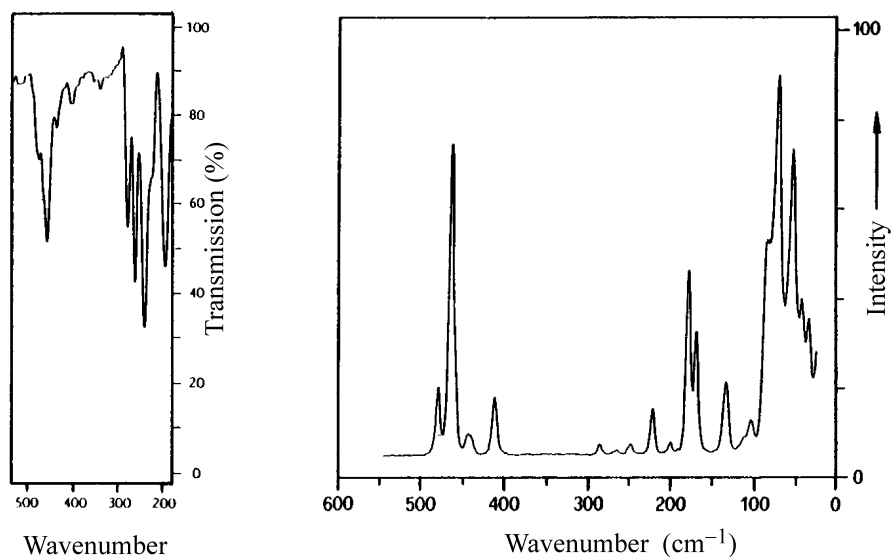


**Fig. 23** Infrared and Raman spectra of solid  $S_{11}$  at  $-100\text{ }^{\circ}\text{C}$  [162]

### 3.2.6

#### $S_{11}$

*Cyclo*-Undecasulfur  $S_{11}$  was first prepared in 1982 and vibrational spectra served to identify this orthorhombic allotrope as a new phase of elemental sulfur [160]. Later, the molecular and crystal structures were determined by X-ray diffraction [161, 162]. The  $S_{11}$  molecules are of  $C_2$  symmetry but occupy sites of  $C_1$  symmetry. The vibrational spectra show signals for the SS stretching modes between  $410$  and  $480\text{ cm}^{-1}$  and the bending, torsion and lattice vibrations below  $290\text{ cm}^{-1}$  [160, 162]. For a detailed list of wavenumbers, see [160]. The vibrational spectra of solid  $S_{11}$  are shown in Fig. 23.

### 3.2.7

#### $S_{12}$ and $S_{12}\cdot\text{CS}_2$

The molecule  $S_{12}$ , like  $S_6$ , is of  $D_{3d}$  symmetry but in the solid state it occupies sites of the much lower  $C_{2h}$  symmetry [163]. Due to the low solubility and the thermal decomposition on melting only solid state vibrational spectra have been recorded [2,79]. However, from carbon disulfide the compound  $S_{12}\cdot\text{CS}_2$  crystallizes in which the  $S_{12}$  molecules occupy sites of the high  $S_6$  symmetry which is close to  $D_{3d}$  [163]. The spectroscopic investigation of this adduct has resulted in a revision [79] of the earlier vibrational assignment [2] and therefore also of the earlier force constants calculation [164]. In Fig. 24 the low-temperature Raman spectra of  $S_{12}$  and  $S_{12}\cdot\text{CS}_2$  are shown.

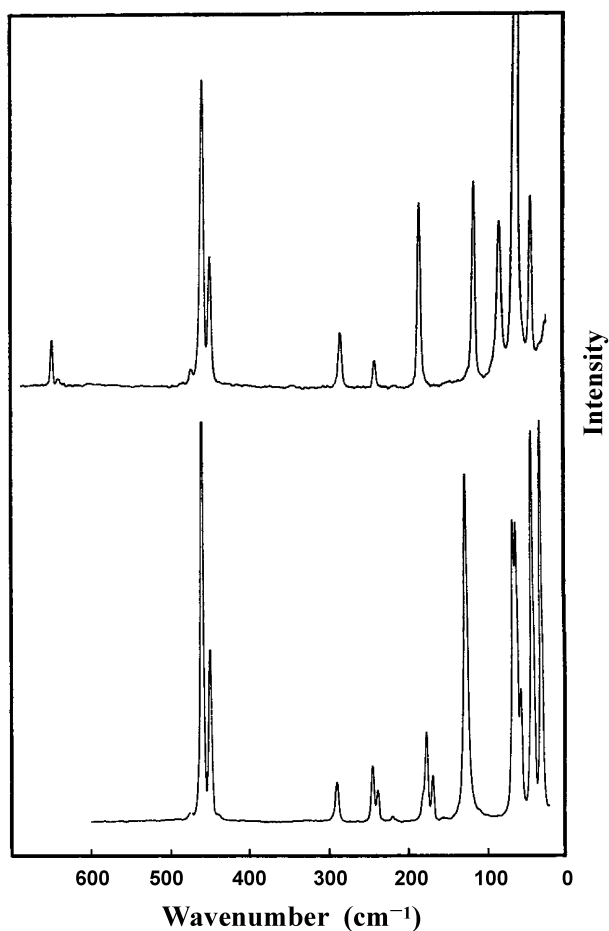


**Fig. 24** Raman spectra of solid S<sub>12</sub> (*bottom*) and of S<sub>12</sub>·CS<sub>2</sub> (*top*) at -80 °C. The weak line at 651 cm<sup>-1</sup> (with isotopic satellite) originates from CS<sub>2</sub> [79]

The full vibrational spectra and the assignment of the observed infrared and Raman signals are presented in Table 10.

The spectra of S<sub>12</sub> and S<sub>12</sub>·CS<sub>2</sub> clearly reflect the differing site symmetries of the S<sub>12</sub> molecule: The two E<sub>g</sub> vibrations at 188 and 245 cm<sup>-1</sup>, degenerate in S<sub>12</sub>·CS<sub>2</sub>, split into their components in pure S<sub>12</sub> with its non-degenerate site symmetry of C<sub>2h</sub>. The valence force constants calculated for S<sub>12</sub> reproduce the observed wavenumbers within ±14 cm<sup>-1</sup> [79]. The two most interesting constants are  $f_r = 2.41$  and  $f_{rr} = 0.60$  N cm<sup>-1</sup>.

**Table 10** Vibrational spectra of  $S_{12}$  and  $S_{12}\cdot CS_2$  (infrared spectra at 20 °C, Raman spectra at –80 °C) [79]. Assignment of the  $S_{12}$  vibrations on the basis of  $D_{3d}$  symmetry. For intensity labels, see Table 7

$S_{12}$ , IR	$S_{12}$ , Raman	$S_{12}\cdot CS_2$ , IR	$S_{12}\cdot CS_2$ , Raman	Assignment
870 w				449+425
830 w				425+410 <sup>a</sup>
705 vw				460+250
		651		$CS_2$
	475 vw		476 vw	$E_g$
465 m				$A_{2u}$ and $E_u$
	460 vs		461 vs	$A_{1g}$
	449 s		451 m-s	$E_g$
425 vw				$E_u$
		389		$CS_2$
	289 m		287 m	$A_{1g}$
265 vs		270 vs		$A_{2u}$
250 vs		248 vs		$E_u$
	245/238 w-m		245 w	$E_g$
	177/179 m-s		188 s-vs	$E_g$
165 vs				$E_u$
	127 vs		117 s-vs	$A_{1g}$
72 m				$A_{2u}$
	67 s		85 s	lattice
62 m				$E_u$
	63 vs		64 vvs	lattice
	58 m-s			$E_g$ (?)
	43 vs			lattice
	31 vs			lattice

<sup>a</sup> Inactive  $A_{2g}$  mode. For the three combination bands there are also other assignments possible [164]

### 3.2.8

#### $S_{13}$

*Cyclo*-tridecasulfur  $S_{13}$  was first prepared in 1982 and vibrational spectra served to identify this monoclinic allotrope as a new phase of elemental sulfur [160]. Later, the molecular and crystal structures were determined by X-ray diffraction [162]. The  $S_{13}$  molecules are of  $C_2$  symmetry but occupy sites of  $C_1$  symmetry. The vibrational spectra show signals for the SS stretching modes between 385 and 500  $cm^{-1}$  and the bending, torsion and lattice vibrations below 290  $cm^{-1}$  [160, 162]. For a detailed list of wavenumbers, see [160]. The vibrational spectra of solid  $S_{13}$  are shown in Fig. 25.

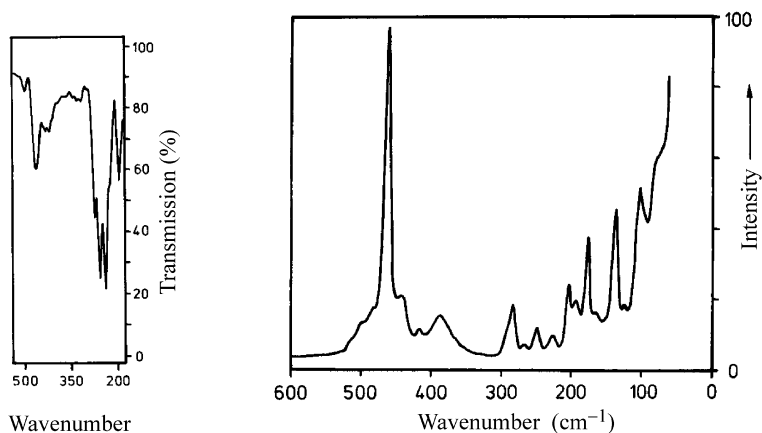


**Fig. 25** Infrared and Raman spectrum of solid  $S_{13}$  at  $-100\text{ }^{\circ}\text{C}$  [162]

**Table 11** Raman lines of crystalline  $S_{14}$  at  $-100\text{ }^{\circ}\text{C}$ . Wavenumbers in  $\text{cm}^{-1}$ ; relative intensities in parentheses (sh: shoulder) [165]

Stretching modes	Bending modes	Bending, torsion, and lattice modes
483 (7)	270 (7)	128 (48)
474 (5)	252 (2)	122 (7)
468 (25)	243 (5)	90 (23)
462 sh	234 (23)	79 (14)
460 (59)	212 (2)	69 (59)
453 sh	198 (18)	61 (41)
447 (11)	189 (7)	57 (36)
444 (11)	177 (11)	47 (100)
	163 (25)	34 (23)
	153 (16)	

### 3.2.9

#### $S_{14}$

The intense yellow rodlike crystals of  $S_{14}$  contain molecules of approximate  $C_s$  symmetry on sites of  $C_1$  symmetry [165]. Their Raman spectra recorded at  $-100\text{ }^{\circ}\text{C}$  exhibit the expected pattern: Stretching modes give rise to lines between  $440$  and  $485\text{ cm}^{-1}$ . This rather narrow region reflects the very narrow bond distance distribution in  $S_{14}$  molecules ( $204.7$ – $206.1\text{ pm}$ ). As usual, the bending, torsional and lattice modes show up below  $300\text{ cm}^{-1}$  (see Table 11 and Fig. 26).

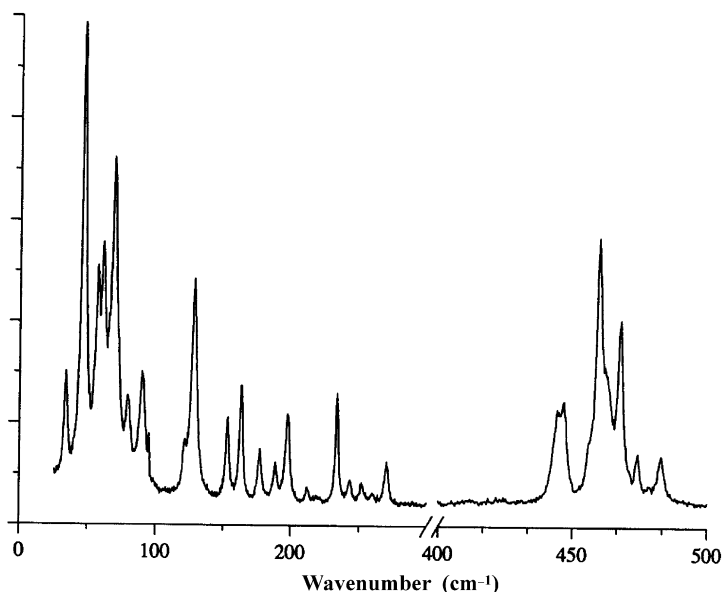


**Fig. 26** Raman spectrum of solid  $S_{14}$  at  $-100\text{ }^{\circ}\text{C}$  [166]

### 3.2.10

#### $S_{15}$ , $S_{18}$ , $S_{20}$ , and Other Large Rings ( $S_x$ )

Homocyclic  $S_{15}$  has been obtained as a lemon-yellow powder which was mainly characterized by its Raman spectrum since single-crystals could not be grown [167]. Once again, this spectrum turned out to be highly characteristic and different from those of other sulfur allotropes. The observation that the SS stretching modes give rise to Raman lines in the region  $400\text{--}495\text{ cm}^{-1}$  indicates that the bond lengths in  $S_{15}$  are in the range  $203\text{--}209\text{ pm}$  since there is a relationship between these quantities [168]. Density functional calculations on  $S_{15}$  resulted in a conformation of  $C_2$  symmetry with bond lengths in the range  $205.3\text{--}206.6\text{ pm}$  [169]. No Raman lines were observed between  $400$  and  $300\text{ cm}^{-1}$ .

The sulfur allotropes  $S_{16}$ ,  $S_{17}$ ,  $S_{19}$ , and  $S_{>20}$  have not yet been prepared as pure materials and therefore no vibrational spectra are known. However, a mixture of large sulfur rings,  $S_x$  with  $x = 12\text{--}35$ , has been isolated from quenched liquid sulfur [145]. The low temperature Raman spectrum of this mixture is very simple: It shows two rather broad lines in the SS stretching region, a very strong line at  $460$  and a weak line at  $416\text{ cm}^{-1}$  as well as a quasi-continuum of lines below  $290\text{ cm}^{-1}$  representing the bending and torsion modes. Obviously, the continuum is the result of many closely neighboring lines of the various rings which probably exist in several differing conformations. This analysis is in agreement with the observation that all sulfur rings

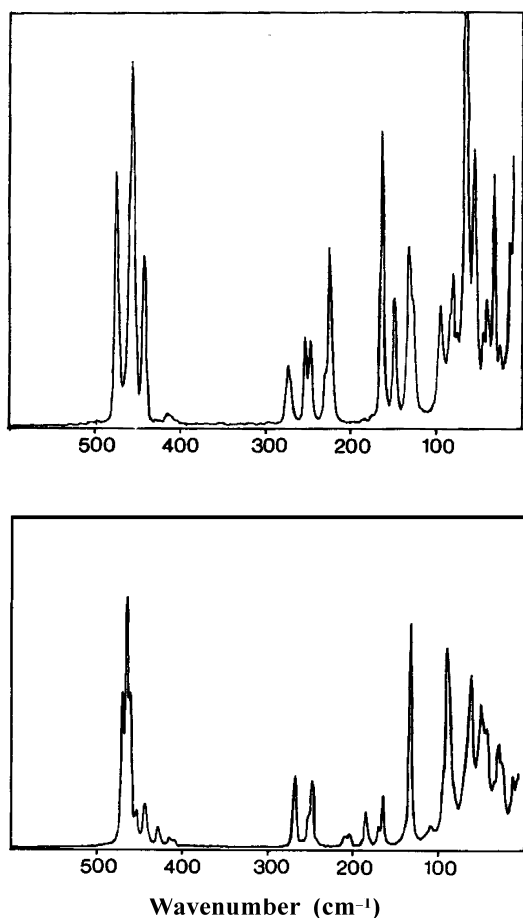


**Fig. 27** Raman spectra of *endo*-S<sub>18</sub> (top) and S<sub>20</sub> (bottom) at  $-100\text{ }^{\circ}\text{C}$  [145]

S<sub>n</sub> except S<sub>6</sub> and S<sub>7</sub> have their SS stretching modes in the  $400\text{--}500\text{ cm}^{-1}$  region and the bending modes below  $300\text{ cm}^{-1}$ .

From the S<sub>x</sub> ring mixture pure *endo*-S<sub>18</sub> and S<sub>20</sub> were prepared and their infrared and Raman spectra measured [145]. The geometrical structures of both molecules belong to non-degenerate point groups. Therefore, 18 respectively 20 SS stretching vibrations are to be expected. However, the Raman spectra of both solids exhibit only 4 and 8 lines, respectively, in the  $400\text{--}500\text{ cm}^{-1}$  region and none between 400 and  $300\text{ cm}^{-1}$ . Evidently, incidental degeneracies play a major role. Both the IR and the Raman spectrum are highly characteristic in the region of bending and torsion vibrations  $< 300\text{ cm}^{-1}$  [145]. The Raman spectra of *endo*-S<sub>18</sub> and S<sub>20</sub> are shown in Fig. 27. Vibrational spectra of *exo*-S<sub>18</sub> have not been published yet.

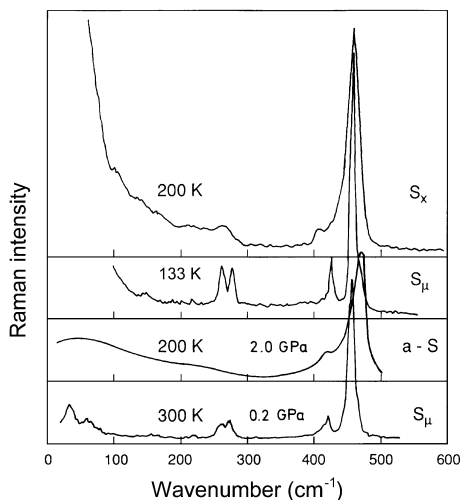


**Fig. 28** Raman spectra of polymeric sulfur ( $S_{\mu}$ ) prepared by various methods [109,173], of large disordered rings ( $S_x$ ) [182], and of photo-induced amorphous sulfur (a-S) [119], respectively. The spectrum of a-S has been smoothed for clarity. The position of the stretching vibration of a-S is pressure-shifted to higher wavenumbers. The very weak signals in the spectra of  $S_{\mu}$  at ca. 150 and 220  $\text{cm}^{-1}$  are probably caused by the presence of  $S_8$ . In addition, the weak shoulder at ca. 470  $\text{cm}^{-1}$  observed in spectra of  $S_{\mu}$  may originate from  $S_8$ , too

### 3.3

#### Polymeric Sulfur

The Raman spectrum of polymeric sulfur is relatively simple compared to other sulfur allotropes. It consists of one strong and one weak band in the stretching region (at  $\sim 460$  and  $\sim 425$   $\text{cm}^{-1}$ ) and two weak bands in the bending region (at  $\sim 275$  and  $\sim 260$   $\text{cm}^{-1}$ ); cf. Fig. 28 [170]. In samples of a higher degree of crystallinity additional bands were observed at  $\sim 65$  and  $\sim 25$   $\text{cm}^{-1}$ , respectively. In general, the Raman spectra of polymeric sulfur allotropes, obtained by different techniques of preparation, are rather similar. For example, spectra have been reported for samples quenched from the gas phase [171], from the melt above the polymerization transition [172–174], for commercially available polymeric sulfur like Crystex or “flowers of sulfur” [174–177], for polymerized samples of  $S_7$ , for mixtures of large disordered rings ( $S_x$ , see below) [173], for sulfur samples after temperature-pressure quenching from 555  $^{\circ}\text{C}$  and 3.5 GPa [178], as well as from a high-pressure allotrope (p-S, see below and [1]) upon decompression [109, 119]. In all cases, the spectra show more or less the same number of bands, band profiles and relative intensities as well as lines at almost the same wavenumbers. However, the bandwidths and relative intensities of these spectra differ probably caused by the varying crystalline quality of the samples. In addition, Raman lines of  $S_8$  can sometimes be seen in the spectra of the polymers

due either to the presence of  $\alpha$ -S<sub>8</sub> as an impurity from the preparation or by back-transformation of the polymer into the STP stable form which is initiated by heat, irradiation or nucleophilic catalysts (cf. [1]).

At first sight, the spectral similarity of such different samples may be surprising. Evidently, this observation indicates a close similarity of the molecular structures of the various helical allotropes as has previously been claimed by Tuinstra [179]; see also [1].

Infrared spectral studies of polymeric sulfur are scarce and mainly the overtone region was studied [142, 180]. In the range of the stretching vibrations, two bands at ca. 460 cm<sup>-1</sup> (strong) and ca. 423 cm<sup>-1</sup> (medium) were reported for Crystex after extraction of the soluble ring fraction by CS<sub>2</sub> [180]. The results of the literature are summarized in Table 12.

First attempts to model the vibrational spectrum of polymeric sulfur have been reported by Dultz et al. who assumed a planar zig-zag chain structure [172]. The calculated vibrational DOS was in qualitative agreement with the observed Raman spectrum of fibrous sulfur. However, some details of the spectrum like the relative intensities of the modes as well as the size of the gap between stretching and bending vibrations could not be reproduced exactly by this simplified model [172].

Vibrational wavenumbers and dispersion curves have been calculated by quantum-mechanical methods in an oligomer approach (H<sub>2</sub>S<sub>5</sub> as a model for helical sulfur) [181]. The wavenumbers of the sulfur vibrations, obtained after scaling with empirical type-of-vibration dependent factors, were in fair agreement with those observed in polymeric sulfur. For example, the wavenumbers of the SS stretching modes were overestimated by only 10–20 cm<sup>-1</sup> and those of the bending modes were in good agreement (Table 12). Furthermore, the authors discussed the Raman and IR activities of vibrations for a perfect helical structure of sulfur. Accordingly, four only Raman active modes (2 stretching, 1 bending, 1 torsional) and two Raman *and* IR active modes are to be expected (1 stretching and 1 bending). The calculated intensity distribution, however, differ significantly from the experiment.

Interestingly, the Raman spectra of certain highly disordered solid forms of sulfur such as S<sub>x</sub> and photo-induced amorphous sulfur (a-S) resemble those of polymeric sulfur (Fig. 28). S<sub>x</sub> is a mixture of large rings prepared from liquid sulfur [182]. An average molecular size of  $\langle x \rangle \sim 25$  was determined, while  $x$  extends over a range of about 15–35 at least but probably up to 50. This material was interpreted in terms of large disordered rings (e.g., characterized by the absence of regular motifs). On the other hand, a-S was found as a result of photo-induced ring-opening in  $\alpha$ -S<sub>8</sub> at high pressure [1, 58, 119]. The Raman spectra of these disordered forms of solid sulfur are characterized by broad bands since the whole vibrational DOS gains optical activity due to the loss of translational symmetry [183]. The Raman bands in the range of 400–500 cm<sup>-1</sup> are caused by the stretching vibrations while the almost unstructured spectrum below the cut-off at about 280 cm<sup>-1</sup> comes from the manifold of bending and torsional vibrations as well as from intermolecular vibrations. Qualitatively, the spectra of S<sub>x</sub> and a-S can be obtained by broadening a Raman spectrum of polymeric sulfur (Fig. 28).

**Table 12** Vibrational spectra of polymeric sulfur in the fundamental region reported for samples obtained by various methods (see text). Lines of  $S_8$  are omitted. Wavenumbers in  $\text{cm}^{-1}$ 

Sample <sup>a</sup>	Assignment				Temperature (K)	Ref.
	Stretching	Bending	Torsion	Lattice?		
Raman						
Crystex	456 vs 418 w	273 w			ca. 300	[175]
"Purple sulfur"	466 s 418 w	273 w			ca. 77	[171]
Sulfur XII	457 s 424 m				ca. 300	[178]
Fibrous sulfur	453 418	273			ca. 300	[172]
Polymeric sulfur <sup>b</sup>	473 sh, 460 vs 429 w, 425 sh	282 m 286 w			173±10	[174]
$S_{\omega 1}$	469 sh, 458 s 430 w	268 vw			ca. 100	[176]
$S_{\omega 2}$	468 sh, 458 s 430 sh, 424 w	280 w 268 vw				
Insoluble sulfur <sup>c</sup>	452 s 416 w	270 m (261) w		23	?	[177]
$S_{\mu}^d$	460 s 427 m	275 w 260 (263+257) w	65	25	ca. 300	[109]
Infrared						
Sulfur XII	457 418				ca. 300	[178]
Polymeric sulfur <sup>e</sup>	460 s 423 m				ca. 300 ?	
Theory						
$H_2S_5$ model <sup>f</sup>	480 w (Ra), 471 m (Ra, IR) 436 s (Ra)	278 s (Ra, IR) 267 s (Ra)	52 s (Ra)	-	-	[181]

<sup>a</sup> Nomenclature by the present authors according to the cited literature

<sup>b</sup> Obtained from commercial polymeric sulfur by extraction with  $CS_2$  and drying in a vacuum [174]

<sup>c</sup> Insoluble sulfur obtained by  $CS_2$  extraction of commercial Crystex N; data taken from conventional Raman studies using an Ar laser [177]

<sup>d</sup> Sample obtained from p-S in high-pressure experiments, wavenumbers extrapolated to ambient pressure [58, 109, 119]

<sup>e</sup> Polymeric sulfur obtained from Crystex after extraction with dichloromethane followed by drying in a vacuum [180]

<sup>f</sup> Wavenumbers scaled by optimized factors. Intensities for Raman active modes classified by the present authors on the basis of the calculated values. The intensities of two IR active vibrations were calculated to be equal; (Ra) = Raman active, (IR) = infrared active [181]

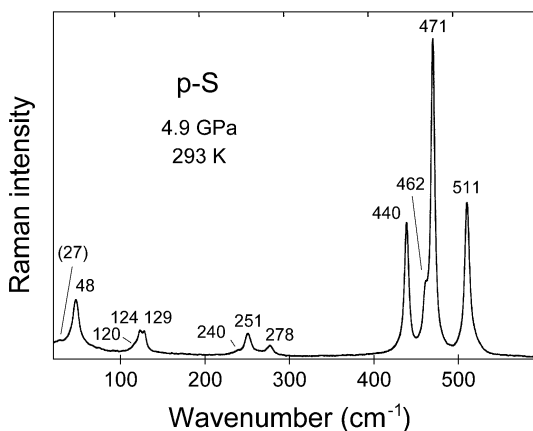


**Fig. 29** Raman spectrum of p-S at high pressure and room temperature [109]. The wavenumbers indicated are given for the actual pressure. No signals of other allotropes have been detected. The line at  $48\text{ cm}^{-1}$  (ca.  $25\text{ cm}^{-1}$  at  $p \sim 0\text{ GPa}$ ) may arise from lattice vibrations, while the other lines resemble the typical pattern of internal vibrations of sulfur molecules

### 3.4

#### High-Pressure Allotropes of Sulfur

Since the vibrational spectra of sulfur allotropes are characteristic for their molecular and crystalline structure, vibrational spectroscopy has become a valuable tool in structural studies besides X-ray diffraction techniques. In particular, Raman spectroscopy on sulfur samples at high pressures is much easier to perform than IR spectroscopical studies due to technical demands (e.g., throughput of the IR beam, spectral range in the far-infrared). On the other hand, application of laser radiation for exciting the Raman spectrum may cause photo-induced structural changes. High-pressure phase transitions and structures of elemental sulfur at high pressures were already discussed in [1].

At least five high-pressure allotropes of sulfur have been observed by Raman spectroscopy up to about 40 GPa the spectra of which differ significantly from those of  $\alpha\text{-S}_8$  at high pressures: photo-induced amorphous sulfur (a-S) [57, 58, 109, 119, 184–186], photo-induced sulfur (p-S) [57, 58, 109, 119, 184, 186–191], rhombohedral  $\text{S}_6$  [58, 109, 137, 184, 186, 188, 191], “high-pressure low-temperature” sulfur (hp-lt-S) [137, 184, 192], and polymeric sulfur ( $\text{S}_\mu$ ) [58, 109, 119, 193]. The Raman spectra of two of these allotropes, a-S and  $\text{S}_\mu$ , were discussed in the preceding section. The Raman spectra of p-S and hp-lt-S have only been reported for samples at high-pressure conditions. The structure of both allotropes are unknown. The Raman spectrum of  $\text{S}_6$  at STP conditions is discussed below.

A Raman spectrum of p-S is shown in Fig. 29. While the Raman lines in the stretching region ( $430\text{--}520\text{ cm}^{-1}$ ) are of high intensity, exceeding those

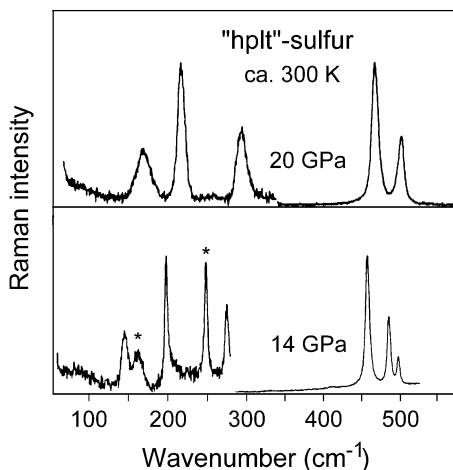


**Fig. 30** Raman spectra of “high-pressure low-temperature” sulfur at two different pressures [184]. The peaks marked by asterisks were reported as originating from another high-pressure allotrope (presumably p-S). The intensities of the spectra at lower wavenumbers (below ca. 300–350  $\text{cm}^{-1}$ ) have been magnified (factor has not been reported)

of  $\alpha\text{-S}_8$  at ambient conditions (!), the low energetic vibrations are relatively weak. The frequency shifts of the modes under variation of pressure have systematically been studied [58, 119, 184, 189, 191]. Unique for sulfur allotropes studied so far, the most intense mode (ca. 476  $\text{cm}^{-1}$  at  $p \rightarrow 0$  GPa) has a negative frequency shift,  $d\omega/dp$ , with increasing pressure. Obviously, a weakening of the bond responsible for this mode appears under pressure. In combination with the large positive shift of the less intense mode at 444  $\text{cm}^{-1}$  (at  $p \rightarrow 0$  GPa) a crossing of the modes occur at about 7 GPa which makes only three lines observable around this pressure. Upon increasing pressure, the 496  $\text{cm}^{-1}$  (at  $p \rightarrow 0$  GPa) line gains relative intensity while the lines at 437 and 444  $\text{cm}^{-1}$  (at  $p \rightarrow 0$  GPa) lose intensity, and the intensity of the 476  $\text{cm}^{-1}$  line remains more or less constant. The intensities of the stretching vibrations with respect to the vibrations at lower wavenumbers resemble the intensity ratios of the different types of vibrations of polymeric sulfur [194]. In addition, the negative slope of the 476  $\text{cm}^{-1}$  line under pressure was interpreted in terms of a chain structure for p-S by analogy with results of high-pressure studies on selenium allotropes [189, 195, 196]. The kinetics of the formation of p-S has been studied by time-dependent Raman spectroscopy, and it was found that the transition from  $\alpha\text{-S}_8$  to p-S is a two-stage process in which the amorphous phase is an intermediate [186].

The phase “hplt-S” appeared in Raman spectra of sulfur at about 12 GPa and above, and this allotrope could be observed up to about 40 GPa [137, 184]. The high-pressure sample was evidently a mixture as the Raman spectra consisted of lines of both  $\text{S}_6$  and p-S. Raman spectra at two different pressures are shown in Fig. 30. Three peaks were observed in the stretching

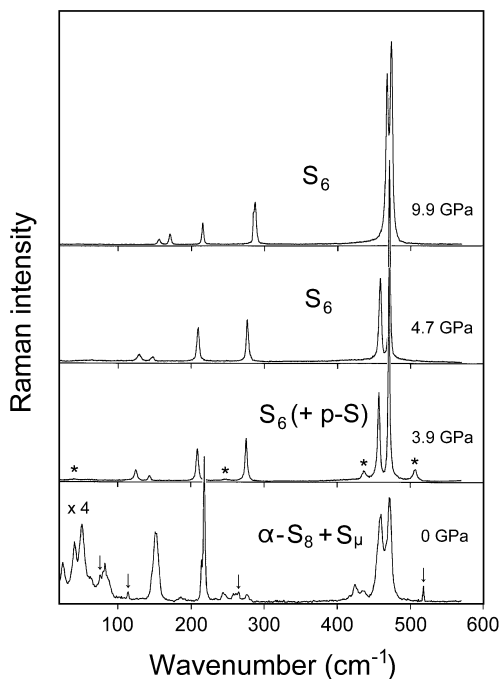


**Fig. 31** Evolution of the Raman spectra of a high-pressure and photo-induced sample of  $S_6$  while decreasing the pressure at ca. 300 K [109]. The spectrum at 3.9 GPa shows the onset of the transformation  $S_6 \rightarrow$  p-S. The asterisks indicate the Raman signals typical for p-S whereas the peaks of two stretching vibrations of p-S coincide with those of  $S_6$  at about  $458\text{ cm}^{-1}$  and  $471\text{ cm}^{-1}$  (not indicated by asterisks). The Raman spectrum of the sample recovered at ambient pressure (0 GPa) is evidently a superposition of the spectra of  $\alpha$ - $S_8$  and polymeric sulfur,  $S_\mu$  (arrows indicate plasma lines of the Ar ion laser at 515 nm, which have been used for calibration). For Raman spectra under increasing pressure, see Fig. 23 in [1] and references cited therein

region ( $497, 485, 458\text{ cm}^{-1}$  at ca. 12 GPa), and three relatively broad and weak bands were recorded at lower wavenumbers ( $273, 196, 142\text{ cm}^{-1}$  at ca. 12 GPa). The pressure dependence of Raman frequencies has been reported [137, 184]. Since the  $485\text{ cm}^{-1}$  mode has a larger frequency shift with increasing pressure than the other stretching modes, the position of this Raman line coincides with that of the  $497\text{ cm}^{-1}$  mode above ca. 17 GPa (ca.  $505\text{ cm}^{-1}$  at 20 GPa). As in the case of a-S, p-S and  $S_6$  the formation of hplt-S is likely to be photo-induced.

Rhombohedral  $S_6$  was found as a high-pressure allotrope of sulfur above 9–10 GPa by several groups [58, 137, 150, 184, 186, 188, 191]. The pressure dependence of frequencies [137, 150, 184] as well as the kinetics of the transition from p-S to  $S_6$  [186] have been investigated systematically by Raman spectroscopy. The pressure dependent frequency shifts of chemically prepared  $S_6$  and of high-pressure  $S_6$  have been found to be identical [137, 150].

In addition, the variation of Raman intensities as a function of pressure has been evaluated [150]. For example, the evolution of Raman spectra of  $S_6$  upon decreasing pressure is shown in Fig. 31 (see also Fig. 23 of Chapter 1 in [1]). The intensities of the bending vibrations as well as of the  $77\text{ cm}^{-1}$  libration, which are strong at STP conditions (Fig. 20), decrease dramatically with increasing pressure in favor of the stretching vibrations (Fig. 31). Furthermore, the intensity ratio of the librations changes under pressure which made possible an assignment of the librations to their symmetry class (cf. Table 6) [150]. Amongst the sulfur allotropes, which had so far been studied under pressure, the two librations in  $S_6$  have very large frequency shifts  $d\omega/dp$  (ca.  $40\text{--}50\text{ cm}^{-1}/\text{GPa}$  at  $0\text{--}1\text{ GPa}$ ) comparable only with the  $26\text{ cm}^{-1}$  mode of polymeric sulfur (ca.  $65\text{ cm}^{-1}/\text{GPa}$ ) [109]. Therefore, the intermolecular potential of rhombohedral  $S_6$  is more anharmonic than that of  $\alpha\text{-S}_8$ , for example. Due to their differing frequency shifts, the Raman lines of the stretching modes are crossing at about 13 GPa and those of the librations overlap at above 20 GPa [137, 184].

### 3.5

#### General Observations

The vibrational spectrum of each sulfur allotrope is characteristic due to its molecular (and crystal) structure and, therefore, can serve as a fingerprint in detecting single members  $S_n$  in mixtures of sulfur homocycles, for example. On the other hand, the fundamental vibrations of solid allotropes are distributed in a typical pattern over the spectral range below  $530\text{ cm}^{-1}$ . The SS stretching vibrations of most of the cyclic molecules  $S_n$  ( $n > 5$ ) were observed in the range  $410\text{--}480\text{ cm}^{-1}$ . The wavenumbers of the SSS bending modes cover the range below ca.  $300\text{ cm}^{-1}$  down to around  $100\text{ cm}^{-1}$ . While in almost all  $S_n$  molecules ( $n > 5$ ) a distinct gap between the stretching and bending vibrations exists, the ranges of bending and torsional modes are close together if not overlapping (ca.  $50\text{--}150\text{ cm}^{-1}$ ). Moreover, in many cases the lattice modes follow directly the torsional modes at lower wavenumbers ( $<100\text{ cm}^{-1}$ ), and there is some mixing of the external modes with the torsions as was theoretically shown for  $\alpha\text{-S}_8$ . Unfortunately, the vibrational spectra of only a few homocycles ( $S_6$ ,  $S_7$ ,  $S_8$ ,  $S_{12}$ ) have been thoroughly analyzed by force constant calculations which allowed the assignment of the observed wavenumbers to the normal modes of the molecules. Therefore, the vibrational lines in the bending and torsional region as well as in the lattice region of the less studied allotropes cannot unambiguously be distinguished.

Generally, the stretching vibrations mainly depend on the bond distances while the bending and torsional vibrations are basically determined by the size and symmetry of the ring [80]. For example, the wavenumbers of the stretching vibrations in low symmetrical rings ( $S_7$ :  $C_8$ ,  $S_{13}$ :  $C_2$ ) extends the "normal" range of  $410\text{--}480\text{ cm}^{-1}$  ( $S_7$ :  $360\text{--}530\text{ cm}^{-1}$ ,  $S_{13}$ :  $385\text{--}500\text{ cm}^{-1}$ ) due to the presence of unusual long bonds neighbored by two short bonds ( $S_7$ : 218, 199 pm,  $S_{13}$ :  $\sim 209$ , 200 pm). The phenomenon of alternating bond

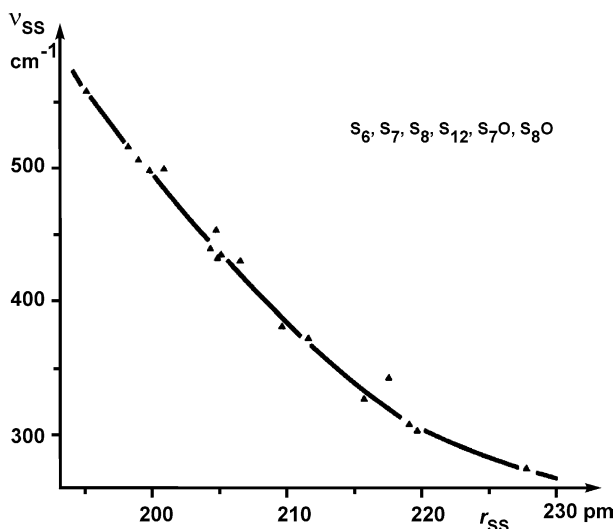


**Fig. 32** Relationship between the S–S stretching vibration  $\nu_{SS}$  (in  $\text{cm}^{-1}$ ) of the bonds in the listed homocyclic sulfur molecules and the bond length  $r_{SS}$  of that bond (in pm) [198]

lengths of adjacent bonds has already been discussed ([1] and references cited therein). The bond length of a sulfur ring,  $r$ , and the wavenumber of the related stretching vibration,  $\nu_{SS}$ , are connected via a relationship shown in Fig. 32, which is almost linear above ca.  $400 \text{ cm}^{-1}$ :

$$r_{SS} = 2.53 - 1.04 \cdot 10^{-3} \cdot \nu_{SS} \quad (1)$$

with  $r_{SS}$  in pm and  $\nu_{SS}$  in  $\text{cm}^{-1}$  [197–199].

Thus, from the measurement of stretching wavenumbers it is possible to estimate the bond lengths in sulfur molecules of unknown structure, e.g., in newly synthesized rings or in high-pressure allotropes like p-S. This has clearly been demonstrated in the case of *cyclo*-nonsulfur, for example [156, 157].

The correlation of stretching wavenumbers to the bond lengths is a spectroscopical expression of the dependence of the valence force constant  $f_r$  from the bond length  $r$  [197–199] which is presented in Fig. 33:

$$f_r = 460 \cdot r^{-7.26} \quad (2)$$

where  $f_r$  is in N/cm, and  $r$  is in 100 pm, respectively. The above-mentioned relationships can easily be understood in terms of a simple spring-mass model. Accordingly, the mean vibrational frequency (or wavenumber) is related to the bond distance by Eq. (3):

$$\overline{\nu_{SS}^2} \propto f_r \propto r^{-7.26} \quad (3)$$

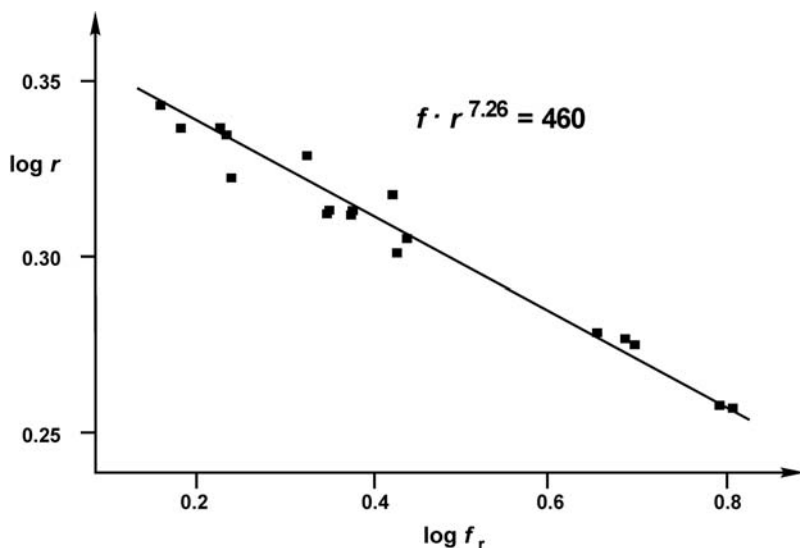


**Fig. 33** Relationship between the logarithm of the bond stretching force constant  $f_r$  of an S-S bond and the logarithm of its length  $r_{SS}$  [198]

giving low wavenumbers for long bonds and vice versa. The force constant,  $f_r$ , represents the “stiffness” of the intramolecular potential. Therefore, the vibrations of shorter bonds are more controlled by the repulsive part of the intramolecular potential than the larger ones.

By means of force constant calculations based on a UBFF it has turned out that the force constant responsible for the interaction of neighboring bonds  $f_{rr}$  is relatively high ( $f_{rr}/f_r \sim 0.25$ ) [80]. The variation of bond length  $\Delta r$  of one bond with length  $r$  causes an opposite variation of the adjacent bond(s) with length  $r'$  by  $-\Delta r'$ ; Eq. (4):

$$\frac{f_{rr'}}{f_r} = -\frac{\Delta r'}{\Delta r} \sim 0.25 \quad (4)$$

Correspondingly, the bond alternation observed in many sulfur homocycles and molecules with cumulated sulfur bonds can be attributed to the relatively strong interaction of neighboring bonds.

The wavenumber of the totally symmetric bending vibration,  $\delta_{SSS}$ , of  $S_n$  rings ( $n = 6, 7, 9, 10, 12$ ), on the other hand, is mainly a function of the ring size and not a function of the quite different bond angles in these molecules, as one may expect. The empirically obtained relation is given by

$$\delta_{SSS} = 400 - 22.8 \cdot n \quad (5)$$

where  $\delta_{SSS}$  is in  $\text{cm}^{-1}$ , and  $n$  is the number of S atoms of the ring, respectively [200].

While the vibrations (stretching, bending, torsion) in high symmetrical rings ( $S_6$ ,  $S_8$ ,  $S_{12}$ ) are almost uncoupled [80], the vibrations in the low symmetrical  $S_7$  ring are heavily mixed, especially the bending and torsional modes [81].

The wavenumber of the torsional vibrations in high symmetrical rings depend also on the ring size:  $S_6 \sim 180 \text{ cm}^{-1}$ ,  $S_8 \sim 86 \text{ cm}^{-1}$ ,  $S_{12} \sim 50\text{--}85 \text{ cm}^{-1}$ . Accordingly, the torsional force constant,  $f_t$ , decreases with the ring size, and this is connected to the increasing tendency in approaching an ideal value for the torsional angle in larger rings ( $S_6 \sim 75^\circ$ ,  $S_8 \sim 99^\circ$ ,  $S_{12} \sim 88^\circ$ ). Obviously, the higher the wavenumber of the torsional vibration the stiffer the ring.

Since the molecular bond parameters of helical sulfur are similar to those of high symmetrical rings, in particular to those of  $S_{12}$ , and since the variation of bond parameters is zero in an ideal helix, it is possible to apply the aforementioned systematics found for rings to the helical sulfur allotrope. From the bond length in polymeric sulfur (ca. 206.6 pm, cf. [1]) one obtains an average wavenumber of the stretching vibrations of  $446 \text{ cm}^{-1}$  from Eq. (1) which agrees very well with the average of the observed wavenumbers, ca.  $444 \text{ cm}^{-1}$ . Therefore, it is reasonable to estimate the stretching force constant of polymeric sulfur molecule with the help of Eq. (2) to about  $2.37 \text{ N cm}^{-1}$  which is close to values of  $S_8$  and  $S_{12}$  ( $2.366$ ,  $2.367 \text{ N cm}^{-1}$ , UBFF [80]). The ratio of the stretching constant to the bending constant was reported to about 8.85 on the basis of a planar zig-zag chain model [172], while for the rings  $S_6$ ,  $S_8$ ,  $S_{12}$  a ratio of about 9.6 to 10 was calculated [79, 80]. The bending force (UBFF) constant of the planar chain model thus is about  $0.27 \text{ N cm}^{-1}$  and slightly larger than in the symmetrical rings  $S_6$ ,  $S_8$ ,  $S_{12}$  [79, 80] but agrees with the relatively high experimentally observed wavenumbers of  $260\text{--}275 \text{ cm}^{-1}$ . On the other hand, the low energetic Raman band around  $65 \text{ cm}^{-1}$  might probably be assigned to a torsional vibration (see above) which indicates the torsional constant (UBFF) to be as low as calculated for  $S_{12}$  ( $f_t \sim 0.03 \text{ N cm}^{-1}$  [79, 80]) in agreement with the large flexibility of the helix molecule.

## 4 Mass Spectra

Since 1960 mass spectrometry has always been an important tool to investigate the molecular composition of sulfur vapor, sulfur melts, and the solid allotropes [201]. Mostly spectra obtained by electron impact (EI) ionization have been reported, except for one study in which the main species present in sulfur vapor ( $S_2\text{--}S_8$ ) were studied by photoionization mass spectrometry [202]. The following ionization potentials were reported (in eV) [202]:

$$S_2: 9.36 \pm 0.02 \quad S_5: 8.60 \pm 0.05 \quad S_7: 8.67 \pm 0.03$$

$$S_3: 9.68 \pm 0.03 \quad S_6: 9.00 \pm 0.03 \quad S_8: 9.04 \pm 0.03$$

EI mass spectra of the solid allotropes  $S_6$  [203],  $S_7$  [204],  $S_8$  [202, 203, 205],  $S_9$  [206, 207],  $S_{10}$  [204], and  $S_{12}$  [208] have been reported, and in all

cases signals for the molecular ions were observed. However, electron impact ionization triggers extensive fragmentation processes which are as more severe as higher the electron beam energy [204]. The main fragment ion is usually  $S_2^+$  (at 70 eV electron energy). In addition, the heating necessary to evaporate the sulfur allotropes initiates thermal decomposition reactions. Therefore, the EI mass spectra of  $S_{11}$ ,  $S_{13}$ , and  $S_{14}$  exhibit only peaks for fragment ions  $S_n^+$  with  $n = 1-9$ . Consequently, an accurate analysis of sulfur mixtures by mass spectrometry is a challenging task. The quantitative analysis of hot sulfur vapors by mass spectrometry has been reviewed elsewhere [9].

Natural sulfur samples contain 4.22%  $^{34}\text{S}$ , 0.75%  $^{33}\text{S}$ , and 0.02%  $^{36}\text{S}$  besides 95.02%  $^{32}\text{S}$  [4]. Evidently, there must be isotopomers of sulfur molecules. For example, in natural samples of  $S_8$  every fourth molecule has the composition  $^{34}\text{S}^3\text{S}_7$ . The probability to find one  $^{34}\text{S}$  atom besides seven  $^{32}\text{S}$  atoms in a molecule of eight atoms is  $8 \times (0.042) \times (0.95)^7 = 0.236$  (24%). Therefore, the mass spectrum of natural  $S_8$  exhibits the molecular ions  $^{32}\text{S}_8^+$  at  $m/e = 256$  and  $^{34}\text{S}^3\text{S}_7^+$  at  $m/e = 258$  in an intensity ratio of ca. 3:1 (besides smaller peaks due to other isotopomers such as  $^{33}\text{S}^3\text{S}_7$  at  $m/e = 257$  and  $^{34}\text{S}_2^3\text{S}_6$  at  $m/e = 260$ ).

The mass spectrum of polymeric sulfur  $S_\mu$ , prepared from either liquid sulfur or by extraction of commercial "flowers of sulfur", has been measured and interpreted in terms of  $S_8$ ,  $S_7$ , and  $S_6$  molecules leaving the polymer on heating and depolymerization [203]. This result is in agreement with depolymerization studies in solution which also show  $S_8$  and  $S_7$  as the major thermal degradation products [174].

Under special conditions sulfur cations with up to 56 atoms have been observed [209]. Evaporation of liquid sulfur and cooling the vapor in an atmosphere of a cold buffer gas (He) at low pressures followed by adiabatic expansion into the vacuum of a mass spectrometer and EI ionization produced mass spectra of clusters of sulfur molecules with  $m/e$  ratios up to ca. 1800. The intensity pattern shows that the species  $(S_8)_n^+$  are most abundant ( $n = 1-7$ ) followed by  $(S_7)(S_8)_{n-1}^+$  clusters and  $(S_6)(S_8)_{n-1}^+$  clusters. The latter have the same mass as  $(S_7)_2(S_8)_{n-2}^+$  clusters; see Fig. 34. Thus, the composition of the clusters reflects the composition of liquid sulfur near the melting point which contains  $S_8$ ,  $S_7$  and  $S_6$  molecules as the majority species [34, 210].

In field desorption mass spectra all ions up to  $S_{22}^+$  have been observed [211]. For this purpose gaseous  $S_2$  was generated in an electrochemical Knudsen cell (from  $\text{Ag}_2\text{S}$ ), built into a mass spectrometer, and continuously condensed on the tungsten tip of a field emitter which from time to time was exposed to a high electric field to initiate desorption. Depending on the flow of  $S_2$  molecules, the tip temperature, the field strength and other conditions (e.g., the reaction time on the tip before desorption) the molecular species observed corresponded either to the ones present in equilibrium sulfur vapor ( $S_n$  with  $n = 2-8$ ), or large molecules up to  $S_{22}$  were observed in addition. The ionization was assumed to take place in the gas-phase after desorption of the adsorbed sulfur molecules and neither fragmentation nor cluster

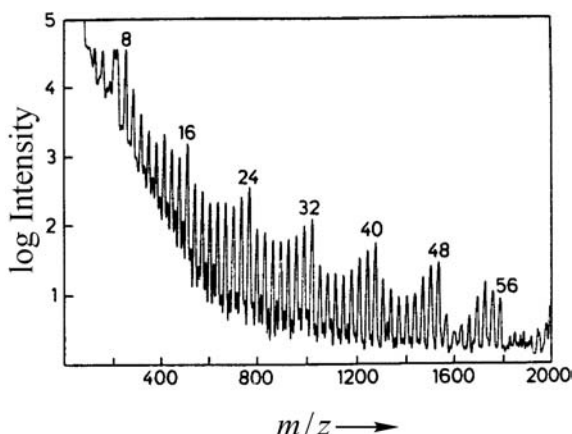
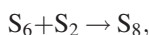
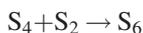
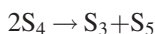
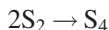


**Fig. 34** Mass spectrum of sulfur clusters obtained by evaporation of liquid sulfur followed by cooling and adiabatic expansion of the vapor [209]. The figures at the peaks give the number of  $S_8$  molecules which represent this particular mass

formation was assumed. The sulfur layers on the tip consist of a chemisorbed  $\alpha$ -layer which is tightly bound to the metal surface and on top of this there exists a physically adsorbed  $\beta$ -layer of liquid-like structure and behavior. The formation of the larger molecules was explained by a sequence of  $S_2$  addition reactions taking place in the  $\beta$ -layer, e.g.,



All of these reactions are exothermic but some of them violate the law of spin conservation since  $S_2$  is a triplet molecule while all species on the right side of the above equations are singlet molecules in the ground state. Therefore, a radical-chain reaction has been assumed.  $S_3$  may also be formed from  $S_2$  by picking a sulfur atom up from a di- or polysulfide in the  $\alpha$ -layer.

## 5 XANES Spectra

X-ray absorption near edge structure (XANES) spectroscopy is a non-destructive and sensitive probe of the coordination number and geometry as well as of the effective charge of a chosen atom within a molecule and therefore also of the formal oxidation number. Recently, there have been a number of XANES studies at the sulfur K-edge demonstrating the sensitivity of

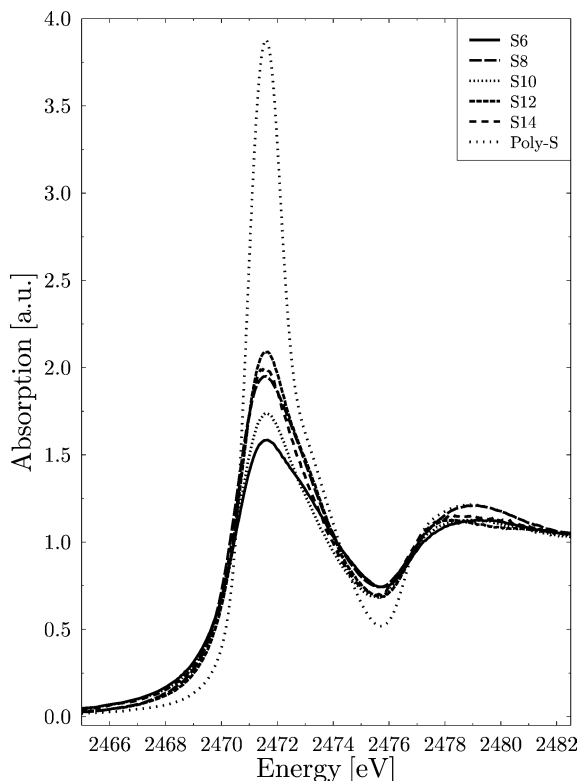


**Fig. 35** K-edge XANES spectra of solid  $S_6$ ,  $S_8$ ,  $S_{10}$ ,  $S_{12}$ ,  $S_{14}$  and polymeric sulfur normalized at 2482 eV. Figure kindly provided by A. Prange [222]

the spectra to the local geometric and electronic environment of the sulfur atoms [212–215]. Due to the penetration strength of X-rays, in situ measurements are possible in many cases. Structural information deduced from XANES measurements by a fingerprint method is often sufficient for solving analytical problems. This has been demonstrated, for example, in studies on the rather complex sulfur speciation in coal [216], in electrically conduction polymers [217] as well as in rubber vulcanized by sulfur [218, 219].

The method involves the irradiation of a sample with polychromatic X-rays (synchrotron radiation) which inter alia promote electrons from the innermost  $1s$  level of the sulfur atom to the lowest unoccupied molecular orbitals. In the present case these are the S-S antibonding  $\sigma^*$ -MOs. The intensity of the absorption lines resulting from these electronic excitations are proportional to the number of such bonds in the molecule. Therefore, the spectra of sulfur compounds show significant differences in the positions and/or the relative intensities of the absorption lines [215, 220, 221]. In principle, solid, liquid and gaseous samples can be measured.

The XANES spectra of  $S_6$ ,  $S_8$ ,  $S_{10}$ ,  $S_{12}$ ,  $S_{14}$  [222] and polymeric sulfur [223, 224] are all very similar as far as the peak positions are concerned but the relative intensities of the two peaks differ considerably. The spectra are characterized by an absorption line at 2471.7 eV (so-called white line) and a broad absorption in the region 2477–2480 eV [222]; see Fig. 35 (energies calibrated to the white line of  $ZnSO_4$  defined as 2481.4 eV). Since the spectra of the components of a mixture are additive, quantitative analyses are possible, even for mixtures of samples as similar as  $S_8$  and polymeric sulfur, for instance [224]. The interpretation of the spectra is, however, still somewhat controversial; see [225].

Thus, XANES spectroscopy of elemental sulfur has mainly been used to detect the particular sulfur species in samples not accessible to other spectroscopic methods, e.g., in cultures of sulfur bacteria [215, 221, 222, 224]. However, the main application is in the area of sulfur compounds with other elements. For a recent review, see [226].

**Acknowledgements** This work has been supported by the Deutsche Forschungsgemeinschaft, the Verband der Chemischen Industrie, the European Community (LENS facility) and the NATO (grants for international collaboration in research).

## References

1. R. Steudel, B. Eckert, *Top. Curr. Chem.* **2003**, *230*, in print
2. R. Steudel, M. Rebsch, *J. Mol. Spectrosc.* **1974**, *51*, 189
3. R. Steudel, M. Rebsch, *J. Mol. Spectrosc.* **1974**, *51*, 334
4. J. Emsley, *The Elements*, 2nd edn, Clarendon, Oxford, **1991**
5. H.C.E. McFarlane, W. McFarlane, in *Multinuclear NMR* (J. Mason, ed.), Plenum, New York, **1987**, p. 417
6. A. Chatelain, J. Buttet, in *Elemental Sulfur* (B. Meyer, ed.), Interscience, New York, **1965**, p. 209
7. A. Chatelain, *Helv. Phys. Acta* **1969**, *42*, 117
8. R. Steudel, J. Albertsen, K. Zink, *Ber. Bunsenges. Phys. Chem.* **1989**, *93*, 502
9. Review: R. Steudel, Y. Steudel, M.W. Wong, *Top. Curr. Chem.* **2003**, *230*, in print
10. R. Steudel, G. Holdt, A.T. Young, *J. Geophys. Res.* **1986**, *91*, 4971
11. A.M. Bass, *J. Chem. Phys.* **1953**, *21*, 80
12. B. Meyer, T. Stroyer-Hansen, T.V. Oommen, *J. Mol. Spectrosc.* **1972**, *42*, 335
13. H. Braune, E. Steinbacher, *Z. Naturforsch. Part A* **1952**, *7*, 486
14. G. Weser, F. Hensel, W.W. Warren, *Ber. Bunsenges. Phys. Chem.* **1978**, *82*, 588. F. Hensel, *Angew. Chem.* **1980**, *92*, 598
15. V.A. Krasnopolsky, *Adv. Space Res.* **1987**, *7*, 25
16. M.H. Moore, B. Donn, R.L. Hudson, *Icarus* **1988**, *74*, 399
17. P. Hassanzadeh, L. Andrews, *J. Phys. Chem.* **1992**, *96*, 6579
18. T.B. Brill, *Light – Its Interaction with Art and Antiquities*, Plenum, New York, **1980**, p. 65
19. R.I. Billmers, A.L. Smith, *J. Chem. Phys.* **1991**, *95*, 4242–4245
20. B. Meyer, M. Gouterman, D. Jensen, T.V. Oommen, K. Spitzer, T. Stroyer-Hansen, *Adv. Chem. Ser.* **1972**, *110*, 53
21. R.J.H. Clark, D.G. Cobbold, *Inorg. Chem.* **1978**, *17*, 3169. R.J.H. Clark, T. J. Dines, M. Kurmoo, *Inorg. Chem.* **1983**, *22*, 2766. F. Seel, H.-J. Güttler, A.J. Wieckowski, B. Wolf, *Z. Naturforsch. Part B* **1979**, *34*, 1671. G. Geismar, U. Westphal, *Chemiker-Ztg.* **1988**, *112*, 177

22. B. Meyer, *Chem. Rev.* **1976**, *76*, 367
23. E. Isoniemi, L. Khriachtchev, M. Petterson, M. Räsänen, *Chem. Phys. Lett.* **1999**, *311*, 47
24. A. Morelle, *Doctoral Dissertation*, University of Washington, Seattle, USA, **1971**; cited after ref. [20]
25. A. Kumar, P.K. Chowdhury, K.V.S. Rama Rao, J.P. Mittal, *Chem. Phys. Lett.* **1992**, *198*, 406
26. K.P. Huber, G. Herzberg, *Constants of Diatomic Molecules*, Van Nostrand Reinhold, New York, **1979**, p. 565
27. L. Brewer, G.D. Brabson, *J. Chem. Phys.* **1966**, *44*, 3274
28. V.E. Bondybey, J.H. English, *J. Chem. Phys.* **1978**, *69*, 1865
29. R.F. Barrow, R.P. du Parcq, in *Elemental Sulfur* (B. Meyer, ed.), Interscience, New York, **1965**, p. 251
30. B. Meyer, D. Jensen, T. Oommen, in *Sulfur in Organic and Inorganic Chemistry*, Vol. 2 (A. Senning, ed.), Dekker, New York, **1972**, p. 13
31. N.A. Narasimham, V. Sethuraman, K. V. S. R. Apparao, *J. Mol. Spectrosc.* **1976**, *59*, 142
32. G. Theodorakopoulos, S.D. Peyerimhoff, R.J. Buenker, *Chem. Phys. Lett.* **1981**, *81*, 413
33. A.J. Hynes, R.C. Richter, A.R. Rosendahl, C.D. Clark, *Chem. Phys. Lett.* **1998**, *295*, 25
34. Review: R. Steudel, *Top. Curr. Chem.* **2003**, *230*, in print
35. M.W. Wong, Y. Steudel, R. Steudel, *Chem. Phys. Lett.* **2002**, *364*, 387
36. For color pictures of piles of sulfur and of the melt at different temperatures, see R. Steudel, *Chemie unserer Zeit* **1996**, *30*, 226 and **1980**, *14*, 73
37. B. Meyer, T.V. Oommen, D. Jensen, *J. Phys. Chem.* **1971**, *75*, 912
38. K. Tamura, H.P. Seyer, F. Hensel, *Ber. Bunsenges. Phys. Chem.* **1986**, *90*, 581
39. S. Hosokawa, T. Matsuoka, K. Tamura, *J. Phys.: Condens. Matter* **1994**, *6*, 5273
40. M. Zanini, J. Tajuc, *J. Non-Cryst. Solids* **1977**, *23*, 349
41. K. Bröllos, G. M. Schneider, *Ber. Bunsenges. Phys. Chem.* **1974**, *78*, 296
42. R. Steudel, D. Jensen, P. Göbel, P. Hugo, *Ber. Bunsenges. Phys. Chem.* **1988**, *92*, 118
43. R. Steudel, R. Strauss, L. Koch, *Angew. Chem.* **1985**, *97*, 58; *Angew. Chem. Int. Ed. Engl.* **1985**, *24*, 59
44. J.C. Koh, W. Klement, *J. Phys. Chem.* **1970**, *74*, 4280
45. H. Rau, T. R. N. Kutty, J. R.F. Guedes de Carvalho, *J. Chem. Thermod.* **1973**, *5*, 833
46. P. Lenain, E. Picquenard, J. Corset, D. Jensen, R. Steudel, *Ber. Bunsenges. Phys. Chem.* **1988**, *92*, 859
47. This isomer was first obtained by density functional calculations: R.O. Jones, D. Hohl, *Int. J. Quantum Chem. Quantum Chem. Symp.* **1990**, *110*, 4703
48. R. Steudel, R. Reinhardt, T. Sandow, *Angew. Chem.* **1977**, *89*, 757; *Angew. Chem. Int. Ed. Engl.* **1977**, *16*, 716
49. For reviews on homocyclic sulfur oxides, see R. Steudel, *Comments Inorg. Chem.* **1982**, *5*, 313, and *Top. Curr. Chem.* **2003**, *231*, in print
50. H.L. Casal, J.S. Scaiano, *J. Photochem.* **1985**, *30*, 253
51. R. Steudel, E.-M. Strauss, *Z. Naturforsch. Part B* **1987**, *42*, 682
52. A.K. Abass, N.H. Ahmad, *J. Phys. Chem. Solids* **1986**, *47*, 143; A.K. Abass, A.K. Hasen, R. H. Misho, *J. Appl. Phys.* **1985**, *58*, 1640; A.K. Abass, N.H. Ahmad, *Phys. Stat. Sol. Part (a)* **1985**, *91*, 627
53. T.E. Slykhouse, H.G. Drickamer, *J. Phys. Chem. Solids* **1958**, *7*, 275
54. M.J. Peanasky, C.W. Jurgensen, H.G. Drickamer, *J. Chem. Phys.* **1984**, *81*, 6407
55. K. Syassen, unpublished results
56. H. Luo, S. Desgreniers, Y.K. Vohra, A.L. Ruoff, *Phys. Rev. Lett* **1991**, *67*, 2998
57. B. Lorenz, I. Orgzall, in: *High Pressure Science and Technology* (S. C. Schmidt, J.W. Shaner, G.A. Samara, M. Ross; eds.), American Institute of Physics, New York, **1994**, p. 259, and unpublished results
58. B. Eckert, R. Schumacher, H.J. Jodl, P. Foggi, *High Press. Res.* **2000**, *17*, 113
59. R. Steudel, B. Holz, *Z. Naturforsch. Part B* **1988**, *43*, 581

60. R. Steudel, E.-M. Strauss, M. Papavassiliou, P. Brätter, W. Gatschke, *Phosphorus Sulfur* **1986**, 29, 17
61. R. Steudel, unpublished results
62. W. Nehb, K. Vydra in *Ullmann's Encyclopedia of Industrial Chemistry*, Vol. A25, VCH, Weinheim, **1994**, p. 507
63. D.B. Nash, *Icarus* **1987**, 72, 1
64. [http://dir.yahoo.com/Science/Astronomy/Solar\\_System/Planets/Jupiter/Moons/Io/](http://dir.yahoo.com/Science/Astronomy/Solar_System/Planets/Jupiter/Moons/Io/)
65. W.E. Spear, A.R. Adams, *J. Phys. Chem. Solids* **1966**, 27, 281. B. E. Cook, W.E. Spear, *J. Phys. Chem. Solids* **1969**, 30, 1125
66. W.R. Salaneck, N.O. Lipari, A. Paton, R. Zallen, K.S. Liang, *Phys. Rev. B* **1975**, 12, 1493
67. N.V. Richardson, P. Weinberger, *J. Electron Spectrosc. Relat. Phenom.* **1975**, 6, 109
68. R.L. Emerald, R.E. Drews, R. Zallen, *Phys. Rev. B* **1976**, 14, 808
69. H.F. Radford, F.O. Rice, *J. Chem. Phys.* **1960**, 33, 774
70. O. V. Krasovska, B. Winkler, E.E. Krasovskii, V.N. Antonov, B. Yu. Yavorsky, *J. Phys.: Condens. Matter* **1998**, 10, 4093
71. R.E. Barletta, H.H. Claassen, R.L. McBeth, *J. Chem. Phys.* **1971**, 55, 5409
72. L. Brewer, G.D. Brabson, B. Meyer, *J. Chem. Phys.* **1965**, 42, 1385. B. Meyer, *J. Chem. Phys.* **1971**, 54, 4305
73. R. Steudel, *Z. Naturforsch. Part B* **1972**, 27, 469
74. E. Picquenard, O. El Jaroudi, J. Corset, *J. Raman Spectrosc.* **1993**, 24, 11
75. G.D. Brabson, Z. Mielke, L. Andrews, *J. Phys. Chem.* **1991**, 95, 79
76. M. S. Boumediene, J. Corset, E. Picquenard, *J. Raman Spectrosc.* **1999**, 30, 463
77. Each atom has three degrees of motional freedom ( $3 \times 8 = 24$ ). From this total number three degrees of translational and three of rotational motion of the whole molecule have to be subtracted in order to obtain the number of intramolecular degrees of freedom ( $24 - 2 \times 3 = 18$ )
78. D.W. Scott, J.P. McCullough, F.H. Kruse, *J. Mol. Spectrosc.* **1964**, 13, 313
79. R. Steudel, H.-J. Mäusle, *Z. Naturforsch., Part A* **1978**, 33, 951
80. R. Steudel, *Spectrochim. Acta* **1975**, 31A, 1065
81. R. Steudel, F. Schuster, *J. Mol. Spectrosc.* **1978**, 44, 143
82. E. Venuti, P.R. Salvi, G. Cardini, *J. Mol. Struct.* **1992**, 266, 229
83. H.H. Eysel, *J. Mol. Struct.* **1982**, 78, 203
84. K. Raghavachari, C. McMichael Rohlfing, J.S. Binkley, *J. Chem. Phys.* **1990**, 93, 5862
85. D.A. Dixon, E. Wasserman, *J. Phys. Chem.* **1990**, 94, 5772
86. W.T. King, *Spectrochim. Acta Part A* **1975**, 31A, 1421
87. C. Domingo, S. Montero, *J. Chem. Phys.* **1981**, 74, 862
88. In order to distinguish between symmetry species of the free molecule and of the crystal we have chosen capital letters for the species in case of the molecule and small letters for those of the crystal
89. W.G. Fateley, F. R. Dollish, N. T. Devitt, F. F. Bentley, *Infrared and Raman Selection Rules for Molecular and Lattice Vibrations: The Correlation Method*, Wiley, New York, **1972**
90. G. Turrell, *Infrared and Raman Spectra of Crystals*, Academic Press, London, **1972**
91. The resonance splitting of intramolecular modes in the crystalline state is often called "Davydov splitting" or "factor group splitting". In contrast to the static field effects of the crystal, this splitting is due to the dynamical interaction of the constituents in the primitive cell
92. K.W.F. Kohlrausch, *Ramanspektren*, Heyden & Son, London **1972** (reprinted from 1943)
93. *Gmelin Handbuch der Anorganischen Chemie*, 8. Auflage, Teil 9A, Verlag Chemie, Weinheim, **1953**
94. H.L. Strauss, J. A. Greenhouse, in: *Elemental Sulfur, Chemistry and Physics* (B. Meyer, ed.), Interscience Publ., New York, **1965**, p. 241
95. A.T. Ward, *J. Phys. Chem.* **1968**, 72, 744
96. A. Anderson, Y.T. Loh, *Can. J. Chemistry* **1969**, 47, 879

97. V. S. Gorelik, L.T. Koldavea, M. M. Sushinskii, *Soviet Physics—Solid State* **1971**, *12*, 2648
98. V. S. Gorelik, in: *Temporal Characteristics of Laser Pulses and Interaction of Laser Radiation with Matter*, N. G. Basov (ed.), Consultants Bureau, New York, **1977**
99. A. Karonen, F. Stenman, *Report Series in Physics HU-P-152*, University of Helsinki, **1979**
100. P.D. Harvey, I. S. Butler, *J. Raman Spectrosc.* **1986**, *17*, 329
101. A. Anderson, L. Y. Wong, *Can. J. Chem.* **1969**, *47*, 2713
102. A. Anderson, P. G. Boczar, *Chem. Phys. Lett.* **1976**, *43*, 506
103. G.A. Ozin, *J. Chem. Soc. A* **1969**, 116
104. J.W. Arthur, G.A. Mackenzie, *J. Raman Spectrosc.* **1974**, *2*, 199
105. R. Bini, unpublished results
106. G. Gautier, M. Debeau, *Spectrochim. Acta, Part A* **1974**, *30A*, 1193
107. M. Becucci, R. Bini, E. Castellucci, B. Eckert, H.J. Jodl, *J. Phys. Chem. Part B* **1997**, *101*, 2132
108. B. Eckert, R. Bini, H.J. Jodl, S. Califano, *J. Chem. Phys.* **1994**, *100*, 912
109. B. Eckert, Doctoral Thesis, University of Kaiserslautern, **2001**
110. M. Becucci, private communication
111. D.A. Dows, private communication
112. R.P. Rinaldy, G.S. Pawley, *Nuovo Cimento, Part B* **1973**, *16B*, 55
113. R.P. Rinaldi, G.S. Pawley, *J. Phys. C: Solid State Phys.* **1975**, *8*, 599
114. M. Becucci, E. Castellucci, P. Foggi, S. Califano, D.A. Dows, *J. Chem. Phys.* **1992**, *96*, 98
115. T. Luty, G.S. Pawley, *Phys. Stat. Sol. B* **1975**, *69*, 551
116. J. V.E. Kurittu, *Physica Scripta* **1980**, *21*, 194
117. C.M. Gramaccioli, G. Filippini, *Chem. Phys. Lett.* **1984**, *108*, 585
118. E. Venuti, G. Cardini, E. Castellucci, *Chem. Phys.* **1992**, *165*, 313
119. B. Eckert, H.O. Albert, H.J. Jodl, P. Foggi, in: *Frontiers of High Pressure Research* (H.D. Hochheimer, R. D. Ethers, eds.), Plenum Press, New York, **1991**, p. 143
120. B. Eckert, H.O. Albert, H.J. Jodl, P. Foggi, *J. Phys. Chem.* **1996**, *100*, 8212
121. C. Biermann, R. Winter, C. Benmore, P. A. Egelstaff, *J. Non-Cryst. Solids* **1998**, *232–234*, 309
122. C. Pastorino, Z. Gamba, *Chem. Phys.* **2000**, *261*, 317; C. Pastorino, Z. Gamba, *Chem. Phys. Lett.* **2000**, *319*, 20
123. M. Ezzine, A. Pellegatti, C. Minot, R.J.-M. Pellenq, *J. Phys. Chem. A* **1998**, *102*, 452
124. A. Abraha, D.E. Williams, *Inorg. Chem.* **1999**, *38*, 4224
125. C. Pastorino, Z. Gamba, *J. Chem. Phys.* **2001**, *15*, 9421
126. In the case of translational modes simply the mass of the rings has to be considered, while in the case of librational modes the moment of inertia has to be taken into account
127. P. Foggi, V. Schettino, *Rivista del Nuovo Cimento* **1992**, *15*, 1
128. A.A. Maradudin, S. Califano, *Phys. Rev. B* **1993**, *48*, 12628
129. T. Held, I. Pfeiffer, W. Kuhn, *Phys. Rev. B* **1997**, *55*, 231
130. R. Bini, S. Califano, B. Eckert, H.J. Jodl, *J. Chem. Phys.* **1997**, *106*, 511
131. E. Venuti, G. Cardini, private communication
132. G. Herzberg, *Molecular Spectra and Molecular Structure, Vol. II – Infrared and Raman Spectra of Polyatomic Molecules*, Van Nostrand Reinhold, New York, **1945**
133. In the crystalline state, it is more convenient to speak about multi-phonon processes since the modes from the whole dispersion range of the first Brillouin zone are allowed to contribute according to the conservation of energy and momentum of the phonons involved in the process
134. P.J. Carroll, J.S. Lannin, *Journal de Physique Colloqu.* **1981**, *42*, C6–643; P.J. Carroll, J.S. Lannin, *Phys. Rev B* **1983**, *27*, 1028
135. R. Zallen, *Phys. Rev. B* **1974**, *9*, 4485; R. Zallen, M.L. Slade, *Phys. Rev. B* **1978**, *18*, 5775; B. A. Weinstein, R. Zallen, in: *Light Scattering in Solids Vol. IV* (M. Cardona, G. Güntherodt, eds.), Springer, Berlin, **1984**, p. 463

136. L. Wang, Y. Zhao, R. Lu, Y. Meng, Y. Fan, H. Luo, Q. Cui, G. Zou, in: *High Pressure Research in Mineral Physics* (M.H. Manghani, Y. Syono, eds.), Terra Scientific Publ., Tokyo, 1987, p. 299
137. W. Häfner, J. Kritzenberger, H. Olijnyk, A. Wokaun, *High Press. Res.* 1990, 6, 57
138. A. Anderson, W. Smith, J.F. Wheeldon, *Chem. Phys. Lett.* 1996, 263, 133
139. G.A. Saunders, Y.K. Yoğurtçu, J.E. Macdonald, G.S. Pawley, *Proc. R. Soc. (London)*, Part A 1986, 407, 325
140. G.S. Pawley, K. Mika, *Phys. Stat. Sol. Part B* 1974, 66, 679
141. J.V.E. Kurittu, *Physica Scripta* 1980, 21, 200
142. A.M. Taylor, E. K. Rideal, *Proc. Roy. Soc. (London)*, Part A 1927, 115, 589
143. G.G. Dumas, F. Vovelle, *Spectrochim. Acta, Part A* 1977, 33, 169
144. Y. Sasaki, Y. Nishina, *J. Physique C6* 1981, 42, 556
145. R. Steudel, H.-J. Mäusle, *Z. Anorg. Allg. Chem.* 1981, 478, 156
146. G. Gautier, M. Debeau, *Spectrochim. Acta, Part A* 1976, 32, 1007
147. J. Steidel, J. Pickardt, R. Steudel, *Z. Naturforsch., Part B* 1978, 33, 1554
148. J. Berkowitz, W.A. Chupka, E. Bromels, R.L. Belford, *J. Chem. Phys.* 1967, 47, 4320. The infrared spectrum in this paper is distorted by additional bands of CS<sub>2</sub> and polymeric sulfur
149. L.A. Nimon, V.D. Neff, R.E. Cantley, R.O. Buttlar, *J. Mol. Spectrosc.* 1967, 22, 105. L.A. Nimon, V. D. Neff, *J. Mol. Spectrosc.* 1968, 26, 175
150. R. Schumacher, B. Eckert, H.J. Jodl, *High Press. Res.* 1996, 15, 105
151. R. Steudel, J. Steidel, R. Reinhardt, *Z. Naturforsch., Part B* 1983, 38, 1548
152. M.W. Wong, personal communication, 2003
153. J. Weidlein, U. Müller, K. Dehnicke, *Schwingungsspektroskopie*, 2. Aufl., Thieme, Stuttgart, 1988
154. R. Steudel, J. Steidel, J. Pickardt, F. Schuster, R. Reinhardt, *Z. Naturforsch., Part B* 1980, 35, 1378
155. M. Gardner, A. Rogstad, *J. Chem. Soc., Dalton Trans.* 1973, 599
156. R. Steudel, T. Sandow, J. Steidel, *Z. Naturforsch., Part B* 1985, 40, 594
157. R. Steudel, K. Bergemann, J. Buschmann, P. Luger, *Inorg. Chem.* 1996, 35, 2184
158. R. Reinhardt, R. Steudel, F. Schuster, *Angew. Chem.* 1978, 90, 55; *Angew. Chem. Int. Ed. Engl.* 1978, 17, 57
159. R. Steudel, J. Steidel, T. Sandow, F. Schuster, *Z. Naturforsch., Part B* 1978, 33, 1198
160. T. Sandow, J. Steidel, R. Steudel, *Angew. Chem.* 1982, 94, 782; *Angew. Chem. Int. Ed. Engl.* 1982, 21, 794
161. J. Steidel, R. Steudel, *J. Chem. Soc. Chem. Commun.* 1982, 1312
162. R. Steudel, J. Steidel, T. Sandow, *Z. Naturforsch., Part B* 1986, 41, 958
163. J. Steidel, R. Steudel, A. Kutoglu, *Z. Anorg. Allg. Chem.* 1981, 476, 171
164. R. Steudel, D. F. Eggers, *Spectrochim. Acta* 1975, 31A, 879
165. R. Steudel, O. Schumann, J. Buschmann, P. Luger, *Angew. Chem.* 1998, 110, 2502; *Angew. Chem. Int. Ed.* 1998, 37, 2377
166. O. Schumann, *Doctoral Dissertation*, Technische Universität Berlin, 1999
167. R. Strauss, R. Steudel, *Z. Naturforsch., Part B* 1988, 43, 1151
168. R. Steudel, *Z. Naturforsch., Part B* 1975, 30, 281
169. L. Peter, *Phosphorus Sulfur Silicon* 2001, 168, 287
170. Sometimes, a shoulder at about 470 cm<sup>-1</sup> has been observed, too. However, it is not clear if the origin of this Raman signal can unambiguously be assigned to polymeric sulfur
171. R.E. Barletta, C.W. Brown, *J. Phys. Chem.* 1971, 75, 4059
172. W. Dultz, H.D. Hochheimer, W. Müller-Lierheim, in: *Proc. 5th Int. Conf. Amorphous and Liquid Semiconductors* (J. Stuke, W. Brenig, eds.), Taylor and Francis, London, 1974, p. 1281
173. H.-J. Mäusle, R. Steudel, *Z. Anorg. Allg. Chem.* 1981, 478, 177
174. R. Steudel, S. Passlack-Stephan, G. Holdt, *Z. Anorg. Allg. Chem.* 1984, 517, 7
175. A.T. Ward, *J. Phys. Chem.* 1968, 72, 4133

176. F. Michaud, J. Fourcade, E. Philippot, M. Maurin, M. Discours, in: *Proc. International Symposium on Elemental Sulfur in Agriculture*, Vol. 2, Syndicat Française du Soufre, Marseille, 1987, p. 789
177. P. Hendra, P. Wallen, A. Chapman, K. Jackson, J. Loadman, M. van Duin, B. Kip, *Kautschuk, Gummi, Kunststoffe* 1993, 46, 694
178. G.C. Vezzoli, R.J. Zeto, *Inorg. Chem.* 1970, 9, 2478
179. F. Tuinstra, *Structural Aspects of the Allotropy of Sulfur and the Other Divalent Elements*, Waltman, Delft, 1967
180. F. Cataldo, *Angew. Makromol. Chem.* 1997, 249, 137. The author has assigned an absorption at  $1509\text{ cm}^{-1}$  to polymeric sulfur, but this absorption originates from a  $\text{CS}_2$  impurity of the sulfur sample
181. C.X. Cui, M. Kertesz, *J. Chem. Phys.* 1990, 93, 5257
182. R. Steudel, H.-J. Mäusle, *Z. Anorg. Allg. Chem.* 1981, 478, 156
183. R. Shuker, R.W. Gammon, *Phys. Rev. Lett.* 1970, 25, 222; R. Shuker, R.W. Gammon, in: *Proc. 2<sup>nd</sup> Int. Conf. Light Scattering in Solids* (M. Balkanski, ed.), Flammarion Sciences, Paris, 1971, p. 334
184. P. Rossmanith, W. Häfner, A. Wokaun, H. Olijnyk, *High Press. Res.* 1993, 11, 183
185. H. Luo, R.G. Greene, A.L. Ruoff, *Phys. Rev. Lett.* 1993, 71, 2943
186. I. Orgzall, B. Lorenz, *High Press. Res.* 1995, 13, 215
187. Various names for this allotropes were in use: intermediate phase sulfur (ip-S) [184], high-pressure unknown phase (HPU phase) [191], and photo-sensitive or, more recently, photo-induced sulfur (p-S) [57, 58, 119, 186], respectively. We are inclined to make use of the term “photo-induced” since it has clearly turned out that the formation of this allotrope is induced when employing laser light of suitable power density and wavelength [1]
188. P. Wolf, B. Baer, M. Nicol, H. Cynn, in: *Molecular Systems under High Pressure* (R. Pucci, G. Piccitto, eds.), Elsevier, Amsterdam, 1991, p. 263
189. K. Nagata, T. Nishio, H. Taguchi, Y. Miyamoto, *Jpn. J. Appl. Phys.* 1992, 31, 1078
190. H. Luo, A.L. Ruoff, in: *High Pressure Science and Technology* (S. C. Schmidt, J.W. Shaner, G.A. Samara, M. Ross; eds.), American Institute of Physics, New York, 1994, p. 43
191. A. Yoshioka, K. Nagata, *J. Phys. Chem. Solids* 1995, 56, 581
192. The term “high-pressure low-temperature” has to be understood as high-pressure room-temperature
193. For convenience, we will use the abbreviation  $S_\mu$  for high-pressure polymeric sulfur since the spectra are analogous to the STP polymer which is often called  $S_\mu$
194. However, it is a general observation for sulfur allotropes that the stretching modes gain relative intensity upon increasing pressure. For example, the Raman intensities of  $S_6$  at pressures above ca. 2 GPa are strong for the stretching vibrations at the expense of the bending and librational modes [150]. Similar observations were made for the vibrations in  $\alpha\text{-S}_8$  [120]. Therefore, the intensity ratios of different species of vibrations in sulfur allotropes at high pressures may not necessarily reflect the ratios at STP conditions
195. K. Nagata, T. Ishikawa, Y. Miyamoto, *Jpn. J. Appl. Phys.* 1983, 22, 1129
196. This interpretation is in contrast to the observation that the frequencies of polymeric sulfur under increasing pressure clearly show positive shifts [109,119]. Furthermore, not only for the selenium chain (trigonal Se) but also for the symmetrical stretching vibrations in the ring molecules  $\text{Se}_6$  and  $\text{Se}_8$  negative shifts have been found experimentally [195]. This behavior was explained by an increased “interference” between the intermolecular and intramolecular bonds under pressure. Unlike selenium, the stretching vibrations in the rings  $\text{S}_8$  and  $\text{S}_6$  have positive slopes of  $d\omega/dp$  up to about 12 GPa [137,150,184]. In fact, the ratio of intramolecular to intermolecular distances is about 1.7 for sulfur and about 1.5 for selenium at STP conditions. Negative slopes for  $d\omega/dp$ , although slightly, were reported for the  $a_g$  stretching mode in  $\text{S}_6$  above ca. 15 GPa [137,184], which may indicate an onset of “interference” between the two different types of bonding. Thus it was concluded that the interaction between intramo-

- molecular and intermolecular bonding at high pressure is likely to be different for sulfur and selenium [109]
197. R. Steudel, *Angew. Chem.* **1975**, *87*, 683; *Angew. Chem. Int. Ed. Engl.* **1975**, *14*, 655
  198. R. Steudel, *Top. Curr. Chem.* **1982**, *102*, 149
  199. R. Steudel, *Z. Naturforsch., Part B* **1975**, *30*, 281
  200. For  $S_9$  and  $S_{10}$  it was assumed that the vibrational lines with highest intensity in the bending region can be regarded as the totally symmetric bending mode. However, for larger rings it is difficult to draw an analogous conclusion since the differences in intensity are less pronounced
  201. J. Berkowitz, J. R. Marquardt, *J. Chem. Phys.* **1963**, *39*, 275 and publications cited therein
  202. J. Berkowitz, C. Lifshitz, *J. Chem. Phys.* **1968**, *48*, 4346
  203. J. Berkowitz, W.A. Chupka, *J. Chem. Phys.* **1964**, *40*, 287
  204. U.-I. Zahorsky, *Angew. Chem.* **1968**, *80*, 661
  205. G. Dudek, E.P. Dudek, *J. Chem. Educ.* **1989**, *66*, 304
  206. M. Schmidt, E. Wilhelm, *J. Chem. Soc., Chem. Commun.* **1970**, 111
  207. R. Steudel, K. Bergemann, J. Buschmann, P. Luger, *Inorg. Chem.* **1996**, *35*, 2184
  208. J. Buchler, *Angew. Chem.* **1966**, *78*, 1021
  209. T.P. Martin, *J. Chem. Phys.* **1984**, *80*, 170
  210. R. Steudel, R. Strauss, L. Koch, *Angew. Chem.* **1985**, *97*, 58; *Angew. Chem. Int. Ed. Engl.* **1985**, *20*, 59
  211. P.R. Davis, E. Bechtold, J.H. Block, *Surface Science* **1974**, *45*, 585. D. L. Cocke, G. Abend, J.H. Block, *J. Phys. Chem.* **1976**, *80*, 524. D. L. Cocke, G. Abend, J.H. Block, *Int. J. Mass Spectr. Ion Phys.* **1977**, *24*, 271. G. Abend, R.-G. Abitz, J.H. Block, in *Nonlinear Behavior of Molecules, Atoms and Ions in Electric, Magnetic or Electromagnetic Fields*, Elsevier, **1979**, p. 261
  212. C. Dezernaud, M. Tronc, A. Modelli, *Chem. Phys.* **1991**, *156*, 129
  213. A.P. Hitchcock, R. S. DeWitte, J.M. Van Esbroeck, P. Aebi, C. L. French, R. T. Oakley, N. P. C. Westwood, *J. Electron Spectrosc. Relat. Phenom.* **1991**, *57*, 165
  214. M. Dezernaud, M. Tronc, A.P. Hitchcock, *Chem. Phys.* **1990**, *142*, 455
  215. A. Prange, C. Dahl, H.G. Trüper, M. Behnke, J. Hahn, H. Modrow, J. Hormes, *Eur. Phys. J.* **2002**, *D20*, 589
  216. G.P. Huffman, F.E. Huggins, S. Mitra, N. Shah, in *X-Ray Absorption Fine Structure* (S. Hasnain, ed.), Ellis Horwood, Chichester, **1991**, p. 161
  217. I. Winter, J. Hormes, M. Hiller, *Nucl. Instr. Methods* **1995**, *B97*, 287
  218. R. Chauvistré, J. Hormes, D. Brück, K. Sommer, H.-W. Engels, *Kautschuk Gummi Kunststoffstoffe* **1992**, *45*, 808
  219. H. Modrow, J. Hormes, F. Visel, R. Zimmer, *Rubber Chem. Technol.* **2001**, *74*, 281
  220. Chauvistré, R.; Hormes, J.; Hartmann, E.; Etzenbach, N.; Hosch, R.; Hahn, J. *Chem. Phys.* **1997**, *223*, 293
  221. I.J. Pickering, G.N. George, E.Y. Yu, D.C. Brune, C. Tuschak, J. Overmann, J.T. Beatty, R.C. Prince, *Biochemistry* **2001**, *40*, 8138
  222. A. Prange, I. Arzberger, C. Engemann, H. Modrow, O. Schumann, H.G. Trüper, R. Steudel, C. Dahl, J. Hormes, *Biochim. Biophys. Acta* **1999**, *1428*, 446
  223. J.M. Durand, J. Olivier-Fourcade, J.C. Jumas, M. Womes, C.M. Teodorescu, A. Elafif, J.M. Esteva, R.C. Karnatak, *J. Phys. B* **1996**, *29*, 5773
  224. A. Prange, R. Chauvistré, H. Modrow, J. Hormes, H.G. Trüper, C. Dahl, *Microbiology* **2002**, *148*, 267
  225. G.N. George, I.J. Pickering, E.Y. Yu, R.C. Prince, *Microbiology* **2002**, *148*, 2267. A. Prange, C. Dahl, H.G. Trüper, R. Chauvistré, H. Modrow, J. Hormes, *Microbiology* **2002**, *148*, 2268
  226. A. Prange, H. Modrow, *Rev. Environm. Sci. Biotechn.* **2002**, *1*, 259

# Inorganic Polysulfanes $H_2S_n$ with $n > 1$

Ralf Steudel

Institut für Chemie, Sekr. C2, Technische Universität Berlin, 10623 Berlin, Germany  
E-mail: steudel@schwefel.chem.tu-berlin.de

**Abstract** The sulfanes  $H_2S_n$  form a long series of homologous chain-like molecules, starting with hydrogen sulfide and running at least up to  $H_2S_{35}$ . These molecules are the parent compounds of numerous derivatives with either organic or inorganic substituents. In this chapter the preparation, structures, physical and chemical properties as well as the spectra of the sulfanes with  $\geq 2$  sulfur atoms are reviewed. In the literature these species are termed either sulfanes, polysulfanes, or hydrogen polysulfides.

**Keywords** Sulfur hydrides · Molecular structures · Reactivity · Spectra · Acidities · Application

1	Introduction . . . . .	100
2	Preparation. . . . .	102
2.1	General . . . . .	102
2.2	Crude Sulfane Oil (“Rohöl”, “Raw Sulfane”). . . . .	102
2.3	Di-, Tri-, and Tetrasulfane from Crude Sulfane Oil. . . . .	105
2.4	Higher Sulfanes by Condensation Reactions. . . . .	105
2.5	Sulfanes from Silyl Derivatives . . . . .	106
3	Physical Properties. . . . .	106
3.1	Freezing and Boiling Points . . . . .	106
3.2	Densities and Viscosities . . . . .	107
3.3	Thermodynamics . . . . .	107
3.4	Solubility . . . . .	107
4	Molecular Structures . . . . .	108
4.1	Disulfane . . . . .	108
4.2	Trisulfane . . . . .	109
4.3	Tetrasulfane . . . . .	109
4.4	Higher Sulfanes . . . . .	111
4.5	Branched Isomers of the Sulfanes . . . . .	111
5	Molecular Spectra . . . . .	112
5.1	$^1H$ NMR Spectra. . . . .	112
5.2	Vibrational Spectra. . . . .	113
5.2.1	Disulfane . . . . .	113
5.2.2	Trisulfane . . . . .	114
5.2.3	Tetrasulfane . . . . .	114

5.2.4	Higher Sulfanes . . . . .	114
5.3	UV-Vis Spectra . . . . .	115
5.4	Other Spectra . . . . .	115
<b>6</b>	<b>Reactions . . . . .</b>	<b>115</b>
6.1	Thermal and Photochemical Decomposition . . . . .	115
6.1.1	Thermolysis . . . . .	116
6.1.2	Photolysis. . . . .	118
6.2	Protonation and Deprotonation. . . . .	118
6.2.1	Protonation. . . . .	119
6.2.2	Deprotonation. . . . .	119
6.3	Nucleophilic Displacement Reactions . . . . .	120
6.4	Condensation Reactions . . . . .	121
<b>7</b>	<b>Applications . . . . .</b>	<b>122</b>
	<b>References . . . . .</b>	<b>123</b>

### List of Abbreviations

TMS	Tetramethylsilane
XANES	X-ray absorption near edge structure

## 1 Introduction

The rather high bond enthalpy of sulfur-sulfur single bonds as in  $S_8$  ( $264 \text{ kJ mol}^{-1}$ ) has the consequence that numerous compounds exist in which sulfur atoms form homoatomic chains, rings or clusters. The sulfanes or hydrogen polysulfides  $H_2S_n$  are the most basic of these species and all other chain-like sulfur-rich compounds may be considered to be derivatives thereof. For example, the dihalogenosulfanes  $S_nCl_2$  [1], the diorganylsulfanes  $R_2S_n$  [2], the sulfane oxides  $R_2S_nO$  [2, 3], and the inorganic polysulfides  $S_n^{2-}$  [4]. The latter are simply the dianions of the Brønsted acids  $H_2S_n$  and protonation of these anions is a convenient method to prepare sulfane mixtures. The name sulfane has been created in analogy to the boranes, alkanes, silanes, and phosphanes [5].

Mixtures of polysulfanes  $H_2S_n$  are easy to make and probably occur even naturally but the pure compounds are relatively unstable and can therefore be prepared only with some experimental skills and observing certain technical precautions. Detailed prescriptions exist how to make di-, tri-, tetra-, and higher sulfanes in gram quantities. However, as longer the sulfur chain grows as more difficult it becomes to obtain pure compounds. In general, all

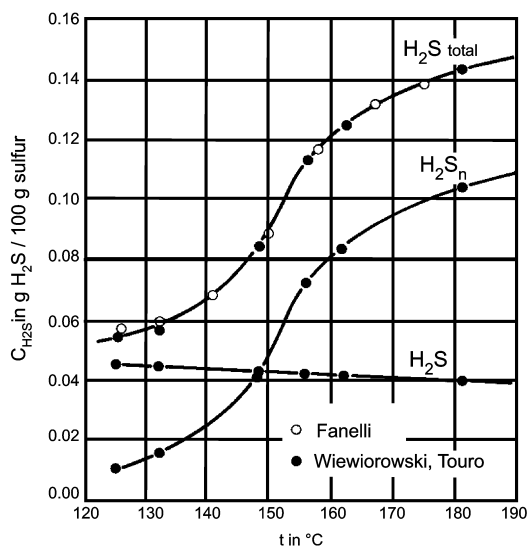
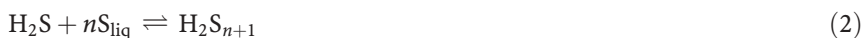


**Fig. 1** Contribution of  $H_2S$  and  $H_2S_n$  to the total solubility of hydrogen sulfide ( $H_2S_{total}$ ) in liquid sulfur as a function of temperature at  $p(H_2S)=1.013$  bar (data from [8, 10])

polysulfanes tend to decompose to elemental sulfur ( $S_8$ ) and hydrogen sulfide:



The  $H_2S$  usually escapes and the sulfur crystallizes; as a consequence the reaction will always be quantitative after long enough reaction times or in the presence of a catalyst. On the other hand, liquid sulfur and  $H_2S$  react to give a mixture of long-chain polysulfanes:



For this reason the solubility of gaseous  $H_2S$  in liquid sulfur dramatically *increases* with increasing temperature in the range 120–200 °C while the (physical) solubility of gases usually *decreases* with increasing temperature [6]. At 150 °C and 1013 mbar equal amounts of  $H_2S$  are dissolved physically and chemically (the latter as  $H_2S_n$  with  $n>5$ ) in liquid sulfur (ca. 420 ppm each) while at 200 °C ca. 400 ppm are dissolved physically and 1100 ppm chemically (1 ppm = 1 mg/1000 g sulfur); see Fig. 1 [7–10]. At higher temperatures a plateau is reached until the solubility decreases again and reaches a minimum at the boiling point (445 °C).

Since hydrogen sulfide and elemental sulfur occur together in hot underground deposits of natural gas (so-called “sour gas”) the formation of sulfur-rich polysulfanes under these high-pressure conditions is very likely. If the gas is produced and in this context the pressure and temperature lowered, the decomposition reaction (Eq. 1) takes place and the precipitated sol-

id elemental sulfur may cause clogging of pipelines and valves creating serious problems [11].

Short reviews on the chemistry of sulfanes have been published in 1968 by Burton and Machmer [12], and in 1973 by Schmidt and Siebert [13]. However, the most comprehensive and reliable review on the chemistry and physics of hydrogen sulfide and the lower sulfanes including the radicals HS· and HS<sub>2</sub>· can be found in Gmelin covering the literature till 1981 [10].

Certain older reports [14] on the existence of extremely sulfur-rich sulfanes in mixtures of high sulfur content obtained from sodium thiosulfate and hydrochloric acid are in error since elemental sulfur was shown to be the main component besides traces of H<sub>2</sub>S<sub>n</sub> [15].

## 2 Preparation

### 2.1

#### General

Sulfanes are very sensitive compounds the decomposition of which is catalyzed by many substances including alkaline materials, nucleophiles, metals, dust, cork, sea sand, magnesium oxide, rough surfaces, and even traces of water. Therefore, all glassware used for the preparation of sulfanes must be carefully cleaned and dried. After rinsing with a mixture of concentrated nitric acid and hydrochloric acid followed by distilled water the glassware should be carefully dried in a dust-free environment. Ground glass joints must be sealed by polysiloxane (silicone) grease. In laboratories where sulfanes are to be prepared there should be neither ammonia cylinders, aqueous ammonia or ammonium sulfide solutions stored [16]. Because of the poor thermal stability of the higher sulfanes sample temperatures above 30 °C should be avoided.

Disulfane is usually made from a sulfane mixture known as crude sulfane oil while various methods are available for the preparation of the higher sulfanes. Deuterated sulfanes may be prepared by isotopic exchange with DCl [17].

### 2.2

#### Crude Sulfane Oil ("Rohöl", "Raw Sulfane")

A mixture of sulfanes is obtained when aqueous sodium polysulfide is rapidly acidified with concentrated hydrochloric acid at low temperatures [16, 18]:



If 50 g of  $\text{Na}_2\text{S}\cdot 9\text{H}_2\text{O}$  are heated with 25 g of  $\text{S}_8$  to ca. 100 °C an aqueous solution of composition  $\text{Na}_2\text{S}_{5.5}$  is obtained which after dilution by 40 ml  $\text{H}_2\text{O}$  is filtered and slowly added to an excess of concentrated aqueous  $\text{HCl}$  ( $c = 6 \text{ mol l}^{-1}$ ) at  $-10$  °C whereupon the water-insoluble  $\text{H}_2\text{S}_n$  precipitates and settles at the bottom of the flask as a yellow oil of camphor-like odor (ca. 25 g). After rinsing the oil with aqueous  $\text{HCl}$  and separation from the aqueous phase some  $\text{P}_4\text{O}_{10}$  is added which stabilizes the sulfane mixture so that it can be stored at 0 °C for several weeks without decomposition. Prior to use the  $\text{P}_4\text{O}_{10}$  is filtered off using a glass frit treated as mentioned above. Crude sulfane does not crystallize on cooling but forms a glass. The gross composition varies between  $\text{H}_2\text{S}_{4.5}$  and  $\text{H}_2\text{S}_7$ .

The molecular composition of crude sulfane oil has been determined by  $^1\text{H}$  NMR spectroscopy after dissolution in  $\text{CS}_2$ ,  $\text{CCl}_4$ , or benzene. The chemical shift of the protons strongly depends on the length of the sulfur chain and on the solvent. All members of the homologous series up to  $\text{H}_2\text{S}_{35}$  have been detected [19]. However, in benzene solution the shift also depends on the concentration. Freshly prepared crude sulfane oil (type "A" in Table 1) consists mainly of tetra-, penta-, hexa-, and trisulfane (in this order decreasing concentrations) with small amounts of hepta-, octa-, nona-, and decasulfane as well as all the higher sulfanes up to  $\text{H}_2\text{S}_{25}$  while di- and monosulfane are present only in traces. From  $\text{H}_2\text{S}_4$  onwards the concentrations decrease with increasing chain-length. In addition, a few percent of  $\text{S}_8$  are present which can be determined by Raman spectroscopy [19].

On aging by storage (even at temperatures as low as  $-60$  °C) the composition of crude sulfane oil changes to type "B" of Table 1. The content of the highest sulfanes up to  $\text{H}_2\text{S}_{35}$  increases as does the  $\text{S}_8$  content. Since these long-chain members are less soluble in benzene a homogeneous mixture in this solvent is obtained only by addition of some  $\text{CS}_2$  which is by far the best solvent for crude sulfane oil [19]. Evidently, the following reactions take place on aging:



Since the chain-lengths of the molecules present in crude sulfane oil is different from the chain-length of the anions in the original sodium polysulfide solution one has to conclude that in addition to the reaction at Eq. (4) the reactions at Eqs. (5) and (6) also take place during the preparation by protonation of the polysulfide anions.

There are a number of other methods to prepare crude sulfane oils, e.g., from liquid  $\text{H}_2\text{S}$  and elemental chlorine or bromine [10] or by reaction of  $\text{H}_2\text{S}$  with sulfur fluorides [10] or sulfur chlorides [20] but these processes are of little practical importance.

**Table 1** Concentration of the sulfanes H<sub>2</sub>S<sub>n</sub><sup>a</sup> and of S<sub>8</sub><sup>b</sup> in two crude sulfane oils “A” and “B” (δ: chemical shift in ppm vs TMS; after [19])

	Oil “A”		Oil “B”	
	δ( <sup>1</sup> H)	mol%	δ( <sup>1</sup> H)	mol%
H <sub>2</sub> S	0.523	0.65	0.466	0.54
H <sub>2</sub> S <sub>2</sub>	2.499	0.94	2.414	0.50
H <sub>2</sub> S <sub>3</sub>	3.842	11.25	3.746	11.21
H <sub>2</sub> S <sub>4</sub>	3.899	28.91	3.799	27.28
H <sub>2</sub> S <sub>5</sub>	4.027	18.11	3.919	16.87
H <sub>2</sub> S <sub>6</sub>	4.120	12.91	4.014	11.06
H <sub>2</sub> S <sub>7</sub>	4.148	7.88	4.039	7.03
H <sub>2</sub> S <sub>8</sub>	4.177	5.18	4.067	4.87
H <sub>2</sub> S <sub>9</sub>	4.182	4.03	4.072	3.90
H <sub>2</sub> S <sub>10</sub>	4.195	2.62	4.080	3.12
H <sub>2</sub> S <sub>11</sub>	4.205	1.71	4.088	2.08
H <sub>2</sub> S <sub>12</sub>	4.212	1.20	4.092	1.57
H <sub>2</sub> S <sub>13</sub>	4.221	0.75	4.099	1.13
H <sub>2</sub> S <sub>14</sub>	4.229	0.53	4.106	0.81
H <sub>2</sub> S <sub>15</sub>	4.237	0.37	4.112	0.62
H <sub>2</sub> S <sub>16</sub>	4.246	0.26	4.120	0.46
H <sub>2</sub> S <sub>17</sub>	4.253	0.16	4.126	0.34
H <sub>2</sub> S <sub>18</sub>	4.261	0.14	4.133	0.26
H <sub>2</sub> S <sub>19</sub>	4.268	0.09	4.139	0.20
H <sub>2</sub> S <sub>20</sub>	4.274	0.07	4.145	0.15
H <sub>2</sub> S <sub>21</sub>	4.280	0.04	4.151	0.11
H <sub>2</sub> S <sub>22</sub>	4.286	0.03	4.156	0.09
H <sub>2</sub> S <sub>23</sub>	4.291	0.03	4.160	0.07
H <sub>2</sub> S <sub>24</sub>	4.296	0.02	4.165	0.06
H <sub>2</sub> S <sub>25</sub>	4.301	0.02	4.169	0.05
H <sub>2</sub> S <sub>26</sub>			4.735	0.04
H <sub>2</sub> S <sub>27</sub>			4.776	0.03
H <sub>2</sub> S <sub>28</sub>			4.181	0.03
H <sub>2</sub> S <sub>29</sub>			4.185	0.02
H <sub>2</sub> S <sub>30</sub>			4.189	0.02
H <sub>2</sub> S <sub>31</sub>			4.192	0.02
H <sub>2</sub> S <sub>32</sub>			4.196	0.02
H <sub>2</sub> S <sub>33</sub>			4.199	0.02
H <sub>2</sub> S <sub>34</sub>			4.202	0.01
H <sub>2</sub> S <sub>35</sub>			4.205	0.01
S <sub>8</sub>		2.1		5.4

<sup>a</sup> By integration of the <sup>1</sup>H NMR signals (sample A: homogeneous mixture of oil A and C<sub>6</sub>D<sub>6</sub> in a volume ratio of 3:2; sample B: homogeneous mixture of oil B, C<sub>6</sub>D<sub>6</sub> and CS<sub>2</sub> in a volume ratio of 1:1:0.42)

<sup>b</sup> Determined by Raman spectroscopy

### 2.3

#### Di-, Tri-, and Tetrasulfane from Crude Sulfane Oil

Disulfane is prepared by thermal cracking of crude sulfane oil and simultaneous distillation. As mentioned above, crude sulfane oil does not contain substantial amounts of disulfane [19] but it is the decomposition that generates the lower sulfanes with one to three sulfur atoms by thermal cracking reactions; the heat sensitive products are immediately distilled off [16, 21]. Obviously, the reactions shown in Eqs. (5) and (6) take place. A relatively simple apparatus for the cracking-distillation process has been described by Hahn et al. [21]; it consists of a rotary evaporator connected to a vertical multiple coil condenser and several traps. The crude sulfane oil is cracked at 80 °C/16 mbar (100 Pa) in the rotating flask (oil bath). The most volatile products H<sub>2</sub>S and H<sub>2</sub>S<sub>2</sub> pass through the condenser and are collected in traps cooled to -78 °C and -196 °C, respectively, while trisulfane and higher sulfanes condense in the vertical condenser (cooled to -10 °C) and are collected separately. From 140 ml crude sulfane oil 30 ml of disulfane were obtained [21]. Using a more sophisticated equipment it is possible to prepare di-, tri-, and tetrasulfane from crude sulfane oil. In each case, the products have to be purified by distillation in a vacuum [16, 22-24].

Trace amounts of disulfane have been obtained in the gas phase by recombination of HS· radicals generated by oxidation of hydrogen sulfide by oxygen atoms which in turn are produced from molecular oxygen in a microwave discharge [25]:

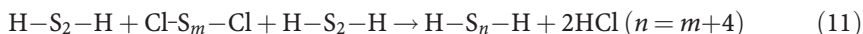
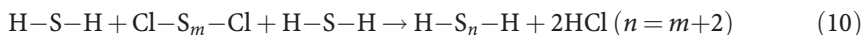


Side products of this reaction are SO and S<sub>2</sub>O.

### 2.4

#### Higher Sulfanes by Condensation Reactions

The higher sulfanes H<sub>2</sub>S<sub>*n*</sub> with *n*>3 are usually prepared by condensation reactions since their volatility is low and vacuum distillation is difficult if not impossible. The starting products are the lower sulfanes and certain dichlorosulfanes S<sub>*m*</sub>Cl<sub>2</sub> which provide all members up to octasulfane by reactions of the following types:



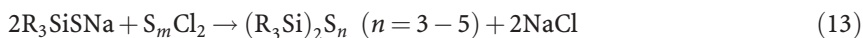
The liquid components are mixed at -78 °C. To suppress side reactions the sulfane component is applied in a large excess (>10:1). The unreacted starting sulfane and hydrogen chloride are distilled off after the reaction has

been completed at 0 °C. No solvent is used [16, 26–28]. Evidently, this procedure will not produce sulfanes of analytical purity since the products may also react with the starting materials producing even higher sulfanes. However, for preparative purposes the purity is usually sufficient.

## 2.5

### Sulfanes from Silyl Derivatives

Hahn and Altenbach designed a method to prepare specific sulfanes with 2 to 5 sulfur atoms in small quantities in solution by the following reactions ( $R_3Si = MePh_2Si$ ) [29]:



Reactions at Eqs. (12) and (13) are carried out in toluene solution. The yellow crystalline products are purified by recrystallization from pentane and stored in a dry atmosphere at  $-20$  °C. Reaction at Eq. (14) takes place slowly at 20 °C in benzene. The sulfane product  $H_2S_n$  is separated from the silylester side product by distillation together with the benzene solvent (in the case of  $n=2-4$ ) or by phase separation (for  $n=4, 5$ ). For certain preparative purposes the ester and the solvent may not interfere. If deuterated trifluoroacetic acid is used in the reaction at Eq. (14) the fully deuterated sulfane is obtained [29].

## 3

### Physical Properties

#### 3.1

##### Freezing and Boiling Points

The sulfanes  $H_2S_2$  to  $H_2S_8$  which have been prepared as more or less pure substances are yellow liquids at 20 °C. The intensity of the color increases with the sulfur content.  $H_2S_2$  freezes at  $-90$  °C,  $H_2S_3$  at  $-53$  °C and  $H_2S_4$  at  $-85$  °C. For the higher sulfanes neither freezing nor boiling points are known due to the thermal instability and the tendency to form glasses on cooling [16]. However, from vapor pressure measurements the boiling points at 1.013 bar (0.101 MPa) have been estimated as follows using the Clausius-Clapeyron equation [30]:



**Table 2** Density (g cm<sup>-3</sup>) and dynamic viscosity (mPa s) of liquid sulfanes at 20 °C

Sulfane	Density	Viscosity
H <sub>2</sub> S <sub>2</sub>	1.334	0.616
H <sub>2</sub> S <sub>3</sub>	1.491	1.32
H <sub>2</sub> S <sub>4</sub>	1.582	2.63
H <sub>2</sub> S <sub>5</sub>	1.644	5.52
H <sub>2</sub> S <sub>6</sub>	1.688	11.0
H <sub>2</sub> S <sub>7</sub>	1.721	22.8
H <sub>2</sub> S <sub>8</sub>	1.744	46.8

### 3.2

#### Densities and Viscosities

The densities *d* and dynamic viscosities  $\eta$  of the sulfanes at 20 °C are given in Table 2. The densities expectedly increase with the chain-length [31] as does the viscosity which practically doubles with each additional sulfur atom [24, 27, 32]. There is a linear relationship between log  $\eta$  and the number of sulfur atoms in the molecule.

### 3.3

#### Thermodynamics

Fehér and Hitzemann [30] determined the enthalpies of evaporation  $\Delta_v H^\circ_{293}$  of the sulfanes H<sub>2</sub>S<sub>*n*</sub> with *n*=2–5 calorimetrically. Interestingly, there exists a linear relationship between  $\Delta_v H^\circ_{293}$  (in kJ mol<sup>-1</sup>) and the number of sulfur atoms:

$$\Delta_v H^\circ_{293} = 10.67 + 11.54 \cdot n$$

The dissociation enthalpies for the SS and SH bonds of the lower sulfanes have been determined by high-level ab initio MO calculations. For gaseous disulfane  $D^\circ(\text{SH})=313$  kJ mol<sup>-1</sup> and  $D^\circ(\text{SS})=271$  kJ mol<sup>-1</sup> were obtained at 0 K by the G2(MP2) method [33]. At the CCSD(T)/6-311++G(2df,p)//MP2/6-311++G\*\* level of theory the following SS bond dissociation energies at 0 K were calculated: H<sub>2</sub>S<sub>2</sub> 260, H<sub>2</sub>S<sub>3</sub> 212, H<sub>2</sub>S<sub>4</sub> 169 kJ mol<sup>-1</sup> (central bond) [34].

### 3.4

#### Solubility

The sulfanes are soluble in carbon disulfide, benzene, tetrachloromethane, and dry diethylether (decreasingly so in that order) while alcohols and aqueous systems initiate rapid decomposition. For this reason a report on the chromatographic separation of the sulfanes H<sub>2</sub>S<sub>*n*</sub> by reversed-phase HPLC using methanol as an eluent [35] was shown to be in error: The peaks observed in the chromatogram have to be assigned to bismethoxy oligosulfanes

(MeO)<sub>2</sub>S<sub>n</sub> [36]. These evidently originated from the reaction of the dichlorosulfanes with the methanol solvent used in the preparation of the “sulfanes” by mixing sodium polysulfide with dichlorosulfanes.

## 4 Molecular Structures

Only the structures of di- and trisulfane have been determined experimentally. For a number of other sulfanes structural information is available from theoretical calculations using either density functional theory or ab initio molecular orbital theory. In all cases the unbranched chain has been confirmed as the most stable structure but these chains can exist as different rotamers and, in some cases, as enantiomers. However, by theoretical methods information about the structures and stabilities of additional isomeric sulfane molecules with branched sulfur chains and cluster-like structures was obtained which were identified as local minima on the potential energy hypersurface (see later).

### 4.1 Disulfane

The molecular conformation of gaseous disulfane is analogous to the structure of hydrogen peroxide. Both molecules are of C<sub>2</sub> symmetry and therefore chiral. The two enantiomers differ just in the signs of the torsional angles. The molecular structure of H<sub>2</sub>S<sub>2</sub> has been studied by electron diffraction [37] as well as by microwave spectroscopy [21, 38]. The parameters from [21] shown in Table 3 have been derived using additional data of partially deuterated disulfane. They agree best with the results of theoretical calculations [34] and, therefore, seem to be the most reliable data.

The barriers for the rotation around the SS bond have been estimated from microwave data [40] and ab initio MO calculations [41, 42] as 34–36 kJ mol<sup>-1</sup> (*cis*-barrier) and 24–25 kJ mol<sup>-1</sup> (*trans*-barrier), respectively. They are explained as the result of three effects: First, the repulsion of the two 3*p* lone pairs at the sulfur atoms is lowest for τ=90°. Second, the 3*p* lone pair electrons are partly delocalized into the antibonding σ\* orbitals of the SH bonds originating from the neighboring sulfur atom. This hyperconjugation or π bond is at its maximum for τ=90° but disappears for τ=0° and 180°. Third,

**Table 3** Geometrical parameters of gaseous disulfane (H<sub>2</sub>S<sub>2</sub> and D<sub>2</sub>S<sub>2</sub>)

Method	<i>d</i> <sub>SS</sub> (pm)	<i>d</i> <sub>SH</sub> (pm)	α(SSH)	τ(HSSH)	Reference
Electron diffraction on H <sub>2</sub> S <sub>2</sub>	205.5(1)	132.7	92.0(5)°	90.60°	[37]
MW spectroscopy of D <sub>2</sub> S <sub>2</sub>	205.5(1)	132.4(3)	91.3(5)°	90.23(3)	[38]
MW and FTIR spectroscopy on H <sub>2</sub> S <sub>2</sub> , HDS <sub>2</sub> and D <sub>2</sub> S <sub>2</sub>	205.64(1)	134.21(2)	97.88(5)°	90.3(2)°	[21, 39]

**Table 4** Geometrical parameters of two conformational isomers of gaseous trisulfane (r<sub>e</sub> bond lengths; data from ref. [17])

	d <sub>SS</sub> (pm)	d <sub>SH</sub> (pm)	α(SSH)	β(SSS)	τ(HSSS)
<i>cis</i> -H <sub>2</sub> S <sub>3</sub>	205.30(1)	134.35(14)	97.37(15) <sup>o</sup>	106.919(3) <sup>o</sup>	90.82(16) <sup>o</sup>
<i>trans</i> -H <sub>2</sub> S <sub>3</sub>	205.39(4)	(134.35) <sup>a</sup>	97.2(7) <sup>o</sup>	107.02(2) <sup>o</sup>	87.7(4) <sup>o</sup>

<sup>a</sup> Assumed value

the hydrogen atoms repel each other and this effect is maximum at  $\tau=0^\circ$ ; therefore, the *cis*-barrier is substantially higher than the *trans*-barrier [41, 43, 44].

## 4.2

### Trisulfane

The trisulfane molecule exists as two conformers which have been termed as *cis*- and *trans*-H<sub>2</sub>S<sub>3</sub>. While the *trans*-form is a helical molecule of C<sub>2</sub> symmetry with the motif ++ (or – – for the enantiomer), the *cis*-form is of C<sub>s</sub> symmetry with the motif +- (identical to -+). Both forms have been detected by rotational spectroscopy [17, 45, 46]. The motif gives the order of the signs of the torsion angles at the SS bonds. The geometrical parameters [17] are presented in Table 4. The *trans*-isomer is by only 1 kJ mol<sup>-1</sup> more stable than the *cis*-form but the barrier to internal rotation from *trans* to *cis* is 35 kJ mol<sup>-1</sup> [46]. The dipole moments were calculated by ab initio MO theory at the QCISD/TZ+P level as 0.68 D (*trans*) and 2.02 D (*cis*) [46]. For geometrical parameters of *cis*- and *trans*-trisulfane calculated at the MP2/6-311++G\*\* level, see [34].

## 4.3

### Tetrasulfane

The molecule H<sub>2</sub>S<sub>4</sub> exists as three conformers with the motifs (symmetries) +++(C<sub>2</sub>), ++-(C<sub>1</sub>), and +-(C<sub>2</sub>); see Fig. 2.

According to ab initio MO calculations at the MP2/6-311G\*\*//MP2/6-311G\*\* level of theory the conformer of C<sub>1</sub> symmetry (motif + + -) is the most stable one at 0 K, followed by the C<sub>2</sub> form with the motif + - + which is by only 0.4 kJ mol<sup>-1</sup> less stable [47]. The helical form of C<sub>2</sub> symmetry is by 0.7 kJ mol<sup>-1</sup> less stable than the C<sub>1</sub> form. The activation energies for the rotation about the central SS bond are 32 kJ mol<sup>-1</sup> for the *cis*-barrier and 27 kJ mol<sup>-1</sup> for the *trans*-barrier [47]. At the G2 level of theory the Gibbs energy difference at 298 K between the isomers of motifs + + - (most stable; C<sub>1</sub> symmetry) and + - + (C<sub>2</sub>) is 0.9 kJ mol<sup>-1</sup> [48].

The geometrical parameters of the three isomers of H<sub>2</sub>S<sub>4</sub> are rather similar excepting the signs of the torsional angles. The following data were obtained at the MP2/6-311G\*\* level: d<sub>SS</sub>=207.3–207.7 pm, d<sub>SH</sub>=133.7–133.8 pm, α(HSS)=97.3–98.0°, β(SSS)=106.8–107.4°, τ(HSSS)=82.9–92.3°, τ(SSSS)=

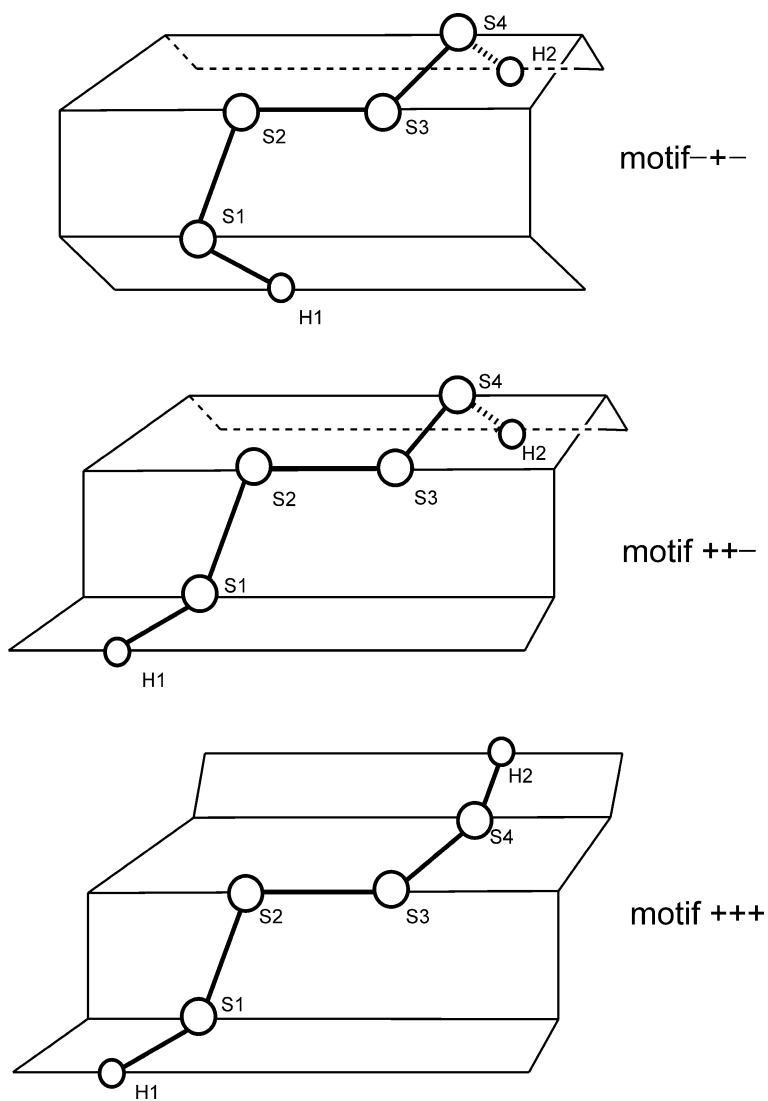


**Fig. 2** Three conformational isomers of the tetrasulfane molecule  $\text{H}_2\text{S}_4$  differing by the signs of the torsional angles at the three SS bonds (after [47])

79.9–80.5° [47]. Very similar values were calculated at the MP2(full)/6-31G\* level [48] and at the MP2/6-311++G\*\* level [34]. No experimental structure determination has been reported for tetrasulfane.

#### 4.4

##### Higher Sulfanes

No experimental studies on the molecular structures of the higher polysulfanes  $H_2S_n$  with  $n > 4$  are known but a number of ab initio MO calculations on these molecules have been published. Of these, only those will be cited here which used a decent level of theory by today's standards. In particular, the correction for electron correlation has to be included in the geometry optimization. The rotational isomerism of the sulfur chains gets more and more complex as the chain-length increases. In theory,  $2^m$  permutations for the signs of the torsion angles exist for a sulfane molecule with  $m$  S-S bonds. Of these, all molecules of  $C_n$  symmetry ( $n=1, 2$ ) will be chiral. However, only the helical isomers of  $C_2$  symmetry have so far been calculated at a high level, for example  $H_2S_5$  and  $H_2S_6$  [42].

#### 4.5

##### Branched Isomers of the Sulfanes

By ab initio MO and density functional theoretical (DFT) calculations it has been shown that the branched isomers of the sulfanes are local minima on the particular potential energy hypersurface. In the case of disulfane the thiosulfide isomer  $H_2S=S$  of  $C_s$  symmetry is by 138 kJ mol<sup>-1</sup> less stable than the chain-like molecule of  $C_2$  symmetry at the QCISD(T)/6-31+G\*\*//MP2/6-31G\*\* level of theory at 0 K [49]. At the MP2/6-311G\*\*//MP2/6-311G\*\* level the energy difference is 143 kJ mol<sup>-1</sup> and the activation energy for the isomerization is 210 kJ mol<sup>-1</sup> at 0 K [50]. Somewhat smaller values (117/195 kJ mol<sup>-1</sup>) have been calculated with the more elaborate CCSD(T)/ANO-L method [50]. The high barrier of ca. 80 kJ mol<sup>-1</sup> for the isomerization of the pyramidal  $H_2S=S$  back to the screw-like disulfane structure means that the thiosulfide, once it has been formed, will not decompose in an unimolecular reaction at low temperature, e.g., in a matrix-isolation experiment. The transition state structure is characterized by a hydrogen atom bridging the two sulfur atoms.

The symmetrical thiosulfide isomer of tetrasulfane  $(HS)_2S=S$  is also of  $C_s$  symmetry and by 123 kJ mol<sup>-1</sup> less stable than the chain-like ground state of  $C_2$  symmetry (at the MP2/6-31G\*\*//HF/4-31G\* level of theory) [51]. However, at the much higher G3(MP2) level the energy difference is only 93 kJ mol<sup>-1</sup> [52]. Similarly, the two hexasulfane isomers  $(HSS)_2S=S$  ( $C_s$  symmetry) and  $(HS)(HSSS)S=S$  ( $C_1$  symmetry) have recently been calculated at the G3X(MP2) level to be by 53 and 54 kJ mol<sup>-1</sup>, respectively, less stable than the helical chain of  $C_2$  symmetry [52]. The decreasing energy difference be-

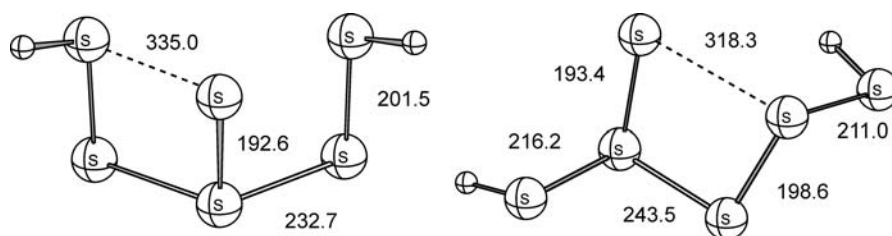


**Fig. 3** Structures of two branched isomers of hexasulfane  $\text{H}_2\text{S}_6$  calculated at the B3LYP/6-31G(2df) level of theory (internuclear distances in pm) [52]

tween helical and cluster-like conformations is explained by the stabilization of the latter by  $\pi^*-\pi^*$  bonds between the sulfur atoms (see Fig. 3).

The activation energies for the formation of the branched species from the unbranched chains are not known yet but will be ca. 200  $\text{kJ mol}^{-1}$  according to calculations on a related cyclic organic pentasulfane (pentathiepin) [53].

## 5 Molecular Spectra

The most important analytical tool to characterize sulfane molecules is  $^1\text{H}$  NMR spectroscopy followed by Raman spectroscopy while the UV-Vis spectra are rather uncharacteristic.

### 5.1 $^1\text{H}$ NMR Spectra

Schmidbaur et al. discovered in 1964 that the sulfanes  $\text{H}_2\text{S}_n$  with  $n=1-6$  can be detected in solution by their  $^1\text{H}$  NMR spectra (60 MHz) since the chemical shifts are sufficiently different [54]. These shifts depend somewhat on the solvent but change monotonically towards lower fields with increasing number of sulfur atoms, e.g., in  $\text{CCl}_4$  (values in ppm):  $\text{H}_2\text{S}$  0.67,  $\text{H}_2\text{S}_2$  2.63,  $\text{H}_2\text{S}_3$  3.98,  $\text{H}_2\text{S}_4$  4.00,  $\text{H}_2\text{S}_5$  4.14. At that time the peaks originating from the species  $\text{H}_2\text{S}_{>6}$  could not be resolved enough to make a definite assignment. Nevertheless, it became possible to determine the approximate molecular composition of crude sulfane mixtures and to check the purity of so-called pure sulfane samples. This technique has later been applied to solutions of the lower sulfanes in liquid sulfur which eventually results in the formation of equilibrium mixtures of very long-chain polysulfanes; see Eq. (2) [8]. These solutions were made either by reaction of  $\text{H}_2\text{S}$  with liquid sulfur at 180  $^\circ\text{C}$  for 24 h (type "A") or by dissolution of crude sulfane oil in liquid sulfur at 130  $^\circ\text{C}$  (type "B"). The samples were measured at 130  $^\circ\text{C}$  with TMS as external standard. The  $\text{H}_2\text{S}$  solution showed only signals of higher polysulfanes ( $n \gg 5$ ) and  $\text{H}_2\text{S}$  while the sample of type "B" initially exhibited signals of

the lower sulfanes but these disappeared within 100 h in favor of the signal of the long-chain  $H_2S_n$  species [8].

The most elaborate investigation of the proton NMR spectra of polysulfanes in various solvents and in crude sulfane oil has been published by Hahn [19] who succeeded to resolve the signals of all members up to  $H_2S_{35}$  in mixtures using a 300 MHz spectrometer. The downfield shift differences of the higher members are almost constant but the absolute shift values depend strongly on the concentration (especially in benzene) as well as on the solvent which has been explained by hydrogen bonding between the sulfane molecules and/or between benzene and sulfane molecules (see Table 1).

## 5.2

### Vibrational Spectra

Infrared and Raman spectra of the lower sulfanes as well as of sulfane mixtures and of crude sulfane oil have been published. Obtaining reliable infrared spectra is relatively unproblematic but the formation of hydrogen bonds to certain solvents and between sulfane molecules has to be taken into account. The latter effect results in a certain dependence of the SH stretching and bending vibrations on the concentration. Reliable Raman spectra, on the other hand, can only be obtained if the light-sensitivity of the sulfanes is taken into account which means that blue and green laser lines must not be used while red lines (e.g., krypton ion laser) or infrared lines (Nd:YAG laser) can be recommended. Furthermore, the samples should be cooled to ca.  $-100\text{ }^\circ\text{C}$  to prevent thermal and photochemical decomposition. The low temperature at the same time results in narrower lines and therefore a better resolution. In the older literature (prior to 1970) Raman spectra excited with the green line of a mercury lamp have been described and the spectra of the sulfanes accordingly show the lines of the decomposition product  $S_8$  in addition. Fortunately, some of the Raman lines of  $S_8$  do not interfere with the sulfane spectra thus allowing the quantitative determination of  $S_8$  dissolved in sulfanes by Raman spectroscopy.

#### 5.2.1

##### *Disulfane*

The vibrational spectra of  $H_2S_2$  and  $D_2S_2$  have been studied both in the gas phase and in solution. Table 5 summarizes the results for gaseous  $H_2S_2$  [55], liquid  $H_2S_2$  [56], and gaseous  $D_2S_2$  [56]. Although in the pointgroup  $C_2$  all fundamental modes are both infrared active and Raman allowed, their intensities in the two types of spectra are quite different. While  $\nu_1$ ,  $\nu_4$ ,  $\nu_5$ , and  $\nu_6$  are strong in the infrared spectrum,  $\nu_2$  and  $\nu_3$  are best observed by Raman spectroscopy.

For harmonic wavenumbers and force constants, see [57].

**Table 5** Vibrational spectra of H<sub>2</sub>S<sub>2</sub> and D<sub>2</sub>S<sub>2</sub> observed by infrared spectroscopy

Symmetry class	No.	Type of mode	H <sub>2</sub> S <sub>2</sub> (gas)	H <sub>2</sub> S <sub>2</sub> (liquid)	D <sub>2</sub> S <sub>2</sub> (gas)
A	$\nu_1$	SH stretch	2556	2505	
A	$\nu_2$	SH bend	883		
A	$\nu_3$	SS stretch	517		
A	$\nu_4$	Torsion	417	420	306
B	$\nu_5$	SH stretch	2559	2505	1863
B	$\nu_6$	SH bend	880	870	646

### 5.2.2

#### *Trisulfane*

The infrared and Raman spectra of trisulfane have been assigned assuming a molecular  $C_2$  symmetry [58]. Due to strong coupling between bending and torsion modes the assignment given in Table 6 should be considered as only approximate.

### 5.2.3

#### *Tetrasulfane*

The infrared and Raman spectra of dissolved tetrasulfane have been assigned assuming a molecular  $C_2$  symmetry [58]. Due to strong coupling between bending and torsion modes the assignment given in Table 7 is only approximate. However, the assignment is supported by the results of high-level ab initio MO calculations [47].

### 5.2.4

#### *Higher Sulfanes*

Older Raman data obtained using a mercury lamp are available for the sulfanes H<sub>2</sub>S<sub>*n*</sub> (*n*=5–8) and for crude sulfane oil. However, there is some suspicion that the lines observed near 150 and 217 cm<sup>-1</sup> result from S<sub>8</sub> as a by-product of the preparation reactions or as a photochemical decomposition

**Table 6** Vibrational spectra of trisulfane (after [58]; wavenumbers in cm<sup>-1</sup>)

Symmetry class	IR (in CCl <sub>4</sub> )	Raman (in CS <sub>2</sub> )	Assignment
A	2540		SH stretch
A	868	867	SSH bend
A	487	488	SS stretch
A		320	SSSH torsion
A		211	SSS bend
B	2532		SH stretch
B	856	857	SSH bend
B	477	470	SS stretch
B		320	SSSH torsion

**Table 7** Vibrational spectra of tetrasulfane (after [58]; wavenumbers in  $cm^{-1}$ )

Symmetry class	IR (in $CCl_4$ )	Raman (in $CS_2$ )	Assignment
A	2450		SH stretch
A	863	864	SSH bend
A		484	SS stretch
A	450	454	SS stretch
A		320	SSSH torsion
A		184	SSS bend
A		77	SSSS torsion
B	2532		SH stretch
B	851	854	SSH bend
B	487		SS stretch
B		320	SSSH torsion
B		225	SSS bend

product [24, 27, 59]. For more recent infrared and laser Raman spectra of crude sulfane (also containing some  $S_8$ ), see [15].

### 5.3

#### UV-Vis Spectra

Fehér and Münzner [60] recorded the UV-Vis spectra (200–400 nm) of the sulfanes  $H_2S_n$  with  $n=1-8$  in cyclohexane. The spectra are characterized by a strong absorption in the region 200–230 nm and a slow decrease of the extinction coefficient towards longer wavelengths. As longer the sulfur chain, as higher the molar absorbance at a given wavelength and as more red-shifted the spectra become. In the 260–330 region there is also an absorption maximum or a broad plateau which gets more and more pronounced as more sulfur atoms are present.

### 5.4

#### Other Spectra

The ionization energy of gaseous disulfane has been determined by photoionization efficiency spectroscopy as  $9.40 \pm 0.02$  eV [25] and by photoelectron spectroscopy as 9.41 eV [61]. Recently, XANES spectra of  $H_2S$  and  $H_2S_2$  have been reported which show distinct differences [62].

## 6

### Reactions

#### 6.1

##### Thermal and Photochemical Decomposition

All sulfane molecules are thermally and photochemically sensitive and tend to decompose into hydrogen sulfide and elemental sulfur ( $S_8$ ). As mentioned

earlier this reaction is accelerated by many substances. While the enthalpies of formation of the lower sulfanes are all negative at standard conditions (liquid sulfanes), the decomposition according to Eq. (1) is always exothermic. In other words, the sulfanes are metastable compounds. Even if the hydrogen sulfide is not allowed to escape (as in a calorimetric steel bomb) the reaction at Eq. (1) goes to completion at 298 K, especially in the presence of a catalyst like MgO [63]. In this way the standard enthalpies of formation (from H<sub>2</sub> and orthorhombic S<sub>8</sub>) have been determined as follows (kJ mol<sup>-1</sup>) [63]:



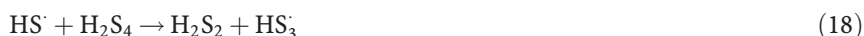
### 6.1.1

#### *Thermolysis*

The decomposition of tri- and tetrasulfane in CCl<sub>4</sub> solution (0.2 mol l<sup>-1</sup>) at 70 °C and in the absence of oxygen has been studied by <sup>1</sup>H NMR spectroscopy [64]. Initially, tetrasulfane decomposes to a mixture of tri- and pentasulfane but slowly and after an induction period hydrogen sulfide and disulfane are formed in addition. These results have been interpreted in terms of a radical-chain reaction. The initial step is assumed to be the homolytic cleavage of the central SS bond which has by far the lowest dissociation enthalpy of the molecule:



The further products depend on the site at which the generated radicals attack the starting material:



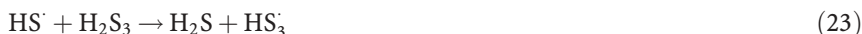
Only HS<sup>·</sup> radicals are able to abstract hydrogen atoms from sulfanes:



Recombination of the radicals may also occur. After about 200 h the composition of the solution was about the same as for the trisulfane decomposition but the final products were just H<sub>2</sub>S and S<sub>8</sub>.

The initial products in the trisulfane decomposition are H<sub>2</sub>S<sub>4</sub> and approximately equal amounts of H<sub>2</sub>S and H<sub>2</sub>S<sub>2</sub>. This reaction is much faster than the tetrasulfane decomposition despite the higher dissociation enthalpy. Therefore, it was assumed that the radicals formed in the initial step are more reactive [64]:





It should be pointed out however that there is no proof for the intermediate formation of free radicals and other mechanisms may explain the product distribution equally well. Such an alternative may be an ionic mechanism, possibly catalyzed by impurities or the walls of the container. In the above experiments Pyrex tubes were used [64].

The SS bond dissociation energies ( $\Delta E^0$ ) at 298 K are 247 kJ mol<sup>-1</sup> for disulfane, 201 kJ mol<sup>-1</sup> for trisulfane, and 159 kJ mol<sup>-1</sup> for the central bond of tetrasulfane, all calculated at the CCSD(T)/6-311++G(2df,p)//MP2/6-311G\*\* level of theory. The corresponding Gibbs energies for these reactions are 212, 157, and 112 kJ mol<sup>-1</sup>, respectively [34].

In the literature tetrathiosulfuranes have been discussed as possible intermediates in the thermal decomposition of sulfanes and other polysulfur compounds. High-level ab initio MO calculations have in fact revealed that such species are local minima on the potential energy hypersurface [34]. However, recent results show that both the Gibbs reaction energies as well as the activation enthalpies for reactions of the type



are higher than the bond dissociation energies of the starting materials [34]. Therefore, tetrathiosulfuranes can be ruled out as intermediates in the interconversion reactions discussed in this chapter.

Fehér and Weber [65] have shown that liquid disulfane on heating to 50 °C decomposes initially according to Eq. (25):

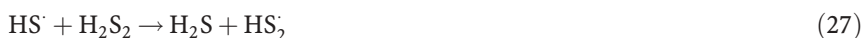


As the reaction proceeds higher sulfanes and finally S<sub>8</sub> are formed. The reaction is autocatalytic which makes any kinetic analysis difficult. The authors discussed a number of reaction mechanisms which are, however, obsolete by today's standards. Also, the reported Arrhenius activation energy of 107±17 kJ mol<sup>-1</sup> is questionable since it was derived from the study of the decomposition of a mixture of disulfane and higher sulfanes. Nevertheless, the observed autocatalytic behavior may be explained by the easier homolytic SS bond dissociation of the higher sulfanes formed as intermediate products compared to the SS bond of disulfane (see above). The free radicals formed may then attack the disulfane molecule with formation of H<sub>2</sub>S on the one hand and higher and higher sulfanes on the other hand from which eventually an S<sub>8</sub> molecule is split off.

### 6.1.2

#### Photolysis

Flash photolysis of either  $\text{H}_2\text{S}$  [66] or  $\text{H}_2\text{S}_2$  [67, 68] in the gas phase at low partial pressures produces, inter alia,  $\text{HS}_2\cdot$  radicals which were detected by their UV absorption spectrum in the 307–380 nm region. In addition, singlet and triplet  $\text{S}_2$  molecules as well as  $\text{SH}\cdot$  radicals are formed from  $\text{H}_2\text{S}_2$ , and the following reaction mechanism has been proposed (photolysis in the region 200–300 nm in the presence of excess  $\text{CO}_2$ ) [67]:



Irradiation of disulfane in an argon matrix at 7.5 K by photons of wavelength 266 nm resulted in dissociation according to the following equations in an approximate 1:1 ratio [69]:



The  $\text{HS}_2\cdot$  radical was detected by its infrared absorption spectrum and the  $\text{S}_2$  molecule by luminescence spectroscopy. In addition, infrared bands assigned to dimers of disulfane molecules were observed at higher  $\text{H}_2\text{S}_2$  concentrations. The  $\text{HS}_2\cdot$  radicals may further be split into hydrogen atoms and  $\text{S}_2$  molecules during the photolysis since the concentration of  $\text{HS}_2\cdot$  first increases and then decreases while that of  $\text{S}_2$  steadily increases. No evidence for the thiosulfoxide  $\text{H}_2\text{S}=\text{S}$  was found, and the probably formed  $\text{HS}\cdot$  radicals are assumed to be unable to leave their cage in the matrix and either recombine to  $\text{H}_2\text{S}_2$  or form  $\text{H}_2+\text{S}_2$  [69].

## 6.2

### Protonation and Deprotonation

Interestingly, the sulfanes  $\text{H}_2\text{S}_n$  are both proton acceptors and donors. In the first case sulfonium ions  $\text{H}_3\text{S}_n^+$  are formed, in the second case hydrogen polysulfide anions  $\text{HS}_n^-$  are the result. While the latter have never been isolated in salts, several salts with sulfonium cations derived from the sulfanes with  $n = 1, 2,$  and  $4$  have been published. However, none of these salts has been structurally characterized by a diffraction technique. Therefore, the structures of the  $\text{H}_3\text{S}_n^+$  cations and  $\text{HS}_n^-$  anions are known from theoretical calculations only.

### 6.2.1

#### Protonation

In an extensive ab initio MO study the structures, energies and vibrational spectra of the sulfonium ions H<sub>3</sub>S<sub>*n*</sub><sup>+</sup> with *n*=1–4 were studied at the MP2/6-311(2df,2pd) level of theory [70]. It was confirmed that H<sub>3</sub>S<sup>+</sup> is of C<sub>3v</sub> symmetry with *d*<sub>SH</sub>=134.6 pm and bond angles of 94.2°. This cation had previously been isolated as a component of the salt [H<sub>3</sub>S][SbF<sub>6</sub>] [71] and had been observed spectroscopically [72]. The experimental gas phase *r*<sub>e</sub> geometry is *d*<sub>SH</sub>=135.02 pm and α<sub>HSH</sub>=94.189° [72] which agrees well with the ab initio calculated values by Botschwina et al.: *d*<sub>SH</sub>=135.0 pm, α<sub>HSH</sub>=94.2° [73].

The cation [H<sub>2</sub>S-SH]<sup>+</sup> derived from disulfane is of C<sub>s</sub> symmetry with an SS bond of length 206.4 pm and the hydrogen atoms in a *transoid* configuration [70]. This ion is contained in the salts [H<sub>3</sub>S<sub>2</sub>][AsF<sub>6</sub>] [74] and [H<sub>3</sub>S<sub>2</sub>][SbF<sub>6</sub>] [75]. At the (rather low) SCF/4-31G\* level of theory the rotational barrier of [H<sub>2</sub>S-SH]<sup>+</sup> has been studied and the maximum energy was obtained at torsional angles close to 90° and 270° (a torsion angle of 180° was assigned to the ground state conformation of C<sub>s</sub> symmetry) [76]. The barrier for the shift of the excess proton from one sulfur atom to the other has been calculated as 160 kJ mol<sup>-1</sup> at the MP4/6-31G\*\*/HF/6-31G\* level of theory; the transition state is of C<sub>2</sub> symmetry [77].

In the case of trisulfane the protonation may occur either at a terminal or at the central sulfur atom. Both ions were found to be of C<sub>1</sub> symmetry. On the basis of their Gibbs energies the ion [H<sub>2</sub>S-S-SH]<sup>+</sup> is by 9 kJ mol<sup>-1</sup> more stable than the tautomer [HS-S(H)-SH]<sup>+</sup> at 298 K. While the SS bonds in the latter ion are of almost identical length (205.4 and 205.7 pm), they are rather different in the former ion (214.9 and 200.9 pm) with the longer one originating from the three-coordinate atom [70]. These two ions have not been observed yet.

Tetrasulfane may form the ions [H<sub>2</sub>S-S-S-SH]<sup>+</sup>, [HS-S(H)-S-SH]<sup>+</sup>, and [S(SH)<sub>3</sub>]<sup>+</sup> which seem to be the most reasonable connectivities. The latter has been isolated in the salt [S(SH)<sub>3</sub>][SbCl<sub>6</sub>] [75]. The ion [HS-S(H)-S-SH]<sup>+</sup> is of C<sub>1</sub> symmetry and represents the global minimum on the potential energy hypersurface. Its SS bonds are, from left to right, of lengths 205.7, 211.5, and 203.3 pm. The gaseous ions [H<sub>2</sub>S-S-S-SH]<sup>+</sup> and [S(SH)<sub>3</sub>]<sup>+</sup> are by only 1 and 7 kJ mol<sup>-1</sup> less stable (Gibbs energies at 298 K) and are of C<sub>1</sub> and C<sub>3</sub> symmetry, respectively [70].

### 6.2.2

#### Deprotonation

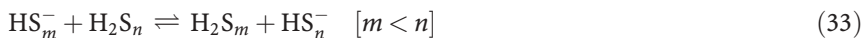
In the gas phase all sulfane molecules are relatively strong Brønsted acids. Their acidity is defined by the enthalpy or, alternatively, by the Gibbs energy of the following deprotonation reaction:



According to high-level ab initio MO calculations by the G2 method the gas phase acidities of sulfanes increase with the number of sulfur atoms in the molecule [48]. Obviously, the delocalization of the excess electron in the generated anions is as easier as larger the anion becomes. Gaseous trisulfane is as strong a proton donor as hydrogen chloride and tetrasulfane is even stronger but less so than HBr. The corresponding Gibbs energies of reaction (32) at 298 K are as follows (in kJ mol<sup>-1</sup>): H<sub>2</sub>S 1444; H<sub>2</sub>S<sub>2</sub> 1406; H<sub>2</sub>S<sub>3</sub> 1370; H<sub>2</sub>S<sub>4</sub> 1347. Since the increase in acidity from H<sub>2</sub>S<sub>3</sub> to H<sub>2</sub>S<sub>4</sub> is still considerable it can be expected that H<sub>2</sub>S<sub>5</sub> and H<sub>2</sub>S<sub>6</sub> will be even stronger proton donors [48]. The acidity data calculated for H<sub>2</sub>S and H<sub>2</sub>S<sub>2</sub> are in excellent agreement with the experimental values [78]. No experimental data are available for the higher sulfanes.

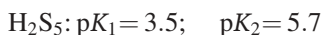
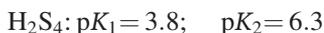
The monoanions HS<sub>*n*</sub><sup>-</sup> formed in the reaction at Eq. (32) exhibit interesting structures with alternating SS bond lengths indicative for strong hyperconjugation effects [4, 48]. It has been suspected that the high acidity of the sulfanes may be responsible for the corrosion of steel pipes used to produce “sour gas” which is a natural gas rich in hydrogen sulfide and containing lower sulfanes like H<sub>2</sub>S<sub>2</sub> [48].

Since the gas phase acidities of the sulfanes increase with the chain-length the equilibria



will always be on the right side.

The acidity of some polysulfanes in aqueous solution has been estimated by Schwarzenbach and Fischer from the results of elegant titration experiments in a flow apparatus [79]. Using solutions of sodium tetra- and pentasulfide and measuring the pH value immediately after addition of certain amounts of hydrochloric acid the p*K*<sub>a</sub> values were determined as follows:

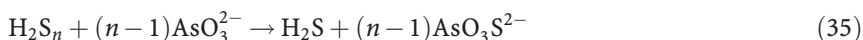


However, since the authors assumed that no hexasulfide and negligible amounts of tri- and disulfide ions were present in their solutions at pH values of 11–12, these data can be only approximately correct. In any case, it is obvious that the acidity of aqueous sulfanes increases with increasing sulfur content, as it does in the gas phase.

### 6.3

#### Nucleophilic Displacement Reactions

Like other polysulfur compounds, the sulfanes are subject to degradation if treated with strong nucleophiles like aqueous sulfite, arsenite or cyanide:



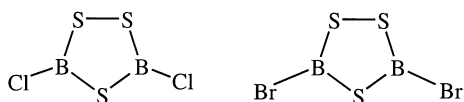


Since the reactivity of the sulfanes, dissolved in ether or chloroform, towards such reagents is higher than that of S<sub>8</sub> a separate determination of these components in mixtures is possible [80]. However, nowadays the sulfanes can be more easily determined by <sup>1</sup>H NMR spectroscopy and the dissolved sulfur by Raman spectroscopy (see above).

## 6.4

### Condensation Reactions

The chlorides and bromides of certain non-metals react with H<sub>2</sub>S and higher sulfanes with liberation of hydrogen halides and formation of novel non-metal-sulfur bonds. For example, the reaction of H<sub>2</sub>S<sub>2</sub> with BCl<sub>3</sub> in CS<sub>2</sub> at -40 °C gives 3,5-dichloro-1,2,4,3,5-trithioadiborolane in 2.5% yield along with HCl and elemental sulfur. The reaction of BBr<sub>3</sub> with H<sub>2</sub>S<sub>2</sub> in CS<sub>2</sub> at 0 °C gives the corresponding 3,5-dibromoborolane in 95% yield along with HBr and elemental sulfur (see Scheme 1) [81].



**Scheme 1**

The reactions of disulfane with PhBCl<sub>2</sub> or MeBBr<sub>2</sub> in CS<sub>2</sub> at 20 °C give the corresponding 3,5-diphenyl- and 3,5-dimethylborolanes in yields of 50% and 73% respectively [82].

Dichlorosulfanes S<sub>m</sub>Cl<sub>2</sub> (and, in an analogous manner, dibromosulfanes) react with sulfanes by the general equations



or



depending on which component is applied in excess. These reactions may be used for the preparation of either higher sulfanes (see above) or of higher dichlorosulfanes. If the starting materials are mixed in a molar ratio of 1:1 a reaction with quantitative evolution of HCl takes place and elemental sulfur is formed which consists mainly of polymeric “μ-sulfur” but contains also the homocycles S<sub>12</sub>, S<sub>18</sub>, and S<sub>20</sub>:



The mentioned homocycles have been extracted from the sulfur mixture by carbon disulfide [83].

The condensation of an excess of  $\text{H}_2\text{S}_2$  with  $\text{SCl}_2$  at  $-60\text{ }^\circ\text{C}$  followed by evaporation of the unreacted disulfane together with the  $\text{HCl}$  yields almost pure pentasulfane  $\text{H}_2\text{S}_5$  [16, 27, 54]. If  $\text{H}_2\text{S}_2$  is allowed to react with a large excess of  $\text{SCl}_2$  at  $-78\text{ }^\circ\text{C}$  [16, 84] or  $-10$  to  $0\text{ }^\circ\text{C}$  [85] dichlorotetrasulfane is produced in high yield and good purity. If an inert solvent like  $\text{CCl}_4$  is used, no excess of  $\text{SCl}_2$  is required [86].

The reaction of organic sulfenyl chlorides  $\text{RSCl}$  or chlorodisulfanes  $\text{RSSCl}$  with sulfanes provides organic polysulfanes in preparative quantities [2]:



For example, trichloromethyl sulfenylchloride yields the corresponding tri- and tetrasulfanes on reaction with disulfane [87]:



The trisulfane  $\text{R}_2\text{S}_3$  probably results from the decomposition of  $\text{H}_2\text{S}_2$  to  $\text{H}_2\text{S}$  followed by condensation with  $\text{CCl}_3\text{SCl}$ .

The homocyclic sulfur oxide  $\text{S}_8\text{O}$  was prepared by condensation of thionylchloride with crude sulfane oil at  $-40\text{ }^\circ\text{C}$  applying the dilution principle. It is believed that the product results from the heptasulfane content of the sulfane oil [88]:



From 95 g of  $\text{SOCl}_2$  and 183 g of  $\text{H}_2\text{S}_m$ , both dissolved in  $\text{CS}_2$  and added simultaneously but slowly (within 8 h) to a mixture of 0.75 l  $\text{CS}_2$  and 0.35 l  $\text{Me}_2\text{O}$ , ca. 4 g of pure  $\text{S}_8\text{O}$  were obtained after repeated recrystallization.  $\text{S}_8\text{O}$  forms needle-shaped yellow crystals of m.p.  $78\text{ }^\circ\text{C}$  (dec.). The molecules consists of a crown-shaped  $\text{S}_8$  rings with exocyclic oxygen atoms in axial positions [89].

## 7 Applications

In the Introduction it has already been mentioned that sulfanes are likely to occur in underground sulfur-rich deposits of sour natural gas. This gas is freed from  $\text{H}_2\text{S}$  by washing with an alkaline solvent from which the hydrogen sulfide is later expelled by heating. The Claus process is then applied to convert  $\text{H}_2\text{S}$  into elemental sulfur:



However, since the latter reaction is an equilibrium process the Claus sulfur still contains traces of  $\text{H}_2\text{S}$  (200–350 ppm, mostly in the form of polysulfanes) which causes serious problems since the  $\text{H}_2\text{S}$  partly escapes on cooling or solidification of the sulfur. Obviously, the  $\text{H}_2\text{S}$  content needs to be controlled because of the extreme toxicity of hydrogen sulfide and its ability

to form explosive mixtures with air (lower explosive limit in air at 150 °C: 3.5 vol.% H<sub>2</sub>S). Another concern is the corrosive nature of hydrogen sulfide. The removal of H<sub>2</sub>S physically and chemically dissolved in liquid sulfur is therefore an important process [9]. There are several degassing methods. The principle is always to accelerate the decomposition of the polysulfanes to hydrogen sulfide and sulfur and to remove the physically dissolved H<sub>2</sub>S by a sweep gas (usually hot air). The acceleration can be achieved by either agitation or spraying of the liquid as well as by adding a catalyst like ammonia, urea or other amines. However, some of the catalysts may result in plugging problems if the sulfur is later burned for sulfuric acid production. The oxygen in the sweep gas helps to oxidize dissolved H<sub>2</sub>S according to Eqs. (43) and (44) [9]. The remaining H<sub>2</sub>S concentration should be well below 10 ppm.

## References

1. *Gmelin Handbuch der Anorganischen Chemie*, 8th ed., *Sulfur Halides*, Springer, Berlin, 1978
2. R. Steudel, *Chem. Rev.* **2002**, *102*, 3905
3. E.L. Clennan, K.L. Stensaas, *Org. Prep. Proc. Int.* **1998**, *30*, 551
4. R. Steudel, *Top. Curr. Chem.* **2004**, *231*, in print
5. F. Fehér, W. Laue, *Z. Naturforsch. Part B* **1953**, *8*, 687
6. R. Fanelli, *Ind. Eng. Chem.* **1949**, *41*, 2031 and **1946**, *38*, 39
7. T.K. Wiewiorowski, F. J. Touro, *J. Chem. Phys.* **1966**, *70*, 234
8. J.B. Hyne, E. Muller, T.K. Wiewiorowski, *J. Chem. Phys.* **1966**, *70*, 3733
9. Anonymous, *Sulphur* **1994**, *233*, 35
10. *Gmelin Handbook of Inorganic Chemistry*, 8th ed., *Sulfanes*, Springer, Berlin, 1983
11. J.B. Hyne, G. D. Derald, *World Oil*, October **1980**, 111
12. K. W. C. Burton, P. Machmer, in: *Inorganic Sulfur Chemistry* (G. Nickless, ed.), Chapter 10, Elsevier, Amsterdam, **1968**, p. 335
13. M. Schmidt, W. Siebert, in: *Comprehensive Inorganic Chemistry*, Vol. 2, Chapter 23, Pergamon, Oxford **1973**, p. 795
14. F. Fehér, H.J. Berthold, *Z. Anorg. Allg. Chem.* **1952**, *267*, 251
15. R. Steudel, H.-J. Mäusle, *Z. Anorg. Allg. Chem.* **1979**, *457*, 165
16. F. Fehér in: *Handbuch der Präparativen Anorganischen Chemie* (G. Brauer, ed.), Vol. 1, Chapter 6, Enke, Stuttgart, **1975**, p. 356
17. M. Liedtke, K.M.T. Yamada, G. Winnewisser, J. Hahn, *J. Mol. Struct.* **1997**, *413–414*, 265
18. F. Fehér, W. Laue, *Z. Anorg. Allg. Chem.* **1956**, *288*, 103
19. J. Hahn, *Z. Naturforsch. Part B* **1985**, *40*, 263
20. E. Muller, J.B. Hyne, *Can. J. Chem.* **1968**, *46*, 2341
21. J. Hahn, P. Schmidt, K. Reinartz, J. Behrend, G. Winnewisser, K.M.T. Yamada, *Z. Naturforsch. Part B* **1991**, *46*, 1338
22. I. Bloch, F. Höhn, *Ber. Dtsch. Chem. Ges.* **1908**, *41*, 1971, 1975
23. F. Fehér, M. Baudler, *Z. Anorg. Allg. Chem.* **1947**, *254*, 289
24. F. Fehér, W. Laue, G. Winkhaus, *Z. Anorg. Allg. Chem.* **1956**, *288*, 113
25. B.-M. Cheng, W.-C. Hung, *J. Phys. Chem.* **1996**, *100*, 10210
26. F. Fehér, L. Meyer, *Z. Naturforsch. Part B* **1956**, *11*, 605
27. F. Fehér, G. Winkhaus, *Z. Anorg. Allg. Chem.* **1956**, *288*, 123
28. F. Fehér, W. Kruse, *Z. Anorg. Allg. Chem.* **1957**, *293*, 302
29. J. Hahn, K. Altenbach, *Z. Naturforsch. Part B* **1986**, *41*, 675
30. F. Fehér, G. Hitzemann, *Z. Anorg. Allg. Chem.* **1957**, *294*, 50
31. F. Fehér, W. Laue, G. Winkhaus, *Z. Anorg. Allg. Chem.* **1957**, *290*, 52

32. F. Fehér, W. Kruse, W. Laue, *Z. Anorg. Allg. Chem.* **1957**, 292, 203
33. S. Antonello, R. Benassi, G. Gavioli, F. Taddei, F. Maran, *J. Am. Chem. Soc.* **2002**, 124, 7529
34. R. Steudel, Y. Steudel, K. Miaskiewicz, *Chem. Eur. J.* **2001**, 7, 3281
35. H.J. Möckel, *Fresenius Z. Anal. Chem.* **1984**, 318, 116
36. R. Steudel, T. Göbel, H. Schmidt, G. Holdt, *Fresenius Z. Anal. Chem.* **1989**, 334, 266
37. M. Winnewisser, J. Haase, *Z. Naturforsch. Part A* **1958**, 23, 56
38. G. Winnewisser, *J. Mol. Spectrosc.* **1972**, 41, 534
39. J. Behrend, P. Mittler, G. Winnewisser, K.M.T. Yamada, *J. Mol. Spectrosc.* **1991**, 150, 99
40. E. Herbst, G. Winnewisser, *Chem. Phys. Lett.* **1989**, 155, 572
41. G.I. Cárdenas-Jirón, C. Cárdenas-Lailhacar, A. Toro-Labbé, *J. Mol. Struct. (Theochem)* **1993**, 282, 113
42. O.M. Suleimenov, T.-K. Ha, *Chem. Phys. Lett.* **1998**, 290, 451
43. G. Winnewisser, M. Winnewisser, W. Gordy, *J. Chem. Phys.* **1968**, 49, 3465
44. D.A. Dixon, D. Zeroka, J.J. Wendoloski, Z.R. Wasserman, *J. Phys. Chem.* **1985**, 89, 5334. G. Grein, *Chem. Phys. Lett.* **1985**, 116, 323
45. D. Mauer, G. Winnewisser, K.M.T. Yamada, *J. Mol. Struct.* **1988**, 190, 457
46. M. Liedtke, A.H. Saleck, K.M.T. Yamada, G. Winnewisser, D. Cremer, E. Kraka, A. Dolgner, J. Hahn, S. Dobos, *J. Phys. Chem.* **1993**, 97, 11204
47. Y. Drozdova, K. Miaskiewicz, R. Steudel, *Z. Naturforsch. Part B* **1995**, 50, 889
48. A.H. Otto, R. Steudel, *Eur. J. Inorg. Chem.* **1999**, 2057
49. F.M. Bickelhaupt, M. Solà, P. von R. Schleyer, *J. Comput. Chem.* **1995**, 16, 465
50. R. Steudel, Y. Drozdova, K. Miaskiewicz, R.H. Hertwig, W. Koch, *J. Am. Chem. Soc.* **1997**, 119, 1990
51. R.S. Laitinen, T.A. Pakkanen, R. Steudel, *J. Am. Chem. Soc.* **1987**, 109, 710
52. M.W. Wong, Y. Steudel, R. Steudel, *Chem. Phys. Lett.* **2002**, 364, 387
53. A. Greer, *J. Am. Chem. Soc.* **2001**, 123, 10379
54. H. Schmidbaur, M. Schmidt, W. Siebert, *Chem. Ber.* **1964**, 97, 3374
55. P. Mittler, K.M.T. Yamada, G. Winnewisser, M. Birk, *J. Mol. Spectrosc.* **1994**, 164, 390
56. B.P. Winnewisser, M. Winnewisser, *Z. Naturforsch. Part A* **1968**, 23, 832
57. C.J. Marsden, B.J. Smith, *J. Phys. Chem.* **1988**, 92, 347
58. H. Wieser, P.J. Krueger, E. Muller, J.B. Hyne, *Can J. Chem.* **1969**, 47, 1633
59. F. Fehér, M. Baudler, *Z. Anorg. Allg. Chem.* **1949**, 258, 132
60. F. Fehér, H. Münzner, *Chem. Ber.* **1963**, 96, 1131
61. D.C. Frost, S.T. Lee, C. A. McDowell, N. P. C. Westwood, *J. Electron Spectrosc. Relat. Phenom.* **1977**, 12, 95
62. A. Prange, C. Dahl, H.G. Trüper, M. Behnke, J. Hahn, H. Modrow, J. Hormes, *Eur. Phys. J.* **2002**, D20, 589
63. F. Fehér, G. Winkhaus, *Z. Anorg. Allg. Chem.* **1957**, 292, 210
64. E. Muller, J.B. Hyne, *J. Am. Chem. Soc.* **1969**, 91, 1907
65. F. Fehér, H. Weber, *Z. Elektrochem., Ber. Bunsenges. Phys. Chem.* **1956**, 61, 285
66. G. Porter, *Discussions Faraday Soc.* **1950**, 9, 60
67. O.P. Strausz, R.J. Donovan, M. deSorgo, *Ber. Bunsenges. Physik. Chem.* **1968**, 72, 253
68. R.K. Gosavi, M. deSorgo, H.E. Gunning, O.P. Strausz, *Chem. Phys. Lett.* **1973**, 21, 318
69. E. Isoniemi, L. Khriachtchev, M. Petterson, M. Räsänen, *Chem. Phys. Lett.* **1999**, 311, 47
70. A.H. Otto, R. Steudel, *Z. Anorg. Allg. Chem.* **2000**, 626, 2063
71. K.O. Christe, *Inorg. Chem.* **1975**, 14, 2230
72. T. Nakanaga, T. Amano, *J. Mol. Spectrosc.* **1989**, 133, 201
73. P. Botschwina, A. Zilch, H.-J. Werner, P. Rosmus, E.-A. Reinsch, *J. Chem. Phys.* **1986**, 85, 5107
74. R. Minkwitz, A. Kornath, W. Sawodny, J. Hahn, *Inorg. Chem.* **1996**, 35, 3622
75. R. Minkwitz, R. Krause, H. Härtner, W. Sawodny, *Z. Anorg. Allg. Chem.* **1991**, 593, 137
76. M. Loos, J.-L. Rivail, I.G. Csizmadia, *J. Mol. Struct. (Theochem)* **1990**, 204, 389
77. R. Cimiriaglia, J. Tomasi, R. Cammi, H.-J. Hofmann, *Chem. Phys.* **1989**, 136, 399

78. H<sub>2</sub>S: J.E. Bartmess, *Negative Ion Energetics Data in NIST Chemistry WebBook*, W. G. Mallard, P. J. Linstrom, Eds., NIST Standard Reference Database Number 69, November 1998, National Institute of Standards and Technology, Gaithersburg, MD, USA (<http://webbook.nist.gov/chemistry>). H<sub>2</sub>S<sub>2</sub>: R. A.J. O'Hair, C.H. DePuy, V. M. Bierbaum, *J. Phys. Chem.* **1993**, *97*, 7955
79. G. Schwarzenbach, A. Fischer, *Helv. Chim. Acta* **1960**, *43*, 1365
80. M. Schmidt, G. Talsky, *Z. Anal. Chem.* **1959**, *166*, 274. M. Schmidt, R. R. Wägerle, *Chem. Ber.* **1963**, *96*, 3293
81. M. Schmidt, W. Siebert, *Z. Anorg. Allg. Chem.* **1966**, *345*, 87
82. M. Schmidt, W. Siebert, *Chem. Ber.* **1969**, *102*, 2752 and *Angew. Chem.* **1964**, *76*, 687; *Angew. Chem. Int. Ed. Engl.* **1964**, *3*, 637
83. M. Schmidt, E. Wilhelm, T. Debaerdemaeker, E. Hellner, A. Kutoglu, *Z. Anorg. Allg. Chem.* **1974**, *405*, 153. M. Schmidt, G. Knippschild, E. Wilhelm, *Chem. Ber.* **1968**, *101*, 381
84. F. Fehér, K. Naussed, H. Weber, *Z. Anorg. Allg. Chem.* **1957**, *290*, 303
85. F. Fehér, J. Goebell, F.-R. Minz, *Z. Anorg. Allg. Chem.* **1966**, *342*, 146
86. F. Fehér, H. Kulus, *Z. Anorg. Allg. Chem.* **1969**, *364*, 241
87. F. Fehér, H.J. Berthold, *Chem. Ber.* **1955**, *88*, 1634
88. R. Steudel, M. Rebsch, *Z. Anorg. Allg. Chem.* **1975**, *413*, 252
89. P. Luger, H. Bradaczek, R. Steudel, M. Rebsch, *Chem. Ber.* **1976**, *109*, 180



# Inorganic Polysulfides $S_n^{2-}$ and Radical Anions $S_n^{\cdot-}$

Ralf Steudel

Institut für Chemie, Sekr. C2, Technische Universität Berlin, 10623 Berlin, Germany  
E-mail: [steudel@schwefel.chem.tu-berlin.de](mailto:steudel@schwefel.chem.tu-berlin.de)

**Abstract** Inorganic polysulfide anions  $S_n^{2-}$  and the related radical anions  $S_n^{\cdot-}$  play an important role in the redox reactions of elemental sulfur and therefore also in the geobiochemical sulfur cycle. This chapter describes the preparation of the solid polysulfides with up to eight sulfur atoms and univalent cations, as well as their solid state structures, vibrational spectra and their behavior in aqueous and non-aqueous solutions. In addition, the highly colored and reactive radical anions  $S_n^{\cdot-}$  with  $n = 2, 3,$  and  $6$  are discussed, some of which exist in equilibrium with the corresponding diamagnetic dianions.

**Keywords** Sulfur chains · Molecular structures · Radical anions · Spectra · Redox reactions

1	Introduction . . . . .	128
2	Preparation of Solid Polysulfides . . . . .	130
2.1	Alkali Metal Polysulfides . . . . .	130
2.2	Sulfur-Rich Polysulfides with Complex Univalent Cations. . . . .	132
2.2.1	General . . . . .	132
2.2.2	Tetrasulfides . . . . .	133
2.2.3	Pentasulfides . . . . .	133
2.2.4	Hexasulfides . . . . .	133
2.2.5	Heptasulfides. . . . .	134
2.2.6	Octasulfides . . . . .	134
3	Properties of Solid Alkali Polysulfides . . . . .	134
4	Structures of Polysulfide Dianions . . . . .	135
5	Polysulfide Solutions . . . . .	137
5.1	Aqueous Solutions . . . . .	137
5.2	Non-Aqueous Solutions . . . . .	141
5.2.1	Electrochemical Studies . . . . .	141
6	Vibrational Spectra . . . . .	142
7	Reactions in Solution . . . . .	143
8	Polysulfide Radical Anions . . . . .	145
8.1	General . . . . .	145
8.2	The Radicals $S_2^{\cdot-}$ and $S_3^{\cdot-}$ . . . . .	145

8.3	The Radical $S_4^{\cdot-}$ . . . . .	147
8.4	The Radical $S_6^{\cdot-}$ . . . . .	148
8.5	Calculated Structures . . . . .	148
	References . . . . .	149

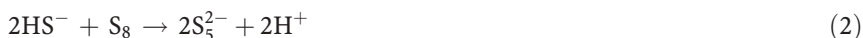
## List of Abbreviations

crypt-2.2.2	$N(C_2H_4OC_2H_4OC_2H_4)_3N$
en	Ethylenediamine
hmpa	Hexamethylphosphoric triamide
pmdeta	$N,N,N',N'',N'''$ -pentamethyldiethylenetriamine
teeda	Tetraethylethylenediamine
tmeda	Tetramethylethylenediamine

## 1

### Introduction

Inorganic polysulfides are ionic substances containing chain-like dianions  $S_n^{2-}$ . Such ions are formed in numerous reactions, e.g., by oxidation of monosulfide ions  $HS^-$  in water or other polar solvents as well as by reaction of aqueous monosulfide with sulfur-rich compounds including elemental sulfur:



Therefore, polysulfide ions play a major role in the global geological and biological sulfur cycles [1, 2]. In addition, they are reagents in important industrial processes, e.g., in desulfurization and paper production plants. It should be pointed out however that only sulfide, elemental sulfur and sulfate are thermodynamically stable under ambient conditions in the presence of water, their particular stability region depending on the redox potential and the pH value [3]:



On the other hand, the large activation energy for the formation of sulfate from  $S_8$  and water makes it possible to prepare polysulfides as well as other reduced sulfur compounds as metastable products in aqueous solution at ambient conditions.

Polysulfides are the key reactants in the high-density sodium-sulfur and lithium-sulfur batteries [4] which are based on the following reversible redox reaction taking place in the polysulfide melt:



In melts and polar solvents polysulfide dianions are usually present as mixtures of species of different chain-lengths as a result of the following types of equilibria which are rapidly established even at 20 °C [5]:



The chemistry of polysulfide dianions is closely related to that of the radical-monoanions  $S_n^{\cdot-}$  since both types of anions are in equilibrium with each other in solution and in high-temperature melts, e.g.:



Furthermore, polysulfide anions are subject to autoxidation if molecular oxygen is present, e.g.:



In solution this reaction is rather rapid but in the solid state autoxidation takes place much slower. Nevertheless, commercial sulfides and polysulfides of the alkali and alkali earth metals usually contain thiosulfate (and anions of other sulfur oxoacids) as impurities [6]. For all these reasons the chemistry of polysulfides is rather complex, and some of the earlier studies on polysulfides (prior to ca. 1960) are not very reliable experimentally and/or describe erroneous interpretations of the experimental results.

Polysulfides have been prepared with many different types of cations, both monoatomic like alkali metal ions and polyatomic like ammonium or substituted ammonium or phosphonium ions. In this chapter only those salts will be discussed in detail which contain univalent main-group cations although a large number of transition metal polysulfido complexes have been prepared [7–9].

A truly comprehensive review on the chemistry of inorganic (ionic) polysulfides has never been published. Szekeres [10] as well as Hanley and Czech [11] reviewed the classical analytical chemistry (titrimetric and gravimetric analysis) of sulfur acids including sulfides and polysulfides in 1974 and 1970, respectively. Chivers reviewed the chemistry of polychalcogenide anions including the radical monoanions (with the stress on the latter) in 1977 [12]. Hamilton critically reviewed the literature on aqueous polysulfide solutions and proposed a speciation model of his own [13].

**Table 1** Properties of some ionic polysulfides

Compound	Color (20 °C)	Melting point [14, 15]	Density (g cm <sup>-3</sup> ) (20 °C)
Na <sub>2</sub> S <sub>2</sub>	Yellow	470±10 °C ( $\beta$ )	Two allotropes
Na <sub>2</sub> S <sub>4</sub>	Orange-yellow	290±5 °C	2.08
Na <sub>2</sub> S <sub>5</sub>	Brown-yellow	265±5 °C	2.08
K <sub>2</sub> S <sub>2</sub>	Pale yellow	487 °C	1.973
K <sub>2</sub> S <sub>3</sub>	Yellow-brown	302 °C	2.102
K <sub>2</sub> S <sub>4</sub>	Orange-yellow	154 °C	
K <sub>2</sub> S <sub>5</sub>	Orange	206 °C	2.128
K <sub>2</sub> S <sub>6</sub>	Red	189 °C	2.02

## 2 Preparation of Solid Polysulfides

### 2.1 Alkali Metal Polysulfides

The rather complex equilibrium phase diagrams of the sodium-sulfur system [14] and of the potassium-sulfur system [15] have been critically reviewed by Sangster and Pelton in 1997. In the sodium-sulfur system the compounds Na<sub>2</sub>S,  $\alpha$ -Na<sub>2</sub>S<sub>2</sub>,  $\beta$ -Na<sub>2</sub>S<sub>2</sub>, Na<sub>2</sub>S<sub>4</sub>, and Na<sub>2</sub>S<sub>5</sub> exist but neither Na<sub>2</sub>S<sub>3</sub> nor polysulfides higher than the pentasulfide do [16]. Na<sub>2</sub>S<sub>2</sub> exists as  $\alpha$ -form below 160 °C and as  $\beta$ -form above this temperature; both are of hexagonal crystal symmetry.  $\beta$ -Na<sub>2</sub>S<sub>2</sub> melts incongruently at 470 °C while the tetra- and pentasulfides show congruent melting points (peritectic) [14]. As higher the sulfur content as lower the melting points (see Table 1). Liquid sodium polysulfides easily supercool and form relatively stable glasses. By Raman spectroscopy it was found that Na<sub>2</sub>S<sub>4</sub> and Na<sub>2</sub>S<sub>5</sub> can be obtained as several metastable phases depending on the preparation conditions [17,18]. The thermodynamically stable forms at ambient conditions are designated by  $\alpha$ .

In the potassium-sulfur system the compounds K<sub>2</sub>S, K<sub>2</sub>S<sub>2</sub>, K<sub>2</sub>S<sub>3</sub>, K<sub>2</sub>S<sub>4</sub>, K<sub>2</sub>S<sub>5</sub>, and K<sub>2</sub>S<sub>6</sub> exist and there are six eutectics [15]. All sodium and potassium sulfides and polysulfides are hygroscopic and some of them form well defined hydrates.

The preparation of anhydrous Na<sub>2</sub>S<sub>2</sub>, Na<sub>2</sub>S<sub>4</sub>, Na<sub>2</sub>S<sub>5</sub>, K<sub>2</sub>S<sub>2</sub>, K<sub>2</sub>S<sub>3</sub>, K<sub>2</sub>S<sub>4</sub>, K<sub>2</sub>S<sub>5</sub>, and K<sub>2</sub>S<sub>6</sub> has been described in detail by Fehér et al. [16, 19–21]. These procedures are based on the following reactions (M: Na or K):





$Na_2S_2$ ,  $K_2S_2$ ,  $Na_2S_4$ ,  $K_2S_4$ , and  $K_2S_5$  may be prepared from the elements in liquid ammonia according to Eq. (10) in a special apparatus which allows the strict exclusion of moisture and oxygen. The alkali metals are soluble in liquid ammonia and reduce the sulfur stoichiometrically. After evaporation of the solvent the product is homogenized by heating under vacuum to a temperature just below the melting point.

Anhydrous  $Na_2S_2$  and  $K_2S_2$  may also be prepared according to Eq. (11), e.g., by heating of the components in an evacuated glass ampoule to 500 °C until a homogeneous melt is obtained which is then allowed to cool slowly. High-melting glass should be used for the ampoule.

Sodium disulfide for the in situ preparation of organic disulfanes  $R_2S_2$  may also be prepared from the elements in 1,2-dimethoxyethane at 70 °C in the presence of catalytic amounts of an aromatic hydrocarbon or ketone [22].

The reaction at Eq. (12) allows the preparation of  $Na_2S_4$  and  $K_2S_5$  from the alkali metals, hydrogen sulfide and sulfur in anhydrous ethanol (ROH). First the metal is dissolved in the alcohol with formation of ethanolate (MOR) and hydrogen. Bubbling of  $H_2S$  into this solution produces the hydrogen sulfide (MHS). To obtain the polysulfide the solution is refluxed with the calculated amount of elemental sulfur. After partial evaporation of the solvent and subsequent cooling the product precipitates.

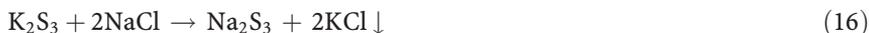
The alcoholic solution of  $Na_2S_4$  prepared as described above may be reduced to  $Na_2S_2$  by addition of the calculated amount of sodium and refluxing under pure nitrogen; see Eq. (13).

$K_2S_6$  is obtained if  $K_2S_5$  and sulfur are heated in an evacuated glass ampoule to 220–280 °C for several hours followed by cooling to 20 °C within 10 h; see Eq. (14).

The mechanism of the reaction of solid  $\alpha$ - $Na_2S_2$  with  $S_8$  has been studied by Raman spectroscopy [18]. The reaction begins at the melting temperature of  $S_8$  (120 °C) and the primary product is  $\alpha$ - $Na_2S_4$ . Near 160 °C the remaining  $\alpha$ - $Na_2S_2$  first transforms to  $\beta$ - $Na_2S_2$  which also reacts with  $S_8$  to  $\alpha$ - $Na_2S_4$ . If  $Na_2S$  is used as a starting material it first reacts with  $S_8$  to  $Na_2S_2$ . Heating of  $\alpha$ - $Na_2S_4$  to 500 °C followed by cooling to 120 °C results in a glassy material which on annealing at this temperature forms crystalline  $\gamma$ - $Na_2S_4$  as a metastable phase which melts at ca. 230 °C. If a mixture of  $Na_2S$  and  $\alpha$ - $Na_2S_4$  is heated to 200 °C the Raman lines of  $\beta$ - $Na_2S_2$  can be observed:



$Na_2S_3$  is not stable in the solid state, and cooling of a melt of composition  $Na_2S_3$  leads to an eutectic mixture of  $Na_2S_2$  and  $Na_2S_4$  [18, 23]. However, the Raman spectra of melts of this composition show a line at 462  $cm^{-1}$  which has been assigned to  $S_3^{2-}$  ions [18], and at low temperatures in liquid ammonia a metastable phase of  $Na_2S_3$  has evidently been prepared by the following reaction [24]:



The potassium chloride precipitates from the solution shifting the equilibrium to the right side. On heating to 100 °C this  $\text{Na}_2\text{S}_3$  sample decomposed exothermically to a 1:1 mixture of  $\text{Na}_2\text{S}_2$  and  $\text{Na}_2\text{S}_4$  similar to the one described above.

Heating of  $\alpha$ - $\text{Na}_2\text{S}_4$  with an excess of sulfur to 500 °C yields mixtures of  $\alpha$ -,  $\beta$ -,  $\gamma$ -, and  $\delta$ - $\text{Na}_2\text{S}_5$  with the  $\gamma$ -form predominating. This allotrope converts to the  $\alpha$ -form on annealing at 200 °C for 21 h while the  $\beta$ - and  $\delta$ -form slowly convert to the  $\alpha$ -allotrope on cooling also. In other words, these phases are metastable at any temperature [18].

Although solid  $\text{Na}_2\text{S}_6$  does not exist the adduct  $[\text{Na}(\text{tea})]_2\text{S}_6$  has been isolated as red crystals which were crystallographically characterized (tea = triethanolamine) [25].

The sulfur pressure over liquid sodium polysulfides has been measured in the temperature range 400–1000 °C [26].

For the preparation of rubidium and cesium polysulfides, see [27].

To check the identity and purity of the products obtained in the above reactions it is not sufficient to analyze for the sulfur content since a mixture may incidentally have the same S content. Either X-ray diffraction on single crystals or Raman spectra of powder-like or crystalline samples will help to identify the anion(s) present in the product. However, the most convincing information comes from laser desorption Fourier transform ion cyclotron resonance (FTICR) mass spectra in the negative ion mode (LD mass spectra). It has been demonstrated that pure samples of  $\text{K}_2\text{S}_3$  and  $\text{K}_2\text{S}_5$  show peaks originating from  $\text{S}_n^{\cdot-}$  radical anions which are of the same size as the dianions in the particular sample; no fragment ions of this type were observed [28].

## 2.2

### Sulfur-Rich Polysulfides with Complex Univalent Cations

#### 2.2.1

##### General

A large number of polysulfides with up to eight sulfur atoms in the anion have been prepared, mostly from non-aqueous solvents. The following donor ligands served to coordinate the alkali metal cations: en = ethylenediamine, tmeda = tetramethylethylenediamine, teeda = tetraethylethylenediamine, hmpa = hexamethylphosphoric triamide, pmdeta =  $N,N,N',N'',N'''$ -pentamethyldiethylenetriamine, crypt-2.2.2 =  $\text{N}(\text{C}_2\text{H}_4\text{OC}_2\text{H}_4\text{OC}_2\text{H}_4)_3\text{N}$ . Often the polysulfide chain-length in the product is different from that in the starting material because of the reactions at Eqs. (5) and (6) taking place in solution. Since the polysulfides are often hygroscopic and air-sensitive their preparation has to be performed under an atmosphere of dry nitrogen or argon.

### 2.2.2

#### Tetrasulfides

$\text{Na}(\text{Et}_4\text{N})\text{S}_4$  was obtained from  $\text{Na}_2\text{S}_4$  and  $\text{Et}_4\text{NCl}$  in ethanol and was characterized by X-ray diffraction on single-crystals [29]. Orange needles of  $[\text{Li}(\text{pmdeta})]_2\text{S}_4$  crystallized from solutions of pmdeta in toluene in which  $\text{Li}_2\text{S}_2$  or  $\text{Li}_2\text{S}_4$  was suspended. In the case of  $\text{Li}_2\text{S}_4$  the yield is, of course, much higher [30].

### 2.2.3

#### Pentasulfides

Ammonium pentasulfide is usually prepared according to Eq. (17) by suspending elemental sulfur in aqueous ammonia (35%) and bubbling hydrogen sulfide into the solution [20, 31, 32]:

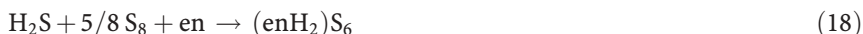


On cooling  $(\text{NH}_4)_2\text{S}_5$  crystallizes as yellow to orange-yellow needles which melt at 95 °C in a sealed glass tube but decompose in air [reverse reaction at Eq. (17)] and on dissolution in water.  $(\text{Et}_4\text{N})_2\text{S}_5$  is obtained by reaction of  $\text{Et}_4\text{NCl}$  with  $\text{Na}_2\text{S}_5$  in ethanol [33].

### 2.2.4

#### Hexasulfides

Dark-red needles of  $(\text{Bu}_4\text{N})_2\text{S}_6$  were obtained by treatment of an "alloy" of composition  $\text{Na}_2\text{S}_3$  (prepared from  $\text{Na}_2\text{S} + 1/4 \text{S}_8$ ) with aqueous  $(\text{Bu}_4\text{N})\text{Br}$  followed by recrystallization from acetone [34]. In a similar fashion  $(\text{Me}_4\text{N})_2\text{S}_6$  was prepared from  $\text{Na}_2\text{S}_5$  and  $\text{Me}_4\text{NCl}$  in  $\text{H}_2\text{O}$  with exclusion of oxygen [35]. Ethylenediamine reacts with sulfur and  $\text{H}_2\text{S}$  to give  $(\text{enH}_2)_2\text{S}_6$  containing diprotonated ligands [36]:



In contrast, the reaction of  $\text{H}_2\text{S}$ ,  $\text{S}_8$  and ethylenediamine *in ethanol* at 65 °C produces orange crystals of  $(\text{enH})_2\text{S}_6$  which still contain some elemental sulfur [37]. If trimethylamine is used the product is  $(\text{Me}_3\text{NH})_2\text{S}_6$  [38]. Dark-red  $[\text{K}(\text{crypt-2.2.2})]_2\text{S}_6$  crystallizes from a solution of  $\text{K}_2\text{S}_5$ ,  $\text{S}_8$  and crypt-2.2.2 in ethylenediamine [39]. Orange crystals of  $[\text{Li}(\text{tmeda})]_2\text{S}_6$  were obtained by extracting  $\text{Li}_2\text{S}_2$  repeatedly with tetrahydrofuran (THF), evaporation of the solvent from the extracts and suspending the latter in a solution of tmeda in toluene followed by addition of THF and cooling [40,41]. In a similar fashion  $[\text{Li}(\text{hmpa})]_2\text{S}_6$ ,  $[\text{Li}(\text{pmdeta})]_2\text{S}_6$ ,  $[\text{Na}(\text{pmdeta})]_2\text{S}_6$ , and  $[\text{K}(\text{hmpa})]_2\text{S}_6$  [41] as well as  $[\text{Li}(\text{teeda})]_2\text{S}_6$  [30] were prepared. The reaction of triorganotellurium chlorides  $\text{R}_3\text{TeCl}$  ( $\text{R} = \text{Me}, \text{Ph}, \text{etc.}$ ) with  $\text{Na}_2\text{S}_x$  ( $x = 4-6$ ) in methanol at 50 °C yields the corresponding bis(triorganotelluroni-

um) hexasulfides  $(R_3Te)_2S_6$  regardless of the employed sodium polysulfide or the size of the telluronium cation [42].

### 2.2.5

#### Heptasulfides

Bis(tetrapropylammonium)heptasulfide  $(Pr_4N)_2S_7$  was obtained from the reaction of  $Pr_4NBr$  and  $Na_2S_5$  in water [43].  $[K(\text{crypt-2.2.2})_2]_2S_7$  crystallizes together with other products from a solution of  $K_2S_5$ ,  $S_8$  and crypt-2.2.2 in ethylenediamine. The red crystals easily lose the solvent molecule [39]. Triclinic orange-red crystals of  $(Ph_4P)_2S_7$  have been obtained from a mixture of  $(Et_4N)_2MoS_9$ , diethyldithiocarbamate trihydrate, and  $Ph_4PCl$  in  $CH_3CN$  [44]. The compound  $(Ph_4P)_2S_7$  and the derivative  $(Ph_4P)(NH_4)S_7 \cdot CH_3CN$  are also accessible from  $Ph_4PBr$ , polysulfide,  $S_8$ ,  $H_2S$ , and  $NH_3$  in  $CH_3CN$  but the details of this synthesis have not been disclosed yet [45]. The reaction of  $[PPN]SH$  with  $S_8$  in ethanol yields crystalline  $[PPN]_2S_7 \cdot 2EtOH$  in high purity  $[PPN = (Ph_3P)_2N^+]$  [46]. Saturation of a solution of diisobutylamine and  $S_8$  in a 1:1 mixture of formamide and dimethylformamide with  $H_2S$  provides  $[(i-C_4H_9)_2NH_2]_2S_7$  [47].

### 2.2.6

#### Octasulfides

Treatment of  $Na_2S_4$  with  $(Ph_4P)_2Cl$  in ethanol yields  $(Ph_4P)_2S_8$  [48]:



Orange-red crystals of  $(Et_3NH)_2S_8$  are formed on reaction of triethanolamine with sulfur and  $H_2S$  in formamide at 60 °C and subsequent cooling to 20 °C [49]:



There is also a report on the preparation of the *dodecasulfide*  $(PPN)_2S_{12}$  [50] but the experimental evidence for such an anion is rather weak.

Polysulfides with two-valent complex cations, e.g.,  $[M(N\text{-methylimidazole})_6]S_8$  have been prepared with  $M = Mn, Fe, Ni, Mg$  [51].

## 3

### Properties of Solid Alkali Polysulfides

The alkali polysulfides are hygroscopic crystalline substances which show a pronounced thermochromic effect. The higher members decompose on heating and sinter before melting. The densities given in Table 1 were determined by the pycnometric method [52]. As far as the colors and melting points are concerned rather differing reports can be found in the literature. The melting temperatures cited in Table 1 are "best values" and the colors were taken from Fehér's work.

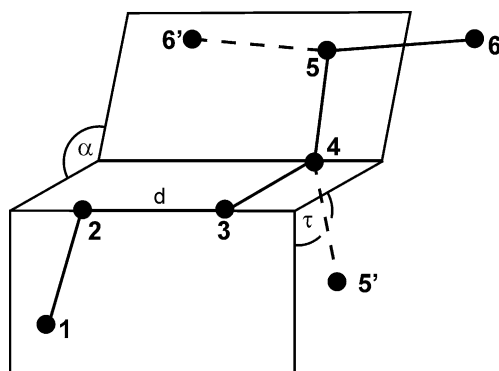


**Fig. 1** Possible conformations of the pentasulfide anion  $S_5^{2-}$  and of the hexasulfide ion  $S_6^{2-}$  depending on the signs of the torsion angles

#### 4 Structures of Polysulfide Dianions

Many of the polysulfides described above have been investigated by X-ray diffraction on either powders or single crystals. In all cases the more sulfur-rich anions ( $n > 3$ ) form unbranched chains the symmetry of which varies between  $C_1$ ,  $C_2$ , and  $C_s$ . According to Fig. 1 the symmetry  $C_2$  results if all torsion angles have the same sign (right-handed helix: + + +...; left-handed helix: - - -...). If the different torsion angles of the anion vary between + and - the symmetry may be  $C_s$  or  $C_1$ . The order of the signs of the torsion angles along the chain is called the "motif" of the anion. For structural details, see Table 2.

For powder diffraction studies of  $Na_2S_2$  (hexagonal),  $\alpha$ - $Na_2S_4$  (tetragonal), and  $\alpha$ - $Na_2S_5$  (orthorhombic), see [16, 53]; for those of  $K_2S_2$ ,  $K_2S_3$ ,  $K_2S_4$ ,  $K_2S_5$ , and  $K_2S_6$ , see [21]. The hexagonal structures of  $\alpha$ - and  $\beta$ - $Na_2S_2$  contain disulfide anions with SS bonds of length 215 pm (in both cases) while 210 pm were derived for  $K_2S_2$  [54]. The orthorhombic structure of  $K_2S_3$  contains anions of  $C_{2v}$  symmetry with SS bonds of 208.3(1) pm and a bond angle of 105.4(1) $^\circ$  [55].

$\alpha$ - $Na_2S_4$  crystallizes in a tetragonal space group with  $Z=8$ . The anions are located on a twofold axis ( $C_2$  symmetry) with internuclear SS distances of 207.4(1) pm for the terminal bonds and 206.1(1) pm for the central bond, an SSS bond angle of 109.76(2) $^\circ$  and a torsion angle of 97.81 $^\circ$  [56].

The crystals of  $\alpha$ - $Na_2S_5$  are orthorhombic and contain anions of  $C_s$  symmetry (*cis* conformation) with SS bond lengths of 206.1(2) pm (terminal) and 206.6(2) pm (central), SSS angles of 107.3(1) $^\circ$  (terminal) and 108.1(1) $^\circ$  (central), and torsion angles of 88.6 $^\circ$ . The terminal sulfur atoms have four, their next neighbors two and the central S atom one sodium cation in the distance range 285–303 pm [57]. In contrast, the anions of  $K_2S_5$  [58],  $Rb_2S_5$  [59],  $Cs_2S_5 \cdot H_2O$  [60] and  $Tl_2S_5$  [61] are all of  $C_2$  symmetry (helical conformation). The only alkali metal hexasulfide which has been studied by single

**Table 2** Structure data of sulfur-rich polysulfides with univalent cations (for abbreviations, see text)

Anion	Cations	Symmetry <sup>a</sup>	$d_{ss}$ (pm)	$\alpha_{SSS}$ (°)	$\tau_{SSSS}$ (°)	Ref.
S <sub>4</sub> <sup>2-</sup>	2 Na <sup>+</sup> ( $\alpha$ )	C <sub>2</sub>	206.1/207.4	109.76	97.81	[56]
	Na <sup>+</sup> , NEt <sub>4</sub> <sup>+</sup>	(C <sub>2</sub> )	206.1–207.9	109.6/110.3	81.84	[29]
	2 Li(pmdeta) <sup>+</sup>		204.8–206.7	109.9/109.3	92.1	[30]
	2 Na <sup>+</sup> ( $\alpha$ )	C <sub>s</sub>	206.1/206.6	107.3/108.1	88.6	[57]
	2 NH <sub>4</sub> <sup>+</sup>	(C <sub>2</sub> )	205.8–207.3	106.4–109.0	67.1/68.0	[32]
	2 K <sup>+</sup>	(C <sub>2</sub> )	203.7–207.5	106.4–109.7	68.7/73.6	[58]
	2 Rb <sup>+</sup>	(C <sub>2</sub> )	201.9–210.9	107.5–111.2	68.7/74.5	[59]
	2 Cs <sup>+</sup> (H <sub>2</sub> O) <sup>b</sup>	(C <sub>2</sub> )	204.8–207.0	106.9–107.9	69.2/75.7	[60]
	2 Tl <sup>+</sup>	(C <sub>2</sub> )	206–216	107–109	67/73	[61]
	2 Cs <sup>+</sup>	(C <sub>2</sub> )	199–212	108.1–109.5	61.4/78.6/81.9	[63]
S <sub>6</sub> <sup>2-</sup>	2 Li(teeda) <sup>+</sup>	(C <sub>2</sub> )	disordered			[30]
	2 Bu <sub>4</sub> N <sup>+</sup>	C <sub>2</sub>	206.2–209.0	109.5/110.5		[34]
	2 Me <sub>4</sub> N <sup>+</sup>	C <sub>2</sub>	202.2–210.1	108.2/112.1	65.3/88.5	[35]
	enH <sub>2</sub> <sup>2+</sup>	C <sub>1</sub>	202.6–207.7	106.7–109.8	58.9–82.0	<XAppendix>[36]
	2 enH <sup>+</sup>	(C <sub>2</sub> )	202.3–206.7	107.2–110.8	71.2–85.0	[37]
	2 Li(tmada) <sup>+</sup>	C <sub>2</sub>	disordered			[40,41]
	2 Me <sub>3</sub> NH <sup>+</sup>	C <sub>2</sub>	203.4–207.9	108.8/111.0	75.5/85.5	[38]
	2 Ph <sub>3</sub> Te <sup>+</sup>	(C <sub>2</sub> )	203.6–210.3	108.7–113.0	84.7–110.4	[42]
	2 Na(tea) <sup>+</sup>	(C <sub>2</sub> )	203.3–205.9			[25]
	2 K(crypt-2.2.2) <sup>+</sup>	C <sub>2</sub>	200.7–207.6	111.8/112.1	83.2/93.0	[39]
S <sub>7</sub> <sup>2-</sup>	2 Pr <sub>4</sub> N <sup>+</sup>	(C <sub>2</sub> )	201.0–209.8	107.5–111.4	65.3–78.7	[43]
	2 K(crypt-2.2.2) <sup>+</sup> (en) <sup>b</sup>	(C <sub>2</sub> )	199.8–208.0	108.8–110.9	75.9–81.5	[39]
	2 Ph <sub>4</sub> P <sup>+</sup>	(C <sub>2</sub> )	199.0–206.2	106.8–111.3	65.2–79.9	[44]
	Ph <sub>4</sub> P <sup>+</sup> , NH <sub>4</sub> <sup>+</sup> (CH <sub>3</sub> CN) <sup>b</sup>	C <sub>1</sub>	196.3–205.9		71.3–96.2	[45]
	2 PPN <sup>+</sup> (2 EtOH) <sup>b</sup>	(C <sub>2</sub> )	202.6–207.2	107.9–110.9	71.8–94.2	[46]
	2 <sup>i</sup> Bu <sub>2</sub> NH <sub>3</sub> <sup>+</sup>	(C <sub>s</sub> )	202.0–205.2	106.3–111.0	74.8–85.5	[47]
	2 Et <sub>3</sub> NH <sup>+</sup>	C <sub>2</sub>	204.1–207.3	107.3–110.4	84.3–97.7	[49]

<sup>a</sup> Symmetry of the anion in the crystal. Data in parentheses give the approximate (non-crystallographic) symmetry<sup>b</sup> Solvent molecule(s) in the crystal structure

crystal X-ray structural analysis is  $Cs_2S_6$  which also contains helical anions [62, 63].

For structures of polysulfides with two-valent cations, see the original literature:  $SrS_2$ ,  $BaS_2$ ,  $SrS_3$ , and  $BaS_3$  in [64] and  $BaS_4 \cdot H_2O$  in [65].

The structures of isolated polysulfide dianions  $S_n^{2-}$  with  $n = 2-8$  have been studied by ab initio molecular orbital calculations with the DZPD basis set [66]. Generally, small dianions cannot exist as isolated particles but either spontaneously lose one electron ("electron autodetachment") or dissociate into two singly charged fragments ("Coulomb explosion"). In the case of the polysulfide dianions it was found that at least seven sulfur atoms are needed to accommodate two negative charges. In the ground state all dianions exhibit a helical structure of  $C_2$  symmetry; other chain-like conformers are only slightly less stable. The negative charges are essentially localized at the terminal atoms ( $0.7 e^-$  each in the case of hepta- and octasulfide). The dissociation of  $S_7^{2-}$  and  $S_8^{2-}$  into polyatomic monoanions is exothermic and most so if the two fragments are of similar or identical size. On the other hand, the dissociation into  $S^-$  and  $S_{n-1}^-$  is endothermic and there may be a substantial activation barrier for this process. In other words, all polysulfide dianions are either unstable or metastable in the gas phase. Surprisingly, branched polysulfide dianions like the tetrahedral  $S_5^{2-}$  ion (analogous to the sulfate ion) and the  $D_{3d}$  structure of  $S_8^{2-}$  (in analogy to the dithionate ion,  $S_2O_6^{2-}$ ) are also local minima but much less stable than the helical chain isomers.

## 5 Polysulfide Solutions

### 5.1 Aqueous Solutions

Water-soluble sulfides like those of the alkali and alkali earth metals dissolve in  $H_2O$  with hydrolysis to give strongly alkaline solutions:



This equilibrium is practically completely on the right side and therefore the pH of sodium sulfide solutions increases from 12 at a concentration of  $0.04 \text{ mol l}^{-1}$  to 13 at  $1.00 \text{ mol l}^{-1}$  [67]. In other words, the pH of these solutions are almost identical to those which one would obtain if pure NaOH had been dissolved instead of  $Na_2S$ . Due to the extremely low value of the second dissociation constant of  $H_2S$  the sulfide ion  $S^{2-}$  exists in water at extremely high pH values only but even then it remains a minority species compared to the  $HS^-$  ion [68]. The value of  $K_{a2}(H_2S)$  is not known exactly and depends on the ionic strength but has been estimated experimentally at  $20^\circ C$  as somewhere between  $10^{-14}$  and  $10^{-17} \text{ mol l}^{-1}$  [68-70] with the latter value being more likely in strongly alkaline solutions (high ionic strength).

Remarkably, in the structure of the solid hydrate  $\text{Na}_2\text{S}\cdot 9\text{H}_2\text{O}$  the sulfide ion is coordinated by 12 hydrogen atoms but no  $\text{SH}^-$  ion is formed [71].

Solutions containing the nucleophiles  $\text{S}^{2-}$  and/or  $\text{HS}^-$  dissolve elemental sulfur by reactions according to the following equations (nucleophilic degradation):



The generated polysulfide dianions of different chain-lengths then establish a complex equilibrium mixture with all members up to the octasulfide at least; see Eqs. (5) and (6). For this reason, it is not possible to separate the polysulfide dianions by ion chromatography [6]. The maximum possible chain-length can be estimated from the preparation of salts with these anions in various solvents (see above). However, since the reactions at Eqs. (22) and (23) are reversible and  $\text{S}_8$  precipitates from such solutions if the pH is lowered below a value of 6, the nonasulfide ion must be present also to generate the  $\text{S}_8$  molecules by the reverse of the reaction at Eq. (22). The latter reaction (precipitation of  $\text{S}_8$  on acidification) may be used for the gravimetric determination of polysulfides [11]. There is no evidence for the presence of monoprotonated polysulfide ions  $\text{HS}_n^-$  in aqueous solutions [67, 72].

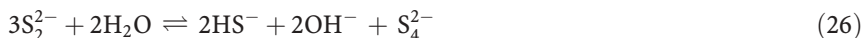
If  $\text{S}_8$  is dissolved in a polysulfide solution the reactions according to Eqs. (24) and (25) are faster than the reactions at Eqs. (22) and (23) since disulfide (and also trisulfide) anions are evidently stronger nucleophiles than  $\text{HS}^-$ :



Consequently, sulfur dissolves in polysulfide solutions much faster than in equimolar monosulfide solutions [73]. In this context it is of interest that the analogous decaselenium dianion  $\text{Se}_{10}^{2-}$  has been prepared and structurally characterized in solid  $[\text{PPN}]_2\text{Se}_{10}$  [74]. This anion is however bicyclic.

Many authors have tried to determine the speciation of the various polysulfide anions in water as a function of sulfur content, pH value, concentration, and temperature. However, since there is no direct method to determine single species either analytically or spectroscopically the results are somewhat speculative and rest on certain assumptions. Most authors agree that tetra- and pentasulfide ions are the dominating species at higher sulfur concentrations and that  $\text{S}_n^{2-}$  ions with  $n > 6$  can be neglected to a first approximation [67]. Schwarzenbach and Fischer [69] demonstrated that aqueous alkali polysulfides can be titrated with hydrochloric acid in a flow apparatus allowing a very rapid mixing with simultaneous measurement of the pH value and exclusion of dioxygen. The authors concluded that at polysul-

fide concentrations of  $0.05 \text{ mol l}^{-1}$  only  $\text{Na}_2\text{S}_5$  dissolves undecomposed, while di-, tri-, and tetrasulfides (of Na or K) hydrolyze almost quantitatively according to the following equations (at  $20^\circ\text{C}$ ):



Therefore, the pH values of these solutions are between 11 and 12. The speciation model used by Schwarzenbach and Fischer is certainly too simple but these authors have been the first to demonstrate the strong dependence of the polysulfide anion distribution on the alkalinity. According to Eqs. (26)–(28) higher pH values in dilute solutions will favor smaller anion sizes.

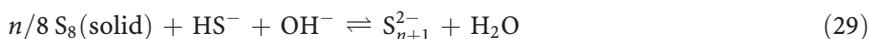
Teder has been the first to analyze successfully aqueous sodium polysulfide solutions by UV-Vis absorption spectroscopy in the range of 200–600 nm and at pH values ranging from 11 to 13.8 [75]. He observed eight overlapping bands one of which could be assigned to the  $\text{HS}^-$  ion (at 230 nm) while the other seven (240–400 nm) all seemed to have contributions from polysulfide ions with up to six sulfur atoms. The spectra were analyzed by varying the alkalinity, the ratio of sulfide: polysulfide excess sulfur (i.e., the sulfur atoms of formal oxidation number zero in the polysulfide chain) and the temperature (25 and  $80^\circ\text{C}$ ). The results could be interpreted with the assumption that tetra-, penta-, and hexasulfide ions are the dominating species besides trisulfide ions and hydrogen monosulfide while the concentration of  $\text{S}^{2-}$  was negligible at  $25^\circ\text{C}$ . Also, monoprotonated polysulfide ions were not observed. However, several models with differing polysulfide species could explain the experimental data equally well! The mean size of the polysulfide ions increased with temperature and decreased with increasing alkalinity (see Eq. 23) and reached maximum values of 5 atoms at  $25^\circ\text{C}$  and 6.5 atoms at  $80^\circ\text{C}$ . Interestingly, in ethanolic solution the maximum size of the polysulfide ions is even larger resulting in additional absorption bands in the visible region at 476 and 588 nm. The wings of the polysulfide bands in the near UV stretching into the visible region cause the yellow color of dilute polysulfide solutions. At higher concentrations the color changes via orange to red; it has been shown above that solid hexa-, hepta- and octasulfides are red (see above).

The composition of sodium polysulfide solutions *saturated* with sulfur of zero oxidation number ( $\text{S}^0$ ) has also been studied at 25 and  $80^\circ\text{C}$  (solutions in contact with elemental sulfur) [76]. In this case the ratio  $\text{S}^0:\text{S}^{2-}$  per polysulfide ion increases with increasing alkalinity. The maximum average number of sulfur atoms per polysulfide molecule was obtained as 5.4 at  $25^\circ\text{C}$  and 6.0 at  $80^\circ\text{C}$  and pH values of  $>12$ . Equilibrium constants for reactions as in Eqs. (26) and (27) have been derived assuming various models with differing numbers of polysulfide ions present.

The isotopic exchange between radioactive elemental sulfur containing traces of  $^{35}\text{S}$  and aqueous polysulfide at  $\text{pH}=7.6$  has been shown to be very rapid. Within less than 2 min half of the tracer from  $^{35}\text{S}^0$  had exchanged [77].

Optical measurements on polysulfide solutions at  $20\text{ }^\circ\text{C}$  similar to those described above have also been carried out by Giggenbach who varied the  $\text{pH}$  value between 6.8 and 17.5 and recorded spectra of *dilute solutions* at wavelengths of between 250 and 500 nm [5]. Depending on the concentrations of  $\text{OH}^-$ ,  $\text{SH}^-$ , and  $\text{S}^0$  the spectra showed five absorption bands which were assigned to specific ions as follows:  $\text{S}_2^{2-}$ : 358,  $\text{S}_3^{2-}$ : 417,  $\text{S}_4^{2-}$ : 368,  $\text{S}_5^{2-}$ : 375 nm. This order is rather surprising since one would expect the wavelengths to steadily increase with increasing chain-length as has been observed for covalent polysulfanes [78]. On the other hand, the  $\lambda_{\text{max}}$  values for tetra- and pentasulfide are in agreement with earlier measurements [69]. These absorption bands are however too close to each other for an accurate quantitative analysis. The maximum average number of 4.5 sulfur atoms in the polysulfide ions derived by Giggenbach for solutions saturated with sulfur at temperatures of between  $20$  and  $180\text{ }^\circ\text{C}$  and an ionic strength of 0.4 [72] is relatively low and in contrast to the results of Teder [76] and Jordan et al. [79] which was explained by the lower concentrations [80]. Giggenbach later extended his studies up to temperatures of  $240\text{ }^\circ\text{C}$  [80]. Licht et al. [81] duplicated Giggenbach's work using a different numerical analysis of the data without obtaining more reliable results, partly because ions larger than  $\text{S}_5^{2-}$  were neglected. The following peaks were assigned to the polysulfide ions considered (wavelengths in nm):  $\text{S}^{2-}$ : 358,  $\text{S}_3^{2-}$ : 429,  $\text{S}_4^{2-}$ : 372,  $\text{S}_5^{2-}$ : 377.

Hamilton [13] assumed the presence of all ions  $\text{S}_n^{2-}$  with  $n$  ranging from 1 to 8 in aqueous polysulfide solutions which is by far the most acceptable model but since there is insufficient experimental data available this model cannot be worked out quantitatively without additional assumptions. The general idea is that those species are most abundant which are close to the average composition of the particular solution, e.g.,  $\text{S}_4^{2-}$  and  $\text{S}_5^{2-}$  for a solution of composition  $\text{Na}_2\text{S}_{4.5}$ , and that the larger and smaller ions are symmetrically less abundant. Equilibrium constants for the various reactions



in water were derived for a number of different speciation models ( $n = 1-7$ ). The presence of several ions larger than  $\text{S}_5^{2-}$  in aqueous polysulfide solutions has in fact been demonstrated by laser desorption mass spectroscopy [28].

Giggenbach observed that the absorption band of  $\text{HS}^-$  at 230 nm in solutions of  $\text{H}_2\text{S}$  in concentrated aqueous  $\text{NaOH}$  developed a shoulder at ca. 250 nm with increasing  $\text{OH}^-$  concentration; he assigned the new band to the hydrated sulfide ion  $\text{S}^{2-}(\text{aq})$  [68].

## 5.2

### Non-Aqueous Solutions

Ionic polysulfides dissolve only in media of high polarity like water, liquid ammonia, alcohols, nitriles, amines, and similar solvents. In all of these solvents  $S_8$  can be reduced electrochemically to polysulfide anions. On the other hand, the electrochemical oxidation of polysulfide anions produces elemental sulfur:



The chemistry of elemental sulfur and sulfur-rich molecules including polysulfides in liquid ammonia [82] and in primary as well as secondary amines [83] is complex because of the possible formation of sulfur-nitrogen compounds. Therefore, polysulfide solutions in these solvents will not be discussed here. Inert solvents which have often been used are dimethylformamide (DMF) [84–86], tetrahydrofuran (THF) [87], dimethylsulfoxide (DMSO) [87], and hexamethylphosphoric triamide (HMPA) [86, 88].

Ionic polysulfides dissolve in DMF, DMSO, and HMPA to give air-sensitive colored solutions. Chivers and Drummond [88] were the first to identify the blue  $S_3^{\cdot-}$  radical anion as the species responsible for the characteristic absorption at 620 nm of solutions of alkali polysulfides in HMPA and similar systems while numerous previous authors had proposed other anions or even neutral sulfur molecules (for a survey of these publications, see [88]). The blue radical anion is evidently formed by reactions according to Eqs. (5)–(8) since the composition of the dissolved sodium polysulfide could be varied between  $Na_2S_3$  and  $Na_2S_{14}$  with little impact on the visible absorption spectrum. On cooling the color of these solutions changes via green to yellow due to dimerization of the radicals which have been detected by magnetic measurements, ESR, UV-Vis, infrared and resonance Raman spectra [84, 86, 88, 89]; see later.

### 5.2.1

#### Electrochemical Studies

The electrochemical reduction and oxidation of sulfur and of polysulfide dianions at inert electrodes has been studied in aprotic solvents and in liquid ammonia. In the latter case, sulfur-nitrogen compounds are involved and these systems [90] will not be discussed here.

The electrochemical reduction of  $S_8$  in aprotic solvents like DMSO [87, 91, 92], DMF [92, 93], dimethylacetamide [94], acetonitrile [95], or methanol [95] yields primarily  $S_8^{2-}$  ions which then equilibrate with other dianions and radical anions like  $S_3^{\cdot-}$  and others; see Eqs. (4)–(8). In a second reduction step tetrasulfide ions are formed:



However, the actual mechanism of tetrasulfide formation may be as follows [93]:



Besides  $\text{S}_8$ , the homocycles  $\text{S}_6$  and  $\text{S}_7$  have been reduced electrochemically in methanol (Au electrode); the reported half-wave potentials are  $-0.50$ ,  $-0.54$ , and  $-0.63$  V ( $\pm 0.03$  V each) for  $\text{S}_6$ ,  $\text{S}_7$ , and  $\text{S}_8$ , respectively [95].

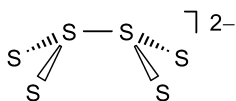
## 6 Vibrational Spectra

Vibrational spectroscopy and in particular Raman spectroscopy is by far the most useful spectroscopic technique to qualitatively characterize polysulfide samples. The fundamental vibrations of the polysulfide dianions with between 4 and 8 atoms have been calculated by Steudel and Schuster [96] using force constants derived partly from the vibrational spectra of  $\text{Na}_2\text{S}_4$  and  $(\text{NH}_4)_2\text{S}_5$  and partly from *cyclo*- $\text{S}_8$ . It turned out that not only species of differing molecular size but also rotational isomers like  $\text{S}_5^{2-}$  of either  $C_2$  or  $C_s$  symmetry can be recognized from pronounced differences in their spectra. The latter two anions are present, for instance, in  $\text{Na}_2\text{S}_5$  ( $C_s$ ) and  $\text{K}_2\text{S}_5$  ( $C_2$ ), respectively (see Table 2).

Reliable spectra of  $\text{K}_2\text{S}_3$  [97],  $\text{BaS}_3$  [98],  $\text{Na}_2\text{S}_4$  [99–101],  $\text{Cs}_2\text{S}_4$  [101],  $\text{Na}_2\text{S}_5$  [99],  $\text{Rb}_2\text{S}_5$  [101],  $\text{K}_2\text{S}_5$  [97, 99],  $\text{K}_2\text{S}_6$  [97],  $\text{Cs}_2\text{S}_6$  [101], as well as of  $(\text{NH}_4)_2\text{S}_5$  [96] have been published. Corset et al. studied the reactions of sodium sulfide and disulfide with elemental sulfur at high temperatures and identified the solid phases  $\alpha$ - and  $\beta$ - $\text{Na}_2\text{S}_2$ ,  $\alpha$ -,  $\gamma$ -, and glassy  $\text{Na}_2\text{S}_4$ , as well as  $\alpha$ -,  $\beta$ -,  $\gamma$ -,  $\delta$ -, and glassy  $\text{Na}_2\text{S}_5$  by Raman spectroscopy [18].

For Raman spectra of hexa- [30, 40] and heptasulfides [46] with complex univalent cations, see the original literature.

Several authors studied the changes in the Raman spectra of alkali polysulfides on heating. Heating of pure  $\text{Na}_2\text{S}_4$  or mixtures of this salt with KSCN to 300 °C produces the radical anions  $\text{S}_3^{\cdot-}$  (detected by their resonance Raman effect) [102]. The thermal behavior of the tetra-, penta-, and hexasulfides of Na, Rb, and Cs up to 400 °C were studied by Ziemann and Bues [101] and the formation of  $\text{S}_3^{\cdot-}$  radicals in the melt of  $\text{Cs}_2\text{S}_4$  (but not in the case of  $\text{Na}_2\text{S}_4$ ) was observed. Evidently  $\text{S}_3^{\cdot-}$  results from the reactions according to Eqs. (5) and (8).  $\text{Cs}_2\text{S}_6$  turns black on melting, and the spectrum of the rapidly quenched melt is different from the original hexasulfide which has been interpreted in terms of a hexasulfide isomer with the structure shown in Scheme 1.



Scheme 1

This black material changed back to the ordinary structure of  $Cs_2S_6$  on annealing. The formation of the isomeric hexasulfide (analogous to the structure of the isoelectronic dithionite anion) was explained by recombination of two trisulfide radical anions [101].

## 7

### Reactions in Solution

Under special conditions the rapid protonation of aqueous polysulfide ions by hydrochloric acid at temperatures of below 0 °C produces polysulfanes:



However, some interconversion reactions take place simultaneously and therefore the composition of the sulfane mixture is not a mirror image of the composition of the polysulfide solution [103]. The sulfane mixture forms a yellow oily hydrophobic liquid which precipitates from the aqueous phase. At 20 °C it decomposes more or less rapidly to  $H_2S$  and  $S_8$ .

Sulfite ions react with polysulfide ions at 50 °C in neutral solution to thio-sulfate and monosulfide, e.g.:



This reaction has also been used for the titrimetric determination of polysulfides [10, 11].

In a similar fashion, cyanide ions desulfurize polysulfide ions at 100 °C to the monosulfide level, e.g.:



After acidification with  $H_3PO_3$  the extremely poisonous  $HCN$  and  $H_2S$  formed may be evaporated by refluxing under a fume hood; subsequently the thiocyanate can be titrated [10, 11]. The degradation of the polysulfide in the reactions at Eqs. (35) and (36) results in discoloration of the solutions.

Alkaline hydrogen peroxide oxidizes polysulfides to sulfate, e.g.:



Titration of the unreacted hydroxide with standard sulfuric acid allows the determination of the polysulfide [10, 11].

Aqueous polysulfide solutions are thermodynamically unstable with respect to thiosulfate and sulfide. Therefore, on heating to 150–240 °C under anaerobic conditions polysulfide ions disproportionate reversibly [72, 80, 104], e.g.:



This equilibrium can be approached from both sides. In other words, thiosulfate and sulfide react at 240 °C to a solution containing polysulfide.

Below 150 °C the forward reaction is very slow because of the high activation energy. The color of a polysulfide solution at a pH around 7 changes on heating from a deepening yellow through green to blue (formation of  $S_3^{2-}$ , see the following section). At temperatures above 200 °C the color starts to fade with the solution becoming almost colorless at 240 °C due to the reaction at Eq. (38). On lowering the temperature all of the above changes can be observed in reverse order [72]. The reaction rates and activation energies of the forward and reverse reactions have been determined under various conditions [105, 106]. At temperatures above 250 °C thiosulfate also disproportionates or hydrolyzes according to the Eq. (39) [107]:



Aqueous polysulfide  $S_n^{2-}$  rapidly takes up molecular oxygen to produce thiosulfate and, for chain-lengths  $n > 2$ , elemental sulfur [6, 108]:



Since this is a spin-forbidden reaction it has been suspected that the reactive species is a radical anion like  $S_2^-$  or  $S_3^-$  produced by homolytic dissociation of an appropriate polysulfide dianion; see Eqs. (7) and (8) as well as the following section. During the course of the reaction at Eq. (40) the originally yellow solution becomes colorless.

Very often inorganic polysulfides have been used to synthesize organic polysulfanes by reaction with, for example, alkyl or aryl halides [109, 110], e.g.:



Finally, it should be mentioned that polysulfides are formed on oxidation of hydrogen sulfide ions in water, either electrochemically [111] or by oxidation with molecular oxygen:



The latter reaction has been studied numerous times because of its relevance for the autoxidation of hydrogen sulfide in seawater and other aqueous systems [112, 113]. Since the polysulfide ions can be further oxidized to elemental sulfur which precipitates from the solution, these reactions are the basis for several industrially important desulfurization processes (e.g., the Stretford, Sulfolin, Lo-Cat, SulFerox, and Bio-SR processes) [114]:



The latter reactions are catalyzed by a number of transition metal ions which can exist in several oxidation states in aqueous solution, e.g.,  $Fe^{2+/3+}$  [28]:



The tetrasulfide radical anion will dimerize to  $S_8^{2-}$  which equilibrates with longer chains from which eventually  $S_8$  is formed by the back reaction shown in Eq. (22).

## 8 Polysulfide Radical Anions

### 8.1

#### General

The chemistry of polysulfide radical anions  $S_n^{\cdot-}$  ( $n = 2-4$ ) was reviewed by Chivers [12] in 1977, including a historical discussion describing the difficult route to the final identification of these ubiquitous and highly colored species. However, since that time considerable progress has been made. Only the species  $S_2^{\cdot-}$ ,  $S_3^{\cdot-}$ , and  $S_6^{\cdot-}$  have been experimentally characterized in detail while the existence of  $S_4^{\cdot-}$  has only been suspected. The nature of the color centers in ultramarine-type solids ( $S_2^{\cdot-}$ ,  $S_3^{\cdot-}$ ) has been reviewed by Reinen and Lindner [115].

### 8.2

#### The Radicals $S_2^{\cdot-}$ and $S_3^{\cdot-}$

The yellow disulfide radical anion and the brilliant blue trisulfide radical anion often occur together for what reason some authors of the older literature (prior to 1975) got mixed up with their identification. Today, both species are well known by their ESR, infrared, resonance Raman, UV-Vis, and photoelectron spectra, some of which have been recorded both in solutions and in solid matrices. In solution these radical species are formed by the homolytic dissociation of polysulfide dianions according to Eqs. (7) and (8). Since these dissociation reactions are of course endothermic the radical formation is promoted by heating as well as by dilution. Furthermore, solvents of lower polarity than that of water also favor the homolytic dissociation. However, in solutions at 20 °C the equilibria at Eqs. (7) and (8) are usually on the left side (excepting extremely dilute systems) and only the very high sensitivity of ESR, UV-Vis and resonance Raman spectroscopy made it possible to detect the radical anions in liquid and solid solutions; see above.

The addition of elemental sulfur to systems containing  $S_2^{\cdot-}$  or  $S_3^{\cdot-}$  results in the formation of more sulfur-rich species [89]:



Therefore, on addition of sulfur the color of a solution of  $\text{Na}_2\text{S}_4$  in DMF changes from originally yellow-green ( $\text{S}_2^{\cdot-}$ ) via blue ( $\text{S}_3^{\cdot-}$ ) to red (maybe  $\text{S}_4^{\cdot-}$ ) [89]. The existence of  $\text{S}_4^{\cdot-}$  is, however, still disputed (see below).

Heating of certain alkali halides with elemental sulfur also produces colored materials containing the anions  $\text{S}_2^{\cdot-}$  or  $\text{S}_3^{\cdot-}$  which replace the corresponding halide ions. For example, NaCl and KI crystals when heated in the presence of sulfur vapor incorporate di- and trisulfide monoanions [116–119] which can be detected, inter alia, by resonance Raman spectroscopy [120, 121]:



In a KI matrix the electronic absorption maximum of  $\text{S}_2^{\cdot-}$  is observed at 400 nm, and the SS stretching vibration by a Raman line at  $594 \text{ cm}^{-1}$ .  $\text{S}_3^{\cdot-}$  shows a Raman line at  $546 \text{ cm}^{-1}$  and an infrared absorption at  $585 \text{ cm}^{-1}$  which were assigned to the symmetric and antisymmetric stretching vibrations, respectively. The bromides and iodides of Na, K, and Rb have also been used to trap  $\text{S}_2^{\cdot-}$  but the wavenumbers of the SS stretching vibration differ by as much as  $18 \text{ cm}^{-1}$  from the value in KI. The anion  $\text{S}_3^{\cdot-}$  has been trapped in the chlorides, bromides and iodides of Na, K, and Rb [120]. While the disulfide monoanion usually occupies a single anion vacancy [116, 122], the trisulfide radical anion prefers a trivacancy (one cation and two halide anions missing) [119].

With the same technique  $\text{S}_3^{\cdot-}$  has been detected in the mineral ultramarine (lapislazuli) [120]. Lapislazuli is one of the oldest precious stones which was already in use in the Sumerian civilization about 5500 years ago. The underlying pigment ultramarine contains the color centers  $\text{S}_2^{\cdot-}$  and  $\text{S}_3^{\cdot-}$  incorporated into the cages of the mineral sodalite  $\text{Na}_8[\text{Al}_6\text{Si}_6\text{O}_{24}]\text{Cl}_2$ , an aluminosilicate which belongs to the class of zeolites. The colorless sodalite turns more or less blue if the radical anions  $\text{S}_2^{\cdot-}$  (yellow) and  $\text{S}_3^{\cdot-}$  (blue) substitute the chloride anions (as well as a sodium cation) partly or completely, a typical composition being  $\text{Na}_{6.9}[\text{Al}_{5.6}\text{Si}_{6.4}\text{O}_{24}]\text{S}_{2.0}$ . Depending on the concentration ratio between the two radical anions the material will be either violet-blue (high ratio  $\text{S}_3^{\cdot-}:\text{S}_2^{\cdot-}$ ), steel-blue or green (low ratio) [86, 115]. The concentration of  $\text{S}_3^{\cdot-}$  in commercial blue ultramarine pigments has been determined by quantitative ESR spectrometry. Only one out of two  $\beta$  cages of the sodalite structure were occupied by  $\text{S}_3^{\cdot-}$  ions (maximum of  $54 \times 10^{19}$  spins per gram). These ions are coordinated by four sodium cations. In addition,  $\text{S}_2^{\cdot-}$  ions were detected [123].

In certain pink and red colored ultramarine varieties an additional red colored species absorbing at  $\lambda_{\text{max}}=520 \text{ nm}$  has been detected but its identity has been disputed; it may be the radical anion  $\text{S}_4^{\cdot-}$  or the neutral molecule  $\text{S}_4$  [86, 124–126]. In fact, the *cis*-planar isomer of the latter absorbs at  $\lambda_{\text{max}}=520 \text{ nm}$  in the gas phase and one of its fundamental vibrations ( $678 \text{ cm}^{-1}$ ) [127] matches exactly a resonance Raman line of the red chro-

mophore in pink ultramarine. Thus, the assignment to the  $C_{2v}$  isomer of  $S_4$  seems justified.

Nowadays, ultramarine-type pigments are produced synthetically. Inside the zeolite structure the highly reactive sulfur radical anions are well protected which explains the stability of the blue color over thousands of years in air. However, the species responsible for the blue color should not be confused with the sulfur radical *cations* responsible for the blue color of sulfur solutions in fuming sulfuric acid (oleum) and similar oxidizing mixtures [128] or with the blue anion  $S_4N^-$  ( $\lambda_{\max}=580$  nm) which is also present in solutions of sulfur in liquid ammonia in addition to the radical anion  $S_3^{\cdot-}$  [129].  $S_4N^-$  is a planar chain-like anion of connectivity SSNS [130].

The wavenumbers of the stretching vibrations of the radical anions  $S_2^{\cdot-}$  and  $S_3^{\cdot-}$  are higher than those of the corresponding dianions (see above) but lower than those of the corresponding neutral molecules. Since there is a systematic relationship between the bond distances and the bond stretching force constants as well as the wavenumbers of polysulfur compounds [131] it can be concluded that the bond lengths in the monoanions are between those of the dianions and the neutrals; the same holds for the bond strengths. In both anions the unpaired electron occupies an antibonding molecular orbital.

The blue color of  $S_3^{\cdot-}$  has been observed in numerous experiments. For example, a brilliant blue color occurs if a potassium thiocyanate melt is heated to temperatures above 300 °C [132] or if eutectic melts of LiCl-KCl (containing some sulfide) are in contact with elemental sulfur [132, 133], if aqueous sodium tetrasulfide is heated to temperatures above 100 °C [134], if alkali polysulfides are dissolved in boiling ethanol or in polar aprotic solvents (see above), or if borate glasses are doped with elemental sulfur [132]. In most of these cases mixtures of much  $S_3^{\cdot-}$  and little  $S_2^{\cdot-}$  will have been present demonstrating the ubiquitous nature of these radicals [12].

The photoelectron spectrum of gaseous  $S_2^{\cdot-}$  has been measured and analyzed; it provided the value of the ionization energy of this ion as 1.67 eV [135].

### 8.3

#### The Radical $S_4^{\cdot-}$

The red tetrasulfide radical anion  $S_4^{\cdot-}$  has been proposed as a constituent of sulfur-doped alkali halides, of alkali polysulfide solutions in DMF [84, 86], HMPA [89] and acetone [136] and as a product of the electrochemical reduction of  $S_8$  in DMSO or DMF [12]. However, in all these cases no convincing proof for the molecular composition of the species observed by either ESR, Raman, infrared or UV-Vis spectroscopy has been provided. The problem is that the red species is formed only in sulfur-rich solutions where long-chain polysulfide dianions are present also and these are of orange to red color, too (for a description of this dilemma, see [89]). Furthermore, the presence of the orange radical anion  $S_6^{\cdot-}$  (see below) cannot be excluded in such systems.

More recently,  $S_4^-$  may have been identified by ESR spectroscopy of solutions of  $Li_2S_n$  ( $n > 6$ ) in DMF at 303 K. The lithium polysulfide was prepared from the elements in liquid ammonia. These polysulfide solutions also contain the trisulfide radical anion ( $g = 2.0290$ ) but at high sulfur contents a second radical at  $g = 2.031$  (Lorentzian lineshape) was formed which was assumed to be  $S_4^-$  generated by dissociation of octasulfide dianions; see Eq. (32) [137].

The more reasonable formation of the tetrasulfide radical by the reaction shown in Eq. (51)

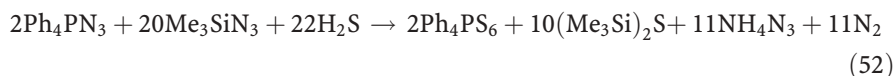


was not considered by the authors despite the presence of both radicals in the same solution. Most authors discussing the solutions of polysulfide dianions in aprotic solvents assumed the presence of tri-, tetra-, hexa-, and octasulfide ions but usually ignored the equally likely existence of penta- and heptasulfide anions in these systems; see Eqs. (5)–(8) and (51).

## 8.4

### The Radical $S_6^-$

This species has been isolated as the tetraphenylphosphonium salt  $(Ph_4P)S_6$  which is produced in the following complex reaction at 20 °C [138]:



$Ph_4PS_6$  forms orange needle-like air-sensitive crystals which were characterized by X-ray diffraction. The anions are cyclic and adopt a chair-conformation of  $C_{2h}$  symmetry. These rings can be considered to be composed of two  $S_3$  units connected by two extremely long bonds of 263 pm. The ESR spectrum of  $Ph_4PS_6$  at 115 K ( $g$ : 2.056/2.036/2.003) is different from those of  $S_2^-$  and  $S_3^-$  and it is possible that the  $S_6^-$  radical is identical to the species which many authors have taken for  $S_4^-$  (see above).

## 8.5

### Calculated Structures

The electronic structure and the UV-Vis spectrum of  $S_3^-$  have been studied by high-level ab initio MO calculations [139].

The molecular structures of the isolated polysulfide monoanions  $S_n^-$  with  $n = 2-9$  have been studied by density functional calculations and those of the smaller ions also by ab initio MO calculations. Compared to the neutral  $S_n$  molecules the extra electron occupies an antibonding orbital resulting in longer SS bonds. The species  $S_3^-$  is bent and of  $C_{2v}$  symmetry ( $\alpha = 115^\circ$ ) [140, 141].  $S_4^-$  was calculated to be a planar ion of  $C_{2v}$  symmetry (similar to the neutral molecule  $S_4$ ) but the planar  $C_{2h}$  structure is only slightly less stable [140, 141]. The most stable isomer of  $S_5^-$  is a chain of  $C_s$  symmetry sim-

ilar to the anion structure in  $Na_2S_5$  (torsion angle motif  $+ - a$ ). However,  $S_5^{\cdot-}$  chains of  $C_1$  and  $C_2$  symmetry are by less than  $10 \text{ kJ mol}^{-1}$  less stable than the global minimum [140, 141]. In the case of  $S_6^{\cdot-}$  a chain-like isomer of  $C_2$  symmetry is the global minimum but a ring of the same symmetry (chair conformation) is by only  $2 \text{ kJ mol}^{-1}$  less stable [138, 141]. The  $S_7^{\cdot-}$  anion also exists as many local minima on the potential energy hypersurface. Most stable is a chair-like ring as in the case of neutral  $S_7$  molecules but with one extremely long bond of 289 pm. The global minimum isomer of  $S_8^{\cdot-}$  has a geometry which is a distortion of the crown-shaped  $S_8$  molecule. On addition of the extra electron two bonds on opposite sides of the ring increase in length resulting in a lowering of the molecular symmetry from  $D_{4d}$  to  $D_2$ . The anion  $S_9^{\cdot-}$  also forms chain-like and cyclic isomers; most stable is a chain of  $C_1$  symmetry [141].

By mass spectrometry sulfur radical anions with up to 25 atoms have been detected and there is photoelectron spectroscopic evidence for chain-like as well as cyclic isomers of  $S_6^{\cdot-}$  and  $S_7^{\cdot-}$  [141].

## References

1. C. Dahl, A. Prange, R. Steudel, in *Biopolymers*, Vol. 9 (A. Steinbüchel, S. Matsumura, eds.), Chapter 5, Wiley-VCH, Weinheim, 2002, and references cited therein
2. *Environmental Technologies to Treat Sulfur Pollution* (P. Lens, L. Hulshoff Pol, eds.), IWA Publishing, London, 2000
3. G.H. Kelsall, I. Thompson, *J. Appl. Electrochem.* 1993, 23, 279
4. J.L. Sudworth, A.R. Tilley, *The Sodium Sulfur Battery*, Chapman & Hall, New York, 1985
5. W. Giggenschbach, *Inorg. Chem.* 1972, 11, 1201
6. R. Steudel, G. Holdt, T. Göbel, *J. Chromatogr.* 1989, 475, 442
7. F. Hulliger, *Struct. Bonding (Berlin)* 1968, 4, 83–229
8. K. Matsumoto, T. Koyama, T. Furuhashi, in *Transition Metal Sulfur Chemistry* (E. I. Stiefel, K. Matsumoto, eds.), Chapter 15, ACS Symp. Ser. 653, Washington, D. C. 1996, p. 251
9. Polysulfido complexes: M. Draganjac, T.B. Rauchfuss, *Angew. Chem.* 1985, 97, 745; *Angew. Chem. Int. Ed. Engl.* 1985, 24, 742. N. Takeda, N. Tokitoh, R. Okazaki, *Top. Curr. Chem.* 2003, 231, in print
10. L. Szekeres, *Talanta* 1974, 21, 1
11. A.V. Hanley, F.W. Czech, in *The Analytical Chemistry of Sulfur and its Compounds*, Part I (J.H. Karchmer, ed.), Wiley, New York, 1970, Chapter 5, p. 285
12. Review: T. Chivers, in: *Homoatomic Rings, Chains and Macromolecules of Main-Group Elements* (A.L. Reihngold, ed.), Chapter 22, Elsevier, Amsterdam, 1977, p.499
13. E. McCampbell Hamilton, Ph. D. Thesis, University of Minnesota, Ann Arbor, USA, 1991
14. J. Sangster, A.D. Pelton, *J. Phase Equilibria* 1997, 18, 89
15. J. Sangster, A.D. Pelton, *J. Phase Equilibria* 1997, 18, 82
16. F. Fehér, H.J. Berthold, *Z. Anorg. Allg. Chem.* 1953, 273, 144
17. G.J. Janz, J.R. Downey, E. Roduner, G.J. Wasilczyk, J.W. Coutts, A. Eluard, *Inorg. Chem.* 1976, 15, 1759
18. O. El Jaroudi, E. Picquenard, N. Gobeltz, A. Demortier, J. Corset, *Inorg. Chem.* 1999, 38, 2917
19. F. Fehér, H.J. Berthold, *Z. Anorg. Allg. Chem.* 1953, 274, 223
20. F. Fehér in *Handbuch der Präparativen Anorganischen Chemie*, Vol.1 (G. Brauer, ed.), Enke, Stuttgart, 1975, Chapter 6, p. 356

21. F. Fehér, H.J. Berthold, *Z. Anorg. Allg. Chem.* **1953**, 274, 223
22. T. Takata, D. Saeki, Y. Makita, N. Yamada, N. Kihara, *Inorg. Chem.* **2003**, 42, 3721
23. D.-G. Oei, *Inorg. Chem.* **1973**, 12, 435
24. D.-G. Oei, *Inorg. Chem.* **1973**, 12, 438
25. Y. Chen, Q. Liu, Y. Deng, H. Zhu, C. Chen, H. Fan, D. Liao, E. Gao, *Inorg. Chem.* **2001**, 40, 3725
26. A. Teder, J. Tiberger, *Acta Chem. Scand.* **1970**, 24, 991
27. F. Fehér, K. Naused, *Z. anorg. Allg. Chem.* **1956**, 283, 79
28. E.T. Clarke, T. Solouki, D.H. Russel, A.E. Martell, D. McManus, *Anal. Chem. Acta* **1994**, 299, 97
29. I. Sens, D. Bacher, U. Müller, *Z. Naturforsch. Part B* **1992**, 47, 819
30. K. Tatsumi, H. Kawaguchi, K. Inoue, K. Tani, R. E. Cramer, *Inorg. Chem.* **1993**, 32, 4317
31. H. Mills, P.L. Robinson, *J. Chem. Soc. (London)* **1928**, 2326
32. H.G. von Schnering, N. K. Goh, K. Peters, *Z. Kristallogr.* **1985**, 172, 153
33. A.D. Bacher, I. Sens, U. Müller, *Z. Naturforsch. Part B* **1992**, 47, 702
34. R.G. Teller, L. J. Krause, R. C. Haushalter, *Inorg. Chem.* **1983**, 22, 1809
35. P.Böttcher, W. Flamm, *Z. Naturforsch. Part B* **1986**, 41, 405
36. P. Böttcher, H. Buchkremer, J. Baron, *Z. Naturforsch. Part B* **1984**, 39, 416
37. P. Böttcher, H. Buchkremer-Hermanns, *Z. Naturforsch. Part B* **1987**, 42, 267
38. C. Müller, P. Böttcher, *Z. Naturforsch. Part B* **1994**, 49, 489
39. P. Böttcher, H. Buchkremer-Hermanns, *Z. Naturforsch. Part B* **1987**, 42, 272
40. K. Tatsumi, Y. Inoue, A. Nakamura, R.E. Cramer, W. VanDoorne, J.W. Gilje, *Angew. Chem.* **1990**, 102, 455
41. A.J. Banister, D. Barr, A.T. Brooker, W. Clegg, M.J. Cunnington, M.J. Doyle, S.R. Drake, W.R. Gill, K. Manning, P.R. Raithby, R. Snaith, K. Wade, D.S. Wright, *J. Chem. Soc., Chem Commun.* **1990**, 105
42. M. Wieber, R. Habersack, *Z. Naturforsch. Part B* **1994**, 49, 1314
43. P. Böttcher, W. Flamm, *Z. Naturforsch. Part B* **1986**, 41, 1000
44. M.G. Kanatzidis, N. C. Baenziger, D. Coucouvanis, *Inorg. Chem.* **1983**, 22, 290
45. A. Müller, E. Krickmeyer, M. Zimmermann, M. Römer, H. Bögge, M. Penk, K. Schmitz, *Inorg. Chim. Acta* **1984**, 90, L69
46. T. Chivers, F. Edelmann, J. F. Richardson, K. J. Schmidt, *Can. J. Chem.* **1986**, 64, 1509
47. C. Müller, P. Böttcher, *Z. Naturforsch. Part B* **1993**, 48, 1732
48. B. Czeska, K. Dehnicke, *Z. Naturforsch. Part B* **1985**, 40, 120
49. A. Schliephake, H. Falius, H. Buchkremer-Hermanns, P. Böttcher, *Z. Naturforsch. Part B* **1988**, 43, 21
50. F. Seel, M. Wagner, *Z. Naturforsch. Part B* **1985**, 40, 762
51. S. Dev, E. Ramli, T.B. Rauchfuss, S.R. Wilson, *Inorg. Chem.* **1991**, 30, 2514
52. F. Fehér, H.J. Berthold, *Z. Anorg. Allg. Chem.* **1954**, 275, 241
53. E. Rosén, R. Tegman, *Acta Chem. Scand.* **1971**, 25, 3329
54. H. Föppl, E. Busmann, F.-K. Frorath, *Z. Anorg. Allg. Chem.* **1962**, 314, 12
55. P. Böttcher, *Z. Anorg. Allg. Chem.* **1977**, 432, 167
56. R. Tegman, *Acta Cryst. Ser. B* **1973**, 29, 1463
57. P. Böttcher, R. Keller, *Z. Naturforsch. Part B* **1984**, 39, 577
58. B. Kelly, P. Woodward, *J. Chem. Soc. Dalton Trans.* **1976**, 1314
59. P. Böttcher, *Z. Kristallogr.* **1979**, 150, 65
60. P. Böttcher, G. Trampe, *Z. Naturforsch. Part B* **1985**, 40, 321
61. B. Leclerc, T.S. Kabré, *Acta Cryst. B* **1975**, 31, 1675
62. S.C. Abrahams, E. Grison, *Acta Cryst.* **1953**, 6, 206
63. A. Hordvik, E. Sletten, *Acta Chem. Scand.* **1968**, 22, 3029
64. H.G. von Schnering, N. K. Goh, *Naturwissenschaften* **1974**, 61, 272. S. Yamaoka, J. T. Lemley, J. M. Jenks, H. Steinfink, *Inorg. Chem.* **1975**, 14, 129
65. S.C. Abrahams, *Acta Cryst.* **1954**, 7, 423
66. V. Berghof, T. Sommerfeld, L.C. Cederbaum, *J. Phys. Chem. A* **1998**, 102, 5100
67. P.L. Cloke, *Geochim. Cosmochim. Acta* **1963**, 27, 1265

68. W. Giggenbach, *Inorg. Chem.* **1971**, *10*, 1333
69. G. Schwarzenbach, A. Fischer, *Helv. Chim. Acta* **1960**, *43*, 1365
70. D.J. Phillips, S.L. Phillips, *J. Chem. Eng. Data* **2000**, *45*, 981
71. A. Preisinger, K. Mereiter, O. Baumgartner, G. Heger, W. Mikenda, H. Steidl, *Inorg. Chim. Acta* **1982**, *57*, 237
72. W.F. Giggenbach, *Inorg. Chem.* **1974**, *13*, 1720
73. H. Gerischer, *Z. Anorg. Allg. Chem.* **1949**, *259*, 220
74. D. Fenske, G. Kräuter, K. Dehnicke, *Angew. Chem.* **1990**, *102*, 420
75. A. Teder, *Arkiv Kemi* **1969**, *30*, 379 and **1969**, *31*, 173
76. A. Teder, *Acta Chem. Scand.* **1971**, *25*, 1722
77. H. Fossing, B.B. Jørgensen, *Biogeochemistry* **1990**, *9*, 223
78. Y. Minoura, T. Moriyoshi, *J. Chem. Soc. Faraday Trans.* **1962**, *59*, 1019
79. J. Jordan, reports by the U.S. Department of Energy, cited in ref. [13]
80. W.F. Giggenbach, *Inorg. Chem.* **1974**, *13*, 1724 and 1730
81. S. Licht, G. Hodes, J. Manassen, *Inorg. Chem.* **1986**, *25*, 2486
82. P. Dubois, J.P. Lelieur, G. Lepoutre, *Inorg. Chem.* **1988**, *27*, 73 and 1883, and **1989**, *28*, 2489. C. Jehoulet, A. Demortier, J.P. Lelieur, *J. Electroanal. Chem.* **1990**, *292*, 153
83. F.P. Daly, C.W. Brown, *J. Phys. Chem.* **1975**, *79*, 350 and **1976**, *80*, 480
84. F. Seel, H.-J. Güttler, *Angew. Chem.* **1973**, *85*, 416; *Angew. Chem Int. Ed. Engl.* **1973**, *12*, 420
85. J. Badoz-Lambling, R. Bonnaterre, G. Cauquis, M. Delamar, G. Demange, *Electrochim. Acta* **1976**, *21*, 119
86. R.J.H. Clark, D.G. Cobbold, *Inorg. Chem.* **1978**, *17*, 3169
87. R.D. Rauh, F.S. Shuker, J. M. Marston, S. B. Brummer, *J. Inorg. Nucl. Chem.* **1977**, *39*, 1761
88. T. Chivers, I. Drummond, *Inorg. Chem.* **1972**, *11*, 2525 and references cited therein. T. Chivers, I. Drummond, *J. Chem. Soc. Dalton Trans.* **1974**, 631
89. F. Seel, H.-J. Güttler, G. Simon, A. Wieckowski, *Pure Appl. Chem.* **1977**, *49*, 45
90. E. Levillain, F. Gaillard, A. Demortier, J.P. Lelieur, *J. Electroanal. Chem.* **1996**, *405*, 85 and references cited therein
91. R.P. Martin, W.H. Doub, J.L. Roberts, D.T. Sawyer, *Inorg. Chem.* **1973**, *12*, 1921
92. R. Bonnaterre, G. Cauquis, *J. Chem. Soc. Chem. Commun.* **1972**, 293. J. Badoz-Lambling, R. Bonnaterre, G. Cauquis, M. Delamar, G. Demange, *Electrochim. Acta* **1976**, *21*, 119
93. F. Gaillard, J.P. Levillain, *J. Electrochem. Soc.* **1995**, *389*, 77. E. Levillain, F. Gaillard, P. Leghie, A. Demortier, J.P. Lelieur, *J. Electrochem. Soc.* **1997**, *420*, 167. F. Gaillard, E. Levillain, J.P. Lelieur, *J. Electrochem. Soc.* **1997**, *432*, 129
94. J. Paris, V. Plichon, *Electrochim. Acta* **1981**, *26*, 1823
95. J.B. Richard, M. Aparicio-Razo, D.K. Roe, *J. Electrochem. Soc.* **1990**, *137*, 2143
96. R. Steudel, F. Schuster, *Z. Naturforsch Part A* **1977**, *32*, 1313
97. G.J. Janz, J.W. Coutts, J.R. Downey, E. Roduner, *Inorg. Chem.* **1976**, *15*, 1755
98. G.J. Janz, E. Roduner, J.W. Coutts, J.R. Downey, *Inorg. Chem.* **1976**, *15*, 1751
99. H.H. Eysel, G. Wieghardt, H. Kleinschmager, G. Weddigen, *Z. Naturforsch. Part B* **1976**, *31*, 415
100. R. Steudel, *J. Phys. Chem.* **1976**, *80*, 1516
101. H. Ziemann, W. Bues, *Z. Anorg. Allg. Chem.* **1979**, *455*, 69
102. H.H. Eysel, D. Nöthe, *Z. Naturforsch. Part B* **1976**, *31*, 411
103. See the Chapter on Inorganic Polysulfanes by R. Steudel, *Top. Curr. Chem.* **2004**, *231*, in print.
104. E. Schulek, E. Körös, L. Maros, *Acta Chim. (Budapest)* **1955**, *10*, 291. J.E. Olson, O. Samuelson, *Svensk Papperstidn.* **1966**, *69*, 703. I. Gustafsson, A. Teder, *Svensk Papperstidn.* **1969**, *72*, 249
105. W.F. Giggenbach, *Inorg. Chem.* **1974**, *13*, 1731
106. S. Licht, J. Davis, *J. Phys. Chem. B* **1997**, *101*, 2540
107. W.A. Pryor, *J. Am. Chem. Soc.* **1960**, *82*, 4794
108. R. Steudel, G. Holdt, R. Nagorka, *Z. Naturforsch. Part B* **1986**, *41*, 1519

109. R. Steudel, M. Kustos, in *Encyclopedia of Inorganic Chemistry*, R. B. King (ed.), Vol. 7, Wiley, Chichester, 1994, p.4009
110. R. Steudel, *Chem. Rev.* **2002**, *102*, 3905
111. J. Szyrak, P.G. Komorowski, J.C. Donini, *Electrochim. Acta* **1994**, *15*, 2285
112. J.W. Bowers, M.J. A. Fuller, J.E. Packer, *Chem. Ind. (London)* **1966**, 65
113. K.Y. Chen, J.C. Morris, *Environm. Sci. Technol.* **1972**, *6*, 529
114. R. Steudel, *Ind. Eng. Chem. Res.* **1996**, *35*, 1417 and references cited therein
115. Review: D. Reinen, G.-G. Lindner, *Chem. Soc. Rev.* **1999**, *28*, 75
116. L.E. Vanotti, J.R. Morton, *Phys. Rev.* **1967**, *161*, 282
117. J. Rolfe, *J. Chem. Phys.* **1968**, *49*, 4193
118. L. Schneider, B. Dischler, A. Räuber, *Phys. Stat. Sol.* **1966**, *13*, 141
119. J. Suwalski, H. Seidel, *Phys. Stat. Sol.* **1966**, *13*, 159
120. W. Holzer, M.F. Murthy, H.J. Bernstein, *J. Mol. Spectrosc.* **1969**, *32*, 13
121. H. Fabian, F. Fischer, *J. Raman Spectrosc.* **1989**, *20*, 639
122. S. Van Doorslaer, F. Maes, F. Callens, P. Matthyss, E. Boesman, *J. Chem. Soc., Faraday Trans.* **1996**, *92*, 1579. S. Van Doorslaer, F. Maes, F. Callens, P. Moens, E. Boesman, *J. Chem. Soc., Faraday Trans.* **1994**, *90*, 2541. F. Callens, F. Maes, P. Matthyss, E. Boesman, *J. Phys.: Condens. Matt.* **1989**, *1*, 6921
123. N. Gobeltz-Hautecoeur, A. Demortier, B. Lede, J.P. Lelieur, C. Duhayon, *Inorg. Chem.* **2002**, *41*, 2848
124. R.J.H. Clark, T.J. Dines, M. Kurmoo, *Inorg. Chem.* **1983**, *22*, 2766
125. F. Seel, H.-J. Güttler, A.J. Wieckowski, B. Wolf, *Z. Naturforsch. Part B* **1979**, *34*, 1671
126. G. Geismar, U. Westphal, *Chemiker-Ztg.* **1988**, *112*, 177
127. R. Steudel, Y. Steudel, M.W. Wong, *Top. Curr. Chem.* **2004**, *231*, in print
128. See the Chapter on Polysulfur Cations by I. Krossing, *Top. Curr. Chem.* **2003**, *230*, in print
129. T. Chivers, C. Lau, *Inorg. Chem.* **1982**, *21*, 453
130. T. Chivers, W.G. Laidlaw, R. T. Oakley, M. Trsic, *J. Am. Chem. Soc.* **1980**, *102*, 5773
131. R. Steudel, *Z. Naturforsch. Part B* **1975**, *30*, 281
132. W. Giggenschbach, *Inorg. Chem.* **1971**, *10*, 1308
133. D.M. Gruen, R. L. McBeth, A.J. Zielen, *J. Am. Chem. Soc.* **1971**, *93*, 6691
134. W. Giggenschbach, *Inorg. Chem.* **1971**, *10*, 1306
135. S. Moran, G.B. Ellison, *J. Phys. Chem.* **1988**, *92*, 1794
136. F. Seel, M. Wagner, *Z. Naturforsch. Part B* **1987**, *42*, 801
137. E. Levillain, P. Leghié, N. Gobeltz, J.P. Lelieur, *New. J. Chem.* **1997**, *21*, 335
138. B. Neumüller, F. Schmock, R. Kirmse, A. Voigt, A. Diefenbach, F.M. Bickelhaupt, K. Dehnicke, *Angew. Chem.* **2000**, *112*, 4753
139. C. Heinemann, W. Koch, G.-G. Lindner, D. Reinen, *Phys. Rev. A* **1995**, *52*, 1024. W. Koch, J. Natterer, C. Heinemann, *J. Chem. Phys.* **1995**, *102*, 6159. H. Johansen, *Acta Chem. Scand.* **1995**, *49*, 79
140. V.G. Zakrzewski, W. von Niessen, *Theor. Chim. Acta* **1994**, *88*, 75
141. S. Hunsicker, R.O. Jones, G. Ganteför, *J. Chem. Phys.* **1995**, *102*, 5917. G. Ganteför, S. Hunsicker, R.O. Jones, *Chem. Phys. Lett.* **1995**, *236*, 43

# Polysulfido Complexes of Main Group and Transition Metals

Nobuhiro Takeda<sup>1</sup> · Norihiro Tokitoh<sup>1</sup> · Renji Okazaki<sup>2</sup>

<sup>1</sup> Institute for Chemical Research, Kyoto University, 611-0011, Gokasho, Uji, Kyoto, Japan

*E-mail: ntakeda@boc.kuicr.kyoto-u.ac.jp*

*E-mail: tokitoh@boc.kuicr.kyoto-u.ac.jp*

<sup>2</sup> Department of Chemical and Biological Sciences, Faculty of Science, Japan Women's University, Mejirodai, 2-8-1, 112-8681, Bunkyo-ku, Tokyo, Japan

*E-mail: okazaki@fc.jwu.ac.jp*

**Abstract** Main group and transition metals form complexes with polysulfido ligands of a remarkable structural variety and complexity. These compounds are of high scientific interest but in addition have the potential for serving as catalysts in important industrial processes. The size of the polysulfido ligands can vary between  $S_2^{2-}$  and  $S_9^{2-}$  and the complexes may be mononuclear, polynuclear or even cluster-like. The type of compound formed depends not only on the metal and its oxidation number but to a large extent also on the other ligands present and in particular on their bulkiness. This review describes the progress made in the area of polysulfido complexes with regard of their synthesis, structures and reactions.

**Keywords** Sulfur · Main group metal · Transition metal · Polysulfido complex

1	<b>Introduction</b> . . . . .	154
2	<b>Synthesis</b> . . . . .	155
2.1	Reaction of Low-Valent Metal Compounds with Elemental Sulfur or Other Sulfur Sources . . . . .	155
2.2	Reaction of Metals with Elemental Sulfur in Donor Solvents . . . . .	161
2.3	Oxidation of Ligands on the Metal by Elemental Sulfur. . . . .	162
2.4	Insertion of Sulfur Atoms into M-C or M-M Bonds . . . . .	165
2.5	Reactions of Metal Halides with Polysulfide Dianions . . . . .	166
2.6	Synthesis from Compounds with Formal Metal-Sulfur Double Bonds . . . . .	169
2.7	Synthesis from Hydrogensulfido Complexes. . . . .	170
2.8	Other Synthetic Methods . . . . .	172
3	<b>Structural Properties</b> . . . . .	174
3.1	$S_2^{2-}$ Complexes . . . . .	174
3.2	$S_n^{2-}$ Complexes ( $n > 2$ ) . . . . .	177
3.3	A Tetranuclear Rh Complex with a Rectangular $S_4$ Unit . . . . .	178
4	<b>Reactions</b> . . . . .	180
4.1	Thermal Equilibrium between Polysulfido Complexes . . . . .	180
4.2	Desulfurization by Phosphines . . . . .	181

4.3	Oxidation Reactions . . . . .	184
4.4	Sulfur Transfer Reactions. . . . .	185
4.5	Reactions with Carbenes . . . . .	189
4.6	Reactions with Unsaturated Organic Molecules. . . . .	190
4.7	Reactions with Transition Metal Complexes. . . . .	195
4.8	Reductions by Metals . . . . .	197
4.9	Other Reactions . . . . .	198
	<b>References</b> . . . . .	199

## 1 Introduction

Metal polysulfido complexes have attracted much interest not only from the viewpoint of fundamental chemistry but also because of their potential for applications. Various types of metal polysulfido complexes have been reported as shown in Fig. 1. The diversity of the structures results from the nature of sulfur atoms which can adopt a variety of coordination environments (mainly two- and three-coordination) and form catenated structures with various chain lengths. On the other hand, transition metal polysulfides have attracted interest as catalysts and intermediates in enzymatic processes and in catalytic reactions of industrial importance such as the desulfurization of oil and coal. In addition, there has been much interest in the use of metal polysulfido complexes as precursors for metal-sulfur clusters. The chemistry of metal polysulfido complexes has been studied extensively, and many reviews have been published [1–10].

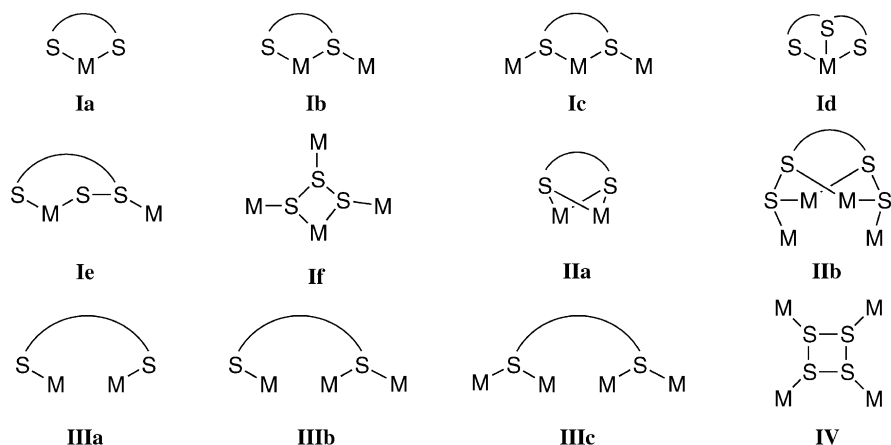


**Fig. 1** Important structure types of polysulfido complexes

In this review, we describe the topics reported during the last ten years for the synthesis, structure, and reactivity of polysulfido complexes of main group and transition metals.

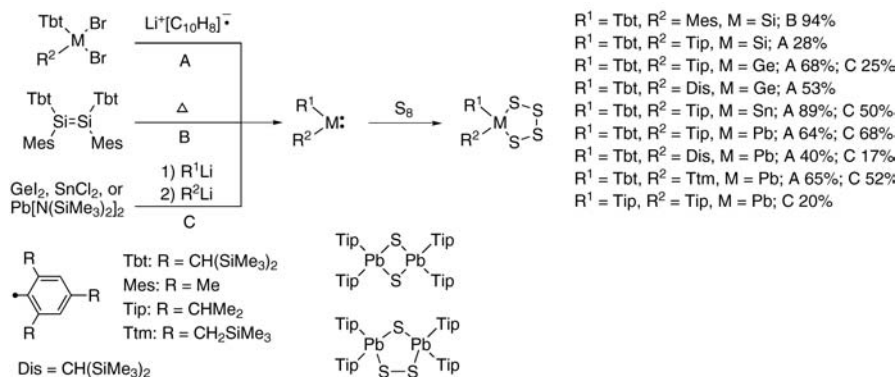
## 2 Synthesis

Metal-polysulfido complexes have been synthesized by a variety of methods using various reagents as sulfur sources, e.g.,  $S_8$ ,  $M_2S_n$  ( $M$ =alkali metal),  $P_2S_5$ ,  $H_2S$ , organic polysulfanes, etc. The nature of the resulting polysulfido complexes often depends on the reaction conditions such as the ratio of starting materials, solvents, reaction temperature, and reaction time. In addition, the use of different ligands leads to the different results in most cases. This section shows typical synthetic methods for metal-polysulfido complexes based on recent reports on their syntheses.

### 2.1

#### Reaction of Low-Valent Metal Compounds with Elemental Sulfur or Other Sulfur Sources

The tetrasulfides  $R^1R^2MS_4$  with  $M$ =Si, Ge, Sn, or Pb bearing bulky substituents on the group 14 element were synthesized by the reaction of the corresponding divalent species  $R^1R^2M$ , which are heavier analogues of the carbenes, with elemental sulfur (see Scheme 1) [11–20]. The divalent species

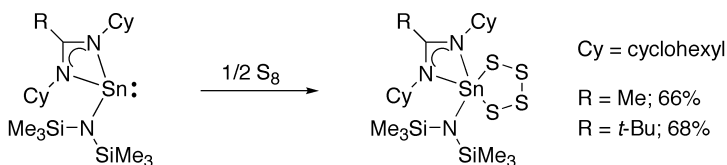


**Scheme 1** Synthesis of group 14 elements polysulfido complexes from divalent compounds bearing bulky substituents

$R^1R^2M$  were prepared by reduction of the dibromides  $R^1R^2MBr_2$  with lithium naphthalenide (method A), by thermolysis of a disilene (method B), and the ligand exchange of divalent group 14 element species (method C). In all cases except for the synthesis of  $\text{Tip}_2\text{PbS}_4$ , exclusively tetrasulfides  $R^1R^2MS_4$

were isolated as stable compounds. It is assumed that the tetrasulfides are thermodynamically controlled products in these cases. The reaction of  $\text{Tip}_2\text{Pb}$  with elemental sulfur gave  $\text{Tip}_2\text{PbS}_4$  together with two byproducts, i.e., dithiadiplumbetane  $(\text{Tip}_2\text{Pb})_2(\mu\text{-S})_2$  (13%) and trithiadiplumbolane  $(\text{Tip}_2\text{Pb})_2(\mu\text{-S})(\mu\text{-S}_2)$  (14%). On the other hand, Steudel et al. have reported that diphenyltetra-thiametallolanes  $\text{Ph}_2\text{MS}_4$  ( $\text{M}=\text{Si}, \text{Ge}$ ) are stable only below  $-20^\circ\text{C}$  [21, 22]. These results strongly suggest that the extremely bulky Tbt group contributes to the stabilization of the tetrathiametallolane rings.

Reactions of stannylenes  $\text{Sn}[\text{N}(\text{SiMe}_3)_2][(\text{NCy})_2\text{CR}]$  ( $\text{R}=\text{Me}, t\text{-Bu}$ ) stabilized by bulky trialkyl amidinates with elemental sulfur proceeded efficiently to afford the corresponding tetrathiastannolane  $\text{Sn}[\text{N}(\text{SiMe}_3)_2][(\text{NCy})_2\text{CR}]_4\text{S}_4$  [23]. This is in sharp contrast to the reaction of  $\text{M}[\text{N}(\text{SiMe}_3)_2]_2$  ( $\text{M}=\text{Ge}, \text{Sn}$ ) with elemental sulfur giving the bridged dimer  $[\text{M}\{\text{N}(\text{SiMe}_3)_2\}_2\text{S}]_2$  [24, 25] (Scheme 2).

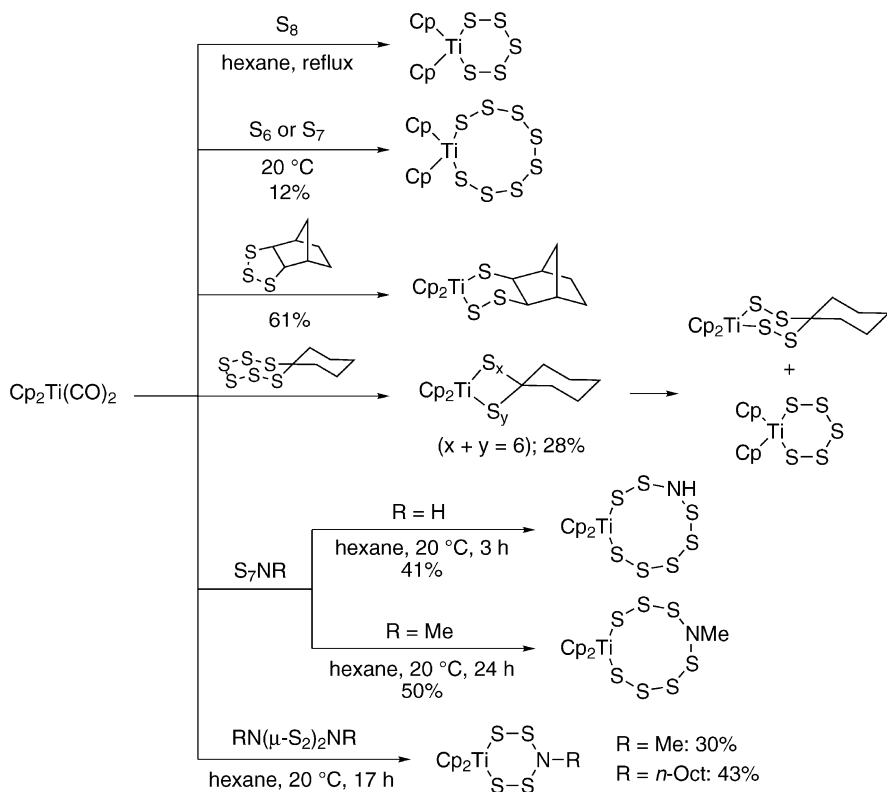


**Scheme 2** Synthesis of five-coordinated tin tetrasulfido complexes from *N*-coordinated divalent tin compounds

A variety of polysulfido complexes of transition metals has also been synthesized by the reactions of low-valent metal complexes with elemental sulfur.

Tatsumi et al. reported that the oxidative addition of cyclooctasulfur to rhodium(I) complexes having P-N hybrid ligands,  $\text{RhCl}(\text{edpp})_2$  and  $\text{RhCl}(\text{edmp})_2$  ( $\text{edpp}=(2\text{-aminoethyl})\text{diphenylphosphine}$ ,  $\text{edmp}=(2\text{-aminoethyl})\text{dimethylphosphine}$ ), yielded the corresponding tetra- and pentasulfido complexes,  $\text{RhClS}_n(\text{edpp})_2$  ( $n=4, 5$ ) and  $\text{RhClS}_n(\text{edmp})_2$  ( $n=4, 5$ ), respectively (Scheme 3) [26]. The coordination geometries of these complexes were different from each other:  $\text{RhClS}_n(\text{edpp})_2$  and  $\text{RhClS}_n(\text{edmp})_2$  have *trans*(*P,N*) and *trans*(*N,N'*) geometries, respectively. The structural differences in these complexes are most likely due to the different steric congestion between the ligands and the relative lability of the coordinated amino donor group between the edmp and edpp ligands. It is noteworthy that the rhodium(I) complexes having bisphosphine ligands,  $(\text{Ph}_2\text{PCH}_2)_2$  and  $(\text{Me}_2\text{PCH}_2)_2$  [27], a bisarsine ligand  $[(\text{Ph}_2\text{AsCH}_2)_2]$  [28], and a trisphosphine ligand  $[\text{PhP}[(\text{CH}_2)_3\text{PPh}_2]_2]$  [29] react with elemental sulfur to afford the corresponding  $\eta^2\text{-S}_2$  complexes  $[\text{Rh}(\eta^2\text{-S}_2)\text{L}_2]^+$ , whereas the oxidative addition of  $\text{S}_8$  to  $\text{RhCp}(\text{PPh}_3)_2$  results in the formation of the corresponding tetra-, penta-, and hexasulfido complexes  $\text{RhCp}(\text{S}_n)(\text{PPh}_3)$  ( $n=4\text{--}6$ ) [30].



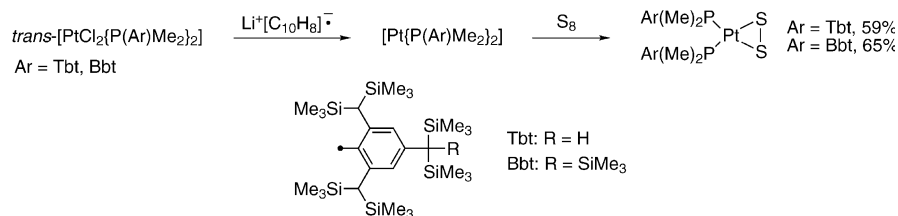


**Scheme 5** Synthesis of titanium polysulfido complexes from  $\text{TiCp}_2(\text{CO})_2$

Titanocene dicarbonyl,  $\text{TiCp}_2(\text{CO})_2$ , is also a good precursor for polysulfido complexes of titanium. The S-S bonds of cyclooctasulfur ( $\text{S}_8$ ) do not react with  $\text{TiCp}_2(\text{CO})_2$  at room temperature, but refluxing in hexane for several days resulted in the pentasulfido complex,  $\text{TiCp}_2\text{S}_5$  [33]. Steudel et al. [34] reported that the reactions of  $\text{TiCp}_2(\text{CO})_2$  with cyclohexasulfur ( $\text{S}_6$ ) and cycloheptasulfur ( $\text{S}_7$ ) in hexane at 20 °C yield precipitates consisting of several  $\text{TiCp}_2\text{S}_n$  molecules ( $n=5, 7$ , and 8 in both cases). Recrystallization of the mixture from  $\text{CS}_2$  gave almost pure  $\text{TiCp}_2\text{S}_8$  as a dark-red solid. The oxidative addition of other sulfur sources such as 1,2,3-trithiolane and hexathiepane to  $\text{TiCp}_2(\text{CO})_2$  resulted in the formation of the expected titanium polysulfido complexes,  $\text{TiCp}_2(\text{C}_7\text{H}_{10}\text{S}_3)$  and  $\text{TiCp}_2(\text{C}_6\text{H}_{10}\text{S}_6)$ , respectively [34]. A grass-green solution of  $\text{TiCp}_2(\text{C}_6\text{H}_{10}\text{S}_6)$  decomposed with the formation of the thermodynamically stable compounds,  $\text{TiCp}_2(\text{C}_6\text{H}_{10}\text{S}_4)$  and  $\text{TiCp}_2\text{S}_5$ . This result suggests that  $\text{TiCp}_2(\text{C}_6\text{H}_{10}\text{S}_6)$  having six sulfur atoms is a kinetically controlled product. In addition,  $\text{TiCp}_2(\text{CO})_2$  reacted with  $\text{S}_7\text{NR}$  ( $\text{R}=\text{H}, \text{Me}$ ) to afford  $\text{TiCp}_2(\text{S}_7\text{NR})$  ( $\text{R}=\text{H}, \text{Me}$ ) via the insertion of the Ti atom to the S-S bond [35]. Interestingly, the structure characterized by X-ray structural analysis is  $\text{TiCp}_2(\mu\text{-S}_2)(\mu\text{-S}_5)\text{NH}$  in the case of  $\text{R}=\text{H}$  while in the case of

R=Me the connectivity is  $\text{TiCp}_2(\mu\text{-S}_3)(\mu\text{-S}_4)\text{NMe}$ . This different behavior between the  $\text{S}_7\text{NH}$  and  $\text{S}_7\text{NMe}$  systems cannot be attributed to either recognizable steric or electronic reasons. By contrast, the reaction with  $\text{RN}(\mu\text{-S}_2)_2\text{NR}$  (R=Me, *n*-Oct) in hexane at 20 °C gave not the expected seven-membered ring compound but a six-membered metallacycle,  $\text{TiCp}_2(\mu\text{-S}_2)\text{NR}$  [36] (Scheme 5).

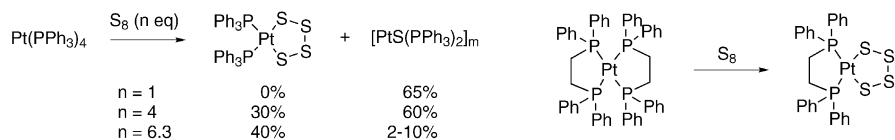
Very recently, the first disulfur complexes of a tetracoordinated transition metal  $\text{PtS}_2[\text{P}(\text{Ar})\text{Me}_2]_2$  (Ar=Tbt, Bbt) were synthesized by the reaction of zerovalent platinum complexes  $\text{Pt}[\text{P}(\text{Ar})\text{Me}_2]_2$ , generated by treatment of the dichloride complexes  $\text{PtCl}_2[\text{P}(\text{Ar})\text{Me}_2]_2$  with lithium naphthalenide, with elemental sulfur (Scheme 6) [37]. Since the use of excess elemental sulfur also



**Scheme 6** Synthesis of platinum disulfido complexes from zerovalent platinum complexes

resulted in the formation of the disulfur complexes  $\text{PtS}_2[\text{P}(\text{Ar})\text{Me}_2]_2$  as the main products they are considered to be thermodynamically controlled products.

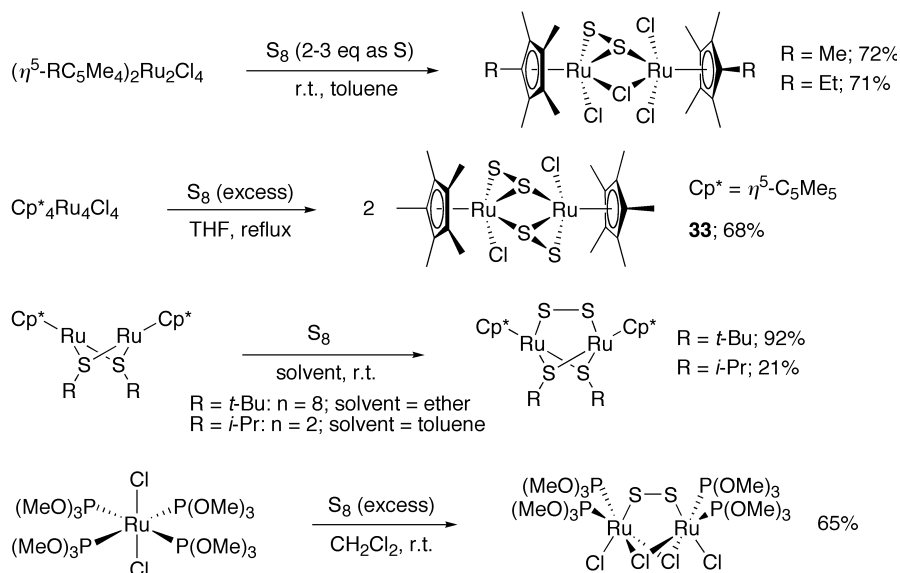
By contrast,  $\text{Pt}(\text{PPh}_3)_4$  reacted with elemental sulfur to give the corresponding tetrasulfido complexes,  $\text{PtS}_4(\text{PPh}_3)_2$ , together with oligomers of  $\text{PtS}(\text{PPh}_3)_2$  units (Scheme 7) [38, 39]. In addition, the reaction of  $\text{Pt}(\text{dppe})_2$



**Scheme 7** Synthesis of platinum tetrasulfido complexes from zerovalent platinum complexes

[dppe=1,2-bis(diphenylphosphino)ethane] with elemental sulfur gave the corresponding tetrasulfido complex,  $\text{PtS}_4(\text{dppe})_2$  (Scheme 7) [38]. The differences in the lengths of the sulfur chain may be interpreted in terms of the different bulkiness of the ligands leading to a change in the thermodynamic stabilities of the platinum-containing cyclic polysulfides.

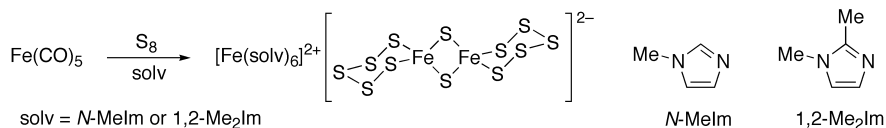
Some disulfide-bridged diruthenium complexes have been synthesized by the reaction of Ru(II) or Ru(III) complexes with elemental sulfur. The binuclear Ru(III) complexes  $\text{Ru}_2(\eta^5\text{-RC}_5\text{Me}_4)_2\text{Cl}_4$  ( $\text{R}=\text{Me}$ ,  $\text{Et}$ ) readily react with  $\text{S}_8$  to afford the disulfido complexes  $\text{Ru}_2(\eta^5\text{-RC}_5\text{Me}_4)_2\text{Cl}_4\text{S}_2$  bearing two non-equivalent ruthenium(IV) atoms in good yields, while the reaction of the Ru(II) complex  $\text{Ru}_4\text{Cp}^*_4\text{Cl}_4$  with excess of  $\text{S}_8$  results in the efficient formation of the diruthenium complex  $\text{Ru}_2\text{Cp}^*_2\text{Cl}_2\text{S}_4$  which has two equivalent ruthenium(IV) atoms (Scheme 8) [40]. In addition, the reaction of a binuclear



**Scheme 8** Synthesis of ruthenium polysulfido complexes from low-valent ruthenium complexes

Ru(II) complex  $(\text{RuCp}^*)_2(\mu\text{-SR})_2$  and a mononuclear Ru(II) complex  $\text{RuCl}_2\{\text{P}(\text{OMe})_3\}_4$  with  $\text{S}_8$  results in the formation of the corresponding disulfide-bridged binuclear ruthenium(III) complexes  $(\text{RuCp}^*)_2(\mu\text{-S}_2)(\mu\text{-SR})_2$  and  $\{\text{RuCl}\{\text{P}(\text{OMe})_3\}_2\}_2(\mu\text{-Cl})_2(\mu\text{-S}_2)$ , respectively [41–43].

The use of *N*-alkylimidazoles as a solvent promotes the reaction of  $\text{Fe}(\text{CO})_5$  with  $\text{S}_8$  [44]. The reaction in *N*-methylimidazole (*N*-MeIm) using 0.5 molar amounts of  $\text{S}_8$  gives the mixed-valence salt  $[\text{Fe}(\text{N-MeIm})_6][\text{Fe}_2\text{S}_{12}]$ , while an equimolar amount of  $\text{S}_8$  resulted in the formation of the octasulfide  $[\text{Fe}(\text{N-MeIm})_6]\text{S}_8$ . The reaction in 1,2-dimethylimidazole (1,2-Me<sub>2</sub>Im) led to  $[\text{Fe}(1,2\text{-Me}_2\text{Im})_6][\text{Fe}_2\text{S}_{12}]$  even in the presence of excess sulfur, probably because the coordinating power of 1,2-Me<sub>2</sub>Im is lower than that of *N*-MeIm due to its steric hindrance (Scheme 9).

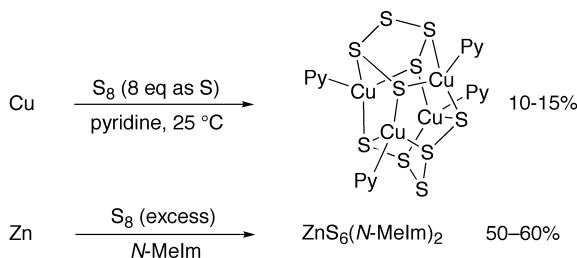


**Scheme 9** Synthesis of iron polysulfido complexes from Fe(CO)<sub>5</sub>

## 2.2

### Reaction of Metals with Elemental Sulfur in Donor Solvents

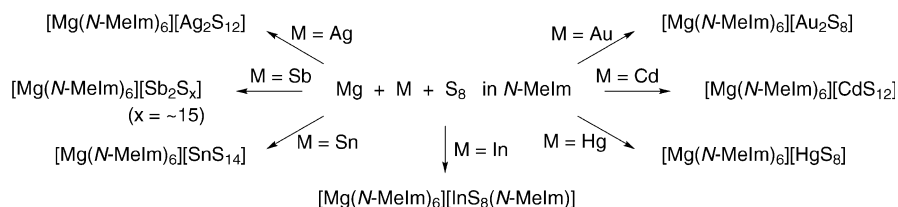
Some compounds with network structures are synthesized by high-temperature reactions of metals with elemental sulfur [2, 8]. Rauchfuss et al. exploited the low-temperature synthesis of metal polysulfides by the reaction of metals with elemental sulfur in strong donor solvents. The reaction of copper powder with S<sub>8</sub> in pyridine gives a copper polysulfide cluster Cu<sub>4</sub>(S<sub>5</sub>)<sub>2</sub>(-py)<sub>4</sub> as orange crystals (Scheme 10) [45]. Furthermore, zinc powder reacts



**Scheme 10** Synthesis of copper and zinc polysulfido complexes by the reaction of a metal with S<sub>8</sub> in donor solvents

with S<sub>8</sub> in *N*-MeIm, tetramethylethylenediamine (TMEDA), 4-(*N,N*-dimethylamino)pyridine (DMAP), or pyridine to give the corresponding hexasulfido complexes, ZnS<sub>6</sub>(*N*-donor) [46, 47]. It has been revealed that the order of the relative stability (DMAP > *N*-MeIm > TMEDA > pyridine) is consistent with that of the basicity of the *N*-donor ligands.

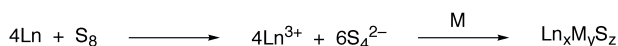
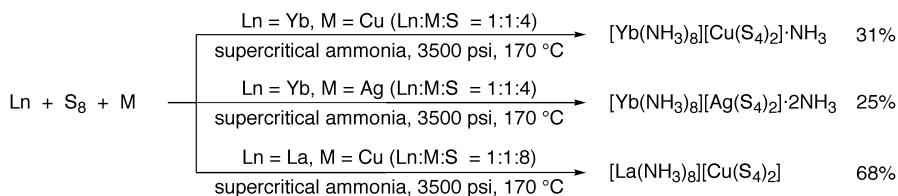
The above-mentioned method is useful but metals that form strong M-S bonds (e.g., Hg, Ag, Sn) do not dissolve in *N*-MeIm solutions of sulfur. This problem has been solved by the addition of Mg to the reaction mixture. Metal polysulfides having a variety of metals can be synthesized by the *N*-MeIm/M+Mg/S<sub>8</sub> method (Scheme 11) [48]. For example, a mixture of Mg, Sb powder (1 eq.), S<sub>8</sub> (15 eq. as S) and *N*-MeIm is heated at 80 °C for 48 h to afford the orange powder of [Mg(*N*-MeIm)<sub>6</sub>]Sb<sub>2</sub>S<sub>*x*</sub> (*x*; ~15) in 88% yield. Rauchfuss et al. proposed the mechanism of these reactions as follows. First, the reduction of S<sub>8</sub> with Mg occurs to give the [Mg(*N*-MeIm)<sub>6</sub>] salt of S<sub>8</sub><sup>2-</sup>, which is probably in equilibrium with S<sub>8</sub>, S<sub>6</sub><sup>2-</sup>, S<sub>3</sub><sup>-</sup> and other species. Independently, the sulfuration of the thiophilic metal takes place. Next, the polysulfide an-



**Scheme 11** Synthesis of metal polysulfido complexes by reaction of a metal with  $\text{S}_8$  in the presence of magnesium

ions attack the polymeric metal sulfide leading to the final product (Scheme 11).

Kolis et al. reported the synthesis of some metal sulfide salts of homoleptic lanthanide ammine complexes using supercritical ammonia as a reaction medium (Scheme 12) [49]. They proposed that these reactions proceed via a



**Scheme 12** Synthesis of metal polysulfido complexes using supercritical ammonia as a solvent

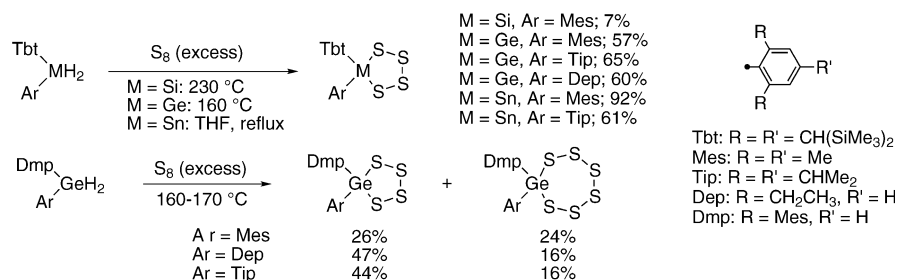
reduction of elemental sulfur by lanthanide metals in supercritical ammonia followed by the reaction of the resulting polysulfide anions with metal powder.

## 2.3

### Oxidation of Ligands on the Metal by Elemental Sulfur

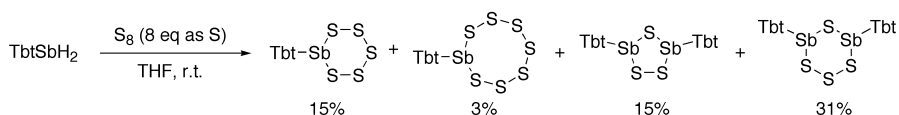
Certain dihydrides of main-group and transition metals are good precursors for metal polysulfides. The reactions of the dihydrides with  $\text{S}_8$  proceed without a change in the oxidation state of the metals.

Dihydrides of heavier group 14 elements bearing bulky substituents such as  $\text{Tbt}(\text{Ar})\text{MH}_2$  react with elemental sulfur to give the corresponding tetrasulfides  $\text{Tbt}(\text{Ar})\text{MS}_4$  (Scheme 13) [50–52]. Sulfuration of germanium dihydride bearing a Dmp group give the corresponding tetra- and hexasulfides,  $\text{Dmp}(\text{Ar})\text{GeS}_x$  ( $x=4, 6$ ). The selectivity on the formation of the hexasulfide  $\text{Dmp}(\text{Ar})\text{GeS}_6$  is higher in the reaction of  $\text{Dmp}(\text{Ar})\text{GeH}_2$  having a less bulky Ar group [53].



**Scheme 13** Synthesis of group 14 element polysulfido complexes from the corresponding metal dihydrides

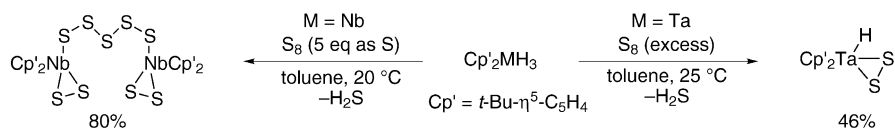
The reaction of dihydrostibine TbtSbH<sub>2</sub> with S<sub>8</sub> at room temperature resulted in the formation of mono- and dinuclear polysulfides (Scheme 14) [54]. On the other hand, the dropwise addition of a THF solution of TbtSbH<sub>2</sub> to a suspension of excess of S<sub>8</sub> in THF at -30 °C led to quite a different re-



**Scheme 14** Synthesis of antimony polysulfido complexes from the corresponding antimony dihydride

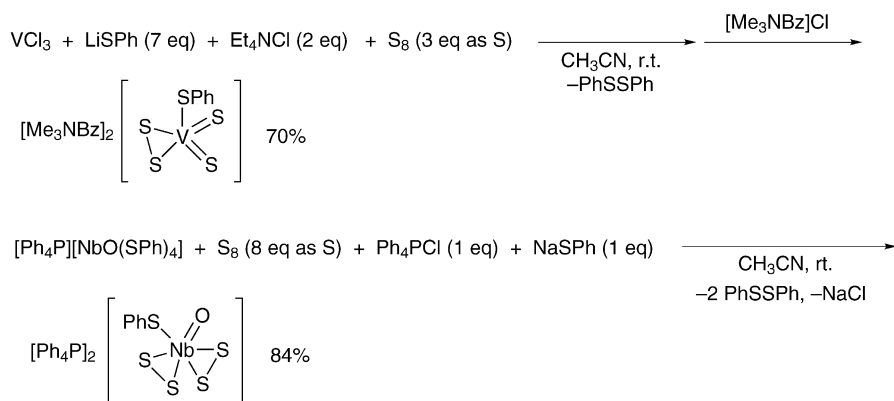
sult, i.e., the formation of the mononuclear polysulfides TbtSbS<sub>5</sub> (49%) and TbtSbS<sub>7</sub> (12%) together with trace amounts of dinuclear polysulfides. The dinuclear polysulfides Tbt<sub>2</sub>Sb<sub>2</sub>S<sub>x</sub> (x=3, 4) originate from the reaction of initially formed TbtSbS<sub>5</sub> and TbtSbS<sub>7</sub> with TbtSbH<sub>2</sub>.

Wachter et al. reported the synthesis of polysulfido complexes of group 5 metals by the reaction of the corresponding trihydrides with elemental sulfur (Scheme 15). The reaction of Cp'<sub>2</sub>NbH<sub>3</sub> with S<sub>8</sub> gives the dinuclear poly-



**Scheme 15** Synthesis of group 5 metal polysulfido complexes from the metal trihydrido complexes



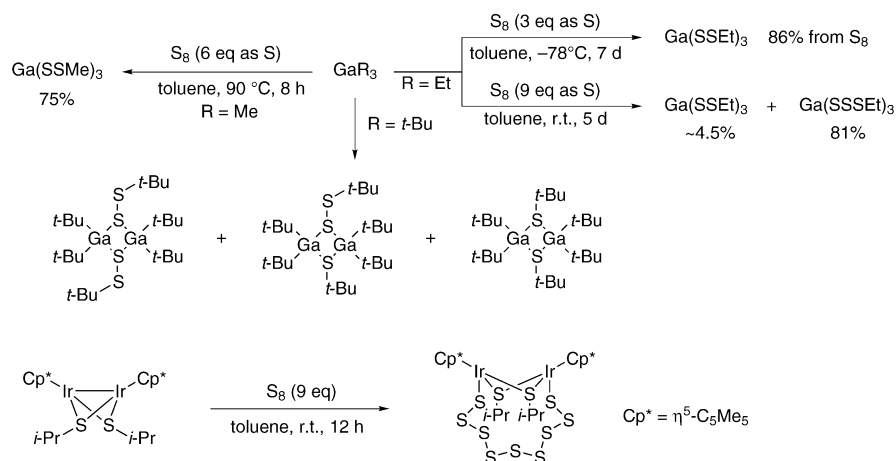


**Scheme 18** Synthesis of group 5 metal disulfido complexes from the metal thiolato complexes

## 2.4

### Insertion of Sulfur Atoms into M-C or M-M Bonds

Some metal polysulfido complexes are synthesized by insertion of sulfur into the M-C or M-M bond. The reaction of  $\text{GaEt}_3$  with 3 equivalents of sulfur in the form of  $\text{S}_8$  at  $-78^\circ\text{C}$  results in the formation of  $\text{Ga}(\text{S}_2\text{Et})_3$  in good yield, while the reaction using 9 equivalents of sulfur at room temperature gives  $\text{Ga}(\text{S}_3\text{Et})_3$  as the main product together with small amounts of  $\text{Ga}(\text{S}_2\text{Et})_3$  (Scheme 19) [60]. The reaction with 12 equivalents of sulfur also af-



**Scheme 19** Synthesis by the insertion reaction of sulfur atoms into the M-C and M-M bond

fords  $\text{Ga}(\text{S}_3\text{Et})_3$ . Therefore, it is assumed that three sulfur atoms are the maximum extent of the sulfur insertion into the Ga-C bonds. Monitoring of these reactions by  $^1\text{H}$  NMR spectroscopy indicated that  $\text{Ga}(\text{S}_3\text{Et})_3$  is the kinetic product, and  $\text{Ga}(\text{S}_2\text{Et})_3$  is formed by the elimination of the sulfur atoms from the initially formed  $\text{Ga}(\text{S}_3\text{Et})_3$ . The reactions of  $\text{GaMe}_3$  with various amounts (3–9 eq) of sulfur in toluene at 90 °C yielded only  $\text{Ga}(\text{S}_2\text{Me})_3$ . On the other hand,  $\text{Ga}(t\text{-Bu})_3$  undergoes the insertion of sulfur atoms into only one Ga-C bond to afford  $[(t\text{-Bu})_2\text{Ga}(\mu\text{-SS}t\text{-Bu})_2]$ ,  $[(t\text{-Bu})_2\text{Ga}(\mu\text{-St-Bu})(\mu\text{-SS}t\text{-Bu})\text{Ga}(t\text{-Bu})_2]$ , and trace amounts of  $[(t\text{-Bu})_2\text{Ga}(\mu\text{-St-Bu})_2]$  [64]. These results are to be compared with the reaction of the dimethyltitanium complex  $\text{TiMe}_2[\text{N}=\text{P}(t\text{-Bu})_3]_2$  with  $\text{S}_8$  proceeding via elimination of the methyl groups (Scheme 17) [58]. Insertion reaction of sulfur atoms into an Ir-Ir bond takes place in the treatment of  $\text{Cp}^*\text{Ir}(\mu\text{-SiPr})_2\text{IrCp}^*$  with  $\text{S}_8$  to give a unique dinuclear iridium complex having a  $\mu$ -nonasulfide ligand [65] (Scheme 19).

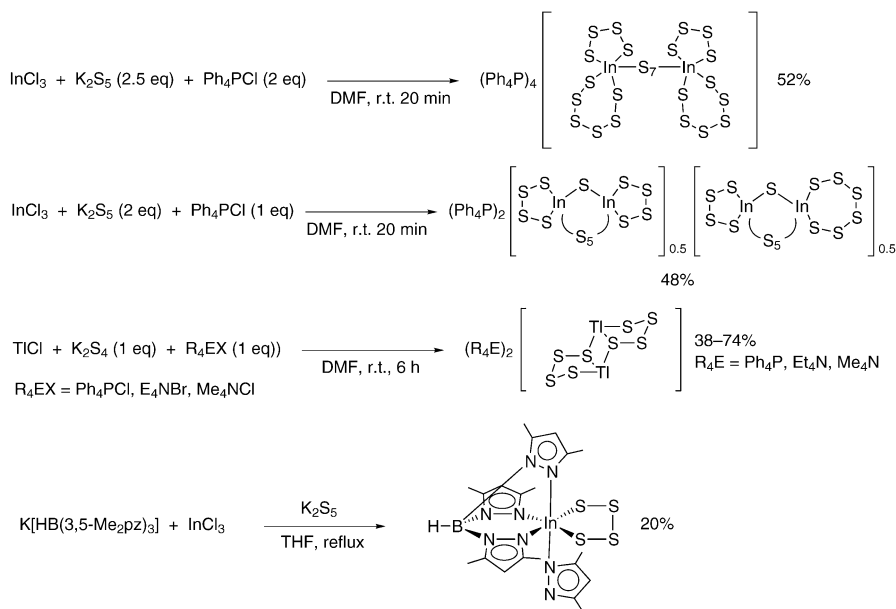
## 2.5

### Reactions of Metal Halides with Polysulfide Dianions

Reactions of metal halides with polysulfide dianions are useful methods for the synthesis of polysulfido complexes of main group elements and transition metals. In most of these reactions, similarly to other methods, the chain lengths and coordination types of the polysulfide ligands depend on the other ligands coordinated to the metal, on the ratio between the metal and sulfur, on the reaction temperature, and other parameters.

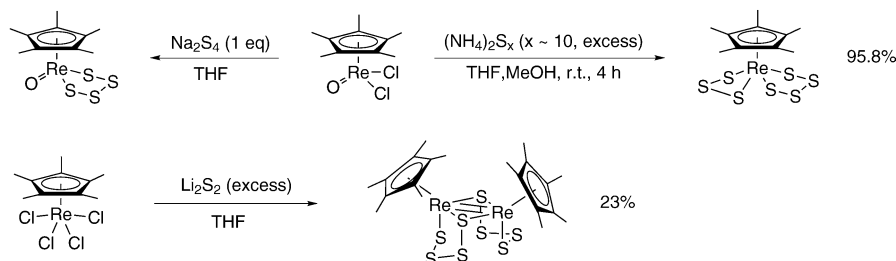
Some polysulfido complexes of group 13 elements are synthesized by reaction of the metal chlorides with  $\text{K}_2\text{S}_5$ . A mixture of  $\text{InCl}_3$ ,  $\text{K}_2\text{S}_5$ , and  $\text{Ph}_4\text{PCl}$  in a 2.5:4 molar ratio is stirred in DMF at room temperature to give pale-yellow crystals of  $(\text{Ph}_4\text{P})_4[\text{In}_2(\text{S}_4)_2(\text{S}_6)_2(\mu\text{-S}_7)]$  in 52% yield (Scheme 20) [66]. A similar reaction with the ratio of  $\text{InCl}_3:\text{K}_2\text{S}_5:\text{Ph}_4\text{PCl}=1:2:1$  results in the formation of  $(\text{Ph}_4\text{P})_2[\text{In}_2(\text{S}_4)_2(\mu\text{-S})(\mu\text{-S}_5)]_{0.5}[\text{In}_2(\text{S}_4)(\text{S}_6)(\mu\text{-S})(\mu\text{-S}_5)]_{0.5}$ . On the other hand, the reaction of  $\text{TlCl}$  with  $\text{K}_2\text{S}_5$  in the presence of one of the cations  $\text{Ph}_4\text{P}^+$ ,  $\text{Et}_4\text{N}^+$ , or  $\text{Me}_4\text{N}^+$  affords novel stable complexes containing the anion  $[\text{Tl}_2(\text{S}_4)_2]^{2-}$  in each case [67]. The use of  $\text{K}_2\text{S}_x$  ( $x=4\text{--}6$ ) in this reaction does not affect the composition of the final product. The reaction of  $\text{In}(\text{Cl}_2)[\text{HB}(3,5\text{-Me}_2\text{pz})_3]$ , prepared from  $\text{InCl}_3$  and the tridentate ligand  $[\text{HB}(3,5\text{-Me}_2\text{pz})_3]^-$ , with  $\text{K}_2\text{S}_5$  results in the formation of the mononuclear tetrasulfido complex  $\text{In}(\text{S}_4)[\text{HB}(3,5\text{-Me}_2\text{pz})_3](3,5\text{-Me}_2\text{pz})$  [68].

The reaction of the dichlororhenium complex  $\text{Cp}^*\text{Re}(\text{O})\text{Cl}_2$  ( $\text{Cp}^*=\eta^5\text{-C}_5\text{Me}_5$ ) with an equimolar amount of  $\text{Na}_2\text{S}_4$  results in almost quantitative formation of the corresponding tetrasulfido complex  $\text{Cp}^*\text{Re}(\text{O})\text{S}_4$  [69]. Increasing amounts of  $\text{Na}_2\text{S}_4$  in this reaction lead to the formation of  $\text{Cp}^*\text{Re}(\text{S}_3)(\text{S}_4)$ , and treatment of  $\text{Cp}^*\text{Re}(\text{O})\text{Cl}_2$  with an excess of  $(\text{NH}_4)_2\text{S}_x$  ( $x=10$ ) gives  $\text{Cp}^*\text{Re}(\text{S}_3)(\text{S}_4)$  in quantitative yield. The reaction of  $\text{Cp}^*\text{ReCl}_4$  with an excess of  $\text{Li}_2\text{S}_2$  gives the dinuclear polysulfido complex  $\text{Cp}_2\text{Re}_2(\mu\text{-S}_4)_2$  containing a Re-Re bond [70] (Scheme 21).



**Scheme 20** Synthesis of group 13 polysulfido complexes by the reaction of the corresponding metal halides with polysulfide dianions

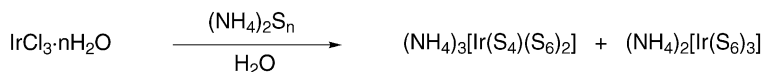
The reaction of  $\text{IrCl}_3 \cdot n\text{H}_2\text{O}$  with 25 wt%  $(\text{NH}_4)_2\text{S}_n$  in water at 30–50 °C gives  $(\text{NH}_4)_3[\text{Ir}(\text{S}_6)_3]$  as the main product together with small amounts of  $(\text{NH}_4)_3[\text{Ir}(\text{S}_4)(\text{S}_6)_2]$  [71, 72]. The use of 20 wt%  $(\text{NH}_4)_2\text{S}_n$  in this reaction led to the predominant formation of  $(\text{NH}_4)_3[\text{Ir}(\text{S}_4)(\text{S}_6)_2]$  (Scheme 22). This result



**Scheme 21** Synthesis of rhenium complexes by the reaction of the rhenium chlorides with polysulfide dianions

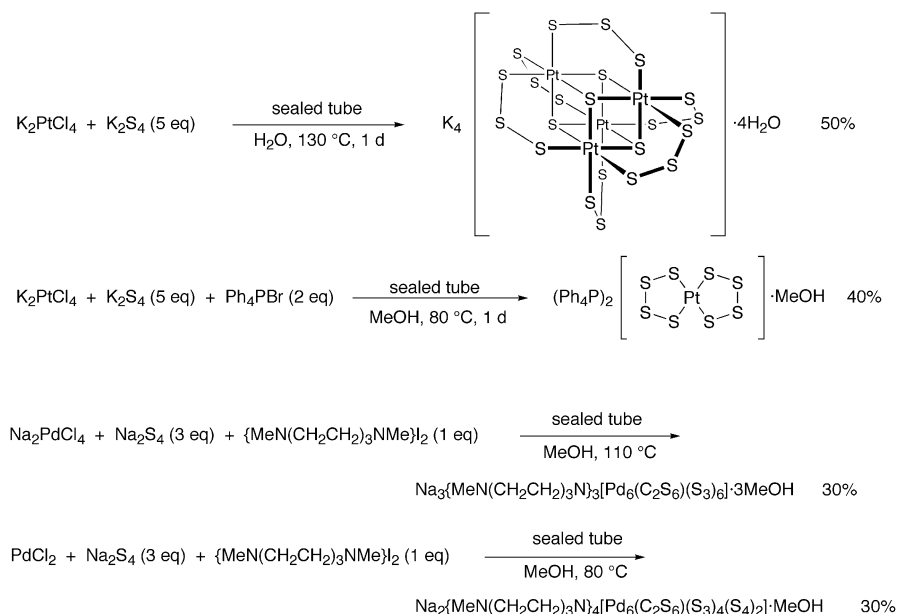
is in sharp contrast to the reaction of  $\text{RhCl}_3 \cdot n\text{H}_2\text{O}$  with  $(\text{NH}_4)_2\text{S}_n$  under identical conditions yielding only  $(\text{NH}_4)_3[\text{Rh}(\text{S}_6)_3] \cdot 3\text{H}_2\text{O}$  [73, 74].

The solvothermal reaction between metal halides and polysulfide anions is also a useful method for the synthesis of metal-polysulfide clusters. Hydrothermal reaction of  $\text{K}_2\text{PtCl}_4$  with  $\text{K}_2\text{S}_4$  (5 eq) at 130 °C in a sealed tube



**Scheme 22** Synthesis of iridium polysulfido complexes by the reaction of  $\text{IrCl}_3 \cdot n\text{H}_2\text{O}$  with polysulfide dianions

gives reddish-black trigonal prismatic crystals of  $\text{K}_4[\text{Pt}_4\text{S}_{22}] \cdot 4\text{H}_2\text{O}$ , while a MeOH solution of  $\text{K}_2\text{PtCl}_4$ ,  $\text{K}_2\text{S}_4$  and  $\text{Ph}_4\text{PBr}$  in a molar ratio of 1:2:5 heated to 80 °C gives  $(\text{Ph}_4\text{P})_2[\text{Pt}(\text{S}_4)_2] \cdot \text{CH}_3\text{OH}$  as reddish-orange rectangular rodlike crystals [75]. The methanothermal reaction of  $\text{Na}_2\text{PdCl}_4$ ,  $\text{Na}_2\text{S}_4$  and  $\{\text{MeN}(\text{CH}_2\text{CH}_2)_3\text{NMe}\}_2$  in a 1:3:1 molar ratio at 110 °C yields reddish-black hexagonal rodlike crystals of  $\text{Na}_3\{\text{MeN}(\text{CH}_2\text{CH}_2)_3\text{N}\}_3[\text{Pd}_6(\text{C}_2\text{S}_6)(\mu\text{-S}_3)_6] \cdot 3\text{MeOH}$  containing the unprecedented hexathioorthooxalate ligand  $[\text{C}_2\text{S}_6]^{6-}$  [76]. On the other hand, a similar reaction at 80 °C using  $\text{PdCl}_2$  instead of  $\text{Na}_2\text{PdCl}_4$  resulted in the formation of  $\text{Na}_2\{\text{MeN}(\text{CH}_2\text{CH}_2)_3\text{N}\}_4[\text{Pd}_6(\text{C}_2\text{S}_6)(\mu\text{-S}_3)_4(\mu\text{-S}_4)_2] \cdot \text{MeOH}$  as reddish-black rectangular rodlike crystals. Since the similar reaction at 110 °C gives the  $[\text{Pd}_6(\text{C}_2\text{S}_6)(\mu\text{-S}_3)_6]^{6-}$  cluster as the main product, it is assumed that the latter anion is thermodynamically more stable than the  $[\text{Pd}_6(\text{C}_2\text{S}_6)(\mu\text{-S}_3)_4(\mu\text{-S}_4)_2]^{6-}$  cluster (Scheme 23). Although the mechanism for the formation of these clusters has not been fully revealed yet, it has been proposed that the cation  $[\text{MeN}(\text{CH}_2\text{CH}_2)_3\text{N}]^+$  is formed by the elimination of a methyl cation from



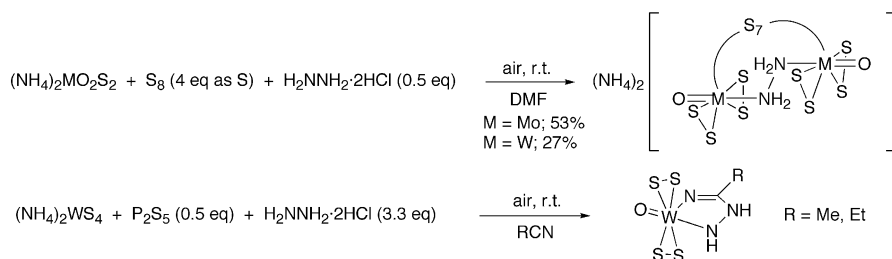
**Scheme 23** Synthesis of group 10 metal polysulfido complexes by the reaction of the metal chlorides with polysulfide dianions

the starting dication  $[\text{MeN}(\text{CH}_2\text{CH}_2)_3\text{NMe}]^{2+}$  and the  $[\text{C}_2\text{S}_6]^{6-}$  ligand originates either from such liberated methyl cations or from  $-\text{CH}_2\text{CH}_2-$  groups of the starting dication.

## 2.6

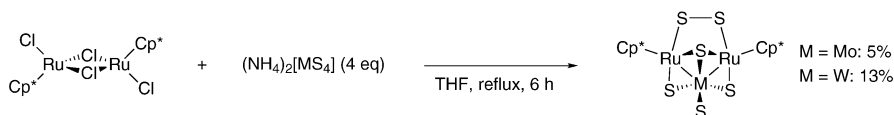
### Synthesis from Compounds with Formal Metal-Sulfur Double Bonds

Some polysulfido complexes of group 6 metals have been synthesized by the addition of sulfur atoms from reagents such as elemental sulfur or organic polysulfanes to formal metal-sulfur double bonds. The reaction of  $\text{MO}_m\text{S}_{4-n}$  ( $\text{M}=\text{Mo}, \text{W}$ ) with elemental sulfur in  $\text{CH}_3\text{CN}$  or DMF solvent gives the polysulfido complexes  $[\text{Mo}(\text{S})(\text{S}_4)_2]^{2-}$ ,  $[\text{Mo}(\text{O})(\text{S}_4)_2]^{2-}$ , and  $[\{\text{M}(\text{S})(\text{S}_4)\}_2(\mu\text{-S})_2]^{2-}$  ( $\text{M}=\text{Mo}, \text{W}$ ) [3, 77, 78]. Xintao et al. developed the reaction system of  $\text{MO}_2\text{S}_2^{2-}/\text{S}_x/\text{H}_2\text{NNH}_2 \cdot 2\text{HCl}$  ( $\text{M}=\text{Mo}, \text{W}$ ), and obtained doubly bridged complexes  $[\{\text{MO}(\text{S}_2)_2\}_2\{\mu_2\text{-S}_7\}(\mu_2\text{-H}_2\text{NNH}_2)]^{2-}$  ( $\text{M}=\text{Mo}, \text{W}$ ) containing bridging  $\text{S}_7^{2-}$  and hydrazine ( $\text{H}_2\text{NNH}_2$ ) ligands [79, 80]. The use of  $[\text{WS}_4]^{2-}$  and  $\text{P}_2\text{S}_5$  instead of  $[\text{MO}_2\text{S}_2]^{2-}$  and  $\text{S}_x$  in this reaction system in RCN solvents ( $\text{R}=\text{Me}, \text{Et}$ ) results in the formation of oxo-thiotungstate amidrazone compounds  $\text{WO}(\text{S}_2)_2\{\text{NH}=\text{C}(\text{R})\text{NHNH}\}$  ( $\text{R}=\text{Me}, \text{Et}$ ) via the reaction with the solvents [81] (Scheme 24).



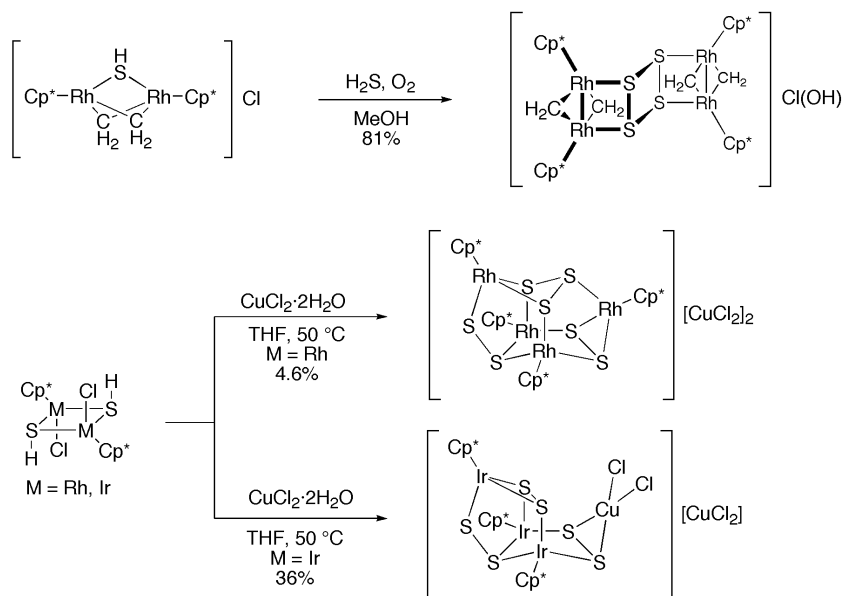
**Scheme 24** Synthesis of group 6 metal disulfido complexes

Trinuclear heterometallic clusters with bridging disulfide and sulfide ligands  $[(\mu_2\text{-S}_2)(\text{Cp}^*\text{Ru})_2(\mu_3\text{-S})(\mu_2\text{-S})_2\text{MS}]$  ( $\text{M}=\text{Mo}, \text{W}$ ) are synthesized by the reaction of  $[\text{Cp}^*\text{RuCl}(\mu\text{-Cl})_2\text{RuCp}^*\text{Cl}]$  with an excess of  $[\text{MS}_4]^{2-}$  ( $\text{M}=\text{Mo}, \text{W}$ ) in THF under reflux [82]. In these complexes, the  $\text{Cp}^*\text{Ru}$  units are connected by bridging  $\text{MS}_4$  and  $\text{S}_2$  ligands. The  $\text{S}_2$  moiety apparently arises from the degradation of the  $[\text{MS}_4]^{2-}$  anion (Scheme 25).



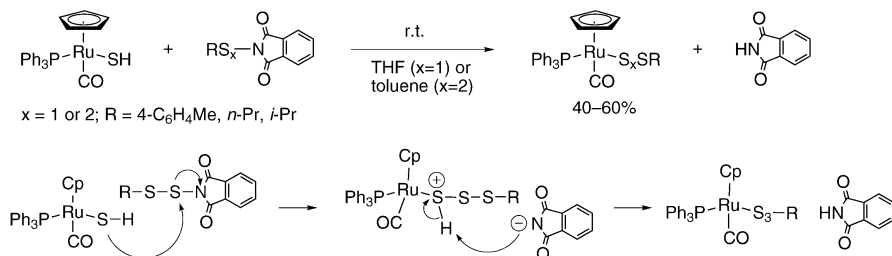
**Scheme 25** Synthesis of trinuclear heterometallic clusters





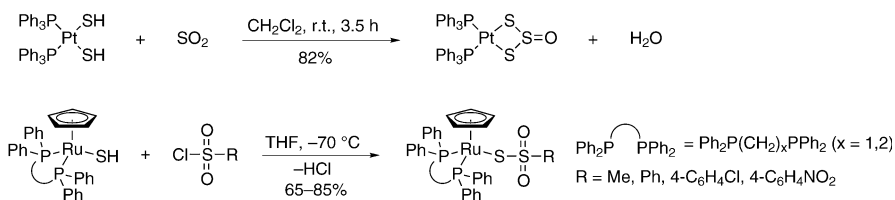
**Scheme 27** Synthesis of rhodium, iridium, and copper polysulfido clusters from the corresponding  $\mu$ -hydrogensulfido complexes

byproducts. The formation of  $\text{RuCp}(\text{S}_3\text{R})(\text{CO})(\text{PPh}_3)$  can be explained in terms of an attack of the thiol on the  $\alpha$ -sulfur atom followed by proton-abstraction with the resulting phthalimido anion as shown below. If the  $\beta$ -sulfur atom is attacked along with the dissociation of the  $\text{Sphth}^-$  group,  $\text{RuCp}(\text{CO})(\text{PPh}_3)_2\text{S}_2\text{R}$  is formed.



**Scheme 28** Synthesis of ruthenium polysulfido complexes from the corresponding hydrogensulfido complexes

Treatment of  $\text{cis}[\text{Pt}(\text{SH})_2(\text{PPh}_3)_2]$  with  $\text{SO}_2$  resulted in the formation of  $\text{Pt}(\text{S}_3\text{O})(\text{PPh}_3)_2$  and  $\text{H}_2\text{O}$  (Scheme 29) [88]. In analogy to the above reaction, the initial attack of the thiol on the sulfur atom of  $\text{SO}_2$  leads to the formation of the S-S bond. Details of the reaction mechanism will be discussed later



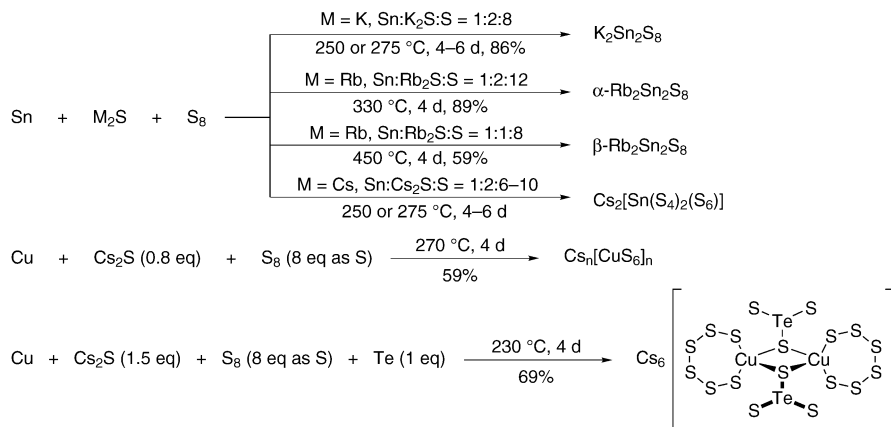
**Scheme 29** Synthesis of oxidized polysulfido complexes from the corresponding hydrogensulfido complexes

(Scheme 67). In addition, the reaction of hydrogensulfido complexes  $\text{RuCp}(\text{SH})[(\text{PPh}_2)_2(\text{CH}_2)_x]$  ( $x=1, 2$ ) with various sulfonylchlorides in THF at  $-70^\circ\text{C}$  afforded the thiosulfonato complexes  $\text{RuCp}(\text{SSO}_2\text{R})[(\text{PPh}_2)_2(\text{CH}_2)_x]$  ( $x=1, 2$ ) accompanied by the abstraction of HCl [89].

## 2.8

### Other Synthetic Methods

The preparation of some polychalcogenide solids can be achieved at 200–450 °C by molten salt (flux) methods. The reaction of tin with alkali metal sulfides in the presence of  $\text{S}_8$  at 200–450 °C gives a variety of alkali metal tin sulfides depending on the ratio of the starting materials, the reaction temperature, and the alkali metals (Scheme 30) [90]. These alkali metal tin sul-

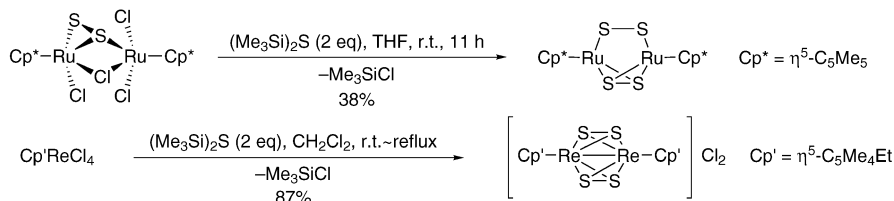


**Scheme 30** Synthesis of metal polysulfido complexes by the reaction of metals with  $\text{S}_8$

fides are probably formed by the reaction of Sn with molten alkali polysulfide salts ( $\text{M}_2\text{S}_x$ ; M = K, Rb, Cs) originating from the alkali sulfide and elemental sulfur. On the other hand, if Cu powder is treated with  $\text{Cs}_2\text{S}$  in the presence of  $\text{S}_8$  the polymeric anions  $[\text{Cu}(\text{S}_6)]_n^{n-}$  are formed with  $\text{CuS}_6$  sev-

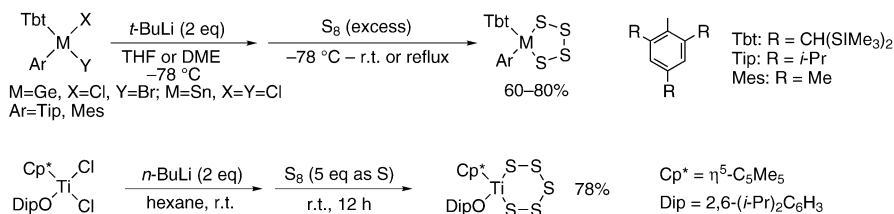
en-membered rings [91]. The addition of Te in this reaction resulted in the formation of  $\text{Cs}_6[\text{Cu}_2(\text{S}_6)_2(\text{TeS}_3)_2]$ . The formation of these copper polysulfides can be interpreted in terms of the reaction of Cu with the initially formed molten  $\text{Cs}_2\text{S}_x$  or  $\text{Cs}_2\text{S}_x\text{Te}_y$  salts.

The reaction of the transition metal chlorides  $\text{Ru}_2\text{Cp}^*\text{Cl}_4\text{S}_2$  ( $\text{Cp}^* = \eta^5\text{-C}_5\text{Me}_5$ ) and  $\text{ReCp}'\text{Cl}_4$  ( $\text{Cp}' = \eta^5\text{-C}_5\text{Me}_4\text{Et}$ ) with  $(\text{Me}_3\text{Si})_2\text{S}$  leads to the formation of the corresponding metal polysulfides  $\text{Ru}_2\text{Cp}^*\text{S}_4$  and  $\text{Re}_2\text{Cp}'\text{S}_4$ , respectively, and  $\text{Me}_3\text{SiCl}$  as the leaving group [40, 92] (Scheme 31).



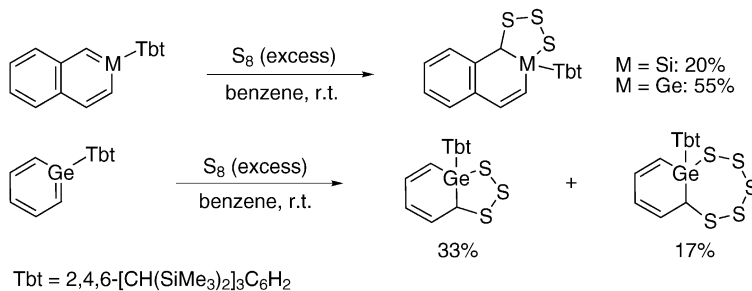
**Scheme 31** Synthesis of ruthenium and rhenium disulfido complexes by the use of  $(\text{TMS})_2\text{S}$  as a sulfur reagent

The reaction of dihalogermane  $\text{Tbt}(\text{Ar})\text{Ge}(\text{Br})\text{Cl}$  ( $\text{Ar} = \text{Mes}$ ,  $\text{Tip}$ ) with 2 equivalents of *tert*-butyllithium followed by the treatment with  $\text{S}_8$  resulted in the formation of the corresponding tetrathiagermolanes  $\text{Tbt}(\text{Ar})\text{GeS}_4$  in good yields ( $\text{R} = \text{Mes}$ : 79%,  $\text{R} = \text{Tip}$ : 81%) [52]. The analogous reaction of the dichlorostannane  $\text{Tbt}(\text{Ar})\text{SnCl}_2$  ( $\text{Ar} = \text{Mes}$ ,  $\text{Tip}$ ) also gave the corresponding tetrathiaastannolanes  $\text{Tbt}(\text{Ar})\text{SnS}_4$  [51]. These reactions are considered to proceed via  $\text{Tbt}(\text{Ar})\text{M}(\text{H})\text{Li}$  ( $\text{M} = \text{Ge}$ ,  $\text{Sn}$ ) as key intermediates. The reaction of  $\text{Tbt}(\text{Ar})\text{M}(\text{H})\text{Li}$  ( $\text{M} = \text{Ge}$ ,  $\text{Sn}$ ) generated from dihydrometallanes such as  $\text{Tbt}(\text{Ar})\text{MH}_2$  ( $\text{M} = \text{Ge}$ ,  $\text{Sn}$ ;  $\text{Ar} = \text{Mes}$ ,  $\text{Tip}$ ) and equimolar amounts of *t*-BuLi with an excess of  $\text{S}_8$  also yielded the tetrathiametallolanes  $\text{Tbt}(\text{Ar})\text{MS}_4$  in moderate yields (45–73%). In addition, a titanium pentasulfide complex  $\text{Ti}(\text{Cp}^*)(\text{ODip})\text{S}_5$  is synthesized by a similar type of reaction, i.e., treatment of  $\text{TiCl}_2(\text{Cp}^*)\text{ODip}$  with 2 equivalents of *n*-butyllithium followed by the addition of  $\text{S}_8$  [93]. In contrast to the formation of the above polysulfides of heavier group 14 elements, the Ti(II) complex was postulated as a key intermediate in this reaction (Scheme 32).



**Scheme 32** Synthesis of metal polysulfido complexes from the corresponding dihalide complexes

Very recently, it has been reported that silaaromatic and germaaromatic compounds, stabilized by steric protection, react with  $S_8$  to afford the corresponding trithiametallolanes and/or pentathiametallepanes via the addition across the M-C (M=Si, Ge) double bond [94–96] (Scheme 33).



**Scheme 33** Synthesis of group 14 element polysulfido complexes

### 3 Structural Properties

The structural properties of metal-polysulfido complexes have already been reviewed by Müller et al. in 1982 and 1987 [2, 8]. This section presents a brief update on the structural properties of metal- $S_n$  complexes ( $n>1$ ) including a novel  $Rh_4S_4$  complex with a rectangular  $S_4$  unit.

#### 3.1 $S_2^{2-}$ Complexes

Various types of metal-disulfido complexes have been reported as shown in Fig. 2. The comparison of their S-S bond lengths (197–215 pm) and  $\nu(S-S)$  vibrational wavenumbers (480–600  $cm^{-1}$ ) with those of  $S_2$  ( $^3\Sigma_g^-$ : 189 pm, 725  $cm^{-1}$ ) [97–100],  $S_2^-$  ( $^2\Pi_g^-$ : 200 pm, 589  $cm^{-1}$ ) [100, 101] and  $S_2^{2-}$  ( $^1\Sigma_g^+$ : 213 pm, 446  $cm^{-1}$ ) [8, 102] leads to the conclusion that the charge distribu-

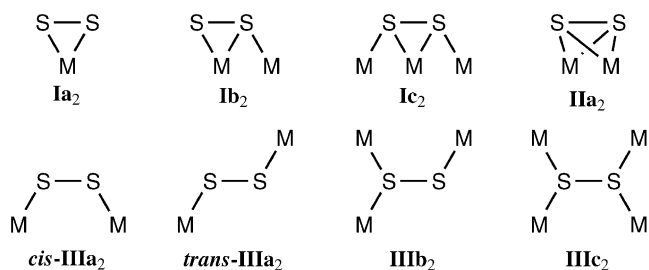
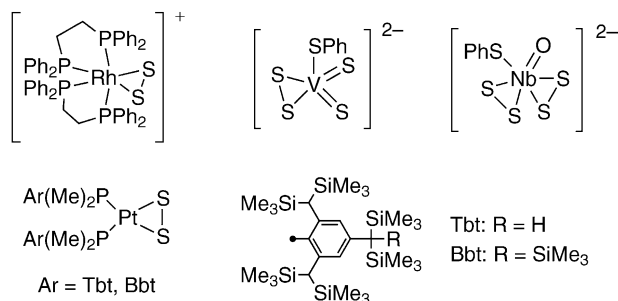


**Fig. 2** Important structure types of disulfido complexes

tion in disulfido complexes lies between those for  $S_2^-$  and  $S_2^{2-}$ . Therefore, the bond order of the S-S bond in  $S_2$  complexes is intermediate between 1.5 and 1.

Type  $Ia_2$  complexes favor high coordination numbers on the metal since the S-M-S angles are small (e.g.,  $[Rh(\eta^2-S_2)(Ph_2PCH_2CH_2PPh_2)_2]^+$  [27],  $[VS_2(\eta^2-S_2)(SPh)]^{2-}$  [62],  $[NbO(\eta^2-S_2)_2(SPh)]^{2-}$  [63]; see Scheme 34). More-



**Scheme 34** Type  $Ia_2$  complexes

over, high coordination numbers have an effect of hindering the nucleophilic attack of reagents on the metal centers. As for the type  $Ia_2$  complexes, the species  $PtS_2[P(Ar)Me_2]_2$  ( $Ar=Tbt, Bbt$ ) [37] has been synthesized as the only examples of stable tetracoordinated complexes taking advantage of the effects of the bulky phosphine ligands  $P(Ar)Me_2$  ( $Ar=Tbt, Bbt$ ).

The principal bonding interactions in type  $Ia_2$  complexes are illustrated schematically in Fig. 3. According to the qualitative Dewar-Chatt-Duncanson bonding scheme [103, 104] the coordination of the  $S_2$  ligand to the central metal can be depicted by the primary bonding interaction between the  $\pi_z$  ( $\pi_h$ ) orbital of the  $S_2$  ligand and the metal  $d_{z^2}$  orbital ( $\sigma$ -bonding) and between the  $\pi_z^*$  ( $\pi_h^*$ ) orbital of the  $S_2$  ligand and the metal  $d_{xz}$  orbital ( $\pi$ -bonding). It is assumed that the interaction of the  $\pi_y$  ( $\pi_v$ ) and the  $\pi_y^*$  ( $\pi_v^*$ ) orbitals is negligible. The  $\pi$ -bonding is considered to be the dominating interaction in type  $Ia_2$  complexes. On the other hand, SCF- $X\alpha$ -SW calculations on  $[MS_2(PH_3)_4]$  ( $M=Rh, Ir$ ) suggest that there is also a contribution of the  $p$ -orbitals of the metals and the  $p_\sigma$  orbitals of the  $S_2$  ligands to the bonding in addition to the above-mentioned interaction [105]. These molecular orbital

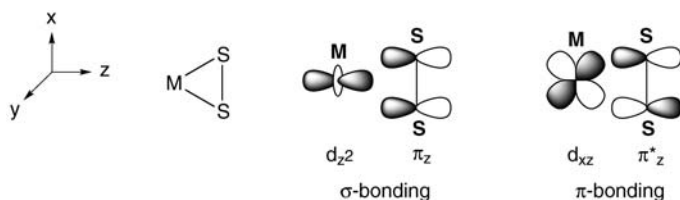
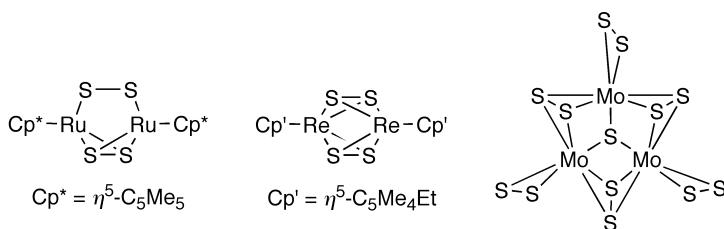


**Fig. 3** Schematic bonding interactions in disulfido complexes

calculations propose that the M-S<sub>2</sub> bond consists of an in-plane  $\pi$  overlap of the S<sub>2</sub>  $\pi_z^*$  ( $\pi_h^*$ ) orbital with the metal  $p_x+d_{xz}$  hybrid of predominantly  $p_x$  character and of  $\sigma$  overlap between the S<sub>2</sub>  $\pi_z$  ( $\pi_h$ ) and  $p\sigma$  orbitals with the metal  $d_z^2$  hybrid.

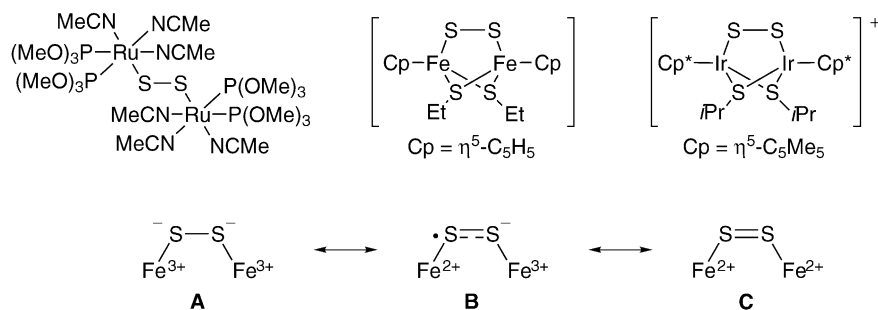
In the electronic spectra of type **Ia**<sub>2</sub> complexes, an absorption band is observed in the visible region. For example, the spectrum of WO(S<sub>2</sub>)<sub>2</sub>{NH=C(R)NHNH} (R=Me, Et) shows the longest wavelength bands at 460 nm ( $\epsilon$  1.95×10<sup>3</sup>) (R=Me) and 465 nm ( $\epsilon$  0.68×10<sup>3</sup>) (R=Et) [80]. The antibonding orbital  $\pi^*$  of the S<sub>2</sub> ligand splits into two components, i.e., the in-plane  $\pi_z^*$  ( $\pi_h^*$ ) orbital and the  $\pi_y^*$  ( $\pi_v^*$ ) orbital perpendicular to the MS<sub>2</sub> plane (cf. Fig. 3). The longest wavelength bands in the visible region are assigned to the ligand-to-metal charge-transfer (LMCT) transitions of the type  $\pi_v^*(S) \rightarrow d(M)$ , while the LMCT transitions of type  $\pi_h^*(S) \rightarrow d(M)$  are observed at higher energies in the UV region [2, 8]. These assignments are considered to be applicable to the other type **Ia**<sub>2</sub> complexes containing metal atoms in a high oxidation state. Meanwhile, the assignments of the absorption in the electronic spectra with the SCF-X $\alpha$ -SW calculations have been performed for [MS<sub>2</sub>(Ph<sub>2</sub>PCH<sub>2</sub>CH<sub>2</sub>PPh<sub>2</sub>)<sub>2</sub>] (M=Rh, Ir) [105]. Their lowest energy absorption bands [M=Rh: 629 nm ( $\epsilon$  62); M=Ir: 582 nm ( $\epsilon$  13)] are assigned to the intraligand transitions  $\pi_v^*(S) \rightarrow \pi_h^*(S)$ ,  $p\sigma^*(S)$ ,  $d_{xz}(M)$ .

Similarly to type **Ia**<sub>2</sub> complexes, type **IIa**<sub>2</sub> complexes favor high coordination numbers on the metal because of the small S-M-S angles (e.g., Ru<sub>2</sub>Cp\*<sub>2</sub>S<sub>4</sub> (Cp\*= $\eta^5$ -C<sub>5</sub>Me<sub>5</sub>) [40] and Re<sub>2</sub>Cp'<sub>2</sub>S<sub>4</sub> (Cp'= $\eta^5$ -C<sub>5</sub>Me<sub>4</sub>Et) [92]). Their bonding interaction is described as follows, using the qualitative Dewar-Chatt-Duncanson bonding scheme. The bonding interaction similar to that in type **Ia**<sub>2</sub> complexes occurs twice. That is, interaction between  $\pi_z^*$  of S<sub>2</sub> and M1 and between  $\pi_y^*$  of S<sub>2</sub> and M2 occurs (Fig. 3). If M2 is a positively charged metal ion with few  $d$ -electrons, the coordination of the S<sub>2</sub> ligand to M2 in type **IIa**<sub>2</sub> complexes lead to a lower electron density on the S<sub>2</sub> ligand compared to type **Ia**<sub>2</sub> complexes. This depopulation of the  $\pi^*$  orbitals of the S<sub>2</sub> ligands results in an enhanced sensitivity to nucleophilic attack together with shorter S-S bond lengths and higher  $\nu(S-S)$  vibrational wavenumbers in type **IIa**<sub>2</sub> complexes compared to type **Ia**<sub>2</sub> complexes. For example, [Mo<sub>3</sub>S(S<sub>2</sub>)<sub>6</sub>]<sup>2-</sup> having both types **Ia**<sub>2</sub> and **IIa**<sub>2</sub> S<sub>2</sub> ligands shows slightly shorter S-S bond lengths (200.0, 203.1 pm) in the bridging S<sub>2</sub> ligand (type **IIa**<sub>2</sub>) compared to those in the terminal S<sub>2</sub> ligand (type **Ia**<sub>2</sub>) [ $d(S-S)$ =204.5, 207.7 pm] [106] (Scheme 35).



**Scheme 35** Type **IIa**<sub>2</sub> complexes

As for type **IIIa<sub>2</sub>** complexes, both  $\nu(\text{S-S})$  and the totally symmetric  $\nu(\text{M-S})$  vibrations are practically forbidden in the IR spectrum, while these vibrations can be observed in the Raman spectrum. Most of type *cis*- and *trans*-**IIIa<sub>2</sub>** complexes have planar M-S-S-M units, although the C-S-S-C torsion angles of organic disulfanes are normally close to 90°. In addition, type **IIIa<sub>2</sub>** complexes have shorter S-S bond lengths and higher vibrational wavenumbers than those of  $\text{S}_2^{2-}$  (213 pm, 446  $\text{cm}^{-1}$ ) (e.g.,  $[\text{Ru}(\text{CH}_3\text{CN})_3\{\text{P}(\text{OMe})_3\}_2(\mu\text{-S}_2)](\text{PF}_6)_3$ :  $d(\text{S-S})=199.5$  pm,  $\nu(\text{S-S})=591$   $\text{cm}^{-1}$  [43];  $\text{Fe}_2\text{Cp}_2(\mu\text{-S}_2)(\mu\text{-SEt})_2$  ( $\text{Cp}=\eta^5\text{-C}_5\text{H}_5$ ):  $d(\text{S-S})=202.3$  pm [107];  $[\text{Ir}_2\text{Cp}^*(\mu\text{-S}_2)(\mu\text{-SET})_2](\text{BPh}_4)$  ( $\text{Cp}^*=\eta^5\text{-C}_5\text{Me}_5$ ):  $d(\text{S-S})=199.7$  pm [65]). These properties may be explained in terms of the large contribution of resonance structure **B**, which has some extent of double bond character in the S-S bond (Scheme 36).



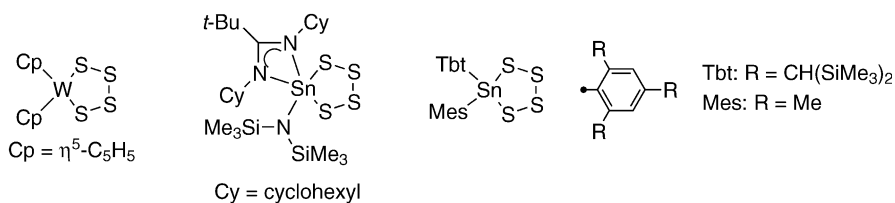
**Scheme 36** Type **IIIa<sub>2</sub>** complexes

### 3.2

#### $\text{S}_n^{2-}$ Complexes ( $n > 2$ )

The geometries of disulfido complexes have been systematically studied by means of X-ray structural analysis, spectroscopic analysis, and theoretical calculations, as mentioned above. However, systematic considerations on the structural features of  $\text{S}_n^{2-}$  ( $n > 2$ ) complexes are difficult due to their diversity. In general, the alternation of the S-S bond lengths is less pronounced in these complexes, and the charge distribution for the  $\text{S}_n^{2-}$  ligands is assumed to be intermediate between those for  $\text{S}_n$  and  $\text{S}_n^{2-}$  species. The conformations of the polysulfido-metal rings are different from each other depending on the central metal and/or ligands.

Some tetrasulfido complexes of Mo and W with high oxidation states show a shortening of the central S(2)-S(3) bond of the  $[-\text{S}(1)\text{-S}(2)\text{-S}(3)\text{-S}(4)]^{2-}$  ligand [e.g.,  $\text{W}(\eta^5\text{-C}_5\text{H}_5)_2\text{S}_4$ : S(1)-S(2) 210.5(7), S(2)-S(3) 201.6(8), S(3)-S(4) 211.6(9) pm] [108]. A similar bond shortening has been observed in the tetrasulfido tin complex  $\text{Sn}[\text{N}(\text{SiMe}_3)_2][(\text{NCy})_2\text{C}(t\text{-Bu})\text{S}_4]$  [23] although the X-ray analysis of another tin tetrasulfide,  $\text{Tbt}(\text{Mes})\text{SnS}_4$ , does not show such an effect [51] (Scheme 37).



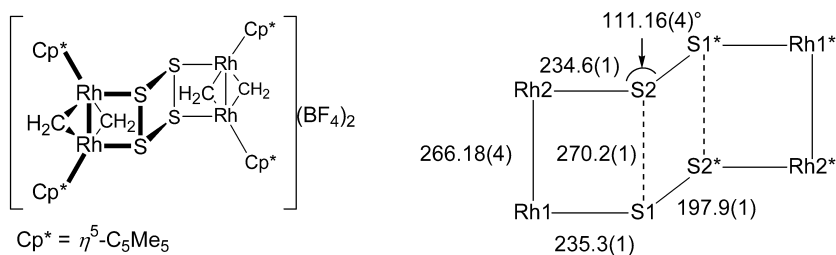
**Scheme 37** Metal tetrasulfido complexes

Infrared absorption bands of  $\text{S}_n^{2-}$  ( $n > 2$ ) complexes are usually of low intensity, while the Raman spectra often show intense and characteristic lines. However, the assignments are difficult because of their complexity. The absorptions in electronic spectra are often assigned to intraligand transitions, and it is known that the increasing length of the polysulfido chain leads to an increasing red shift of the absorption band.

### 3.3

#### A Tetranuclear Rh Complex with a Rectangular $\text{S}_4$ Unit

The tetranuclear complex  $[\{\text{Rh}_2\text{Cp}^*(\mu\text{-CH}_2)_2\}_2(\mu\text{-S}_4)](\text{BF}_4)_2$  ( $\text{Cp}^* = \eta^5\text{-C}_5\text{Me}_5$ ) with a rectangular  $\text{S}_4$  unit has been synthesized (Scheme 27) [85]. The X-ray structural analysis shows that the rectangular planar  $\text{S}_4$  unit and the two planar  $\text{Rh}_2\text{S}_2$  rings form the  $\text{Rh}_4\text{S}_4$  eight-membered ring with a centrosymmetric chair-like core. The molecule has a symmetry center (Scheme 38). The



**Scheme 38** Structure of the  $\text{Rh}_4\text{S}_4$  complex

$\text{S1-S2}^*$  and  $\text{S1}^*\text{-S2}$  bond lengths [197.9(1) pm] lie between those of gaseous  $\text{S}_2$  (189 pm) [98] and  $\text{H}_2\text{S}_2$  (205.5 pm) [109]. This short S-S distance indicates a considerable double bond character. The other two S-S bonds ( $\text{S1-S2}$  and  $\text{S1}^*\text{-S2}^*$ ) are quite long [270.2(1) pm] although shorter than the sum of the van der Waals radii of sulfur atoms (350 pm). The Rh-Rh [266.18(4) pm] and Rh-S [235.3(1) and 234.6(1) pm] bonds are in the range of single bonds.

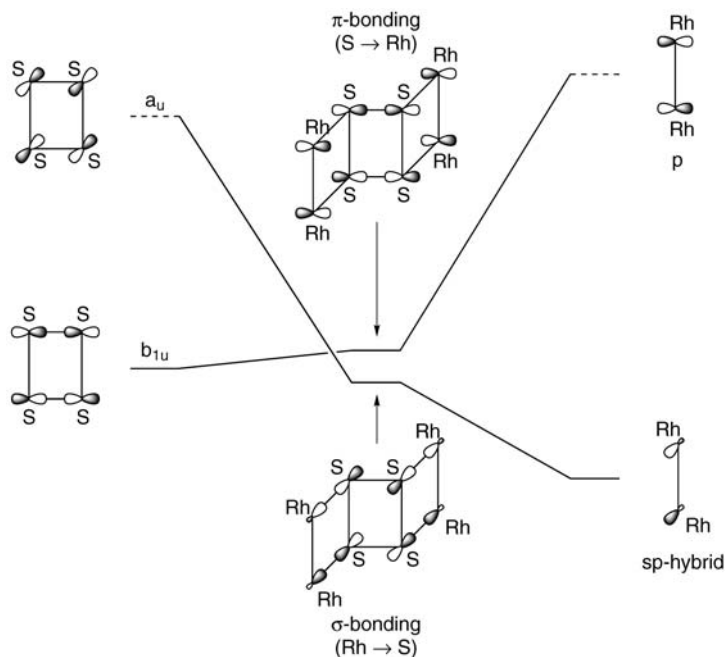


**Fig. 4** Schematic bonding interactions in the  $\text{Rh}_4\text{S}_4$  complex

The  $\nu(\text{S-S})$  stretching mode is observed in the Raman spectrum at  $579\text{ cm}^{-1}$ , suggesting some S-S double-bond character. The stretching vibration of the weak S-S bond has not been observed in the Raman spectrum.

The estimation of the charge on the  $\text{S}_4$  ligand of the model molecule  $[\{\text{Rh}_2(\eta^5\text{-C}_5\text{H}_5)_2(\mu\text{-CH}_2)_2\}_2(\mu\text{-S}_4)]^{2+}$  has been performed by ab initio molecular orbital calculations [110]. The population analysis gives the total charge on the  $\text{S}_4$  unit as about  $-0.7\text{ e}$ . This result is consistent with the above-mentioned X-ray structural analysis, i.e., the  $\text{S}_4$  unit of the complex is close to  $\text{S}_4^-$ . The bonding interaction of the  $\text{S}_4$  unit with the Rh atoms in this complex has been depicted as  $\sigma$ -back donation from the Rh atoms to the  $\text{S}_4$  ligand accompanied by  $\pi$ -donation from the  $\text{S}_4$  ligand to the Rh atoms (Fig. 4). The  $\sigma$ -bond is the interaction between the LUMO of neutral  $\text{S}_4$  (SOMO of  $\text{S}_4^-$ ) and occupied MOs of the  $\text{Rh}_2$  moieties consisting mostly of  $sp$ -hybrid orbitals of the metal atoms. The  $\pi$ -bond is formed by the interaction of the occupied  $b_{1u}$  MO of the hypothetical rectangular  $\text{S}_4$  unit and an unoccupied MO of the  $\text{Rh}_2$  units containing mostly  $p$ -AOs of the Rh atoms.

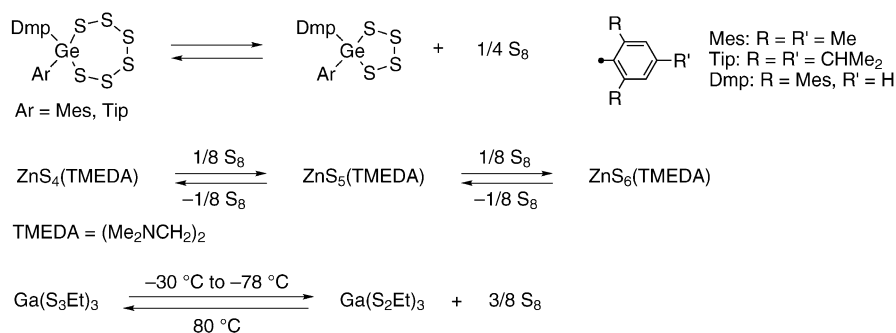
## 4 Reactions

The reactivities of metal polysulfido complexes have previously been reviewed [2–4, 8]. In this section we describe some of the recent progress made in this area.

### 4.1

#### Thermal Equilibrium between Polysulfido Complexes

In hexane solution, hexathiagermepanes,  $\text{Dmp}(\text{Ar})\text{GeS}_6$  ( $\text{Ar}=\text{Mes}$ ,  $\text{Tip}$ ), gradually convert to a mixture of the corresponding tetrathiagermolanes,  $\text{Dmp}(\text{Ar})\text{GeS}_4$ , and  $\text{S}_8$  (Scheme 39) [53]. This transformation is accelerated



**Scheme 39** Thermal equilibrium between metal polysulfido complexes

by heat. The equilibrium ratios are  $\text{Dmp}(\text{Ar})\text{GeS}_6 : \text{Dmp}(\text{Ar})\text{GeS}_4 = 1:1$  ( $\text{Ar}=\text{Mes}$ ) and  $1:4$  ( $\text{Ar}=\text{Tip}$ ). These differing equilibrium ratios depending on the substituents indicate that the ring size of the polysulfides is thermodynamically controlled by the size of the substituents on germanium.

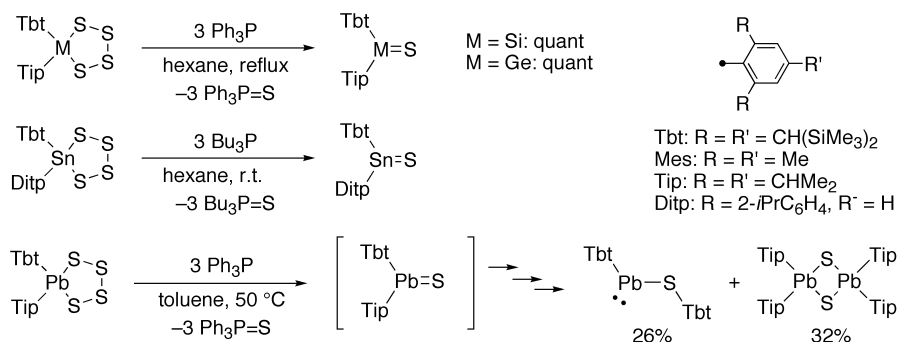
An equilibrium among polysulfido complexes of zinc,  $\text{ZnS}_n(\text{TMEDA})$  ( $n=4, 5, 6$ ), has also been observed in  $\text{MeCN}$  solution (see Scheme 39), although solutions in pyridine or  $\text{CH}_2\text{Cl}_2$  do not show such an equilibrium [111]. The equilibrium ratio among these three complexes is  $\text{ZnS}_4(\text{TMEDA}) : \text{ZnS}_5(\text{TMEDA}) : \text{ZnS}_6(\text{TMEDA}) = 1:1.5:12$ .

Acyclic polysulfido complexes of gallium show similar equilibrium reactions, for instance between  $\text{Ga}(\text{S}_3\text{Et})_3$  and  $\text{Ga}(\text{S}_2\text{Et})_3$  [60]. If  $\text{Ga}(\text{S}_3\text{Et})_3$  is cooled at  $-30$  °C and  $-78$  °C for 2 and 1 weeks, respectively, it affords  $\text{Ga}(\text{S}_2\text{Et})_3$  quantitatively. Heating of a mixture of  $\text{Ga}(\text{S}_2\text{Et})_3$  and  $\text{S}_8$  (3 eq as S) results in the quantitative formation of  $\text{Ga}(\text{S}_3\text{Et})_3$ .

## 4.2

## Desulfurization by Phosphines

Reaction of cyclic tetrasulfido complexes of heavier group 14 elements bearing bulky substituents such as  $\text{Tbt}(\text{Ar})\text{MS}_4$  ( $\text{M}=\text{Si}$ ,  $\text{Ar}=\text{Tip}$ ;  $\text{M}=\text{Ge}$ ,  $\text{Ar}=\text{Tip}$ ;  $\text{M}=\text{Sn}$ ,  $\text{Ar}=\text{Ditp}$ ) with 3 equivalents of phosphines afforded the successful isolation of the first stable double-bonded compounds between heavier group 14 elements and sulfur atom (heavy ketones),  $\text{Tbt}(\text{Ar})\text{M}=\text{S}$ , accompanied by the quantitative formation of the corresponding phosphine sulfides (Scheme 40) [13, 15, 112, 113]. On the other hand, their lead an-



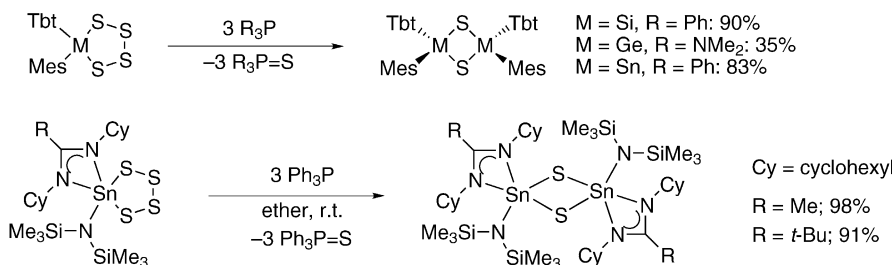
**Scheme 40** Synthesis of doubly bonded compounds between group 14 elements and sulfur by the desulfurization of the corresponding tetrasulfides

alog  $\text{Tbt}(\text{Tip})\text{PbS}_4$  reacts with 3 equivalents of  $\text{Ph}_3\text{P}$  to give the aryl(arythio)plumbylene  $\text{Tbt}(\text{TbtS})\text{Pb}$  and 1,3,2,4-dithiaplumbetane  $(\text{Tip}_2\text{Pb})_2(\mu\text{-S})_2$  which are assumed to be formed via the corresponding plumbanethione  $\text{Tbt}(\text{Tip})\text{Pb}=\text{S}$  [114].

Desulfurization of the less-hindered tetrathiametallolanes  $\text{Tbt}(\text{Mes})\text{MS}_4$  ( $\text{M}=\text{Si}$ ,  $\text{Ge}$ ,  $\text{Sn}$ ) by phosphines gives the corresponding 1,3,2,4-dithiadimetal-letanes  $\{\text{Tbt}(\text{Mes})\text{M}\}_2(\mu\text{-S})_2$ , the formation of which is explained in terms of the insufficient steric protection leading to the dimerization of the intermediates  $\text{Tbt}(\text{Mes})\text{M}=\text{S}$  [13, 115, 116]. The five-coordinated tetrathiasnolananes  $[\text{N}(\text{SiMe}_3)_2][(\text{NCy})_2\text{CR}]\text{SnS}_4$  ( $\text{R}=\text{Me}$ , *t*-Bu) also react with  $\text{Ph}_3\text{P}$  to afford the dimer of the *N*-coordinating stannanethione  $\{[\text{N}(\text{SiMe}_3)_2][(\text{NCy})_2\text{CR}]\text{Sn}\}_2(\mu\text{-S})_2$  [23] (Scheme 41).

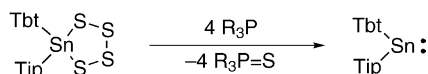
The use of 4 equivalents of  $\text{Me}_3\text{P}$  in the desulfurization of the tetrathiasnolanane  $\text{Tbt}(\text{Tip})\text{SnS}_4$  results in the formation of the corresponding divalent species  $[\text{Tbt}(\text{Tip})\text{Sn}]$  [117] (Scheme 42). By contrast, treatment of the germanium analog  $\text{Tbt}(\text{Tip})\text{GeS}_4$  with excess of  $\text{Ph}_3\text{P}$  gives only the corresponding doubly bonded species  $\text{Tbt}(\text{Tip})\text{Ge}=\text{S}$ .

1,2,3,5-Tetrathia-4-germacyclohexanes with  $\text{S}_3$  and  $\text{S}$  bridging ligands such as  $\text{Tbt}(\text{Ar})\text{Ge}(\text{S}_3)(\text{S})\text{CPh}_2$  ( $\text{Ar}=\text{Mes}$ ,  $\text{Tip}$ ) are readily desulfurized by  $\text{P}(\text{NMe}_2)_3$  at room temperature and 1,2,4-trithia-3-germacyclopentane



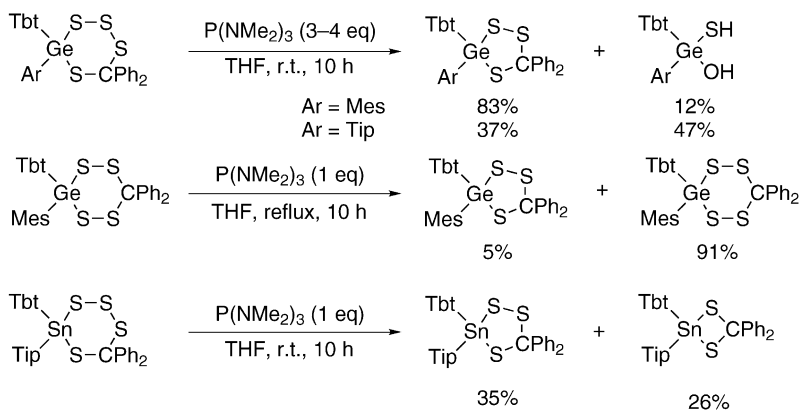
**Scheme 41** Synthesis of 1,3,2,4-dithiadimetallanes by the desulfurization of the corresponding tetrasulfides

Tbt(Ar)Ge(S<sub>2</sub>)(S)CPh<sub>2</sub>, is obtained together with Tbt(Ar)Ge(OH)(SH), the formation of which can be explained in terms of the hydrolysis of the intermediately generated germanethiones Tbt(Ar)Ge=S (Scheme 43) [52, 118]. By contrast, the reaction of 1,2,4,5-tetrathia-3-germacyclohexane Tbt(Mes)-



**Scheme 42** Synthesis of a stannylene by desulfurization of the corresponding tetrasulfide

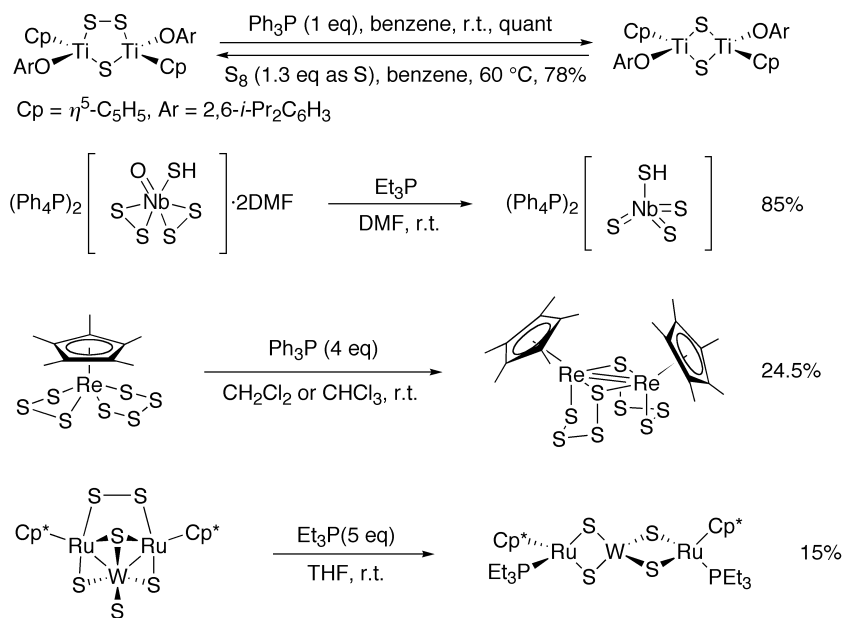
Ge(S<sub>2</sub>)<sub>2</sub>CPh<sub>2</sub> with P(NMe<sub>2</sub>)<sub>3</sub> hardly proceeds even in refluxing THF, and affords only Tbt(Mes)Ge(S<sub>2</sub>)(S)CPh<sub>2</sub> in 5% yield accompanied by the starting material (91%). This fact indicates that the 2-position of the former 1,2,3,5-tetrathia-4-germacyclohexanes is exposed to an attack by the phosphorus



**Scheme 43** Desulfurization of tetrathiametallacyclohexanes

reagent, while both sulfurs in the latter 1,2,4,5-tetrathia-3-germacyclohexane are sterically protected. The reaction of a tin analog,  $\text{Tbt}(\text{Tip})\text{Sn}(\text{S}_3)(\text{S})\text{CPh}_2$ , with equimolar amounts of  $\text{P}(\text{NMe}_2)_3$  results in the formation of  $\text{Tbt}(\text{Mes})\text{Sn}(\text{S}_2)(\text{S})\text{CPh}_2$  and  $\text{Tbt}(\text{Mes})\text{Sn}(\text{S})_2\text{CPh}_2$  in 35 and 26% yields, respectively [119, 120].

Desulfurization reactions of transition metal-polysulfido complexes have also been reported. The treatment of a dimetallic complex of titanium,  $[\{\text{Ti}(\text{Cp})(\text{OAr})\}_2(\mu\text{-S})(\mu\text{-S}_2)]$  ( $\text{Cp}=\eta^5\text{-C}_5\text{H}_5$ ,  $\text{Ar}=2,6\text{-}i\text{-Pr}_2\text{C}_6\text{H}_3$ ), with an equimolar amount of  $\text{Ph}_3\text{P}$  results in the quantitative formation of  $[\{\text{Ti}(\text{Cp})(\text{OAr})\}_2(\mu\text{-S})_2]$  via the transformation of the  $\mu\text{-S}_2$  ligand to a  $\mu\text{-S}$  ligand (Scheme 44) [93]. The reverse reaction of  $[\{\text{Ti}(\text{Cp})(\text{OAr})\}_2(\mu\text{-S})_2]$  with  $\text{S}_8$  proceeds in a good yield.



**Scheme 44** Desulfurization of transition metal polysulfido complexes

The reaction of  $(\text{Ph}_4\text{P})_2[\text{Nb}(\text{O})(\text{S}_2)_2(\text{SH})] \cdot 2\text{DMF}$  with  $\text{Et}_3\text{P}$  in DMF gives  $(\text{Ph}_4\text{P})_2[\text{Nb}(\text{S})_3(\text{SH})]$  together with  $\text{Et}_3\text{PO}$  and  $\text{Et}_3\text{PS}$  (Scheme 44) [84]. The formation of  $\text{Et}_3\text{PO}$  suggests that the abstraction of the oxygen atom from the  $\text{Nb}=\text{O}$  group occurs to afford an intermediary  $\text{Nb}(\text{III})$  species which is subsequently reoxidized to the final  $\text{Nb}(\text{V})$  compound. As mentioned above (Scheme 26),  $(\text{Ph}_4\text{P})_2[\text{Nb}(\text{S})_3(\text{SH})]$  reacts with  $\text{BzSSSBz}$  ( $\text{Bz}=\text{benzoyl}$ ) in wet  $\text{CH}_3\text{CN}$  to give  $(\text{Ph}_4\text{P})_2[\text{Nb}(\text{O})(\text{S}_2)_2(\text{SH})]$ .

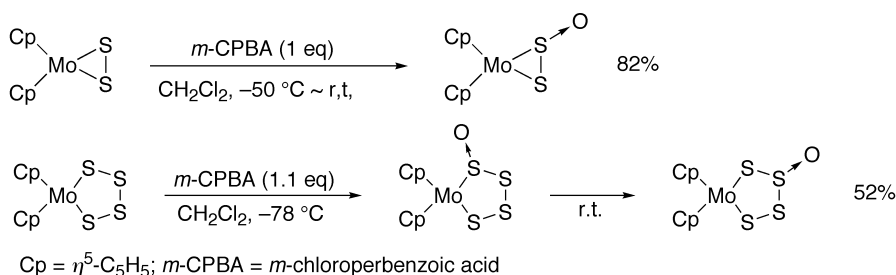
In addition, it has been reported that the rhenium polysulfido complex  $[\text{Re}(\text{Cp}^*)(\text{S}_3)(\text{S}_4)]$  ( $\text{Cp}^*=\eta^5\text{-C}_5\text{Me}_5$ ) undergoes desulfurization with  $\text{Ph}_3\text{P}$  to

the binuclear complex  $[\{\text{Re}(\text{Cp}^*)(\text{S}_4)\}_2]$  (Scheme 44) [69]. The trinuclear heterometallic cluster  $[(\mu_2\text{-S}_2)(\text{RuCp}^*)_2(\mu_2\text{-S})_2(\mu_3\text{-S})\text{W}(\text{S})]$  with bridging sulfur ligands reacts with excess  $\text{Et}_3\text{P}$  to give  $[\text{RuCp}^*(\text{PET}_3)(\mu\text{-S})_2\text{W}(\mu\text{-S})_2\text{RuCp}^*(\text{PET}_3)]$  in 15% yield via the loss of the  $\text{S}_2$  ligand [82].

### 4.3

#### Oxidation Reactions

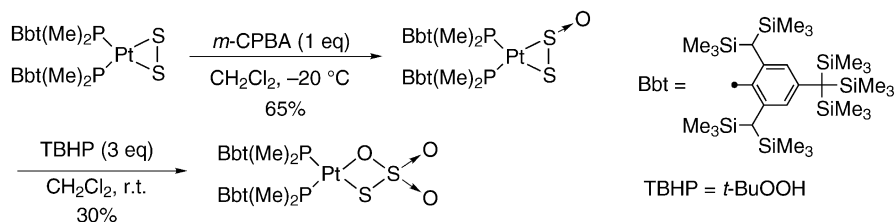
Oxidation of  $\text{MoCp}_2(\text{S}_2)$  ( $\text{Cp}=\eta^5\text{-C}_5\text{H}_5$ ) by *m*-CPBA (*m*-chloroperbenzoic acid) gives the corresponding  $\text{S}_2\text{O}$  complex  $\text{MoCp}_2(\text{S}_2\text{O})$  in a good yield (Scheme 45) [121]. The tetrasulfido complex  $\text{MoCp}_2(\text{S}_4)$  treated with *m*-CPBA at  $-78^\circ\text{C}$  affords the 2-oxo isomer of  $\text{MoCp}_2(\text{S}_4\text{O})$  as the final product



**Scheme 45** Oxidation of molybdenum polysulfido complexes

in 52% yield. Monitoring of this oxidation reaction by  $^1\text{H}$  NMR spectroscopy revealed the initial formation of the 1-oxo isomer, followed by an oxygen migration to give the 2-oxo isomer, which is the thermodynamically stable product.

The monooxidation of the disulfido complex of platinum  $[\text{Pt}(\text{S}_2)\{\text{P}(\text{Bbt})\text{Me}_2\}_2]$  with an equimolar amount of *m*-CPBA in  $\text{CH}_2\text{Cl}_2$  is complete at  $-20^\circ\text{C}$  within 2 h and gives the  $\text{S}_2\text{O}$  complex  $[\text{Pt}(\text{S}_2\text{O})(\text{PBbtMe}_2)_2]$  (Scheme 46) [122]. Further oxidation of the  $\text{S}_2\text{O}$  com-



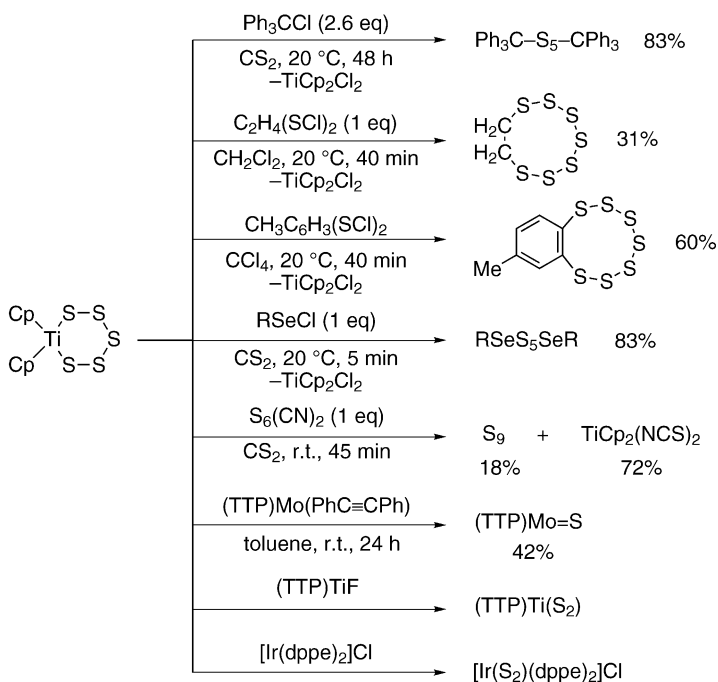
**Scheme 46** Oxidation of platinum disulfido complexes

plex using 3 equivalents of TBHP (*tert*-butyl hydroperoxide) unexpectedly yields the  $S_2O_3$  complex  $[Pt(S_2O_3)(PBBtMe_2)_2]$ . These results are in contrast to the reported exhaustive oxidation of a disulfido complex of iridium,  $[Ir(S_2)(dppe)_2]^+$  ( $dppe=1,2$ -bis(diphenylphosphino)ethane), to the  $S_2O_2$  complex  $[Ir(S_2O_2)(dppe)_2]^+$  via  $[Ir(S_2O)(dppe)_2]^+$  [123].

#### 4.4

##### Sulfur Transfer Reactions

Titanocene pentasulfide  $TiCp_2(S_5)$  has been used as a sulfur transfer reagent in the synthesis of a variety of organic and inorganic sulfur compounds. The reactions of  $TiCp_2(S_5)$  with  $Ph_3CCl$ ,  $C_2H_4(SCl)_2$ ,  $CH_3C_6H_3(SCl)_2$ , and  $RSeCl$  ( $R=4-ClC_6H_4$ ) result in the exchange of the  $S_5^{2-}$  unit with the  $Cl^-$  ligands to give  $Ph_3CS_5CPh_3$ ,  $C_2H_4S_7$ ,  $CH_3C_6H_3S_7$ , and  $RSeS_5SeR$ , respectively, along with  $Ti(Cp)_2Cl_2$  (Scheme 47) [124, 125]. The driving force of these reactions is

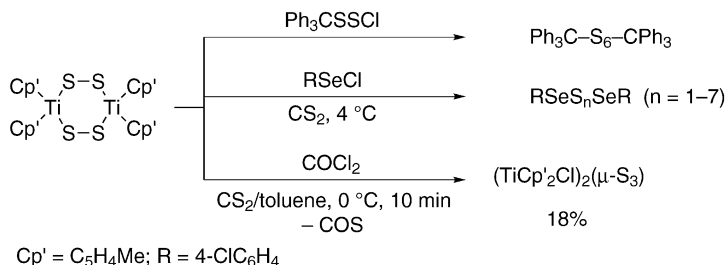


$Cp = \eta^5-C_5H_5$ ;  $R = 4-ClC_6H_4$ ;  $dppe = (Ph_2PCH_2)_2$ ;  $TTP = meso$ -tetra-*p*-tolylporphyrinato

**Scheme 47** Sulfur transfer reactions by the use of  $TiCp_2S_5$

the strong affinity of the titanium atom toward the  $\text{Cl}^-$  ligand. The exchange reaction with the  $\text{SCN}^-$  ligand also takes place in the reaction of  $\text{TiCp}_2(\text{S}_5)$  with  $\text{S}_6(\text{CN})_2$  to yield cyclononasulfur [126]. In the reaction with low-valent metal compounds such as  $(\text{TTP})\text{Mo}(\text{PhC}\equiv\text{CPh})$  ( $\text{TTP}=\text{meso-tetra-}p\text{-tolylporphyrinato}$ ),  $(\text{TTP})\text{TiF}$ , and  $[\text{Ir}(\text{dppe})_2]\text{Cl}$  ( $\text{dppe}=(\text{Ph}_2\text{PCH}_2)_2$ ),  $\text{TiCp}_2(\text{S}_5)$  acts as a transfer reagent for  $\text{S}^{2-}$  or  $\text{S}_2^{2-}$  units to afford  $(\text{TTP})\text{Mo}=\text{S}$ ,  $(\text{TTP})\text{Ti}(\text{S}_2)$ , and  $[\text{Ir}(\text{S}_2)(\text{dppe})_2]\text{Cl}$ , respectively [127, 128].

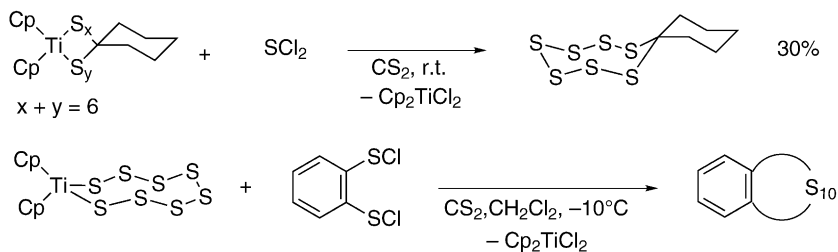
The dinuclear complex  $(\text{TiCp}'_2)_2(\mu\text{-S}_2)_2$  ( $\text{Cp}'=\text{C}_5\text{H}_4\text{Me}$ ) transfers the  $\text{S}_2^{2-}$  unit in the reaction with  $\text{Ph}_3\text{CSSCl}$  to yield  $(\text{Ph}_3\text{C})_2\text{S}_6$  (Scheme 48) [129].



**Scheme 48** Sulfur transfer reactions by the use of  $(\text{TiCp}'_2)_2(\mu\text{-S}_2)_2$

However, the reaction with  $\text{RSeCl}$  ( $\text{R}=4\text{-ClC}_6\text{H}_4$ ) gives a mixture of  $(\text{RSe})_2\text{S}_n$  ( $n=1-7$ ) and  $\text{R}_2\text{Se}_2$  [125]. Heating of this mixture results in the formation of a more complicated mixture,  $(\text{RSe})_2\text{S}_n$  ( $n=0-10$ ), instead of the convergence to a thermodynamically stable compound. When a toluene solution of phosgene is added to a solution of  $(\text{TiCp}'_2)_2(\mu\text{-S}_2)_2$  in  $\text{CS}_2$ , the acyclic trisulfido complex  $(\text{TiCp}'_2\text{Cl})_2(\mu\text{-S}_3)$  is obtained in 18% yield [130].

The chelate complexes  $\text{TiCp}_2(\text{S}_6\text{C}_6\text{H}_{10})$  and  $\text{TiCp}_2\text{S}_8$  undergo exchange reactions of the polysulfido ligands with chloride anions. The former reacts with  $\text{SCL}_2$  to afford 7,8,9,10,11,12,13-heptathiaspiro[5.7]tridecane, and the reaction of the latter with 1,2-benzodisulfenylchloride gives benzodecathionundecene (Scheme 49) [34].

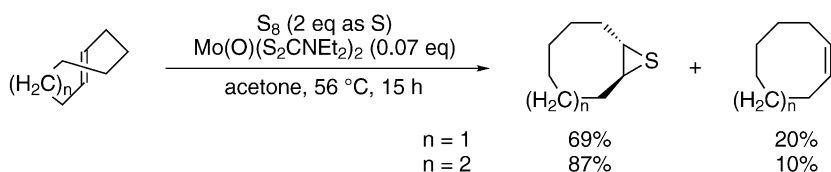


**Scheme 49** Sulfur transfer reactions by the use of  $\text{TiCp}_2(\text{S}_6\text{C}_6\text{H}_{10})$  and  $\text{TiCp}_2\text{S}_8$



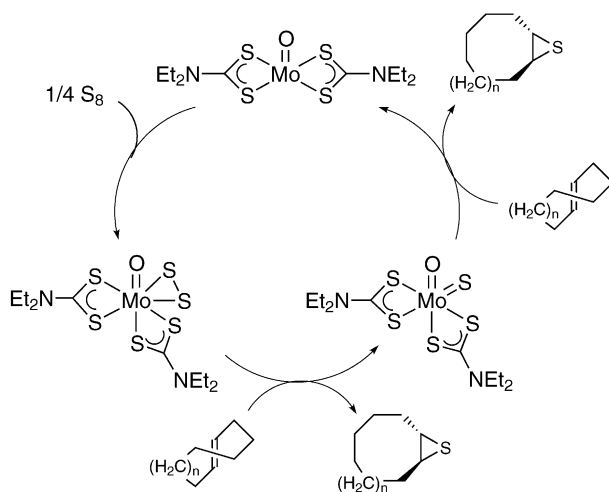
$\text{Zn}(\text{S}_6)(\text{TMEDA})$  is superior to  $\text{TiCp}_2\text{S}_5$  in the sulfur transfer ability. The usefulness of  $\text{ZnS}_6(\text{TMEDA})$  as an  $\text{S}_6$  transfer reagent is demonstrated in the reaction with  $\text{Se}_2\text{Cl}_2$  to give  $\text{S}_6\text{Se}_2$  via the exchange between  $\text{S}_6^{-2}$  ligand and the chloride anions.

A catalytic episulfidation of the strained olefins (*E*)-cyclooctene and (*E*)-cyclononene has been achieved by taking advantage of the sulfur transfer reaction from a molybdenum disulfido complex,  $\text{Mo}(\text{O})(\text{S}_2)(\text{S}_2\text{CNET}_2)_2$ , toward olefins [133]. Heating of a mixture of (*E*)-cyclooctene or (*E*)-cyclononene, 2 equivalents of S as  $\text{S}_8$ , and catalytic amounts (0.07 eq.) of  $\text{Mo}(\text{O})(\text{S}_2\text{CNET}_2)_2$  in acetone at 56 °C for 15 h results in the formation of the corresponding *trans*-episulfide together with the (*Z*)-isomers of the olefins (Scheme 52). In



**Scheme 52** Catalytic episulfidation of strained olefins by the use of  $\text{Mo}(\text{O})(\text{S}_2)(\text{S}_2\text{CNET}_2)_2$

these reactions,  $\text{Mo}(\text{O})(\text{S}_2)(\text{S}_2\text{CNET}_2)_2$ , generated from  $\text{Mo}(\text{O})(\text{S}_2\text{CNET}_2)_2$  and  $\text{S}_8$ , transfers a sulfur atom toward the strained olefin, and the further abstraction of the sulfur atom from the resulting  $\text{Mo}(\text{O})(\text{S})(\text{S}_2\text{CNET}_2)_2$  gives the initial oxo complex,  $\text{Mo}(\text{O})(\text{S}_2\text{CNET}_2)_2$ , again (Scheme 53).

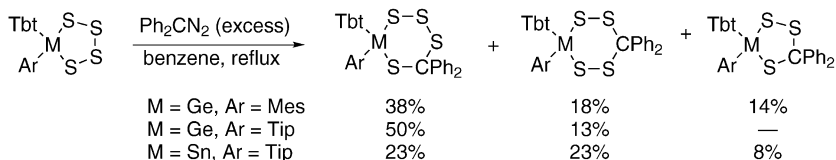


**Scheme 53** Plausible mechanism for catalytic episulfidation of strained olefins by the use of  $\text{Mo}(\text{O})(\text{S}_2)(\text{S}_2\text{CNET}_2)_2$

## 4.5

## Reactions with Carbenes

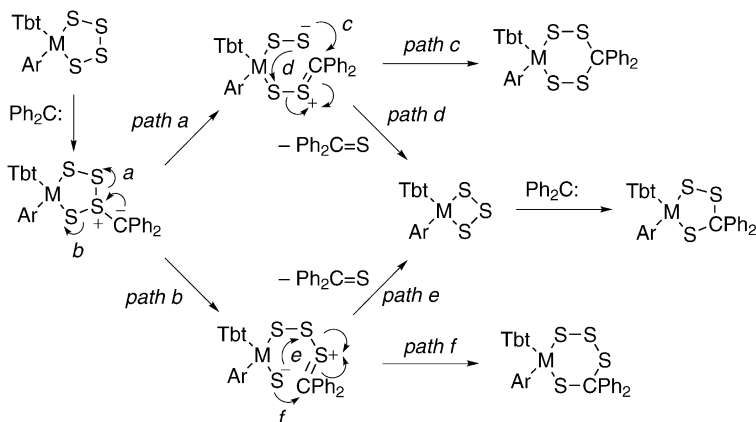
Reactions of cyclic tetrasulfides containing a heavier group 14 element,  $\text{Tbt}(\text{Ar})\text{MS}_4$  ( $\text{M}=\text{Ge}$ ,  $\text{Ar}=\text{Mes}$  or  $\text{Tip}$ ;  $\text{M}=\text{Sn}$ ,  $\text{Ar}=\text{Tip}$ ), with diphenyl diazomethane gives 1,2,3,5-tetrathia-4-metallacyclohexanes, 1,2,4,5-tetrathia-3-metallacyclohexanes, and 1,2,4-trithia-3-metallacyclopentanes (Scheme 54) [52, 118–120].



$\text{Tbt} = 2,4,6\text{-}[\text{CH}(\text{SiMe}_3)_2]_3\text{C}_6\text{H}_2$ ;  $\text{Mes} = 2,4,6\text{-Me}_3\text{C}_6\text{H}_2$ ;  $\text{Tip} = 2,4,6\text{-}(\text{CHMe}_2)_3\text{C}_6\text{H}_2$

**Scheme 54** Reaction of cyclic tetrasulfides containing a heavier group 14 element with diphenyl diazomethane

These tetrathiametallacyclohexanes are probably formed via the initial attack of diphenylcarbene, generated from the corresponding diazo compound, on a sulfur atom and subsequent ring expansion (Scheme 55). The



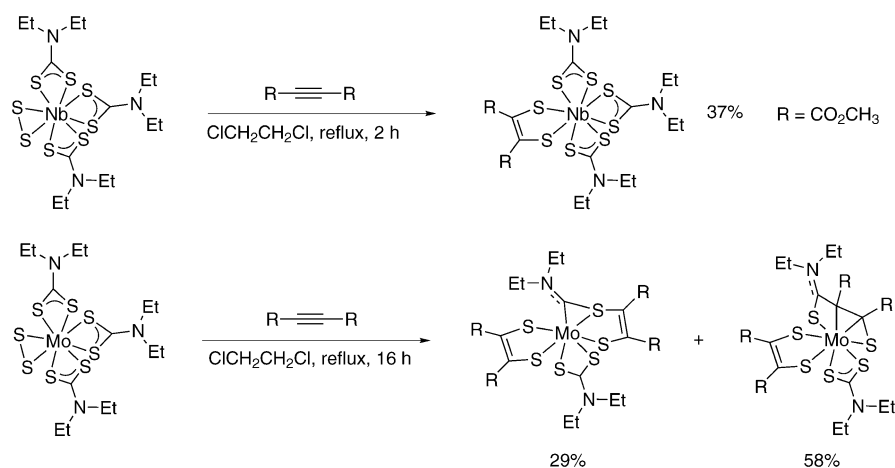
**Scheme 55** Possible mechanism for the reaction of cyclic tetrasulfides containing a heavier group 14 element with diphenyl diazomethane

formation mechanism for the trithiametallacyclopentanes is interpreted in terms of the ring extraction accompanied by the elimination of thiobenzophenone after the above-mentioned attack of the carbene, followed by the second attack of the carbene on the sulfur atom of the resulting  $\text{Tbt}(\text{Ar})\text{MS}_3$ .

#### 4.6

##### Reactions with Unsaturated Organic Molecules

The insertion reaction of dimethyl acetylenedicarboxylate (DMAD) into the S-S bond of a cyclic disulfido complex of niobium,  $\text{Nb}(\text{S}_2)(\text{S}_2\text{CNET}_2)_3$ , takes place to give the corresponding dithiolene complex,  $\text{Nb}\{\text{S}_2\text{C}_2(\text{CO}_2\text{Me})_2\}(\text{S}_2\text{CNET}_2)_3$  (Scheme 56) [134].



**Scheme 56** Reaction of niobium and molybdenum disulfido complexes with alkyne

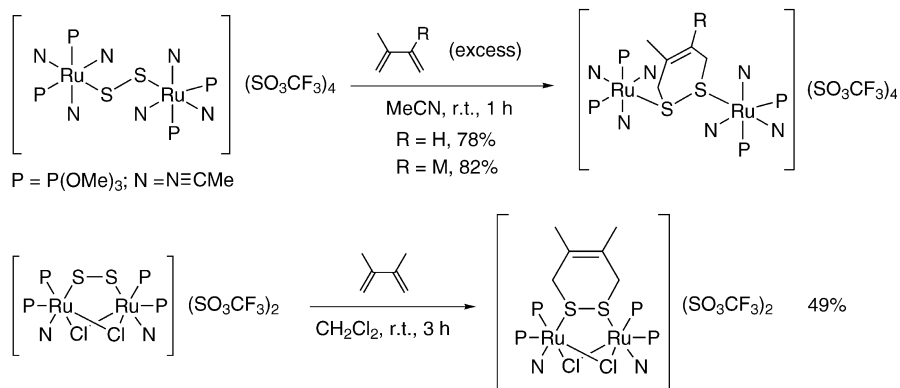
By contrast, the reaction of the molybdenum disulfido complex  $\text{Mo}(\text{S}_2)(\text{S}_2\text{CNET}_2)_3$  with DMAD results in the formation of  $\text{Mo}\{\text{SC}(\text{CO}_2\text{Me})=\text{C}(\text{CO}_2\text{Me})\text{SCNET}_2\}\{\text{S}_2\text{C}_2(\text{CO}_2\text{Me})_2\}(\text{S}_2\text{CNET}_2)$  and  $\text{Mo}\{\text{SC}(\text{CO}_2\text{Me})\text{C}(\text{CO}_2\text{Me})\text{C}(\text{NET}_2)\text{S}\}\{\text{S}_2\text{C}_2(\text{CO}_2\text{Me})_2\}(\text{S}_2\text{CNET}_2)$ . The formation of these complexes may be explained in terms of the initial insertion of DMAD into the S-S bond, followed by the elimination of a dithiocarbamyl radical with concomitant incorporation of the second DMAD unit and formation of thiuram disulfide,  $(\text{S}_2\text{CNET}_2)_2$ .

The dinuclear rhenium disulfido complex with  $\mu, \eta^2$ - $\text{S}_2$  ligands  $(\text{ReCp}')_2(\mu\text{-S}_2)_2$  ( $\text{Cp}' = \eta^5\text{-C}_5\text{Me}_4\text{Et}$ ) (type **IIa**<sub>2</sub> complex in Fig. 2) undergoes an insertion reaction of acetylene and ethylene into the S-S bond according to Scheme 57.

The zinc tetrasulfido complex  $\text{ZnS}_4(\text{PMDETA})$  (PMDETA=pen-tamethyldiethylenetriamine) reacts with alkynes and  $\text{CS}_2$  to give the dithio-lene complexes  $\text{ZnS}_2\text{C}_2(\text{CO}_2\text{Me})_2(\text{PMDETA})$  and  $\text{ZnS}_3\text{CS}(\text{PMDETA})$ , respec-

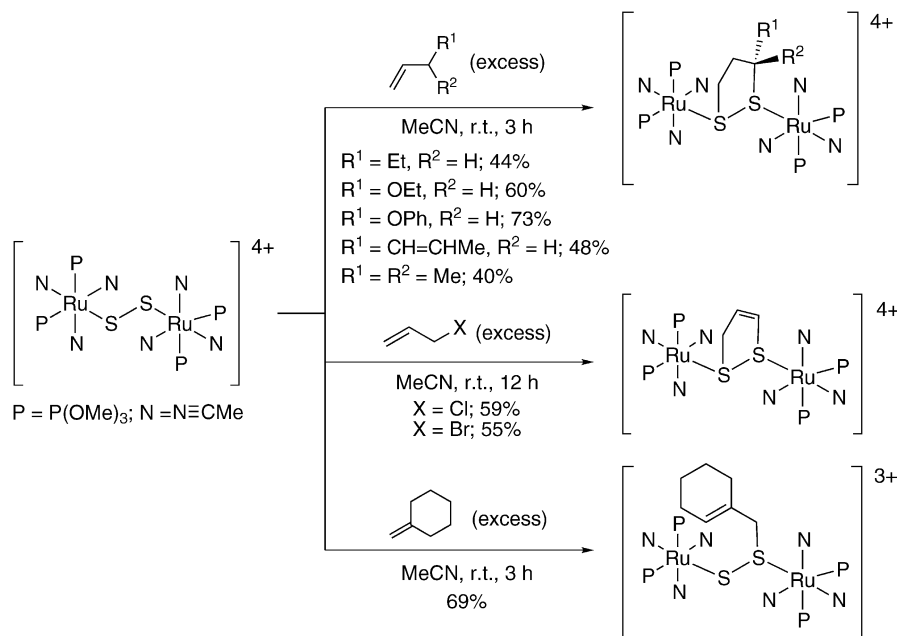


(R)=C(Me)CH<sub>2</sub>S}}] <sup>4+</sup>, respectively, via [2+4]cycloaddition reactions (Scheme 59) [135, 136]. It has been proposed that these reactions can be explained as Diels-Alder type additions. These reactivities are similar to those of unstable free disulfur prepared in situ, and different from those of their



**Scheme 59** Reaction of diruthenium disulfido complexes with 1,3-dienes

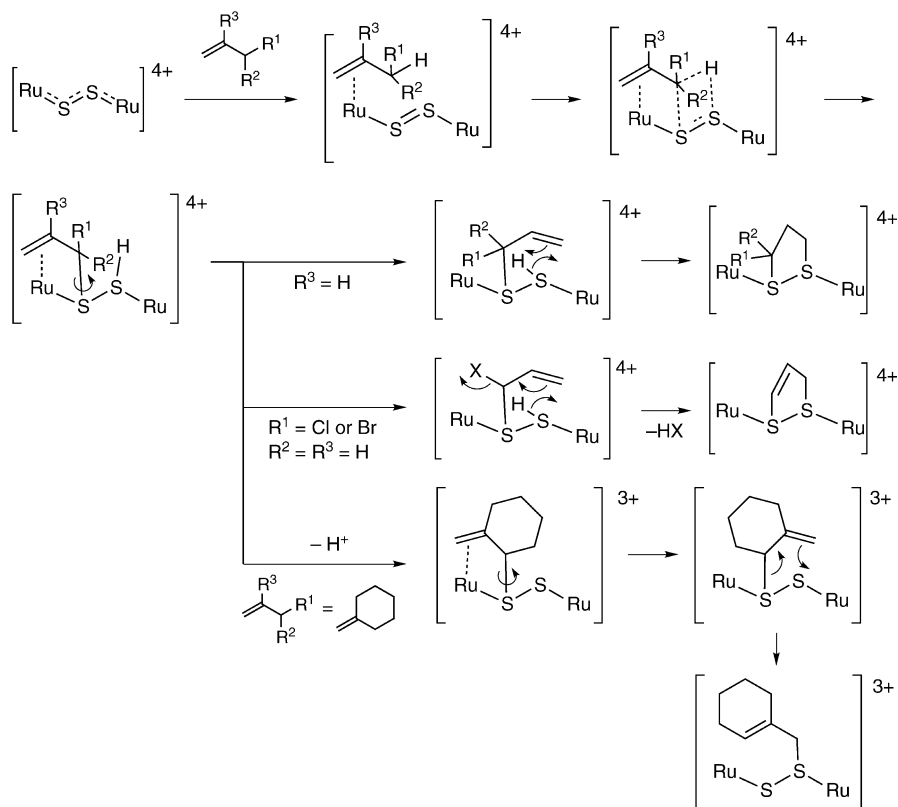
PMe<sub>3</sub> analogues, [Ru(MeCN)(PMe<sub>3</sub>)<sub>2</sub>]<sub>2</sub>(μ-S<sub>2</sub>)] <sup>4+</sup> and [Ru(MeCN)(PMe<sub>3</sub>)<sub>2</sub>(μ-Cl)<sub>2</sub>(μ-S<sub>2</sub>)] <sup>2+</sup>, and other bridging disulfido complexes such as [Ru(NH<sub>3</sub>)<sub>5</sub>]<sub>2</sub>(μ-S<sub>2</sub>)] <sup>4+</sup> and [Ru(Cp)(PPh<sub>3</sub>)<sub>2</sub>(μ-S<sub>2</sub>)] <sup>2+</sup>.



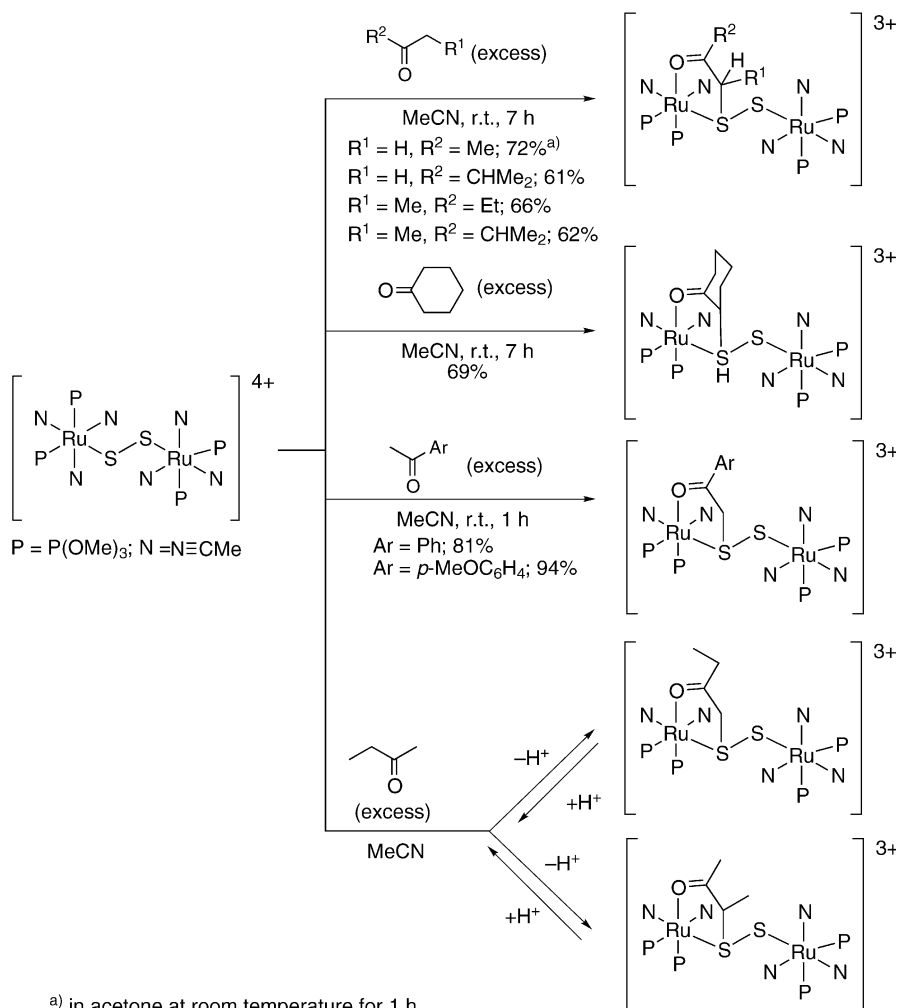
**Scheme 60** Reaction of a diruthenium disulfido complex with olefins

In addition, Matsumoto et al. reported that the reaction of  $[\{\text{Ru}(\text{MeCN})_3(\text{P}(\text{OMe})_3)_2\}_2(\mu\text{-S}_2)](\text{CF}_3\text{SO}_4)_4$  with various types of alkenes results in a C-H bond activation on the bridging disulfur ligand of the diruthenium complex. The diruthenium disulfido complex reacts with terminal alkenes such as 1-pentene, allylethylether, allylphenylether, and 1,4-hexadiene at room temperature to give the complexes with a  $\text{C}_3\text{S}_2$  five-membered ring,  $[\{\text{Ru}(\text{MeCN})_3(\text{P}(\text{OMe})_3)_2\}_2(\mu\text{-SCH}_2\text{CH}_2\text{CR}^1\text{R}^2\text{S})](\text{CF}_3\text{SO}_4)_4$  (Scheme 60) [137, 138].

On the other hand, the reaction with allyl halide and methylenecyclohexane results in the formation of  $[\{\text{Ru}(\text{MeCN})_3(\text{P}(\text{OMe})_3)_2\}_2(\mu\text{-SCH}_2\text{CH}=\text{CHS})](\text{CF}_3\text{SO}_4)_4$  and  $[\{\text{Ru}(\text{MeCN})_3(\text{P}(\text{OMe})_3)_2\}_2\{\mu\text{-S}(\text{CH}_2\text{C}_6\text{H}_9)\text{S}\}](\text{CF}_3\text{SO}_4)_4$ , respectively (Scheme 60) [137–139]. The key steps in all of these reactions might be the addition of an allylic C-H bond to the S-S bond to form the C-S and S-H bonds (Scheme 61). In the case of  $\text{R}^3=\text{H}$ , the liberated hydrogen



**Scheme 61** Plausible mechanism for the reaction of diruthenium disulfido complexes with olefins



**Scheme 62** Reaction of a diruthenium disulfido complex with ketones

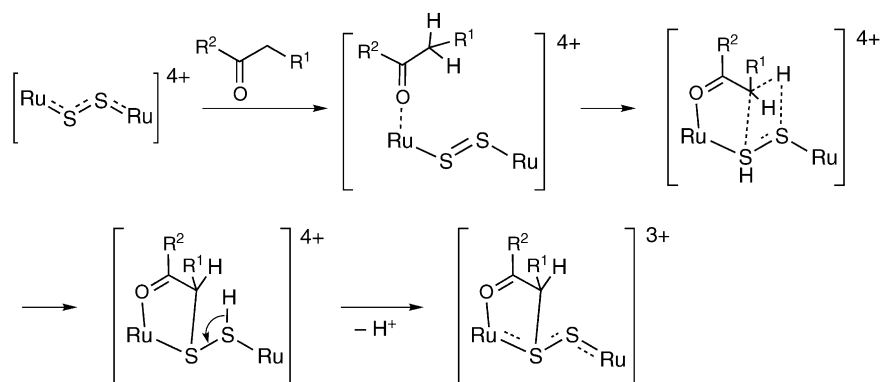
atom of the S-H bond seems to be transferred to the neighboring carbon atom after the C-S bond rotation, and then the terminal carbon atom forms the second C-S bond to give the  $\text{C}_3\text{S}_2$  ring. In the reaction with allyl halide, the ring closure accompanied by the elimination of HX ( $\text{X} = \text{Cl}, \text{Br}$ ) occurred to afford the product having a 1,2-dithiolene ring. The deprotonation from the key intermediate before the C-S bond rotation, which is hindered by the bulky substituent, takes place in the reaction with methylenecyclohexane, and the subsequent migration gives the final product.

In addition, the reactions of  $[\{\text{Ru}(\text{MeCN})_3(\text{P}(\text{OMe})_3)_2\}_2(\mu\text{-S}_2)](\text{CF}_3\text{SO}_4)_4$  with haloalkenes [139], alkynes [140] and hydroxyl substituted alkenes and

alkynes [141] have been reported to proceed via the above-mentioned C-H bond activation on the S-S bond of the diruthenium disulfido complex  $[\{\text{Ru}(\text{MeCN})_3(\text{P}(\text{OMe})_3)_2\}_2(\mu\text{-S}_2)](\text{CF}_3\text{SO}_4)_4$ .

Another type of C-H activation on S-S bonds has been observed in the reaction of  $[\{\text{Ru}(\text{MeCN})_3(\text{P}(\text{OMe})_3)_2\}_2(\mu\text{-S}_2)]^{4+}$  with ketones. Treatment of  $[\{\text{Ru}(\text{MeCN})_3(\text{P}(\text{OMe})_3)_2\}_2(\mu\text{-S}_2)]^{4+}$  with various ketones results in the formation of the corresponding ketonated complexes,  $[\{\text{Ru}(\text{MeCN})_3(\text{P}(\text{OMe})_3)_2\}_2\{\mu\text{-SS}(\text{CHR}^1\text{COR}^2)\}]^{4+}$  (Scheme 62) [142, 143].

In the reaction with butanone, an equilibrium between the  $\text{CH}_3$ -activated complex and the  $\text{CH}_2$ -activated complex is observed and it is revealed that the former is a thermodynamic product and the latter is a kinetic product. These results indicate that the relative reactivity of the C-H bonds is in the order of  $2 > 1 > 3$ , and the large and electron-withdrawing substituents retard the reaction. A plausible mechanism is shown in Scheme 63. When the oxy-



**Scheme 63** Plausible mechanism for reaction of a diruthenium disulfido complex with ketones

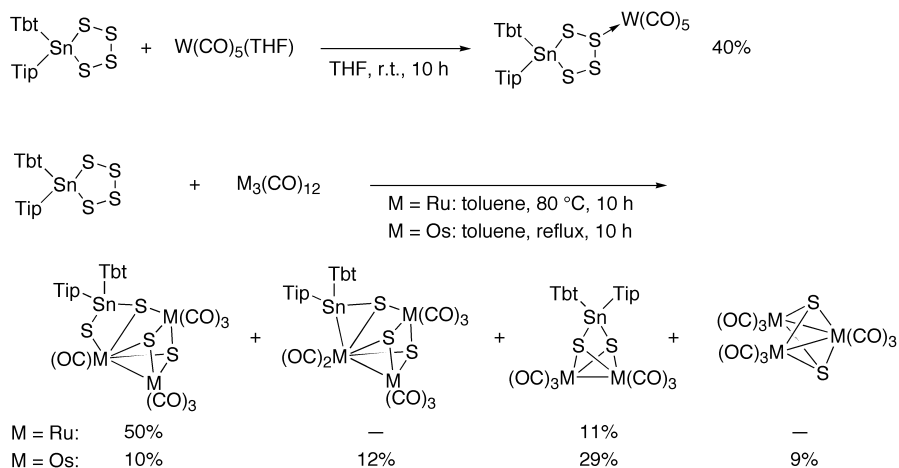
gen atom of the ketone is coordinated to the Ru center and the  $\alpha$ -C-H bond of the ketone is oriented parallel to the  $\text{S}_2$  moiety, metathesis could occur between the C-H  $\sigma$  bond and the formal S=S  $\pi$  bond to form the C-S and S-H bonds. The reaction is completed by the deprotonation of the S-H bond.

#### 4.7

##### Reactions with Transition Metal Complexes

Reactions of tetrathiaastannolanes bearing bulky substituents with groups 6 and 8 transition metal carbonyls have been reported.  $\text{Tbt}(\text{Tip})\text{SnS}_4$  reacts with  $\text{W}(\text{CO})_5(\text{THF})$  in THF at room temperature to give  $\text{Tbt}(\text{Tip})\text{SnS}_4\cdot\text{W}(\text{CO})_5$  in 40% yield (Scheme 64) [144].

The reaction of  $\text{Tbt}(\text{Tip})\text{SnS}_4$  with  $\text{Ru}_3(\text{CO})_{12}$  results in the formation of the triruthenium complex  $[\{\text{Ru}(\text{CO})\}_3\{\text{Ru}(\text{CO})_3\}_2\{\text{Sn}(\text{Tbt})(\text{Tip})\}(\mu_2\text{-S})(\mu_3\text{-S})_3]$

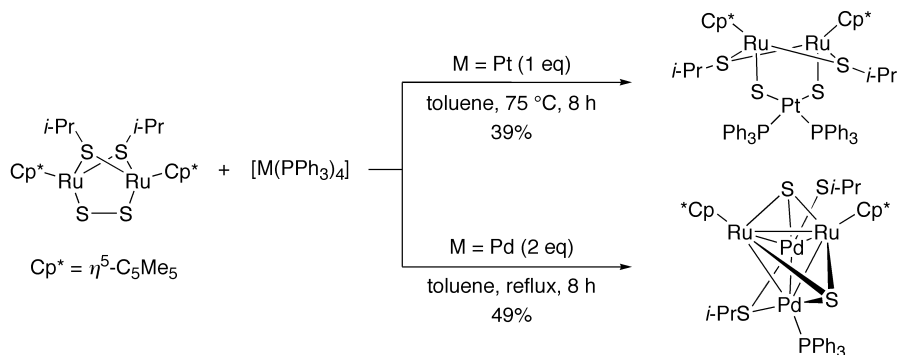


Tbt = 2,4,6-[CH(SiMe<sub>3</sub>)<sub>2</sub>]<sub>3</sub>C<sub>6</sub>H<sub>2</sub>; Tip = 2,4,6-(CHMe<sub>2</sub>)<sub>3</sub>C<sub>6</sub>H<sub>2</sub>

**Scheme 64** Reaction of tin tetrasulfide with transition metal complexes

and the diruthenium complex [ $\{\text{Ru}(\text{CO})_3\}_2\{\text{Sn}(\text{Tbt})(\text{Tip})\}(\mu_3\text{-Y})_2$ ] [144]. Furthermore, the triosmium complexes [ $\{\text{Os}(\text{CO})_2\}\{\text{Os}(\text{CO})_3\}_2\{\text{Sn}(\text{Tbt})(\text{Tip})\}(\mu_3\text{-S})_3$ ] and [ $\{\text{Os}(\text{CO})_3\}_3(\mu_3\text{-S})_2$ ] have been isolated together with the osmium analogues of the above-mentioned ruthenium complexes in the reaction of Tbt(Tip)SnS<sub>4</sub> with Os<sub>3</sub>(CO)<sub>12</sub> [144, 145]. The formation of these complexes containing group 8 metals and tin is explained in terms of the initial formation of [ $\{\text{M}(\text{CO})_3\}_3(\mu_3\text{-S})_2$ ] (M=Ru, Os), which are known to be generated in the reaction of M(CO)<sub>12</sub> with elemental sulfur.

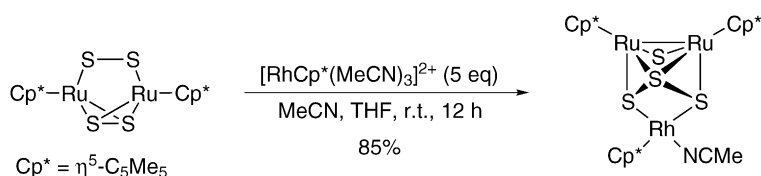
Hidai et al. have reported the reaction of a diruthenium complex, (RuCp<sup>\*</sup>)<sub>2</sub>(μ-Si-Pr)<sub>2</sub>(μ-S<sub>2</sub>), with zerovalent complexes of group 10 metals, [M(PPh<sub>3</sub>)<sub>4</sub>] (M=Pd, Pt) (Scheme 65) [146]. The reaction with the Pt complex



**Scheme 65** Reaction of (RuCp<sup>\*</sup>)<sub>2</sub>(μ-Si-Pr)<sub>2</sub>(μ-S<sub>2</sub>) with zerovalent platinum and palladium complexes

results in the insertion reaction of the Pt atom into the S-S bond of the diruthenium complex to give  $[(\text{Ph}_3\text{P})_2\text{Pt}(\mu\text{-S})_2(\text{RuCp}^*)_2(\mu\text{-Si-Pr})_2]$ . By contrast, the tetranuclear cluster  $[\text{Pd}_2(\text{PPh}_3)(\text{Si-Pr})(\mu\text{-Si-Pr})(\mu_3\text{-S})_2(\text{RuCp}^*)_2]$  is obtained in 47% yield from the reaction with the Pd complex.

In addition, the reaction of the diruthenium complex  $[\text{Ru}_2\text{Cp}^*_2\text{S}_4]$  with  $[\text{RhCp}^*(\text{MeCN})_3](\text{PF}_6)_2$  has been reported to afford the trinuclear cluster  $[\text{RhRu}_2\text{Cp}^*_3\text{S}_4(\text{MeCN})](\text{PF}_6)_2$  in 85% yield (Scheme 66) [147].

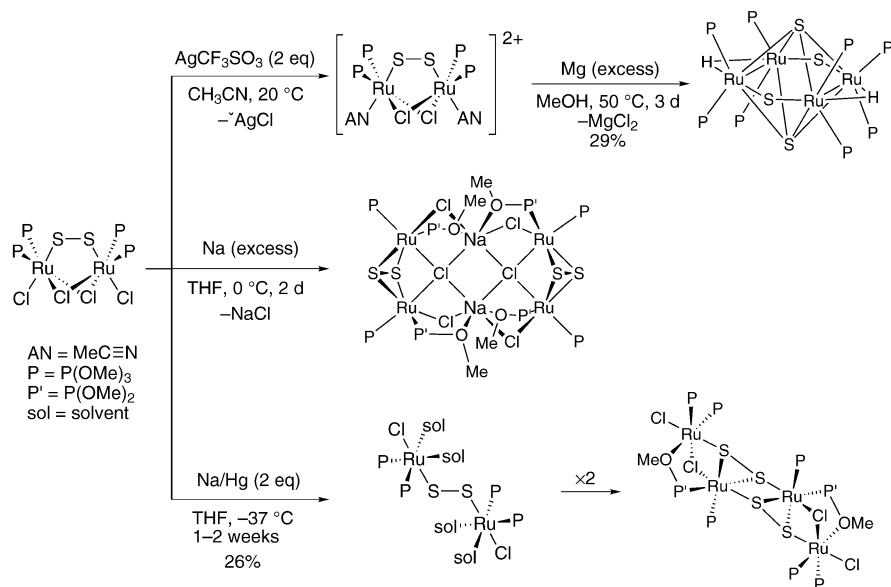


**Scheme 66** Reaction of  $[\text{Ru}_2\text{Cp}^*_2\text{S}_4]$  with a rhodium complex

## 4.8

### Reductions by Metals

Tetraruthenium cluster complexes have been synthesized by the reaction of  $[\{\text{Ru}(\text{Cl})(\text{P}(\text{OMe})_3)_2\}_2(\mu\text{-Cl})_2(\mu\text{-S}_2)]$  with Mg, Na, or Na amalgam (Scheme 67). The removal of the terminal chlorine atoms from



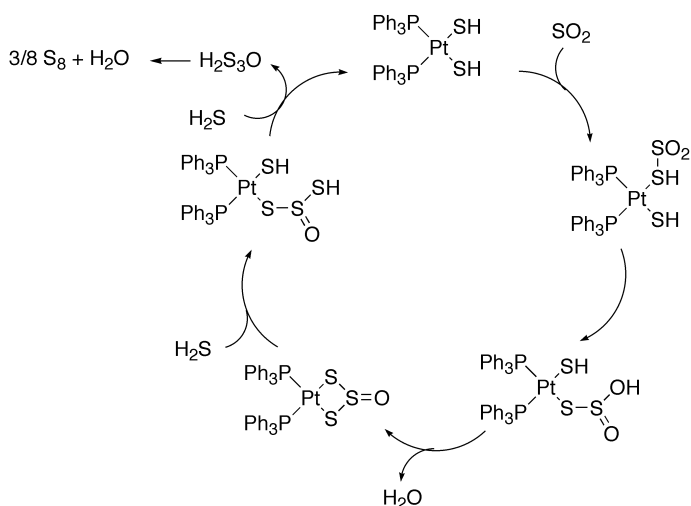
**Scheme 67** Reaction of a diruthenium disulfido complex with metals

$[\{\text{Ru}(\text{Cl})\text{P}(\text{OMe})_3\}_2(\mu\text{-Cl})_2(\mu\text{-S}_2)]$  with  $\text{Ag}^+$  and the subsequent reduction by  $\text{Mg}$  in  $\text{MeOH}$  results in the formation of the  $\text{Ru}(\text{II})_2\text{Ru}(\text{III})_2$  mixed-valent tetranuclear complex  $[\text{Ru}\{\text{P}(\text{OMe})_3\}_2]_4(\mu\text{-H})_2(\mu\text{-S})_2(\mu_4\text{-S})_2$  (Scheme 67) [148]. While the reduction of  $[\{\text{Ru}(\text{Cl})\text{P}(\text{OMe})_3\}_2(\mu\text{-Cl})_2(\mu\text{-S}_2)]$  with an excess of  $\text{Na}$  in  $\text{THF}$  gives the  $\text{Ru}(\text{II})_4\text{Na}_2$  hexanuclear cluster complex  $[\text{Na}_2\text{Ru}_4\{\text{P}(\text{OMe})_3\}_4(\mu\text{-Cl})_4(\mu_4\text{-Cl})_2(\mu,\eta^2\text{-S}_2)_2(\mu\text{-P}(\text{OMe})_3\text{-P}_2\text{O})_4]\cdot\text{THF}$  [149], the reaction using 2 equivalents of sodium amalgam at  $-37^\circ\text{C}$  leads to the formation of the tetranuclear  $\text{Ru}(\text{II})$  complex  $[\text{RuCl}(\mu\text{-Cl})\{\text{P}(\text{OMe})_3\}_2(\mu,\eta^1,\eta^2\text{-S}_2)\text{Ru}\{\text{P}(\text{OMe})_3\}\{\mu\text{-P}(\text{OMe})_3\text{-P}_2\text{O}\}]_2$  [150]. It has been proposed that the initial step of the latter reaction is the reduction of the two  $\text{Ru}(\text{III})$  centers to  $\text{Ru}(\text{II})$  by 2 equivalents of metallic sodium, concomitant with removal of the bridging chloride ligands by  $\text{Na}^+$  as  $\text{NaCl}$  to afford an intermediate,  $[\text{RuCl}\{\text{P}(\text{OMe})_3\}_2(\text{sol})_2]_2(\mu\text{-S}_2)$ . The subsequent coupling reaction of the intermediate leads to the final product.

#### 4.9

##### Other Reactions

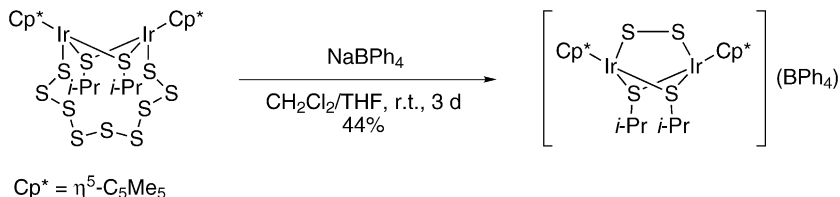
The reaction of  $[\text{Pt}(\text{S}_3\text{O})(\text{PPh}_3)_2]$  with  $\text{H}_2\text{S}$  has been studied from the standpoint of the chemistry of the Claus process [88]. The Claus process implies the reaction between  $\text{H}_2\text{S}$  and  $\text{SO}_2$  over alumina at  $300^\circ\text{C}$  to give sulfur and water with very high efficiency. This process has been used for the disposal of  $\text{H}_2\text{S}$ , which is generated in the hydrodesulfurization (HDS) of sulfur compounds in fossil fuels.  $[\text{Pt}(\text{S}_3\text{O})(\text{PPh}_3)_2]$  reacts with  $\text{H}_2\text{S}$  at room temperature in  $\text{THF}$  to afford the corresponding thiol *cis*- $[\text{Pt}(\text{SH})_2(\text{PPh}_3)_2]$ . Since the reaction of *cis*- $[\text{Pt}(\text{SH})_2(\text{PPh}_3)_2]$  with  $\text{SO}_2$  gives  $[\text{Pt}(\text{S}_3\text{O})(\text{PPh}_3)_2]$  in good yield (see above, Scheme 29),  $[\text{Pt}(\text{SH})_2(\text{PPh}_3)_2]$  and  $[\text{Pt}(\text{S}_3\text{O})(\text{PPh}_3)_2]$  may act as



**Scheme 68** Potential mechanism for the Claus reaction catalyzed by *cis*- $[\text{Pt}(\text{SH})_2(\text{PPh}_3)_2]$

catalysts for the Claus process. Actually, these complexes catalyze the reaction of  $\text{SO}_2$  with  $\text{H}_2\text{S}$  to give  $\text{S}_8$  and  $\text{H}_2\text{O}$  in good yield (Scheme 68).

The diiridium complex  $(\text{IrCp}^*)_2(\mu\text{-S}_9)(\mu\text{-Si-Pr})_2$  reacts with 3 equivalents of  $\text{NaBPh}_4$  in  $\text{CH}_2\text{Cl}_2/\text{THF}$  at room temperature to the formal Ir(III)/Ir(II)



**Scheme 69** Reaction of a diiridium nonasulfido complex with  $\text{NaBPh}_4$

mixed-valent complex  $[(\text{IrCp}^*)_2(\mu\text{-S}_2)(\mu\text{-Si-Pr})_2](\text{BPh}_4)$  via degradation of the  $\mu\text{-S}_9$  ligand accompanied by one-electron oxidation of the dimetallic center (Scheme 69) [65]. The fate of the eliminated " $\text{S}_7^-$ " unit could not be clarified.

## References

1. D. Coucouvanis, *Adv. Inorg. Chem.* **1998**, *45*, 1
2. A. Müller, E. Diemann, *Adv. Inorg. Chem.* **1987**, *31*, 89
3. M. Draganjac, T.B. Rauchfuss, *Angew. Chem. Int. Ed. Engl.* **1985**, *24*, 742
4. J. Wachter, *Angew. Chem. Int. Ed. Engl.* **1989**, *28*, 1613
5. M.R. Dubois, *Chem. Rev.* **1989**, *89*, 1
6. C. Simonnet-Jégat, F. Sécheresse, *Chem. Rev.* **2001**, *101*, 2601
7. J.W. Kois, *Coord. Chem. Rev.* **1990**, *105*, 195
8. A. Müller, W. Jaegermann, J.H. Enemark, *Coord. Chem. Rev.* **1982**, *46*, 245
9. D. Coucouvanis, A. Hadjikyriacou, M. Draganjac, M.G. Kanatzidis, O. Ieperuma, *Polyhedron* **1986**, *5*, 349
10. A. Müller, *Polyhedron* **1986**, *5*, 323
11. H. Suzuki, N. Tokitoh, R. Okazaki, *Bull. Chem. Soc. Jpn.* **1995**, *68*, 2471
12. H. Suzuki, N. Tokitoh, S. Nagase, R. Okazaki, *J. Am. Chem. Soc.* **1994**, *116*, 11578
13. H. Suzuki, N. Tokitoh, R. Okazaki, S. Nagase, M. Goto, *J. Am. Chem. Soc.* **1998**, *120*, 11096
14. N. Tokitoh, K. Manmaru, R. Okazaki, *Organometallics* **1994**, *13*, 167
15. T. Matsumoto, N. Tokitoh, R. Okazaki, *J. Am. Chem. Soc.* **1999**, *121*, 8811
16. N. Tokitoh, M. Saito, R. Okazaki, *J. Am. Chem. Soc.* **1993**, *115*, 2065
17. M. Saito, N. Tokitoh, R. Okazaki, *Organometallics* **1995**, *14*, 3620
18. M. Saito, N. Tokitoh, R. Okazaki, *Organometallics* **1996**, *15*, 4531
19. N. Tokitoh, N. Kano, K. Shibata, R. Okazaki, *Organometallics* **1995**, *14*, 3121
20. N. Kano, K. Shibata, N. Tokitoh, R. Okazaki, *Organometallics* **1999**, *18*, 2999
21. J. Albertsen, R. Steudel, *Phosphorus, Sulfur, and Silicon* **1992**, *65*, 165
22. J. Albertsen, R. Steudel, *J. Organomet. Chem.* **1992**, *424*, 153
23. S.R. Foley, G.P.A. Yap, D.S. Richeson, *Organometallics* **1999**, *18*, 4700
24. P.B. Hitchcock, H.A. Jasim, M.F. Lappert, W.-P. Leung, A.K. Rai, R.E. Taylor, *Polyhedron* **1991**, *10*, 1203
25. P.B. Hitchcock, E. Jang, M.F. Lappert, *J. Chem. Soc., Dalton Trans.* **1995**, 3179

26. K. Kashiwabara, A. Morikawa, T. Suzuki, K. Isobe, K. Tatsumi, *J. Chem. Soc., Dalton Trans.* **1997**, 1075
27. A.P. Ginsberg, W.E. Lindsell, C.R. Sprinkle, K.W. West, R.L. Cohen, *Inorg. Chem.* **1982**, *21*, 3666
28. J.T. Mague, E.J. Davis, *Inorg. Chem.* **1977**, *16*, 131
29. J.T.E. Nappier, D.W. Meek, R.M. Kirchner, J.A. Ibers, *J. Am. Chem. Soc.* **1973**, *95*, 4194
30. Y. Wakatsuki, H. Yamazaki, C. Cheng, *J. Organomet. Chem.* **1989**, *372*, 437
31. M. Kita, K. Kashiwabara, J. Fujita, S. Kurachi, S. Ohba, *Bull. Chem. Soc. Jpn.* **1993**, *66*, 3686
32. T. Suzuki, N. Tsuji, K. Kashiwabara, K. Tatsumi, *Inorg. Chem.* **2000**, *39*, 3938
33. E.G. Müller, J.L. Petersen, L.F. Dahl, *J. Organomet. Chem.* **1976**, *111*, 91
34. R. Steudel, M. Kustos, V. Münchow, U. Westphal, *Chem. Ber.-Recl.* **1997**, *130*, 757
35. K. Bergemann, M. Kustos, P. Krüger, R. Steudel, *Angew. Chem. Int. Ed. Engl.* **1995**, *34*, 1330
36. R. Steudel, O. Schumann, J. Buschmann, P. Luger, *Angew. Chem. Int. Ed.* **1998**, *37*, 492
37. K. Nagata, N. Takeda, N. Tokitoh, *Angew. Chem. Int. Ed. Engl.* **2002**, *41*, 136
38. J. Chatt, D.M.P. Mingos, *J. Chem. Soc. A* **1970**, 1243
39. R.R. Gukathasan, R.H. Morris, A. Walker, *Can. J. Chem.* **1983**, *61*, 2490
40. E.J. Houser, S. Dev, A.E. Ogilvy, T.B. Rauchfuss, S.R. Wilson, *Organometallics* **1993**, *12*, 4678
41. A. Hörnig, C. Rietmann, U. Englert, T. Wagner, U. Kölle, *Chem. Ber.* **1993**, *126*, 2609
42. Y. Mizobe, M. Hosomizu, S. Kuwata, J. Kawabata, M. Hidai, *J. Organomet. Chem.* **1996**, *513*, 231
43. K. Matsumoto, T. Matsumoto, M. Kawano, H. Ohnuki, Y. Shichi, T. Nishide, T. Sato, *J. Am. Chem. Soc.* **1996**, *118*, 3597
44. T.B. Rauchfuss, S. Dev, S.R. Wilson, *Inorg. Chem.* **1992**, *31*, 154
45. R. Emannuel, T.B. Rauchfuss, C.L. Stern, *J. Am. Chem. Soc.* **1990**, *112*, 4043
46. S. Dev, R. Emannuel, T.B. Rauchfuss, C.L. Stern, *J. Am. Chem. Soc.* **1990**, *112*, 6385
47. A.K. Verma, T.B. Rauchfuss, S.R. Wilson, *Inorg. Chem.* **1995**, *34*, 3072
48. P.P. Paul, T.B. Rauchfuss, S.R. Wilson, *J. Am. Chem. Soc.* **1993**, *115*, 3316
49. D.M. Young, G.L. Schimek, J.W. Kolis, *Inorg. Chem.* **1996**, *35*, 7620
50. N. Tokitoh, H. Suzuki, K. Matsumoto, Y. Matsushashi, R. Okazaki, M. Goto, *J. Am. Chem. Soc.* **1991**, *113*, 7047
51. Y. Matsushashi, N. Tokitoh, R. Okazaki, M. Goto, S. Nagase, *Organometallics* **1993**, *12*, 1351
52. K. Matsumoto, N. Tokitoh, R. Okazaki, M. Goto, *Organometallics* **1995**, *14*, 1008
53. T. Matsumoto, Y. Matsui, Y. Nakaya, K. Tatsumi, *Chem. Lett.* **2001**, 60
54. N. Tokitoh, Y. Arai, J. Harada, R. Okazaki, *Chem. Lett.* **1995**, 959
55. H. Brunner, U. Klement, J. Wachter, M. Tsunoda, J.-C. Leblanc, C. Moise, *Inorg. Chem.* **1990**, *29*, 584
56. H.-J. Bach, H. Brunner, J. Wachter, M.M. Kubicki, J.-C. Leblanc, C. Moise, F. Volpato, B. Nuber, M.L. Ziegler, *Organometallics* **1992**, *11*, 1403
57. M.M. Hossain, K. Matsumoto, *Inorg. Chem.* **2000**, *39*, 247
58. C. Ong, J. Kickham, S. Clemens, F. Guérin, D.W. Stephan, *Organometallics* **2002**, *21*, 1646
59. P. Meunier, B. Gautheron, A. Mazouz, *J. Organomet. Chem.* **1987**, *320*, C39
60. G. Shang, M.J. Hampden-Smith, E.N. Duesler, *Inorg. Chem.* **1996**, *35*, 2611
61. S.C. Sendlinger, J.R. Nicholson, E.B. Lobkovsky, J.C. Huffman, D. Rehder, G. Christou, *Inorg. Chem.* **1993**, *32*, 204
62. J.K. Money, J.R. Nicholson, J.C. Huffman, G. Christou, *Inorg. Chem.* **1986**, *25*, 4072
63. J.W. Park, S.M. Koo, *Inorg. Chem.* **1999**, *38*, 4898
64. M.B. Power, J.W. Ziller, A.N. Tyler, A.R. Barron, *Organometallics* **1992**, *11*, 1055
65. M. Nishino, H. Matsuzaka, Y. Mizobe, M. Hidai, *Angew. Chem. Int. Ed. Engl.* **1996**, *35*, 872
66. S.S. Dhingra, M.G. Kanatzidis, *Inorg. Chem.* **1993**, *32*, 3300

67. S.S. Dhingra, M.G. Kanatzidis, *Inorg. Chem.* **1993**, *32*, 2298
68. D.L. Reger, P.S. Coan, *Inorg. Chem.* **1995**, *34*, 6226
69. M. Herberhold, G.-X. Jin, W. Milius, *Angew. Chem. Int. Ed. Engl.* **1993**, *32*, 85
70. G.-X. Jin, Y. Arikawa, K. Tatsumi, *J. Am. Chem. Soc.* **2001**, *123*, 735
71. T.E. Albrecht-Schmitt, J.A. Ibers, *Inorg. Chem.* **1996**, *35*, 7273
72. T.E. Albrecht-Schmitt, J.A. Ibers, *Angew. Chem. Int. Ed. Engl.* **1997**, *36*, 2010
73. R.A. Krause, *Inorg. Nucl. Chem. Lett.* **1971**, *7*, 973
74. P. Cartwright, R.D. Gillard, R. Sillanpaa, J. Valkonen, *Polyhedron* **1987**, *6*, 1775
75. K.-W. Kim, M.G. Kanatzidis, *Inorg. Chem.* **1993**, *32*, 4161
76. K.-W. Kim, M.G. Kanatzidis, *J. Am. Chem. Soc.* **1995**, *117*, 5606
77. M. Draganjac, E. Simhon, L.T. Chan, M.G. Kanatzidis, N.C. Baenziger, D. Coucouvanis, *Inorg. Chem.* **1982**, *21*, 3321
78. S.A. Cohen, E.I. Stiefel, *Inorg. Chem.* **1985**, *24*, 4657
79. X.-T. Wu, N.-Y. Zhu, S.-W. Du, J.-X. Lu, *Angew. Chem. Int. Ed. Engl.* **1992**, *31*, 87
80. S.-W. Du, N.-Y. Zhu, X.-T. Wu, J.-X. Lu, *Inorg. Chem.* **1992**, *31*, 2847
81. S.-W. Du, N.-Y. Zhu, X.-T. Wu, *Polyhedron* **1994**, *13*, 301
82. Y. Mizobe, M. Hosomizu, Y. Kubota, M. Hidai, *J. Organomet. Chem.* **1996**, *507*, 179
83. J.T. Goodman, S. Inomata, T.B. Rauchfuss, *J. Am. Chem. Soc.* **1996**, *118*, 11674
84. B.S. Mandimutsira, S.-J. Chen, K.D. Demadis, D. Coucouvanis, *Inorg. Chem.* **1995**, *34*, 2267
85. K. Isobe, Y. Ozawa, A.V. de Miguel, T.-W. Zhu, K.-M. Zhao, T. Nishioka, T. Ogura, T. Kitagawa, *Angew. Chem. Int. Ed. Engl.* **1994**, *33*, 1882
86. T. Kochi, Y. Tanabe, Z. Tang, Y. Ishii, M. Hidai, *Chem. Lett.* **1999**, 1279
87. A. Shaver, P.-Y. Plouffe, *Inorg. Chem.* **1994**, *33*, 4327
88. A. Shaver, M. El-khateeb, A.-M. Lebuis, *Angew. Chem. Int. Ed. Engl.* **1996**, *35*, 2362
89. M. El-khateeb, B. Wolfsberger, W.A. Schenk, *J. Organomet. Chem.* **2000**, *612*, 14
90. J.-H. Liao, C. Varotsis, M.G. Kanatzidis, *Inorg. Chem.* **1993**, *32*, 2453
91. T.J. McCarthy, X. Zhang, M.G. Kanatzidis, *Inorg. Chem.* **1993**, *32*, 2944
92. M.R. Dubois, B.R. Jagirdar, S. Diets, B.C. Noll, *Organometallics* **1997**, *16*, 294
93. A.V. Firth, D.W. Stephan, *Inorg. Chem.* **1998**, *37*, 4726
94. K. Wakita, N. Tokitoh, R. Okazaki, S. Nagase, P. v. R. Schleyer, H. Jiao, *J. Am. Chem. Soc.* **1999**, *121*, 11336
95. N. Nakata, N. Takeda, N. Tokitoh, *Organometallics* **2003**, *22*, 481
96. N. Nakata, N. Takeda, N. Tokitoh, *Chem. Lett.* **2002**, 818
97. L.R. Maxwell, V.M. Mosley, S.B. Hendricks, *Phys. Rev.* **1936**, *50*, 41
98. B. Meyer, *Chem. Rev.* **1976**, *76*, 367
99. B.C. Bunker, R.S. Drago, D.N. Hendrickson, R.M. Richman, S.L. Kessell, *J. Am. Chem. Soc.* **1978**, *100*, 3805
100. R.J.H. Clark, D.G. Cobbold, *Inorg. Chem.* **1978**, *17*, 3169
101. W. Holzer, W.F. Murphy, H.J. Bernstein, *Mol. Spectrosc.* **1969**, *32*, 13
102. H. Föppl, E. Busmann, F.-K. Frorath, *Z. Anorg. Allg. Chem.* **1962**, *314*, 12
103. M.J.S. Dewar, *Bull. Soc. Chim. Fr.* **1951**, *18*, C71
104. J. Chatt, L.A. Duncanson, *J. Chem. Soc.* **1953**, 2939
105. A.P. Ginsberg, J.H. Osborne, C.R. Sprinkle, *Inorg. Chem.* **1983**, *22*, 254
106. A. Müller, S. Pohl, M. Dartmann, J.P. Cohen, J.M. Bennett, R.M. Kirchner, *Z. Naturforsch.* **1979**, *34b*, 434
107. A. Terzis, R. Rivest, *Inorg. Chem.* **1973**, *12*, 2132
108. B.R. Davis, I. Bernal, H. Köpf, *Angew. Chem. Int. Ed. Engl.* **1971**, *10*, 921
109. G. Winnewisser, H. Winnewisser, W. Gordy, *J. Chem. Phys.* **1968**, *49*, 3465
110. A.M. Mebel, K. Morokuma, K. Isobe, *Inorg. Chem.* **1995**, *34*, 1208
111. R.J. Pafford, T.B. Rauchfuss, *Inorg. Chem.* **1998**, *37*, 1974
112. R. Okazaki, N. Tokitoh, *Acc. Chem. Res.* **2000**, *33*, 625
113. N. Tokitoh, T. Matsumoto, K. Manmaru, R. Okazaki, *J. Am. Chem. Soc.* **1993**, *115*, 8855
114. N. Kano, N. Tokitoh, R. Okazaki, *Organometallics* **1997**, *16*, 4237
115. N. Tokitoh, T. Matsumoto, H. Ichida, R. Okazaki, *Tetrahedron Lett.* **1991**, *32*, 6877

116. N. Tokitoh, Y. Matsuhashi, M. Goto, R. Okazaki, *chem. Lett.* **1992**, 1595
117. M. Saito, N. Tokitoh, R. Okazaki, *Chem. Lett.* **1996**, 265
118. N. Tokitoh, T. Matsumoto, R. Okazaki, *Tetrahedron Lett.* **1991**, 32, 6143
119. N. Tokitoh, Y. Matsuhashi, R. Okazaki, *Tetrahedron Lett.* **1992**, 33, 5551
120. Y. Matsuhashi, N. Tokitoh, R. Okazaki, M. Goto, *Organometallics* **1993**, 12, 2573
121. A.Z. Rys, A.-M. Lebuis, A. Shaver, D.N. Harpp, *Organometallics* **1999**, 18, 1113
122. K. Nagata, N. Takeda, N. Tokitoh, *Chem. Lett.* **2003**, 32, 170
123. G. Schmid, G. Ritter, T. Debaerdemaeker, *Chem. Ber.* **1975**, 108, 3008
124. R. Steudel, S. Förster, J. Albertsen, *Chem. Ber.* **1991**, 124, 2357
125. M. Pridöhl, R. Steudel, F. Baumgart, *Polyhedron* **1993**, 12, 2577
126. R. Steudel, K. Bergemann, J. Buschmann, P. Luger, *Inorg. Chem.* **1996**, 35, 2184
127. L.M. Berreau, V.G. Young, L.K. Woo, *Inorg. Chem.* **1995**, 34, 3485
128. L.K. Woo, J.A. Hays, *Inorg. Chem.* **1993**, 32, 2228
129. M. Kustos, J. Pickardt, J. Albertsen, R. Steudel, *Z. Naturforsch.* **1993**, 48b, 928
130. R. Steudel, M. Kustos, A. Prenzel, *Z. Naturforsch.* **1997**, 52b, 79
131. R. Steudel, K. Bergemann, J. Buschmann, P. Luger, *Angew. Chem. Int. Ed. Engl.* **1996**, 35, 2537
132. A.K. Verma, T.B. Rauchfuss, *Inorg. Chem.* **1995**, 34, 6199
133. W. Adam, R.M. Bargon, *Chem. Commun.* **2001**, 1910
134. P.J. Lim, R.W. Gable, C.G. Young, *Inorg. Chim. Acta* **2000**, 310, 120
135. K. Matsumoto, H. Sugiyama, *Acc. Chem. Res.* **2002**, 35, 915
136. H. Sugiyama, Y.-S. Lin, K. Matsumoto, *Angew. Chem. Int. Ed.* **2000**, 39, 4058
137. M. M. Hossain, Y.-S. Lin, H. Sugiyama, K. Matsumoto, *J. Am. Chem. Soc.* **2000**, 122, 172
138. H. Sugiyama, Y.-S. Lin, M.M. Hossain, K. Matsumoto, *Inorg. Chem.* **2001**, 40, 5547
139. S. Hatemata, H. Sugiyama, S. Sasaki, K. Matsumoto, *Inorg. Chem.* **2002**, 41, 6006
140. H. Sugiyama, Y. Moriya, K. Matsumoto, *Organometallics* **2001**, 20, 5636
141. K. Matsumoto, Y. Moriya, H. Sugiyama, M.M. Hossain, Y.-S. Lin, *J. Am. Chem. Soc.* **2002**, 124, 13106
142. K. Matsumoto, H. Uemura, M. Kawano, *Inorg. Chem.* **1995**, 34, 658
143. H. Sugiyama, M.M. Hossain, Y.-S. Lin, K. Matsumoto, *Inorg. Chem.* **2000**, 39, 3948
144. Y. Matsuhashi, N. Tokitoh, R. Okazaki, *Organometallics* **1994**, 13, 4387
145. N. Tokitoh, Y. Matsuhashi, R. Okazaki, *Organometallics* **1993**, 12, 2894
146. S. Kuwata, Y. Mizobe, M. Hidai, *J. Am. Chem. Soc.* **1993**, 115, 8499
147. A. Venturelli, T.B. Rauchfuss, A. K. Verma, *Inorg. Chem.* **1997**, 36, 1360
148. K. Matsumoto, H. Ohnuki, M. Kawano, *Inorg. Chem.* **1995**, 34, 3838
149. K. Matsumoto, Y. Sano, *Inorg. Chem.* **1997**, 36, 4405
150. T. Koyama, Y. Koide, K. Matsumoto, *Inorg. Chem.* **1999**, 38, 3241

# Sulfur-Rich Oxides $S_nO$ and $S_nO_2$ ( $n>1$ )

Ralf Steudel

Institut für Chemie, Sekr. C2, Technische Universität Berlin, 10623 Berlin Germany  
E-mail: [steudel@schwefel.chem.tu-berlin.de](mailto:steudel@schwefel.chem.tu-berlin.de)

**Abstract** Sulfur is the element with the largest number of binary oxides. In this chapter the lower sulfur oxides are reviewed most of which contain more sulfur than oxygen atoms per molecule and all have at least one sulfur-sulfur bond. They may exist as gaseous compounds consisting of small molecules ( $S_2O$ ,  $S_2O_2$ ), as crystalline materials ( $S_6O$ ,  $S_7O$ ,  $S_7O_2$ ,  $S_8O$ ,  $S_9O$ ,  $S_{10}O$ ), or as polymeric non-stoichiometric materials (polysulfuroxides). In each case the oxygen atoms are present as part of a sulfoxide group. In some cases adducts with Lewis acids have been prepared, e.g.,  $S_8OSbCl_5$ ,  $(S_8O)_2SnCl_4$ , and  $S_{12}O_2(SbCl_5)_2$ . The preparation, thermal stabilities, molecular structures, spectra, and reactions are described.

**Keywords** Lower sulfur oxides · Homocyclic sulfur oxides · Preparation · Spectra · Reactions · Structures · Bonding

1	Introduction . . . . .	204
2	Preparation and Properties . . . . .	204
2.1	Disulfurmonoxide $S_2O$ . . . . .	204
2.1.1	General. . . . .	204
2.1.2	Preparation . . . . .	205
2.1.3	Molecular Structure . . . . .	207
2.1.4	Molecular Spectra . . . . .	208
2.1.4.1	Vibrational Spectra . . . . .	208
2.1.4.2	UV-Vis Spectrum . . . . .	209
2.1.5	Reactions . . . . .	209
2.2	Disulfurdioxide $S_2O_2$ . . . . .	211
2.3	Trisulfurmonoxide $S_3O$ . . . . .	212
2.4	Tetrasulfurmonoxide $S_4O$ . . . . .	213
2.5	Pentasulfurmonoxide $S_5O$ . . . . .	213
2.6	Hexasulfurmonoxide $S_6O$ and Hexasulfurdioxide $S_6O_2$ . . . . .	214
2.7	Heptasulfurmonoxide $S_7O$ . . . . .	216
2.8	Heptasulfurdioxide $S_7O_2$ . . . . .	217
2.9	Octasulfurmonoxide $S_8O$ . . . . .	219
2.10	Nonasulfurmonoxide $S_9O$ . . . . .	223
2.11	Decasulfurmonoxide $S_{10}O$ . . . . .	224
2.12	Polysulfuroxides $(S_nO)_x$ . . . . .	225
3	Bond Properties . . . . .	226
	References . . . . .	228

## 1 Introduction

The sulfur-rich oxides  $S_nO$  and  $S_nO_2$  belong to the group of so-called “lower oxides of sulfur” named after the low oxidation state of the sulfur atom(s) compared to the best known oxide  $SO_2$  in which the sulfur is in the oxidation state +4. Sulfur monoxide  $SO$  is also a member of this class but is not subject of this review. The blue-green material of composition “ $S_2O_3$ ” described in the older literature has long been shown to be a mixture of salts with the cations  $S_4^{2+}$  and  $S_8^{2+}$  and polysulfate anions rather than a sulfur oxide [1, 2]. Reliable reviews on the complex chemistry of the lower sulfur oxides have been published before [1, 3–6]. The present review deals with those sulfur oxides which contain at least one sulfur-sulfur bond and not more than two oxygen atoms. These species are important intermediates in a number of redox reactions of elemental sulfur and other sulfur compounds.

This chapter is organized by compounds of increasing number of sulfur atoms which also means increasing complexity. The simplest species is consequently disulfurmonoxide  $S_2O$ , a well investigated though unstable compound consisting of bent molecules similar to  $SO_2$ . Even less stable are  $S_2O_2$  and  $S_3O$  which have only recently been characterized in some detail. The more sulfur-rich molecules  $S_6O$  till  $S_{10}O$  were isolated as pure crystalline compounds consisting of homocyclic rings bearing exocyclic oxygen atoms in the form of sulfoxide groups. Analogous structures are assumed for  $S_5O$  which is known only in solution and for crystalline  $S_7O_2$ .

## 2 Preparation and Properties

### 2.1 Disulfurmonoxide $S_2O$

#### 2.1.1 *General*

Besides sulfurmonoxide  $SO$ , disulfurmonoxide  $S_2O$  is the most important of the so-called lower oxides of sulfur. It is formed in numerous reactions, often from  $SO$  by disproportionation:



$S_2O$  was first prepared by Schenk in 1933 but he did not recognize it as such but denoted it as sulfurmonoxide [7]. Meschi and Myers [8] showed by mass spectrometry in 1956 that Schenk’s “sulfurmonoxide” was a 1:1 mixture of  $S_2O$  and  $SO_2$  in accordance with Eq. (1). Therefore,  $S_2O$  was usually called “sulfurmonoxide” in the literature before 1956 and to some extent even up to 1960. Sometimes it was erroneously believed that  $S_2O_2$  is present

instead of  $S_2O$  after molecular mass determinations and other observations had indicated a dimerization of SO. In the gas phase  $S_2O$  survives for several days at pressures below 1 mbar (100 Pa) and at temperatures near 20 °C while SO survives only for a few milliseconds. Thus, in each case it is usually clear from the experimental conditions which compound was actually studied in those historic experiments. In liquid solutions  $S_2O$  is not stable but immediately polymerizes with disproportionation. However, in solid solutions at very low temperatures (matrix isolated)  $S_2O$  can be studied for extended periods of time.

### 2.1.2

#### *Preparation*

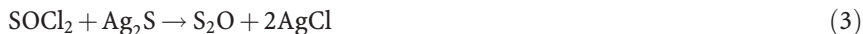
For the preparation of gaseous  $S_2O$  a vacuum line is needed which should be well dried by pumping and baking. The partial pressure of  $S_2O$  has to be kept well below 1 mbar (100 Pa). If only small amounts of  $S_2O$  are needed a mixture of 2 g CuO and 10 g elemental sulfur is heated in a high vacuum to 250–400 °C. The liberated gas is passed through a glass wool filter to remove  $SO_3$  and sulfur vapor; it then contains up to 40%  $S_2O$  besides  $SO_2$  [9]:



Another useful method for the preparation of small quantities of the  $S_2O$  is the thermal decomposition of solid  $S_8O$  in a vacuum (see below).

To generate a continuous flow of gaseous  $S_2O$  (or a mixture rich in  $S_2O$ ) the following three methods can be recommended:

1. Gaseous thionyl chloride is passed through a layer of silver sulfide at 160 °C under a pressure of 0.1–0.5 mbar (10–50 Pa) [10]. The silver sulfide is prepared by precipitating aqueous  $AgNO_3$  with freshly recrystallized  $Na_2S$  followed by repeated washing and decantation until no nitrate can be detected anymore. This sample is then carefully dried by heating in a vacuum. The gas prepared in this way contains up to 96%  $S_2O$  besides  $SO_2$ . Some authors used CdS or CuS instead of  $Ag_2S$ , and some transported the thionyl chloride vapor by a stream of helium gas:



2. A mixture of sulfur dioxide and sulfur vapor is passed through an electrical discharge at 120 °C and a total pressure of 0.5–0.9 mbar (50–90 Pa). Behind the discharge the gas is allowed to react with an excess of elemental sulfur to increase the  $S_2O$  content which reaches 86% at most [11]:



3. Combustion of liquid sulfur, contained in a quartz vessel, in a stream of pure oxygen under reduced pressure (8 mbar, 800 Pa) produces a mixture of SO<sub>2</sub>, S<sub>2</sub>O, and little SO<sub>3</sub>; the latter and any sulfur vapor can be removed by a filter of glass wool [12]. The S<sub>2</sub>O content of the gas then reaches at most 32% and decreases with increasing pressure [13]:



To determine the S<sub>2</sub>O content of a gaseous mixture with SO<sub>2</sub> and other volatile components the decomposition of S<sub>2</sub>O according to Eq. (8) is utilized:



For this purpose, the mixture is condensed at -196 °C in a small weighable trap equipped with two stopcocks. The net mass of the evacuated trap has to be determined before. After weighing the trap containing the condensate at 20 °C, the trap is evacuated at 20 °C to remove all volatile species, and the stopcocks are closed. The residue of polysulfuroxide is then heated to 100 °C for a few minutes to initiate its quantitative decomposition to SO<sub>2</sub> and elemental sulfur. After cooling to 20 °C the trap is evacuated again and weighed. From the mass of the elemental sulfur and the total mass of the original condensate the S<sub>2</sub>O content of the gas mixture can be calculated assuming the decomposition at Eq. (8) [11].

Very approximately the S<sub>2</sub>O content of a gas mixture can be estimated from the color of the condensate at -196 °C in a glass trap (provided that all other components are colorless at this temperature). Due to the formation of highly colored decomposition products the condensate is yellow at <2 mol% S<sub>2</sub>O, orange-yellow at 5–10%, orange at 20–30%, cherry-red at 40–70%, and dark-red at >85% [10]. These colors [14] are caused by small sulfur molecules like S<sub>3</sub> and S<sub>4</sub> [15, 16] as well as by sulfur radicals formed in the radical-chain polymerization of S<sub>2</sub>O to polysulfuroxides (S<sub>n</sub>O)<sub>x</sub> and SO<sub>2</sub> [10, 17]:



The species S<sub>3</sub> (absorbing at 420 nm) and S<sub>4</sub> (absorbing at 530 nm) have been detected by reflection spectra in the condensate but the formation of S<sub>4</sub> is unexplained [16]. S<sub>3</sub> and SO<sub>2</sub> have also been observed by Raman spectroscopy in such samples [15] (the expected S<sub>4</sub> Raman line at 678 cm<sup>-1</sup> was probably obscured by the SS stretching mode of S<sub>2</sub>O at 673 cm<sup>-1</sup> but a shoulder at the high-frequency side of the S<sub>2</sub>O line indicates that some S<sub>4</sub> may have been present). While the reddish colors turn yellow on warming at about -120 °C, the sulfur radicals could be observed by ESR spectroscopy up to 0 °C [10]. If the condensation of S<sub>2</sub>O gas is performed very slowly at -196 °C the condensate is almost colorless and turns red only if the temperature is allowed to increase slowly. Hence, it has been suspected that S<sub>2</sub>O is actually colorless like SO<sub>2</sub>.

In carefully dried (vacuum-baked) and sealed glass containers gaseous  $S_2O$  can be kept at 20 °C and partial pressures of below 1 mbar (100 Pa) for several days but at 180 °C the decomposition to  $SO_2$  and sulfur is complete within 1 min. At higher partial pressures gaseous  $S_2O$  decomposes at 20 °C to  $SO_2$  and a yellow, relatively stable solid polymeric sulfuroxide of composition  $S_{>3}O$  (see below). This decomposition is accelerated by traces of water and by irradiation with UV radiation [18].

If gaseous  $S_2O$ - $SO_2$  mixtures are dissolved in dry solvents such as  $CS_2$ ,  $CCl_4$ ,  $CHCl_3$ ,  $CH_2Cl_2$ , and liquid  $SO_2$  at temperatures between -75 and +25 °C, intense yellow solutions of polysulfuroxides are obtained which have been characterized only very poorly [19]. In contrast to the opinion of some authors [20],  $S_2O$  cannot be detected in such solutions, e.g., by infrared spectroscopy. Most probably, mixtures of cyclic polysulfuroxides are present besides  $SO_2$  (see below, in particular the preparation of  $S_5O$ ), e.g.:



Numerous oxidation reactions of sulfur compounds have been described in which  $S_2O$  or its precursor  $SO$  are formed as intermediates but most of these reactions are not suitable to investigate the properties of  $S_2O$  because of the low yield or the interference from by-products [1]. A relatively clean process is the reaction of oxygen atoms with  $COS$  producing  $SO$  and  $CO$ . The formation of  $S_2O$  from gaseous  $SO$  is a stepwise process according to the following equations ( $M$  is a collision partner) [21]:



The rate constants for the reactions at Eqs. (12) and (13) at 298 K are  $1.6 \times 10^{17} \text{ cm}^6 \text{ mol}^{-2} \text{ s}^{-1}$  and  $2 \times 10^{10} \text{ cm}^3 \text{ mol}^{-1} \text{ s}^{-1}$ , respectively [21].

$S_2O$  and the polysulfuroxide formed from it are also suspected to be components of the surface and the atmosphere of Jupiter's moon Io [22], and  $S_2O$  has been detected in the atmosphere of the planet Venus [23].

### 2.1.3

#### **Molecular Structure**

The structure of the  $S_2O$  molecule has been determined by rotational spectroscopy. The internuclear distances  $d$  and the bond angles  $\alpha$  obtained by two groups are as follows:

- $d_{SO}$ : 146.5(10) pm [24], 146.37(5) pm [25]
- $d_{SS}$ : 188.4(10) pm [24], 188.248(10) pm [25]
- $\alpha_{SSO}$ : 118.0(5)° [24], 118.26(7)° [25]

**Table 1** Geometrical parameters of the S<sub>2</sub>O molecule [26]

Parameter	Ground state ( $r_0$ )	Zero point ( $r_z$ )	Equilibrium ( $r_e$ )
$d_{SO}$ (pm)	145.7(15)	145.86(19)	145.61
$d_{SS}$ (pm)	188.7(12)	188.52(22)	188.42
$\alpha_{SSO}$ (°)	118.0(4)	117.91(17)	117.882

A careful structural analysis using additional microwave data of 95% enriched S<sub>2</sub><sup>18</sup>O resulted in the  $r_0$ ,  $r_z$ , and  $r_e$  geometries compiled in Table 1 [26].

From a similar analysis by Marsden and Smith using all the spectroscopic data available in 1989 the following equilibrium structure was derived [27]:

$$- d_{SO}=145.56(9) \text{ pm}, d_{SS}=188.48(7) \text{ pm}, \alpha_{OSS}=117.858(3)^\circ.$$

The  $r_z$  geometry is very similar.

Ab initio MO calculations at a high level of theory [28] support the open-chain structure for the ground state of S<sub>2</sub>O while density functional calculations predicted a cyclic ground-state structure [29].

The dipole moment of S<sub>2</sub>O derived from the Stark effect in the MW spectrum is  $\mu=1.47\pm 0.02$  D. The dipole moment components in the direction of the SO and SS bonds are 1.58 and 0.30 D, respectively [24].

## 2.1.4

### *Molecular Spectra*

#### 2.1.4.1

#### Vibrational Spectra

Infrared spectra of gaseous [30, 31], condensed [32] and matrix-isolated S<sub>2</sub>O have been measured [33], and Raman spectra of the matrix-isolated molecule were reported [15]. In Table 2 the infrared absorption bands of 5 isotopomers of S<sub>2</sub>O are listed; some bands coincide with other absorptions.

**Table 2** Infrared absorptions of S<sub>2</sub>O in an Ar matrix at 20 K [33]

Isotopomer	$\nu_1$ or $\nu_{SO}$ (cm <sup>-1</sup> )	$\nu_2$ or $\nu_{SS}$ (cm <sup>-1</sup> )	$\nu_3$ or $\delta$ (cm <sup>-1</sup> )
<sup>32</sup> S <sub>2</sub> <sup>16</sup> O	1156.2	672.2	382.0
<sup>34</sup> S <sub>2</sub> <sup>16</sup> O	1144.0	652.9	376.6
<sup>32</sup> S <sub>2</sub> <sup>18</sup> O	1114.8	670.9	371.1
<sup>32</sup> S <sup>34</sup> S <sup>16</sup> O	1144.0	662.8	379.3
<sup>34</sup> S <sup>32</sup> S <sup>16</sup> O	1156.2	662.8	379.3

In the gas-phase only the SO stretching ( $1165\text{ cm}^{-1}$ ) and SS stretching vibrations ( $679\text{ cm}^{-1}$ ) have been observed by infrared spectroscopy (Q branches are given) [30, 31]. If an  $S_2O$ - $SO_2$  mixture is condensed on a KBr disc at 83 K the three fundamentals are observed in the IR at  $1130$  ( $\nu_1$ ),  $673$  ( $\nu_2$ ), and  $384\text{ cm}^{-1}$  ( $\nu_3$ ) together with the combination mode  $\nu_2 + \nu_3$  at  $1060\text{ cm}^{-1}$ . However, the broad  $1130\text{ cm}^{-1}$  band is composed of the SO stretching vibrations of  $SO_2$  ( $\nu_1$ ), of  $S_2O$  and of a polysulfuroxide. Warming of the condensate to 270 K followed by cooling it back to 83 K resulted in the disappearance of the  $S_2O$  absorptions while a broad band at  $1123\text{ cm}^{-1}$  remained which was assigned to the SO stretching vibration of a polysulfuroxide (together with the symmetric stretching vibration of some remaining  $SO_2$  trapped in the polymer); this polymeric oxide contains the structural unit  $-S-S(=O)-S-$  (see below) [31, 32].

The Raman spectrum of  $S_2O$  in an Ar matrix at 20 K consists of three lines at  $1157$ ,  $673$ , and  $382\text{ cm}^{-1}$ . On annealing matrix-isolated  $S_2O$  decomposes primarily to  $SO_2$  and  $S_3$  [15].

Force constants of  $S_2O$  were calculated from infrared and microwave data for a general harmonic force field using the equilibrium geometry; the following data were obtained [34] ( $1\text{ aJ \AA}^{-2} = 1\text{ mdyn \AA}^{-1} = 1\text{ N cm}^{-1}$ ):

$F_{11}$ ( $\text{aJ \AA}^{-2}$ ):	8.55(6)	(SO stretching)
$F_{12}$ ( $\text{aJ \AA}^{-2}$ ):	0.84(10)	(SO/SS bond interaction)
$F_{13}$ ( $\text{aJ \AA}^{-1}$ ):	0.20(4)	(SO bond/angle interaction)
$F_{22}$ ( $\text{aJ \AA}^{-2}$ ):	4.32(3)	(SS stretching)
$F_{23}$ ( $\text{aJ \AA}^{-1}$ ):	0.18(1)	(SS bond/angle interaction)
$F_{33}$ ( $\text{aJ \AA}$ ):	1.376(8)	(SSO bending)

Slightly differing values have been published by Marsden and Smith [27].

#### 2.1.4.2

##### UV-Vis Spectrum

The electronic spectrum of  $S_2O$  has been studied both in absorption and in emission and both in the ultraviolet and the visible regions. The absorption spectrum in the near UV region is extremely intense and well suited to detect  $S_2O$  in gases even at very low partial pressures. Two band systems are located in the UV region at  $340$ – $250\text{ nm}$  and at  $230$ – $190\text{ nm}$  [35] while a third system in the visible region at  $645$ – $575\text{ nm}$  was discovered only by optoacoustic detection [36]. The  $340$ – $250\text{ nm}$  system has also been observed for matrix-isolated  $S_2O$  [37]. For more details see [1, 38–47].

#### 2.1.5

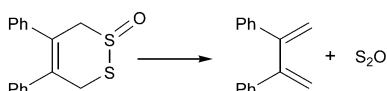
##### Reactions

The ionization energy of  $S_2O$  obtained from photoionization efficiency measurements is  $10.584 \pm 0.005\text{ eV}$  [48] or  $10.60 \pm 0.04\text{ eV}$  [49].

According to *ab initio* MO calculations [50] protonation of  $S_2O$  produces the planar chain-like molecule *cis*-SSOH<sup>+</sup> as the isomer of lowest energy. The *trans*-isomer is by only 2 kJ mol<sup>-1</sup> less stable and S-protonated as well as O-protonated cyclic isomers are next highest in energy.

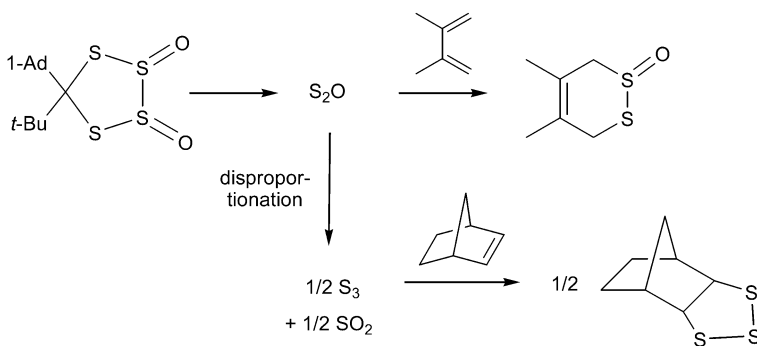
Trimethylamine and gaseous  $S_2O$  react at -30 °C and low pressure to the yellow solid adduct  $Me_3N \cdot S_2O$  which sublimes in a high vacuum (probably with dissociation in the gas-phase and recombination on condensation). This adduct is soluble in organic solvents; it is analogous to but less stable than the colorless  $Me_3N \cdot SO_2$  [51].

A number of metal complexes with disulfurmonoxide as a ligand have been prepared either by oxidation of precursor complexes containing the  $S_2$  ligand or by trapping  $S_2O$  formally produced in situ from a suitable precursor by heating [52]. Such molecules are cyclic di-, tri-, or tetrasulfane monoxides or dioxides such as the one shown in Scheme 1.



**Scheme 1**

$S_8O$  may also function as a precursor for  $S_2O$  units. However, it should be noticed that *free*  $S_2O$  has never been detected *directly* in liquid solutions and that the isolated products most probably arise from a reaction of the  $S_2O$  precursor with the trapping reagent since the reaction temperature is always 20 °C (e.g., by a transition-metal-induced *retro*-Diels-Alder reaction) [52, 53]. An exception may be the thermal decomposition of the substituted tetrathiolane-2,3-dioxide shown in Scheme 2; this compound evidently



**Scheme 2**

yields  $S_2O$  as a primary decomposition product which then decomposes to  $SO_2$  and  $S_3$ ; both  $S_2O$  and  $S_3$  have been trapped at 25 °C [54].

The  $S_2O$  ligand in complexes is coordinated to the metal atom through both sulfur atoms which causes an increase of the SS bond length. Such complexes are also accessible by the reaction of sulfinylimido complexes with  $H_2S$  [52].

For reviews on the cation  $S_2O^+$  and the anion  $S_2O^-$ , see [1].

## 2.2

### Disulfurdioxide $S_2O_2$

The molecule  $S_2O_2$  was discovered by Lovas et al. in 1974 using microwave spectroscopy [55]. Reports about a disulfurdioxide in the older literature (before 1960) are erroneous since the species actually investigated was  $S_2O$  (mixed with  $SO_2$ ). Therefore, these publications are dealt with above.

$S_2O_2$  is the dimerization product of sulfurmonoxide; it therefore is present in all gases containing SO; the connectivity is OSSO:



If  $SO_2$ , flowing in a quartz tube, is exposed to a microwave discharge (80 W, 2.45 GHz) at pressures of 0.1–0.2 mbar (10–20 Pa), approximately 50% is decomposed resulting in a mixture containing 20–30% SO, 5%  $S_2O$ , and 5%  $S_2O_2$  besides  $SO_2$ . In addition, a yellow deposit on the walls of the tube is formed, presumably elemental sulfur. Instead of  $SO_2$  a 1:1 mixture of COS and  $O_2$  may be used; see Eqs. (16)–(18):



The half-life of  $S_2O_2$  at this pressure is of the order of seconds, much longer than that of SO but much shorter than the half-life of  $S_2O$  [55].

The formation of  $S_2O$  from gaseous SO proceeds according to the following equations (M: collision partner):



The rate constants for these reactions at 298 K are  $k(19)=1.6 \times 10^{17} \text{ cm}^6 \text{ mol}^{-2} \text{ s}^{-1}$  and  $k(20)=2 \times 10^{10} \text{ cm}^3 \text{ mol}^{-1} \text{ s}^{-1}$ , respectively [21].

The  $S_2O_2$  molecule exists in a singlet ground state of  $C_{2v}$  symmetry. The molecular parameters of  $^{32}S_2^{16}O_2$  derived from the microwave spectrum (mixed  $r_0/r_s$  structure) are as follows:  $d_{SS}=202.45(6) \text{ pm}$ ,  $d_{SO}=145.8(2) \text{ pm}$ ,  $\alpha_{OSS}=112.7(5)^\circ$ . The dipole moment is  $3.17(10) \text{ D}$  [55]. The ionization energy of  $S_2O_2$  obtained from photoionization efficiency measurements is  $9.93 \pm 0.02 \text{ eV}$  [49].

Hartree-Fock as well as density functional calculations on hypothetical cyclic oligomers  $(SO)_n$  with  $n=2-4$  have been published [56]; these species are all more stable than the corresponding number of monomeric SO mole-

**Table 3** Predicted harmonic wavenumbers for the fundamental modes of two conformers of OSSO as calculated by quantum mechanical methods [34]; values in parentheses from [57]

	Symmetry class	S <sub>2</sub> O <sub>2</sub> (C <sub>2v</sub> )	Symmetry class	S <sub>2</sub> O <sub>2</sub> (C <sub>2h</sub> )
$\nu_1$	A <sub>1</sub>	1158 (1080)	A <sub>g</sub>	1122
$\nu_2$	A <sub>1</sub>	470 (453)	A <sub>g</sub>	530
$\nu_3$	A <sub>1</sub>	134 (130)	A <sub>g</sub>	385
$\nu_4$	A <sub>2</sub>	304 (290)	A <sub>u</sub>	237
$\nu_5$	B <sub>1</sub>	1073 (1029)	B <sub>u</sub>	1058
$\nu_6$	B <sub>1</sub>	494 (461)	B <sub>u</sub>	179

cules in their triplet ground state but most probably less stable than the C<sub>2v</sub> isomer of OSSO detected spectroscopically. A very detailed theoretical investigation of 13 singlet and 6 triplet isomers of composition S<sub>2</sub>O<sub>2</sub> was published by Marsden and Smith [57]. The global minimum corresponds to a planar branched structure of C<sub>2v</sub> symmetry which is formally derived from the trigonal-planar SO<sub>3</sub> structure (D<sub>3h</sub>) by substitution of one oxygen by a sulfur atom. Such a molecule has not been observed yet but at the MP3 level of theory this structure is by 47 kJ mol<sup>-1</sup> more stable than *cis*-planar OSSO (C<sub>2v</sub>); the latter is calculated to be by 60 kJ mol<sup>-1</sup> more stable than two separated SO molecules in their triplet ground state. The *trans*- and *cis*-planar conformers of OSSO were found to be almost degenerate ( $\Delta E < 1$  kJ mol<sup>-1</sup>); the torsional barrier for the internal rotation around the SS bond was estimated from the torsional force constant as 98 kJ mol<sup>-1</sup>. Both  $r_0$  and  $r_z$  structures have been calculated by the authors from the available spectroscopic data [57].

Since vibrational spectra of S<sub>2</sub>O<sub>2</sub> have not yet been observed, the force constants calculated by ab initio MO methods were used to predict the harmonic vibrational wavenumbers of *cis*-S<sub>2</sub>O<sub>2</sub> (C<sub>2v</sub>) and *trans*-S<sub>2</sub>O<sub>2</sub> (C<sub>2h</sub>); see Table 3 [34, 57].

For reviews on the ions S<sub>2</sub>O<sub>2</sub><sup>+</sup> and S<sub>2</sub>O<sub>2</sub><sup>-</sup>, see [1].

### 2.3

#### Trisulfurmonoxide S<sub>3</sub>O

The oxide S<sub>3</sub>O has been identified only in the gas-phase by means of neutralization reionization mass spectrometry [58]. The precursor ion S<sub>3</sub>O<sup>+</sup> was generated by the following sequence of reactions:



The S<sub>3</sub>O<sup>+</sup> ion was then mass selected and neutralized by electron exchange with Xe atoms. The neutral beam was reionized by collision with O<sub>2</sub> and the

spectra of  $S_3O^+$  and its isotopomers were recorded. The lifetime of  $S_3O$  in the gas-phase was estimated as  $\geq 1 \mu s$ . The molecular structure of  $S_3O$  was studied by ab initio MO calculations at the CCSD(T)/6-311+G(3df)//B3LYP/6-311+G(3df) level of theory and the *cis*-planar structure ( $^1A'$ ) analogous to the experimental structures of  $S_2O_2$  and  $S_4$  was found to be most stable (see Scheme 3).



**Scheme 3**

The terminal SS bond (192.2 pm) of  $S_3O$  is considerably shorter than the central bond (204.0 pm) and represents a double bond; the same holds for the SO bond (147.1 pm). The angles SSO ( $112.1^\circ$ ) and SSS ( $111.6^\circ$ ) show the expected values. The *trans*-planar singlet structure is by  $\Delta H_{298}^\circ = 18 \text{ kJ mol}^{-1}$  less stable at this level of theory.

## 2.4

### Tetrasulfurmonoxide $S_4O$

A molecule of composition  $S_4O$  has not been observed yet. Ab initio MO calculations indicate that a cyclic and an open-chain structure have almost the same energy but no details have been released yet [58].

## 2.5

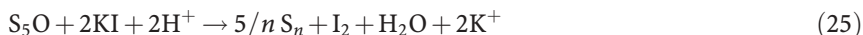
### Pentasulfurmonoxide $S_5O$

This oxide has not yet been prepared as a pure material but was observed only in dilute solution. If liquid sulfur is burned in pure oxygen under reduced pressure a mixture of  $S_2O$ ,  $SO_2$ , and little  $SO_3$  is formed (see above). The latter can be removed by passing the gas through a filter of glass-wool. Bubbling of the  $S_2O$ - $SO_2$  mixture into trichloromethane at  $-60^\circ \text{C}$  results in a yellow solution which can be freed from most of the dissolved  $SO_2$  in a vacuum. The analytical and spectroscopic data then indicate the presence of  $S_5O$  (up to  $77 \text{ mmol l}^{-1}$ ) and of traces of  $SO_2$  in the solution [13]:



The molecular mass determined osmotically corresponds to the formula  $S_5O$ . The SO stretching vibration was observed in the infrared spectrum at  $1119 \text{ cm}^{-1}$  (at  $-65^\circ \text{C}$ ) indicating an exocyclic sulfoxide group similar to the one in  $S_8O$  (see below). At  $-50^\circ \text{C}$  the solution of  $S_5O$  may be kept for several days without decomposition which usually results in a Tyndall effect caused by a colloidal polymeric sulfuroxide which is the expected decomposition product. At  $25^\circ \text{C}$  some decomposition already occurs within

15 min. The dissolved  $S_5O$  reacts with chlorine at  $-60\text{ }^\circ\text{C}$  to give thionyl chloride and other sulfuroxochlorides. With potassium iodide in anhydrous formic acid the stoichiometric amount of iodine is liberated [13]:



Although the evidence for a cyclic oxide  $S_5O$  is relatively weak, its existence is likely in the light of the properties of the homologous oxides  $S_6O$ ,  $S_7O$ , and  $S_8O$  which show analogous spectra and reactions (see below).

## 2.6

### Hexasulfurmonoxide $S_6O$ and Hexasulfurdioxide $S_6O_2$

Oxidation of  $S_6$ , dissolved in dichloromethane, by trifluoroperoxoacetic acid at  $-20\text{ }^\circ\text{C}$  (molar ratio 1:1.2) followed by addition of *n*-pentane and cooling to  $-78\text{ }^\circ\text{C}$  results in the crystallization of  $\alpha$ - $S_6O$  recovered after recrystallization from  $CH_2Cl_2$  in 5.5% yield:

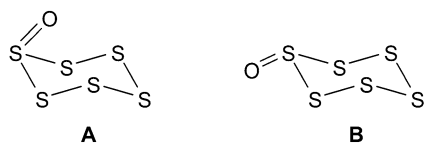


According to the Raman spectrum the product contains traces of  $S_6$  in solid solution which could not be removed by repeated recrystallization. If the oxidation is carried out at  $-25\text{ }^\circ\text{C}$  in a  $CS_2/CH_2Cl_2$  mixture and the molar ratio is increased to 1:2.2,  $\beta$ - $S_6O$  is obtained [59] isolated in 10% yield [60].

$\alpha$ - $S_6O$  forms orange transparent spearhead-shaped crystals melting at  $39\text{ }^\circ\text{C}$  with decomposition to  $SO_2$  and polymeric sulfur.  $\beta$ - $S_6O$  forms dark-orange transparent prismatic or truncated pyramidal crystals of melting point  $34\text{ }^\circ\text{C}$  (dec.). Both forms are moderately soluble in  $CS_2$ ,  $CH_2Cl_2$ , and  $CHBr_3$ . The solutions are unstable at  $25\text{ }^\circ\text{C}$  and turn turbid after a few minutes. The decomposition is complete after 12 h and the solution then contains  $SO_2$ ,  $S_8$  and  $S_7$  as well as traces of  $S_6$ ,  $S_{10}$ , and  $S_{12}$ . At  $25\text{ }^\circ\text{C}$  solid hexasulfuroxide decomposes within 2 h almost quantitatively to  $SO_2$  and elemental sulfur, but at  $-50\text{ }^\circ\text{C}$  no decomposition could be noticed even after storage for several weeks. Heating of  $S_6O$  in a vacuum produces  $S_2O$  instead of  $SO_2$  besides elemental sulfur. The EI mass spectrum exhibits a small peak corresponding to the molecular ion. The infrared spectra of  $\alpha$ - and  $\beta$ - $S_6O$ , dissolved in tribromomethane, are identical.  $\alpha$ - $S_6O$  and  $\beta$ - $S_6O$  may therefore consist of identical molecules in differing packing patterns [59]. However, the observations may also be explained assuming either axial or equatorial positions, respectively, for the oxygen atoms in  $\alpha$ - and  $\beta$ - $S_6O$  while in solution one of these isomers may dominate resulting in identical spectra.

The Raman spectra of solid  $\alpha$ - and  $\beta$ - $S_6O$  show characteristic differences but both spectra can be assigned assuming a chair-like six-membered homocycle with an exocyclic oxygen atom (molecular symmetry  $C_6$ ; see Scheme 4).

The SO stretching vibration gives rise to a very strong infrared absorption at  $1112\text{ cm}^{-1}$  (in  $CHBr_3$ ), and Raman lines of medium intensity have been observed at  $1092\text{ cm}^{-1}$  for  $\alpha$ - $S_6O$  and at  $1102\text{ cm}^{-1}$  for  $\beta$ - $S_6O$ . The SS stretch-



Scheme 4

ing and SSO bending modes have been detected in the range  $293\text{--}506\text{ cm}^{-1}$  [59].

In  $CS_2$  solution,  $S_6O$  reacts with  $SbCl_5$  within one week at  $-50\text{ }^\circ\text{C}$  followed by cooling to  $-78\text{ }^\circ\text{C}$  to orange crystals of  $S_{12}O_2 \cdot 2SbCl_5 \cdot 3CS_2$  which have been characterized by a single-crystal X-ray diffraction analysis at  $-115\text{ }^\circ\text{C}$

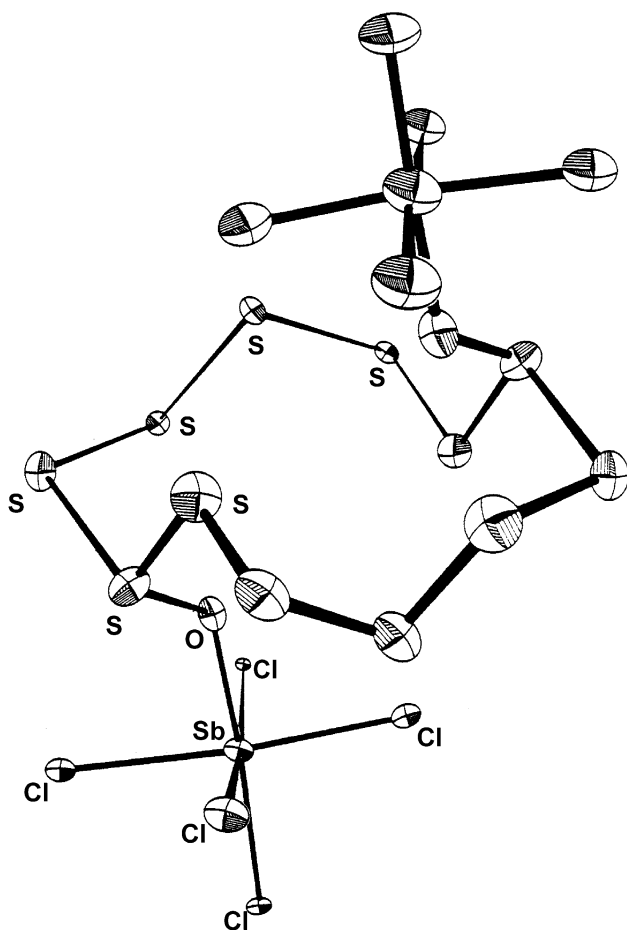


Fig. 1 Molecular structure of the adduct  $S_{12}O_2 \cdot 2SbCl_5$  in the crystal [61]

[61]. Evidently, a dimerization of  $S_6O$  takes place under the influence of the Lewis acid  $SbCl_5$  resulting in the centrosymmetric *cyclo*-dodecasulfurdioxide adduct shown in Fig. 1.

On exposure to air, the initially clear orange crystals of the adduct turn cloudy within 1 min as a result of the loss of  $CS_2$ , and ultimately form a yellow oil. In  $CS_2$  solution the adduct decomposes fairly rapidly at room temperature; the decomposition products  $SOCl_2$ ,  $SO_2$ ,  $S_8$ , and  $SbCl_3$  are already detectable after 10 min. The  $SO$  stretching vibrations of  $S_{12}O_2 \cdot 2SbCl_5$  occur at  $940\text{ cm}^{-1}$  in the infrared spectrum (in  $CS_2$ ) [61]. Free  $S_{12}O_2$  has not been prepared yet.

If  $S_6$  is oxidized by an excess of trifluoroperoxoacetic acid (molar ratio 1:2.4) at  $0\text{ }^\circ\text{C}$  a novel oxide is formed which is much less stable than  $S_6O$  and therefore has not been characterized yet. This oxide, probably  $S_6O_2$ , decomposes in  $CH_2Cl_2$  solution at  $5\text{ }^\circ\text{C}$  within 48 h to  $SO_2$ , polymeric sulfur and  $S_{10}$  which can be prepared in this way from  $S_6$  [62]; see Eqs. (27) and (28):



## 2.7

### Heptasulfurmonoxide $S_7O$

Oxidation of *cyclo*-heptasulfur by trifluoroperoxoacetic acid at  $-20\text{ }^\circ\text{C}$  in  $CH_2Cl_2$  provides  $S_7O$  in 45% yield [63]:



$S_7O$  crystallizes in orange monoclinic crystals which are yellow at  $-80\text{ }^\circ\text{C}$  and melt with decomposition at  $55\text{ }^\circ\text{C}$ . However, even at  $25\text{ }^\circ\text{C}$   $S_7O$  decomposes quantitatively within 24 h in diffuse daylight, more slowly in the dark, to  $SO_2$ , polymeric sulfur and little  $S_8$ . Thermolysis in a high vacuum at  $60\text{ }^\circ\text{C}$  produces  $S_2O$  and elemental sulfur. Therefore, the EI mass spectrum exhibits only ions originating from these decomposition products ( $SO^+$ ,  $S_2O^+$ ,  $S_n^+$ ). In  $CH_2Cl_2$  solution  $S_7O$  decomposes at  $20\text{ }^\circ\text{C}$  within 3 h to  $SO_2$ , polymeric sulfur and  $S_{10}$ ; the latter can be isolated in 7% yield based on the starting material  $S_7$  [62]:



The density of  $S_7O$  has been determined as  $2.15\text{ g cm}^{-3}$  at  $25\text{ }^\circ\text{C}$  and calculated from the lattice constants as  $2.179\text{ g cm}^{-3}$  at  $-110\text{ }^\circ\text{C}$ , measured by a single-crystal X-ray diffraction analysis [1, 64, 65]. The  $S_7O$  molecules are of  $C_1$  symmetry and consist of chair-like seven-membered homocycles with the exocyclic oxygen atom in an axial position; see Fig. 2. Most remarkably are the two almost planar groups O-S-S-S (torsion angle  $\tau=2.9^\circ$ ) and S-S-S-S ( $\tau=6.3^\circ$ ).

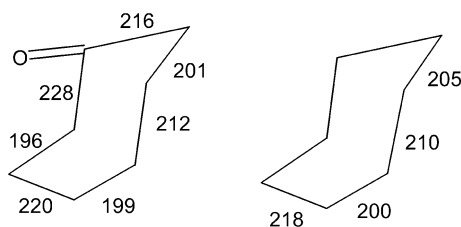


**Fig. 2** Molecular structures of the molecules  $S_7O$  (left) and, for comparison, of  $S_7$  (symmetry  $C_s$ ) in the crystal; SS bond lengths in pm (after [1, 65])

The SO bond length of 147.4 pm is similar to that in sulfurmonoxide (148 pm) and longer than that in  $SO_2$  (143 pm). The SS bonds vary in length between 195.7 and 228.3 pm. These bond lengths alternate around the ring which is of motif  $- - + - + - +$ . The intermolecular  $S \cdots S$  contacts are in accord with the van der Waals distance between two sulfur atoms (350 pm) but there are intermolecular  $S \cdots O$  contacts much shorter than the van der Waals SO distance of 310 pm.

The SO stretching vibration of  $S_7O$  was observed at  $1134 \text{ cm}^{-1}$  in the IR spectrum of a  $CS_2$  solution and at  $1089/1102/1113 \text{ cm}^{-1}$  in the Raman spectrum of a solid sample at  $-90 \text{ }^\circ\text{C}$  (the three very weak Raman lines probably originate from the intermolecular  $S \cdots O$  interactions). The two strongest Raman lines at 292 and  $325 \text{ cm}^{-1}$  have been assigned to the SS stretching vibrations of the particularly weak bonds (see the bond distances in Fig. 2).

Hohl et al. [66] investigated the potential energy hypersurface of  $S_7O$  by a combined molecular dynamics/density functional scheme to calculate the geometries of the local minima. The experimental  $S_7=O$  structure shown in Fig. 2 (symmetry  $C_1$ ) was found to be the global minimum and the observed geometry was well reproduced although the bond lengths were overestimated. The heterocyclic crown-shaped isomer of  $S_7O$  with a structural unit  $-S-O-S-$  (analogous to the  $S_8$  structure but with symmetry  $C_s$ ) represents a local minimum which is by  $12 \text{ kJ mol}^{-1}$  higher in energy (see also below). A conformational isomer of homocyclic  $S_7O$  with the oxygen atom connected to a different ring atom is higher in energy by ca.  $57 \text{ kJ mol}^{-1}$  compared to the most stable structure; in this isomer the  $S_7$  ring is twisted rather than chair-like.

## 2.8

### Heptasulfurdioxide $S_7O_2$

Oxidation of  $S_8$  in dichloromethane at  $-20 \text{ }^\circ\text{C}$  by an excess of trifluoroperoxoacetic acid (molar ratio 1:5) yields  $S_7O_2$  besides  $SO_2$  [67]:



The isolated yields vary between 5 and 10%. The oxides  $S_8O$ ,  $S_8O_2$  and  $S_8O_3$  are probably intermediates in this reaction and it is assumed that  $S_8O_3$

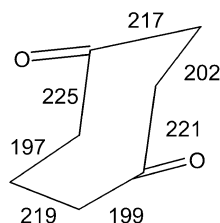


**Fig. 3** Possible structure of  $S_7O_2$  as derived from the Raman spectrum. Estimated SS bond lengths in pm (after [67])

spontaneously decomposes to  $SO_2$  and  $S_7O$  which is then further oxidized to  $S_7O_2$ :



Therefore,  $S_7O_2$  can also be prepared by oxidation of  $S_8O$ ,  $S_7$ , or  $S_7O$  but the isolated yields are either lower or at best identical to the yield of the  $S_8$  oxidation according to Eq. (31) [67].

From  $CS_2$  solution  $S_7O_2$  is obtained as intensely orange colored crystals which on heating spontaneously decompose at 60–62 °C with evolution of sulfur dioxide.  $S_7O_2$  is far less soluble in  $CS_2$  (ca. 1 g l<sup>-1</sup> at 0 °C) than  $S_7O$ . The solution decomposes within 1 h to a mixture of sulfur homocycles and  $SO_2$ . Solid  $S_7O_2$  decomposes at 25 °C within minutes and quantitatively within 2 h, even in the dark. Heating in a high vacuum to 50–60 °C produces  $S_2O$  and elemental sulfur. The EI mass spectrum therefore exhibits peaks due to these decomposition products only [67].

Freshly prepared solutions of  $S_7O_2$  in  $CS_2$  exhibit two strong absorptions at 1127 and 1138 cm<sup>-1</sup> in the infrared spectrum which have been assigned to two sulfoxide groups within the same molecule. The low temperature Raman spectrum of  $S_7O_2$  (-100 °C) shows SO stretching vibrations at 1083, 1103, and 1117 cm<sup>-1</sup> while the SS stretching and SSO bending modes are observed in the region 300–559 cm<sup>-1</sup>. The strongest line at 333 cm<sup>-1</sup> was assigned to the SS stretching mode of a particularly weak bond. For cumulated SS bonds there exists a relationship between the SS stretching wavenumber  $\nu$  (cm<sup>-1</sup>) and the bond length  $d$  [67]:

$$\log d = 2.881 - 0.231 \cdot \log \nu$$

Thus, the wavenumbers of the SS stretching modes may be used to estimate the bond lengths in sulfur homocycles assuming that the corresponding vibrations are not coupled with other modes. The results obtained in this way for  $S_7O_2$  are shown in Fig. 3.

The positions of the oxygen atoms have been tentatively assumed but they are in agreement with the structure of the precursor molecule  $S_7O$  and with the Raman spectrum of  $S_7O_2$ . No crystallographic structure determination has been published for  $S_7O_2$  yet. However, Jones [68] investigated 14 cyclic

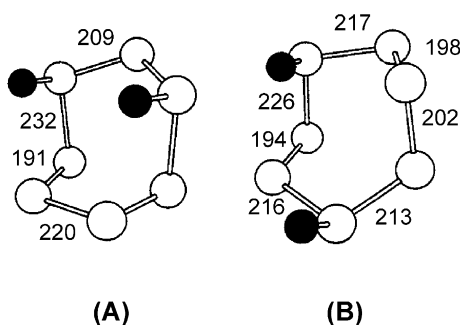


**Fig. 4** Calculated structures of the two most stable isomers of  $S_7O_2$ . Bond lengths in pm. The energies of the two structures A and B are almost identical (after [68])

isomers of composition  $S_7O_2$  by density functional calculations with simulated annealing. The two most stable isomers are shown in Fig. 4.

The two structures shown in Fig. 4 can be derived from the experimental  $S_7O$  structure by adding one exocyclic oxygen atom in such positions that the O atoms form nearly planar four-atomic arrangements with three neighboring sulfur atoms. These nearly planar units SSSS (in  $S_7$ ,  $S_7O$ , and  $S_7O_2$ ) and SSSO (in  $S_7O$  and  $S_7O_2$ ) seem to be more stable than twisted arrangements. According to these calculations, the 1,3-dioxide ( $C_s$  symmetry) is by  $2 \text{ kJ mol}^{-1}$  more stable than the 1,4-isomer ( $C_1$  symmetry), both containing the oxygen atoms in axial positions. Ten other possible isomers with SO groups separated by either one or two sulfur atoms are much less stable (by  $12\text{--}60 \text{ kJ mol}^{-1}$ ). The two investigated *heterocyclic*  $S_7O_2$  species with only one exocyclic oxygen atom and one endocyclic S-O-S bridge are by  $63\text{--}71 \text{ kJ mol}^{-1}$  less stable than the global minimum structure. Isomers with adjacent sulfoxide groups turned out to be unstable on annealing in agreement with the observation that organic *vic*-disulfoxides are generally unstable unless protected by very bulky substituents.

## 2.9

### Octasulfurmonoxide $S_8O$

*Cyclo*-Octasulfurmonoxide was the first homocyclic sulfuroxide prepared as a pure material. Originally it had been prepared in 1972 by condensation of thionyl chloride and heptasulfane [69, 70]. The two components, dissolved in  $CS_2$ , were added to a mixture of  $CS_2$  and  $Me_2O$  at  $-40 \text{ }^\circ\text{C}$  applying the dilution principle:



Since heptasulfane is difficult to prepare, a mixture of polysulfanes known as “crude sulfane oil” was used instead (average composition  $H_2S_{6.2}$ , accessible from sodium polysulfide and hydrochloric acid [71]). From 104 g of

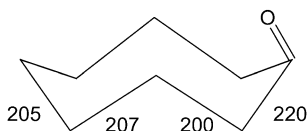
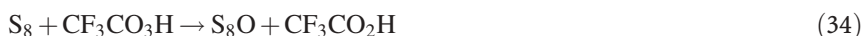


**Fig. 5** Molecular structure of S<sub>8</sub>O in the crystal; SS bond lengths in pm, averaged for C<sub>s</sub> symmetry (after [74, 75])

H<sub>2</sub>S<sub>6.2</sub> and 62 g of SOCl<sub>2</sub> 3 g of pure S<sub>8</sub>O were obtained after repeated recrystallization from CS<sub>2</sub> [69, 70].

A more convenient method uses the oxidation of S<sub>8</sub>, dissolved in CH<sub>2</sub>Cl<sub>2</sub> or CS<sub>2</sub>, by trifluoroperoxoacetic acid at temperatures between -10 and 0 °C (molar ratio 1:1.5):



After the reaction is complete the product is precipitated by addition of hexane and recrystallized from CS<sub>2</sub> (yield 20%) [72, 73].

The needle-shaped orthorhombic crystals of S<sub>8</sub>O are orange at 25 °C but yellow at -78 °C (density from X-ray measurements at +10 °C: 2.11 g cm<sup>-3</sup> [74, 75]; experimental density at 25 °C: 2.126 g cm<sup>-3</sup> [70]). At -20 °C pure S<sub>8</sub>O can be stored for weeks in a desiccator over P<sub>2</sub>O<sub>5</sub> without decomposition; at 25 °C in the dark and with exclusion of moisture S<sub>8</sub>O survives for a few hours. On heating in a nitrogen atmosphere (heating rate 6 K min<sup>-1</sup>) the oxygen is quantitatively liberated as SO<sub>2</sub> at 78 °C; at this “melting point” plastic sulfur is formed which becomes a mobile liquid only at 120 °C [70]. However, if S<sub>8</sub>O is heated to 80–120 °C in a high vacuum, all oxygen is liberated as S<sub>2</sub>O rather than SO<sub>2</sub>. Therefore, the EI mass spectrum (70 eV) shows peaks due to the decomposition products only [73].

According to an X-ray crystallographic analysis the S<sub>8</sub>O molecules consist of crown-shaped S<sub>8</sub> rings with the oxygen atom present as a sulfoxide group in an axial orientation. The molecular symmetry is C<sub>s</sub> but the site symmetry is C<sub>1</sub>. The SS bond lengths vary between 200.1 and 220.1 pm with the longest bonds neighboring the SO group followed by the two shortest bonds [74, 75]; see Fig. 5.

This bond length alternation is very typical for compounds containing cumulated sulfur-sulfur bonds [76, 77]. The axial position of the oxygen atom can be explained by the anomeric effect (delocalization of oxygen 2*p* lone pairs into the unoccupied σ\* molecular orbitals of the neighboring SS bonds). In addition, the SO groups of neighboring molecules interact in the crystal by means of their atomic charges forming infinite and almost planar zig-zag chains S=O...S=O...S=O with *d*(S...O)=293.5 pm [74, 75].

The infrared and Raman spectra of S<sub>8</sub>O [78] reflect the molecular structure. The SO stretching vibration gives rise to very strong IR absorptions at 1133 cm<sup>-1</sup> (CS<sub>2</sub> solution) and at 1104 cm<sup>-1</sup> (CsCl disc) but to a weak Raman line at 1080 cm<sup>-1</sup> (all at 25 °C). Since S<sub>8</sub>O is a strong oxidant, KBr discs should not be used (formation of sulfur bromides). The Raman lines in the

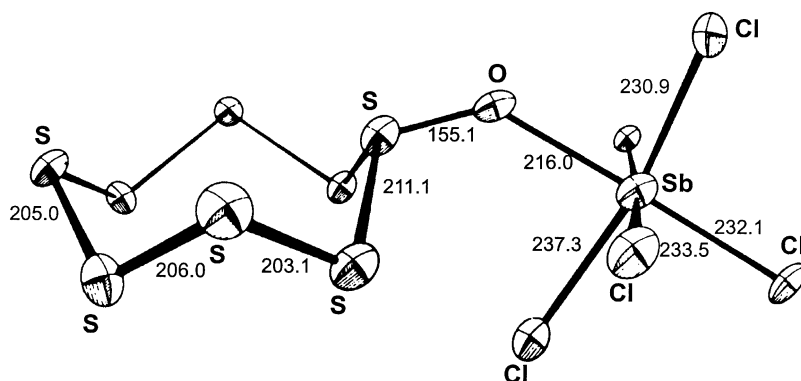


**Fig. 6** Molecular structure of the adduct  $S_8O \cdot SbCl_5$  in the crystal. Bond lengths in pm (after [81])

range 300–516  $cm^{-1}$  have been assigned to the SS stretching and SSO bending modes using a Urey-Bradley force constant calculation as a guidance [79]. Irradiation of solid  $S_8O$  by either green or blue laser lines at 25 °C results in decomposition to  $SO_2$ ,  $S_8$ , and  $S_{12}$  [78] while yellow and red laser lines at –100 °C have no such effect [70].

$S_8O$  is moderately soluble only in  $CS_2$  (8 g  $l^{-1}$  at 25 °C, 3.5 g  $l^{-1}$  at 0 °C), hardly soluble in  $CH_2Cl_2$ ,  $CHCl_3$ , and  $CHBr_3$  and insoluble in hydrocarbons and ether. The solution in  $CS_2$  can be kept at 25 °C for some hours, at –20 °C for several days without decomposition while refluxing for a few minutes results in formation of  $SO_2$ ,  $S_8$ ,  $S_{12}$ , and polymeric sulfur [70].

In its reactions  $S_8O$  shows properties typical for both sulfur homocycles and sulfoxides. With elemental chlorine  $SOCl_2$  and  $S_2Cl_2$  are formed, with bromine  $SOBr_2$  and  $S_2Br_2$  are obtained. Water decomposes  $S_8O$  to  $H_2S$  and  $SO_2$  besides elemental sulfur while cyanide ions expectedly produce thiocyanate. The reaction with iodide in the presence of formic acid is used for the iodometric determination of the oxygen content [70]:



Oxidation of  $S_8$  by an excess of trifluoroperoxoacetic acid does not give any stable dioxide or trioxide of  $S_8$  but instead  $S_7O$  and  $S_7O_2$  are formed together with  $SO_2$ , evidently as a result of the instability of the higher  $S_8$ -oxides [67]; see previous section.

Sulfoxides form adducts with Lewis acids like  $SbCl_5$  and  $SnCl_4$  [80]. In the case of  $S_8O$  the crystalline products  $S_8O \cdot SbCl_5$  [81] and  $(S_8O)_2 \cdot SnCl_4$  [82] have been prepared and characterized by single crystal X-ray diffraction analyses. Reaction of  $S_8O$  with  $SbCl_5$  in  $CS_2$  at 20 °C and subsequent cooling of the solution to –50 °C resulted in orange orthorhombic crystals of  $S_8O \cdot SbCl_5$  in 71% yield. These molecules are of  $C_s$  symmetry; see Fig.6 [81].

In contrast to pure  $S_8O$ , the adduct contains an  $S_8O$  ligand with the oxygen atom in an equatorial position. The coordination at the metal atom is

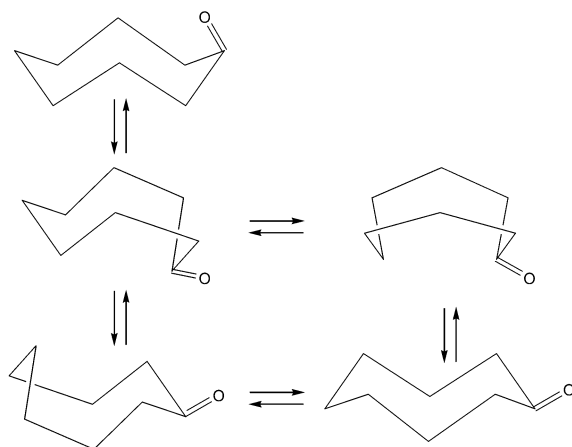


**Fig. 7** Possible pathway for the interconversion of  $S_8O$  with the oxygen atom in either axial or equatorial position (after [81])

approximately octahedral with a mean Sb-Cl distance of 233 pm and bond angles Cl-Sb-Cl between  $86^\circ$  and  $94^\circ$ . The SO bond length has increased from 148.3 pm in  $S_8O$  to 155 pm, while the adjacent SS bonds have decreased in length from 220 pm in  $S_8O$  to 211.1 pm. This observation is in agreement with the assumption of an anomeric effect in  $S_8O$  (see above) which is lifted in the adduct. For this reason the oxygen atom now prefers the equatorial position. The S-O-Sb angle is  $133.3^\circ$ .

At  $25^\circ\text{C}$  the adduct decomposes within 5 min to a mixture of  $SOCl_2$ ,  $SbCl_3$ , and  $S_8$ . On dissolution in acetone and subsequent cooling and recrystallization from  $CS_2$ , pure  $S_8O$  was recovered, the Raman spectrum of which was identical to a freshly prepared sample. Therefore, the liberated ligand must contain the oxygen atom in an axial position. Since pyramidal inversion at the three-coordinate sulfur atom is unlikely at low temperatures, a conformational inversion of the eight-membered ring is probably taking place during preparation and dissociation of the adduct; see Fig. 7.

Yellow monoclinic crystals of  $(S_8O)_2 \cdot SnCl_4$  were prepared from  $S_8O$ , dissolved in  $CS_2$ , and a large excess of  $SnCl_4$  by cooling to  $-35^\circ\text{C}$  (yield 78%) [82]. An X-ray diffraction analysis revealed a molecule with the two ligands in *cis*-position to each other; see Fig. 8.

The coordination sphere at the metal center is approximately octahedral. The two crystallographically independent  $S_8O$  ligands exhibit the same conformation as in pure  $S_8O$  with the oxygen atoms in axial positions. The overall molecular conformation of the  $S_8O$  ligand is identical to that of crystalline  $S_8O$ . However, two significant effects on the bond distances are observed on complex formation. While the SO bond length increases, the amount of SS bond length variation in the homocyclic ring decreases. This is indicated by the lengths of the SS bonds adjacent to the sulfoxide group which are 218 pm long compared to 220 pm in crystalline  $S_8O$ . Compared to  $S_8O \cdot SbCl_5$

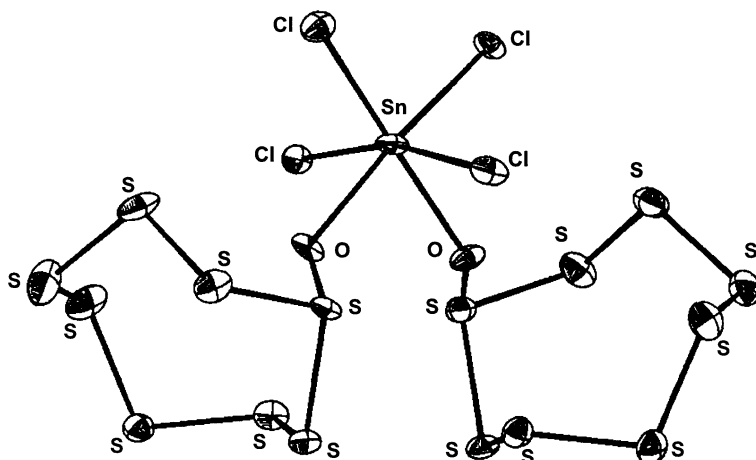


Fig. 8 Structure of the adduct  $(S_8O)_2 \cdot SnCl_4$  in the crystal [82]

the metal-ligand interaction is weaker in  $(S_8O)_2 \cdot SnCl_4$ . This follows from the extent of dissociation in solution. The infrared spectrum of a solution of  $S_8O$  and  $SnCl_4$  in a molar ratio of 1:400 in  $CS_2$  still shows the absorption bands of free  $S_8O$  besides SO stretching vibrations that can be assigned to the 2:1 and 1:1 complexes. The strength of the coordination also follows from the weakening of the SO bond which is of length 148 pm in  $S_8O$ , 152 pm in  $(S_8O)_2 \cdot SnCl_4$ , and 155 pm in  $S_8O \cdot SbCl_5$  [82].

## 2.10

### Nonasulfurmonoxide $S_9O$

Oxidation of *cyclo*- $S_9$ , dissolved in carbon disulfide, by trifloroperoxoacetic acid, dissolved in dichloromethane, at  $-30$  °C provides  $S_9O$  in 12% yield, isolated as intense yellow crystals (after recrystallization from  $CH_2Cl_2$ ) [83]:



On heating  $S_9O$  decomposes at 32–34 °C with melting and  $SO_2$  evolution. At 20 °C the solid oxide decomposes quantitatively within 2 h to  $SO_2$  and a polymeric sulfuroxide  $(S_nO)_x$  with  $n > 9$ . Even dissolved in carbon disulfide  $S_9O$  decomposes within 20 min to a large extent with formation of  $SO_2$  as can be seen from the decrease of the infrared absorption intensity at  $1134$   $cm^{-1}$  ( $S_9O$ ) and the intensity increase at  $1336$   $cm^{-1}$  ( $SO_2$ ). The solubility of  $S_9O$  in  $CS_2$  ( $>21$  g  $l^{-1}$  at 0 °C) is much higher than in  $CH_2Cl_2$  (260 mg  $l^{-1}$  at 0 °C) while the substance is practically insoluble in *n*-pentane, *n*-hexane and tribromomethane. At  $-80$  °C,  $S_9O$  can be stored for longer periods of time without decomposition.

No crystallographic analysis of  $S_9O$  has been reported so far. Therefore, structural information about the  $S_9O$  molecule is available only from the

analysis of the Raman spectrum which was recorded at a sample temperature of  $-100\text{ }^{\circ}\text{C}$ . The SO stretching vibration observed at  $1121\text{ cm}^{-1}$  (in the solid state) is in agreement with an exocyclic oxygen atom rather than an -S-O-S- bridge. The highest possible molecular symmetry is therefore  $C_s$ . Regarding the structure of the nine-membered ring the vibrational spectrum can help to gain some information since there exists a relationship between the S-S bond lengths and the wavenumbers of the S-S stretching vibrations in sulfur homocycles; see above [67, 84]. The molecules of the related sulfur allotrope  $S_9$  form a puckered ring of  $C_s$  symmetry with the motif  $+ + - - + + - + -$  and bond lengths in the range  $203.2\text{--}206.9\text{ pm}$  [85]. This bond distance pattern results in S-S stretching vibrations in the range of  $416\text{--}485\text{ cm}^{-1}$  [83]. In the case of  $S_9O$  the S-S stretching vibrations are observed in the range of  $350\text{--}517\text{ cm}^{-1}$ . Therefore, it can be expected that the bond lengths vary between  $200$  and  $220\text{ pm}$ , approximately. Taking the experiences with the structures of the other homocyclic sulfur oxides into account, the two S-S bonds neighboring to the sulfoxide group will most probably be the longest ( $220\text{ pm}$ ) and the following two S-S bonds will be the shortest ( $200\text{ pm}$ ) of the molecule (see the structures of  $S_7O$  and  $S_8O$  above).

## 2.11

### Decasulfurmonoxide $S_{10}O$

Oxidation of *cyclo*- $S_{10}$ , dissolved in carbon disulfide, by trifloroperoxyacetic acid, dissolved in dichloromethane, at  $-30\text{ }^{\circ}\text{C}$  (molar ratio 1:3) provides  $S_{10}O$  in 14% yield, isolated as orange-colored crystals (after recrystallization from  $\text{CH}_2\text{Cl}_2$ ) [83]:



On heating  $S_{10}O$  decomposes with melting and  $\text{SO}_2$  evolution at  $51\text{ }^{\circ}\text{C}$ . At  $20\text{ }^{\circ}\text{C}$  the solid oxide decomposes quantitatively within 2 h to  $\text{SO}_2$ , elemental sulfur and a polymeric sulfuroxide  $(S_nO)_x$  with  $n > 10$ . This polysulfuroxide also decomposes within 24 h at  $20\text{ }^{\circ}\text{C}$  to  $\text{SO}_2$ ,  $S_8$ , and polymeric sulfur. The solubility of  $S_{10}O$  in  $\text{CS}_2$  is much higher than in  $\text{CH}_2\text{Cl}_2$  while the substance is practically insoluble in *n*-pentane. At  $-80\text{ }^{\circ}\text{C}$ ,  $S_{10}O$  can be stored for longer periods of time without decomposition. The EI mass spectrum shows large peaks for  $\text{SO}^+$  and  $\text{S}_2\text{O}^+$  but no molecular ion [60].

No crystallographic analysis of  $S_{10}O$  has been reported so far. Therefore, structural information about the  $S_{10}O$  molecule is available only from the analysis of the Raman spectrum which was recorded at a sample temperature of  $-100\text{ }^{\circ}\text{C}$ . The SO stretching vibration observed at  $1091\text{ cm}^{-1}$  (in the solid state) is in agreement with an exocyclic oxygen atom rather than an -S-O-S- bridge. The highest possible molecular symmetry is therefore  $C_s$ . Regarding the structure of the ten-membered ring the vibrational spectrum can help to gain some information since there exists a relationship between the S-S bond lengths and the wavenumbers of the S-S stretching vibrations in sulfur homocycles [67, 84]. The molecules of the related sulfur allotrope

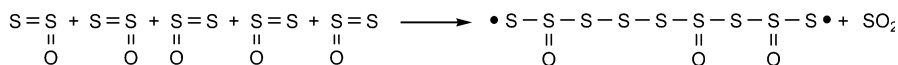
$S_{10}$  form a puckered ring of  $D_2$  symmetry with the motif  $- - + - + - - + - +$  and bond lengths in the range 203.3–208.0 pm [86]. This bond distance pattern results in S-S stretching vibrations in the range of 403–495  $cm^{-1}$  [86]. In the case of  $S_{10}O$  the S-S stretching vibrations are observed in the range of 354–506  $cm^{-1}$  [83]. Therefore, it can be expected that the bond lengths vary between 202 and 220 pm, approximately. Taking the experiences with the structures of the other homocyclic sulfur oxides into account, the two S-S bonds neighboring the sulfoxide group will most probably be the longest (220 pm) and the following two S-S bonds will be the shortest (202 pm) of the molecule (see the structures of  $S_7O$  and  $S_8O$  above).

## 2.12

### Polysulfuroxides ( $S_nO$ )<sub>x</sub>

The spontaneous thermal decomposition of  $S_2O$  on condensation at low temperatures and of some of the homocyclic sulfuroxides on storage at 20 °C results in polysulfuroxides (PSO) of composition  $S_nO$  with  $n>3$ . These products are mixtures of molecules of unknown molecular mass which slowly decompose at 20 °C to elemental sulfur and  $SO_2$ . Consequently, their composition depends on the preparation and changes with time. At 100 °C this decomposition is quantitative within a few minutes.

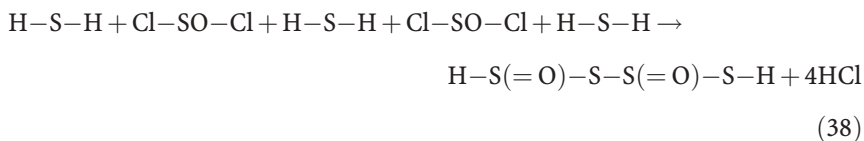
On condensation at low temperatures, on dissolution in inert solvents or on raising its partial pressure substantially above 1 mbar (100 Pa)  $S_2O$  polymerizes with partial disproportionation. Since sulfur radicals have been detected in such condensates by ESR spectroscopy [10] it has been proposed that a radical-chain reaction takes place according to Scheme 5.



Scheme 5

The intermediate product  $S_3$  (see above) will also take part in this polymerization. Infrared spectra of the polysulfuroxide show a strong absorption at 1123  $cm^{-1}$  which was assigned to the structural unit  $-S-S(=O)-S-$  by comparison with model compounds like trisulfane-2-oxides  $(RS)_2S=O$  [31] and  $S_8O$  (see above). In chloroform solution  $S_2O$  reacts at  $-60$  °C to  $S_5O$  and  $SO_2$  (see above).

Yellow insoluble substances of similar composition are obtained on reaction of hydrogen sulfide with either  $SO_2$ ,  $SOCl_2$ , or  $SO_2Cl_2$  and on hydrolysis of  $S_2Cl_2$  [87], e.g.:



The materials obtained by this idealized equation have also been termed polysulfuroxides in the older literature. However, more recent results showed that they also contain hydrogen and therefore are probably polysulfane oxides of the types  $\text{HS}(\text{S}_n\text{O})_x\text{SH}$  or  $\text{HS}(\text{S}_n\text{O})_x\text{OH}$  [3, 88]. Due to the simultaneous thermal decomposition with formation of  $\text{SO}_2$  the sulfur content is higher than expected from Eq. (38) and from the general formula. All these compounds produce  $\text{S}_2\text{O}$  on heating in a high vacuum which is a typical reaction for compounds containing oxidized sulfur chains or rings.

### 3

#### Bond Properties

The most interesting aspect of the bonding in the sulfur-rich oxides is the enormous variation of the SS internuclear distances. The shortest SS bond is observed in  $\text{S}_2\text{O}$  with 188.5 pm and the longest in  $\text{S}_7\text{O}$  neighboring to the oxygen atom with 228.3 pm. One SS bond of  $\text{S}_7\text{O}_2$  (isomer A) calculated by the DFT method is even longer (232 pm); see Fig. 4. Compared to the single bond length of 205 pm in  $\text{S}_8$  and 206 pm in  $\text{H}_2\text{S}_2$  these data indicate a wide variation in bond order.

Cumulated sulfur-sulfur bonds as in homocycles show a unique interdependence in so far as the length of a particular bond depends on the arithmetic mean of the lengths of the two neighboring bonds [77]. This is demonstrated in Fig. 9 for the bonds in the homocycles  $\text{S}_n$  ( $n = 6, 7, 8, 10, 12$ ) and the sulfur-rich oxides  $\text{S}_n\text{O}$  ( $n = 7, 8$ ).

The effect shown in Fig. 9 is a result of the bond-bond interaction which is a characteristic feature for chains and rings of two-valent chalcogen atoms. It can also be recognized from the relatively large bond interaction force constants  $f_{rr}$  of such compounds. The stretching force constants  $f_r(\text{SS})$  of polysulfur compounds depend on the SS bond distances as shown in Fig. 10. The data used in this figure include several excited electronic states of the  $\text{S}_2$  molecule as well as the disulfide anion and a number of sulfur homocycles [77].

Another unusual feature of the homocyclic sulfuroxides are the nearly planar units SSSS (in  $\text{S}_7$ ,  $\text{S}_7\text{O}$ , and  $\text{S}_7\text{O}_2$ ) and SSSO (in  $\text{S}_7\text{O}$  and  $\text{S}_7\text{O}_2$ ). While a torsion angle at cumulated SS bonds in the vicinity of  $80\text{--}100^\circ$  is normal in the most stable structures [76], the mentioned seven-membered rings exhibit some SSSS and SSSO torsion angles which are within  $\pm 6^\circ$  of zero. As a consequence, the central SS bond of these four-atom units is rather long (218–235 pm) and probably responsible for the thermal instability of all of these species. It has been suspected that there exists an attractive interaction between the terminal atoms in these planar SSSO units [89]. That this is in fact the case can be seen from the HOMO of  $\text{S}_7\text{O}$  which shows a positive overlap between the (occupied)  $\pi^*$  orbital of the long SS bond in the planar SSSS unit on the one hand and the (empty)  $\pi^*$  orbital of the SO bond on the other hand, especially between the oxygen atom and the terminal sulfur atom in the planar SSSO unit [89]. This kind of  $\pi^*\text{-}\pi^*$  interaction in nearly

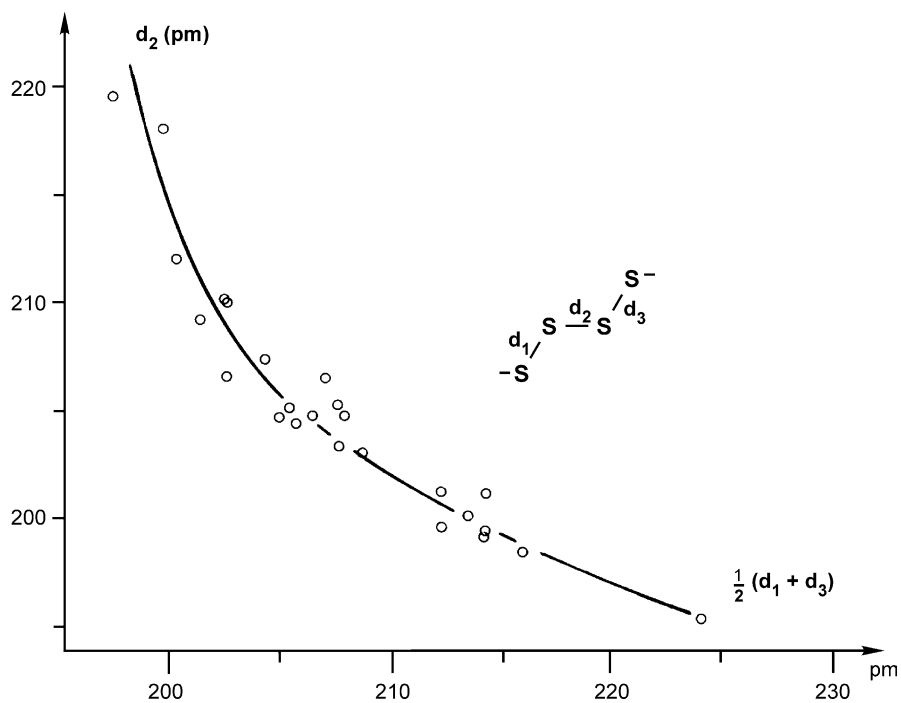


**Fig. 9** Mutual dependence of neighboring internuclear distances in sulfur homocycles (after [77])

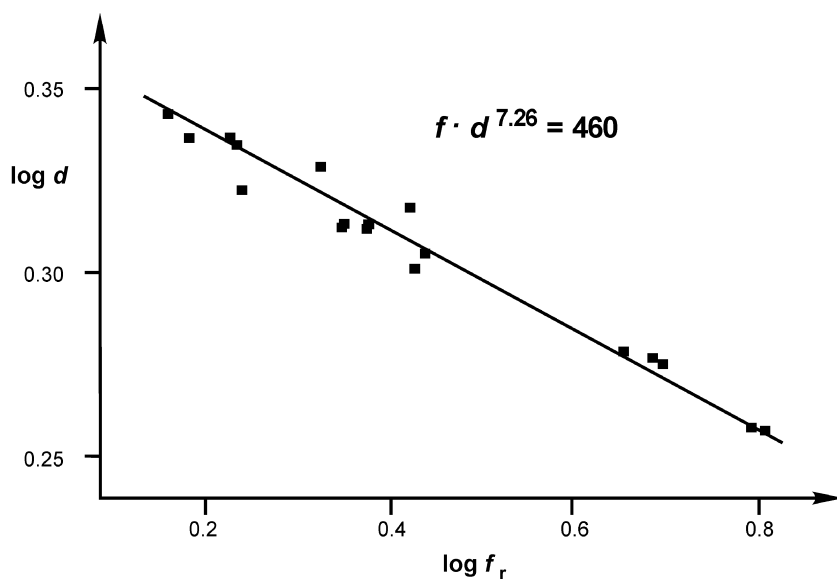


**Fig. 10** Linear relationship between the logarithms of the SS bond length  $d$  and the stretching force constant  $f_r$  of this bond in various sulfur compounds

planar four-atomic units is quite common in certain sulfur-rich molecules including diradical chains.

The oxygen atoms of the homocyclic oxides occupy axial positions in solid  $S_7O$  and  $S_8O$ . In fact, recent ab initio MO calculations at the G3X(MP2) level of theory have demonstrated that these isomers are, by 7 and 9 kJ mol<sup>-1</sup>, respectively, more stable than the alternative structures with the oxygen atoms in equatorial positions [89]. In the case of  $S_6O$ , however, the energy difference is only 1 kJ mol<sup>-1</sup> and the conformation with the oxygen atom in the equatorial position is more stable. This result agrees with the observation that  $S_6O$  exists as two isomeric forms in the solid state depending on the crystallization conditions (see above).

In principle, oxides of composition  $S_nO$  could also exist as heterocycles in which the oxygen atom is part of the ring which is then larger by one atom. Ab initio MO calculations by Wong at the G3X(MP2) level have shown, however, that these isomers are less stable than the homocyclic molecules, by the following relative energies at 0 K (in kJ mol<sup>-1</sup>) [89]:



Interestingly, the energy difference is smallest for  $S_7O$  which as a heterocycle forms a crown-shaped eight-membered ring similar to and isoelectronic with the well known  $S_8$  structure of  $D_{4d}$  symmetry. The transformation of the heterocycle  $S_7O$  into the homocyclic isomer  $S_7=O$  was studied by the molecular dynamics/density functional method but the unrealistically high barrier of 5 eV calculated for this transformation indicates that the system was far from equilibrium during most of the simulation [66].

**Acknowledgements** The invaluable help of Dr. Yana Steudel with the preparation of the figures and stimulating discussions with Prof. M. W. Wong (Singapore) are gratefully acknowledged. This work has been supported for many years by the Deutsche Forschungsgemeinschaft and the Fonds der Chemischen Industrie.

## References

1. R. Steudel in *Gmelin Handbuch der Anorganischen Chemie*, 8. Aufl., Schwefeloxide, Springer, Berlin, 1980, pp. 1–69
2. See the Review on Homocyclic Sulfur Cations by I. Crossing, *Top. Curr. Chem.* **2003**, 230, in print
3. P.W. Schenk, R. Steudel, *Angew. Chem.* **1965**, 77, 437; *Angew. Chem. Int. Ed. Engl.* **1965**, 4, 402
4. P.W. Schenk, R. Steudel in *Inorganic Sulphur Chemistry* (G. Nickless, ed.), Chapter 11, Elsevier, Amsterdam, 1968, p. 367
5. R. Steudel, *Comments Inorg. Chem.* **1982**, 1, 313
6. R. Steudel, *Phosphorus Sulfur* **1985**, 23, 33
7. P.W. Schenk, *Z. Anorg. Allg. Chem.* **1933**, 211, 150; P.W. Schenk, H. Platz, *Z. Anorg. Allg. Chem.* **1933**, 215, 113
8. D.J. Meschi, R.J. Myers, *J. Am. Chem. Soc.* **1956**, 78, 6220
9. S.R. Satyanarayana, A.R. V. Murthy, *Z. Anorg. Allg. Chem.* **1964**, 333, 245
10. P.W. Schenk, R. Steudel, *Z. Anorg. Allg. Chem.* **1966**, 342, 253; P.W. Schenk, R. Steudel, *Angew. Chem.* **1964**, 76, 97; *Angew. Chem. Int. Ed. Engl.* **1964**, 3, 61
11. P.W. Schenk, W. Holst, *Z. Anorg. Allg. Chem.* **1963**, 319, 337

12. For a photograph of the apparatus, designed by W. Genz [13], see R. Steudel, *Bild der Wissenschaft* **1969**, 207
13. W. Genz, P.W. Schenk, *Z. Anorg. Allg. Chem.* **1970**, 379, 300; W. Genz, *Doctoral Dissertation*, Technical University Berlin, Berlin **1969**
14. For a color picture of the orange-red condensate, see R. Steudel, *Bild der Wissenschaft* **1969**, 207
15. S.-Y. Tang, C.W. Brown, *Inorg. Chem.* **1975**, *14*, 2856
16. B. Hapke, F. Graham, *Icarus* **1989**, *79*, 47
17. R. Steudel, *Doctoral Dissertation*, Technische Universität Berlin, Berlin, **1965**
18. H. Cordes, P.W. Schenk, *Z. Anorg. Allg. Chem.* **1933**, *214*, 33
19. P.W. Schenk, *Z. Anorg. Allg. Chem.* **1951**, *265*, 169 and **1941**, *248*, 297 and **1937**, *233*, 385
20. A. R. V. Murthy, T.R.N. Kutty, D. K. Sharma, *Int. J. Sulfur Chem. B* **1971**, *6*, 161
21. J.T. Herron, R.E. Huie, *Chem. Phys. Lett.* **1980**, *76*, 322
22. J.R. Spencer, A. S. McEwen, M. A. McGrath, P. Sartoretto, D. B. Nash, K. S. Noll, D. Gilmore, *Icarus* **1997**, *127*, 221. B. Hapke, *Icarus* **1989**, *79*, 56
23. Y.C. Na, L. W. Esposito, *Icarus* **1997**, *125*, 364
24. D.J. Meschi, R.J. Myers, *J. Mol. Spectrosc.* **1959**, *3*, 405
25. E. Tiemann, J. Hoefl, F.J. Lovas, D.R. Johnson, *J. Chem. Phys.* **1974**, *60*, 5000
26. J. Lindenmayer, H. D. Rudolph, H. Jones, *J. Mol. Spectrosc.* **1986**, *119*, 56. J. Lindenmayer, *J. mol. Spectrosc.* **1986**, *116*, 315
27. C.J. Marsden, B. J. Smith, *Chem. Phys.* **1990**, *141*, 325
28. T. Fueno, R.J. Buenker, *Theor. Chim. Acta* **1988**, *73*, 123; J. Ivanic, G. J. Atchity, K. Ruedenberg, *J. Chem. Phys.* **1997**, *107*, 4307
29. R.O. Jones, *Chem. Phys. Lett.* **1986**, *125*, 221
30. A.V. Jones, *J. Phys. Chem.* **1950**, *18*, 1263
31. R. Steudel, P.W. Schenk, J. Bilal, *Z. Anorg. Allg. Chem.* **1967**, *353*, 250
32. R. Steudel, *Habilitatiosschrift*, Technische Universität Berlin, Berlin, **1969**
33. A.G. Hopkins, F.P. Daly, C.W. Brown, *J. Phys. Chem.* **1975**, *79*, 1849
34. C. D. Paulse, R.A. Porier, R.W. Davis, *Chem. Phys. Lett.* **1990**, *172*, 43
35. G. Lakshminarayana, *J. Mol. Spectrosc.* **1975**, *55*, 141
36. R.N. Dixon, D.A. Haner, C. R. Webster, *Chem. Phys.* **1977**, *22*, 199
37. L.F. Phillips, J. J. Smith, B. Meyer, *J. Mol. Spectrosc.* **1969**, *29*, 230
38. C.L. Chiu, P.C. Sung, L.D. Chen, *J. Mol. Spectrosc.* **1982**, *94*, 343
39. K. Tsukiyama, D. Kobayashi, K. Obi, I. Tanaka, *Chem. Phys.* **1984**, *84*, 337
40. J. Lindenmayer, H. Jones, *J. Mol. Spectrosc.* **1985**, *112*, 71
41. D.J. Clouthier, *J. Mol. Spectrosc.* **1987**, *124*, 179
42. D.J. Clouthier, M. L. Rutherford, *Chem. Phys.* **1988**, *127*, 189
43. M.E. Jacox, *Phys. Chem. Ref. Data* **1990**, *19*, 1387
44. T. Müller, P.H. Vaccaro, F. Pérez-Bernal, F. Iachello, *J. Chem. Phys.* **1999**, *111*, 5038
45. Q. Zhang, P. Dupre, B. Grzybowski, P.H. Vaccaro, *J. Chem. Phys.* **1995**, *103*, 67
46. T. Müller, P.H. Vaccaro, F. Perez-Bernal, F. Iachello, *Chem. Phys. Lett.* **2000**, *329*, 271
47. F. Iachello, F. Perez-Bernal, T. Müller, P.H. Vaccaro, *J. Chem. Phys.* **2000**, *112*, 6507
48. K. Norwood, C.Y. Ng, *Chem. Phys. Lett.* **1989**, *156*, 145
49. B.-M. Cheng, W.-C. Hung, *J. Chem. Phys.* **1999**, *110*, 188
50. R.D. Davy, E Skoumbourdis, *Mol. Phys.* **1998**, *94*, 539
51. P.W. Schenk, R. Steudel, *Z. Anorg. Allg. Chem.* **1966**, *342*, 263
52. Reviews on  $S_2O$  complexes: A. F. Hill, *Adv. Organomet. Chem.* **1994**, *36*, 159; K. K. Pandey, *Progr. Inorg. Chem.* **1992**, *40*, 445; W. A. Schenk, *Angew. Chem.* **1987**, *99*, 101, *Angew. Chem. Int. Ed. Engl.* **1987**, *26*, 98
53. G.A. Urove, M.E. Welker, *Organometallics* **1988**, *7*, 1013; B. L. Hayes, M.E. Welker, *Organometallics* **1998**, *17*, 5534; A. Ishii, T. Kawai, K. Tekura, H. Oshida, J. Nakayama, *Angew. Chem.* **2001**, *113*, 1978, *Angew. Chem. Int. Ed.* **2001**, *40*, 1924
54. A. Ishii, M. Nakabayashi, J. Nakayama, *J. Am. Chem. Soc.* **1999**, *121*, 7959. A. Ishii, M. Nakabayashi, Y.-N. Jin, J. Nakayama, *J. Organomet. Chem.* **2000**, *611*, 127
55. F.J. Lovas, E. Tiemann, D.R. Johnson, *J. Chem. Phys.* **1974**, *60*, 5005
56. C. Groves, E. Lewars, *J. Mol. Struct. (Theochem)* **2000**, *530*, 265

57. C.J. Marsden, B. J. Smith, *Chem. Phys.* **1990**, *141*, 335
58. F. Cacace, G. de Petris, M. Rosi, A. Troiani, *Chem. Commun.* **2001**, 2086
59. R. Steudel, J. Steidel, *Angew. Chem.* **1978**, *90*, 134; *Angew. Chem. Int. Ed. Engl.* **1978**, *17*, 134
60. J. Steidel, *Doctoral Dissertation*, Technische Universität Berlin, **1983**
61. R. Steudel, J. Steidel, J. Pickardt, *Angew. Chem.* **1980**, *92*, 313; *Angew. Chem. Int. Ed. Engl.* **1980**, *19*, 325
62. R. Steudel, J. Steidel, T. Sandow, F. Schuster, *Z. Naturforsch. Part B* **1978**, *33*, 1198
63. R. Steudel, T. Sandow, *Angew. Chem.* **1976**, *88*, 854; *Angew. Chem. Int. Ed. Engl.* **1976**, *15*, 772
64. R. Steudel, R. Reinhardt, T. Sandow, *Angew. Chem.* **1977**, *89*, 757; *Angew. Chem. Int. Ed. Engl.* **1977**, *16*, 716
65. R. Reinhardt, *Doctoral Dissertation*, Freie Universität Berlin, Berlin, **1978**
66. D. Hohl, R.O. Jones, R. Car, M. Parinello, *J. Am. Chem. Soc.* **1989**, *111*, 825. R.O. Jones, D. Hohl, *Int. J. Quantum Chem.: Quant. Chem. Symp.* **1990**, *24*, 141
67. R. Steudel, T. Sandow, *Angew. Chem.* **1978**, *90*, 644; *Angew. Chem. Int. Ed. Engl.* **1978**, *17*, 611
68. R.O. Jones, *Inorg. Chem.* **1994**, *33*, 1340
69. R. Steudel, M. Rebsch, *Angew. Chem.* **1972**, *84*, 344; *Angew. Chem. Int. Ed. Engl.* **1972**, *11*, 302
70. R. Steudel, M. Rebsch, *Z. Anorg. Allg. Chem.* **1975**, *413*, 252
71. R. Steudel, *Top. Curr. Chem.* **2004**, *231*, in print
72. R. Steudel, J. Latte, *Angew. Chem.* **1974**, *86*, 648; *Angew. Chem. Int. Ed. Engl.* **1974**, *13*, 603
73. R. Steudel, T. Sandow, *Inorg. Synthesis* **1982**, *21*, 172
74. R. Steudel, P. Luger, H. Bradaczek, M. Rebsch, *Angew. Chem.* **1973**, *85*, 452; *Angew. Chem. Int. Ed. Engl.* **1973**, *12*, 423
75. P. Luger, H. Bradaczek, R. Steudel, M. Rebsch, *Chem. Ber.* **1976**, *109*, 180
76. R. Steudel, *Angew. Chem.* **1975**, *87*, 683; *Angew. Chem. Int. Ed. Engl.* **1975**, *14*, 655
77. R. Steudel, *Top. Curr. Chem.* **1982**, *102*, 149
78. R. Steudel, M. Rebsch, *J. Mol. Spectrosc.* **1974**, *51*, 334
79. R. Steudel, D. F. Eggers, *Spectrochim. Acta Part A* **1975**, *31*, 871
80. I. Lindquist, *Inorganic Adduct Molecules of Oxo-Compounds*, Springer, Berlin, **1963**
81. R. Steudel, T. Sandow, J. Steidel, *J. Chem. Soc. Chem. Commun.* **1980**, 180
82. R. Steudel, J. Steidel, T. Sandow, *Z. Naturforsch. Part B* **1986**, *41*, 951
83. R. Steudel, T. Sandow, J. Steidel, *Z. Naturforsch. Part B* **1985**, *40*, 594
84. R. Steudel, *Z. Naturforsch. Part B* **1975**, *30*, 281
85. R. Steudel, K. Bergemann, J. Buschmann, P. Luger, *Inorg. Chem.* **1996**, *35*, 2184
86. R. Steudel, J. Steidel, R. Reinhardt, *Z. Naturforsch. Part B* **1983**, *38*, 1548
87. P.W. Schenk, *Z. Anorg. Allg. Chem.* **1941**, *248*, 297 and **1951**, *265*, 169. P.W. Schenk, W. Kretschmer, *Angew. Chem.* **1962**, *74*, 695. M. Schmidt, D. Eichelsdörfer, *Z. Anorg. Allg. Chem.* **1964**, *330*, 130
88. P.W. Schenk, R. Steudel, R. Ludwig, J. Bilal, *Ann. Genie Chim.* **1967**, *3*, 82. R. Ludwig, *Doctoral Dissertation*, Technische Universität Berlin, **1969**
89. M. W. Wong, personal communication of unpublished results, **2002**

---

## Author Index Volumes 201–231

*Author Index Vols. 26–50 see Vol. 50*

*Author Index Vols. 51–100 see Vol. 100*

*Author Index Vols. 101–150 see Vol. 150*

*Author Index Vols. 151–200 see Vol. 200*

*The volume numbers are printed in italics*

- Achilefu S, Dorshow RB (2002) Dynamic and Continuous Monitoring of Renal and Hepatic Functions with Exogenous Markers. *222*: 31–72
- Albert M, see Dax K (2001) *215*: 193–275
- Angyal SJ (2001) The Lobry de Bruyn-Alberda van Ekenstein Transformation and Related Reactions. *215*: 1–14
- Armentrout PB (2003) Threshold Collision-Induced Dissociations for the Determination of Accurate Gas-Phase Binding Energies and Reaction Barriers. *225*: 227–256
- Astruc D, Blais J-C, Cloutet E, Djakovitch L, Rigaut S, Ruiz J, Sartor V, Valério C (2000) The First Organometallic Dendrimers: Design and Redox Functions. *210*: 229–259
- Augé J, see Lubineau A (1999) *206*: 1–39
- Baars MWPL, Meijer EW (2000) Host-Guest Chemistry of Dendritic Molecules. *210*: 131–182
- Balczewski P, see Mikolajczyk M (2003) *223*: 161–214
- Ballauff M (2001) Structure of Dendrimers in Dilute Solution. *212*: 177–194
- Baltzer L (1999) Functionalization and Properties of Designed Folded Polypeptides. *202*: 39–76
- Balzani V, Ceroni P, Maestri M, Saudan C, Vicinelli V (2003) Luminescent Dendrimers. *Recent Advances*. *228*: 159–191
- Barré L, see Lasne M-C (2002) *222*: 201–258
- Bartlett RJ, see Sun J-Q (1999) *203*: 121–145
- Bertrand G, Bourissou D (2002) Diphosphorus-Containing Unsaturated Three-Membered Rings: Comparison of Carbon, Nitrogen, and Phosphorus Chemistry. *220*: 1–25
- Betzemeier B, Knochel P (1999) Perfluorinated Solvents – a Novel Reaction Medium in Organic Chemistry. *206*: 61–78
- Bibette J, see Schmitt V (2003) *227*: 195–215
- Blais J-C, see Astruc D (2000) *210*: 229–259
- Bogár F, see Pipek J (1999) *203*: 43–61
- Bohme DK, see Petrie S (2003) *225*: 35–73
- Bourissou D, see Bertrand G (2002) *220*: 1–25
- Bowers MT, see Wyttenbach T (2003) *225*: 201–226
- Brand SC, see Haley MM (1999) *201*: 81–129
- Bray KL (2001) High Pressure Probes of Electronic Structure and Luminescence Properties of Transition Metal and Lanthanide Systems. *213*: 1–94
- Bronstein LM (2003) Nanoparticles Made in Mesoporous Solids. *226*: 55–89
- Brönstrup M (2003) High Throughput Mass Spectrometry for Compound Characterization in Drug Discovery. *225*: 275–294
- Brücher E (2002) Kinetic Stabilities of Gadolinium(III) Chelates Used as MRI Contrast Agents. *221*: 103–122
- Brunel JM, Buono G (2002) New Chiral Organophosphorus catalysts in Asymmetric Synthesis. *220*: 79–106
- Buchwald SL, see Muci A R (2002) *219*: 131–209
- Bunz UHF (1999) Carbon-Rich Molecular Objects from Multiply Ethynylated *p*-Complexes. *201*: 131–161
- Buono G, see Brunel JM (2002) *220*: 79–106

- Cadierno V, see Majoral J-P (2002) 220: 53–77  
Caminade A-M, see Majoral J-P (2003) 223: 111–159  
Carmichael D, Mathey F (2002) New Trends in Phosphametalocene Chemistry. 220: 27–51  
Caruso F (2003) Hollow Inorganic Capsules via Colloid-Templated Layer-by-Layer Electrostatic Assembly. 227: 145–168  
Caruso RA (2003) Nanocasting and Nanocoating. 226: 91–118  
Ceroni P, see Balzani V (2003) 228: 159–191  
Chamberlin AR, see Gilmore MA (1999) 202: 77–99  
Chivers T (2003) Imido Analogues of Phosphorus Oxo and Chalcogenido Anions. 229: 143–159  
Chow H-F, Leung C-F, Wang G-X, Zhang J (2001) Dendritic Oligoethers. 217: 1–50  
Clarkson RB (2002) Blood-Pool MRI Contrast Agents: Properties and Characterization. 221: 201–235  
Cloutet E, see Astruc D (2000) 210: 229–259  
Co CC, see Hentze H-P (2003) 226: 197–223  
Cooper DL, see Raimondi M (1999) 203: 105–120  
Cornils B (1999) Modern Solvent Systems in Industrial Homogeneous Catalysis. 206: 133–152  
Corot C, see Idee J-M (2002) 222: 151–171  
Crépy KVL, Imamoto T (2003) New P-Chirogenic Phosphine Ligands and Their Use in Catalytic Asymmetric Reactions. 229: 1–40  
Cristau H-J, see Taillefer M (2003) 229: 41–73  
Crooks RM, Lemon III BI, Yeung LK, Zhao M (2001) Dendrimer-Encapsulated Metals and Semiconductors: Synthesis, Characterization, and Applications. 212: 81–135  
Croteau R, see Davis EM (2000) 209: 53–95  
Crouzel C, see Lasne M-C (2002) 222: 201–258  
Curran DP, see Maul JJ (1999) 206: 79–105  
Currie F, see Häger M (2003) 227: 53–74  
Davidson P, see Gabriel J-C P (2003) 226: 119–172  
Davis EM, Croteau R (2000) Cyclization Enzymes in the Biosynthesis of Monoterpenes, Sesquiterpenes and Diterpenes. 209: 53–95  
Davies JA, see Schwert DD (2002) 221: 165–200  
Dax K, Albert M (2001) Rearrangements in the Course of Nucleophilic Substitution Reactions. 215: 193–275  
de Keizer A, see Kleinjan WE (2003) 230: 167–188  
de la Plata BC, see Ruano JLG (1999) 204: 1–126  
de Meijere A, Kozhushkov SI (1999) Macrocyclic Structurally Homoconjugated Oligoacetylenes: Acetylene- and Diacetylene-Expanded Cycloalkanes and Rotanes. 201: 1–42  
de Meijere A, Kozhushkov SI, Khlebnikov AF (2000) Bicyclopropylidene – A Unique Tetra-substituted Alkene and a Versatile C<sub>6</sub>-Building Block. 207: 89–147  
de Meijere A, Kozhushkov SI, Hadjiaraoglou LP (2000) Alkyl 2-Chloro-2-cyclopropylideneacetates – Remarkably Versatile Building Blocks for Organic Synthesis. 207: 149–227  
Dennig J (2003) Gene Transfer in Eukaryotic Cells Using Activated Dendrimers. 228: 227–236  
de Raadt A, Fechter MH (2001) Miscellaneous. 215: 327–345  
Desreux JF, see Jacques V (2002) 221: 123–164  
Diederich F, Gobbi L (1999) Cyclic and Linear Acetylenic Molecular Scaffolding. 201: 43–79  
Diederich F, see Smith DK (2000) 210: 183–227  
Djakovitch L, see Astruc D (2000) 210: 229–259  
Dolle F, see Lasne M-C (2002) 222: 201–258  
Donges D, see Yersin H (2001) 214: 81–186  
Dormán G (2000) Photoaffinity Labeling in Biological Signal Transduction. 211: 169–225  
Dorn H, see McWilliams AR (2002) 220: 141–167  
Dorshow RB, see Achilefu S (2002) 222: 31–72  
Drabowicz J, Mikołajczyk M (2000) Selenium at Higher Oxidation States. 208: 143–176  
Eckert B, see Steudel R (2003) 230: 1–79  
Eckert B, Steudel R (2003) Molecular Spectra of Sulfur Molecules and Solid Sulfur Allotropes. 231: 31–97

- Ehse M, Romerosa A, Peruzzini M (2002) Metal-Mediated Degradation and Reaggregation of White Phosphorus. *220*: 107–140
- Eder B, see Wrodnigg TM (2001) The Amadori and Heyns Rearrangements: Landmarks in the History of Carbohydrate Chemistry or Unrecognized Synthetic Opportunities? *215*: 115–175
- Edwards DS, see Liu S (2002) *222*: 259–278
- Elaissari A, Ganachaud F, Pichot C (2003) Biorelevant Latexes and Microgels for the Interaction with Nucleic Acids. *227*: 169–193
- Esumi K (2003) Dendrimers for Nanoparticle Synthesis and Dispersion Stabilization. *227*: 31–52
- Famulok M, Jenne A (1999) Catalysis Based on Nucleic Acid Structures. *202*: 101–131
- Fechter MH, see de Raadt A (2001) *215*: 327–345
- Ferrier RJ (2001) Substitution-with-Allylic-Rearrangement Reactions of Glycal Derivatives. *215*: 153–175
- Ferrier RJ (2001) Direct Conversion of 5,6-Unsaturated Hexopyranosyl Compounds to Functionalized Glycohexanones. *215*: 277–291
- Frey H, Schlenk C (2000) Silicon-Based Dendrimers. *210*: 69–129
- Förster S (2003) Amphiphilic Block Copolymers for Templating Applications. *226*: 1–28
- Frullano L, Rohovec J, Peters JA, Geraldes CFGC (2002) Structures of MRI Contrast Agents in Solution. *221*: 25–60
- Fugami K, Kosugi M (2002) Organotin Compounds. *219*: 87–130
- Führhop J-H, see Li G (2002) *218*: 133–158
- Furukawa N, Sato S (1999) New Aspects of Hypervalent Organosulfur Compounds. *205*: 89–129
- Gabriel J-C P, Davidson P (2003) Mineral Liquid Crystals from Self-Assembly of Anisotropic Nanosystems. *226*: 119–172
- Gamelin DR, Güdel HU (2001) Upconversion Processes in Transition Metal and Rare Earth Metal Systems. *214*: 1–56
- Ganachaud F, see Elaissari A (2003) *227*: 169–193
- García R, see Tromas C (2002) *218*: 115–132
- Geraldes CFGC, see Frullano L (2002) *221*: 25–60
- Gilmore MA, Steward LE, Chamberlin AR (1999) Incorporation of Noncoded Amino Acids by In Vitro Protein Biosynthesis. *202*: 77–99
- Glasbeek M (2001) Excited State Spectroscopy and Excited State Dynamics of Rh(III) and Pd(II) Chelates as Studied by Optically Detected Magnetic Resonance Techniques. *213*: 95–142
- Glass RS (1999) Sulfur Radical Cations. *205*: 1–87
- Gobbi L, see Diederich F (1999) *201*: 43–129
- Göltner-Spickermann C (2003) Nanocasting of Lyotropic Liquid Crystal Phases for Metals and Ceramics. *226*: 29–54
- Gouzy M-F, see Li G (2002) *218*: 133–158
- Gries H (2002) Extracellular MRI Contrast Agents Based on Gadolinium. *221*: 1–24
- Gruber C, see Tovar GEM (2003) *227*: 125–144
- Güdel HU, see Gamelin DR (2001) *214*: 1–56
- Guga P, Okruszek A, Stec WJ (2002) Recent Advances in Stereocontrolled Synthesis of P-Chiral Analogues of Biophosphates. *220*: 169–200
- Gulea M, Masson S (2003) Recent Advances in the Chemistry of Difunctionalized Organophosphorus and -Sulfur Compounds. *229*: 161–198
- Hackmann-Schlichter N, see Krause W (2000) *210*: 261–308
- Hadjiraoglou LP, see de Meijere A (2000) *207*: 149–227
- Häger M, Currie F, Holmberg K (2003) Organic Reactions in Microemulsions. *227*: 53–74
- Häusler H, Stütz AE (2001) d-Xylose (d-Glucose) Isomerase and Related Enzymes in Carbohydrate Synthesis. *215*: 77–114
- Haley MM, Pak JJ, Brand SC (1999) Macrocyclic Oligo(phenylacetylenes) and Oligo(phenyldiacetylenes). *201*: 81–129
- Harada A, see Yamaguchi H (2003) *228*: 237–258
- Hartmann T, Ober D (2000) Biosynthesis and Metabolism of Pyrrolizidine Alkaloids in Plants and Specialized Insect Herbivores. *209*: 207–243
- Haseley SR, Kamerling JP, Vliegthart JFG (2002) Unravelling Carbohydrate Interactions with Biosensors Using Surface Plasmon Resonance (SPR) Detection. *218*: 93–114

- Hassner A, see Namboothiri INN (2001) 216: 1–49
- Helm L, see Tóth E (2002) 221: 61–101
- Hemscheidt T (2000) Tropane and Related Alkaloids. 209: 175–206
- Hentze H-P, Co CC, McKelvey CA, Kaler EW (2003) Templating Vesicles, Microemulsions and Lyotropic Mesophases by Organic Polymerization Processes. 226: 197–223
- Hergenrother PJ, Martin SF (2000) Phosphatidylcholine-Preferring Phospholipase C from *B. cereus*. Function, Structure, and Mechanism. 211: 131–167
- Hermann C, see Kuhlmann J (2000) 211: 61–116
- Heydt H (2003) The Fascinating Chemistry of Triphosphabenzenes and Valence Isomers. 223: 215–249
- Hirsch A, Vostrowsky O (2001) Dendrimers with Carbon Rich-Cores. 217: 51–93
- Hiyama T, Shirakawa E (2002) Organosilicon Compounds. 219: 61–85
- Holmberg K, see Häger M (2003) 227: 53–74
- Houseman BT, Mrksich M (2002) Model Systems for Studying Polyvalent Carbohydrate Binding Interactions. 218: 1–44
- Hricoviniová Z, see Petruš L (2001) 215: 15–41
- Idee J-M, Tichowsky I, Port M, Petta M, Le Lem G, Le Greneur S, Meyer D, Corot C (2002) Iodinated Contrast Media: from Non-Specific to Blood-Pool Agents. 222: 151–171
- Igau A, see Majoral J-P (2002) 220: 53–77
- Imamoto T, see Crépy KVL (2003) 229: 1–40
- Iwaoka M, Tomoda S (2000) Nucleophilic Selenium. 208: 55–80
- Iwasawa N, Narasaka K (2000) Transition Metal Promoted Ring Expansion of Alkynyl- and Propadienylcyclopropanes. 207: 69–88
- Imperiali B, McDonnell KA, Shogren-Knaak M (1999) Design and Construction of Novel Peptides and Proteins by Tailored Incorporation of Coenzyme Functionality. 202: 1–38
- Ito S, see Yoshifuji M (2003) 223: 67–89
- Jacques V, Desreux JF (2002) New Classes of MRI Contrast Agents. 221: 123–164
- James TD, Shinkai S (2002) Artificial Receptors as Chemosensors for Carbohydrates. 218: 159–200
- Janssen AJH, see Kleinjan WE (2003) 230: 167–188
- Jenne A, see Famulok M (1999) 202: 101–131
- Junker T, see Trauger SA (2003) 225: 257–274
- Kaler EW, see Hentze H-P (2003) 226: 197–223
- Kamerling JP, see Haseley SR (2002) 218: 93–114
- Kashemirov BA, see Mc Kenna CE (2002) 220: 201–238
- Kato S, see Murai T (2000) 208: 177–199
- Katti KV, Pillarsetty N, Raghuraman K (2003) New Vistas in Chemistry and Applications of Primary Phosphines. 229: 121–141
- Kawa M (2003) Antenna Effects of Aromatic Dendrons and Their Luminescence Applications. 228: 193–204
- Kee TP, Nixon TD (2003) The Asymmetric Phospho-Aldol Reaction. Past, Present, and Future. 223: 45–65
- Khlebnikov AF, see de Meijere A (2000) 207: 89–147
- Kim K, see Lee JW (2003) 228: 111–140
- Kirtman B (1999) Local Space Approximation Methods for Correlated Electronic Structure Calculations in Large Delocalized Systems that are Locally Perturbed. 203: 147–166
- Kita Y, see Tohma H (2003) 224: 209–248
- Kleij AW, see Kreiter R (2001) 217: 163–199
- Klein Gebbink RJM, see Kreiter R (2001) 217: 163–199
- Kleinjan WE, de Keizer A, Janssen AJH (2003) Biologically Produced Sulfur. 230: 167–188
- Klibanov AL (2002) Ultrasound Contrast Agents: Development of the Field and Current Status. 222: 73–106
- Klopper W, Kutzelnigg W, Müller H, Noga J, Vogtner S (1999) Extremal Electron Pairs – Application to Electron Correlation, Especially the R12 Method. 203: 21–42
- Knochel P, see Betzemeier B (1999) 206: 61–78
- Koser GF (2003) C-Heteroatom-Bond Forming Reactions. 224: 137–172

- Koser GF (2003) Heteroatom-Heteroatom-Bond Forming Reactions. *224*: 173–183
- Kosugi M, see Fugami K (2002) *219*: 87–130
- Kozhushkov SI, see de Meijere A (1999) *201*: 1–42
- Kozhushkov SI, see de Meijere A (2000) *207*: 89–147
- Kozhushkov SI, see de Meijere A (2000) *207*: 149–227
- Krause W (2002) Liver-Specific X-Ray Contrast Agents. *222*: 173–200
- Krause W, Hackmann-Schlichter N, Maier FK, Müller R (2000) Dendrimers in Diagnostics. *210*: 261–308
- Krause W, Schneider PW (2002) Chemistry of X-Ray Contrast Agents. *222*: 107–150
- Kräuter I, see Tovar GEM (2003) *227*: 125–144
- Kreiter R, Kleij AW, Klein Gebbink RJM, van Koten G (2001) Dendritic Catalysts. *217*: 163–199
- Krossing I (2003) Homoatomic Sulfur Cations. *230*: 135–152
- Kuhlmann J, Herrmann C (2000) Biophysical Characterization of the Ras Protein. *211*: 61–116
- Kunkely H, see Vogler A (2001) *213*: 143–182
- Kutzelnigg W, see Klopper W (1999) *203*: 21–42
- Lammertsma K (2003) Phosphinidenes. *229*: 95–119
- Landfester K (2003) Miniemulsions for Nanoparticle Synthesis. *227*: 75–123
- Lasne M-C, Perrio C, Rouden J, Barré L, Roeda D, Dolle F, Cruzel C (2002) Chemistry of  $b^+$ -Emitting Compounds Based on Fluorine-18. *222*: 201–258
- Lawless LJ, see Zimmermann SC (2001) *217*: 95–120
- Leal-Calderon F, see Schmitt V (2003) *227*: 195–215
- Lee JW, Kim K (2003) Rotaxane Dendrimers. *228*: 111–140
- Le Greneur S, see Idee J-M (2002) *222*: 151–171
- Le Lem G, see Idee J-M (2002) *222*: 151–171
- Leitner W (1999) Reactions in Supercritical Carbon Dioxide ( $scCO_2$ ). *206*: 107–132
- Lemon III BI, see Crooks RM (2001) *212*: 81–135
- Leung C-F, see Chow H-F (2001) *217*: 1–50
- Levitzi A (2000) Protein Tyrosine Kinase Inhibitors as Therapeutic Agents. *211*: 1–15
- Li G, Gouzy M-F, Fuhrhop J-H (2002) Recognition Processes with Amphiphilic Carbohydrates in Water. *218*: 133–158
- Li X, see Paldus J (1999) *203*: 1–20
- Licha K (2002) Contrast Agents for Optical Imaging. *222*: 1–29
- Linclau B, see Maul JJ (1999) *206*: 79–105
- Lindhorst TK (2002) Artificial Multivalent Sugar Ligands to Understand and Manipulate Carbohydrate-Protein Interactions. *218*: 201–235
- Lindhorst TK, see Röckendorf N (2001) *217*: 201–238
- Liu S, Edwards DS (2002) Fundamentals of Receptor-Based Diagnostic Metalloradiopharmaceuticals. *222*: 259–278
- Liz-Marzán L, see Mulvaney P (2003) *226*: 225–246
- Loudet JC, Poulin P (2003) Monodisperse Aligned Emulsions from Demixing in Bulk Liquid Crystals. *226*: 173–196
- Lubineau A, Augé J (1999) Water as Solvent in Organic Synthesis. *206*: 1–39
- Lundt I, Madsen R (2001) Synthetically Useful Base Induced Rearrangements of Aldonolactones. *215*: 177–191
- Loupy A (1999) Solvent-Free Reactions. *206*: 153–207
- Madsen R, see Lundt I (2001) *215*: 177–191
- Maestri M, see Balzani V (2003) *228*: 159–191
- Maier FK, see Krause W (2000) *210*: 261–308
- Majoral J-P, Caminade A-M (2003) What to do with Phosphorus in Dendrimer Chemistry. *223*: 111–159
- Majoral J-P, Igau A, Cadierno V, Zablocka M (2002) Benzyne-Zirconocene Reagents as Tools in Phosphorus Chemistry. *220*: 53–77
- Manners I (2002), see McWilliams AR (2002) *220*: 141–167
- March NH (1999) Localization via Density Functionals. *203*: 201–230
- Martin SF, see Hergenrother PJ (2000) *211*: 131–167
- Mashiko S, see Yokoyama S (2003) *228*: 205–226

- Masson S, see Gulea M (2003) 229: 161–198
- Mathey F, see Carmichael D (2002) 220: 27–51
- Maul JJ, Ostrowski PJ, Ublacker GA, Linclau B, Curran DP (1999) Benzotrifluoride and Derivates: Useful Solvents for Organic Synthesis and Fluorous Synthesis. 206: 79–105
- McDonnell KA, see Imperiali B (1999) 202: 1–38
- McKelvey CA, see Hentze H-P (2003) 226: 197–223
- Mc Kenna CE, Kashemirov BA (2002) Recent Progress in Carbonylphosphonate Chemistry. 220: 201–238
- McWilliams AR, Dorn H, Manners I (2002) New Inorganic Polymers Containing Phosphorus. 220: 141–167
- Meijer EW, see Baars MWPL (2000) 210: 131–182
- Merbach AE, see Tóth E (2002) 221: 61–101
- Metzner P (1999) Thiocarbonyl Compounds as Specific Tools for Organic Synthesis. 204: 127–181
- Meyer D, see Idee J-M (2002) 222: 151–171
- Mezey PG (1999) Local Electron Densities and Functional Groups in Quantum Chemistry. 203: 167–186
- Mikołajczyk M, Balczewski P (2003) Phosphonate Chemistry and Reagents in the Synthesis of Biologically Active and Natural Products. 223: 161–214
- Mikołajczyk M, see Drabowicz J (2000) 208: 143–176
- Miura M, Nomura M (2002) Direct Arylation via Cleavage of Activated and Unactivated C-H Bonds. 219: 211–241
- Miyaura N (2002) Organoboron Compounds. 219: 11–59
- Miyaura N, see Tamao K (2002) 219: 1–9
- Möller M, see Sheiko SS (2001) 212: 137–175
- Morales JC, see Rojo J (2002) 218: 45–92
- Mori H, Müller A (2003) Hyperbranched (Meth)acrylates in Solution, in the Melt, and Grafted From Surfaces. 228: 1–37
- Mrksich M, see Houseman BT (2002) 218: 1–44
- Muci AR, Buchwald SL (2002) Practical Palladium Catalysts for C-N and C-O Bond Formation. 219: 131–209
- Müllen K, see Wiesler U-M (2001) 212: 1–40
- Müller A, see Mori H (2003) 228: 1–37
- Müller G (2000) Peptidomimetic SH2 Domain Antagonists for Targeting Signal Transduction. 211: 17–59
- Müller H, see Klopffer W (1999) 203: 21–42
- Müller R, see Krause W (2000) 210: 261–308
- Mulvaney P, Liz-Marzán L (2003) Rational Material Design Using Au Core-Shell Nanocrystals. 226: 225–246
- Murai T, Kato S (2000) Selenocarbonyls. 208: 177–199
- Muscat D, van Benthem RATM (2001) Hyperbranched Polyesteramides – New Dendritic Polymers. 212: 41–80
- Naka K (2003) Effect of Dendrimers on the Crystallization of Calcium Carbonate in Aqueous Solution. 228: 141–158
- Nakahama T, see Yokoyama S (2003) 228: 205–226
- Nakayama J, Sugihara Y (1999) Chemistry of Thiophene 1,1-Dioxides. 205: 131–195
- Namboothiri INN, Hassner A (2001) Stereoselective Intramolecular 1,3-Dipolar Cycloadditions. 216: 1–49
- Narasaka K, see Iwasawa N (2000) 207: 69–88
- Nierengarten J-F (2003) Fullerodendrimers: Fullerene-Containing Macromolecules with Intriguing Properties. 228: 87–110
- Nishibayashi Y, Uemura S (2000) Selenoxide Elimination and [2,3] Sigmatropic Rearrangements. 208: 201–233
- Nishibayashi Y, Uemura S (2000) Selenium Compounds as Ligands and Catalysts. 208: 235–255
- Nixon TD, see Kee TP (2003) 223: 45–65

- Noga J, see Klopper W (1999) 203: 21–42
- Nomura M, see Miura M (2002) 219: 211–241
- Nubbemeyer U (2001) Synthesis of Medium-Sized Ring Lactams. 216: 125–196
- Nummelin S, Skrifvars M, Rissanen K (2000) Polyester and Ester Functionalized Dendrimers. 210: 1–67
- Ober D, see Hemscheidt T (2000) 209: 175–206
- Ochiai M (2003) Reactivities, Properties and Structures. 224: 5–68
- Okazaki R, see Takeda N (2003) 231:153-202
- Okruszek A, see Guga P (2002) 220: 169–200
- Okuno Y, see Yokoyama S (2003) 228: 205–226
- Onitsuka K, Takahashi S (2003) Metallodendrimers Composed of Organometallic Building Blocks. 228: 39–63
- Osanai S (2001) Nickel (II) Catalyzed Rearrangements of Free Sugars. 215: 43–76
- Ostrowski PJ, see Maul JJ (1999) 206: 79–105
- Otomo A, see Yokoyama S (2003) 228: 205–226
- Pak JJ, see Haley MM (1999) 201: 81–129
- Paldus J, Li X (1999) Electron Correlation in Small Molecules: Grafting CI onto CC. 203: 1–20
- Paleos CM, Tsiourvas D (2003) Molecular Recognition and Hydrogen-Bonded Amphiphilites. 227: 1–29
- Paulmier C, see Ponthieux S (2000) 208: 113–142
- Penadés S, see Rojo J (2002) 218: 45–92
- Perrio C, see Lasne M-C (2002) 222: 201–258
- Peruzzini M, see Ehse M (2002) 220: 107–140
- Peters JA, see Frullano L (2002) 221: 25–60
- Petrie S, Bohme DK (2003) Mass Spectrometric Approaches to Interstellar Chemistry. 225: 35–73
- Petruš L, Petrušová M, Hricovíniová (2001) The Břilik Reaction. 215: 15–41
- Petrušová M, see Petruš L (2001) 215: 15–41
- Petta M, see Idee J-M (2002) 222: 151–171
- Pichot C, see Elaissari A (2003) 227: 169–193
- Pillarsetty N, see Katti KV (2003) 229: 121–141
- Pipek J, Bogár F (1999) Many-Body Perturbation Theory with Localized Orbitals – Kapuy's Approach. 203: 43–61
- Plattner DA (2003) Metalorganic Chemistry in the Gas Phase: Insight into Catalysis. 225: 149–199
- Ponthieux S, Paulmier C (2000) Selenium-Stabilized Carbanions. 208: 113–142
- Port M, see Idee J-M (2002) 222: 151–171
- Poulin P, see Loudet JC (2003) 226: 173–196
- Raghuraman K, see Katti KV (2003) 229: 121–141
- Raimondi M, Cooper DL (1999) Ab Initio Modern Valence Bond Theory. 203: 105–120
- Reinhoudt DN, see van Manen H-J (2001) 217: 121–162
- Renaud P (2000) Radical Reactions Using Selenium Precursors. 208: 81–112
- Richardson N, see Schwert DD (2002) 221: 165–200
- Rigaut S, see Astruc D (2000) 210: 229–259
- Riley MJ (2001) Geometric and Electronic Information From the Spectroscopy of Six-Coordinate Copper(II) Compounds. 214: 57–80
- Rissanen K, see Nummelin S (2000) 210: 1–67
- Røeggen I (1999) Extended Geminal Models. 203: 89–103
- Röckendorf N, Lindhorst TK (2001) Glycodendrimers. 217: 201–238
- Roeda D, see Lasne M-C (2002) 222: 201–258
- Rohovec J, see Frullano L (2002) 221: 25–60
- Rojo J, Morales JC, Penadés S (2002) Carbohydrate-Carbohydrate Interactions in Biological and Model Systems. 218: 45–92
- Romerosa A, see Ehse M (2002) 220: 107–140
- Rouden J, see Lasne M-C (2002) 222: 201258

- Ruano JLG, de la Plata BC (1999) Asymmetric [4+2] Cycloadditions Mediated by Sulfoxides. *204*: 1–126
- Ruiz J, see Astruc D (2000) *210*: 229–259
- Rychnovsky SD, see Sinz CJ (2001) *216*: 51–92
- Salaün J (2000) Cyclopropane Derivates and their Diverse Biological Activities. *207*: 1–67
- Sanz-Cervera JF, see Williams RM (2000) *209*: 97–173
- Sartor V, see Astruc D (2000) *210*: 229–259
- Sato S, see Furukawa N (1999) *205*: 89–129
- Saudan C, see Balzani V (2003) *228*: 159–191
- Scherf U (1999) Oligo- and Polyarylenes, Oligo- and Polyarylenevinylenes. *201*: 163–222
- Schlenk C, see Frey H (2000) *210*: 69–129
- Schmitt V, Leal-Calderon F, Bibette J (2003) Preparation of Monodisperse Particles and Emulsions by Controlled Shear. *227*: 195–215
- Schoeller WW (2003) Donor-Acceptor Complexes of Low-Coordinated Cationic p-Bonded Phosphorus Systems. *229*: 75–94
- Schröder D, Schwarz H (2003) Diastereoselective Effects in Gas-Phase Ion Chemistry. *225*: 129–148
- Schwarz H, see Schröder D (2003) *225*: 129–148
- Schwert DD, Davies JA, Richardson N (2002) Non-Gadolinium-Based MRI Contrast Agents. *221*: 165–200
- Sheiko SS, Möller M (2001) Hyperbranched Macromolecules: Soft Particles with Adjustable Shape and Capability to Persistent Motion. *212*: 137–175
- Shen B (2000) The Biosynthesis of Aromatic Polyketides. *209*: 1–51
- Shinkai S, see James TD (2002) *218*: 159–200
- Shirakawa E, see Hiyama T (2002) *219*: 61–85
- Shogren-Knaak M, see Imperiali B (1999) *202*: 1–38
- Sinou D (1999) Metal Catalysis in Water. *206*: 41–59
- Sinz CJ, Rychnovsky SD (2001) 4-Acetoxy- and 4-Cyano-1,3-dioxanes in Synthesis. *216*: 51–92
- Siuzdak G, see Trauger SA (2003) *225*: 257–274
- Skrifvars M, see Nummelin S (2000) *210*: 1–67
- Smith DK, Diederich F (2000) Supramolecular Dendrimer Chemistry – A Journey Through the Branched Architecture. *210*: 183–227
- Stec WJ, see Guga P (2002) *220*: 169–200
- Stedel R (2003) Aqueous Sulfur Sols. *230*: 153–166
- Stedel R (2003) Liquid Sulfur. *230*: 80–116
- Stedel R (2003) Inorganic Polysulfanes  $H_2S_n$  with  $n > 1$ . *231*: 99–125
- Stedel R (2003) Inorganic Polysulfides  $S_n^{2-}$  and Radical Anions  $S_n^{\cdot-}$ . *231*: 127–152
- Stedel R (2003) Sulfur-Rich Oxides  $S_nO$  and  $S_nO_2$ . *231*: 203–230
- Stedel R, Eckert B (2003) Solid Sulfur Allotropes. *230*: 1–79
- Stedel R, see Eckert B (2003) *231*: 31–97
- Stedel R, Steudel Y, Wong MW (2003) Speciation and Thermodynamics of Sulfur Vapor. *230*: 117–134
- Stedel Y, see Steudel R (2003) *230*: 117–134
- Steward LE, see Gilmore MA (1999) *202*: 77–99
- Stocking EM, see Williams RM (2000) *209*: 97–173
- Streubel R (2003) Transient Nitrilium Phosphanylid Complexes: New Versatile Building Blocks in Phosphorus Chemistry. *223*: 91–109
- Stütz AE, see Häusler H (2001) *215*: 77–114
- Sugihara Y, see Nakayama J (1999) *205*: 131–195
- Sugiura K (2003) An Adventure in Macromolecular Chemistry Based on the Achievements of Dendrimer Science: Molecular Design, Synthesis, and Some Basic Properties of Cyclic Porphyrin Oligomers to Create a Functional Nano-Sized Space. *228*: 65–85
- Sun J-Q, Bartlett RJ (1999) Modern Correlation Theories for Extended, Periodic Systems. *203*: 121–145
- Sun L, see Crooks RM (2001) *212*: 81–135
- Surján PR (1999) An Introduction to the Theory of Geminals. *203*: 63–88

- Taillefer M, Cristau H-J (2003) New Trends in Ylide Chemistry. 229: 41–73
- Takahashi S, see Onitsuka K (2003) 228: 39–63
- Takeda N, Tokitoh N, Okazaki R (2003) Polysulfido Complexes of Main Group and Transition Metals. 231:153–202
- Tamao K, Miyaura N (2002) Introduction to Cross-Coupling Reactions. 219: 1–9
- ten Holte P, see Zwanenburg B (2001) 216: 93–124
- Thiem J, see Werschkun B (2001) 215: 293–325
- Thutewohl M, see Waldmann H (2000) 211: 117–130
- Tichkowsky I, see Idee J-M (2002) 222: 151–171
- Tiecco M (2000) Electrophilic Selenium, Selenocyclizations. 208: 7–54
- Tohma H, Kita Y (2003) Synthetic Applications (Total Synthesis and Natural Product Synthesis). 224: 209–248
- Tokitoh N, see Takeda N (2003) 231:153–202
- Tomoda S, see Iwaoka M (2000) 208: 55–80
- Tóth E, Helm L, Merbach AE (2002) Relaxivity of MRI Contrast Agents. 221: 61–101
- Tovar GEM, Kräuter I, Gruber C (2003) Molecularly Imprinted Polymer Nanospheres as Fully Affinity Receptors. 227: 125–144
- Trauger SA, Junker T, Siuzdak G (2003) Investigating Viral Proteins and Intact Viruses with Mass Spectrometry. 225: 257–274
- Tromas C, García R (2002) Interaction Forces with Carbohydrates Measured by Atomic Force Microscopy. 218: 115–132
- Tsiourvas D, see Paleos CM (2003) 227: 1–29
- Turecek F (2003) Transient Intermediates of Chemical Reactions by Neutralization-Reionization Mass Spectrometry. 225: 75–127
- Ublacker GA, see Maul JJ (1999) 206: 79–105
- Uemura S, see Nishibayashi Y (2000) 208: 201–233
- Uemura S, see Nishibayashi Y (2000) 208: 235–255
- Uggerud E (2003) Physical Organic Chemistry of the Gas Phase. Reactivity Trends for Organic Cations. 225: 1–34
- Valdemoro C (1999) Electron Correlation and Reduced Density Matrices. 203: 187–200
- Valério C, see Astruc D (2000) 210: 229–259
- van Benthem RATM, see Muscat D (2001) 212: 41–80
- van Koten G, see Kreiter R (2001) 217: 163–199
- van Manen H-J, van Veggel FCJM, Reinhoudt DN (2001) Non-Covalent Synthesis of Metallo-dendrimers. 217: 121–162
- van Veggel FCJM, see van Manen H-J (2001) 217: 121–162
- Varvoglis A (2003) Preparation of Hypervalent Iodine Compounds. 224: 69–98
- Verkade JG (2003) P(RNCH<sub>2</sub>CH<sub>2</sub>)<sub>3</sub>N: Very Strong Non-ionic Bases Useful in Organic Synthesis. 223: 1–44
- Vicinelli V, see Balzani V (2003) 228: 159–191
- Vliegenthart JFG, see Haseley SR (2002) 218: 93–114
- Vogler A, Kunkely H (2001) Luminescent Metal Complexes: Diversity of Excited States. 213: 143–182
- Vogtner S, see Klopper W (1999) 203: 21–42
- Vostrowsky O, see Hirsch A (2001) 217: 51–93
- Waldmann H, Thutewohl M (2000) Ras-Farnesyltransferase-Inhibitors as Promising Anti-Tumor Drugs. 211: 117–130
- Wang G-X, see Chow H-F (2001) 217: 1–50
- Weil T, see Wiesler U-M (2001) 212: 1–40
- Werschkun B, Thiem J (2001) Claisen Rearrangements in Carbohydrate Chemistry. 215: 293–325
- Wiesler U-M, Weil T, Müllen K (2001) Nanosized Polyphenylene Dendrimers. 212: 1–40
- Williams RM, Stocking EM, Sanz-Cervera JF (2000) Biosynthesis of Prenylated Alkaloids Derived from Tryptophan. 209: 97–173
- Wirth T (2000) Introduction and General Aspects. 208: 1–5
- Wirth T (2003) Introduction and General Aspects. 224: 1–4

- Wirth T (2003) Oxidations and Rearrangements. *224*: 185–208
- Wong MW, see Steudel R (2003) *230*: 117–134
- Wong MW (2003) Quantum-Chemical Calculations of Sulfur-Rich Compounds. *231*:1-29
- Wrodnigg TM, Eder B (2001) The Amadori and Heyns Rearrangements: Landmarks in the History of Carbohydrate Chemistry or Unrecognized Synthetic Opportunities? *215*: 115–175
- Wytenbach T, Bowers MT (2003) Gas-Phase Confirmations: The Ion Mobility/Ion Chromatography Method. *225*: 201–226
- Yamaguchi H, Harada A (2003) Antibody Dendrimers. *228*: 237–258
- Yersin H, Donges D (2001) Low-Lying Electronic States and Photophysical Properties of Organometallic Pd(II) and Pt(II) Compounds. Modern Research Trends Presented in Detailed Case Studies. *214*: 81–186
- Yeung LK, see Crooks RM (2001) *212*: 81–135
- Yokoyama S, Otomo A, Nakahama T, Okuno Y, Mashiko S (2003) Dendrimers for Optoelectronic Applications. *228*: 205–226
- Yoshifuji M, Ito S (2003) Chemistry of Phosphanylidene Carbenoids. *223*: 67–89
- Zablocka M, see Majoral J-P (2002) *220*: 53–77
- Zhang J, see Chow H-F (2001) *217*: 1–50
- Zhdankin VV (2003) C-C Bond Forming Reactions. *224*: 99-136
- Zhao M, see Crooks RM (2001) *212*: 81-135
- Zimmermann SC, Lawless LJ (2001) Supramolecular Chemistry of Dendrimers. *217*: 95–120
- Zwanenburg B, ten Holte P (2001) The Synthetic Potential of Three-Membered Ring Aza-Heterocycles. *216*: 93–124

---

## Subject Index Vol. 230

- Acidithiobacillus ferrooxidans 167, 177  
Acidoid sol 161, 163  
Agriculture 184–185  
Allochromatium vinosum 172, 174–176  
Allotropes 1, 3–4, 12, 17, 19, 47, 54–57  
–, high-pressure 59  
Aqueous sulfur sol 154  
Assimilatory reduction 169  
Aten's sulfur 17
- $\beta$ -Po structure 70  
Bacteria 171, 172  
–, sulfate reducing 169  
bco sulfur 70  
Beggiatoa alba 172, 174, 176  
Biogas 181  
Bioleaching 167, 184, 186  
Bioreactor 178, 183–184  
Bioscrubber 183  
Biosulfur 168, 183, 185  
Bond length 51  
Branched rings 81, 103–104, 109, 117, 127, 129, 132
- Catenane-like molecules 112  
Cell membrane 172, 174–175, 177, 181  
Claus process 82, 181  
Coordination number 62  
Crystex 15, 45–47, 55, 89  
Cyanobacteria 171  
Cyttoplasmic membrane 181
- Density  
–, crystalline sulfur 56, 176  
–, liquid sulfur 83, 176  
–, sulfur globules 176  
Depolymerization 53  
Desulfurization, wastewater 153–154, 164  
DFT calculation of sulfur cation 139–142  
Diamond anvil cell 60  
Dichlorodisulfane 5, 11  
Dichlorotetrasulfane 8
- Dicyanohexasulfane 8  
Diradical, chain-length 91  
Displacement reaction 91  
Dissimilatory reduction 169  
DLVO-theory 172  
Dynamic light scattering 178
- Engel's sulfur 17
- $F_2S=S$  129  
Flavocytochrome c 180  
Floor temperature 111  
Flowers of sulfur 15  
Frasch process 82  
Free radical 57, 86, 90–91, 103, 105, 112
- Gas absorber 183–184  
Geller's phase I 49
- Halorhodospira abdelmalekii 181  
Helix 41  
Hexasulfane 105  
High-pressure/high-temperature phase 67  
Hydrodesulfurization process 82  
Hydrogen sulfide 157, 164  
–, oxidation 154, 162–163  
–, removal 181
- Isoelectric point 173, 179
- LaMer sulfur sol 157  
Landfill 184  
Liquid sulfur 10, 81–97, 101–113, 118, 122, 125–128  
–, band gap 103  
–, color 102–103, 105  
–, conductivity 107  
–, dielectric constant 107  
–, diradical 127–128  
–, electrical conductivity 106  
–, magnetic susceptibility 91  
–, photochemical polymerization 109

- , photochemistry 105
- , physical properties 83, 92, 109
- , polymer content 88
- , polymerization 90, 108–109
- , properties 81
- , quantitative composition 98
- , Raman spectra 95
- , reflectance spectra 105
- , UV-Vis spectroscopy 102
- , vibrational spectroscopy 94, 97, 104
- , viscosity 92
- , -, impact of halogens 93
- , -, minimum 112
  
- Macromolecular sulfur 41
- Melting point 52
- Metallic state 63
- Metallization 62
- Motif 17, 34, 50
  
- Natural gas 181
  
- Odén's colloidal sulfur 157
- Optical absorption edge 63
  
- Periplasmic space 181
- Phase diagram 60–61
- Photoinduced structural change 63
- Photoreaction 63
- Photosynthesis 171
- Plastic sulfur 43
- Polyelectrolytes 174
- Polymer adsorption 174
  - , preparation 87
  - , rate of formation 90
  - , structure 42
- Polymerization theory 81
- Polysulfanes 92–93
- Polysulfide 176, 179, 183
  - , oxidation 184
- Polythionate 156–159, 161, 164, 167, 176, 178–179, 186
- Protein membrane 177
  
- Quantum chemical calculation, sulfur cation 140–141
  
- Raffo sol 154, 157–160, 162
  - , aging 159–162
  - , density 158–160
  - , sulfur content 156, 158–159
- Raman spectroscopy 64, 176
- Ring, large 81, 88, 90, 110, 112
- Ring opening polymerization 108
  
- S 41
- $S_{\mu}$  15, 43, 89
- $S_{\omega}$  43
- $S_{\omega 1}$  45, 47
- $S_{\omega 2}$  45
- $S_x$  11
- $S_y$  43, 44
- $S_1$  41
- $S_3$  117, 120–122, 124–125, 132
  - , vibrational wavenumber 131
- $S_4$  117–132
  - , fundamental vibration 124
  - , vibrational wavenumber 130
- $S_4^{2+}$ , gas phase dissociation enthalpy 143
- $S_6$  17, 18, 30, 31
  - , high-pressure/high-temperature phase 65
  - , preparation 4, 9
- $S_7$  19–21, 106, 109, 127
  - , allotrope 19
  - , concentration in liquid sulfur 96
  - , preparation 1, 6
  - , pseudorotation 19
  - , strain energy 21
- $S_8$  117–119
  - , allotropes 21
  - , entropy, vibrational assignment 120
  - , molecular structure 22
  - , order-disorder transition 26
  - , preparation 6
  - , strain energy 22
  - , thermal expansion 21
- $S_9$  29
  - , preparation 8
- $S_{10}$  29
  - , preparation 8
- $S_{11}$  32
  - , preparation 9
- $S_{12}$  34
  - , preparation 10
  - ,  $\cdot\text{CS}_2$  11, 96
- $S_{13}$  35
  - , preparation 11
- $S_{14}$  36
  - , preparation 12
- $S_{15}$  37
  - , preparation 12
- $S_{18}$  37
  - , preparation 1, 13
- $S_{20}$  38
  - , preparation 13
- S-S bond 128
  - , dissociation enthalpy 128
  - , distance 51

- Selmi sol 154, 157, 159, 161–164  
Semiconductor 62  
Settler 183  
 $S_n$  molecule, enthalpy/entropy 119–122, 125, 128–129, 132  
 $SO_2$  emission 181, 185  
Sol 153–162  
–, monodispersed 155  
Sour gas 82  
Stabilizer 15  
Steric stabilization 167, 173–174  
Structure, high-pressure phase 69  
Sulfane monosulfonic acid 158, 161–162  
Sulfate reducing bacteria 169  
Sulfide, chemical oxidation 179  
–, oxidation 171  
– radicals 180  
Sulfur, colloidal 153, 154, 164  
–, commercial 6, 92, 102  
–, fibrous 15, 43, 45  
–, flowers 15  
–, high-purity 7  
–, insoluble 15  
–, laminar 45  
–, macromolecular 41  
–, polymeric 14, 56, 81–99, 102, 105–108, 112–113  
–, superconducting 60  
 $\epsilon$ -Sulfur 17  
 $\mu$ -Sulfur 87  
–, properties 81, 84, 89  
 $\pi$ -Sulfur 84, 90, 98–107, 118–128, 153–164  
–, critical parameter 101  
–, helical structure 67  
–, high purity 92  
–, melting curve 61  
–, melting point depression 85  
–, metallic liquid 61  
–, molecular nature 84, 87  
–, preparation 84, 87  
–, properties 81, 84  
–, Raman spectra 94, 96  
–, quantum-chemical calculation 117, 125  
 $\rho$ -Sulfur 17  
Sulfur allotropes 1, 3–4, 12, 17, 19, 47, 54–57  
– –, analysis 59  
– –, density 56  
– –, nomenclature 41  
– –, photochemical behavior 57  
– –, physical properties 52  
– –, Raman spectra 94–95  
– –, solubility 55  
– –, thermal behavior 53  
Sulfur bacteria 153–154, 163–164, 167–169, 171  
Sulfur cation, enthalpy of formation 143  
– –, hyperconjugation 149–150  
– –,  $\pi$  bonding 146–148  
– –, radical 138–139, 144, 146  
– –, solid state structure 137  
– –, solvation energy 144  
– –, synthetic procedure 137  
Sulfur chain, long 14  
– –, –, branched 105  
Sulfur cycle, biological 168  
Sulfur compound oxidizing bacteria 167–181, 185  
–, alkaliphilic 172, 183  
Sulfur globules 167–181, 185  
– –, *Allochromatium vinosum* 176  
– –, *Beggiatoa alba* 176  
Sulfur helix 48  
Sulfur homocycle  
–, enthalpies of formation 101  
–, isomer 39  
–, mean bond energy 101  
–, retention time 98  
Sulfur inclusion envelope 177  
Sulfur melts  
–, birefringence 89  
–, doping 92  
–, ESR spectra 91  
–, fractional crystallization 94  
–, glass-transition temperature 89  
–, HPLC 97  
–, Raman spectra 89, 94–95  
Sulfur molecule, HOMO/LUMO gap 104  
Sulfur radical cation 138–139, 144, 146  
Sulfur ring 55  
– –, branched 128  
– –, Raman spectra 94  
Sulfur sol, hydrophilic/hydrophobic 153–157, 160, 162  
– –, LaMer 157  
Sulfur vapor 117–119, 124–132  
–, composition 117–129, 132  
–, density 121, 124, 126  
–, mass spectrometry 118–127, 132  
–, partial pressure 120–121, 126  
–, speciation, thermodynamic 117, 120–122, 125, 128  
–, UV-Vis spectra 124  
–, vibrational spectra 120–122, 129  
Sulfurdichloride 5  
Sulfuretum 169  
Sulfuric acid production 184–185  
Superconducting state 60, 70  
Surface charge density 179

- Surfactant 56  
Syngas 181
- Ta<sub>4</sub>P<sub>4</sub>S<sub>29</sub> 49  
Tetrathiasulfuranes 113  
Tetrathionate 157, 163  
Thiobacillus spp. 167, 172  
Thiocapsa roseopersicina 177  
Thiosulfate 4, 154, 157–160, 163  
Torsional barrier 50  
Triple Point 61
- van der Waals attraction 172  
Van Niel reaction 171  
Vesicles 167, 178, 185
- Wackenroder's solution 154  
Wastewater desulfurization 153–154, 164  
Weimarn sol 153–156  
– –, stabilization by surfactants 155
- X-ray diffraction 175, 178  
XANES 176, 178
- Zero charge, point of 173

---

## Subject Index Vol. 231

- Ab initio calculations 2  
Acetylene 191  
Acidity 9  
Ag complex 161  
AIM 9  
Alkali metal sulfide 172  
Alkyne 190  
Allotrope 11  
-, solid 88  
Ammonia, supercritical 162  
Anomeric effect 220, 222  
Antimony complex 163  
Aromaticity 21  
Atomisation energy 9
- Barrier for rotation 108  
Basicity 21  
Basis set 2, 3  
Bond dissociation energy 10  
Bond energy 14  
Bond property 226  
Bond-bond interaction 226  
Branched ring/isomer 10, 12  
Brønsted acid 119
- Carbene 189  
Catena-sulfur 11  
Chain-like isomer 17  
Claus process 41, 198  
Claus sulfur 122  
Closed-shell interaction 20  
Cluster cation 18  
Cluster species 13  
Cobalt complex 157  
Condensation reaction 105  
Conformational isomer 7  
Constant, vibrational spectra 88  
Copper complex 161, 171, 172  
Coulomb explosion 137  
Crystex, vibrational spectrum 79  
CS<sub>2</sub>, reactions 191
- Decasulfurmonoxide 224  
Dehydrogenation reaction 9  
Density functional theory 3  
Desulfurization 181  
Dewar-Chatto-Duncanson bonding  
  scheme 175-176  
Dianion/dication 17, 19  
Dichlorosulfane 105  
1,3-Dienes 192  
Diiridium complex 199  
Dilution principle 219  
Dimerization energy 20  
Dipole moment 208  
Diruthenium complex 192, 194, 196-197  
Disproportionation reaction 14  
Disulfane 4  
-, ionization energy 115  
-, molecular structure 108  
-, vibrational spectra 113  
Disulfur dioxide 210  
Disulfur monoxide 204  
-, metal complex 210  
Divalent compound 155  
Donor ligand 132  
Double ionisation 19
- ECP 3  
Episulfidation, catalytic 188  
Equilibrium 180
- Fe complex 161, 177  
Force constant  $f_i(SS)$  226  
Frasch process 41
- Gallium complex 165, 180  
Gaussian series 3  
Geometry optimisation 3  
Germaaromatic 174  
Germanium complex 155, 162, 173-174,  
  180-181, 189  
Group 5 metal complex 163  
Group 6 metal complex 169

- Group 10 metal complex 168  
– –, zerovalent complexes 196  
Group 13 element complex 166  
Group 14 element complex 155, 162, 181, 189
- Hartree-Fock 3  
Helical structure 9  
Hemibond 23  
Heptasulfide 134  
Heptasulfur dioxide 217  
Heptasulfur monoxide 216  
Hexasulfide 133  
– –, isomeric 143  
Hexasulfur dioxide 214  
Hexasulfur monoxide 214  
Hg complex 161  
HOMO-LUMO gap 14  
Homocycle 12  
Hückel approximation 24  
Hybrid functional 3  
Hydrodesulfurization (HDS) 198  
Hydrogen polysulfide 99  
Hydrogen-bonded isomer 24  
Hydrogensulfido complex 170  
Hyperconjugation 9, 108  
Hyperpolarizability 10  
Hypervalent 3
- Indium complex 166  
 $\pi^*$ - $\pi^*$  Interaction 10, 226  
Ionisation energy, adiabatic 18  
Iridium complex 166, 168–171, 177, 199  
Iron complex 161, 177  
Isomerization reaction 5  
Isotopomer, mass spectrum 89
- Ketone 194
- Lanthanide complex 162  
Lapislazuli 146  
Laplacian 20  
Ligand-to-metal charge-transfer (LMCT) transition 176  
Liquid sulfur  
– –, absorption edge 36  
– –, combustion 206  
– –, isomers of S<sub>8</sub> 38  
– –, solubility of gaseous H<sub>2</sub>S 101  
– –, UV-Vis spectrum 36  
Low-valent metal compound 155
- Magnesium complex 161, 162  
Mercury complex 161
- Metal halides, reactions with polysulfides 166  
Metal–disulfido complex 174  
Metal–sulfur double bond 169  
Mixed dimer 25  
Molecular structure 207  
Molecular-dynamics simulation 15  
Molten salt (flux) method 172  
Molybdenum complex 169, 184, 188, 190  
Motif 8, 135  
Multireference calculation 11
- Niobium complex 163–164, 170, 183, 190  
Nonasulfur monoxide 223  
Nucleophilic degradation 138
- Octasulfide 134  
Octasulfur monoxide 219  
Olefin 192  
Oxidation 184
- Palladium complex 168  
Pb complex 155, 181  
Pentasulfide 133  
Pentasulfur monoxide 213  
Phosphine ligand 181  
Platinum complex 159, 167, 171, 184, 198  
Polarizability 10  
Polymeric chains, UV-Vis Spectrum 37  
Polymerization 15  
Polysulfane 7  
– –, acidity 120  
– –, decomposition 101  
– –, organic 122  
Polysulfane oxide 226  
Polysulfide, alkali 130, 134  
– –, anion 138, 141  
– –, aqueous, isotopic exchange 140  
– –, autoxidation 129  
– –, dianion 135, 138, 166  
– –, monoanion, structure 148  
– –, non-aqueous solution 141  
– –, preparation 130  
– –, reactions 143  
– –, solution 137–139  
– –, vibrational spectrum 142  
Polysulfur oxide 207, 225  
– –, SO stretching vibration 209  
Pseudorotation 12  
PSO 225  
Pyramidal inversion 222
- Quasi-aromatic 20
- Radical anion 16  
– –, singly-charged 17

- Radical cation, hemibonded 24  
Radical-chain reaction 116, 225  
Reductions by metal 197  
Resonance hybrid 25  
Rhenium complexes 166, 167, 170, 173,  
176, 183, 190, 191  
Rhodium complexes 156, 170, 171, 178  
-, complex, tetranuclear, with a rectangular  
S<sub>4</sub> unit 178  
Rotamer, non-helical 9  
Ruthenium complexes 160, 164, 169–177,  
184, 191–197
- S<sub>2</sub>, electronic state 36  
-, ionization potential 87  
-, UV-Vis Spectrum 33–34, 36  
-, vibrational spectrum 42  
S<sub>2</sub><sup>-</sup> radical 145  
S<sub>2</sub>O 208  
-, electronic spectrum 209  
-, force constant 209  
-, ligand in complex 211  
-, molecular structure 207  
-, polymerization 225  
-, preparation 205  
-, protonation 210  
-, reaction 210  
-, vibrational spectrum 208  
S<sub>2</sub>O<sub>2</sub> 211  
-, molecular parameter 211  
-, vibrational spectrum 212  
S<sub>3</sub>, ionization potential 87  
-, UV-Vis spectrum 33–34, 37  
-, vibrational spectrum 42  
S<sub>3</sub><sup>-</sup> radical 141, 145  
S<sub>3</sub>O 212  
S<sub>4</sub>  
-, isomers 34  
-, UV-Vis spectrum 33–34, 37, 40  
-, vibrational spectrum 43  
S<sub>4</sub><sup>-</sup> radical 147  
S<sub>4</sub>O 213  
S<sub>5</sub>, ionization potential 88  
S<sub>5</sub>O 213  
S<sub>6</sub>  
-, high pressure 82, 84  
-, ionization potential 88  
-, photolysis 40  
-, UV-Vis spectrum 39, 42  
-, vibrational spectrum 65  
-, XANES spectrum 92  
S<sub>6</sub><sup>-</sup>, radical 148  
S<sub>6</sub>:S<sub>10</sub>, vibrational spectrum 70  
S<sub>6</sub>O, dimerization 216  
α-S<sub>6</sub>O/β-S<sub>6</sub>O 214  
S<sub>6</sub>O<sub>2</sub> 214  
S<sub>7</sub>  
-, ionization potential 88  
-, photolysis 40  
-, UV-Vis spectrum 39  
-, vibrational spectrum 68  
S<sub>7</sub>O 216  
-, potential energy hypersurface 217  
S<sub>7</sub>O<sub>2</sub> 217, 218  
-, heterocyclic 219  
S<sub>8</sub>  
-, ionization potential 88  
-, isomer 37  
-, oxidation 220  
-, photolysis 40  
-, UV-Vis spectrum 33, 39  
-, vibrational spectrum 43  
-, XANES spectrum 92  
α-S<sub>8</sub>, absorption edge 40  
-, high pressure 82  
-, isotopic impurities 57  
-, UV-Vis spectrum 42  
-, vibrational spectrum 45  
β-S<sub>8</sub>, vibrational spectrum 64  
S<sub>8</sub>O 219  
-, infrared and Raman spectrum 220  
-, ligand 221  
-, molecular structure 220  
-, precursor for S<sub>2</sub>O 210  
-, reaction 221  
(S<sub>8</sub>O)<sub>2</sub>:SnCl<sub>4</sub> 221  
S<sub>9</sub>, vibrational spectrum 70  
S<sub>9</sub>O 223  
S<sub>10</sub>, preparation 216  
-, vibrational spectrum 70  
-, XANES spectrum 92  
S<sub>10</sub>O 224  
S<sub>11</sub>, vibrational spectrum 73  
S<sub>12</sub>, photolysis 40  
-, UV-Vis spectrum 39  
-, vibrational spectrum 73  
-, XANES spectrum 92  
S<sub>12</sub>:CS<sub>2</sub>, vibrational spectrum 73  
S<sub>12</sub>O<sub>2</sub>:2SbCl<sub>5</sub> 215  
S<sub>13</sub>, vibrational spectrum 75  
S<sub>14</sub>, vibrational spectrum 76  
-, XANES spectrum 92  
S<sub>15</sub>, vibrational spectrum 77  
S<sub>18</sub>, vibrational spectrum 77  
S<sub>20</sub>, vibrational spectrum 77  
S<sub>n</sub>O heterocycle 228  
S<sub>x</sub>, vibrational spectrum 77  
Sb complex 161, 163  
SCF-Xα-SW calculation 175  
Shared interaction 20

- Si complexes 155, 174, 181  
Silaaromatic 174  
 $S_n$  155–156, 161, 172–173, 177, 181, 183, 189, 195  
(SO)<sub>n</sub>, cyclic oligomer 211  
Sodalite 146  
Solvation 6  
Sour gas 101  
SS bond dissociation energy 117  
–, rotation about 109  
SSSS, planar unit 219, 226  
Sulfane 99  
–, <sup>1</sup>H-NMR spectra 112  
–, applications 122  
–, boiling point 106  
–, branched isomer 111  
–, condensation reaction 121  
–, density/viscosity 107  
–, deuterated 102  
–, dissociation enthalpy 107  
–, enthalpy of evaporation 107  
–, of formation 116  
–, nucleophilic displacement reactions 120  
–, photolysis 118  
–, preparation 102  
–, protonation/deprotonation 118  
–, raw 102  
–, silyl derivative 106  
–, solubility 107  
–, thermolysis 116  
–, UV-Vis spectra 115  
–, vibrational spectra 113  
Sulfane oil, thermal cracking 105  
Sulfonium ion 119  
Sulfoxide, adducts with Lewis acid 221  
Sulfur, electrochemical reduction 141  
–, elemental 155  
–, lower oxide 204  
–, polymeric 92  
–, –, high-pressure 82  
–, –, mass spectrum 89  
–, –, vibrational spectrum 78, 87  
–, solid, UV-Vis spectrum 40  
Sulfur atom, insertion 165  
Sulfur bacterium, XANES spectrum 92  
Sulfur cluster anion 16  
–, –, mass spectrum 89  
Sulfur compound, XANES spectrum 92  
Sulfur dioxide, electrical discharge 205  
Sulfur K-edge 90  
Sulfur melt 88  
Sulfur monoxide 204  
Sulfur radical 206  
Sulfur solution, UV-Vis spectrum 39  
Sulfur transfer reaction 185–187  
Sulfur vapor 88  
–, –, mass spectrum 88  
–, UV-Vis spectrum 33, 35  
Sulfur–sulfur bond, bond enthalpy 100  
Tantalum complex 164  
Tetrasulfane  
–, conformational isomer 110  
–, infrared and Raman spectra 114  
Tetrasulfide 133  
Tetrasulfur monoxide 213  
Tetrathiosulfurane 117  
Thermodynamic properties 15  
Thiirane 25  
Thionyl chloride 205  
Thiosulfoxide 5, 111  
–, organic 5  
Three-coordinate atom 13  
Three-electron bond 23  
Tin complexes 156, 172, 177, 183, 196  
Titanium complexes 158, 164, 173, 183–187  
Titanocene dicarbonyl 158  
Titanocene pentasulfide 185  
TiCl 166  
Transannular bond 20  
Transition metal complex 196  
Transition metal polysulfido complex 129  
Transition state 2  
Trinuclear heterometallic cluster 169  
Triplet diradical 15  
Trisulfane  
–, infrared and Raman spectra 114  
–, molecular structure 109  
Trisulfur monoxide 212  
Tungsten complex 169, 177  
Ultramarine 146  
UV-Vis spectrum  
–, gaseous sulfur 33  
–, liquid sulfur 36  
–, polymeric chains 37  
–, solid sulfur 40  
–, sulfur solution 39  
Valence bond theory 6  
van der Waals complex 23  
Vanadium complex 164  
Vibrational frequency, calculation of 3  
Vibrational spectra, calculation of 14  
XANES spectrum 90  
Zinc complexes 161, 180, 187, 190, 191

# Reviews and Monographs on the Chemistry of Sulfur-Rich Compounds

(ordered chronologically)

*Gmelin Handbook of Inorganic Chemistry*, 8th ed., *Sulfur*, Springer, Berlin:

- 1953: Hydrides and Oxides of Sulfur (in German)
- 1953: Elemental Sulfur (in German)
- 1953: Occurrence and Technology of Sulfur and Its Compounds  
(in German)
- 1960: Sulfur Oxoacids (in German)
- 1963: Sulfur Compounds with Nitrogen, Oxygen and Halides (in German)
- 1977: Sulfur-Nitrogen Compounds, Part 1 (in German)
- 1978: Sulfur Halides (in German)
- 1978: Thionyl Halides (in German)
- 1980: Sulfur Oxides (in German)
- 1983: Sulfanes (in English)
- 1985-1994: Sulfur-Nitrogen Compounds, Parts 2-10 (in English)

B. Meyer, *Elemental Sulfur: Chemistry and Physics*, Interscience, New York,  
1965; with Chapters on the following topics:

1. Nomenclature of Sulfur Allotropes
2. Structures of Solid Sulfur Allotropes
3. Phase Transition Rate Measurements
4. Preparation and Properties of Sulfur Allotropes
5. Properties of Polymeric Sulfur
6. Physical Properties of Liquid Sulfur
7. Molecular Composition of Sulfur Vapor
8. Mechanical Properties of Sulfur
9. High Pressure Behavior of Sulfur
10. Electrical and Photoconductive Properties of Orthorhombic Sulfur Crystals
11. ESR Studies of Unstable Sulfur Forms
12. Vibrational Spectra of Elemental Sulfur
13. Electronic Spectrum and Electronic States of S<sub>2</sub>
14. Reactions of Atomic Sulfur
15. Reactions of the Sulfur-Sulfur Bond

16. Preparation of Unusual Sulfur Rings
17. Liquid Solutions of Sulfur
18. Potential Applications of Sulfur

F. Tuinstra, *Structural Aspects of the Allotropy of Sulfur and the Other Divalent Elements*, Waltman, Delft, **1967**.

G. Nickless (Ed.), *Inorganic Sulfur Chemistry*, Elsevier, Amsterdam, **1968**; with Chapters on the following topics:

1. The Sulfur Atom and its Nucleus
2. Orbitals in Sulfur and its Compounds
3. Stereochemistry of Group 16 Compounds
4. Mechanisms of Sulfur Reactions
5. Structural Studies on Sulfur Compounds
6. Analytical Chemistry of Sulfur Compounds
7. Elemental Sulfur
8. The Biogeochemical Sulfur Cycle
9. Chemistry of the Sulfur-Phosphorus Bond
10. Sulfanes
11. Oxides of Sulfur
12. Compounds with Sulfur-Halogen Bonds
13. Sulfur-Nitrogen Compounds
14. Lower Oxoacids of Sulfur
15. Sulfuric Acid
16. Fluorosulfuric Acid as a Solvent System
17. Amido- and Imidosulfuric Acid
18. Metal Sulfides

M. V. Ivanov, *Microbiological Processes in the Formation of Sulfur Deposits*, Jerusalem, **1968**.

A. V. Tobolsky (Ed.), *The Chemistry of Sulfides*, Interscience, New York, **1968**.

J. A. Karchmer (Ed.), *The Analytical Chemistry of Sulfur and its Compounds*, Part I, Wiley, New York, **1970**; with Chapters on following topics:

1. Elemental Sulfur

2. Total Sulfur
3. Sulfur-Containing Gases
4. Oxygen-Containing Inorganic sulfur Compounds
5. Other Inorganic Sulfur Compounds
6. Thiols

A. Senning (Ed.), *Sulfur in Organic and Inorganic Chemistry*, Vol. 1, Dekker, New York, **1971**, with Chapters on the following topics:

1. The Sulfur-Silicon Bond
2. The Sulfur-Nitrogen Bond
3. The Sulfur-Phosphorus Bond
4. The Sulfur-Oxygen Bond
5. The Sulfur-Sulfur Bond
6. The Sulfur-Fluorine Bond
7. The Sulfur-Chlorine Bond
8. The Sulfur-Bromine Bond
9. The Sulfur-Iodine Bond

A. Senning (Ed.), *Sulfur in Organic and Inorganic Chemistry*, Vol. 2, Dekker, New York, **1972**, with Chapters on the following topics:

1. Chemistry of Atomic Sulfur
2. Diatomic Species Containing Sulfur
3. Bond Energy Terms in the Chemistry of sulfur, Selenium and Tellurium
4. Oxyacids of Sulfur
5. Pharmacology and Toxicology of Inorganic Sulfur Compounds
6. Mass Spectra of Sulfur Compounds
7. Mixed Sulfur Halides
8. Commercially Important Sulfur Compounds
9. Chromatographic Techniques in Sulfur Chemistry

A. Senning (Ed.), *Sulfur in Organic and Inorganic Chemistry*, Vol. 3, Dekker, New York, **1972**, with Chapters on the following topics:

1. Reactions of Elemental Sulfur with Inorganic, Organic and Organometallic Compounds
2. Inorganic and Organic Polysulfides
3. Quantum Chemistry of sulfur Compounds
4. Steric Aspects of Sulfur Chemistry

5. NMR spectra of Sulfur Compounds
6. Labeled Sulfur Compounds
7. Thione-Enethiol Tautomerism
8. Nomenclature of Sulfur Compounds
9. Nucleophilicity of Organic Sulfur Compounds

J. A. Karchmer (Ed.), *The Analytical Chemistry of Sulfur and its Compounds*, Part II, Wiley, New York, **1972**; with Chapters on the following topics:

1. Sulfides
2. Di- and Polysulfides
3. Thiophenes
4. Tetra- and Hexavalent Organosulfur Compounds

D. J. Miller, T. K. Wiewiorowski (Eds.), *Sulfur Research Trends*, Adv. Chem. Ser. 110, ACS, Washington, **1972**; with Chapters on the following topics:

1. Semiempirical MO Calculations on Sulfur-Containing Molecules
2. Electron Behavior in Some Sulfur Compounds
3. Spectra of Sulfur Allotropes
4. Transition Metal Complexes with Sulfur-Donor Ligands
5. Structures of Sulfur-Nitrogen Compounds
6. Influence of High Pressure on Elemental Sulfur
7. Reactions of Mercaptanes with Liquid Sulfur
8. Photolysis of Thiols
9. Addition of Sulfur Atoms to Olefins
10. Sulfur Chlorides and Organochlorides
11. Raman Spectra of Amorphous Chalcogenide Alloys
12. Fluorinated Sulfide Polymers
13. Electrical Conductivity of Liquid Sulfur and Sulfur-Phosphorus Mixtures
14. Chemical-Mechanical Alteration of Elemental Sulfur
15. Potential Applications of Sulfur

M. Schmidt, W. Siebert, in *Comprehensive Inorganic Chemistry*, Vol. 2, Chapter 23 (Sulfur), Pergamon, Oxford, **1973**, pp. 795-933 (579 references).

K. C. Mills, *Thermodynamic Data for Inorganic Sulfides, Selenides and Tellurides*, Butterworths, London, **1974**.

D. M. Greenberg (Ed.), *Metabolic Pathways*, 3rd ed., Vol. VII: *Metabolism of Sulfur Compounds*, Academic Press, New York, **1975**.

G. Brauer (ed.), *Handbuch der Präparativen Anorganischen Chemie*, Vol. 1, Enke, Stuttgart, **1975** (Preparation of basic inorganic sulfur compounds).

B. Meyer, *Sulfur, Energy, and Environment*, Elsevier, Amsterdam, **1977** (containing 1600 references with full titles). Chapters on the following topics:.

1. History of Sulfur
2. Properties of sulfur and Inorganic Sulfur Compounds
3. Analytical Chemistry of Sulfur Compounds
4. Occurrence and Sources of Sulfur
5. The Sulfur Cycles
6. Sulfur Production
7. Recovery of Sulfur from Combustion Gases
8. Environmental Control and Legislation
9. Medical Use and Health Effects
10. Sulfur in Agriculture and Food
11. Industrial Uses of Sulfur and Its Compounds
12. Sulfur Polymers
13. Sulfur Containing Materials
14. Future Trends

D. J. Bourne (Ed.), *New Uses of Sulfur-II*, Adv. Chem. Ser. 165, ACS, Washington, **1978**.

H. G. Heal, *The Inorganic Heterocyclic Chemistry of Sulfur, Nitrogen and Phosphorus*, Academic Press, London, **1980**.

H. Bothe, A. Trebst (Eds.), *Biology of Inorganic Nitrogen and Sulfur*, Springer, Berlin, **1981**.

A. Senning (Ed.), *Sulfur in Organic and Inorganic Chemistry*, Vol.4, Dekker, New York, **1982**, with Chapters on the following topics:

1. The Sulfur-Silicon Bond
2. The Sulfur-Nitrogen Bond
3. The Sulfur-Phosphorus Bond
4. The Sulfur-Fluorine Bond
5. The Sulfur-Chlorine Bond
6. The Sulfur-Bromine Bond
7. The Sulfur-Iodine Bond

M. V. Ivanov, J. R. Freney (Eds.), *The Global Biochemical Sulfur Cycle*, SCOPE 19, Wiley, New York, **1983**.

A. Müller, B. Krebs (Eds.), *Sulfur - Its Significance for Chemistry, for the Geo-, Bio- and Cosmosphere and Technology*, Elsevier, Amsterdam, **1984**; with Chapters on the following topics:

1. Elemental Sulfur and Homocyclic Compounds and Ions (R. Steudel)
2. Sulfur in the Earth's Crust, Its Origin and Natural Cycle (K. H. Wedepohl)
3. Role of Sulfur in Black Powder (F. Seel)
4. Lapislazuli and Ultramarine Pigments (F. Seel)
5. New Developments in Organic Sulfur Chemistry (G. Kresze)
6. Organometallic Sulfur Compounds (H. Vahrenkamp)
7. Thiolates as Ligands in Transition Metal Complexes (J. R. Dilworth)
8. Metal Complexes of Sulfur and Sulfur-Nitrogen Compounds (H. W. Roesky)
9. Sulfido-Complexes of Molybdenum and Tungsten (A. G. Wedd)
10. Interaction of Metal Centers Through Sulfur-Containing Ligands (O. Kahn, J.-J. Girerd)
11. Electronic and Resonance Raman Spectra of Sulfur-Containing Complexes (R. J. H. Clark)
12. Technology of Sulfuric Acid (K. Brändle)
13. Flue Gas Desulfurization (M. Schmidt)
14. Metal Sulfides in Photovoltaic and Photoelectrochemical Energy Conversion (H. Tributsch)
15. Inorganic Chemistry of Rubber Vulcanization (J. A. McCleverty)
16. Biodegradation of Sulfur Minerals (K. Bosecker)
17. Microorganisms and the Sulfur Cycle (H. G. Trüper)

18. Phototrophic Bacteria and Their Sulfur Metabolism (H. G. Trüper)
19. Cytochromes and Iron Sulfur Proteins in Bacterial Sulfur Metabolism (U. Fischer)
20. Sulfur-Containing Ligands in Metalloproteins and Enzymes (W. E. Newton)
21. Genetic Diseases of Sulfur Metabolism in Humans (F. Skovby, S. H. Mudd)

F. Bernardi, I. G. Csizmadia, A. Mangini (Eds.), *Organic Sulfur Chemistry: Theoretical and Experimental Advances*, Elsevier, Amsterdam, **1985**.

I. Hargittai, *The Structure of Volatile Sulfur Compounds*, Reidel Publ., Dordrecht, **1985** (structures determined by electron diffraction and microwave spectroscopy).

R. J. Huxtable, *Biochemistry of Sulfur*, Plenum, New York, **1986**.

W. B. Jakoby, O. W. Griffith (Eds.), *Methods in Enzymology*, Vol. 143: *Sulfur and Sulfur Amino Acids*, Academic Press, Orlando, **1987**.

M. G. Voronkov, N. S. Vyazankin, E. N. Deryagina, A. S. Nakhmanovich, V. A. Usov, *Reactions of Sulfur with Organic Compounds*, Plenum Press, New York, **1987**; with Chapters on the following topics:

1. Structure and Physical Properties of Elemental Sulfur
2. Preparation and Chemical Properties of Sulfur Allotropes
3. Action of Sulfur on Hydrocarbons
4. Reactions with Organic Halides
5. Reactions with Organic Sulfur Compounds
6. Reactions with Oxygen-Containing Compounds
7. Reactions with Nitrogen-Containing Compounds
8. Reactions with Organometallic Compounds

B. Zwanenburg, A. J. H. Klunder (Eds.), *Perspectives in the Organic Chemistry of Sulfur*, Elsevier, Amsterdam, **1987**.

J. A. Cole, S. J. Ferguson (Eds.), *The Nitrogen and Sulfur Cycles*, Cambridge Univ. Press, Cambridge, **1988**.

R. T. Oakley, *Sulfur-Nitrogen Heterocycles*, *Progr. Inorg. Chem.* **1988**, 36, 299-391.

P. Brimblecombe, A. Yu. Lein (Eds.), *Evolution of the Biochemical Sulfur Cycle*, SCOPE 39, Wiley, New York, **1989**.

E. S. Saltzman, W. J. Cooper (Eds.), *Biogenic Sulfur in the Environment*, ACS Symp. Ser. 393, ACS, Washington DC, **1989**.

W. L. Orr, C. M. White, *Geochemistry of Sulfur in Fossil Fuels*, A.C.S. Symp. Ser., Vol. 429, American Chemical Society, Washington, **1990**.

C. Chatgililoglu, K.-D. Asmus (Eds.), *Sulfur-Centered Reactive Intermediates in Chemistry and Biology*, Plenum Press, New York, **1990**; *inter alia* with Chapters on the following topics:

1. Force Field and Molecular Orbital Calculations in Organosulfur Chemistry
2. Electronic Transitions in Sulfur-Centered Radicals
3. Electronic Properties of Sulfur-Containing Substituents and Molecules
4. Reactivity of Sulfur-Centered Nucleophiles
5. Alkenethiylperoxyl Radicals
6. Thermochemistry of Sulfur-Centered Intermediates
7. Single Electron Transfer in Nucleophilic Substitution
8. Electrochemical Reduction of Sulfur Compounds
9. Pulse Radiolysis
10. ESR Spectroscopy of Sulfur-Centered Radicals
11. Three-Electron Bonded Radicals
12. Radical Cations
13. Reaction Kinetics of Sulfur-Centered Biological Radicals
14. Redox Systems with Sulfur-Centered Species
15. Repair in Radiation Biology
16. Actions of the Glutathion/Disulfide System

S. Oae, *Organic Sulfur Chemistry: Structure and Mechanism*, CRC Press, Boca Raton, **1991**.

H. R. Krouse, V. A. Grinenko (Eds.), *Stable Isotopes: Natural and Anthropogenic Sulfur in the Environment*, SCOPE 43, Wiley, New York, **1991**.

R. W. Howarth, J. W. B. Stewart, M. V. Ivanov (Eds.), *Sulfur Cycling on the Continents*, SCOPE 48, Wiley, New York, **1991**.

S. Oae, T. Okuyama (Eds.), *Organic Sulfur Chemistry: Biochemical Aspects*, CRC Press, Boca Raton, **1992**.

R. B. King (Ed.), *Encyclopedia of Inorganic Chemistry*, Vol. 7, Wiley, Chichester, **1994**; *inter alia* with Chapters on the following topics:

1. Inorganic Sulfur Chemistry (D. Woollins)
2. Sulfur-Nitrogen Compounds (T. Chivers)
3. Organic Polysulfanes (R. Steudel, M. Kustos)
4. S-Donor Ligands (M. Schröder)

*Ullmann's Encyclopedia of Industrial Chemistry*, Vol. A25, VCH, Weinheim, **1994**.

C. N. Alpers, D. W. Blowes (Eds.), *Environmental Geochemistry of Sulfide Oxidation*, A.C.S. Symp. Ser., Vol 550, American Chemical Society, Washington D.C., **1994**.

Holleman-Wiberg: *Lehrbuch der Anorganischen Chemie*, 101. Auflage, de Gruyter, Berlin, **1995** (textbook with 75 pages on sulfur chemistry).

M. A. Vairaramurthy, M. A. A. Schoonen (Eds.), *Geochemical Transformations of Sedimentary Sulfur*, ACS Symp. Ser. 612, Washington, **1995**.

L. L. Barton (Ed.), *Sulfate-Reducing Bacteria*, Plenum Press, New York, **1995**.

E. I. Stiefel, K. Matsumoto (Eds.), *Transition Metal Sulfur Chemistry*, A.C.S. Symp. Ser., Vol. 653, American Chemical Society, Washington D.C., **1996**.

N. N. Greenwood, A. Earnshaw, *Chemistry of the Elements*, 2nd ed., Butterworth, Oxford, **1997** (textbook with 101 pages on sulfur chemistry).

R. Steudel, *Chemie der Nichtmetalle*, de Gruyter, Berlin, **1998** (modern textbook with 60 pages on sulfur chemistry).

Z. B. Alfassi (Ed.), *The Chemistry of Sulfur Radicals*, Wiley, Chichester, **1999**.

T. Kabe, A. Ishiara, W. Qian (Eds.), *Hydrodesulfurization and Hydrodenitrogenation*, Wiley-VCH, Weinheim, **1999**.

P. N. L. Lens, L. Hulshoff Pol (Eds.), *Environmental Technologies to Treat Sulfur Pollution: Principles and Engineering*, IWA Publishing, London, **2000**; with

Chapters on the following topics:

1. The Chemical Sulfur Cycle (R. Steudel)
2. The Geochemical Sulfur Cycle (J. J. Middleburg)
3. The Biological Sulfur Cycle (T. Brüser, P. N. L. Lens, H. G. Trüper)
4. Removal of Sulfur from Diesel Oil (H. R. Reinhoudt)
5. Bioleaching of Sulfide Minerals (M. Boon)
6. Sulfur Transformation during Sewage Transport (T. Hvitvedt-Jacobsen, P. H. Nielsen)
7. Biological Treatment of Organic Sulfate-Rich Wastewaters (P. N. L. Lens, F. Omil, J. M. Lema, L. W. Hulshoff Pol)
8. Biological Removal of Sulfurous Compounds from Wastewaters (B. Johnson)
9. Anaerobic Treatment of Sulfate-Rich Wastewaters (J.-P. Steyer, N. Bernet, P. N. L. Lens, R. Moletta)
10. Survey of H<sub>2</sub>S and SO<sub>2</sub> Removal Processes (J. A. Lagas)
11. Novel Biological Processes for the Removal of H<sub>2</sub>S and SO<sub>2</sub> (A. J. H. Janssen, H. Dijkman, G. Janssen)
12. Biological Treatment of Gases Polluted by Volatile Sulfur Compounds (V. Herrygers, H. Van Langenhove, E. Smet)
13. Methods of Odor Measurement and Assessment (R. H. Fenner, R. M. Stuetz)
14. Treatment of Solid Materials Containing Inorganic Sulfur Compounds (R. Tichý)
15. Agricultural Aspects of Sulfur (W. H. O. Ernst)
16. Biodegradation of Sulfonated Aromatic Compounds (N. C. G. Tan, J. A. Field)

17. Metal Effects on Sulfur Cycle Bacteria and Metal Removal by Sulfate Reducing Bacteria (O. J. Hao)
18. Interactions of the Sulfur and Nitrogen Cycles: Microbiology and Process Technology (P. M. Chazal, P. N. L. Lens)
19. Sulfur-Storing Bacteria and Bulking of Activated Sludge ((D. H. Eikelboom)
20. Sulfur Problems in Anaerobic Digestion (V. O'Flaherty, E. Colleran)
21. Corrosion and Sulfur Bacteria (B. J. Little, R. I. Ray, R. K. Pope)
22. Recent Developments in Research on Biogenic sulfuric Acid Attack of Concrete (E. Vincke, J. Montaney, A. Beeldens, N. De Belie, L. Taerve, D. Van Gemert, W. H. Verstraete)

Holleman-Wiberg: *Inorganic Chemistry*, Academic Press, New York, **2001** (most comprehensive inorganic chemistry textbook available).

R. Steudel, *Organic Polysulfanes*  $R_2S_n$  ( $n > 2$ ), *Chem. Rev.* **2002**, *102*, 3905-3945.

More reviews and monographs on (mainly inorganic) sulfur chemistry are cited in the various Chapters of Volumes 230 and 231.